

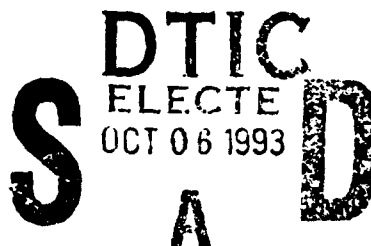


2

**NORWAY/UNITED STATES DESIGN PROTECTIVE
AIRCRAFT SHELTER (PAS) QUANTITY-DISTANCE
PROGRAM 1/3-SCALE TEST SERIES**

**Volume I of V
PAS 1-4 Summary**

**Edward H. Bultmann, Jr.
Bruce A. Schneider**



**New Mexico Engineering Research Institute
The University of New Mexico
Albuquerque, NM 87131-1376**

August 1993

Final Report

Approved for public release; distribution is unlimited.



**PHILLIPS LABORATORY
Advanced Weapons and Survivability Directorate
AIR FORCE MATERIEL COMMAND
KIRTLAND AIR FORCE BASE, NM 87117-5776**

93 10 5 172

93-23403



41370

This final report was prepared by the New Mexico Engineering Research Institute, Albuquerque, New Mexico, under Contract F29601-87-C-0001, Job Orders 41181599 and NORWAYYA, with the Phillips Laboratory, Kirtland Air Force Base, New Mexico. The Laboratory Project Officer-in-Charge was Aaron Perea (WSSD).

When Government drawings, specifications, or other data are used for any purpose other than in connection with a definitely Government-related procurement, the United States Government incurs no responsibility or any obligation whatsoever. The fact that the Government may have formulated or in any way supplied the said drawings, specifications, or other data, is not to be regarded by implication, or otherwise in any manner construed, as licensing the holder, or any other person or corporation; or as conveying any rights or permission to manufacture, use, or sell any patented invention that may in any way be related thereto.

This report has been authored by a contractor of the United States Government. Accordingly, the United States Government retains a nonexclusive, royalty-free license to publish or reproduce the material contained herein, or allow others to do so, for the United States Government purposes.

This technical report has been reviewed by the Public Affairs Office and is releasable to the National Technical Information Service (NTIS). At NTIS, it will be available to the general public, including foreign nationals.

If your address has changed, if you wish to be removed from the mailing list, or if your organization no longer employs the addressee, please notify PL/WSSD, Kirtland AFB, NM 87117-5776 to help maintain a current mailing list.

This technical report has been reviewed and is approved for publication.

FOR THE COMMANDER



AARON PEREA
Project Officer



BRENDAN B. GODFREY, ST
Director, Advanced Weapons
and Survivability Directorate

REPORT DOCUMENTATION PAGE

Form Approved
OMB No. 0704-0188

Public reporting burden for this collection of information is estimated to average 1 hour per response, including the time for reviewing instructions, searching existing data sources, gathering and maintaining the data needed, and completing and reviewing the collection of information. Send comments regarding this burden estimate or any other aspect of this collection of information, including suggestions for reducing this burden, to Washington Headquarters Services, Directorate for Information Operations and Reports, 1215 Jefferson Davis Highway, Suite 1204, Arlington, VA 22202-4302, and to the Office of Management and Budget, Paperwork Reduction Project (0704-0188), Washington, DC 20503.

1. AGENCY USE ONLY (Leave blank)		2. REPORT DATE August 1993		3. REPORT TYPE AND DATES COVERED Final; Jul 91 - Mar 93	
4. TITLE AND SUBTITLE NORWAY/UNITED STATES PROTECTIVE AIRCRAFT SHELTER (PAS) QUANTITY-DISTANCE PROGRAM 1/3-SCALE TEST SERIES Volume I of V: PAS 1-4 Summary				5. FUNDING NUMBERS C: F29601-87-C-0001 PE: 0603790D PR: 4118 TA: 15 WU: 99	
6. AUTHOR(S) Edward H. Bultmann, Jr. and Bruce A. Schneider					
7. PERFORMING ORGANIZATION NAME(S) AND ADDRESS(ES) New Mexico Engineering Research Institute The University of New Mexico Albuquerque, NM 87131-1376				8. PERFORMING ORGANIZATION REPORT NUMBER NMERI SS 2.33(8)	
9. SPONSORING/MONITORING AGENCY NAME(S) AND ADDRESS(ES) Phillips Laboratory 3550 Aberdeen Ave SE Kirtland AFB, NM 87117-5776				10. SPONSORING/MONITORING AGENCY REPORT NUMBER PL-TR--93-1009 Vol. I	
11. SUPPLEMENTARY NOTES This work was funded by the Norwegian Defence Construction Service and the United States Government.					
12a. DISTRIBUTION/AVAILABILITY STATEMENT Approved for public release; distribution is unlimited.				12b. DISTRIBUTION CODE	
13. ABSTRACT (Maximum 200 words) The objective of the Combined Norwegian/U.S. Aircraft Shelter Quantity-Distance Program was to establish an experimental database that could be used to develop explosives safety criteria for a Norwegian-designed aircraft shelter. These shelters have been constructed at various bases in Europe and are used by U.S. and Norwegian air forces. The current criteria for explosives storage in aircraft shelters are based largely on U.S. aircraft shelter designs, which differ significantly in structural details from the Norwegian version. The program included four tests of 1/3-scale models of the Norwegian shelter. Charges varying from 3.7 to 100 kg of C-4 explosive were detonated inside the model shelters. Airblast pressures were measured in the interior and exterior areas surrounding the models. High-speed photography and accelerometers were used to determine structural debris trajectories and velocities. The final distribution of structural debris in the areas surrounding the models was also recorded. Volume I of this report presents a detailed discussion of the results of each test with selected experimental data. Volumes II through V provide a complete set of the experimental data gathered in each of the test events. These data will be provided to those U.S., Norwegian, and NATO agencies responsible for establishing explosives storage safety criteria for the Norwegian aircraft shelter.					
14. SUBJECT TERMS Aircraft Shelters, Quantity-Distance Criteria, Explosives Storage Airblast, Debris Distribution, Accidental Explosions, MK 84 GP Bomb, Explosives Safety				15. NUMBER OF PAGES 420	
				16. PRICE CODE	
17. SECURITY CLASSIFICATION OF REPORT Unclassified	18. SECURITY CLASSIFICATION OF THIS PAGE Unclassified	19. SECURITY CLASSIFICATION OF ABSTRACT Unclassified	20. LIMITATION OF ABSTRACT		

PREFACE

This report was prepared by the New Mexico Engineering Research Institute (NMERI), The University of New Mexico, under Subtask 2.33 of Contract F29601-87-C-0001, with the Phillips Laboratory, Kirtland Air Force Base, New Mexico. The Norwegian/US Aircraft Shelter Quantity-Distance Program under which this test program was conducted was cosponsored by the United States and the Kingdom of Norway. The 1/3-scale aircraft shelter models were designed, constructed, instrumented, and tested by NMERI.

The Phillips Laboratory Program Manager and Subtask Officer for this subtask was Capt Mike Ulshafer of PL/WSB. The Phillips Laboratory Technical Coordinator was Aaron Perea. Arfin Jenssen was the Norwegian Technical Advisor/Coordinator. Dr. Edward H. Bultmann, Jr., of NMERI was the Principal Investigator for the subtask. Bruce Schneider of NMERI was the Alternate Principal Investigator for this subtask. Jon A. Kirst was the Instrumentation Engineer, Curtis Burnett was the Lead Construction (Field) Technician for this subtask. Jesse Martinez was the Lead Instrumentation Technician.

Accession For	
NTIS	CRA&I <input checked="" type="checkbox"/>
DTIC	TAB <input type="checkbox"/>
Unannounced	<input type="checkbox"/>
Justification	
By	
Distribution /	
Availability Codes	
Dist	Avail and/or Special
A1	

CONTENTS

<u>Section</u>		<u>Page</u>
1.0	INTRODUCTION	1
1.1	BACKGROUND	1
1.2	SCOPE	2
2.0	GENERAL TEST DESCRIPTION	3
2.1	TEST STRUCTURES	3
2.2	EXPLOSIVE CHARGES	8
2.3	INSTRUMENTATION PLAN	8
	2.3.1 General	8
	2.3.2 Airblast Measurements	10
	2.3.3 Structural Response Measurements	10
	2.3.4 Photographic Plan	10
	2.3.5 Debris Distribution	11
3.0	PAS-1 TEST	13
3.1	TEST DESCRIPTION	13
	3.1.1 General	13
	3.1.2 Instrumentation Plan	13
3.2	TEST RESULTS	29
	3.2.1 Structural Damage Survey	29
	3.2.2 Data Obtained from Instrumentation	48
	3.2.3 Rock Rubble Berm	82
	3.2.4 Debris Distribution	82
4.0	PAS-3 TEST	84
4.1	TEST DESCRIPTION	84
	4.1.1 General	84
	4.1.2 Instrumentation Plan	91
4.2	TEST RESULTS	105
	4.2.1 Structural Damage Survey	105
	4.2.2 Data Obtained from Instrumentation	133
	4.2.3 Rock Rubble Berm	153
	4.2.4 Debris Distribution	153

CONTENTS (Continued)

<u>Section</u>		<u>Page</u>
5.0	PAS-2 TEST	181
5.1	TEST DESCRIPTION	181
5.1.1	General	181
5.1.2	Instrumentation Plan	181
5.2	TEST RESULTS	198
5.2.1	Structural Damage Survey	198
5.2.2	Data Obtained from Instrumentation	218
5.2.3	Rock Rubble Berm	245
5.2.4	Debris Distribution	245
6.0	PAS-4 TEST	260
6.1	TEST DESCRIPTION	260
6.1.1	General	260
6.1.2	Instrumentation Plan	260
6.2	TEST RESULTS	270
6.2.1	Structural Damage Survey	270
6.2.2	Data Obtained from Instrumentation	313
6.2.3	Rock Rubble Berm	332
6.2.4	Debris Distribution	339
7.0	CONCLUSIONS AND RECOMMENDATIONS	383
7.1	STRUCTURAL RESPONSE	383
7.1.1	General	383
7.1.2	Potential Hazards	389
7.1.3	Considerations for Future Structural Modifications	390
7.2	CONCRETE DEBRIS	391
7.2.1	The Tests	391
7.2.2	Potential Hazards	395

FIGURES

<u>Figure</u>		<u>Page</u>
1.	Longitudinal cross section through test structure.	4
2.	Transverse cross section through test structure.	5
3.	Longitudinal section: Identification key to structural components.	6
4.	Transverse section: Identification key to structural components.	7
5.	Front view of test structure.	9
6.	Side view of test structure.	9
7.	Location of GZ for PAS-1.	14
8.	Explosive charge, 3.7 kg of C-4, PAS-1.	14
9.	Photo pole locations, PAS-1.	15
10.	Locations of aluminum cubes, PAS-1.	16
11.	Instrumentation in floor of structure, PAS-1.	23
12.	Instrumentation on outside of front door at X = 415, PAS-1.	24
13.	Instrumentation on inside surface of front door at X = 498, PAS-1.	25
14.	Instrumentation on arch at X = 645, PAS-1.	26
15.	Instrumentation on arch at X = 3976, PAS-1.	27
16.	Instrumentation on arch at X = 6818, PAS-1.	28
17.	Instrumentation on inner surface of backwall at X = 13010, PAS-1.	30
18.	Free-field airblast gage locations, PAS-1.	31
19.	Camera station locations, PAS-1.	32
20.	Crack pattern in floor slab, around GZ, PAS-1.	33
21.	Cracks in floor slab adjacent to door pit, PAS-1.	34
22.	Cracks in left back corner of floor slab, PAS-1.	36
23.	Gap between floor slab and floor of exhaust port, PAS-1.	36
24.	Cracking at left front wall and parapet, PAS-1.	37
25.	Cracking at right front wall and parapet, PAS-1.	38
26.	Crack pattern in face of parapet, PAS-1.	39
27.	Posttest location of vestibule, PAS-1.	41

FIGURES (Continued)

<u>Figure</u>		<u>Page</u>
28.	Cracks in left wingwall, PAS-1.	42
29.	Debris from top of left wingwall, PAS-1.	43
30.	Crack pattern in right wingwall (front), PAS-1.	43
31.	Pipe vent from backwall, PAS-1.	45
32.	Crack pattern in left corner of the apron slab, PAS-1.	45
33.	Posttest location of front door, PAS-1.	46
34.	Left side hinge bracket and pin of front door, PAS-1.	46
35.	Outward deformation near centerline of front door, PAS-1.	47
36.	Crack pattern in arch, PAS-1.	49
37.	Diagonal crack pattern on right front corner of arch, PAS-1.	50
38.	PAS-1, MN 0604.	52
39.	PAS-1, MN 0602.	55
40.	PAS-1, MN 0603.	56
41.	PAS-1, MN 0401.	57
42.	PAS-1, MN 0402.	58
43.	PAS-1, MN 0403.	59
44.	PAS-1, MN 0405.	60
45.	PAS-1, MN 0201.	62
46.	PAS-1, MN 0203.	63
47.	PAS-1, MN 0701.	65
48.	PAS-1, MN 1601.	67
49.	PAS-1, MN 1602.	70
50.	PAS-1, MN 3401.	73
51.	PAS-1, MN 3403.	74
52.	PAS-1, MN 3402.	76
53.	PAS-1, MN 3404.	77
54.	PAS-1, MN 7401.	79

FIGURES (Continued)

<u>Figure</u>		<u>Page</u>
55.	PAS-1, MN 7402.	80
56.	PAS-1, MN 7403.	81
57.	Location of GZ for PAS-3.	85
58.	Explosive charge, 33.3 kg of C-4, PAS-3.	85
59.	Photo pole locations, PAS-3.	86
60.	Locations of aluminum cubes, PAS-3.	87
61.	The SIFCON cube placement, PAS-3.	88
62.	Section: Debris catcher bin, PAS-3.	89
63.	Locations of debris catcher bins, PAS-3.	90
64.	Instrumentation in floor of structure, PAS-3.	96
65.	Instrumentation on outside surface of front door at $X = 415$, PAS-3.	97
66.	Instrumentation on inside surface of front door at $X = 498$, PAS-3.	98
67.	Instrumentation on arch at $X = 6818$, PAS-3.	99
68.	Instrumentation on inner surface of backwall at $X = 13010$, PAS-3.	100
69.	Free-field airblast gage locations, PAS-3.	101
70.	Locations of WES self-recording accelerometers, PAS-3.	103
71.	The WES self-recording accelerometer, PAS-3.	104
72.	Camera station locations, PAS-3.	106
73.	Impact of front door at 23 m from the structure, PAS-3.	107
74.	Front door, PAS-3.	108
75.	Vestibule and personnel door (foreground), PAS-3.	110
76.	Steel liner at personnel door opening, PAS-3.	110
77.	Part of left wingwall and left front wall, PAS-3.	111
78.	Left wingwall, PAS-3.	111
79.	Elevation: Right wingwall failure plane, PAS-3.	112
80.	Final location of right front wall, PAS-3.	112
81.	Dowel bars in right front wall, PAS-3.	113

FIGURES (Continued)

<u>Figure</u>		<u>Page</u>
82.	Welded joint in steel plate liner and parapet damage at location of door guide bracket, PAS-3.	115
83.	Steel plate liner and parapet at location of missing door guide bracket, PAS-3.	115
84.	Breakup of the arch, PAS-3.	116
85.	Posttest overhead view of PAS-3 test structure.	117
86.	Typical bolt pull-out at liner joint, PAS-3.	119
87.	Edge tear-out of bolts in liner of Section #2, PAS-3.	119
88.	Pull-out of reinforcing bars at transverse failure plane, PAS-3.	120
89.	Broken reinforcing bars at transverse failure plane, PAS-3.	120
90.	Longitudinal failure plane, PAS-3.	121
91.	Tension cracks, PAS-3.	121
92.	Base channel for corrugated liner, PAS-3.	123
93.	Displaced earth backfill, PAS-3.	123
94.	Top edge of backwall, PAS-3.	124
95.	Section: Failure plane between the arch and backwall, PAS-3.	124
96.	Back view of backwall, PAS-3.	125
97.	Wide crack on left side of backwall, PAS-3.	125
98.	Exhaust port endwall failure at sidewall, PAS-3.	127
99.	Final position of exhaust port endwall, PAS-3.	127
100.	Posttest condition of exhaust port, PAS-3.	128
101.	Exhaust port door, PAS-3.	128
102.	Exhaust port door frame, PAS-3.	129
103.	Broken dowel bars in top of the arch foundation, PAS-3.	129
104.	Floor slab expansion joint, PAS-3.	131
105.	Damage to apron slab, PAS-3.	131

FIGURES (Continued)

<u>Figure</u>	<u>Page</u>
106. Gap between foundation and apron slab, PAS-3.	132
107. Top plate of door trench and front foundation, PAS-3.	132
108. Section: Failure plane in backwall foundation, PAS-3.	134
109. Gap between floor slab and backwall, PAS-3.	134
110. PAS-3, MN 0604.	135
111. PAS-3, MN 0602.	136
112. PAS-3, MN 0603.	137
113. PAS-3, MN 0402.	139
114. PAS-3, MN 0202.	140
115. PAS-3, MN 0501.	141
116. PAS-3, MN 0102.	142
117. PAS-3, MN 0601.	143
118. PAS-3, MN 0301.	144
119. PAS-3, MN 0703.	147
120. PAS-3, MN 0704.	148
121. PAS-3, MN 1601.	150
122. Section: Rock rubble berm, PAS-3.	154
123. Structure coordinate system, PAS-3.	155
124. Range and azimuth reference system, PAS-3.	156
125. Dyed concrete and colored beads in arch, PAS-3.	161
126. Five-degree debris collection sectors, PAS-3.	163
127. Number of pieces of debris in each weight interval (scaled to full-size structure).	169
128. Plot of weight of debris versus range of concentric zone.	171
129. Plot of number of pieces of debris versus range of concentric zone.	172
130. Cumulative weight of debris versus range of concentric zone.	174
131. Cumulative number of pieces of debris versus range of concentric zone.	175

FIGURES (Continued)

<u>Figure</u>		<u>Page</u>
132.	Rock rubble debris at structure, PAS-3.	178
133.	Distribution of debris from rock rubble berm, PAS-3.	180
134.	Location of GZ for PAS-2.	182
135.	Explosive charge, 11.1 kg of C-4, PAS-2.	182
136.	Photo pole locations, PAS-2.	183
137.	Locations of aluminum cubes, PAS-2.	184
138.	The SIFCON cube placement, PAS-2.	185
139.	Locations of debris catcher bins, PAS-2.	186
140.	Instrumentation in floor of structure, PAS-2.	192
141.	Instrumentation on outside surface of front door at X = 415, PAS-2.	193
142.	Instrumentation on inside surface of front door at X = 498, PAS-2.	194
143.	Instrumentation on arch at X = 645, PAS-2.	195
144.	Instrumentation on arch at X = 3976, PAS-2.	196
145.	Instrumentation on arch at X = 6818, PAS-2.	197
146.	Instrumentation on inner surface of backwall at X = 13010, PAS-2.	199
147.	Free-field airblast gage locations, PAS-2.	200
148.	Camera station locations, PAS-2.	201
149.	Posttest location of front door, PAS-2.	202
150.	Posttest condition of inside surface of front door, PAS-2.	202
151.	Bent ends of front door, PAS-2.	204
152.	Personnel door inside vestibule, PAS-2.	204
153.	Damage to left wingwall, PAS-2.	205
154.	Impact damage to edge of apron slab, PAS-2.	205
155.	Posttest view of left front wall, PAS-2.	206
156.	Crack pattern in front face of parapet, PAS-2.	206
157.	View of transverse failure plane in arch, PAS-2.	208
158.	Edge tear-out of bolts in line at transverse failure plane, PAS-2.	208
159.	Pull-out of reinforcing bars at transverse failure plane, PAS-2.	209

FIGURES (Continued)

<u>Figure</u>		<u>Page</u>
160.	Transverse cracking pattern in arch, PAS-2.	209
161.	Longitudinal cracks at crown of arch, PAS-2.	210
162.	Condition of liner joints opposite longitudinal cracks, PAS-2.	210
163.	Damage at left front corner of arch, PAS-2.	211
164.	Arch resting on rock rubble, PAS-2.	211
165.	Broken dowel bars in arch foundation, PAS-2.	213
166.	Anchor bolt pull-out at base of arch, PAS-2.	213
167.	Crack at back corners of floor slab, PAS-2.	214
168.	Crack pattern in left side of arch at backwall, PAS-2.	214
169.	Section: Failure plane between the arch and backwall, PAS-2.	216
170.	Section: Failure plane in backwall foundation, PAS-2.	216
171.	Gap between floor slab and backwall, PAS-2.	217
172.	Steel door in right side of exhaust port, PAS-2.	219
173.	Steel door in left side of exhaust port, covered with backfill, PAS-2.	219
174.	PAS-2, MN 0604.	220
175.	PAS-2, MN 0602.	221
176.	PAS-2, MN 0603.	222
177.	PAS-2, MN 0402.	223
178.	PAS-2, MN 0201.	225
179.	PAS-2, MN 0405.	226
180.	PAS-2, MN 0203.	227
181.	PAS-2, MN 0501.	228
182.	PAS-2, MN 0102.	229
183.	PAS-2, MN 0601.	230
184.	PAS-2, MN 0301.	231
185.	PAS-2, MN 0701.	234
186.	PAS-2, MN 0702.	235
187.	PAS-2, MN 1601.	237

FIGURES (Continued)

<u>Figure</u>		<u>Page</u>
188.	PAS-2, MN 3401.	241
189.	PAS-2, MN 3403.	242
190.	PAS-2, MN 3402.	243
191.	PAS-2, MN 3404.	244
192.	Rock rubble ejected from the berm, PAS-2.	246
193.	Structure coordinate system, PAS-2.	248
194.	Range and azimuth reference system, PAS-2.	249
195.	Dyed concrete and colored beads in arch, PAS-2.	252
196.	Five-degree debris collection sectors, PAS-2.	255
197.	Rock rubble distribution, PAS-2.	259
198.	Location of GZ for PAS-4.	261
199.	Explosive charge, 100 kg of C-4, PAS-4.	261
200.	Photo pole locations, PAS-4.	262
201.	Locations of aluminum cubes, PAS-4.	263
202.	The SIFCON cube placement, PAS-4.	264
203.	Locations of debris catcher bins, PAS-4.	265
204.	Instrumentation in floor of structure, PAS-4.	271
205.	Instrumentation on inside surface of front door X = 498, PAS-4.	272
206.	Instrumentation on arch at X = 3976, PAS-4.	273
207.	Instrumentation on arch at X = 6818, PAS-4.	274
208.	Instrumentation on inner surface of backwall at X = 13010, PAS-4.	275
209.	Free-field airblast gage locations, PAS-4.	276
210.	Locations of WES self-recording accelerometers, PAS-4.	277
211.	Camera station locations, PAS-4.	278
212.	Posttest location of front door, PAS-4.	280
213.	Posttest condition of inside surfaces of front door, PAS-4.	280
214.	Bent edges of front door, PAS-4.	281
215.	Left edge of front door, inside surface, PAS-4.	281

FIGURES (Continued)

<u>Figure</u>		<u>Page</u>
216.	Torn weld at inside plate and internal stiffener, PAS-4.	282
217.	Posttest location of vestibule. PAS-4.	283
218.	Vestibule and personnel door (foreground), PAS-4.	283
219.	Right wingwall, PAS-4.	285
220.	Left wingwall, PAS-4.	285
221.	Top plate of door trench and front foundation, PAS-4.	286
222.	Final location of right front wall, PAS-4.	286
223.	Deformed steel plate headworks liner, PAS-4.	287
224.	Rubbleized concrete in parapet, PAS-4.	287
225.	Crack pattern in arch, PAS-4.	289
226.	Posttest locations of large arch sections, PAS-4.	290
227.	Typical bolt pull-out at liner joint, PAS-4.	291
228.	Failure planes and splice locations, PAS-4.	292
229.	Pull-out of reinforcing bars at transverse failure plane, PAS-4.	294
230.	Broken reinforcing bars in transverse failure plane, PAS-4.	294
231.	Locations of longitudinal failure plane, PAS-4.	295
232.	Longitudinal failure plane, PAS-4.	296
233.	Pull-out of reinforcing bars at transverse failure plane, PAS-4.	298
234.	Tension cracks at transverse failure plane, PAS-4.	298
235.	Typical transverse cracks on surface of arch sections, PAS-4.	299
236.	Rubbleized arch section, PAS-4.	299
237.	Top of arch foundation, PAS-4.	300
238.	Broken dowel bars in top of arch foundation, PAS-4.	300
239.	Floor slab at arch foundation, PAS-4.	302
240.	Section: Crack pattern in floor slab at arch foundation, PAS-4.	303
241.	Crater in floor slab, PAS-4.	304
242.	Gap between floor slab and backwall, PAS-4.	304

FIGURES (Continued)

<u>Figure</u>		<u>Page</u>
243.	Crack pattern in floor slab at backwall foundation, PAS-4.	305
244.	Posttest condition of expansion joint, PAS-4.	305
245.	Posttest view of backwall, PAS-4.	307
246.	Thirty-degree backward rotation of backwall, PAS-4.	307
247.	Section: Failure plane between arch and backwall, PAS-4.	308
248.	Top edge of backwall, PAS-4.	308
249.	Limits of ejected earth backfill, PAS-4.	309
250.	Section: Breakup pattern of backwall foundation, PAS-4.	310
251.	Failure of backwall foundation at junction with arch foundation, PAS-4.	311
252.	Exhaust port roof and center section of backwall, PAS-4.	311
253.	Plan: Breakup pattern of exhaust port roof, PAS-4.	312
254.	Left sidewall of exhaust port, PAS-4.	314
255.	Right sidewall of exhaust port, PAS-4.	314
256.	Center wall of exhaust port, PAS-4.	315
257.	Steel door from left side of exhaust port, PAS-4.	315
258.	Steel door from right side of exhaust port, PAS-4.	316
259.	Steel frame for exhaust port door, PAS-4.	316
260.	PAS-4, MN 0602.	318
261.	PAS-4, MN 0603.	319
262.	PAS-4, MN 0601.	320
263.	PAS-4, MN 0301.	321
264.	PAS-4, MN 0402.	322
265.	PAS-4, MN 0202.	323
266.	PAS-4, MN 0501.	324
267.	PAS-4, MN 0102.	325
268.	PAS-4, MN 0703.	328
269.	PAS-4, MN 1601.	330
270.	PAS-4, MN 1603.	333

FIGURES (Concluded)

<u>Figure</u>		<u>Page</u>
271.	PAS-4, MN 1605.	335
272.	Posttest view of rock rubble berm adjacent to arch foundation, PAS-4.	338
273.	Portion of rock rubble berm ejected during test, PAS-4.	338
274.	Structure coordinate system, PAS-4.	340
275.	Range and azimuth reference system, PAS-4.	341
276.	Dyed concrete and colored beads in arch, PAS-4.	346
277.	Five-degree debris collection sectors, PAS-4.	348
278.	Secondary debris from large arch section, PAS-4.	355
279.	Boundaries of secondary debris from large arch sections, PAS-4.	356
280.	Scaled-up mass distribution (no sieve data).	364
281.	Plot of weight of debris versus range of concentric zone.	367
282.	Plot of number of pieces of debris versus range of concentric zone.	368
283.	Cumulative weight of debris versus range of concentric zone.	372
284.	Cumulative number of pieces of debris versus range of concentric zone.	373
285.	Posttest distribution of rocks from left berm.	377
286.	Distribution of rocks from berm.	378
287.	Suggested hazard boundary geometry, PAS-3.	393
288.	Suggested hazard boundary geometry, PAS-4.	394

TABLES

<u>Table</u>	<u>Page</u>
1. List of measurements for PAS-1.	17
2. Summary of interior pressure measurements, PAS-1.	64
3. Summary of free-field pressure measurements, PAS-1.	66
4. Summary of acceleration measurements, PAS-1.	72
5. Summary of strain measurements, PAS-1.	78
6. Summary of displacement measurements, PAS-1.	83
7. List of measurements for PAS-3.	92
8. Summary of interior pressure measurements, PAS-3.	145
9. Summary of free-field pressure measurements, PAS-3.	149
10. Summary of exterior acceleration measurements, PAS-3.	152
11. Summary of strain measurements, PAS-3.	152
12. Pretest and posttest locations of SIFCON cubes, PAS-3.	158
13. Pretest and posttest locations of aluminum cubes, PAS-3.	159
14. Pretest and posttest locations of photo poles, PAS-3.	160
15. Pretest and posttest locations of WES gages, PAS-3.	160
16. Sieve data: 0-deg azimuth (front) sector, PAS-3.	164
17. Sieve data: 90-deg azimuth (right side) sector, PAS-3.	165
18. Sieve data: 180-deg azimuth (back) sector, PAS-3.	165
19. Sieve data: 270-deg azimuth (left side) sector, PAS-3.	166
20. Debris weights scaled up to full-size structure (no sieve data), PAS-3.	168
21. Number of pieces and total weight of debris in concentric zones, PAS-3.	170
22. Cumulative weights and number of pieces of debris in concentric zones, PAS-3.	173
23. Posttest locations of large pieces of structural debris, PAS-3.	177
24. Rock rubble from 5-deg sector, 90-deg azimuth, PAS-3.	177
25. List of measurements for PAS-2.	187
26. Summary of interior pressure measurements, PAS-2.	232

TABLES (Continued)

<u>Table</u>	<u>Page</u>
27. Summary of free-field pressure measurements, PAS-2.	236
28. Summary of acceleration measurements, PAS-2.	240
29. Summary of strain measurements, PAS-2.	246
30. Pretest and posttest locations of SIFCON cubes, PAS-2.	250
31. Pretest and posttest locations of aluminum cubes, PAS-2.	251
32. Concrete debris location data, PAS-2.	256
33. Concrete debris characteristics data, PAS-2.	257
34. Characteristics of debris collected from catcher bins, PAS-2.	258
35. List of measurements for PAS-4.	266
36. Summary of interior pressure measurements, PAS-4.	327
37. Summary of free-field measurements, PAS-4.	329
38. Summary of exterior acceleration measurements, PAS-4.	337
39. Pretest and posttest locations of SIFCON cubes, PAS-4.	342
40. Pretest and posttest locations of aluminum cubes, PAS-4.	343
41. Pretest and posttest locations of photo poles, PAS-4.	344
42. Pretest and posttest locations of WES accelerometers, PAS-4.	344
43. Sieve data: 0-deg azimuth (front) sector, PAS-4.	349
44. Sieve data: 45-deg azimuth (right, front corner) sector, PAS-4.	350
45. Sieve data: 90-deg azimuth (right side) sector, PAS-4.	351
46. Sieve data: 135-deg azimuth (right, back corner) sector, PAS-4.	352
47. Sieve data: 180-deg azimuth (back) sector, PAS-4.	353
48. Sieve data: 270-deg azimuth (left side) sector, PAS-4.	354
49. Weight distribution data from secondary debris regions, PAS-4.	358
50. Number distribution data from secondary debris regions, PAS-4.	359
51. Weight distribution of large pieces from secondary debris regions, PAS-4.	360
52. Number distribution of large pieces from secondary debris regions, PAS-4.	361

TABLES (Concluded)

<u>Table</u>	<u>Page</u>
53. Weight and number densities of small pieces from secondary debris, PAS-4.	362
54. Weight and number densities of large pieces from secondary debris, PAS-4.	362
55. Scaled-up mass distribution (no sieve data), PAS-4.	363
56. Weight and quantity distribution (no sieve data), PAS-4.	365
57. Cumulative weight and quantity distribution, PAS-4.	370
58. Weight distribution of debris from catcher bins, PAS-4.	374
59. Number distribution of debris from catcher bins, PAS-4.	375
60. Larger pieces of debris from catcher bins, PAS-4.	376
61. Locations of large debris, PAS-4.	379
62. Rock rubble from 5-deg sector, 90-deg azimuth, PAS-4.	381
63. Rock rubble from 5-deg sector, 270-deg azimuth, PAS-4.	382

1.0 INTRODUCTION

1.1 BACKGROUND

One of the important factors in siting and operational use of protective aircraft shelters (PAS) is the quantity of explosives that can safely be stored within the shelter. The maximum weight of explosives that can be stored inside a facility depends upon the distance to other inhabited facilities and the distribution of peak overpressures and debris that might result from an accidental detonation of the stored explosives.

Experimental data provide the basis for calculation of minimum separation distances between explosive storage and other types of base facilities. These separation distances are sometimes referred to as explosives quantity-distance (Q-D) criteria and are normally specified as scaled ranges from the source of the explosion. A major objective of the 1981 DISTANT RUNNER test series was to provide an empirical database to assess the validity of the then current Q-D criteria for the US Air Force Third Generation aircraft shelter used by US forces in Europe. A series of aircraft shelter model tests (ASMT) of 1/10-scale models of the Third Generation aircraft shelter conducted in 1985 provided additional experimental data.

A new aircraft shelter designed by the Norwegians is under construction in Norway and will be used by NATO forces. The front door and other structural details of this shelter differ significantly from the US Third Generation design. These differences have raised questions regarding the applicability of the Q-D criteria derived from the DISTANT RUNNER and ASMT tests to the new shelter design. A Memorandum of Understanding signed by the US and Norway proposed an experimental program to generate data that could be used to develop explosives Q-D criteria for the new shelter. The test program included the construction of four 1/3-scale structural models of the Norwegian PAS. These model structures were subjected to internal detonations of various weights of high explosives. The test program included four separate test events. All tests were conducted on the McCormick Ranch test site adjacent to Kirtland Air Force Base.

1.2 SCOPE

Volume I of this report presents a general overview of the test program, a detailed description of the four test events, the structural response observed, and a summary of the data collected in each test. This report provides a detailed description of the four test events with a summary of the data collected in each test. Volumes II through V (Appendices A through D) contain complete sets of electronic measurements data and debris surveys for each of the four tests of the series.

A report documenting the design and construction details of the 1/3-scale PAS will be available in the future. The report will include a complete set of construction drawings, and the results of concrete and reinforcing bar strength tests.

As a follow-on to this program, additional tests were performed on the fifth 1/3-scale US/Norway Protective Aircraft Shelter (PAS-5),¹ a full-size US Third Generation Aircraft Shelter, and a 1/3-scale US Third Generation Aircraft Shelter (TGAS-1).²

The 1/3-scale PAS-5 test used three separate charges totaling 100 kg of C-4 explosives. The charges were located inside the shelter to simulate a typical operational storage arrangement. The full-size US Third Generation used a single, Mark 84 general purpose bomb inside the shelter. The 1/3-scale TGAS-1 test used a steel-cased charge of C-4 explosives to simulate the weapon used in the full-scale test.

¹ Bultmann, Edward H., Jr., and Schneider, Bruce A., *Norway/United States Protective Aircraft Shelter (PAS), 1/3-Scale, Quantity-Distance Program, PAS-5*, Phillips Laboratory, Kirtland AFB, NM, June 1993. NMERI SS 2.33(10)

² Bultmann, Edward H., Jr., and Schneider, Bruce A., *United States Third Generation Aircraft Shelter (TGAS) Quantity-Distance Program, 1/3-Scale Test Series, TGAS-1*, Phillips Laboratory, Kirtland AFB, NM, June 1993. NMERI SS 2.33(11) DRAFT

2.0 GENERAL TEST DESCRIPTION

2.1 TEST STRUCTURES

The test structures were 1/3-scale models of the Norwegian/US design. Longitudinal and transverse cross sections through the model are shown in Figures 1 and 2. Figures 3 and 4 provide a key for identifying major components of the model for reference in the detailed reviews of structural damage presented in the following sections of this report. All structural dimensions and reinforcing details were derived from construction drawings and specifications for the full-size structure. All dimensions are in millimeters except as noted.

The Norwegian/US shelter is similar in concept to the US Third Generation aircraft shelter constructed at many overseas airbases. It includes a reinforced concrete arch constructed with a double-corrugated steel liner on its inner surface. The wall thickness of the model arch varied from 150 to 270 mm. The backwall of the model was 400 mm thick and of reinforced concrete. The geometry of the Norwegian shelter arch differs slightly from the US version, and the Norwegian shelter is more heavily reinforced.

The door of the latter, a one-piece, flat plate, hollow core, steel construction, is raised and lowered by a system of steel cables, pulleys, and winches. When raised into the closed position, the door fits into a slot in the parapet at the front end of the shelter. This slot restrains the door against external or internal airblast loads. In the open position, the door rests in a pit in the shelter floor slab with its outer surface flush with the shelter floor. The door operating system was not included in the 1/3-scale models.

Some simplifications were also made in the exhaust ports for the model structures. The cross-sectional areas of the model's exhaust port were scaled from the full-size structure, but some geometric details beyond the closure doors were modified to facilitate construction. Scaled, non-operating, versions of the exhaust port closures were installed

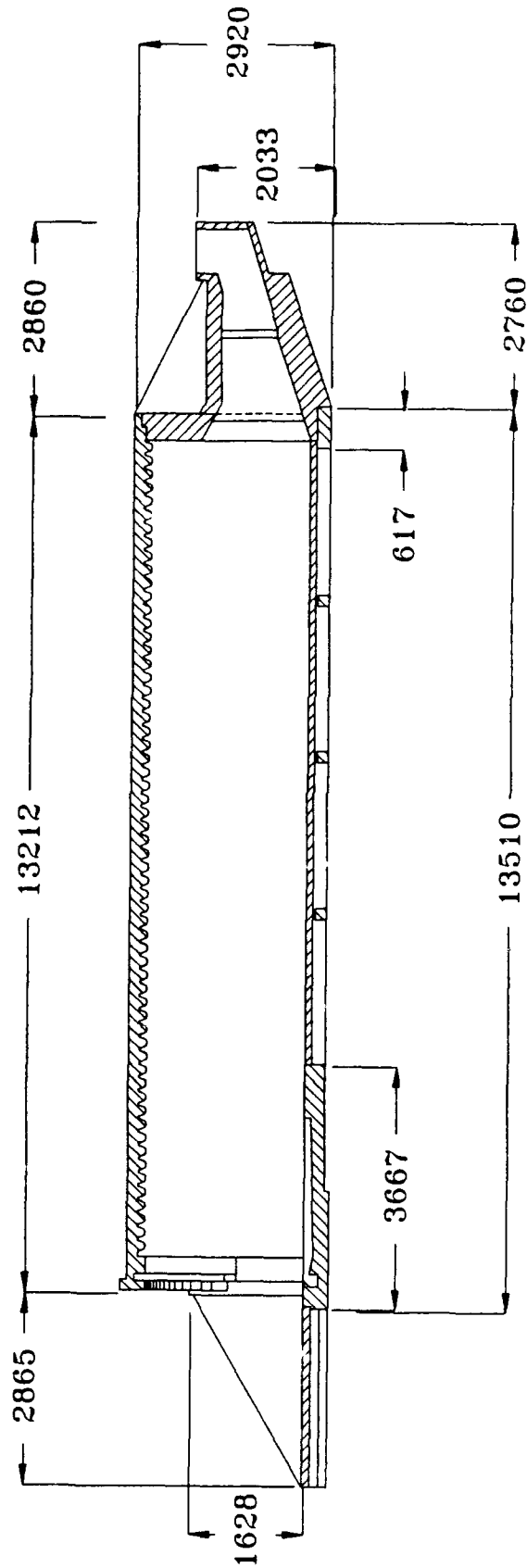


Figure 1. Longitudinal cross section through test structure.

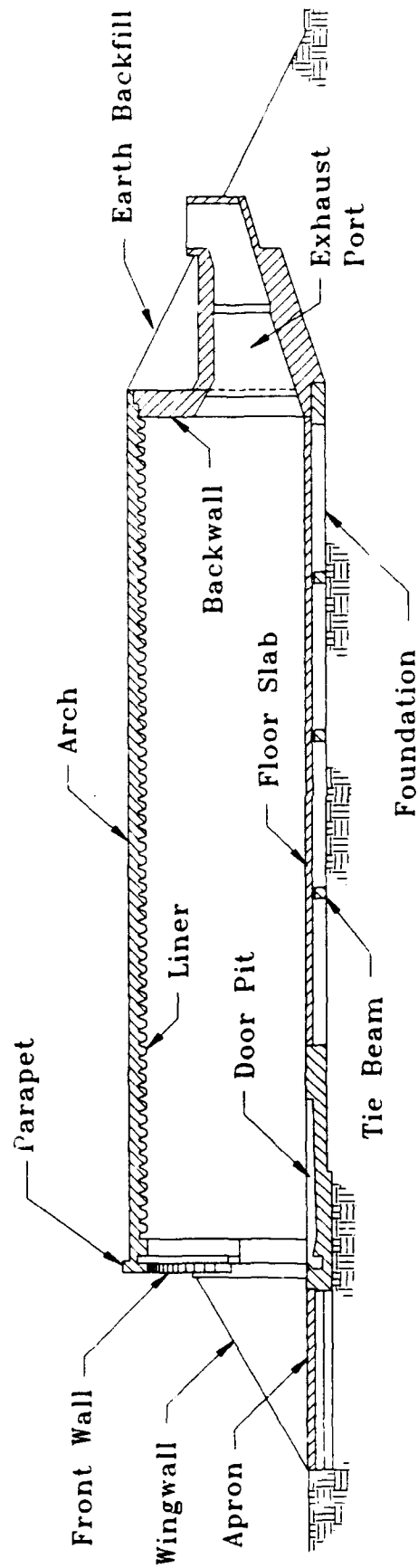


Figure 3. Longitudinal section: Identification key to structural components.

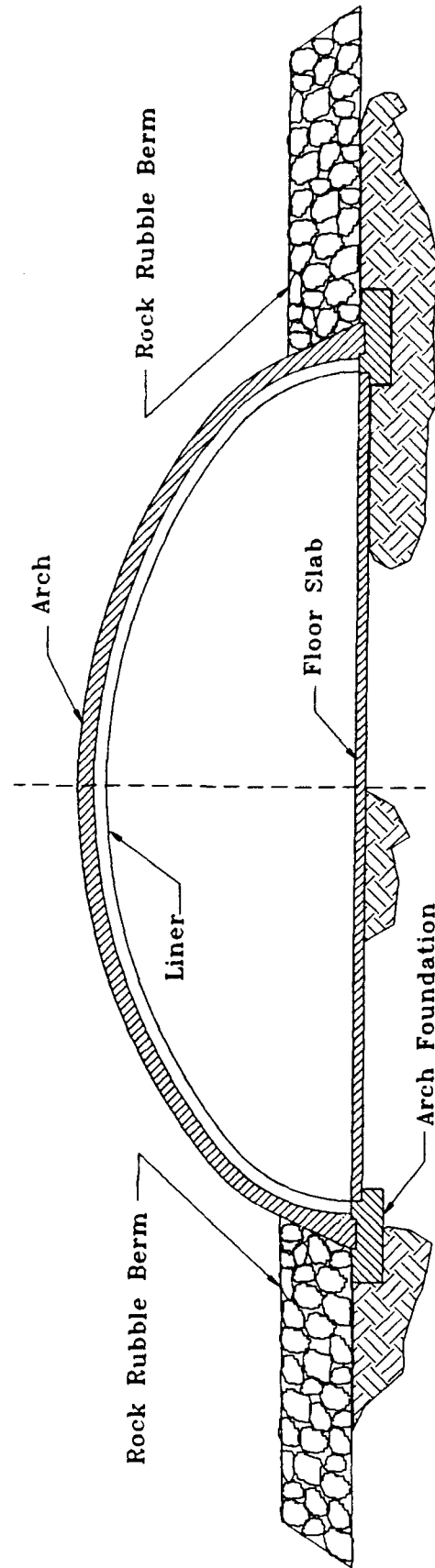


Figure 4. Transverse section: Identification key to structural components.

in the models. A completed 1/3-scale PAS structure, typical of all of the structures tested in this program, is shown in Figures 5 and 6.

The front door framing elements and the doors were fabricated in Norway and shipped to the test site at Kirtland Air Force Base. The double-corrugated steel liner was fabricated by Arch Technology, Inc. (Plato, Illinois). Assembly of the liner and all other construction, instrumentation, and explosives support were provided by NMERI personnel.

2.2 EXPLOSIVE CHARGES

Composition C-4 was used to fabricate the explosive charges for all events in the test series. All charges were uncased spherical charges suspended by cable from the ceiling of the structure. All charges were placed near the center of the structure with the centers of the charges 600 mm above the floor surface.

2.3 INSTRUMENTATION PLAN

2.3.1 General

The instrumentation plan was designed to provide experimental data on the distribution of pressures around the structure. It also included measurements to provide inputs to theoretical predictions of these parameters for full-size structures and data to evaluate the prediction techniques. The following sections of this report include a measurements list for each of the test events. The locations of sensors are referenced to the Shelter Coordinate System (SCS). The origin of the SCS is a point on the centerline of the structure, at the front edge of the foundation, and 367 mm below the elevation of the floor slab. The X coordinates are measured in a direction parallel to the longitudinal axis of the structure. The Y coordinates are measured horizontally from the centerline of the structure, and the Z coordinates are measured in the vertical direction. (Note: As one faces the front of the structure from the inside, orientation may also be given as "left" or "right".)

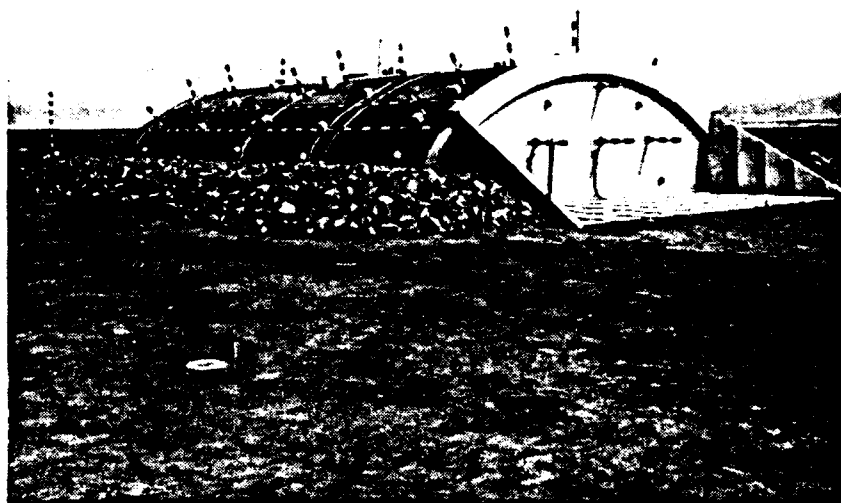


Figure 5. Front view of test structure.

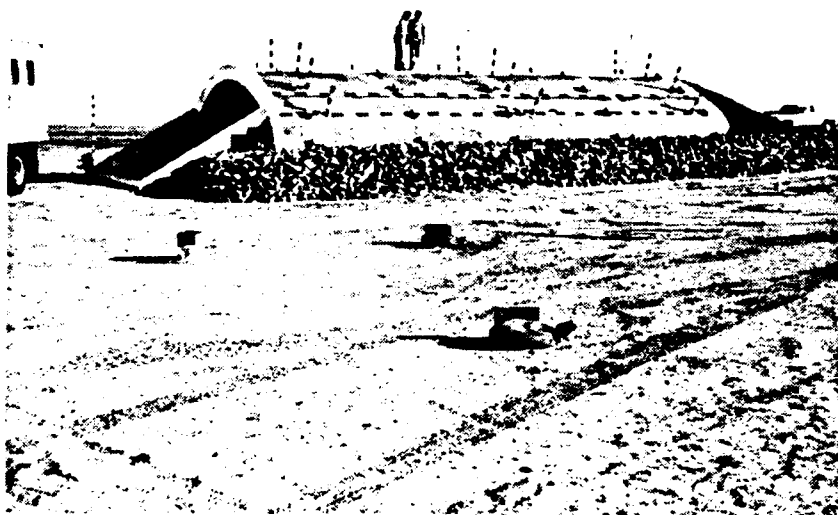


Figure 6. Side view of test structure.

2.3.2 Airblast Measurements

Electronic airblast gages were used to measure blast pressures inside and around the exterior of the test structure. All airblast gages were mounted flush with the surface of the structure or gage mount in which they were installed.

2.3.3 Structural Response Measurements

Accelerometers were installed on the exterior surfaces of the structures in an attempt to record initial motions of shelter debris. In two events, US Army Corps of Engineers Waterways Experiment Station (WES) personnel installed self-recording accelerometers to obtain additional structural response data.

Strain gages were installed on the surfaces of the shelter doors to measure the response of the door to internal and external blast loading.

Displacement gages were only used on the door of PAS-1 to measure deflection.

2.3.4 Photographic Plan

High-speed motion picture and video cameras were provided at various azimuths around the exterior of the structures in all events. Motion picture data were recorded at rates of 400, 500, 1000, and 2000 frames per second. As an aid in determining structural velocities and displacements using motion picture photography, photo poles were attached to the arch in each event. The poles were 60-mm-diameter by 750-mm-long steel pipe mounted on a steel baseplate. They were painted with 150-mm-wide, alternating black and white bands. Wooden photo poles and plastic ground markers were also placed at various locations around the structures as fixed photo reference points.

Various markings were applied to the test structure as a further aid in analysis of high-speed motion picture photography. The crown, front parapet, and back edge of the

arch were painted white. White lines were also painted across the arch to delineate the quarter points along the length of the structure. Two black and white lines were painted horizontally on the side of the arch to provide a dimensional reference for the photography. Each black and white segment of the line was 300 mm long.

2.3.5 Debris Distribution

The distribution of structural debris around the failed structure was an important part of the data to be collected in this test program. The minimum collectable fragment dimensions were based upon prior studies, which established a minimum fragment mass of 136 gm as hazardous to personnel. By applying geometric scaling for a 1/3-scale structure, it was decided that a piece of concrete with dimensions less than 12.7 mm or with a mass less than 5.0 gm would be ignored in this test program.

A debris collection program was developed so that the final resting place and approximate point of origin on the structure could be determined for any piece of debris thrown from the structure. Four colors of concrete additives were used to define four horizontal bands in each side of the arch from the foundation to the crown. Four colors of 10-mm diameter solid, plastic beads were also added to the concrete to delineate four vertical sections from the front to the back of the shelter; thus, each side of the arch was subdivided into 16 identifiable points of origin for shelter debris. The volume of beads used did not exceed 0.5 percent of the volume of concrete. The concrete in the backwall, exhaust port, and front wingwalls was natural gray. The locations of the different colors of concrete and beads varied slightly between tests as noted in the specific section. The area surrounding the structure was graded prior to each test event to facilitate the recovery of any debris produced from the explosion. A posttest survey established the location, size, and weight of each piece of debris.

Aluminum cubes were placed on narrow brackets at various locations on the exterior surface of the arch in all the test events to provide additional data on ejecta hazards from the internal explosion. The aluminum cubes measured 50 mm on each side with an average mass of 0.34 kg. The SIFCON cubes were added in all events after PAS-1.

These cubes measured 152 mm on each side with an average mass of 8.74 kg. Each cube was marked with a unique identifying mark. The SIFCON cubes were painted orange to increase their visibility in high-speed photography. These cubes were ejected outward, along with any structural debris produced by the test. Following the test, the cubes were recovered and their final position recorded. Initial trajectories and velocities can be estimated for these cubes from their known mass, and initial and final positions.

Debris catcher bins were used to determine the areal densities of the debris in a vertical plane. The objective of these bins was to capture pieces of debris without concern for their velocity or trajectory. The number of catcher bins used was determined by the requirement that the frontal area of the bins at each range subtend a solid angle not less than 0.013 steradians. The interiors of the bins were lined with styrofoam to prevent fragment breakup on impact with the bin wall. The debris catcher bins used in the tests were fabricated from plywood. The ranges at which the bins were placed were determined on the basis of the explosive charge weight for each test. The arrangement of the bins is given in the section of this report that describes each specific test.

3.0 PAS-1 TEST

3.1 TEST DESCRIPTION

3.1.1 General

The PAS-1 test was conducted on March 5, 1992. The explosive charge for this event was 3.7 kg of Composition C-4, which is the equivalent of 100 kg of the same explosive in the full-size structure. Figures 7 and 8 show the placement of the charge at GZ (Ground Zero) for the PAS-1 test. Figure 9 shows the placement of photo poles; Figure 10 shows the locations of the aluminum cubes.

3.1.2 Instrumentation Plan

A total of 67 channels of electronic instrumentation were provided for the PAS-1 event. Included were 28 pressure measurements in the interior of the structure, 15 free-field pressure measurements around the exterior of the structure, 15 accelerometers mounted at various locations on the arch, and 3 displacement gages and 6 strain gages on the front door. Table 1 is a measurements list for the PAS-1 event. This list gives the measurement number (MN), the general location, coordinates, type of sensor and its sensing axis, and the predicted maximum amplitude of the recorded data. The predicted maximum amplitudes shown in Table 1 are approximate values used for gage selection and setting recording bandwidths. They are based on pretest calculations, but do not correspond exactly to the results of these calculations. The locations of the various on-structure measurements are shown in Figures 11 through 18. Figure 11 shows the locations of gages mounted in the floor of the structure. The numbers in the rectangular flags are the coordinates of the sensor; measurement numbers are given in the elliptical flags. Figure 12 shows the locations of displacement and strain gages on the outside surface of the front door. Figure 13 shows the locations of sensors mounted on the inner surface of the front door. Figures 14 through 16 show the locations of

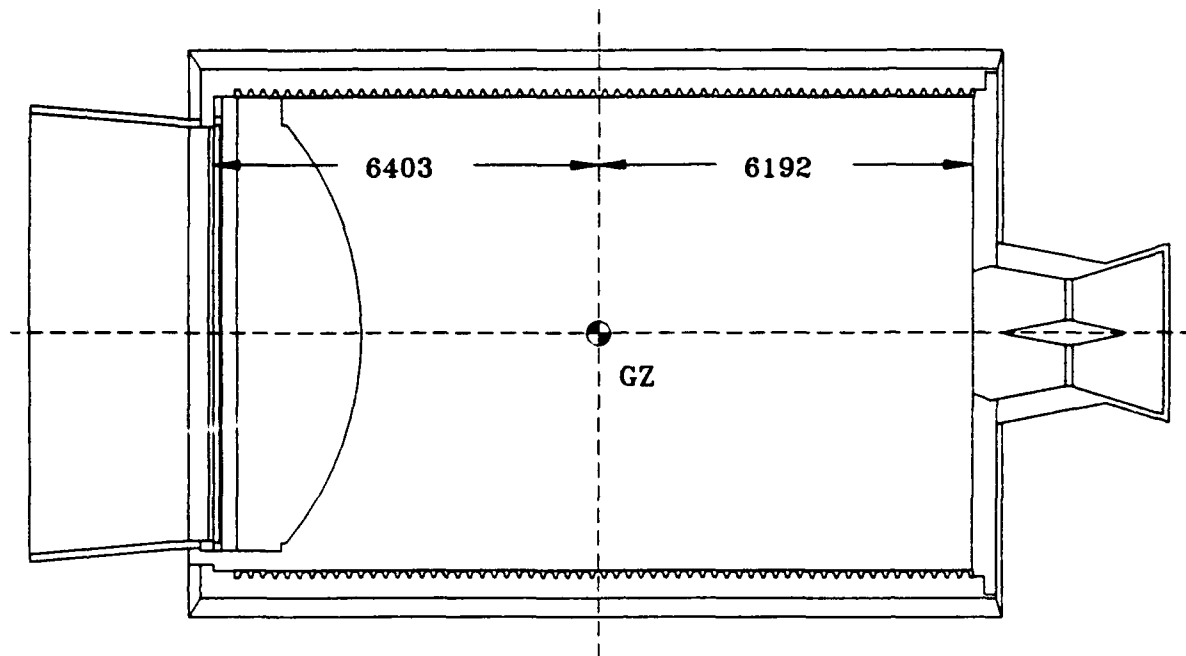


Figure 7. Location of GZ for PAS-1.

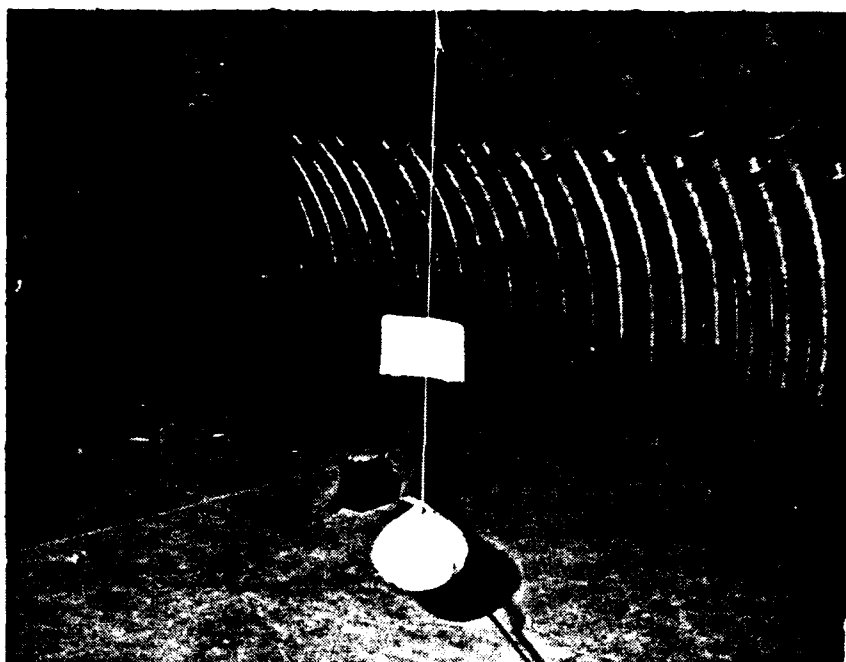
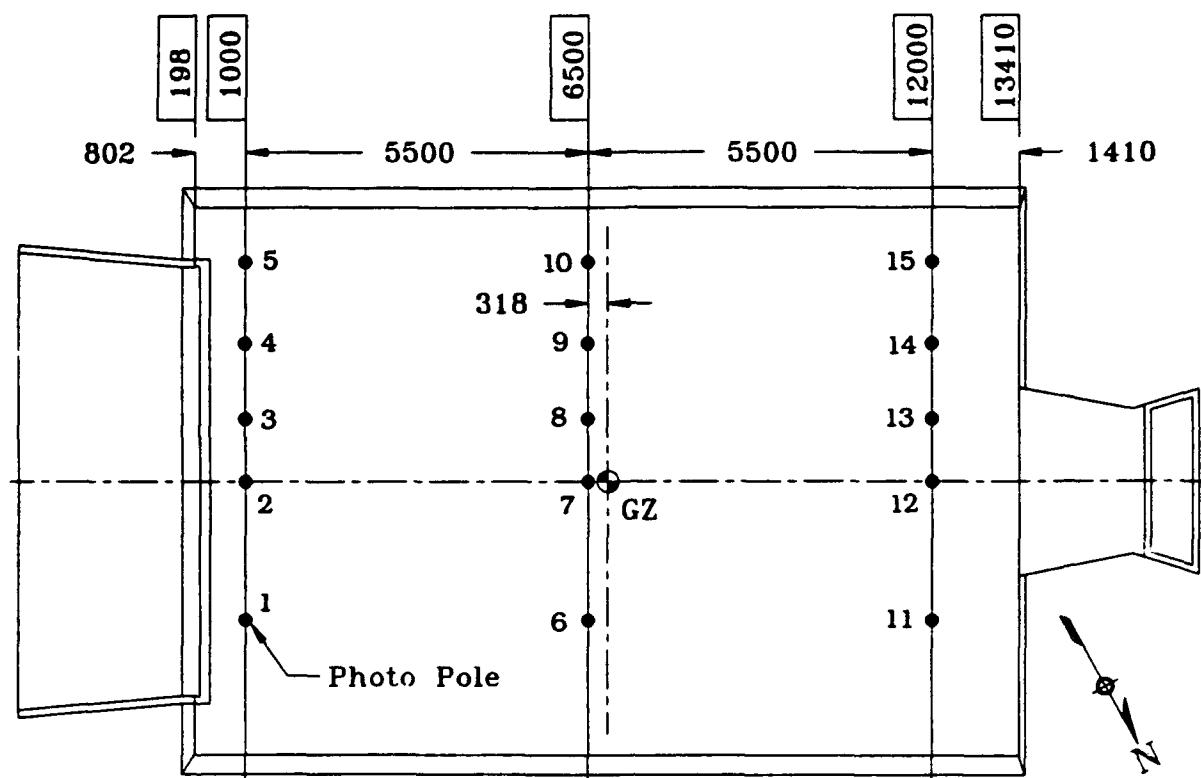
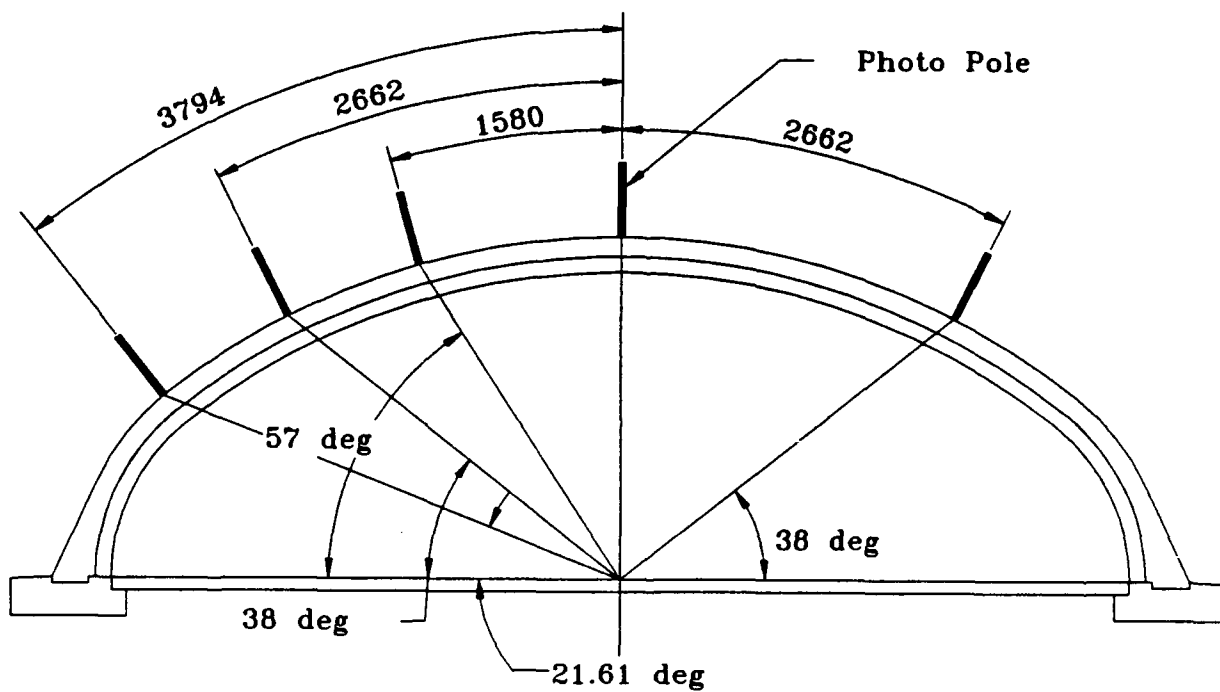


Figure 8. Explosive charge, 3.7 kg of C-4, PAS-1.

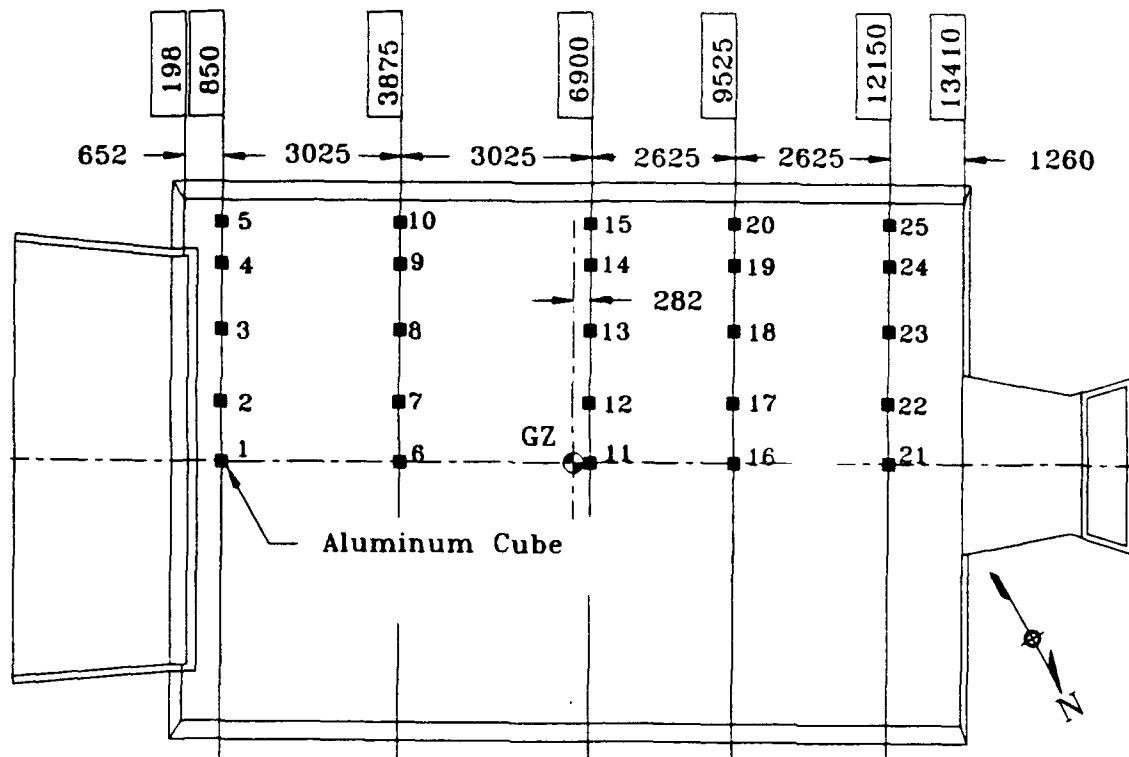


(a) Plan.

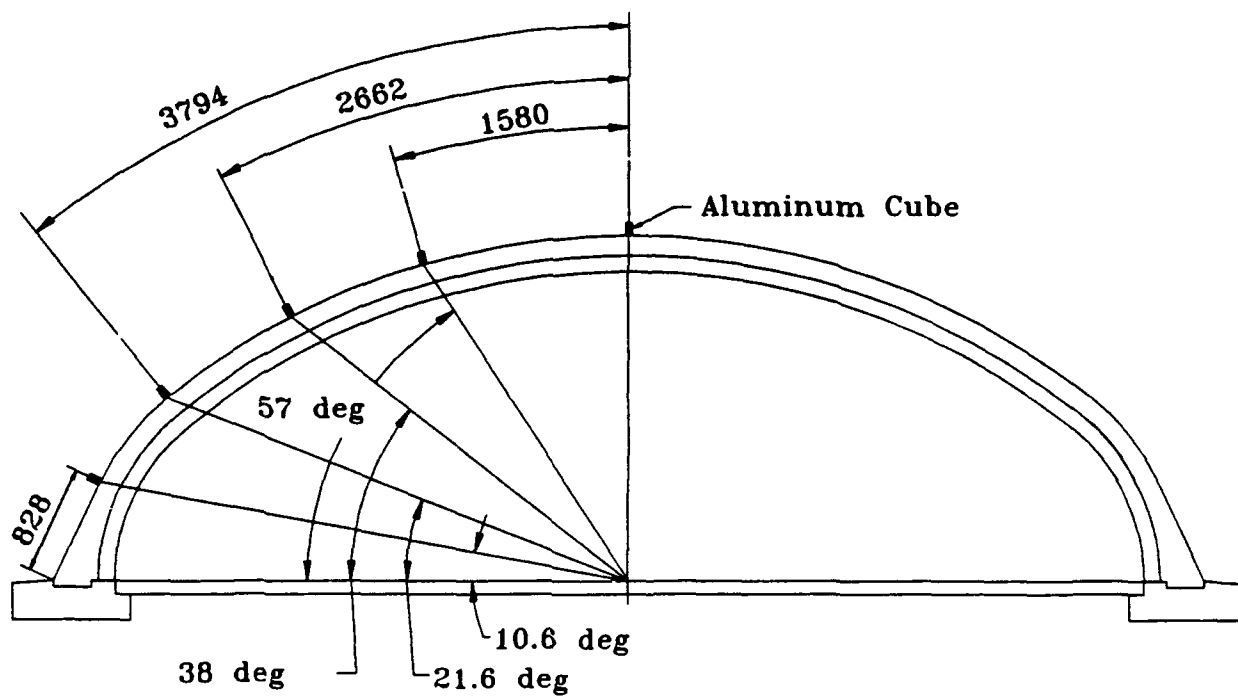


(b) Section.

Figure 9. Photo pole locations, PAS-1.



(a) Plan.



(b) Section.

Figure 10. Locations of aluminum cubes, PAS-1.

Table A-1. List of measurements, PAS-1.

MEASUREMENT LIST														DATE	13 FEB 92	PAGE 1 OF 6 PAGES
TEST EVENT		PAS-1				IE		KIRST				CHANGES				
MEAS NO.	GEN	LOCATION			SENS AXIS	PREC MAX	CONF LEVEL	TRANSDUCER		TRANSDUCER TYPE	TRANSDUCER SERIAL NUMBER	CHANGES				
		X#	Y#	Z#				MODEL	RANGE			ITEM	AUTH	DATE		
0101-1	SF	12807	0	367	Z	413.7 kPa	60	KULITE	689.5 kPa	PRESSURE	(3982-2-184) E18-42					
0102-1	SF	12807	3700	367	Z	689.5 kPa	50	KULITE	1379 kPa	PRESSURE	(2200-2-366) O15-82					
0201-1	BW	13010	100	2500	X	344.7 kPa	50	KULITE	689.5 kPa	PRESSURE	(3982-2-175) E18-35					
0202-1	BW	13010	1700	1475	X	344.7 kPa	50	KULITE	689.5 kPa	PRESSURE	(3982-2-181) E18-40					
0203-1	BW	13010	3700	930	X	482.6 kPa	35	KULITE	1379 kPa	PRESSURE	(3826-4-11) F4-12					
0301-1	SF	3976	0	367	Z	413.7 kPa	60	KULITE	689.5 kPa	PRESSURE	(3982-2-177) E18-37					
0302-1	SF	3976	1850	367	Z	310.3 kPa	60	KULITE	689.5 kPa	PRESSURE	(3982-2-170) E18-31					
0303-1	SF	3976	3700	367	Z	310.3 kPa	60	KULITE	689.5 kPa	PRESSURE	(3982-2-174) E18-34					
0304-1	SC	3976	0	2717	Z	344.7 kPa	50	KULITE	689.5 kPa	PRESSURE	(3982-2-172) E18-32					
0305-1	SC	3976	1749	2424	R1	344.7 kPa	50	KULITE	689.5 kPa	PRESSURE	(3982-2-176) E18-36					
0306-1	SC	3976	3346	1548	R2	344.7 kPa	50	KULITE	689.5 kPa	PRESSURE	(3982-2-168) E18-29					
0307-1	SC	3976	3763	1029	R3	344.7 kPa	50	KULITE	689.5 kPa	PRESSURE	(3982-2-169) E18-30					

NOTES:

= Distance in millimeters
SF = Shelter Floor
SC = Shelter Ceiling

BU = Backwall

Table A-1. Continued.

MEASUREMENT LIST															DATE	25 FEB 92	PAGE 2 OF 8 PAGES
TEST POINT		PAS-1				KIRST		TRANSDUCER		TRANSDUCER	TRANSDUCER	CHANGES					
MEAS NO.	GEN	LOCATION			SENS AXIS	PREC MAX	CONF LEVEL	TRANSDUCER		TRANSDUCER TYPE	SERIAL NUMBER	ITEM	AUTH	DATE			
		X#	Y#	Z#				MODEL	RANGE								
0401-1	FD	498	100	2500	X	344.7 kPa	50 %	KULITE XT-190	689.5 kPa	(Nylon Mount) PRESSURE	(1861-5-92) O7-73						
0402-1	FD	498	100	1475	X	344.7 kPa	50 %	KULITE XT-190	689.5 kPa	(Nylon Mount) PRESSURE	O15-94	QAGE	J.K.	2/25			
0403-1	FD	498	100	450	X	551.6 kPa	45 %	KULITE XT-190	1379 kPa	(Nylon Mount) PRESSURE	(2200-2-361) O15-80						
0404-1	FD	498	1700	1475	X	344.7 kPa	80 %	KULITE XT-190	689.5 kPa	(Nylon Mount) PRESSURE	O15-95						
0405-1	FW	498	3700	930	X	482.6 kPa	40 %	KULITE XT-190	1379 kPa	PRESSURE	(2200-2-324) I13-88						
0501-1	SF	645	3700	367	Z	689.5 kPa	50 %	KULITE XT-190	1379 kPa	PRESSURE	(2200-2-371) O15-87						
0502-1	SC	645	0	2717	Z	482.6 kPa	80 %	KULITE XT-190	689.5 kPa	PRESSURE	(3982-2-173) E18-33						
0503-1	SC	645	1749	2424	R1	482.6 kPa	80 %	KULITE XT-190	689.5 kPa	PRESSURE	(3982-2-185) E18-43						
0504-1	SC	645	3346	1548	R2	482.6 kPa	80 %	KULITE XT-190	689.5 kPa	PRESSURE	(3982-2-180) E18-39						
0601-1	SF	6818	1850	367	Z	1103 kPa	53.3 %	KULITE XT-190	2068 kPa	PRESSURE	(1743-5-145) X6-86						
0602-1	SF	6818	3700	367	Z	551.6 kPa	50 %	KULITE XT-190	1379 kPa	PRESSURE	(2200-2-367) O15-83						
0603-1	SF	6818	-3700	367	Z	551.6 kPa	50 %	KULITE XT-190	1379 kPa	PRESSURE	(2200-2-368) O15-84						
NOTES:															SC = Structure Ceiling		
															SF = Structure Floor		
															FD = Front Door		
															FW = Front Wall		

Table A-1. Continued.

MEASUREMENT LIST																	DATE	13 FEB 92	PAGE 3 OF 8 PAGES
PAS - 1										KIRST									
TEST BODY	MEAS NO.	LOCATION				SCNS AXIS	PRED MAX	CONF LEVEL	TRANSDUCER		TRANSDUCER TYPE	TRANSDUCER SERIAL NUMBER	CHANGES						
		GEN	X#	Y#	Z#				MODEL	RANGE			ITEM	AUTH	DATE				
	0604-1	SC	6818	0	2717	Z	3447 kPa	50 %	KULITE	6895 kPa	PRESSURE	(1906-3-339) F8-38							
	0605-1	SC	6818	1749	2424	R1	1103 kPa	53.3 %	KULITE	2069 kPa	PRESSURE	(1743-5-43) X6-71							
	0606-1	SC	6818	3346	1548	R2	1103 kPa	53.3 %	KULITE	2069 kPa	PRESSURE	(1743-5-143) X6-84							
	0607-1	SC	6818	3763	1029	R3	689.5 kPa	50 %	KULITE	1379 kPa	PRESSURE	(2200-2-365) O15-81							
	0701-1	FF	-3000	0	350	Z	34.47 kPa	100 %	KULITE	34.5 kPa	PRESSURE	(1495-6-94) K7-1							
	0702-1	FF	-5000	0	350	Z	3.447 kPa	25 %	ENDEVCO	13.8 kPa	PRESSURE	PP49							
	0703-1	FF	-7000	0	350	Z	3.447 kPa	25 %	ENDEVCO	13.8 kPa	PRESSURE	RF77							
	0704-1	FF	-9000	0	350	Z	3.447 kPa	25 %	ENDEVCO	13.8 kPa	PRESSURE	TM38							
	0705-1	FF	-3433	8000	350	Z	34.47 kPa	100 %	KULITE	34.5 kPa	PRESSURE	(1495-7-75) K7-7							
	0706-1	FF	-6233	10800	350	Z	3.447 kPa	25 %	ENDEVCO	13.8 kPa	PRESSURE	RF91							
	0707-1	FF	6818	8000	350	Z	34.47 kPa	100 %	KULITE	34.5 kPa	PRESSURE	(1491-2-20) U6-17							
	0708-1	FF	6818	12000	350	Z	3.447 kPa	25 %	ENDEVCO	13.8 kPa	PRESSURE	C61M							
NOTES:																			
# = Distance in millimeters																			
SC = Shelter Ceiling																			
FF = Free Field																			

NOTES: # = Distance in millimeters

SC = Shelter Ceiling

FF = Free Field

Table A-1. Continued.

MEASUREMENT LIST														DATE	13 FEB 92	PAGE 4 OF 8 PAGES
TEST EVENT		PAS-1				KIRST		IF		TRANSDUCER		TRANSDUCER TYPE	TRANSDUCER SERIAL NUMBER	CHANGES		
MEAS NO.	LOCATION		SENS AXIS		PREC MAX	CONF LEVEL	MODEL	RANGE	TRANSDUCER		TRANSDUCER TYPE	TRANSDUCER SERIAL NUMBER	ITEM	AUTH	DATE	
	GEN	X#	Y#	Z#												
0709-1	FF	17041	8000	350	Z	34.474 kPa	100	KULITE	34.5 kPa		PRESSURE	(1491-2-26) U6-20				
0710-1	FF	19841	10800	350	Z	3.4474 kPa	25	ENDEVCO 8510B	13.8 kPa		PRESSURE	C84M				
0711-1	FF	19000	0	350	Z	34.474 kPa	100	ENDEVCO XT-190	34.5 kPa		PRESSURE	(1495-7-76) K7-6				
0712-1	FF	21000	0	350	Z	3.4474 kPa	25	ENDEVCO 8510B	13.8 kPa		PRESSURE	C93M				
0713-1	FF	23000	0	350	Z	3.4474 kPa	25	ENDEVCO 8510B	13.8 kPa		PRESSURE	RF93				
0714-1	FF	6818	-8000	350	Z	34.474 kPa	100	KULITE XT-190	34.5 kPa		PRESSURE	(1491-2-4) U6-16				
0715-1	FF	6818	-12000	350	Z	3.4474 kPa	25	ENDEVCO 8510B	13.8 kPa		PRESSURE	RF60				
1301-1	SR	3976	0	2987	Z	1000 g	100	ENDEVCO 2262	1000 g		ACCELEROMETER	KY63				
1302-1	SR	3976	0	2987	Y	100 g	100	ENDEVCO 2262A	100 g		ACCELEROMETER	LP74				
1303-1	SR	3976	1837	2680	R1	1000 g	100	ENDEVCO 2262	1000 g		ACCELEROMETER	HN02				
1304-1	SR	3976	1837	2680	T1	100 g	100	ENDEVCO 2262	100 g		ACCELEROMETER	LP64				
1305-1	SR	3976	3514	1759	R2	1000 g	100	ENDEVCO 2262	1000 g		ACCELEROMETER	MW04				

NOTES:

= Distance in millimeters

FF = Free Field

SR = Structure Roof

g = Gravitational acceleration

Table A-1. Continued.

MEASUREMENT LIST																	DATE		17 FEB 92		PAGE 9 OF 9 PAGES	
PAS-1										KIRST							IC					
TEST POINT	MEAS NO.	LOCATION				SENS AXIS	PREC MAX	CONF LEVEL	TRANSDUCER		RANGE	TRANSDUCER TYPE	TRANSDUCER SERIAL NUMBER	CHANGES								
		GEN	X#	Y#	Z#				MODEL	ITEM				AUTH	DATE							
	1306-1	SR	3976	3514	1759	T2	100 g	100	%	ENDEVCO 2262A	100 g	ACCELEROMETER	PK28									
	1601-1	SR	6818	0	2987	Z	2000 g	100	%	ENDEVCO 2264A	2000 g	ACCELEROMETER	CC53A									
	1602-1	SR	6818	0	2987	Y	200 g	100	%	ENDEVCO 2262A	200 g	ACCELEROMETER	AP40									
	1603-1	SR	6818	1837	2680	R1	2000 g	100	%	ENDEVCO 2264A	2000 g	ACCELEROMETER	CB24A									
	1604-1	SR	6818	1837	2680	T1	200 g	100	%	ENDEVCO 2262A	200 g	ACCELEROMETER	CG72									
	1605-1	SR	6818	3514	1759	R2	2000 g	100	%	ENDEVCO 2264A	2000 g	ACCELEROMETER	BW95A									
	1606-1	SR	6818	3514	1759	T2	200 g	100	%	ENDEVCO 2262C	200 g	ACCELEROMETER	WB07									
	1607-1	SR	6818	0	2987	Z	30000 g	60	%	ENDEVCO 2264A	50000 g	ACCELEROMETER	CL17E									
	1609-1	SR	6818	1837	2680	R1	30000 g	60	%	ENDEVCO 2264A	50000 g	ACCELEROMETER	CT12E									
	1611-1	SR	6818	3514	1759	R2	30000 g	60	%	ENDEVCO 2264A	50000 g	ACCELEROMETER	CJ75E									
	3401-1	FD	415	0	1475	Y	2000 msn	75	%	AILTECH SG159-11-10-6S	+/- 20000 msn	STRAIN GAGE	N/A									
	3402-1	FD	415	0	1475	Z	2000 msn	75	%	AILTECH SG159-11-10-6S	+/- 20000 msn	STRAIN GAGE	N/A									
NOTES:																	msn = microstrain					
# = Distance in millimeters																						
SR = Shelter Roof																						
FD = Front Door																						

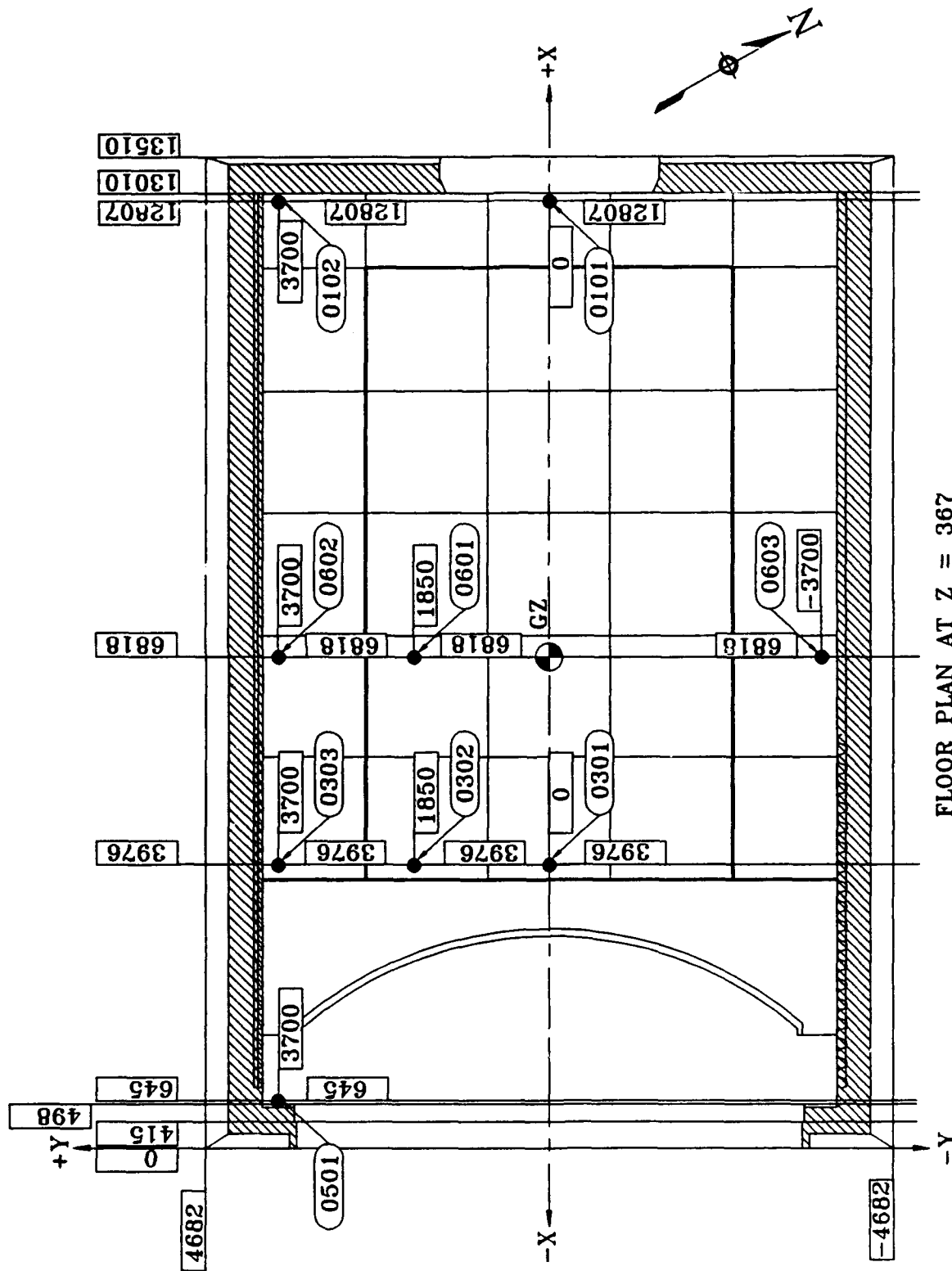
msn = microstrain

= Distance in millimeters

SR = Shelter Roof

FD = Front Door

[illegible]



FLOOR PLAN AT Z = 367

Figure 11. Instrumentation in floor of structure, PAS-1.

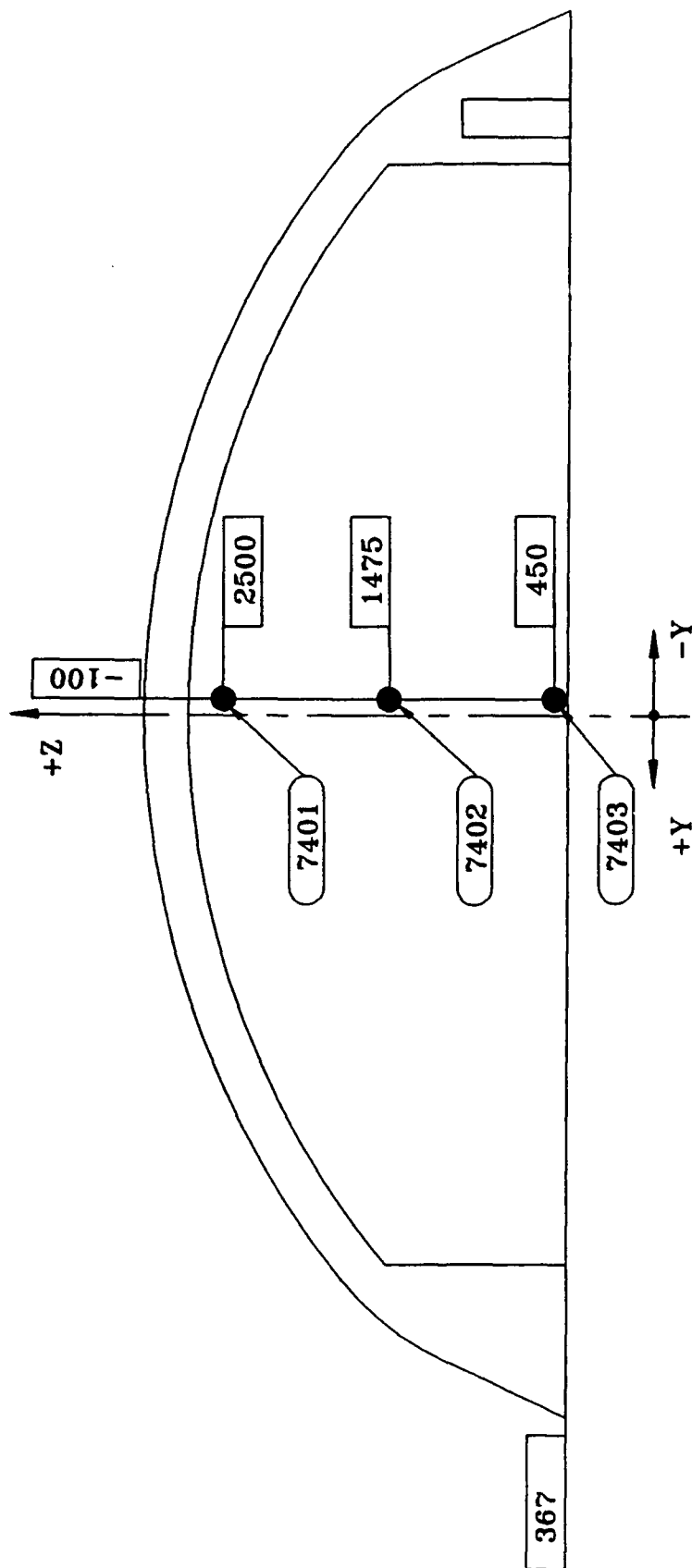


Figure 12. Instrumentation on outside of front door at X = 415, PAS-1.

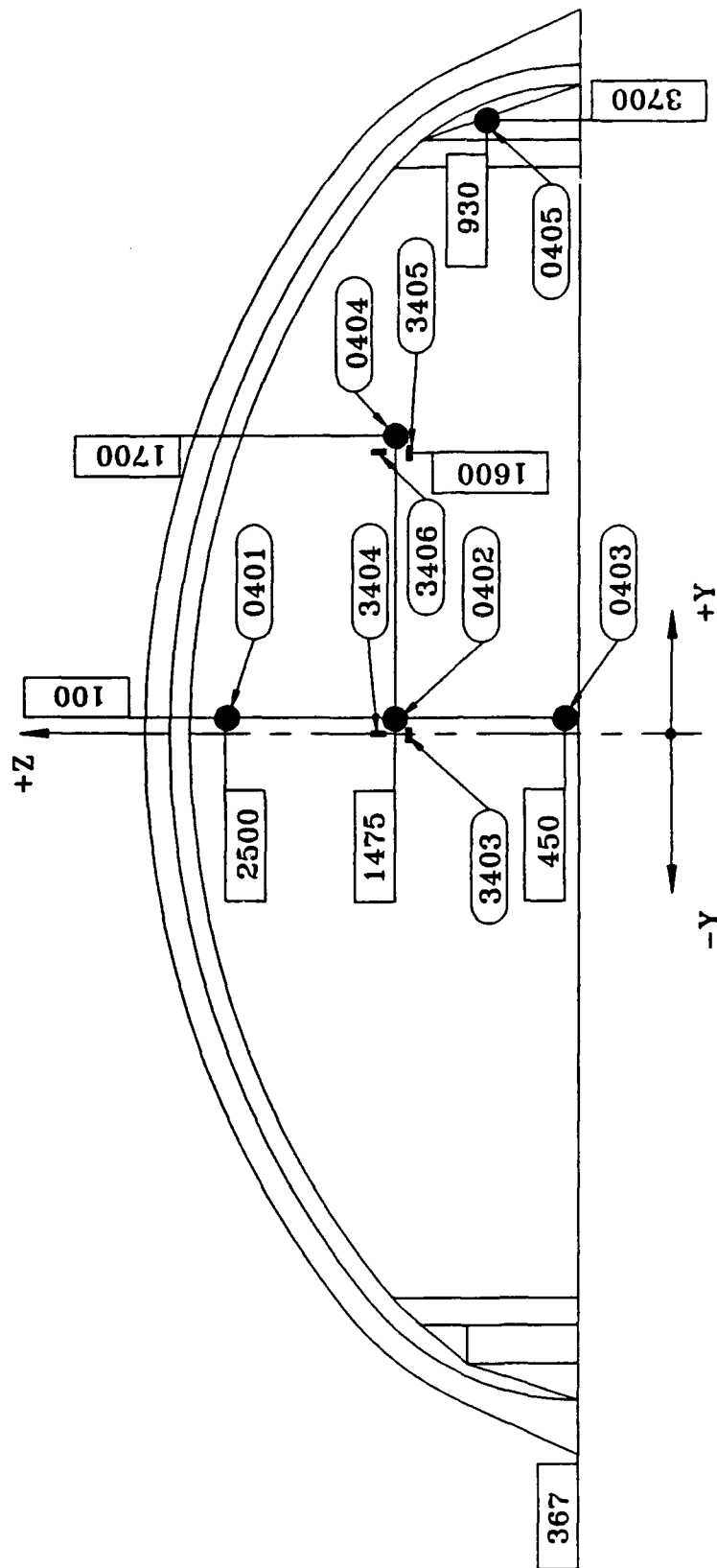


Figure 13. Instrumentation on inside surface of front door at X = 498, PAS-1.

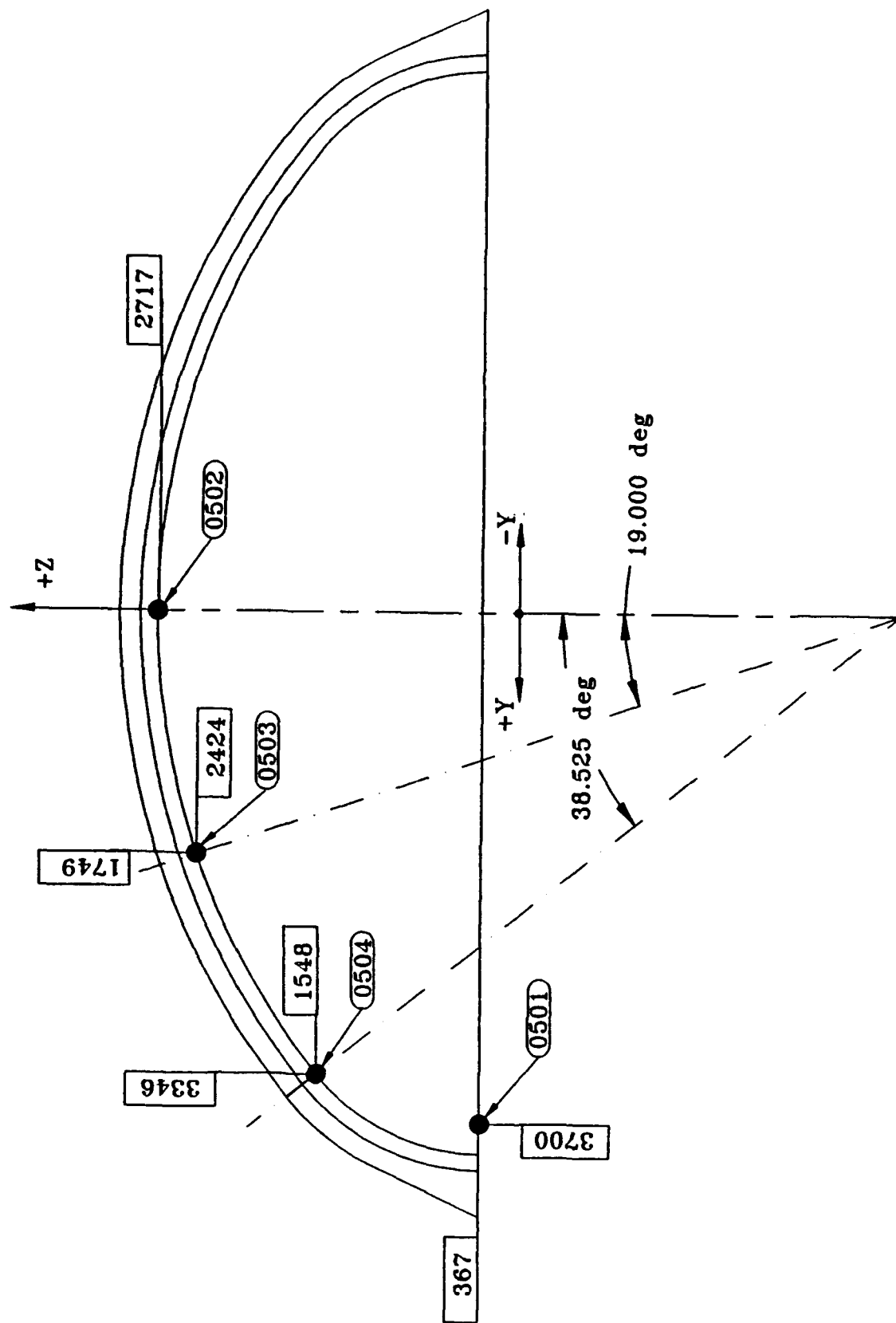


Figure 14. Instrumentation on arch at X = 645, PAS-1.

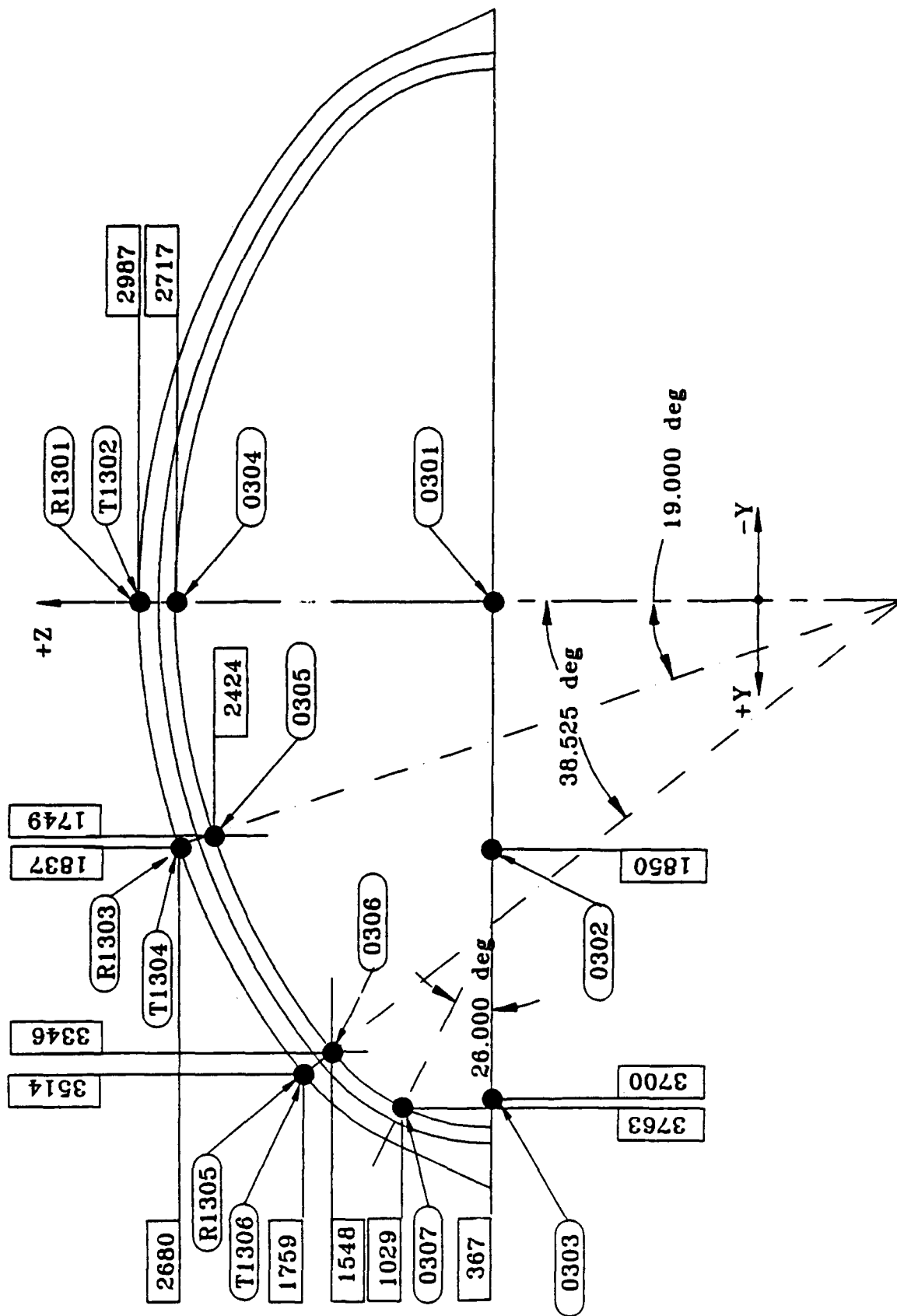


Figure 15. Instrumentation on arch at X = 3976, PAS-1.

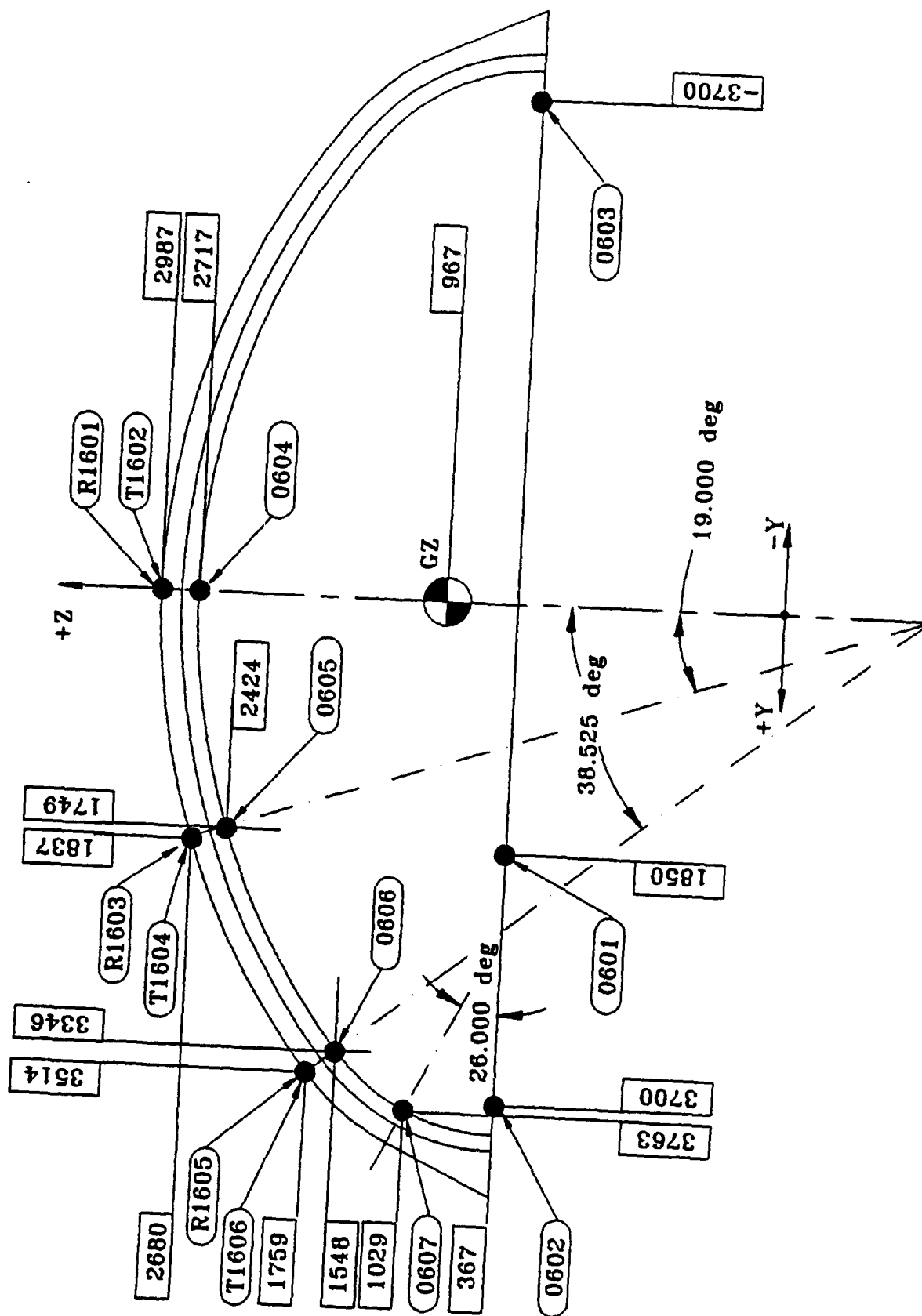


Figure 16. Instrumentation on arch at X = 6818, PAS-I.

sensors mounted at three sections through the arch. The sensing axes of the accelerometers mounted at these locations were oriented to measure radial and tangential accelerations. Figure 17 shows the locations of airblast gages mounted in the backwall. Figure 18 shows the locations of the free-field airblast gages.

Nineteen high-speed motion picture and video cameras were provided at nine camera stations. The locations of these stations for the PAS-1 event are shown in Figure 19. Motion picture data were recorded at rates of 500 and 1000 frames per second.

3.2 TEST RESULTS

3.2.1 Structural Damage Survey

The test structure suffered only minor damage. No cracks were observed in the visible portions of the arch foundation, and there did not appear to be any separation between the top of the arch foundation and the liner base channel. In addition, no separation between the concrete of the arch and the top of the foundation could be detected on the exterior of the structure. There was no discernible outward movement of the arch foundation.

The pattern of hairline cracks shown in Figure 20 was observed in the floor slab around the surface GZ. Within these cracks, and the construction joints, the floor slab was "dished" downward to 18 mm at the GZ.

In the heavily reinforced portion of the floor slab between the door pit and the rest of the floor slab, several hairline cracks were observed running parallel to the axis of the structure (Fig. 21). The location of these cracks appeared to be random, as they did not correspond to any reinforcing bar pattern in the slab. The spacing of these cracks ranged from approximately 450 to 1225 mm.

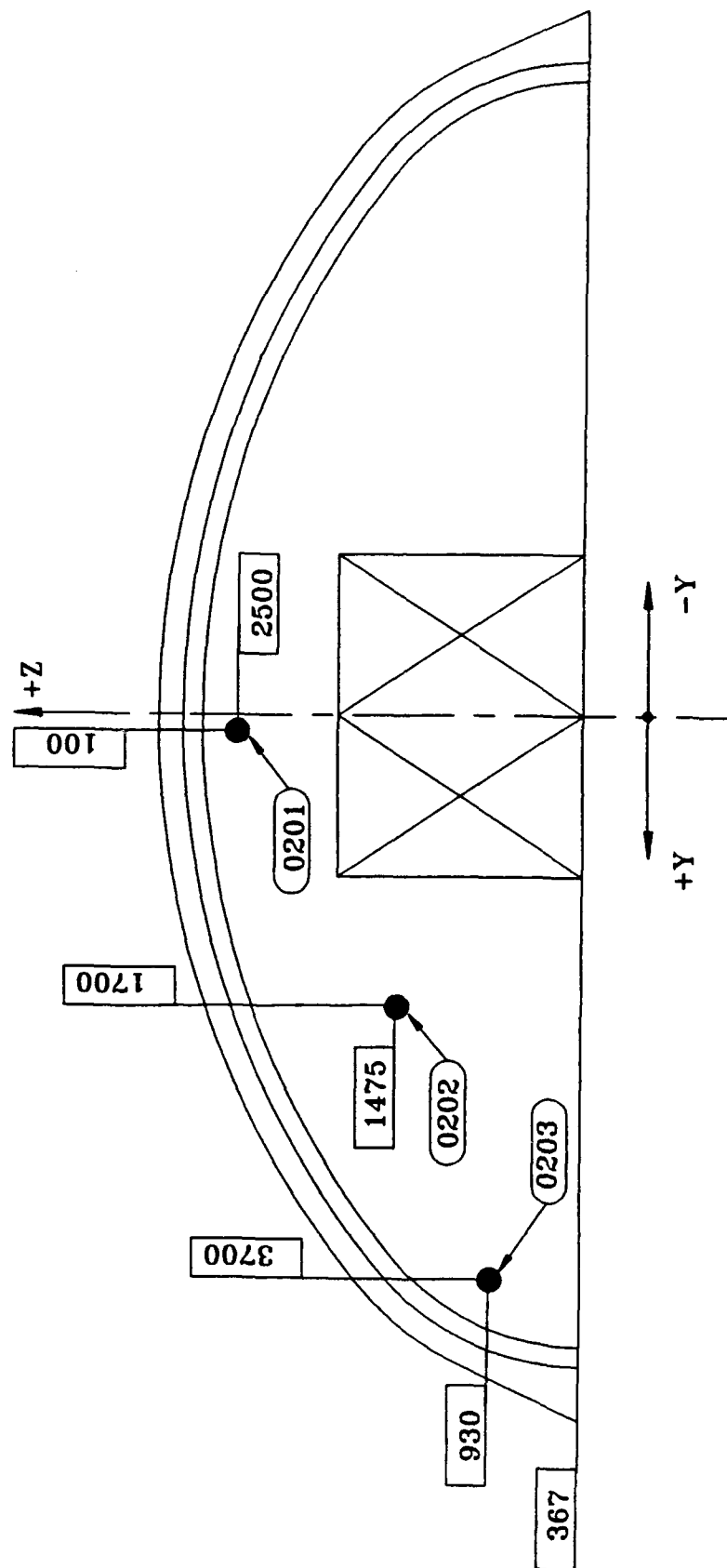
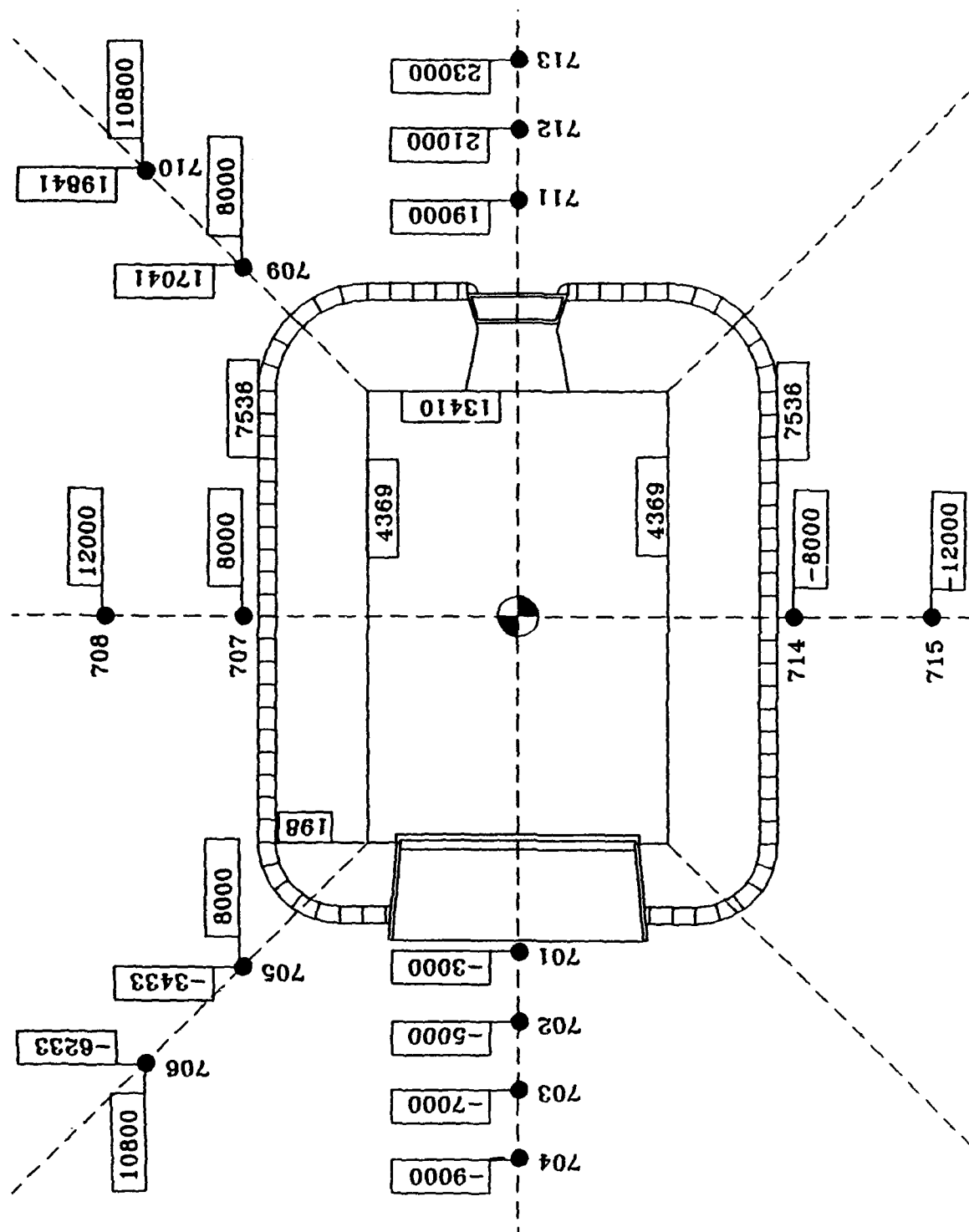


Figure 17. Instrumentation on inner surface of backwall at X = 13010, PAS-1.



Testbed grade at Z = 350
Figure 18. Free-field airblast gage locations, PAS-1.

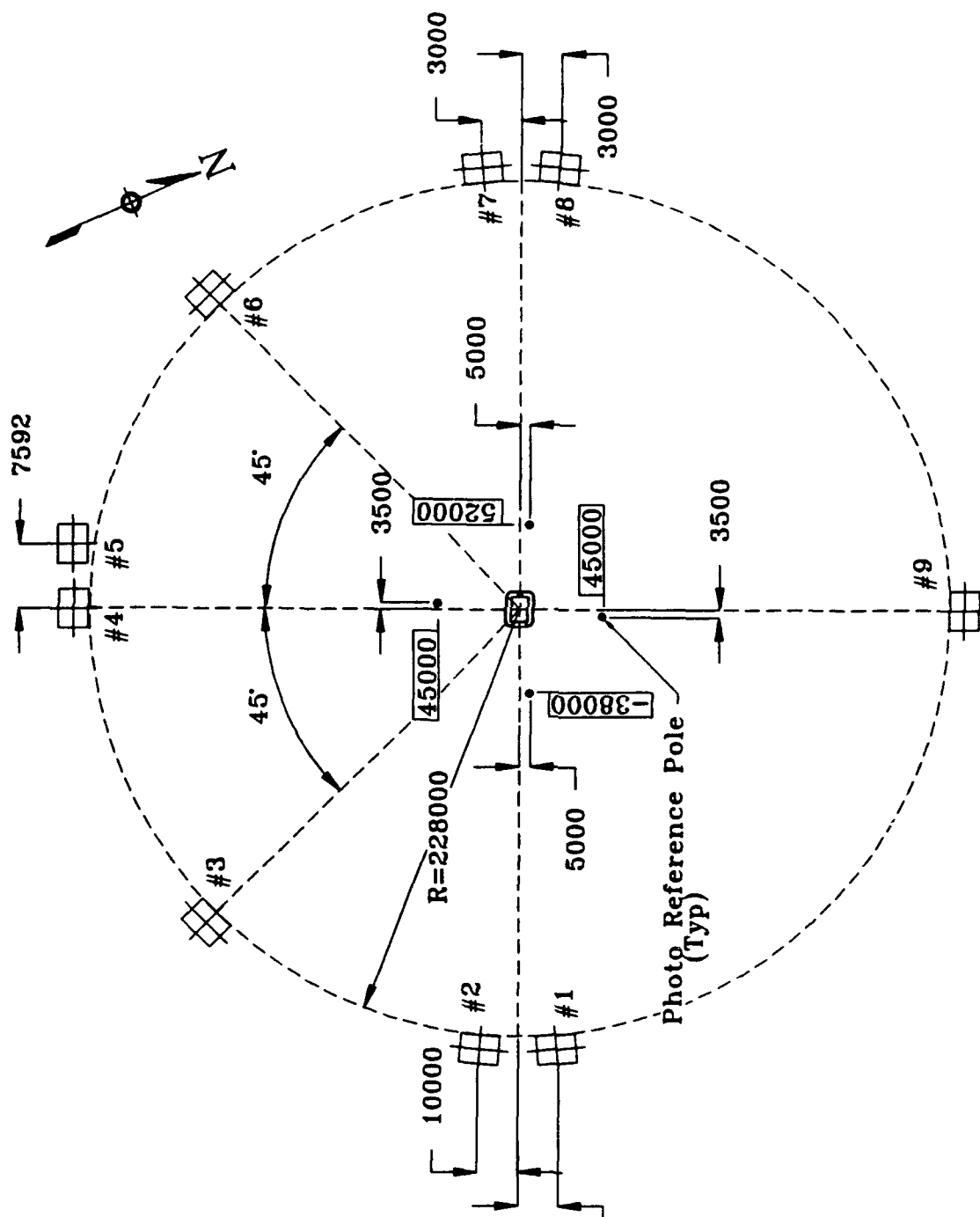


Figure 19. Camera station locations, PAS-1.

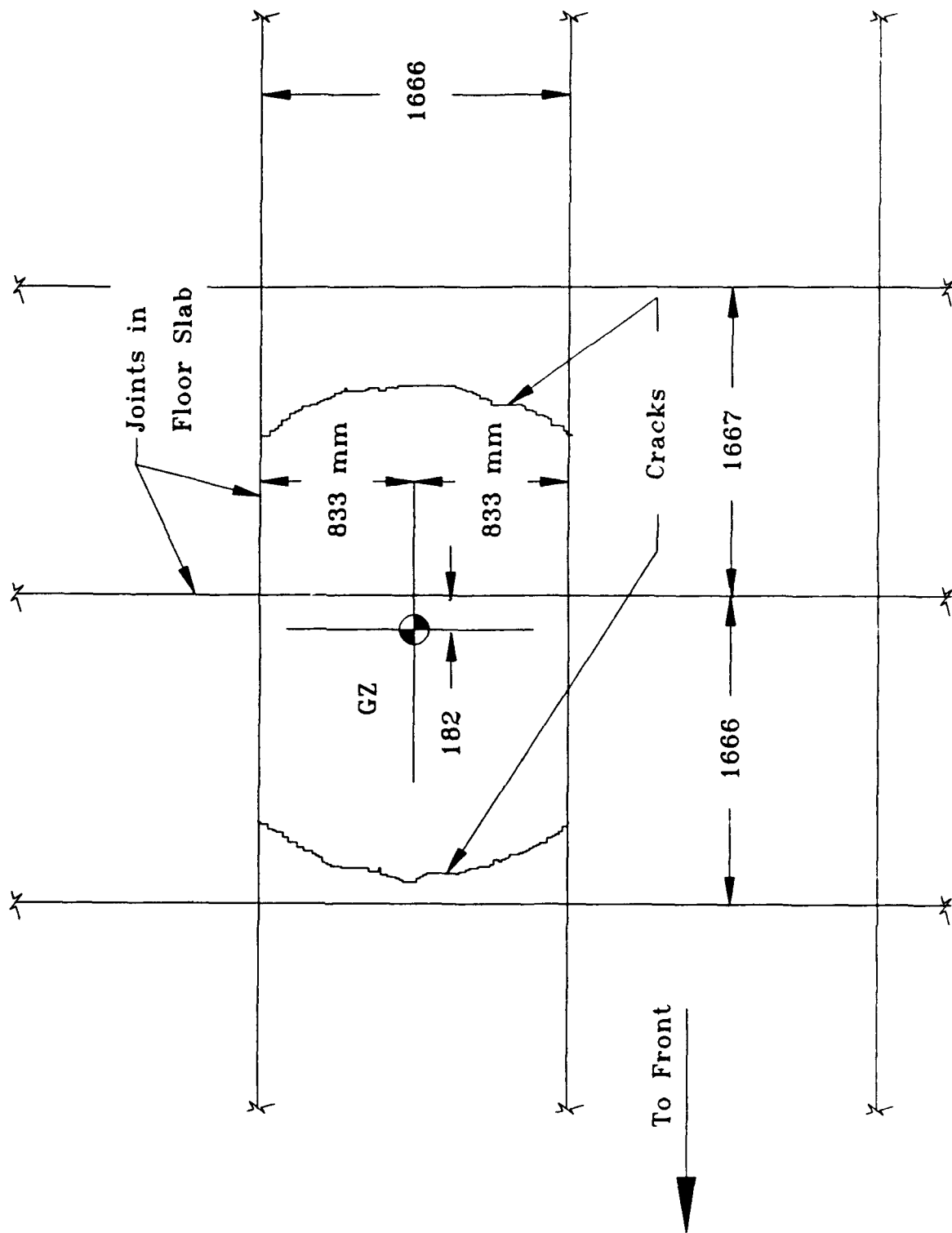


Figure 20. Crack pattern in floor slab, around GZ, PAS-1.



Figure 21. Cracks in floor slab adjacent to door pit, PAS-1.

As shown in Figure 22, a series of hairline cracks was observed in the floor slab near the back corner, on the left side (as one faces the front door from the inside). The pattern of cracks would seem to suggest that the floor slab had been lifted upward near the back corner; however, a similar pattern of cracks was not seen in the back corner on the right side.

A gap was noted between the floor slab and the backwall. The distance of separation ranged from zero at both of the back corners to 3 mm at the edges of the opening of the exhaust port. The gap continued across the opening of the exhaust port, at the joint between the floor slab and the floor of the exhaust port (Fig. 23). It had a fairly uniform width of 4 mm.

A hairline crack was observed at the joint between the top edge of the backwall and the arch concrete. The crack was generally wider at the top of the backwall and became virtually unobservable near the location where the arch radius changes (at an angle of approximately 60 deg from the vertical). Although unobservable by eye, when fingers were run across the crack one could feel a small, but distinct, displacement between the backwall and the arch concrete. The type of displacement would seem to indicate that the backwall had been moved outward relative to the arch concrete. No other cracks were observed in the backwall.

Probably the most dramatic cracking in the structure was found at the intersection of the parapet and the top of the front walls on both sides of the structure. In these areas the concrete was observed to be badly fractured, although it generally still remained in place (Figs. 24 and 25).

A series of hairline cracks could also be seen on the front face of the parapet (Fig. 26). As shown, the cracks near the top of the parapet were generally radial. Moving from the center toward the junction with the front walls, the cracks tended to become more diagonal. Although the crack pattern in the parapet seemed quite symmetrical about the centerline, it was judged that there was slightly more cracking and damage at the right side.



Figure 22. Cracks in left back corner of floor slab, PAS-1.

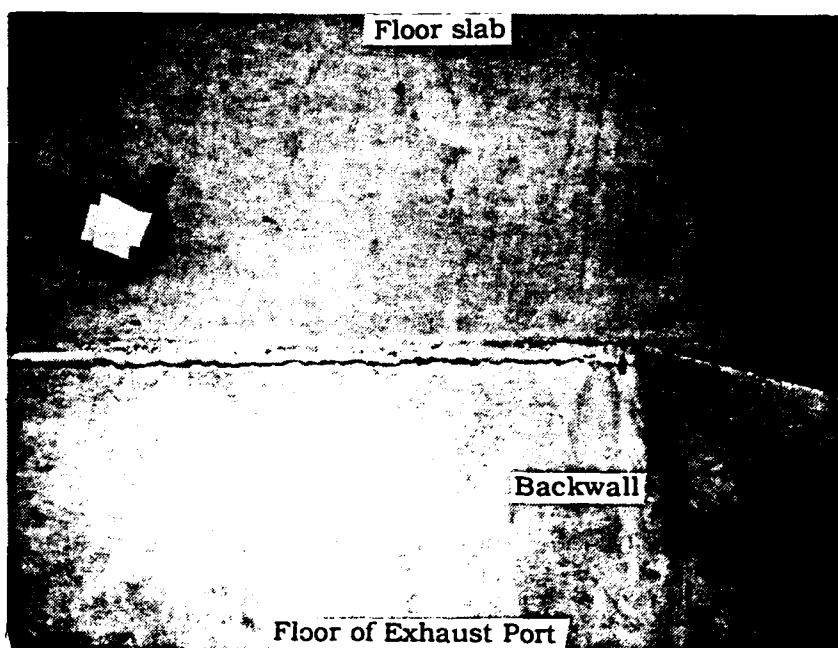
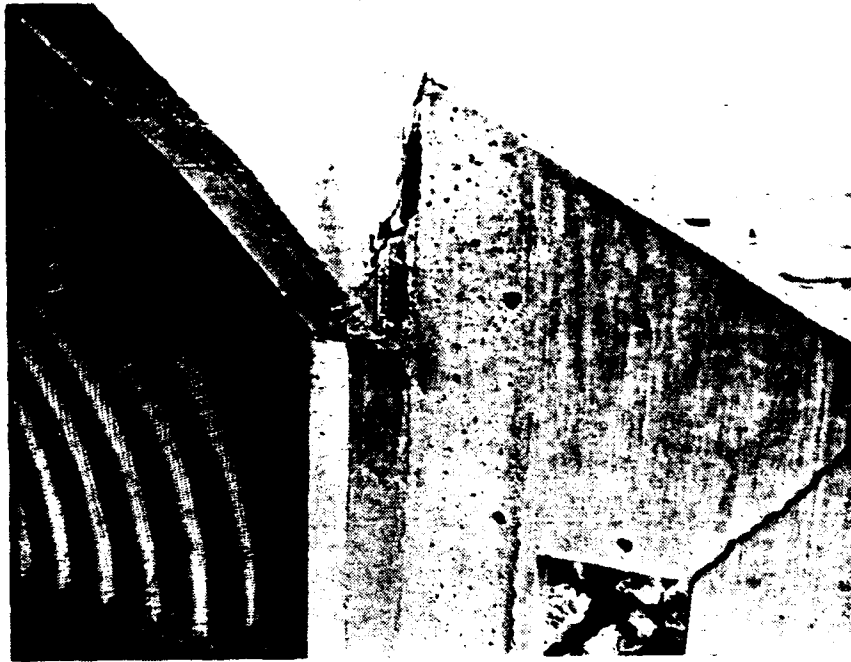


Figure 23. Gap between floor slab and floor of exhaust port, PAS-1.



(a) Front.

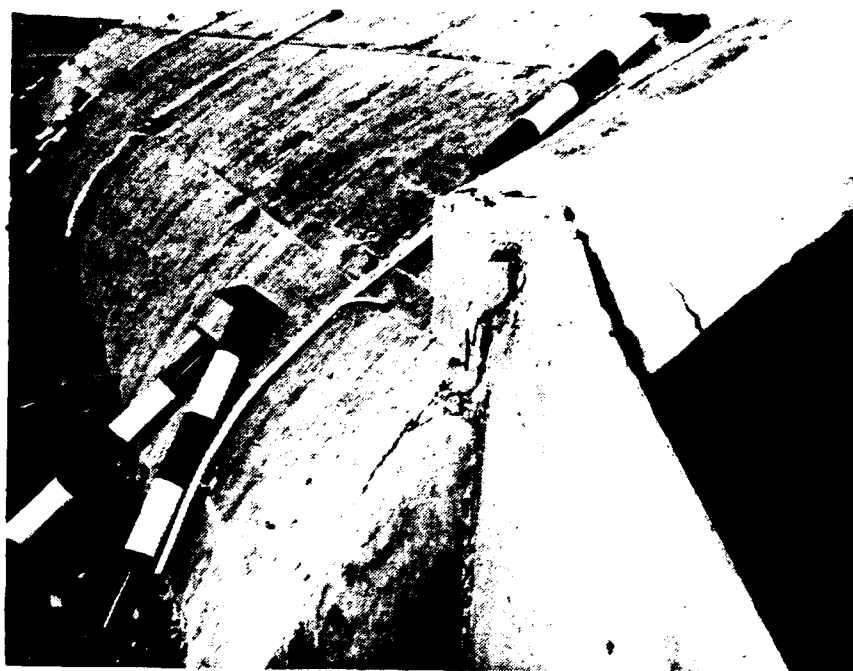


(b) Back.

Figure 24. Cracking at left front wall and parapet, PAS-1.



(a) Front.

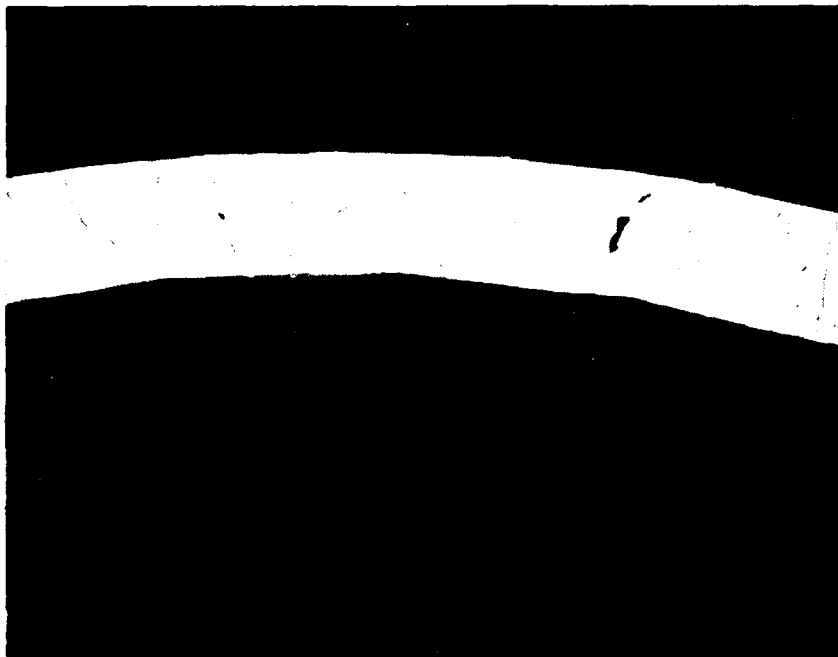


(b) Back.

Figure 25. Cracking at right front wall and parapet, PAS-1.



(a) Right side.



(b) Center.

Figure 26. Crack pattern in face of parapet, PAS-1.

The personnel vestibule was found lying on the rock rubble berm within 1 m of its original position (Fig. 27). The personnel door that had been located in a frame installed in the opening in the left front wall was found inside the vestibule. The door had been bent outward about its vertical centerline, and the welds simulating the hinges and latches had all been broken. The door frame remained intact in the opening.

The left wingwall had three relatively large cracks. One crack ran from both the upper and lower corners of the rectangular opening to the junction of the wingwall and the front wall. The width of both cracks ranged from 2 to 4 mm. The third crack ran from the other upper corner of the opening diagonally upward to the top edge of the wall (Fig. 28a). The width of the third crack on the front face ranged from 6 to 8 mm. In addition, the wall was displaced front-to-back approximately 6 mm at the third crack, with the outer portion of the wall beyond the opening displaced backward relative to the portion joined to the front wall. On the back of the wall, the edges of the third crack had spalled away to a depth approximately one-third the thickness of the wall, exposing the reinforcing bars (Fig. 28b). All of the vertical and horizontal bars were observed to have fractured in tension at the crack line.

Two pieces of concrete debris from the back surface at the top of the left wingwall were found on the rock rubble berm (Fig. 29).

The right wingwall was found to have only two hairline cracks. These cracks ran diagonally from about the mid-point of the top edge of the wall downward toward the front wall foundation (Fig. 30). The cracks ran through the thickness of the wall.

No cracking was observed in any surface or corner of the exhaust port. In addition, no gap or separation was observed between the walls and roof of the exhaust port and the back surface of the backwall.



(c) Left side.

Figure 26. Concluded.

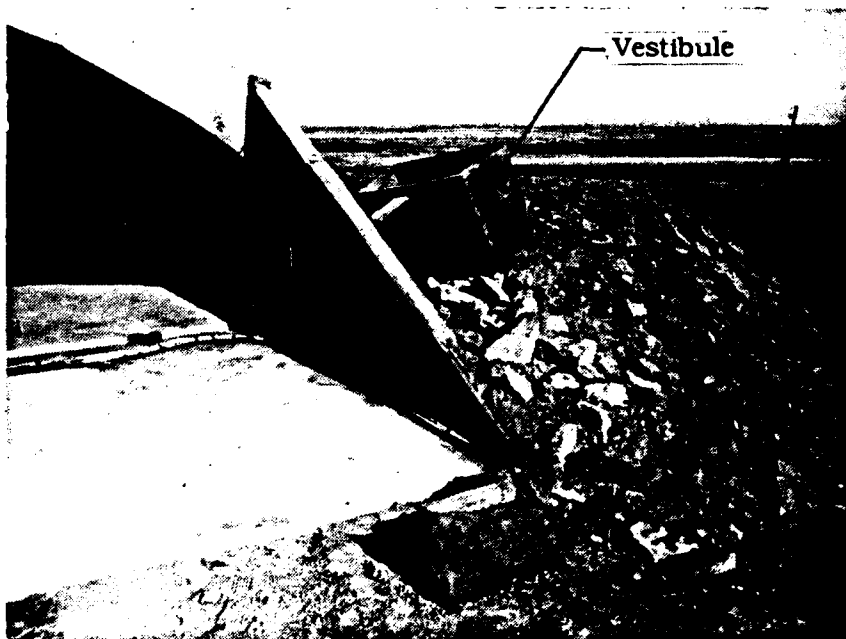
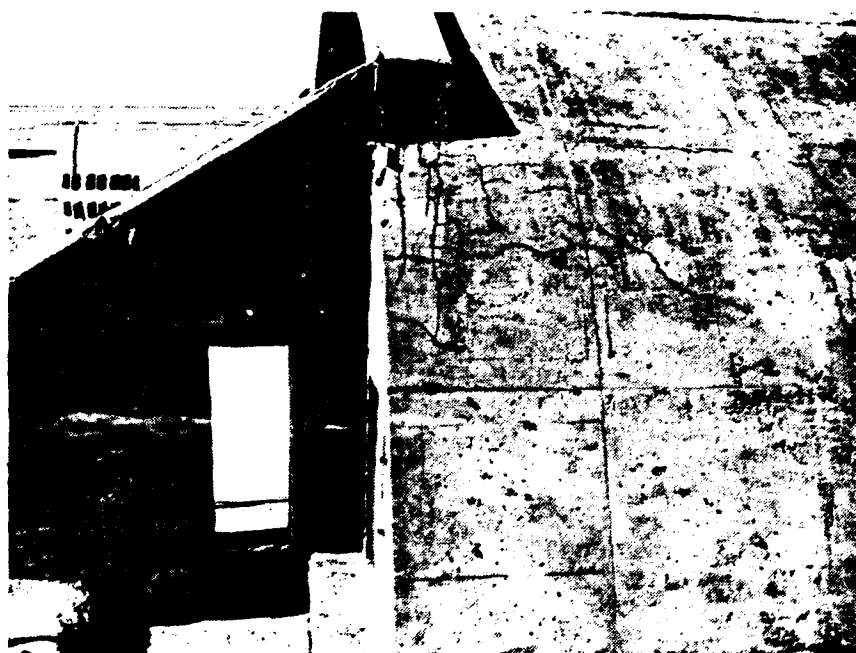


Figure 27. Posttest location of vestibule, PAS-1.



(a) Front.



(b) Back.

Figure 28. Cracks in left wingwall, PAS-1.



Figure 29. Debris from top of left wingwall, PAS-1.

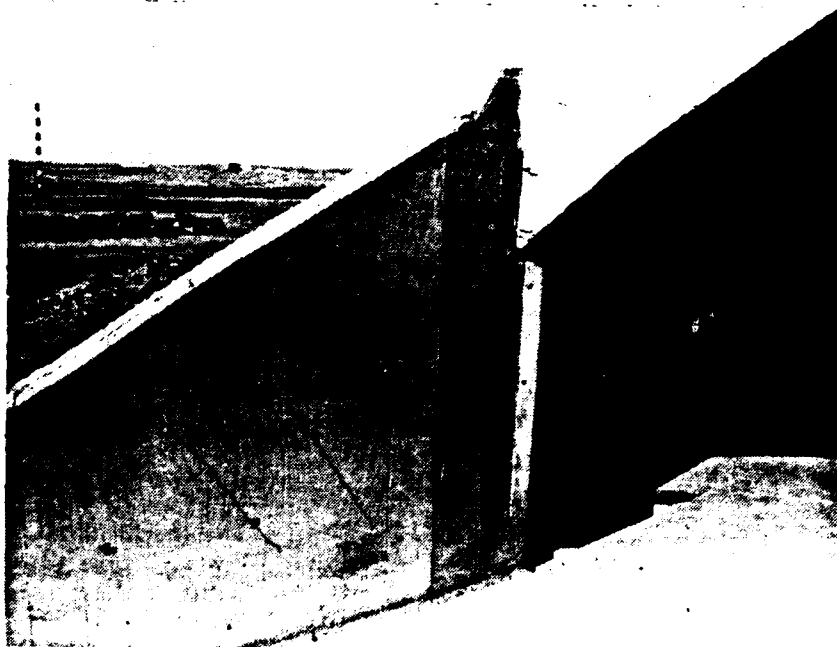


Figure 30. Crack pattern in right wingwall (front), PAS-1.

The polyvinylchloride (PVC) pipe vent located in a hole in the right side of the backwall was found lying on the ground approximately 5 m along a 45-deg line from the right, back corner of the shelter (Fig. 31). The remaining PVC pipe and T-fitting were found in a small blow-out crater in the earth backfill adjacent to the hole in the backwall.

With the exception of a hairline crack in the left corner of the slab (Fig. 32), the apron slab at the front of the shelter was found to be undamaged. No cracking was noted on the right side of the slab. There was no separation or cracking between the apron slab and the front foundation of the shelter.

The front door was found lying inside the shelter in the door pit area (Fig. 33). The right side hinge bracket was still on the hinge pin near the correct position for operation. However, the left hinge bracket had moved off the pin (Fig. 34). The top edge of the door was resting on the steel angle at the edge of the door pit (Fig. 21). No damage to the steel angle was noted. The right support post was found in the door pit area near its original position. The left support post was never found despite an extensive search in front of the shelter. It was assumed that it was blown through the personnel door opening and was buried among the rock rubble and soil.

The door was bent outward about a horizontal line with a permanent deformation of 18 mm at the center (Fig. 35). When the door was raised, it was observed that the inside plate had been locally deformed in an area around the intersection of the horizontal and vertical centerlines, so as to make the locations of most of the vertical ribs in the door just slightly apparent. There were no apparent deformations of the perimeter edges of the door. Later, the door was lifted onto its hinge pins and returned to the closed position with no problems.

One of the two brackets located on either side of the centerline of the parapet, near the top of the steel door frame, was broken off. It was found near the center of the front edge of the apron slab. Plate components in the bracket were buckled, and the welds, originally holding it to the door frame, were observed to be broken. This bracket was

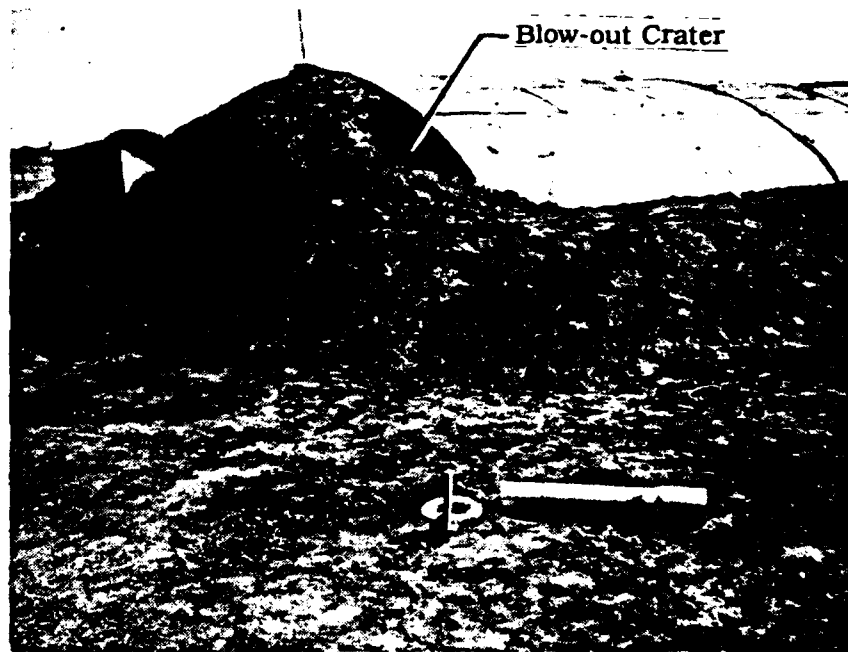


Figure 31. Pipe vent from backwall, PAS-1.



Figure 32. Crack pattern in left corner of the apron slab, PAS-1.

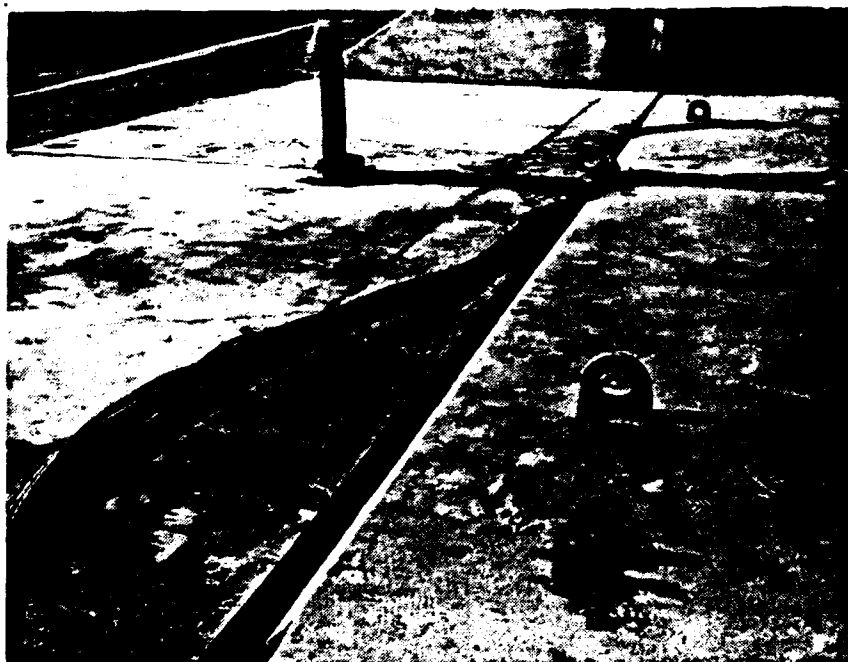


Figure 33. Posttest location of front door, PAS-1.

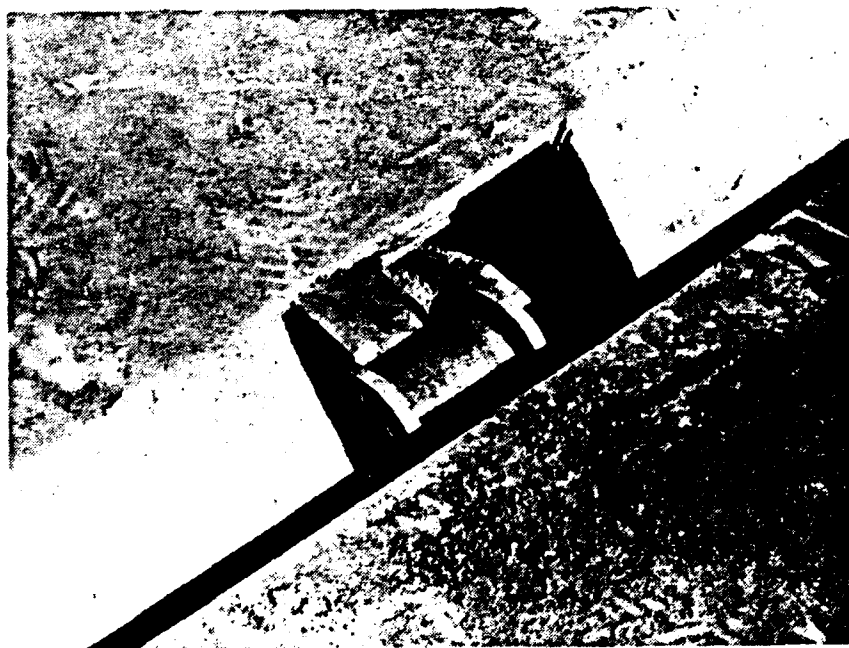


Figure 34. Left side hinge bracket and pin of front door, PAS-1.



Figure 35. Outward deformation near centerline of front door, PAS-1.

the only piece of debris found beyond the perimeter of the structure. The rest of the steel frame was found to be generally undamaged.

A series of hairline cracks was observed in the outer surface of the arch. The cracks were all normal to the longitudinal axis of the structure (Fig. 36). With perhaps one exception, the location of the cracks did not correspond to splices in the reinforcing bars. However, the location of the cracks did seem to correspond closely with the bolted lines of the corrugated steel liner.

In addition to the transverse cracks noted above, a second pattern of hairline cracks was noted on the right front corner of the arch. These cracks appeared to be more diagonal, running from the foundation upward toward the junction of the parapet, front wall, and wingwall (Fig. 37). No similar pattern of cracks was found on the left front corner of the bracket from the top of the front door frame.

The detailed inspection of the model structure described above revealed that the overall damage resulting from the PAS-1 event was minor. It was concluded that the observed damage would have only a minor effect on debris and airblast distribution in a subsequent test where the internal charge would cause catastrophic failure of the structure. Consequently, it was recommended that the structure be retested in the PAS-3 event using 33.3 kg of C-4 explosive.

3.2.2 Data Obtained from Instrumentation

Usable data were obtained from all but one of the electronic sensors. The minimum digitization frequency for data reduction for all records was 100 kHz. Some baseline shifts were noted in many of the records. In a few instances corrections were applied to data to evaluate the effect of these shifts on integrations for impulse or velocities and displacements. The corrections generally did not have a significant effect on the first peaks of the integrated data. Only uncorrected data are presented in this report.

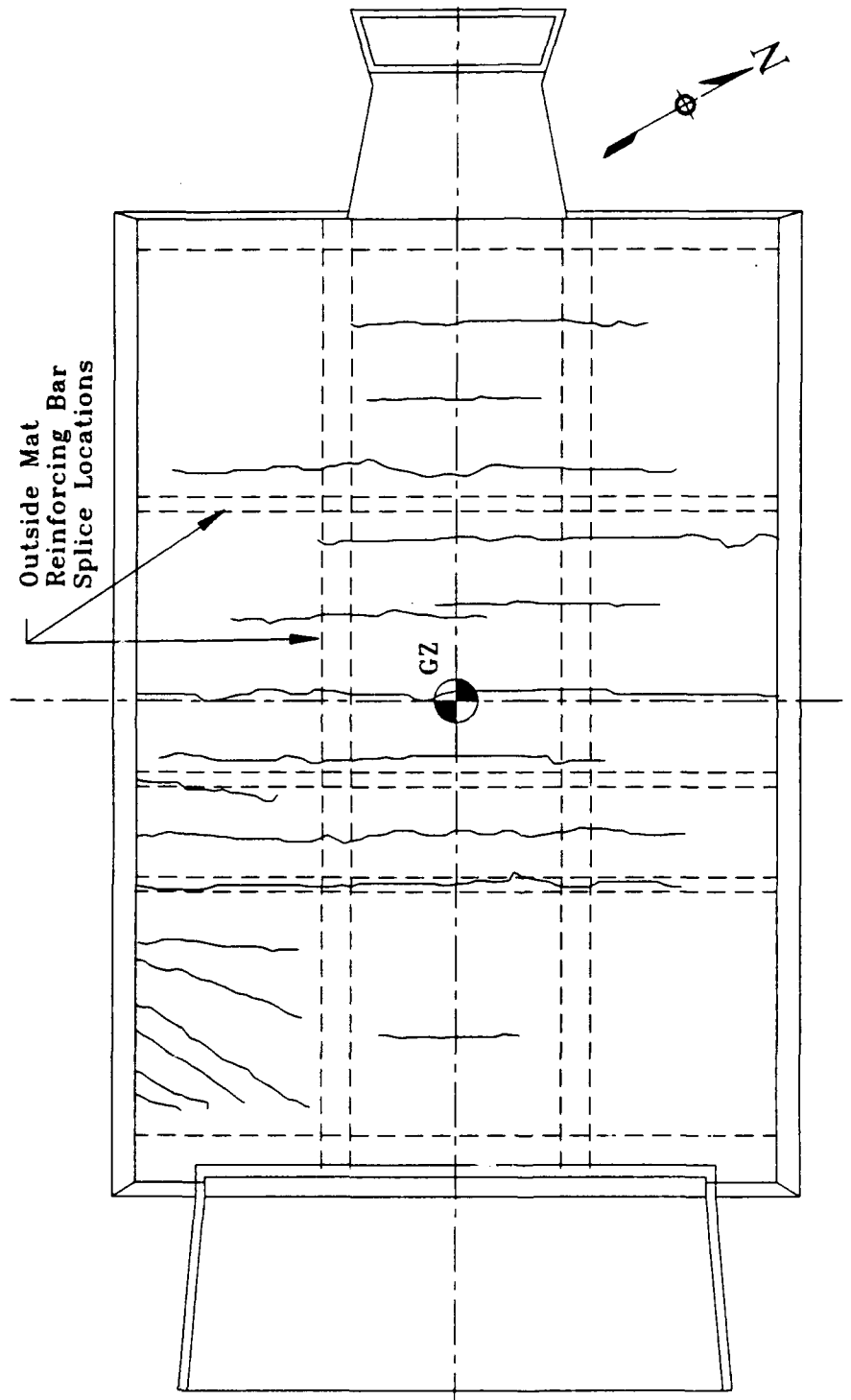


Figure 36. Crack pattern in arch, PAS-1.

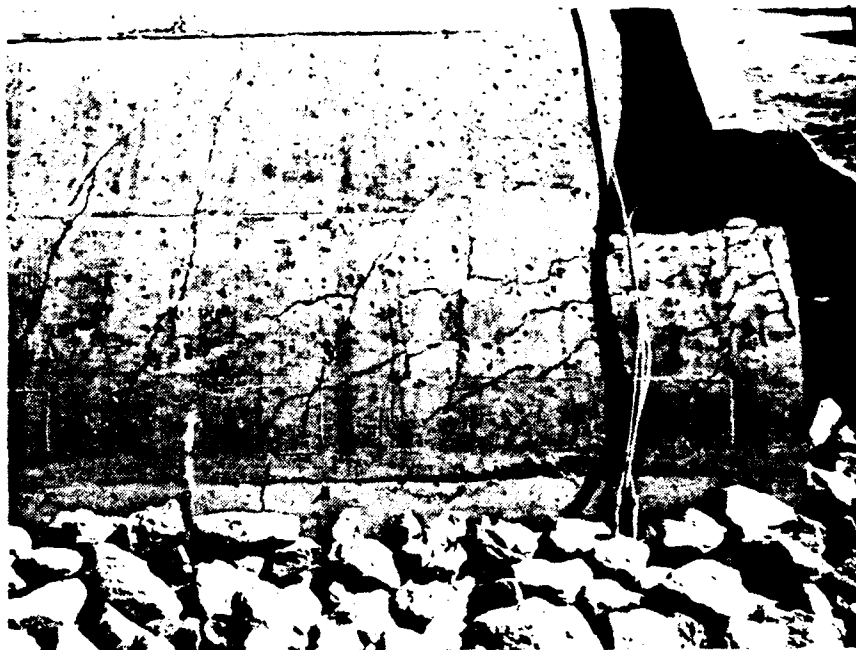


Figure 37. Diagonal crack pattern on right front corner of arch, PAS-1.

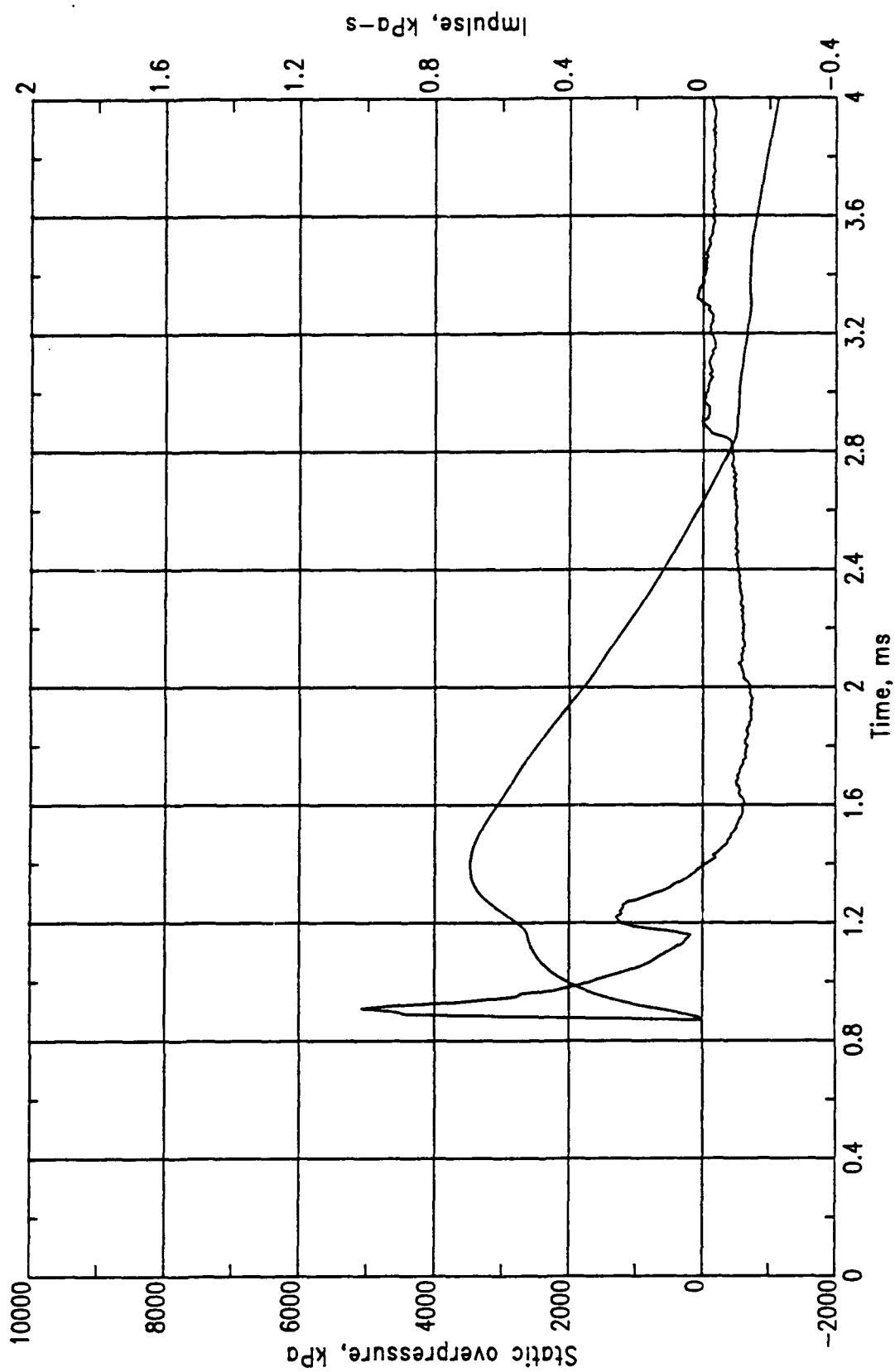
The maximum pressure inside the structure was 5.03 MPa at MN 604, as recorded by a gage located on the ceiling of the arch directly over the explosive charge. The predicted peak reflected pressure at this location was 4.50 MPa. Figure 38 shows 4-, 50-, and 100-ms plots of this record. As might be expected, the peak of the 100-ms plot is reduced somewhat from that observed in the 4-ms plot with its expanded time scale; however, there was no significant difference in the early peak impulse obtained from integration of the pressure record. Multiple peaks were observed in most of the airblast records obtained from gages inside the structure. These multiple peaks are not as pronounced in MN 604 as they are in some other records.

Figures 39 and 40 show the pressures recorded on the floor near the sides of the structure in the same plane as MN 604. The peaks at these two locations were 0.53 and 0.48 MPa. Although the peaks differ slightly, the character of the records are similar.

Figures 41 through 43 show the pressures recorded at the inside centerline of the front door. The peak reflected pressures at the top, mid-height, and bottom of the door were 0.67, 0.76, and 0.49 MPa, respectively. These maximum values occurred between 17 and 18 m/s. The peak reflected pressure at the center of the door was predicted as 0.32 MPa at 9.5 m/s. The predicted value agrees reasonably well with a peak observed in MN 402 at about 9.5 m/s, but it is less than one-half of the maximum value that occurred at about 18 m/s. Measurement Number 405 made on the inner surface of the front wall near the outer edge of the door recorded a peak reflected pressure of 0.77 MPa at 11 m/s (Fig. 44) and showed no peak at 17 m/s. Measurement Number 404 failed at about 11 m/s and did not show the higher peak observed in the other records. A peak pressure impulse of 2.06 kPa-sec was predicted to occur at 54 m/s.

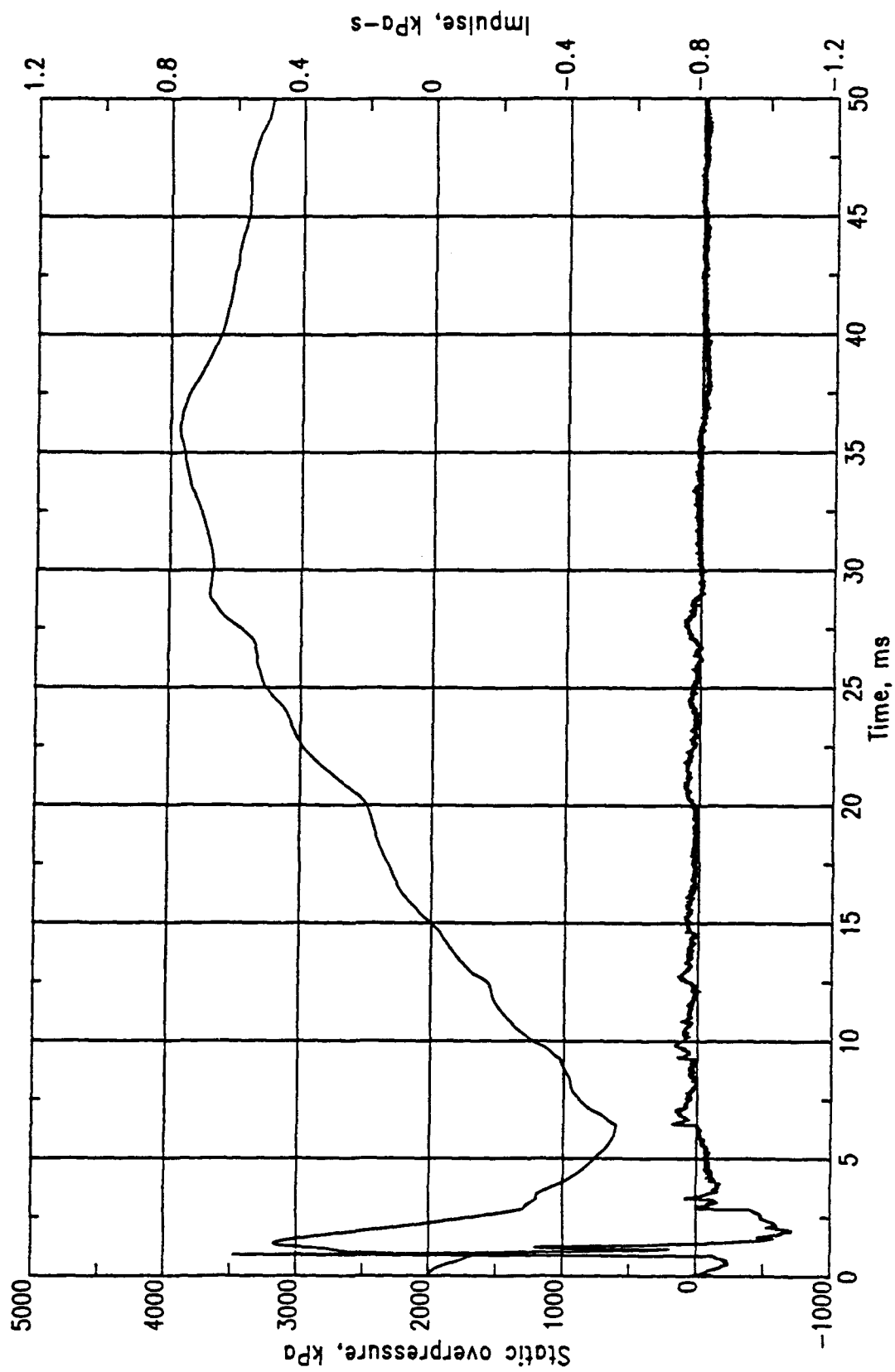
Measurement Number 402 showed a peak of 1.72 kPa-sec at 25 m/s. Pressure impulse at later times is more uncertain due to baseline shifts in the pressure data.

Measurement Numbers 201, 202, and 203 on the inside backwall of the structure had the same Y and Z coordinates as MN 401, MN 404, and MN 405, respectively, on the front door. Since the explosive charge for PAS-1 was 0.128 m closer to the backwall than to the inner surface of the front door, slightly higher pressures and earlier times of arrival (TOA) should be expected from the backwall measurements. The general



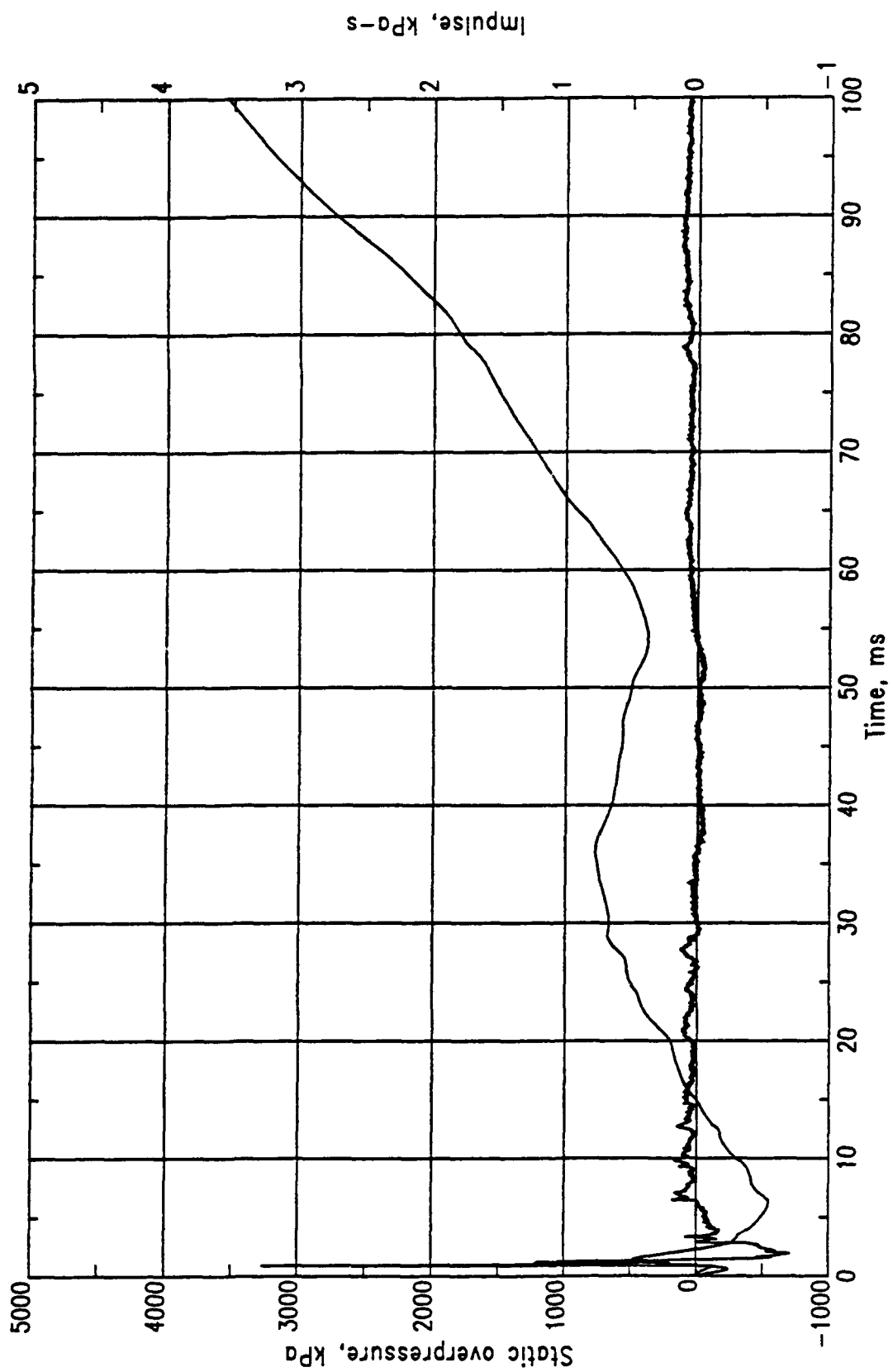
(a) 4-ms plot.

Figure 38. PAS-1, MN 0604.



(b) 50-ms plot.

Figure 38. Continued.



(c) 100-ms plot.

Figure 38. Concluded.

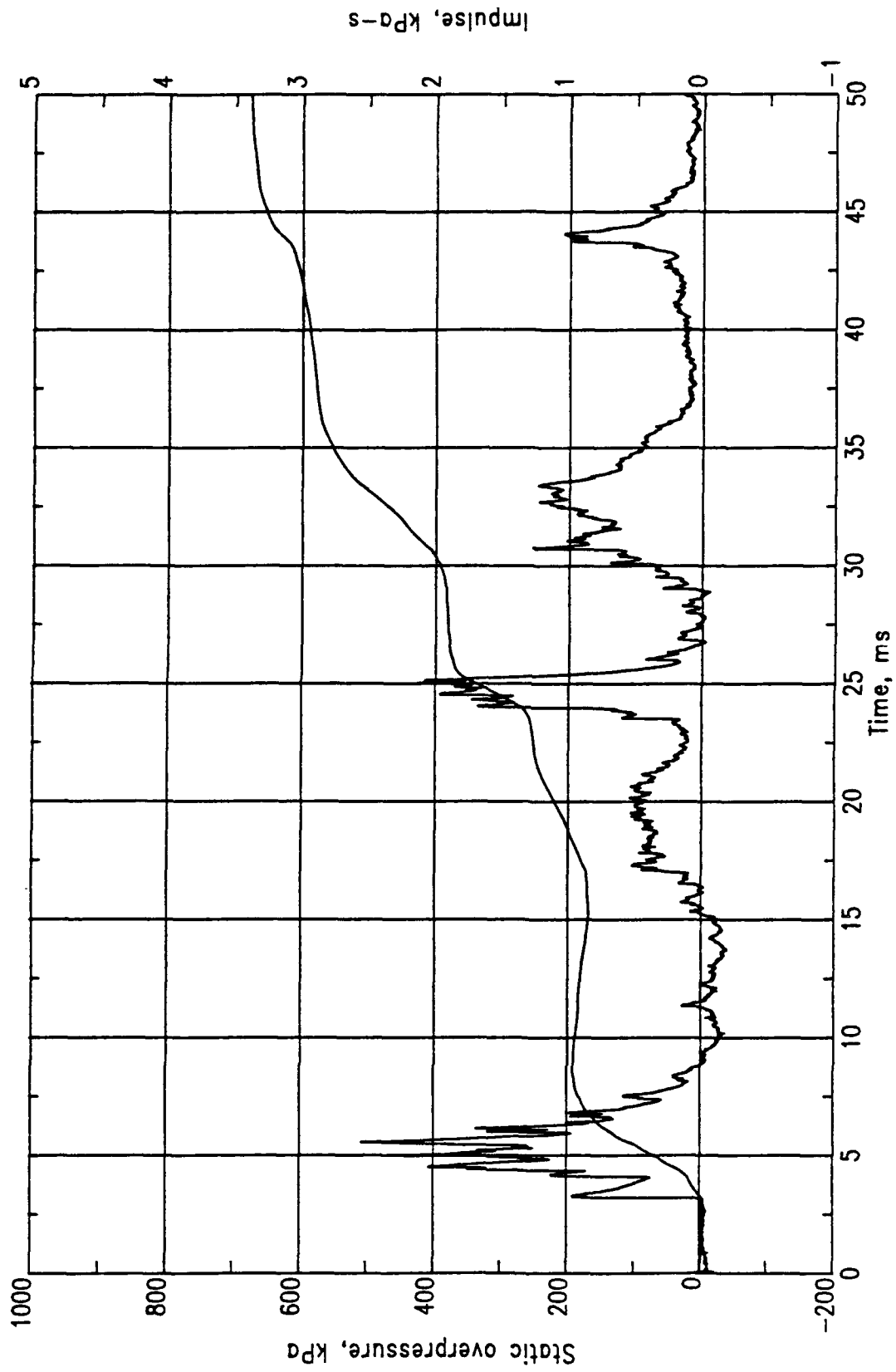


Figure 39. PAS-1, MN 0602.

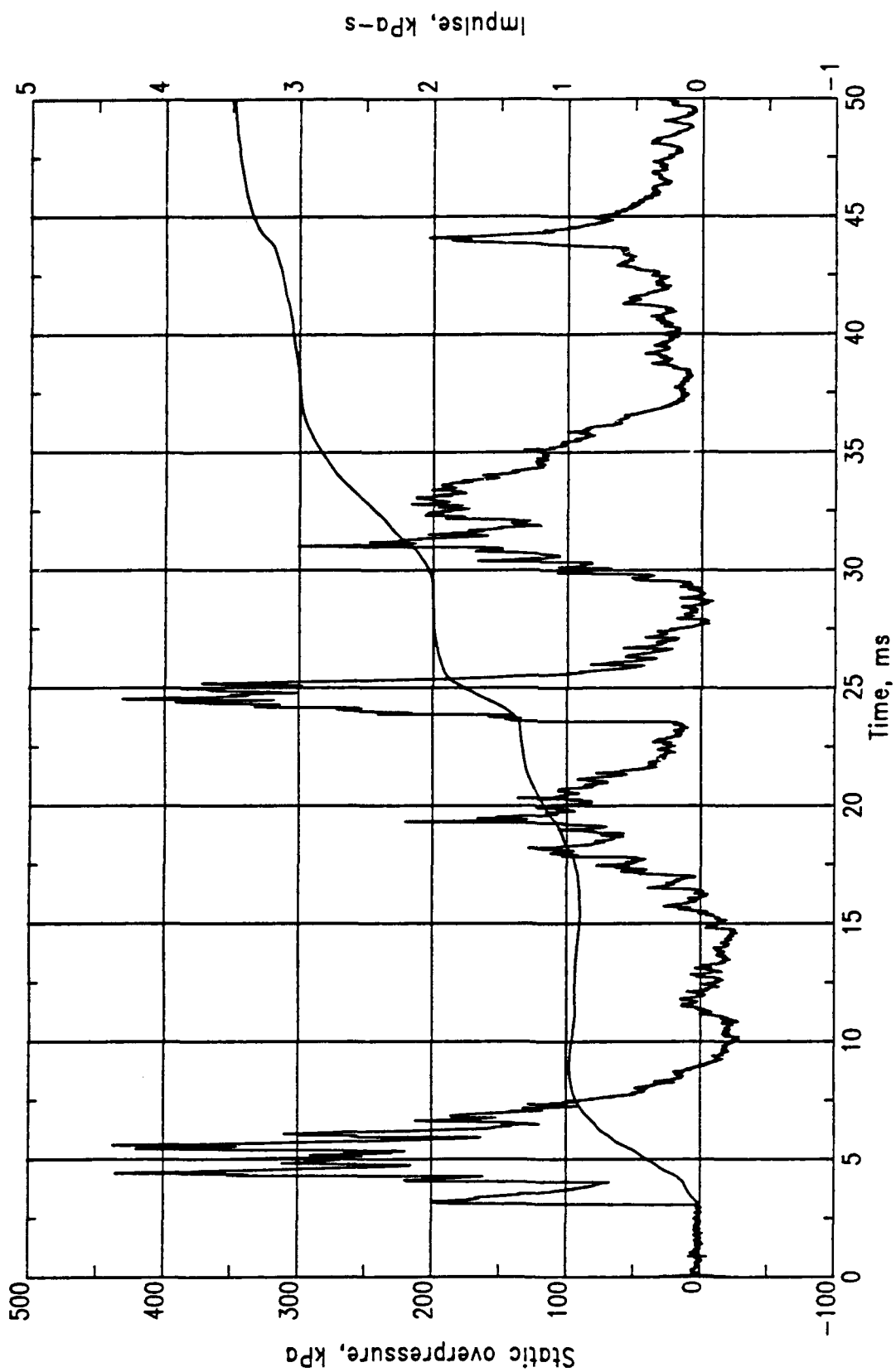


Figure 40. PAS-1, MN 0603.

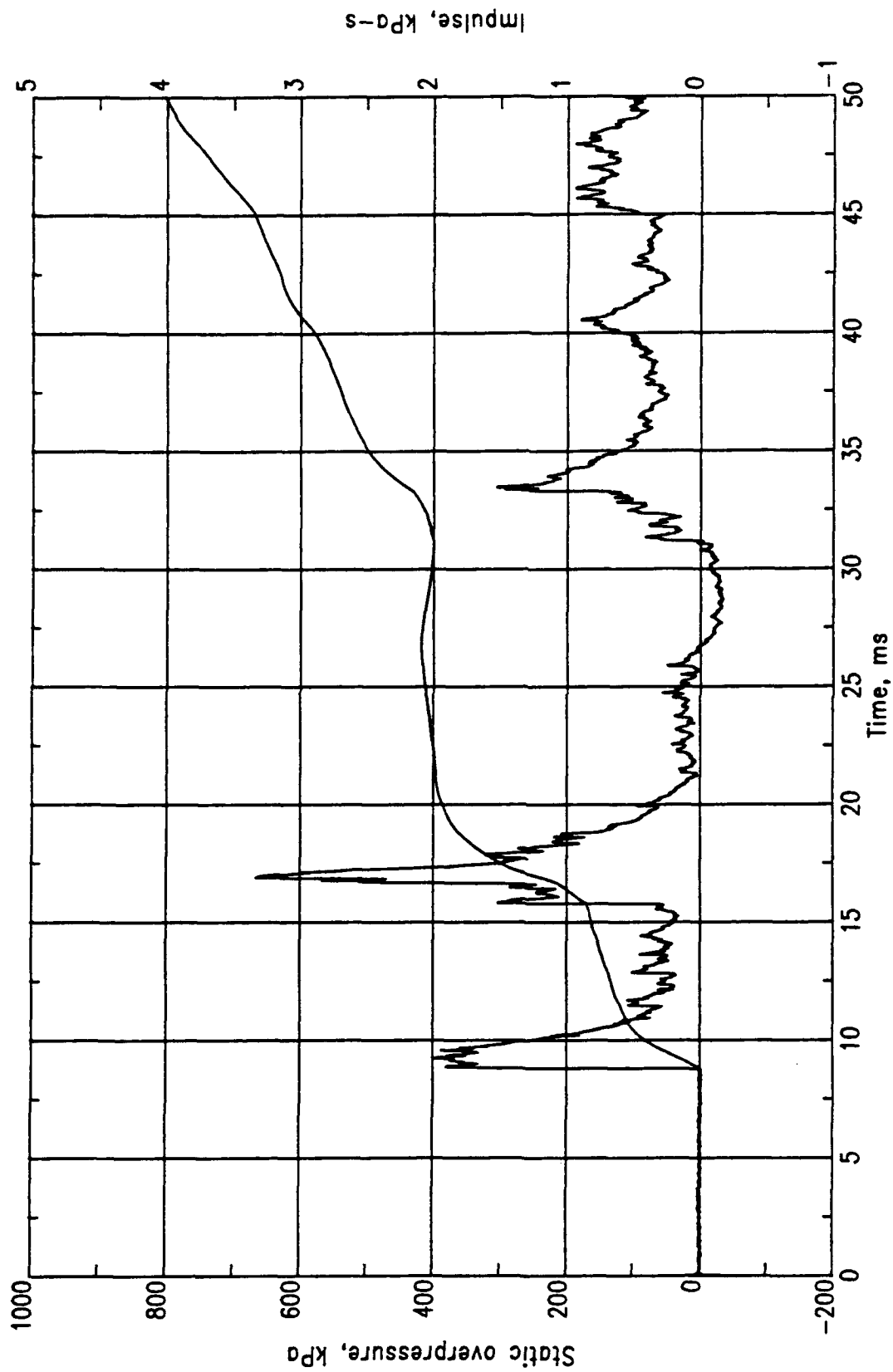


Figure 41. PAS-1, MN 0401.

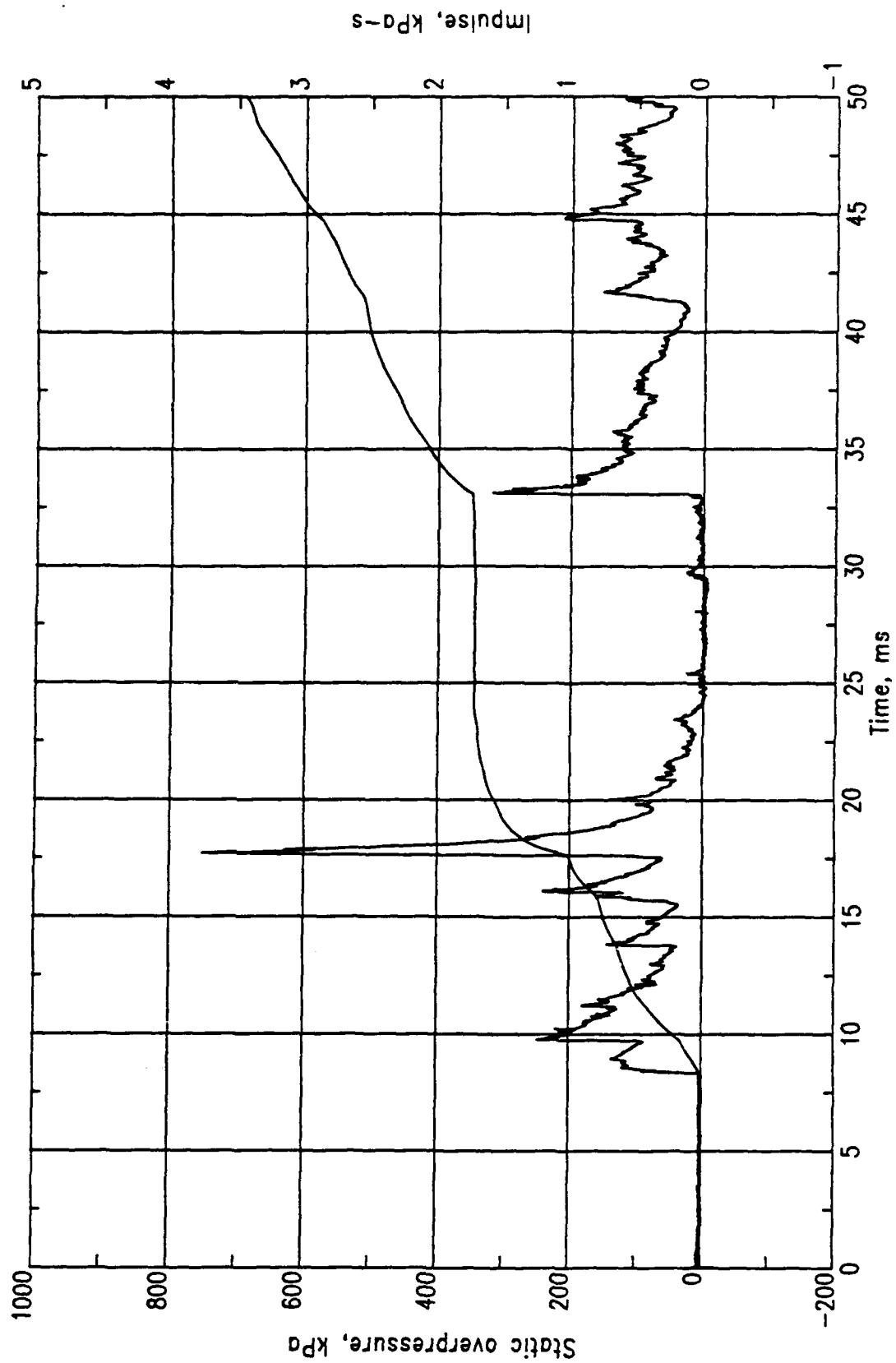


Figure 42. PAS-1, MN 0402.

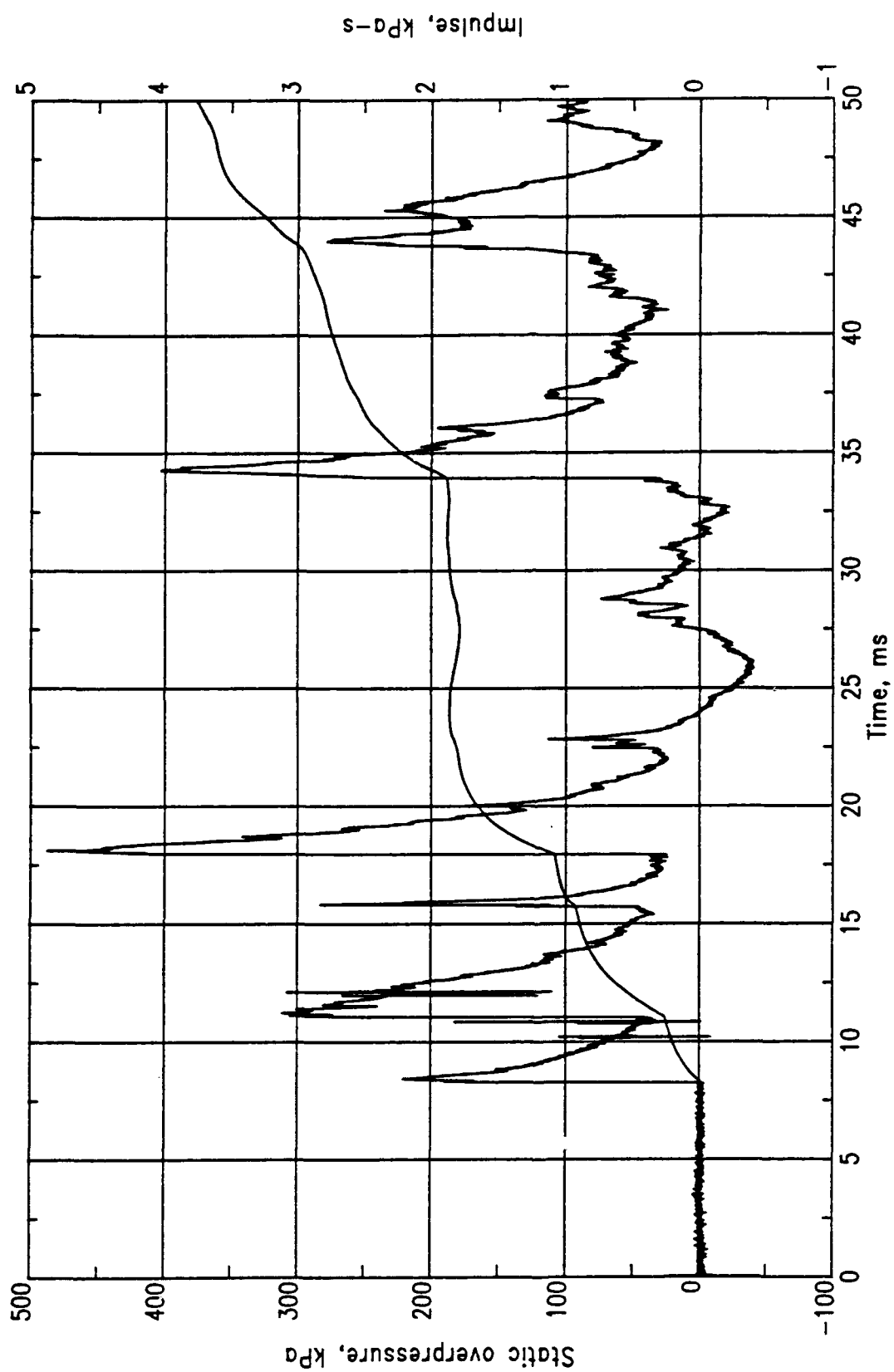


Figure 43. PAS-1, MN 0403.

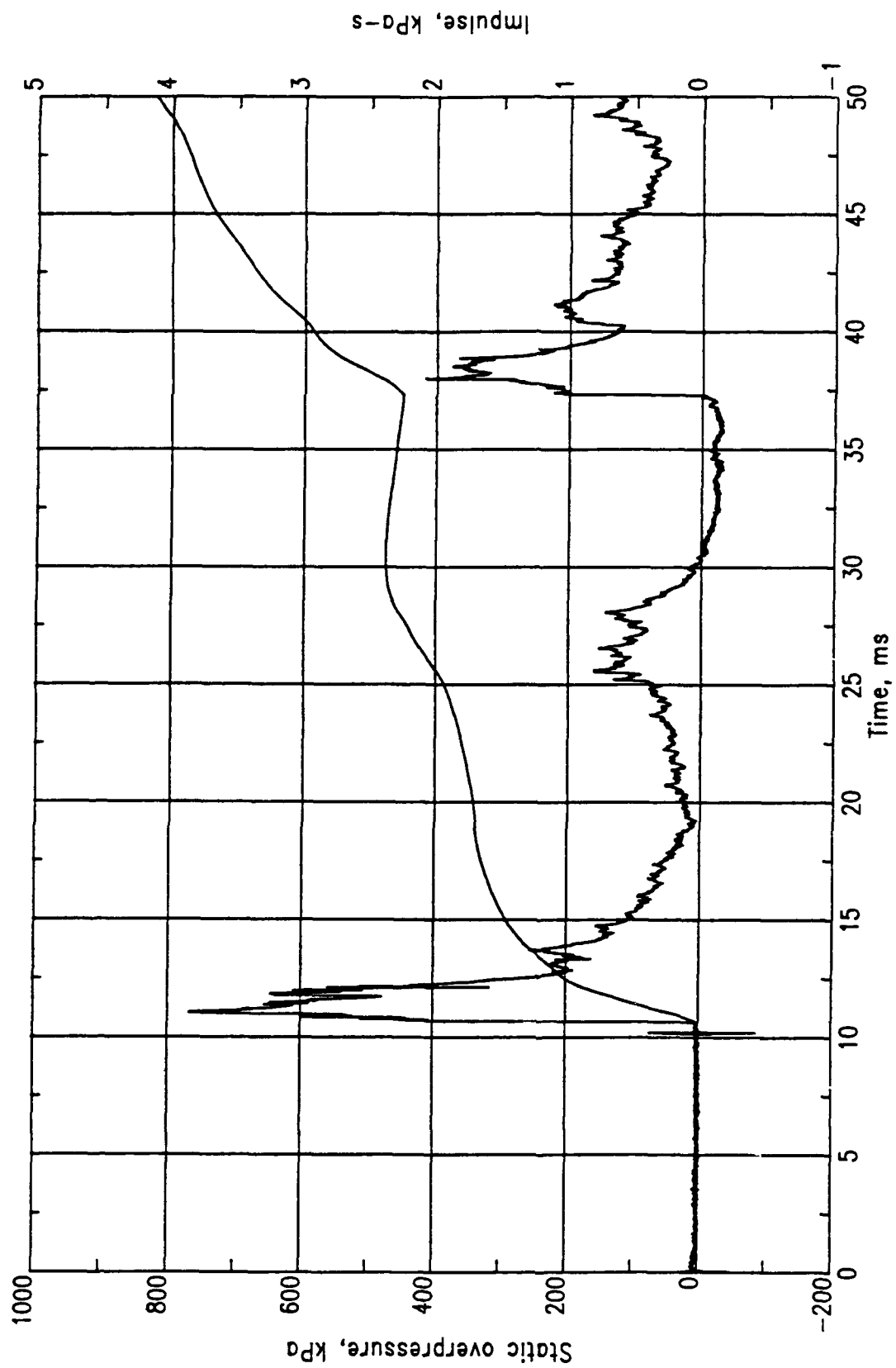


Figure 44. PAS-1, MN 0405.

character of the records obtained from MN 201 and MN 203 is similar to that of MN 401 and MN 405 (Figs. 45 and 46 versus Figs. 41 and 44). The maximum pressure peaks in MN 201 and MN 401 both occur at about 17 m/s; however, the 0.58-MPa peak of MN 201 is slightly less than the 0.67-MPa peak of MN 401. The maximum peaks in MN 203 and MN 405 occurred at about 11 m/s, but the 0.84-MPa peak of MN 203 is slightly greater than the 0.77-MPa peak of MN 405. Pressure impulse on the back wall was about the same as that on the front door. Since MN 404 failed, no comparison can be made between it and MN 202.

Table 2 summarizes selected peaks from interior pressure measurements. A complete set of pressure records is presented in Volume II.

Although electronic noise was observed in many of the records, all of the free-field gages provided usable data. In some instances the noise made the determination of exact TOAs difficult. The entire set of data appears internally consistent, i.e., TOAs increase and peak pressures decrease with increasing distance from the structure. Only one gage exceeded the 6.9-kPa level: MN 701 (Fig. 47), on the centerline of the structure at a range of 3 m from the front door, recorded a peak of 7.76 kPa at 51 m/s. Measurement Number 702, at a range of 5 m, recorded a peak of 6.2 kPa. The highest free-field pressures were measured at the front of the structure. The lowest pressures were measured at the sides.

Table 3 summarizes selected peak pressures from the free-field measurements. A complete set of pressure records is presented in Volume II.

Three pairs of accelerometers were mounted on the exterior surface of the arch in the same cross-sectional plane that included the GZ. The sensing axis in one accelerometer in each pair was oriented to measure radial accelerations; the sensing axis of the other was oriented to measure tangential accelerations. Measurement Numbers 1601 and 1602 were made at the crown of the arch directly above GZ. Figure 48a shows a peak radial acceleration of about 1700 g for MN 1601. Figure 48b, a plot of the first and second integrals of the accelerometer record for MN 1601, shows a peak radial velocity

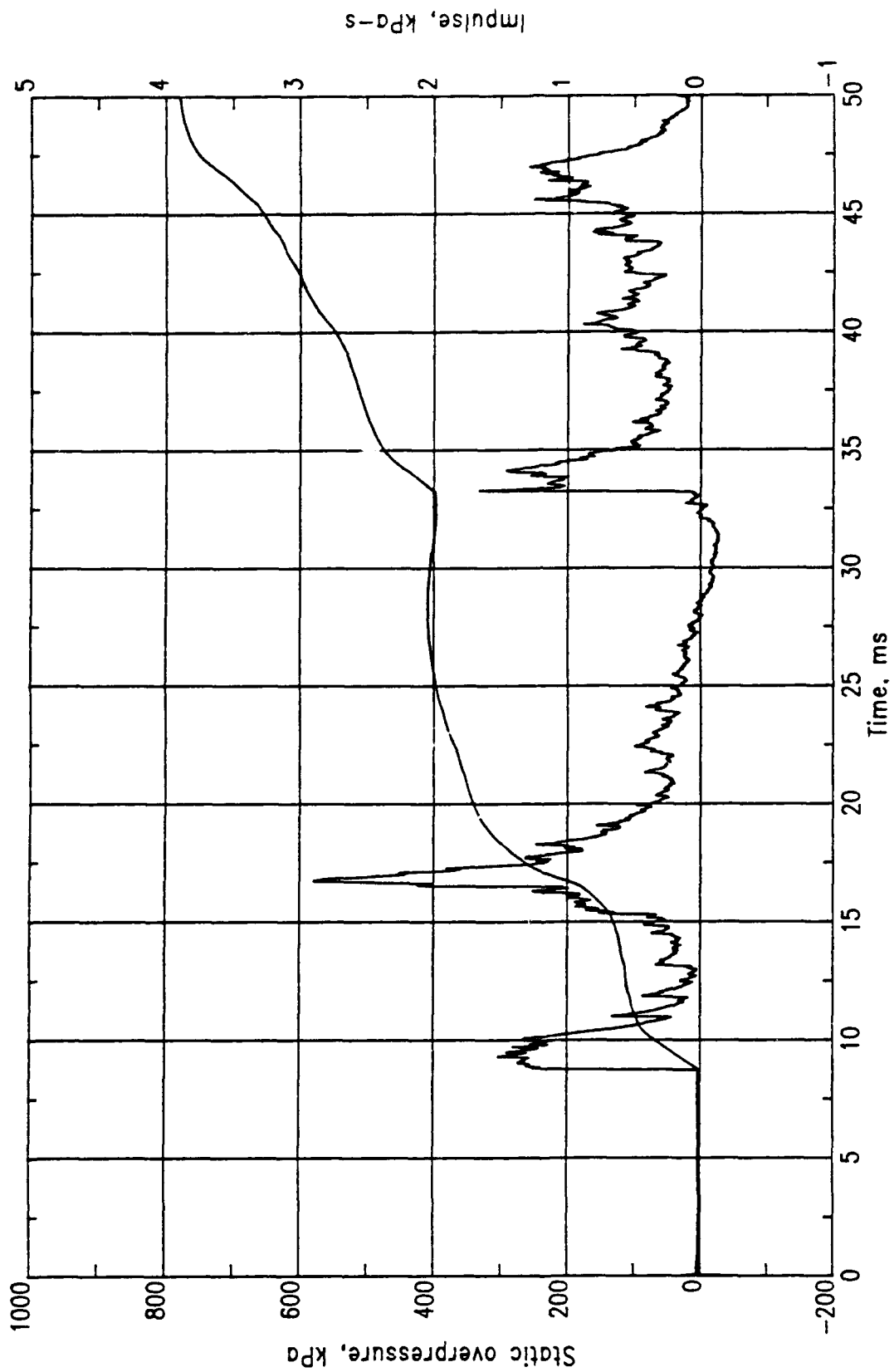


Figure 45. PAS-1, MN 0201.

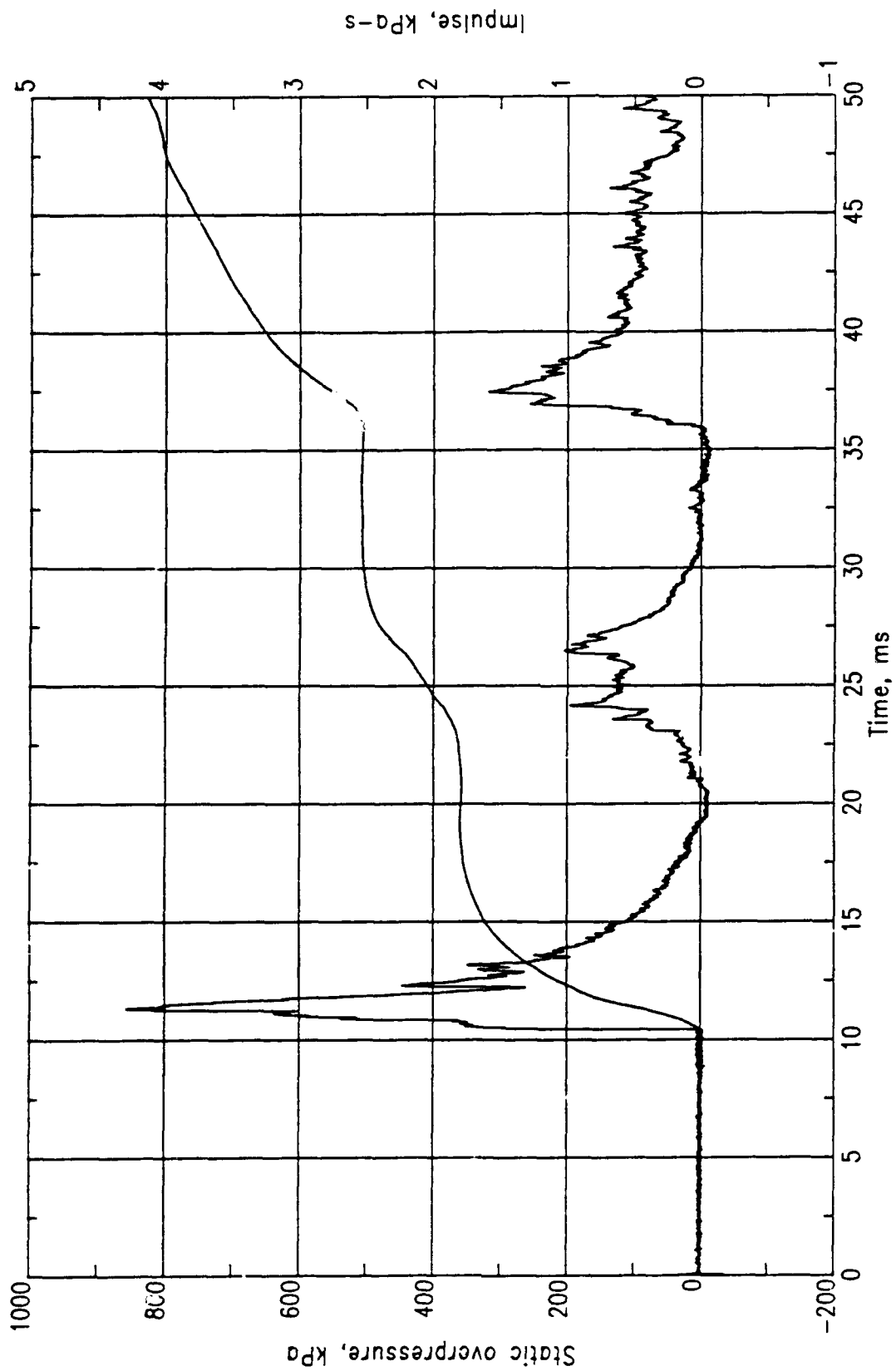


Figure 46. PAS-1, MN 0203.

Table 2. Summary of interior pressure measurements, PAS-1.

Meas. No.	Location	TOA (ms)	Peak (kPa)	Time (ms)	Peak (kPa)	Time (ms)	Peak (kPa)	Time (ms)	Peak (kPa)	Time (ms)	Peak (kPa)	Time (ms)
0101-1	SF	8.20	413.7	18.00	282.7	43.30	317.2	73.0	-	-	-	-
0102-1	SF	10.00	786.0	11.60	275.8	26.00	289.6	37.7	268.9	65.0	-	-
0201-1	BW	8.70	303.4	9.20	579.2	16.60	331.0	33.2	266.1	47.0	206.8	72.0
0202-1	BW	8.70	241.3	9.70	237.9	13.10	182.7	39.5	162.0	47.6	148.2	70.0
0203-1	BW	10.50	841.2	11.30	206.8	26.50	310.3	37.5	413.7	64.8	206.8	94.0
0301-1	SF	2.00	372.3	2.10	193.1	4.80	151.7	12.5	231.0	31.1	-	-
0302-1	SF	2.70	284.1	2.70	173.7	5.50	141.3	6.9	161.3	25.5	148.9	31.5
0303-1	SF	5.00	434.4	6.40	306.8	21.60	272.3	30.3	503.3	45.3	262.0	57.5
0304-1	SC	2.95	329.6	3.80	203.4	27.00	184.8	38.7	172.4	72.0	-	-
0305-1	SC	3.50	544.7	3.60	193.1	10.70	151.7	19.8	-	-	-	-
0306-1	SC	4.50	365.4	4.60	293.0	8.62	199.9	19.2	193.1	46.0	199.9	57.0
0307-1	SC	4.90	303.4	5.80	257.9	20.50	222.0	29.5	304.8	46.3	-	-
0401-1	FD	8.80	399.9	9.20	665.3	16.90	303.4	33.5	303.4	71.0	-	-
0402-1	FD	8.30	758.4	17.70	317.2	33.00	-	-	-	-	-	-
0403-1	FD	8.20	220.6	8.50	310.3	11.10	282.7	15.7	486.1	18.1	386.1	34.1
0404-1	FD	8.80	-	-	-	-	-	-	-	-	-	-
0405-1	FD	10.70	772.2	11.00	413.7	38.00	317.2	64.5	-	-	-	-
0501-1	SF	9.90	296.5	10.30	451.6	12.00	272.3	26.5	262.0	40.1	172.4	48.8
0502-1	SC	8.50	289.6	9.40	524.0	16.30	268.9	33.6	262.0	70.5	213.7	105.5
0503-1	SC	8.80	289.6	9.70	270.3	14.40	150.3	20.7	158.6	40.2	215.1	46.1
0504-1	SC	9.70	358.5	12.10	331.0	37.70	193.1	64.5	175.8	93.5	-	-
0601-1	SF	0.92	992.9	0.96	262.0	3.80	227.5	10.2	-	-	-	-
0602-1	SF	3.10	530.9	5.50	427.5	25.10	317.2	52.0	193.1	80.5	-	-
0603-1	SF	3.10	479.2	4.41	455.1	24.50	317.2	31.0	265.4	52.5	244.8	81.0
0604-1	SC	0.85	5033.2	0.90	1310.0	1.22	-	-	-	-	-	-
0605-1	SC	1.40	1447.9	1.45	1103.2	1.75	-	-	-	-	-	-
0606-1	SC	2.90	634.3	3.00	772.2	3.40	344.7	7.5	282.7	23.1	-	-
0607-1	SC	3.30	641.2	3.90	379.2	24.20	213.7	31.7	237.9	51.5	-	-

NOTE:

The gage for MN 0404-1 apparently malfunctioned or had cable problems. The TOA data appear reliable.

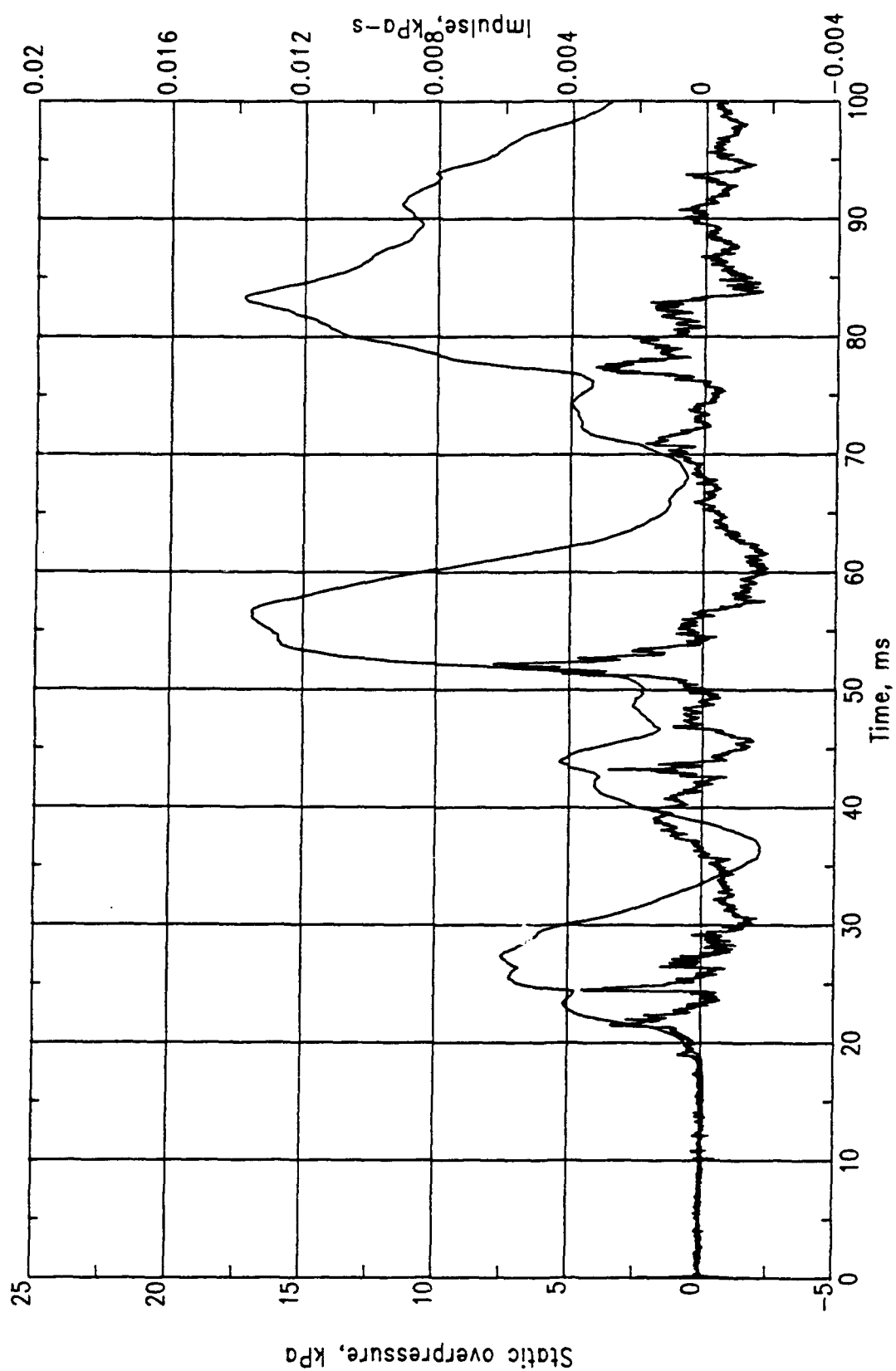


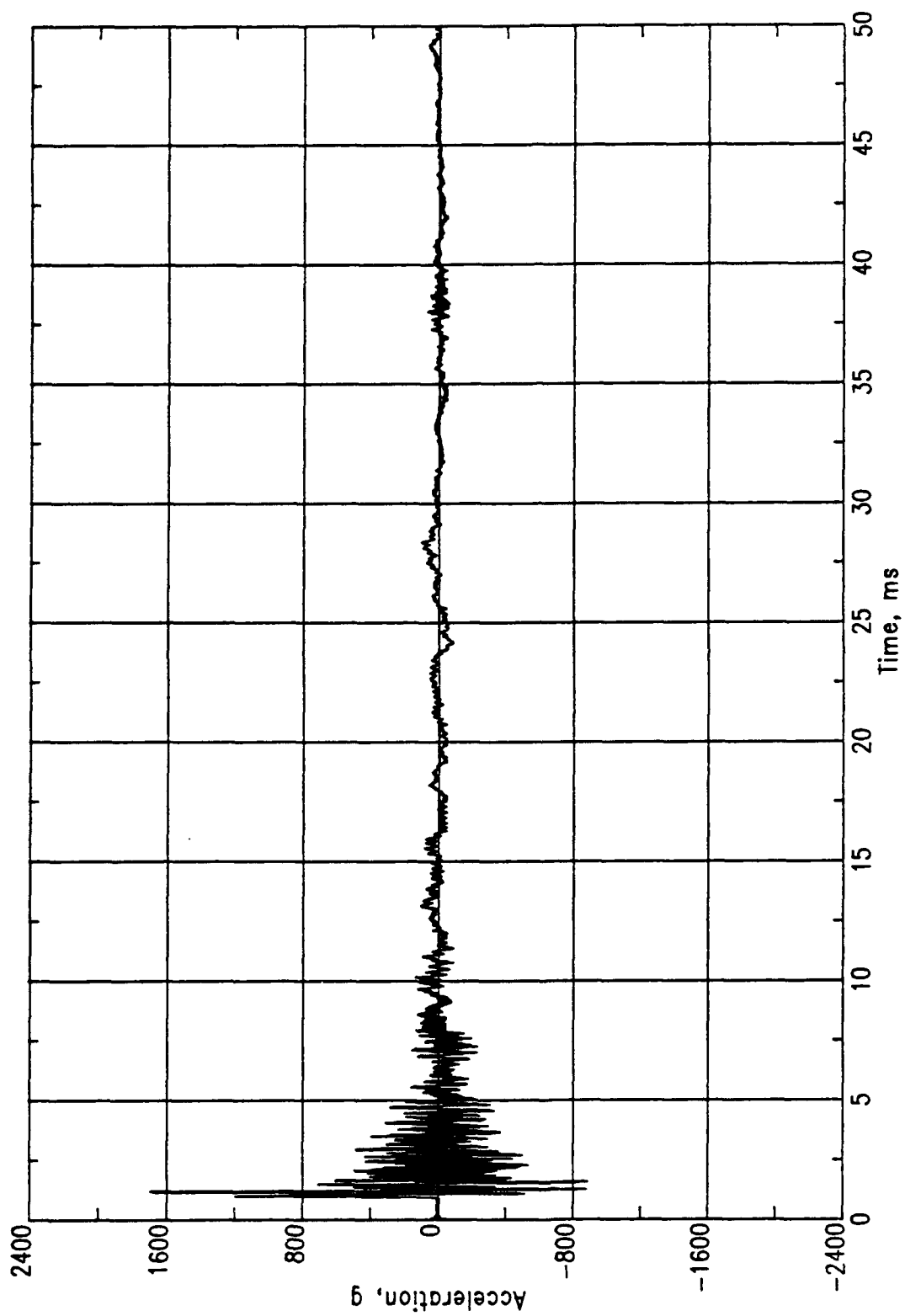
Figure 47. PAS-1, MN 0701.

Table 3. Summary of free-field pressure measurements, PAS-1.

Meas. No.	Location	TOA (ms)	Peak (kPa)	Time (ms)	Peak (kPa)	Time (ms)	Peak (kPa)	Time (ms)	Peak (kPa)	Time (ms)	Peak (kPa)	Time (ms)
701-1	FF	18.8	3.585	22.0	7.757	51.0	4.137	106.0	3.999	167.5	6.205	196.0
702-1	FF	24.5	2.344	26.5	6.205	56.0	4.413	82.5	2.620	111.5	1.724	144.5
703-1	FF	30.0	1.724	32.1	4.137	61.5	3.034	87.5	1.379	126.5	1.310	150.0
704-1	FF	36.5	1.379	37.7	3.378	68.0	2.068	93.0	1.103	132.0	1.103	155.5
705-1	FF	30.0	0.483	30.0	0.483	46.0	1.448	61.0	2.068	74.5	0.689	85.0
706-1	FF	42.0	0.414	57.0	1.103	72.0	1.517	85.0	0.655	96.0	0.483	107.0
707-1	FF	39.0	0.331	39.0	0.414	72.0	0.496	83.5	0.262	139.5	-	-
708-1	FF	46.5	0.290	80.0	0.441	93.0	0.345	110.0	-	-	-	-
709-1	FF	31.0	0.441	31.0	0.345	41.0	0.579	64.5	0.469	90.0	-	-
710-1	FF	42.5	0.379	74.5	0.290	104.0	-	-	-	-	-	-
711-1	FF	26.5	1.310	28.5	0.965	36.0	5.516	46.0	0.290	52.0	-	-
712-1	FF	31.5	0.841	33.5	0.607	41.0	1.862	57.0	0.689	83.5	0.414	106.0
713-1	FF	37.0	0.710	38.3	4.551	45.5	0.345	56.0	0.552	88.0	1.462	62.0
714-1	FF	20-30	0.269	53.5	0.345	72.0	0.379	102.0	0.262	138.0	0.262	157.0
715-1	FF	20-30	0.262	110.0	-	-	-	-	-	-	-	-

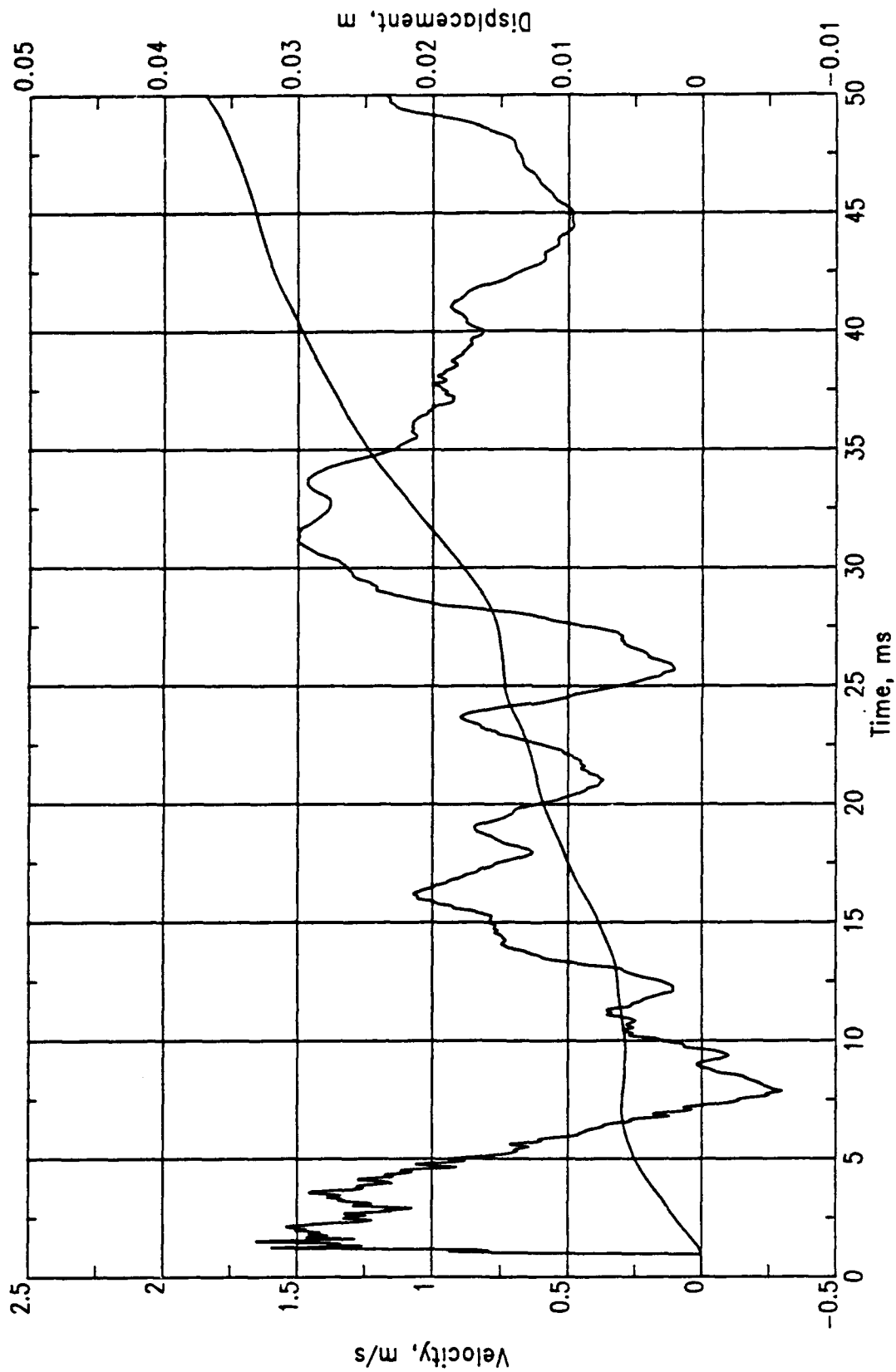
NOTE:

Due to noise, unable to determine exact TOA on MN 714-1 and MN 715-1.



(a) Acceleration.

Figure 48. PAS-1, MN 1601.



(b) Velocity and displacement.

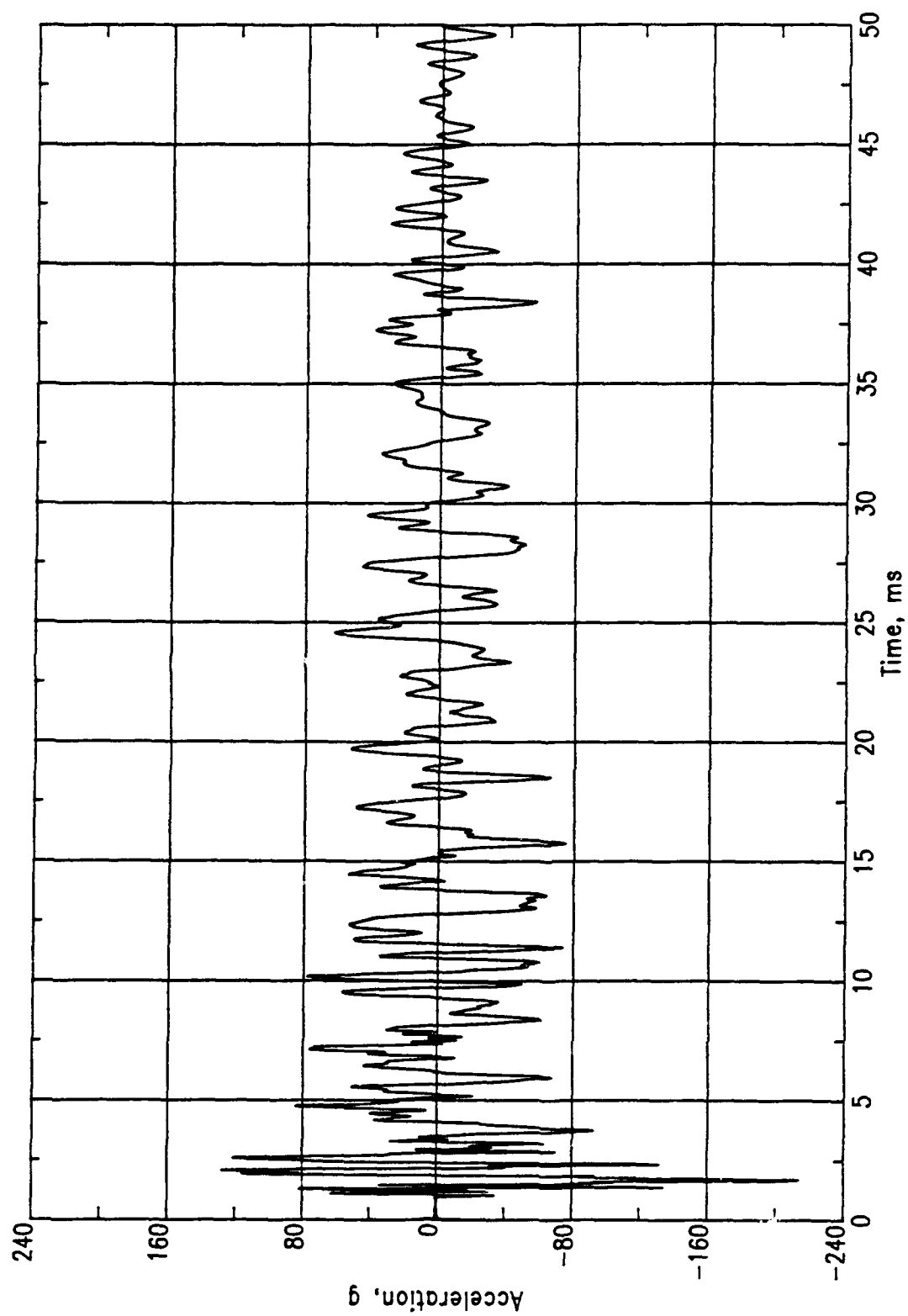
Figure 48. Concluded.

of 1.70 m/s during the first 10 ms of the record. Figure 49a shows a peak tangential acceleration of -220 g for MN 1602; Figure 49b shows a peak velocity of -0.43 ms during the same period for MN 1602. Peak velocities given for times later than 10 ms are subject to greater uncertainties because of baseline shifts in the accelerometer records.

Measurement Numbers 1605 and 1606 were mounted on the side of the arch at a point close to where the radius of curvature changes. Peak accelerations at this point were -440 g radial and -325 g tangential, respectively. Corresponding peak velocities were +0.50 ms and -1.0 ms. Measurement Numbers 1603 and 1604 were mounted on the arch between MN 1601 and 1605, at which point the peak radial acceleration was -1350 g and the peak radial velocity was +0.62 ms. The peak tangential acceleration was -500 g; the peak tangential velocity was -0.50 ms. All of the above measured accelerations were significantly lower than those observed in the Norwegian full-scale shelter tests with smaller charge weights.

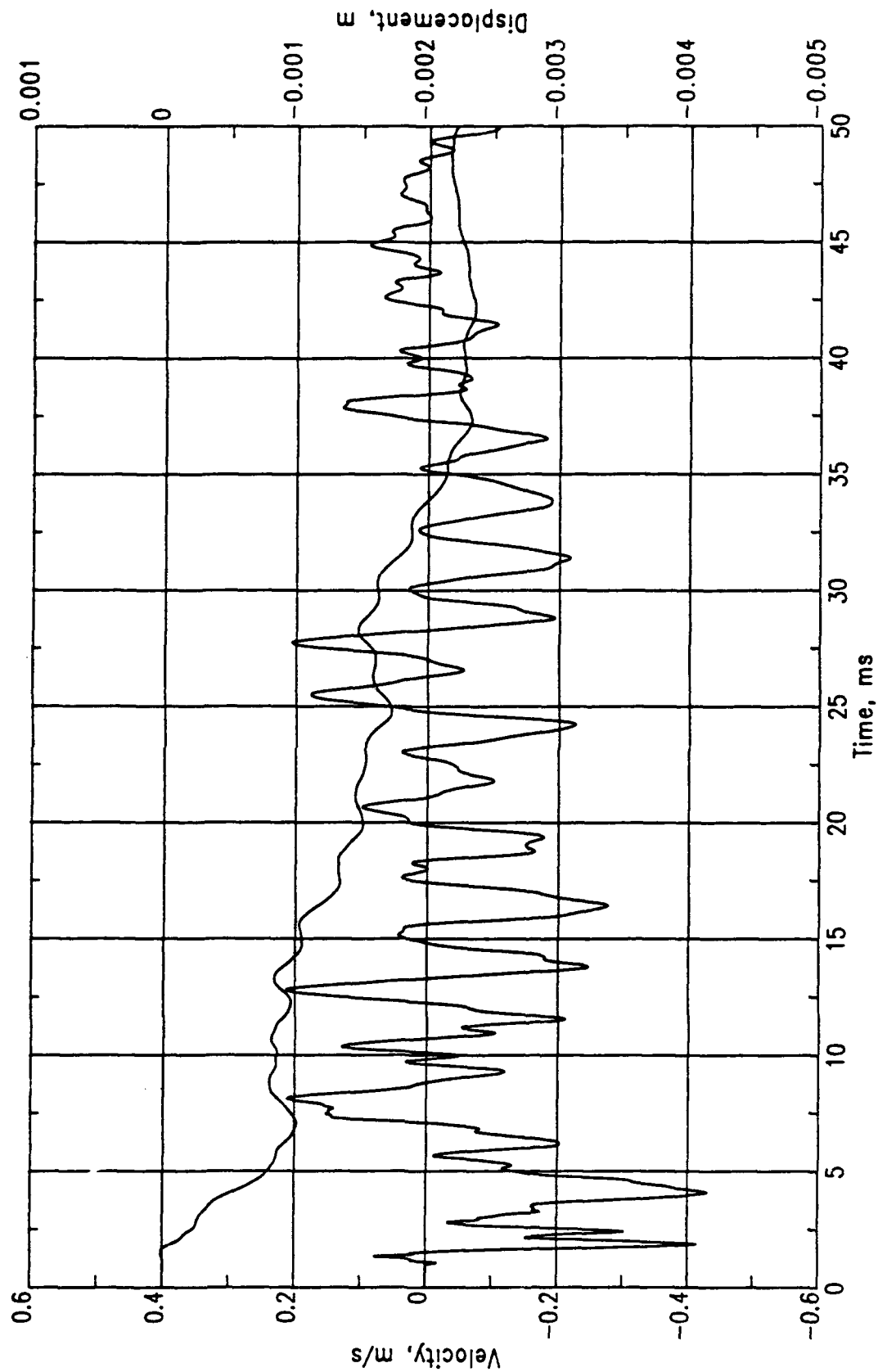
Table 4 summarizes selected peak accelerations from all of the accelerometer records for the PAS-1 event. A complete set of records is presented in Volume II.

Two pairs of strain gages were mounted about mid-height on the centerline of the door. One gage of each pair was mounted on the inner surface of the door and the other on the outer surface. One pair was oriented to measure vertical strains (MN 3402 and MN 3404) and the other to measure horizontal strains (MN 3401 and MN 3403). At about 22 ms, MN 3401 (Fig. 50) shows a horizontal tensile strain of 400 microstrain in the outside plate of the door. At the same time MN 3403 (Fig. 51) shows a tensile strain of 1200 microstrain in the inner plate. The horizontal tensile strains in the inner plate are not consistent with the outward bending of the door. A review of instrumentation setup records appears to eliminate polarity reversal as a cause, and the cause of this discrepancy has not yet been determined. At later times these two gages show tensile residual strains of 800 and 3000 microstrain, respectively.



(a) Acceleration.

Figure 49. PAS-1, MN 1602.



(b) Velocity and displacement.

Figure 49. Concluded.

Table 4. Summary of acceleration measurements, PAS-1.

Meas. No.	Location	TOA (ms)	Peak (g)	Time (ms)	Peak (g)	Time (ms)	Peak (g)	Time (ms)	Peak (g)	Time (ms)	Peak (g)	Time (ms)
1301-1	SR	1.96	-126	2.40	132	2.68	210	3.18	-138	6.65	94	6.97
1302-1	SR	1.92	-103	3.31	89	3.52	-98	6.30	75	6.60	-72	10.00
1303-1	SR	1.95	94	2.45	-148	2.80	120	3.15	150	3.90	72	4.50
1304-1	SR	1.95	-72	2.55	72	3.15	61	4.55	67	8.60	58	11.00
1305-1	SR	2.2-2.5	78	3.40	-132	4.05	234	4.90	100	5.68	-80	6.30
1306-1	SR	2.20	86	3.15	-116	3.94	104	4.29	140	5.55	-167	5.75
1601-1	SR	0.96	1200	1.00	-540	1.10	1680	1.22	-880	1.28	-880	1.59
1602-1	SR	0.97	-136	1.39	-212	1.70	108	2.08	-132	2.35	120	2.60
1603-1	SR	1.25	960	1.55	-1020	1.61	1080	1.64	-1340	1.71	1160	1.77
1604-1	SR	1.23	230	1.58	-510	1.64	-490	1.77	-510	1.85	200	1.98
1605-1	SR	2.06	-420	2.46	-250	3.07	380	3.19	-180	3.36	305	3.45
1606-1	SR	1.90	-204	2.24	213	3.00	-330	3.40	320	4.16	-290	4.70
1607-1	SR	.93	1440	1.00	-620	1.10	1520	1.98	-960	1.26	-880	1.57
1609-1	SR	1.20	1600	0.68	1640	1.52	1680	1.63	1690	3.95	-	-
1611-1	SR	2.36	-416	2.45	320	2.80	-200	2.35	-	-	-	-

NOTE:

Due to noise, unable to determine exact TOA on MN 1305.

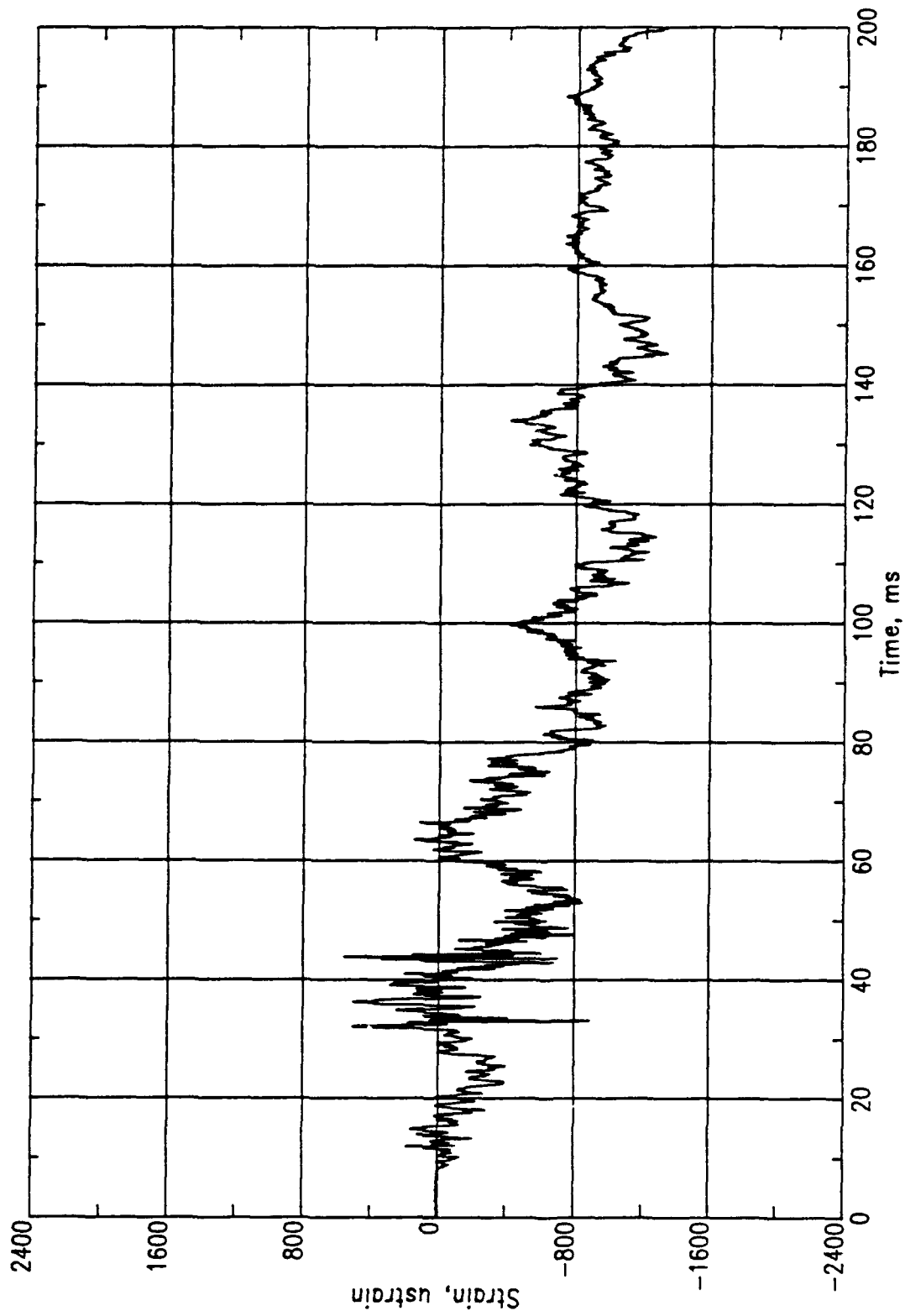


Figure 50. PAS-1, MN 3401.

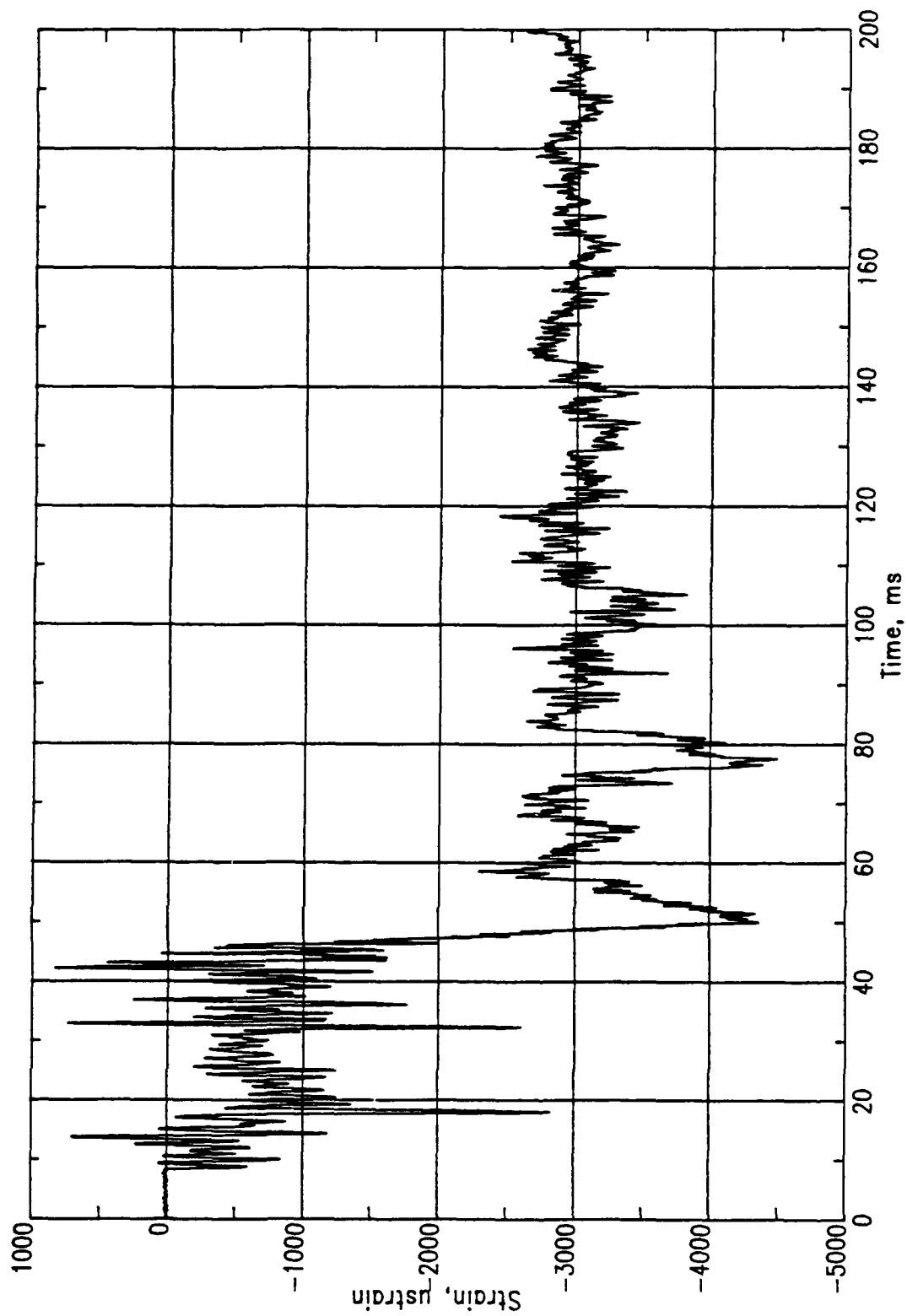


Figure 51. PAS-I, MN 3403.

Vertical strains measured at the center of the door are at least consistent with the outward bending of the door. Measurement Number 3402 (Fig. 52) shows a tensile strain of 1500 microstrain in the outer plate at 21.7 ms. At about the same time MN 3404 (Fig. 53) exceeded its recording bandwidth, but it shows a compressive strain in excess of 4300 microstrain in the inner plate. The higher compressive strains in the inner plate would normally indicate an axial compressive force had been applied to the door; however, this does not appear to be a probable explanation for this measurement discrepancy. Measurement Number 3402 shows a residual tensile strain of about 800 microstrain.

Table 5 summarizes selected peak strains from all strain gages for the PAS-1 event. A complete set of records is presented in Volume II.

Three displacement gages were attached to the front door in a vertical line at its centerline. Measurement Number 7401 (Fig. 54) was attached near the top of the door and showed a peak outward displacement of 2.03 cm at 22.5 ms. Measurement Number 7402 (Fig. 55) attached at mid-height of the door showed a peak outward displacement of 2.79 cm at 26.5 ms, and MN 7403 (Fig. 56) at the bottom of the door showed a peak displacement of 0.98 cm at 22.0 ms. The door appears to have fallen from its supports and into the shelter at 30 to 40 ms, and inward displacements recorded after this time are questionable.

The front door rigid body response observed in PAS-1 would probably not occur in the full-size structure. There are significant differences between the model structure and the full-size shelter in the system that supports the door in the closed position. The door in the full-size shelter is raised and lowered by a cable and pulley system attached to each side of the door near its upper edge. When the door is in the raised and locked position, the cables are slacked off, but remain attached to the door. In the raised position the door rests on a short post at each side of the door. These posts keep the front door in a slot in the parapet and restrained against lateral loads. The posts that hold the door in the slot in the parapet of the full-size shelter are themselves secured in place by a system of hinge pins, springs, and hydraulic rams. These elements hold the

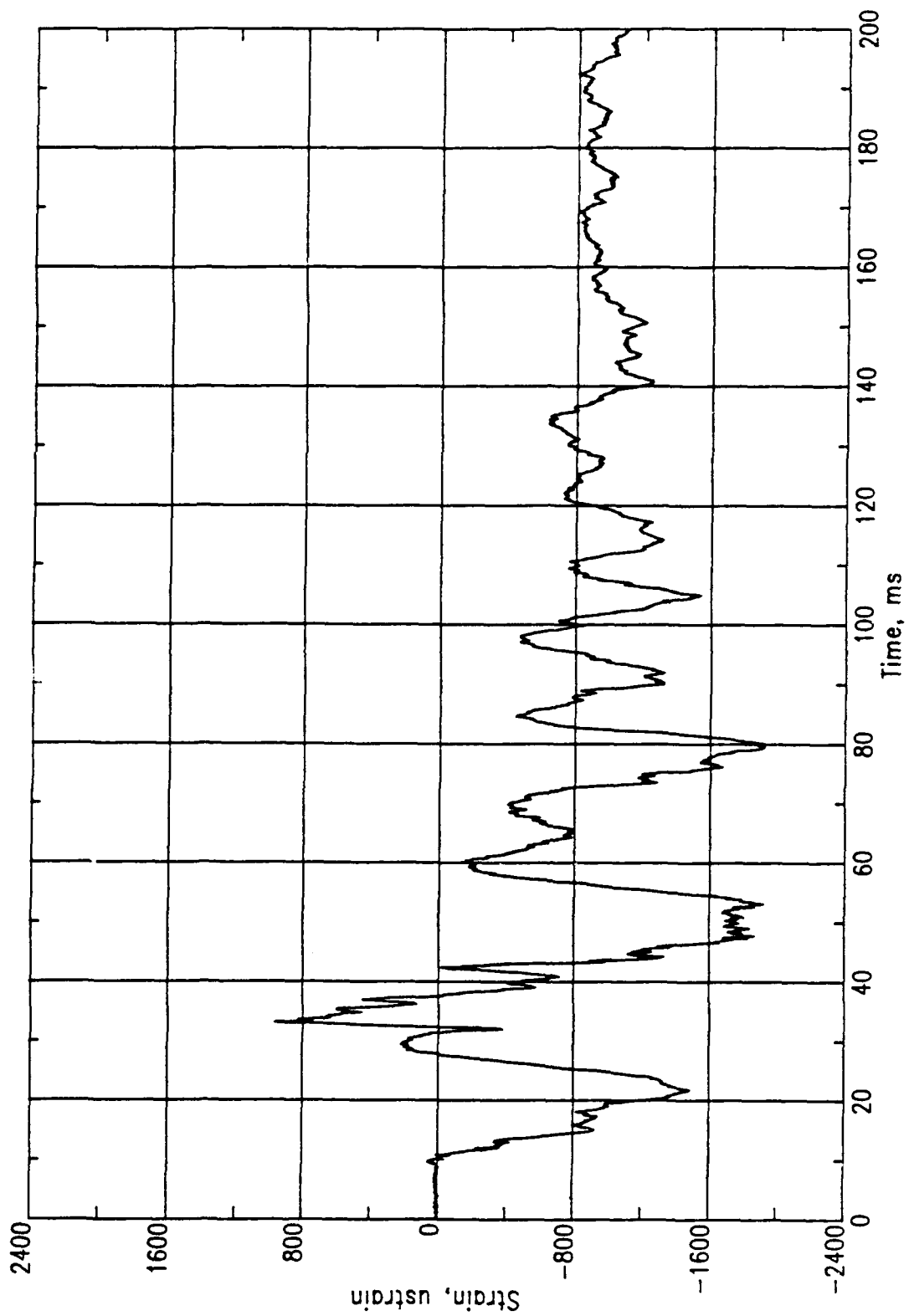


Figure 52. PAS-1, MN 3402.

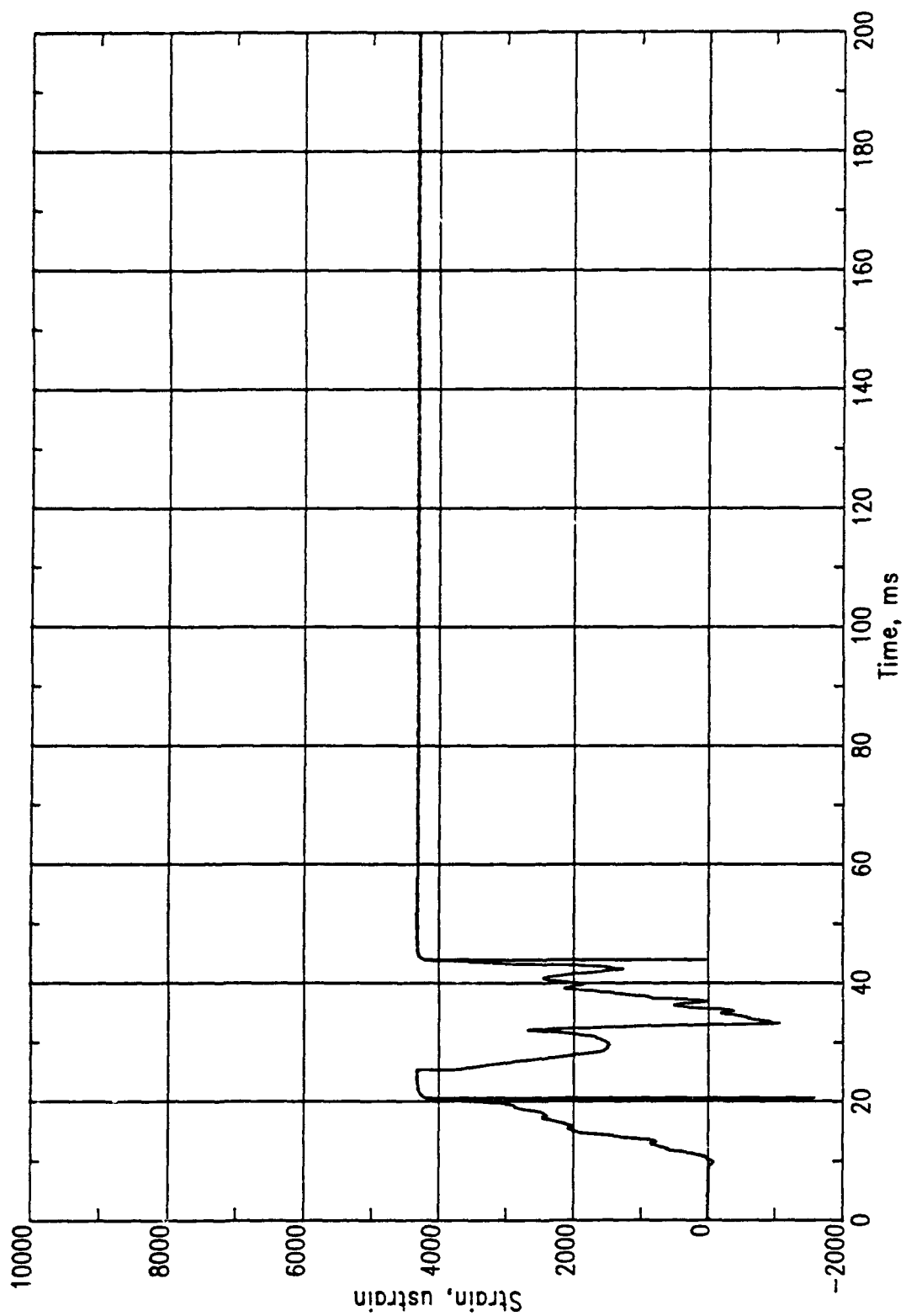


Figure 53. PAS-1, MN 3404.

Table 5. Summary of strain measurements, PAS-1.

Meas. No.	Location	TOA (ms)	Peak (msn)	Time (ms)	Peak (msn)	Time (ms)	Peak (msn)	Time (ms)	Peak (msn)	Time (ms)	Peak (msn)	Time (ms)
3401-1	FD	8.4	500	32.0	-910	33.1	500	36.2	-730	43.5	560	43.9
3402-1	FD	9.5	-1500	21.7	-360	32.0	960	33.0	-1920	53.0	-1920	79.0
3403-1	FD	8.5	-2840	18.0	-272	32.4	750	33.0	850	42.2	-4380	50.0
3404-1	FD	9.4	>4300	22.1	2600	32.0	-1050	33.2	2400	40.9	-	-
3405-1	FD	8.7	3550	18.0	400	42.6	-5500	48.0	-	-	-	-
3406-1	FD	9.5	>3000	21.0	850	35.2	2420	39.5	1120	42.2	2900	63.5

Note:

msn = microstrain

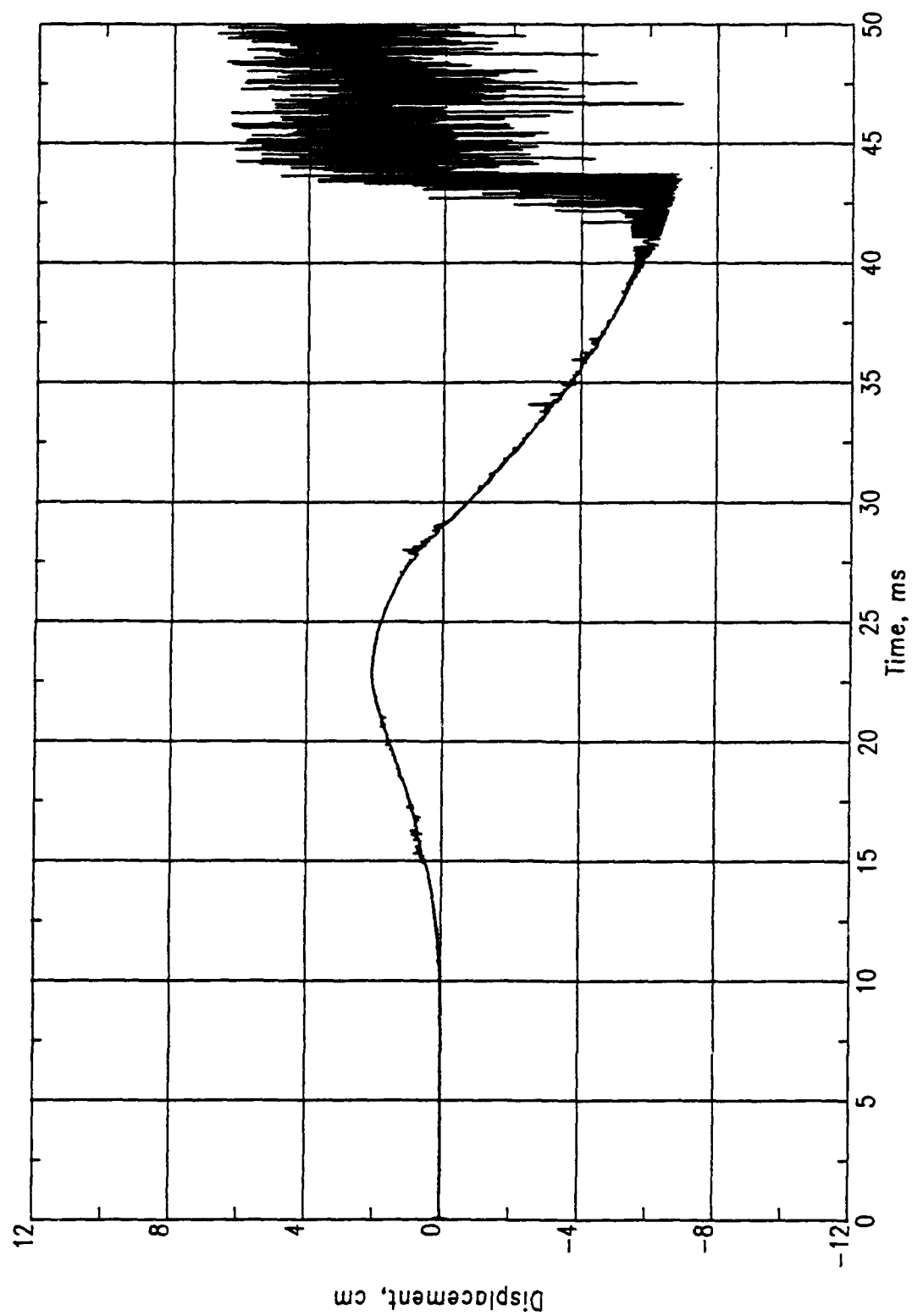


Figure 54. PAS-1, MN 7401.

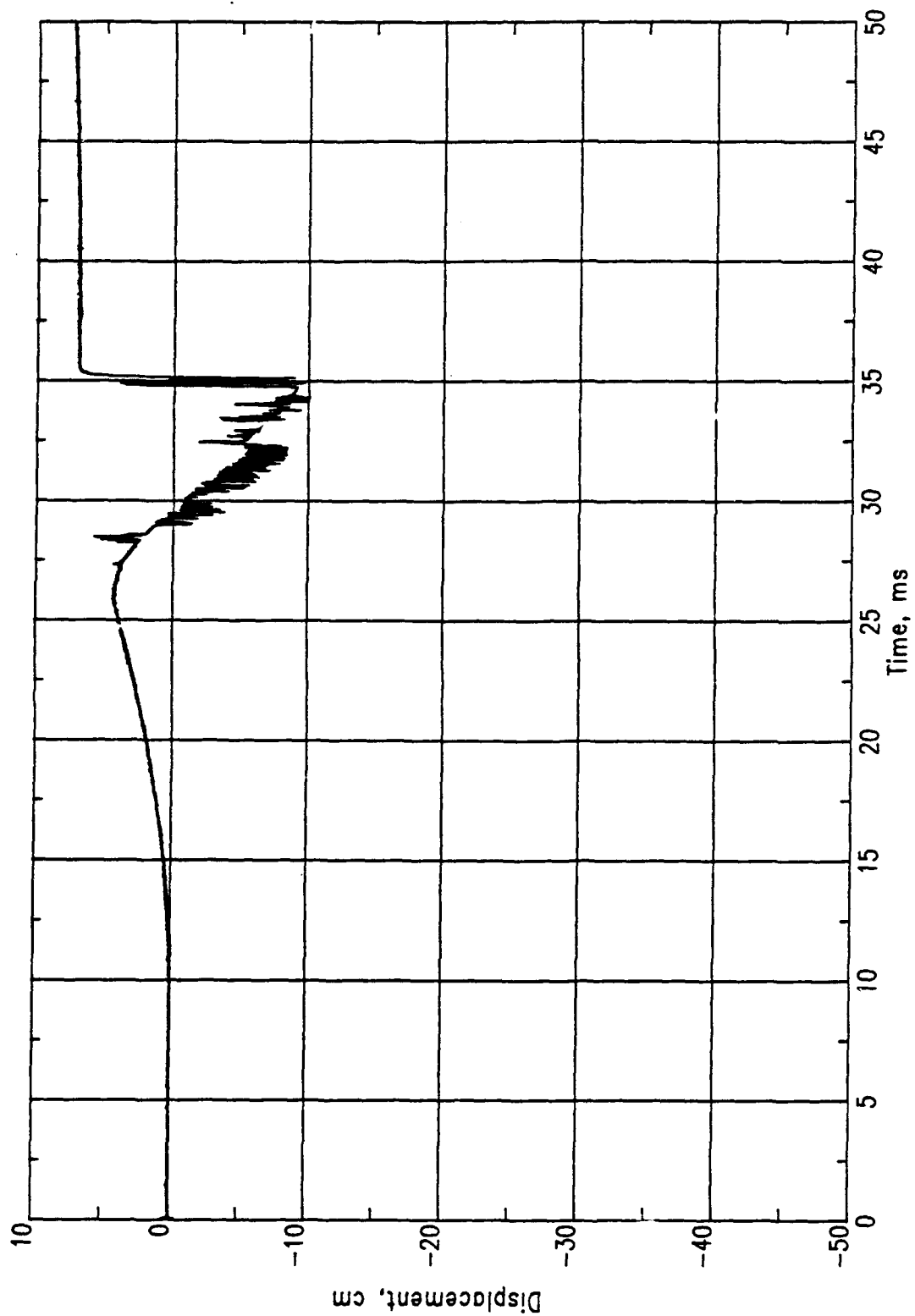


Figure 55. PAS-1, MN 7402.

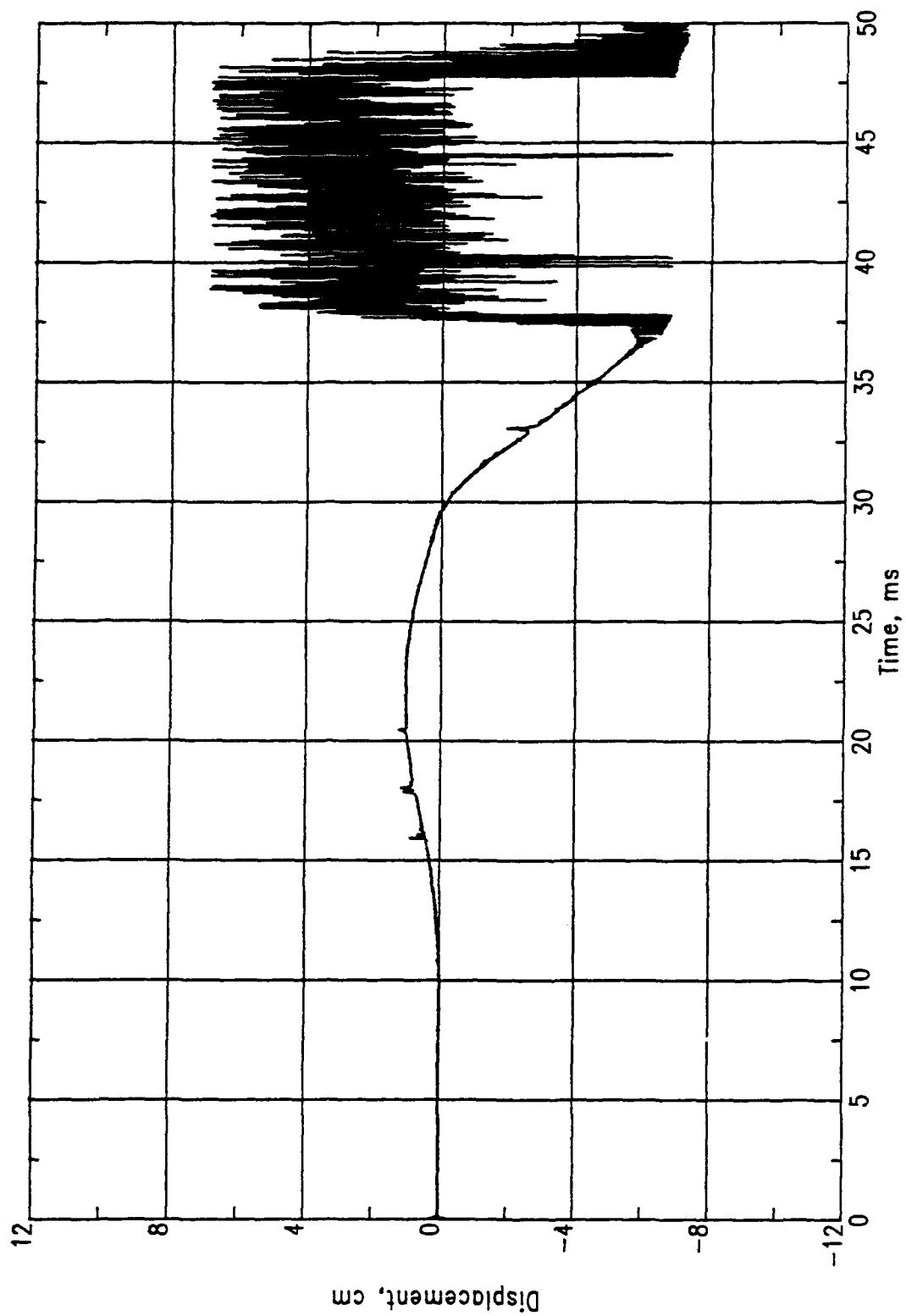


Figure 56. PAS-1, MN 7403.

posts securely in position under the raised door. These door-raising and post-positioning elements were not included in the model. When the model door began moving under internal blast loading in the PAS-1 event, the two posts apparently fell out of position, allowing the door to drop out of the parapet slot and into the shelter.

Table 6 summarizes the first two peaks for the displacement gages. A complete set of records is presented in Volume II.

Since no significant damage to the structure occurred in the PAS-1 event, the high-speed photography yielded very little useful information.

3.2.3 Rock Rubble Berm

With the exception of a few rocks that were displaced at the left front corner at the vestibule and personnel door (Fig. 27), the rock rubble berm remained intact. Only two of the displaced rocks were found beyond the original perimeter of the berm, with the maximum distance from the edge of the berm being slightly less than 2 m.

3.2.4 Debris Distribution

As noted previously, only three pieces of debris from the structure were recovered. Two pieces from the right side wingwall were found on the rock rubble berm. The third, a bracket from the top of the front door frame, was found a few centimeters in front of the concrete apron slab.

Most of the aluminum cubes remained on the structure after the test. Those not on the structure had fallen off the bracket and were found on top of the rock rubble berm against the arch.

Most of the photo poles remained on the structure after the test. Those not on the structure had fallen off and were found on the rock rubble berm against the arch.

Table 6. Summary of displacement measurements, PAS-1.

Meas. No.	Location	TOA (ms)	Peak (cm)	Time (ms)	Peak (cm)	Time (ms)
7401-1	FD	11.2	2.03	22.4	-6.73	43.0
7402-1	FD	13.5	2.79	26.4	-7.62	37.0
7403-1	FD	12.5	1.02	22.0	-6.86	37.8

4.0 PAS-3 TEST

4.1 TEST DESCRIPTION

4.1.1 General

The PAS-3 test was conducted on April 2, 1972. The explosive charge for this event was 33.3 kg of Composition C-4, which is the equivalent of 900 kg of the same explosive in the full-size structure. Figures 57 and 58 show the placement of the charge for PAS-3.

The model structure used for this test was the same as that tested in PAS-1. The earth and rock berm placed alongside the structure for PAS-1 was replaced with a clean rock rubble berm for PAS-3 to reduce the dust problem observed in PAS-1. The personnel entrance vestibule was also modified to divert smoke and other detonation products away from the front door. The pipe vent opening in the backwall was closed for this and all following tests.

Figure 59 shows the placement of photo poles for this test. Figures 60 and 61 show the placement of aluminum and SIFCON cubes for this test.

As an aid in determining debris density, a number of plywood catcher bins (Fig. 62) were placed at various ranges and azimuths around the structure. The bins were arranged end-to-end along several concentric arc lines having their center at the GZ (Fig. 63). The open face of the bins faced the structure. Any debris from the structure passing through the plane of the open side of the bin would be captured in the bottom of the bin.

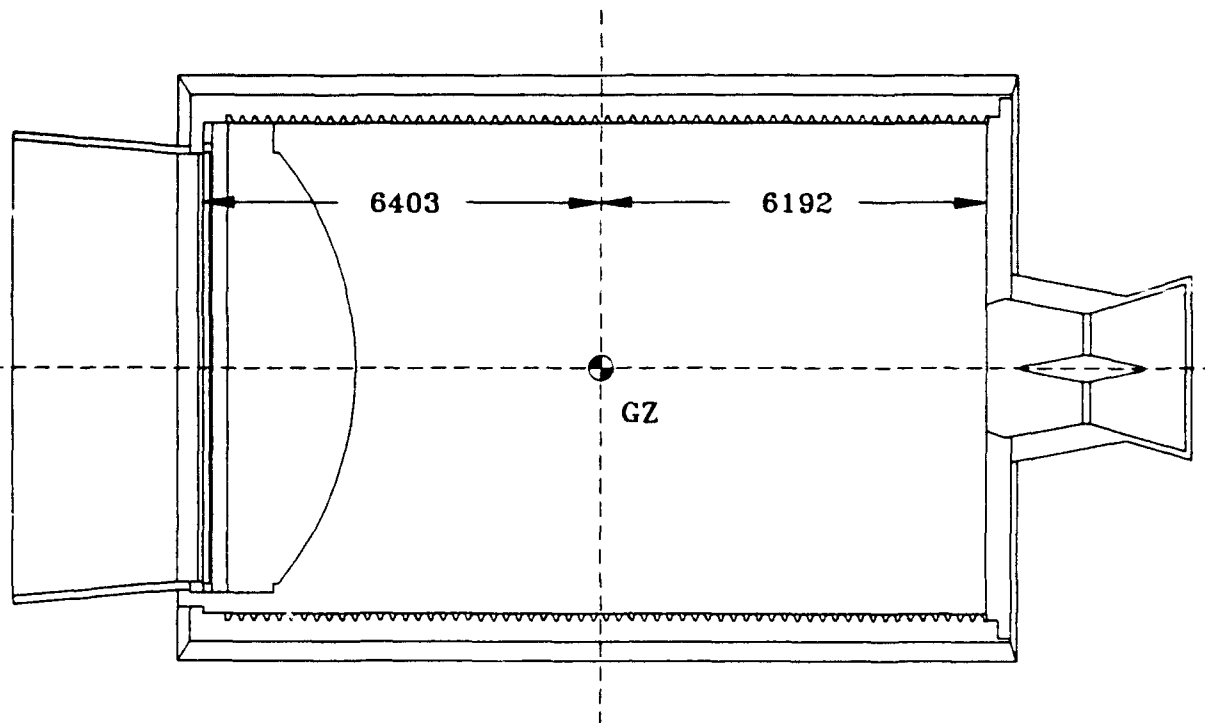
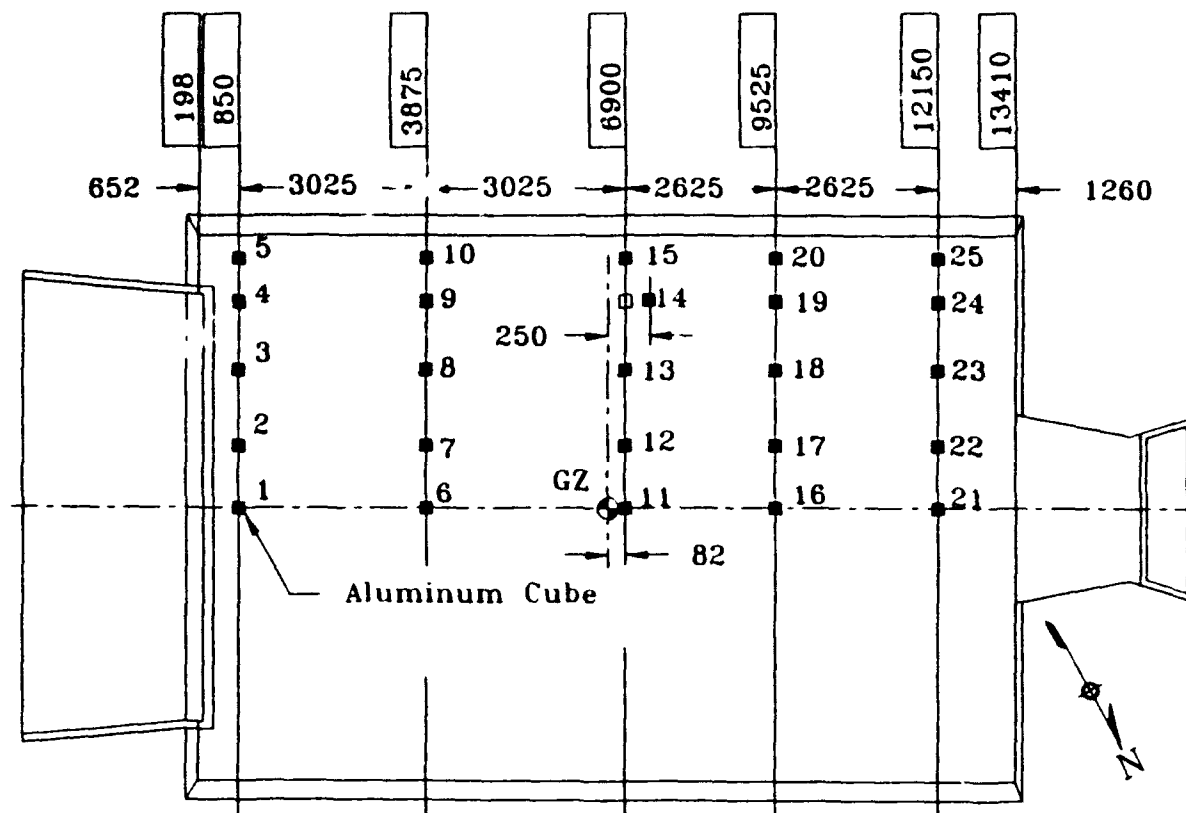


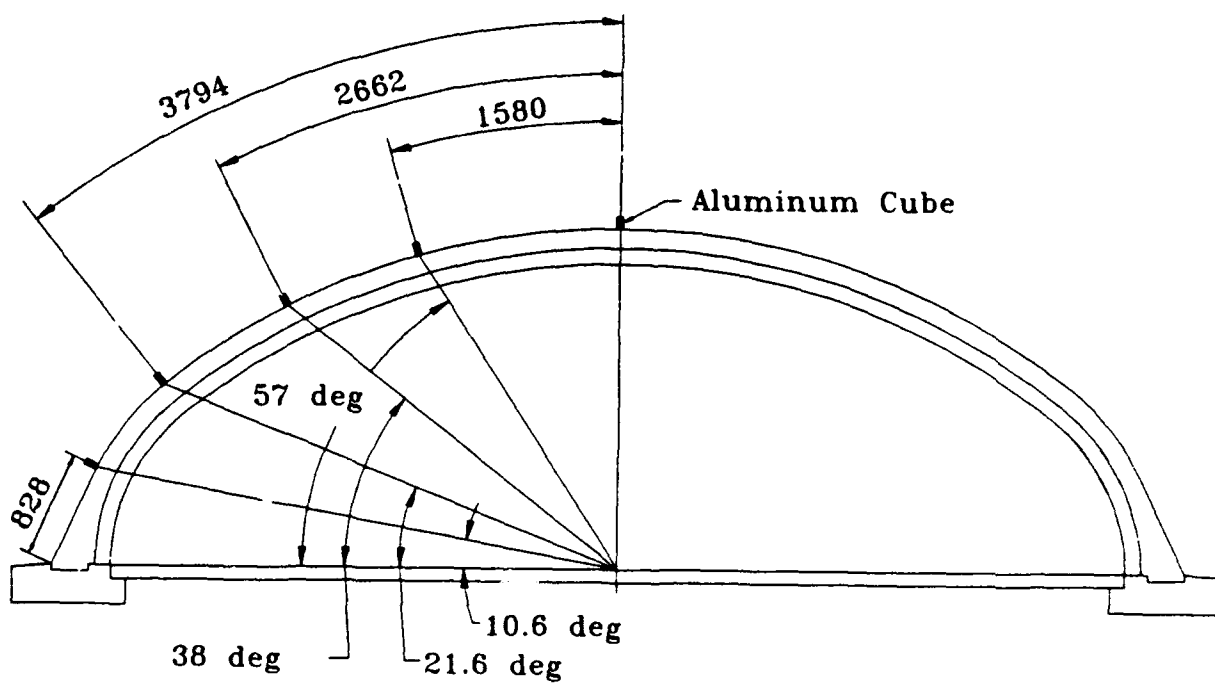
Figure 57. Location of GZ for PAS-3.



Figure 58. Explosive charge, 33.3 kg of C-4, PAS-3.

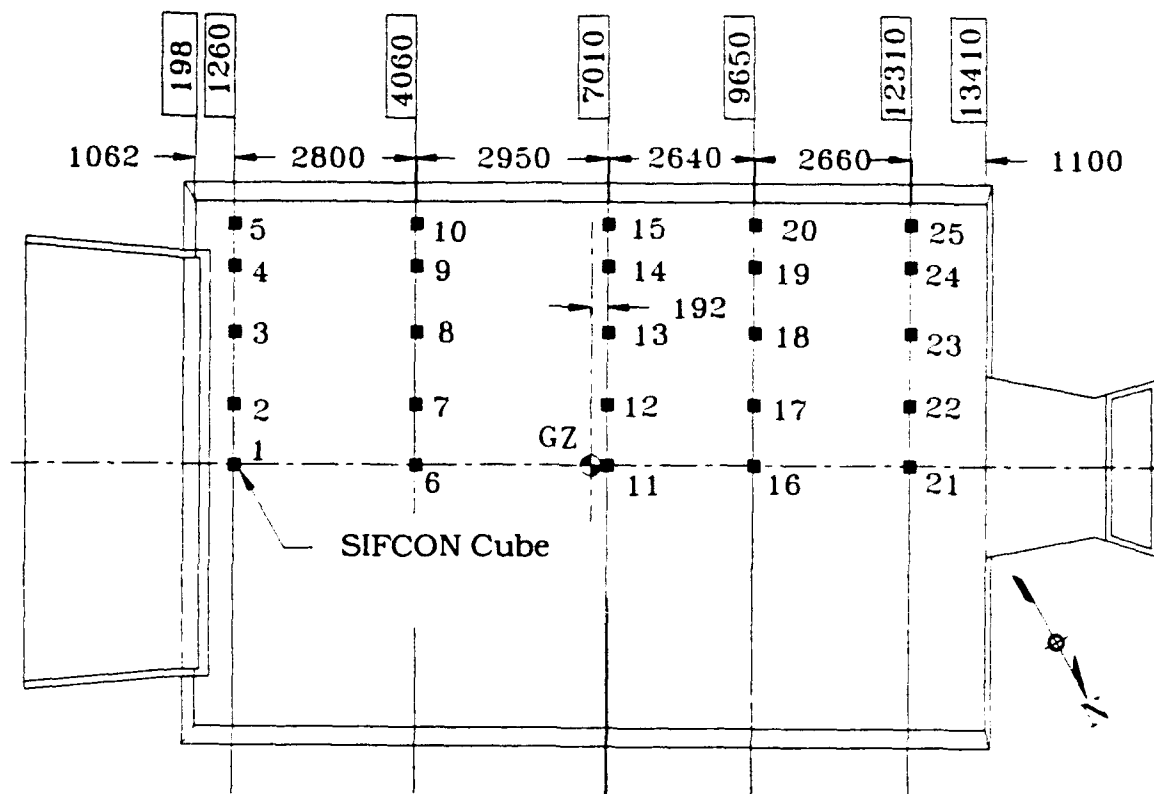


(a) Plan.

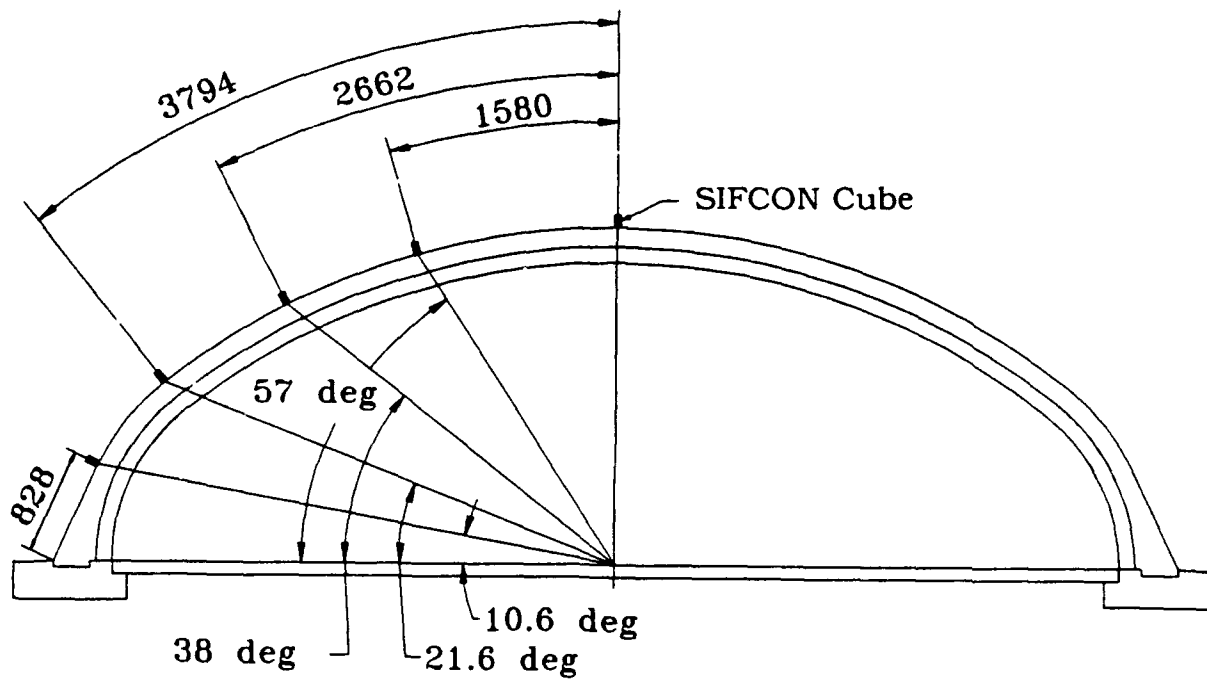


(b) Section.

Figure 60. Locations of aluminum cubes, PAS-3.



(a) Plan.



(b) Section.

Figure 61. The SIFCON cube placement, PAS-3.

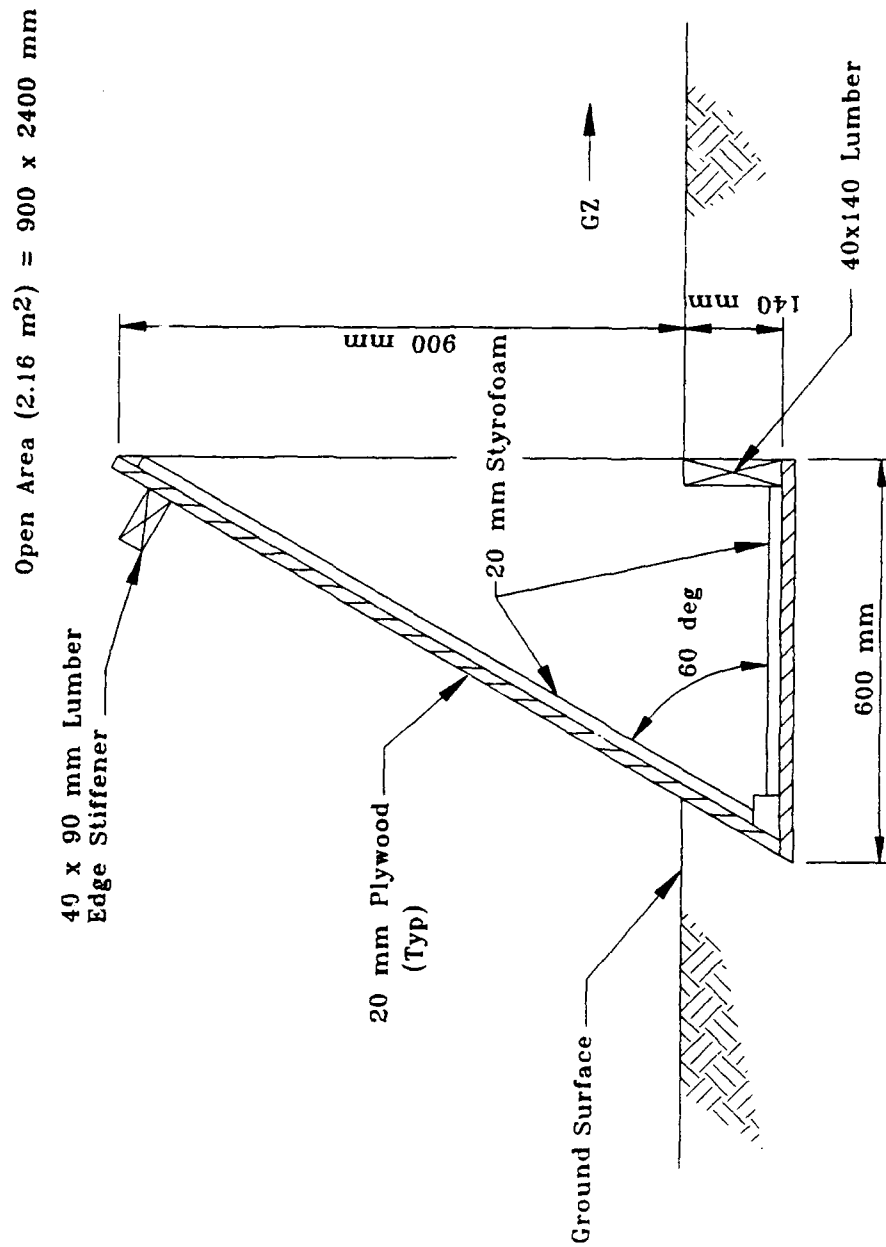


Figure 62. Section: Debris catcher bin, PAS-3.

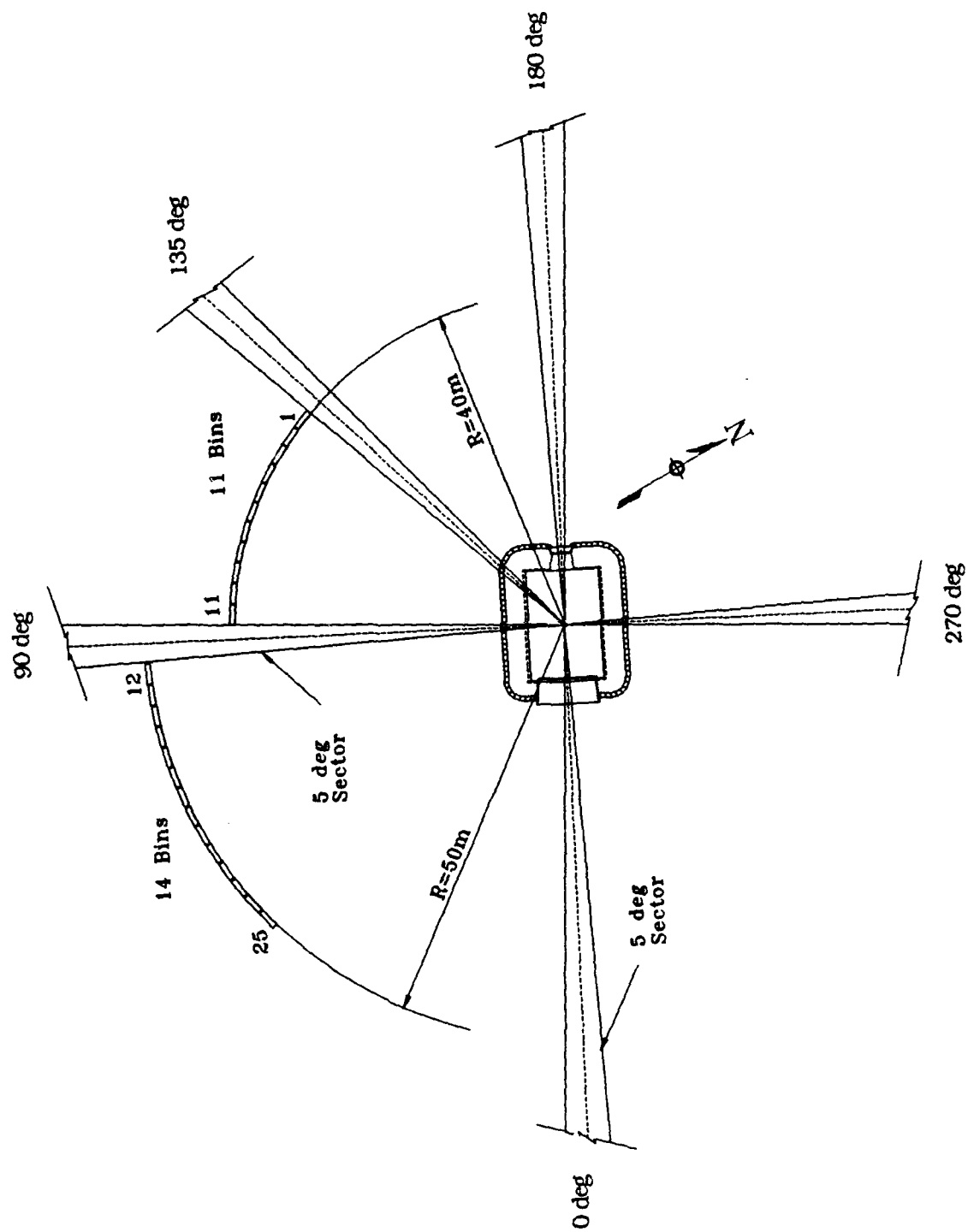


Figure 63. Locations of debris catcher bins, PAS-3.

4.1.2 Instrumentation Plan

A total of 40 channels of electronic instrumentation were provided for the PAS-3 event. Included were 12 pressure measurements in the interior of the structure, 21 free-field pressure measurements around the exterior of the structure, 1 accelerometer mounted at the crown of the structure in the plane of the detonation, and 6 strain gages on the front door. Table 7 is a measurements list for the PAS-3 event. This list gives the MN, the general location, coordinates, type of sensor and its sensing axis, and the predicted maximum amplitude of the recorded data. Similar to the PAS-1 test, the predicted maximum amplitudes shown in Table 7 for PAS-3 are approximate values used for gage selection and setting recording bandwidths. These amplitudes are based on pretest calculations, but do not correspond exactly to the results of these calculations. The locations of the various on-structure measurements are shown in Figures 64 through 68—gages mounted in the floor of the structure (Fig. 64), strain gages placed on the outside surface of the front door (Fig. 65), sensors mounted on the inner surface of the front door (Fig. 66), and sensors mounted on the structure at $X = 6918$ (Fig. 67). This is the only section at which sensors were mounted on the arch in the PAS-3 event. The sensing axis of the accelerometer mounted at the location shown in Figure 67 was oriented to measure radial accelerations. Figure 68 shows the location of the one airblast gage mounted in the rear wall. Figure 69 shows the locations of the free-field airblast gages.

The US Army Corps of Engineers, Waterways Experiment Station (WES) installed three self-recording accelerometers on the structure for the PAS-3 test. Each gage was mounted in an aluminum cube measuring 200 mm on each side and weighing 21.5 kg. The three gages were placed on narrow brackets attached to the outside of the arch at the locations shown in Figure 70. One of the WES gages was positioned between a SIFCON cube and a photo pole (Fig. 71).

Table 7. List of measurements for PAS-3.

MEASUREMENT LIST													
TEST EVENT		PAS-3				190				KIRST			
MEAS NO.	GEN	LOCATION			SENS AXIS	PREC MAX	CONF LEVEL	TRANSDUCER		TRANSDUCER TYPE	TRANSDUCER SERIAL NUMBER	CHANGES	
		X#	Y#	Z#				MODEL	RANGE			ITEM	AUTH
0101-3	SF	12807	0	367	Z	0.689 MPa	50 %	KULITE XT-190	1.379 MPa	PRESSURE	(1743-5-181) G7-35		
0102-3	SF	12807	3700	367	Z	10.342 MPa	50 %	KULITE HKS-11-37	34.47 MPa	PRESSURE	519-2-17		
RDT													
0102-3	SF	12807	3700	367	Z	3.447 MPa	100 %	KULITE HKS-11-37	34.47 MPa	PRESSURE	4319-2-17		
0202-3	BW	13010	1700	1475	X	3.447 MPa	50 %	KULITE XT-190	6.895 MPa	PRESSURE	(1906-3-340) F8-40		
0301-3	SF	3976	0	367	Z	2.068 MPa	50 %	KULITE XT-190	13.79 MPa	PRESSURE	(986-2-25) V6-48		
0302-3	SF	3976	1850	367	Z	1.724 MPa	50 %	KULITE XT-190	3.447 MPa	PRESSURE	(1862-4-100) F7-91		
0303-3	SF	3976	3700	367	Z	2.413 MPa	50 %	KULITE XT-190	6.895 MPa	PRESSURE	(1906-3-297) A8-64		
0402-3	FD	498	100	1475	X	2.758 MPa	50 %	KULITE XT-190	6.895 MPa	PRESSURE	(1862-2-280) L7-3		
0501-3	SF	645	3700	367	Z	10.342 MPa	16.6 %	KULITE HKS-11-37	34.47 MPa	PRESSURE	5246-5-5		
RDT													
0501-3	SF	645	3700	367	Z	3.447 MPa	100 %	KULITE HKS-11-37	34.47 MPa	PRESSURE (Filter)	5246-5-5		
0601-3	SF	6818	1850	367	Z	6.895 MPa	50 %	KULITE HKS-11-37	13.79 MPa	PRESSURE	102-9-9		
0602-3	SF	6818	3700	367	Z	5.171 MPa	50 %	KULITE XT-190	13.79 MPa	PRESSURE	(1944-5-156) C8-4		
NOTES: # = Distance in millimeters SC = Shelter Ceiling													

NOTES: # = Distance in millimeters
 SF = Shelter Floor
 RDT = Redundant
 SC = Shelter Ceiling
 FD = Front Door
 BU = Backwall

Table 7. Continued.

MEASUREMENT LIST																	DATE	25 MAR 92	PAGE 2 OF 4 PAGES	
TEST EVENT		PAS-3					IPO					KIRST								
MEAS NO.	LOCATION			SENS AXIS	PRED MAX	CONF LEVEL	TRANSDUCER		TRANSDUCER TYPE	TRANSDUCER SERIAL NUMBER	CHANGES									
	GEN	X#	Y#				Z#	MODEL			RANGE	ITEM	AUTH	DATE						
0603-3	SF	6818	-3700	367	Z	5.171 MPa	50	KULITE XT-190	13.79 MPa	PRESSURE (Filter)	(1944-4-143) W7-52									
0604-3	SC	6818	0	2717	Z	27.579 MPa	50	KULITE HKS-11-37	68.95 MPa	PRESSURE	2491-3-14									
0701-3	FF	-9000	0	350	Z	48.264 kPa	50	KULITE XT-190	172.4 kPa	PRESSURE	(4073-4-166) M18-58									
0702-3	FF	-24000	0	350	Z	27.579 kPa	50	KULITE XT-190	68.95 kPa	PRESSURE	(3827-4-19) L18-92									
0703-3	FF	-34000	0	350	Z	17.237 kPa	50	KULITE XT-190	34.47 kPa	PRESSURE	(1491-2-4) U6-16									
0704-3	FF	-44000	0	350	Z	6.895 kPa	50	ENDEVCO 8510B	13.79 kPa	PRESSURE	RF86									
0705-3	FF	-54000	0	350	Z	3.447 kPa	50	ENDEVCO 8510B	13.79 kPa	PRESSURE	C93M									
0706-3	FF	-6233	10800	350	Z	41.369 kPa	60	KULITE XT-190	68.95 kPa	PRESSURE	(3827-4-17) L18-91									
0707-3	FF	-16433	21000	350	Z	27.579 kPa	50	KULITE XT-190	68.95 kPa	PRESSURE	(2650-2-110) X8-16									
0708-3	FF	-23433	28000	350	Z	17.237 kPa	50	KULITE XT-190	34.47 kPa	PRESSURE	(1495-7-76) K7-6									
0709-3	FF	-30433	35000	350	Z	6.895 kPa	50	ENDEVCO 8510B	13.79 kPa	PRESSURE	RF69									
0710-3	FF	6818	12000	350	Z	68.948 kPa	50	KULITE XT-190	172.4 kPa	PRESSURE	(4073-4-164) M18-57									
NOTES: # = Distance in millimeters																	SF = Shelter Floor			
FF = Free Field																				
SC = Shelter Ceiling																				

Table 7. Continued.

MEASUREMENT LIST														
TEST EVENT		PAS-3					IIR			KIRST				
		LOCATION			SENS		PRED		CONF		TRANSDUCER		TRANSDUCER	
MEAS NO.	SER	X#	Y#	Z#	AXIS	MAX	LEVEL	MODEL	RANGE	TYPE	SERIAL NUMBER	ITCH	AUTH	DATE
0711-3	FF	6818	40000	350	Z	17.237 kPa	50 %	KULITE XT-190	34.47 kPa	PRESSURE	(1495-6-94) K7-1			
0712-3	FF	6818	50000	350	Z	6.895 kPa	50 %	ENDEVCO 8510B	13.79 kPa	PRESSURE	RF77			
0713-3	FF	17041	8000	350	Z	62.053 kPa	50 %	KULITE XT-190	172.4 kPa	PRESSURE	(4073-4-163) M18-56			
0714-3	FF	19841	10800	350	Z	41.369 kPa	60 %	KULITE XT-190	68.95 kPa	PRESSURE	(2650-2-111) X8-20			
0715-3	FF	30041	21000	350	Z	27.579 kPa	50 %	KULITE XT-190	68.95 kPa	PRESSURE	(3827-4-20) L18-93			
0716-3	FF	30000	0	350	Z	48.264 kPa	50 %	KULITE XT-190	172.4 kPa	PRESSURE	(4073-4-130) M18-37			
0717-3	FF	37000	0	350	Z	27.579 kPa	50 %	KULITE XT-190	68.95 kPa	PRESSURE	(2907-3-114) K9-35			
0718-3	FF	47000	0	350	Z	17.237 kPa	50 %	KULITE XT-190	34.47 kPa	PRESSURE	(1495-7-75) K7-7			
0719-3	FF	57000	0	350	Z	6.895 kPa	50 %	ENDEVCO 8510B	13.79 kPa	PRESSURE	RF60			
0720-3	FF	6818	-12000	350	Z	68.948 kPa	50 %	KULITE XT-190	172.4 kPa	PRESSURE	(4073-4-149) O18-39			
0721-3	FF	6818	-50000	350	Z	6.895 kPa	50 %	ENDEVCO 8510B	13.79 kPa	PRESSURE	PP49			
1601-3	SR	6818	0	2987	Z	10000 g	50 %	ENDEVCO 2264A	2000 g	ACCELEROMETER	DD46D			

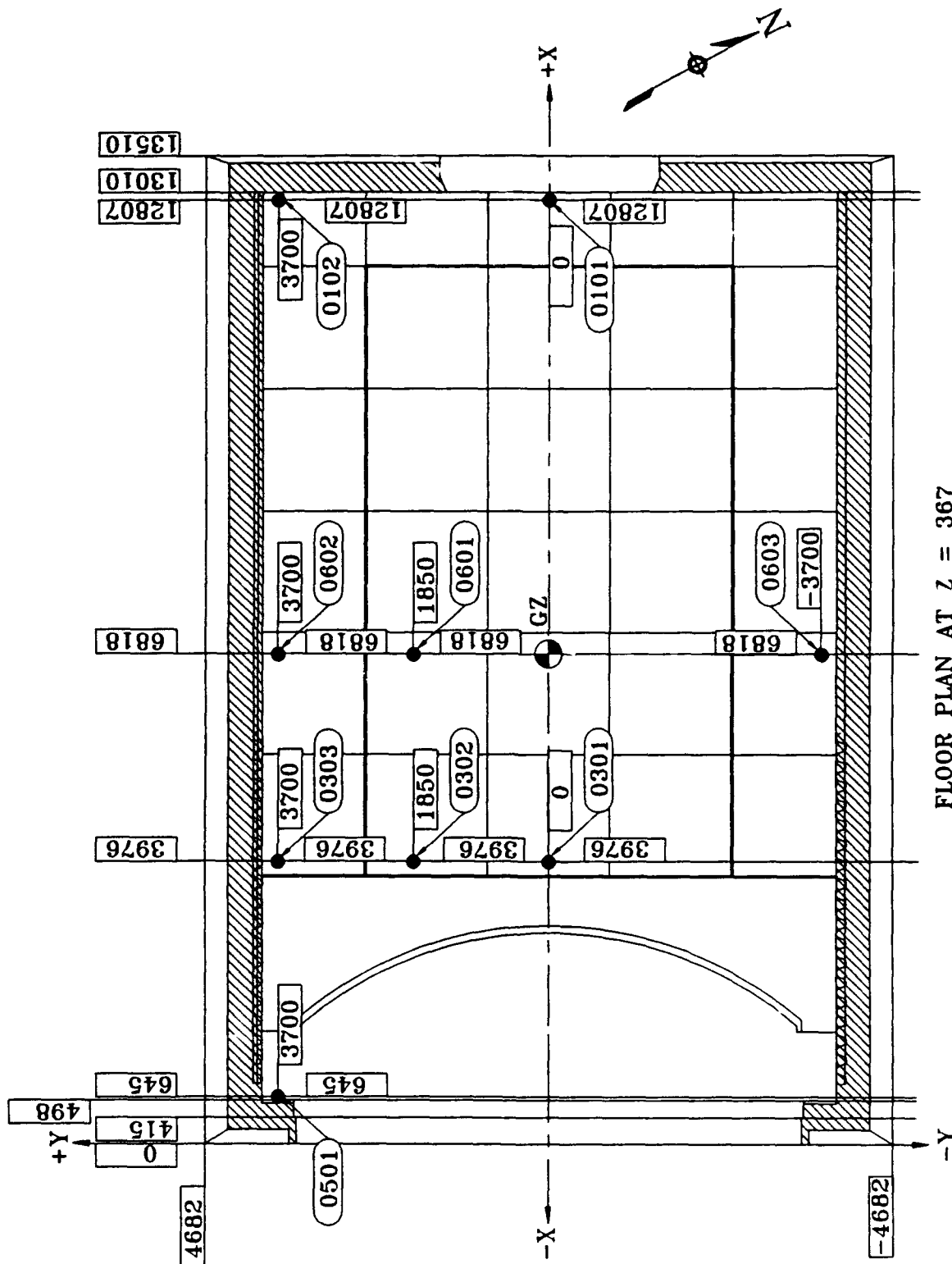
NOTES: # = Distance in millimeters

FF = Free Field

SR = Structure Roof

Table 7. Concluded.

[illegible]



FLOOR PLAN AT $Z = 367$

Figure 64. Instrumentation in floor of structure, PAS-3.

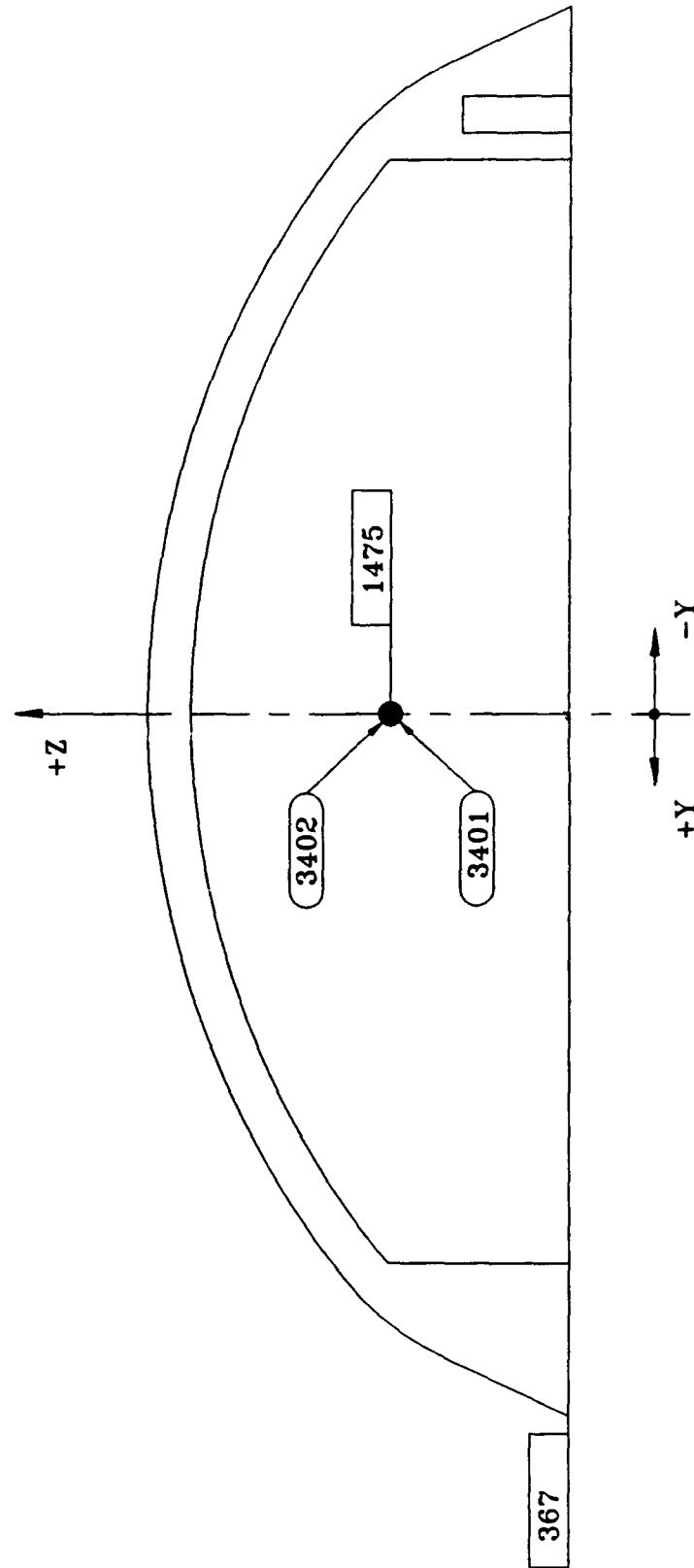


Figure 65. Instrumentation on outside surface of front door at X = 415, PAS-3.

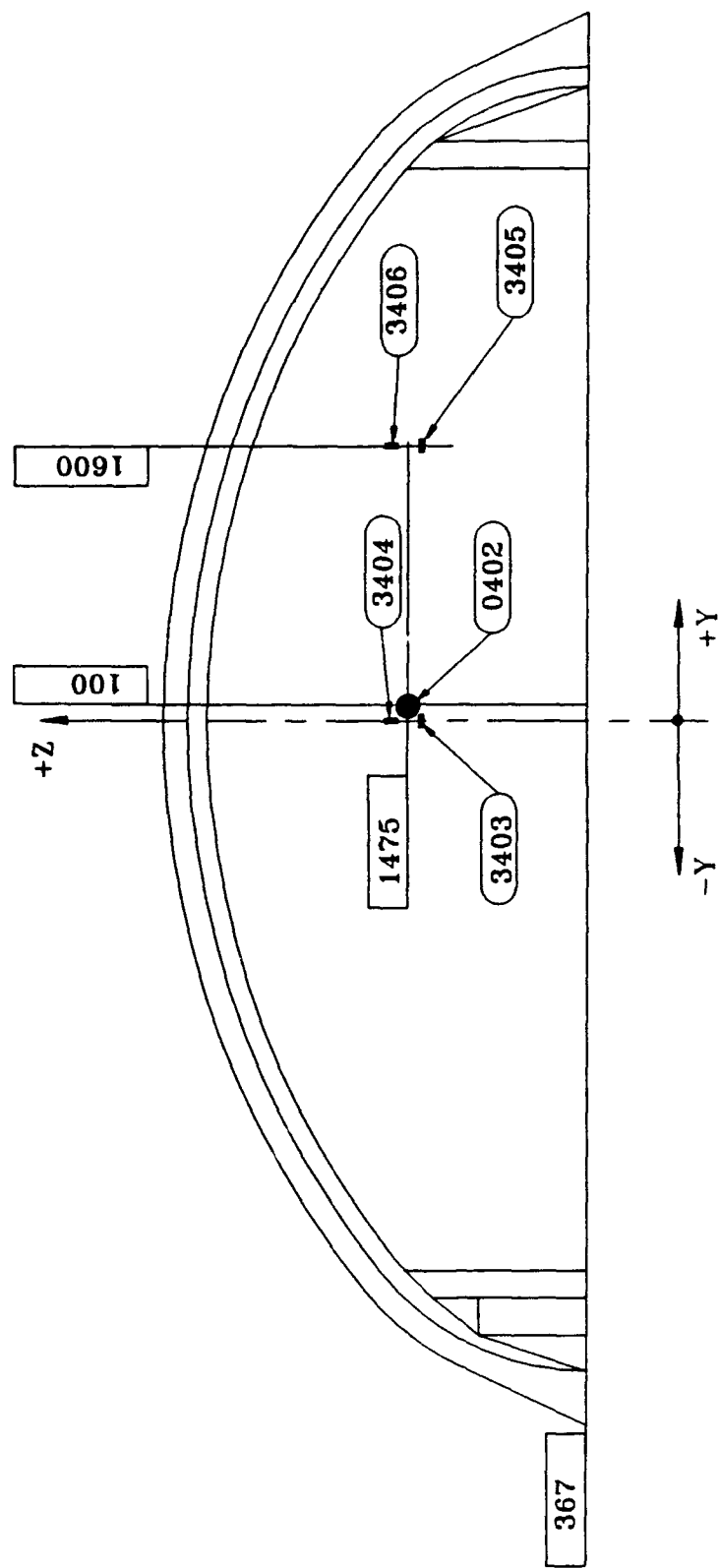


Figure 66. Instrumentation on inside surface of front door at X = 498, PAS-3.

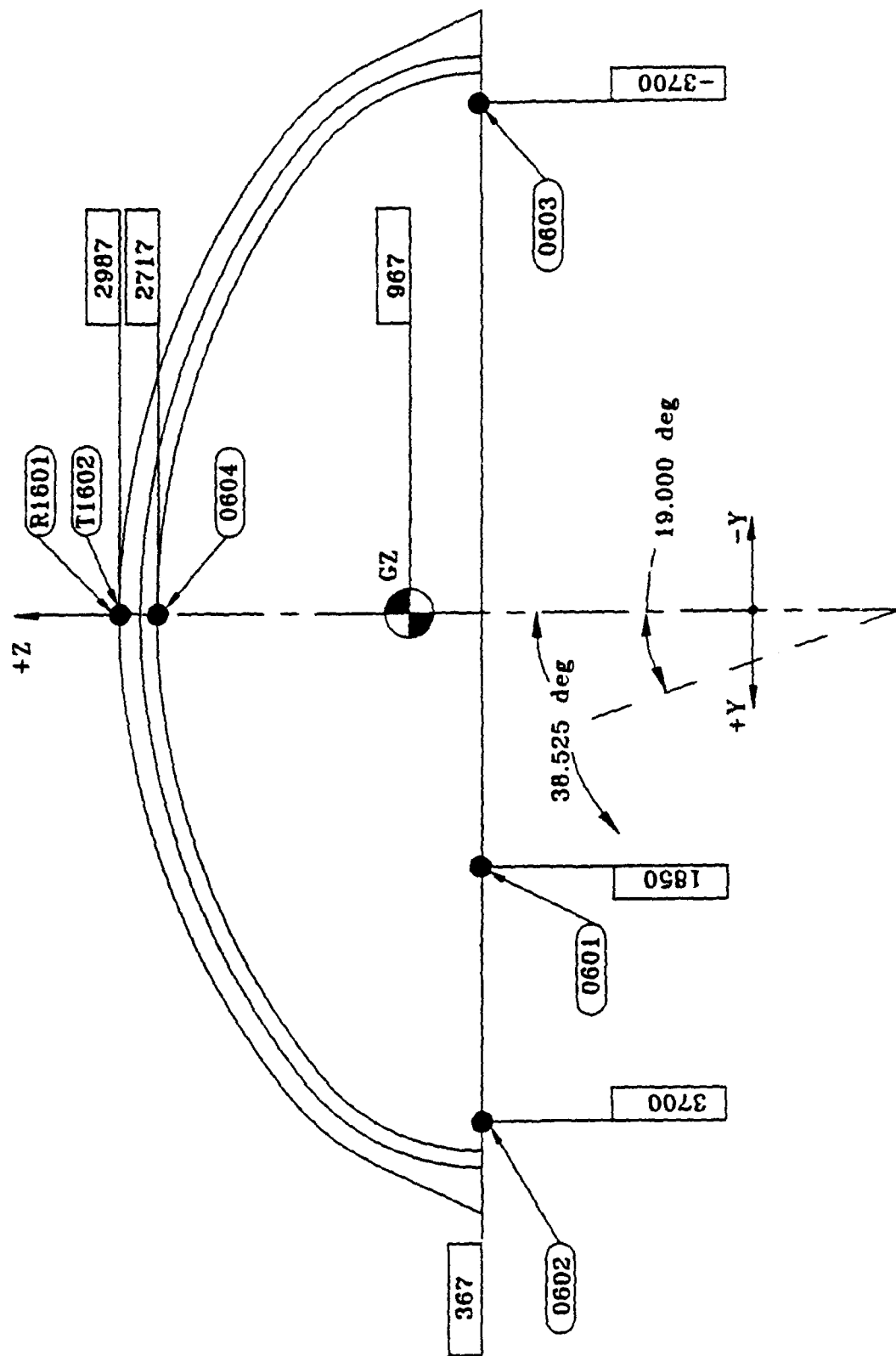


Figure 67. Instrumentation on arch at $X \approx 6818$ PAS-3.

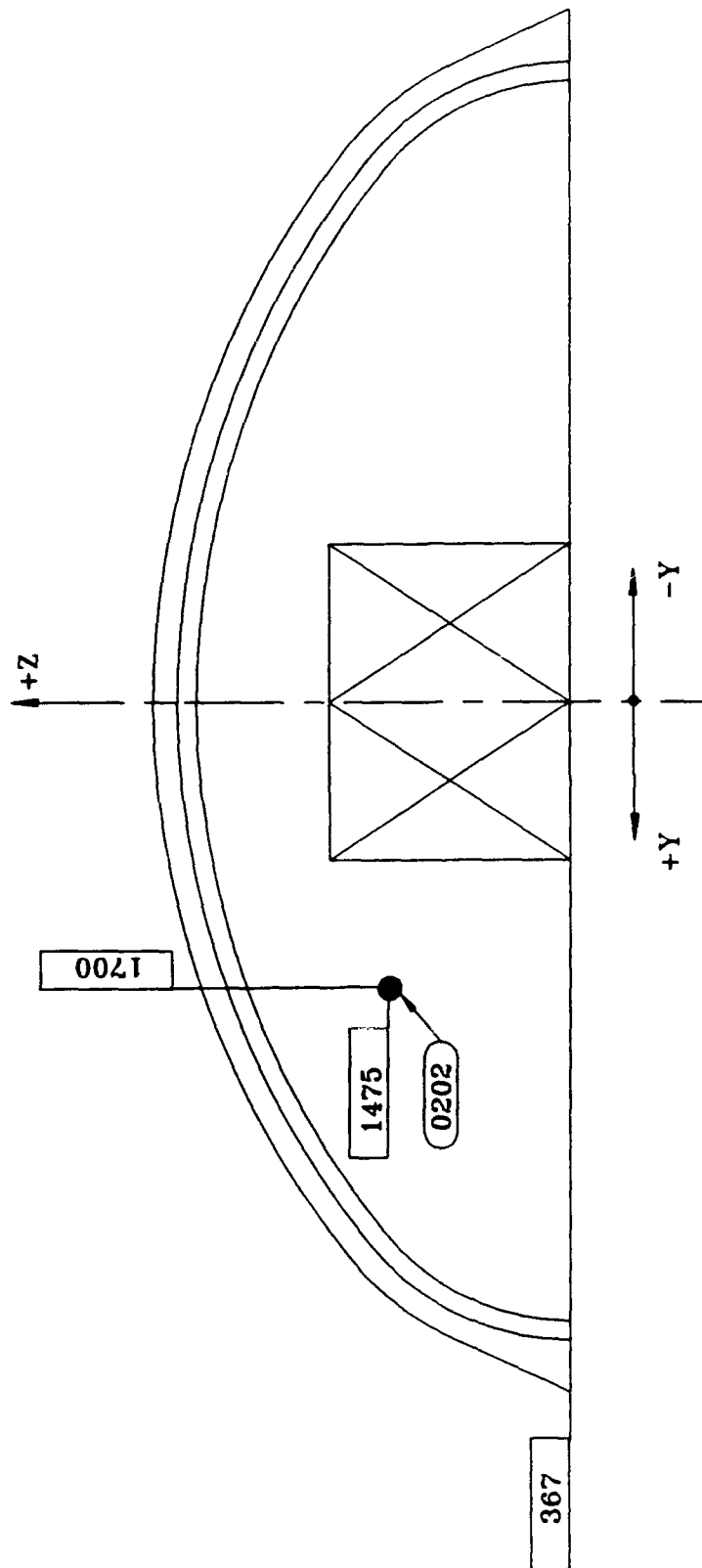
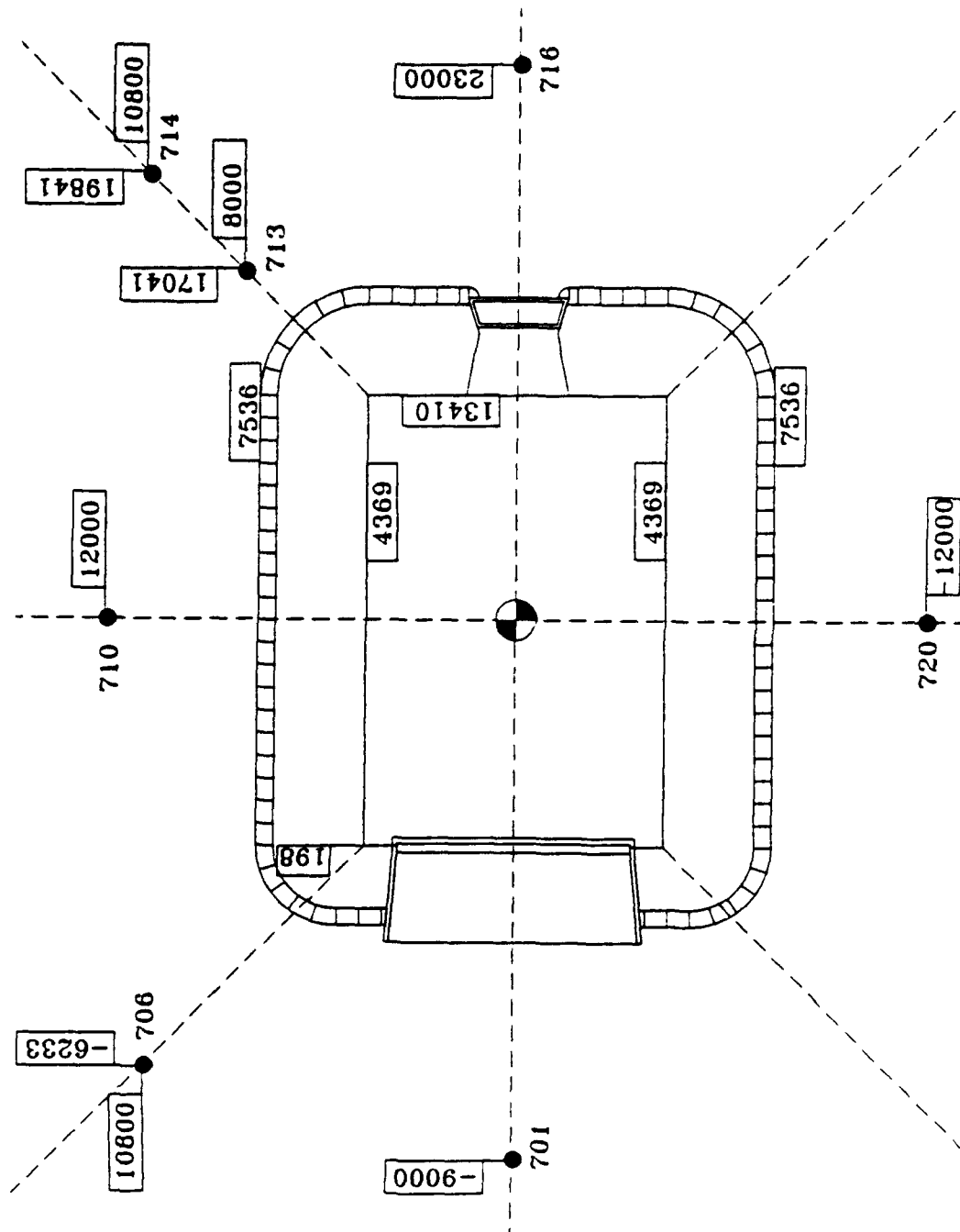
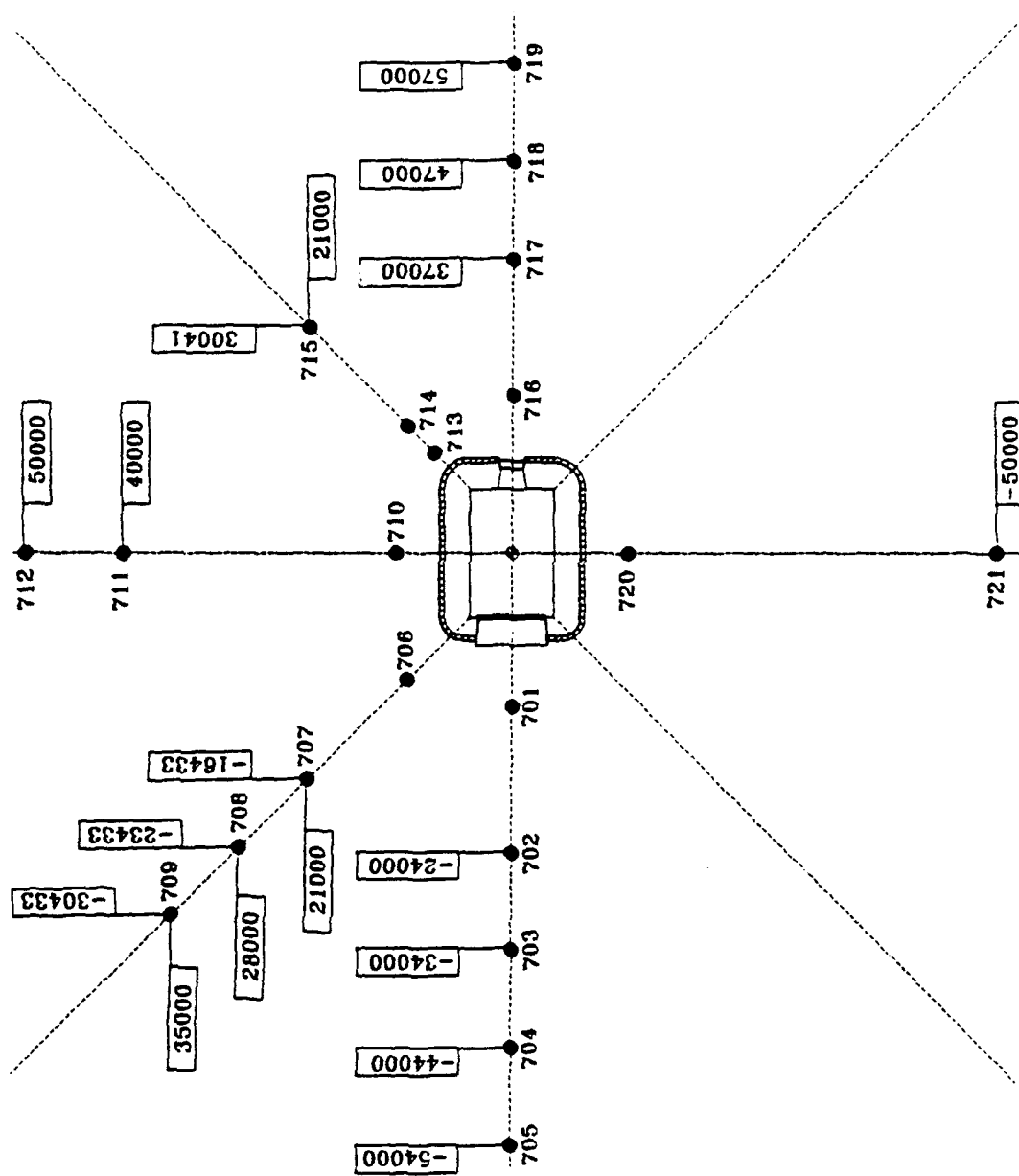


Figure 68. Instrumentation on inner surface of backwall at X = 13010, PAS-3.



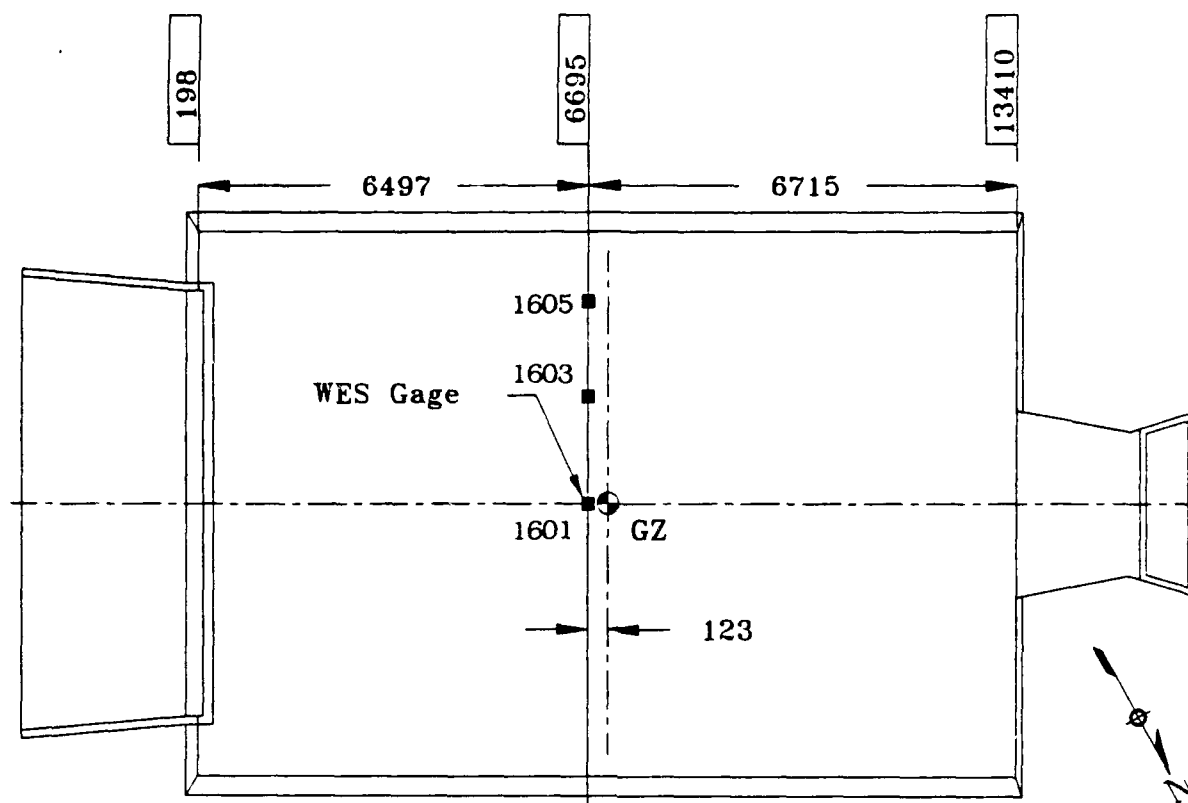
(a) Near free-field.

Figure 69. Free-field airblast gage locations, PAS-3.

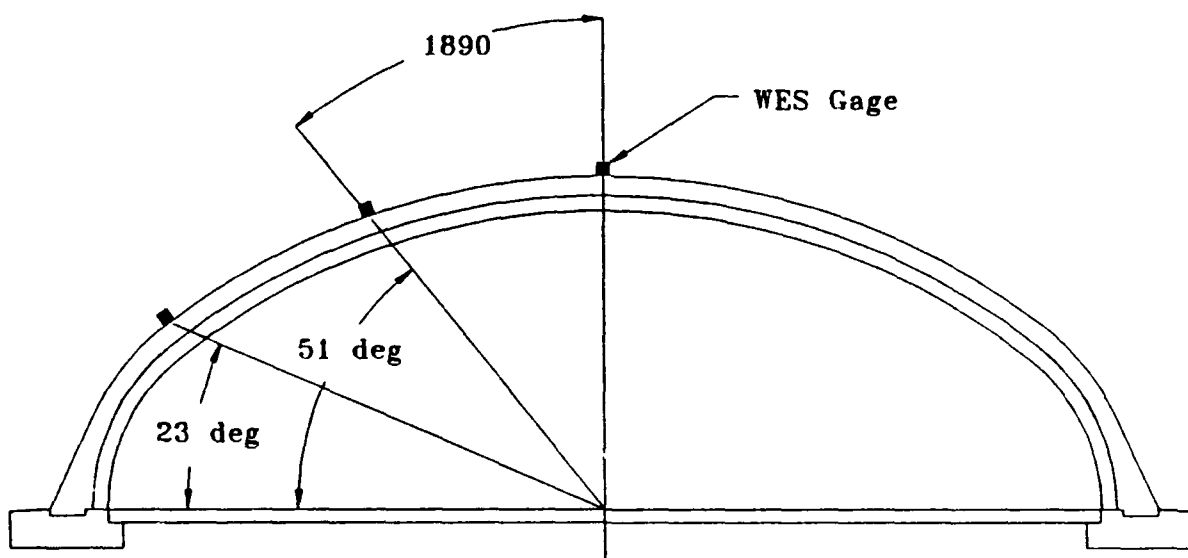


(b) Far free-field.

Figure 69. Concluded.



(a) Plan.



(b) Section.

Figure 70. Locations of WES self-recording accelerometers, PAS-3.

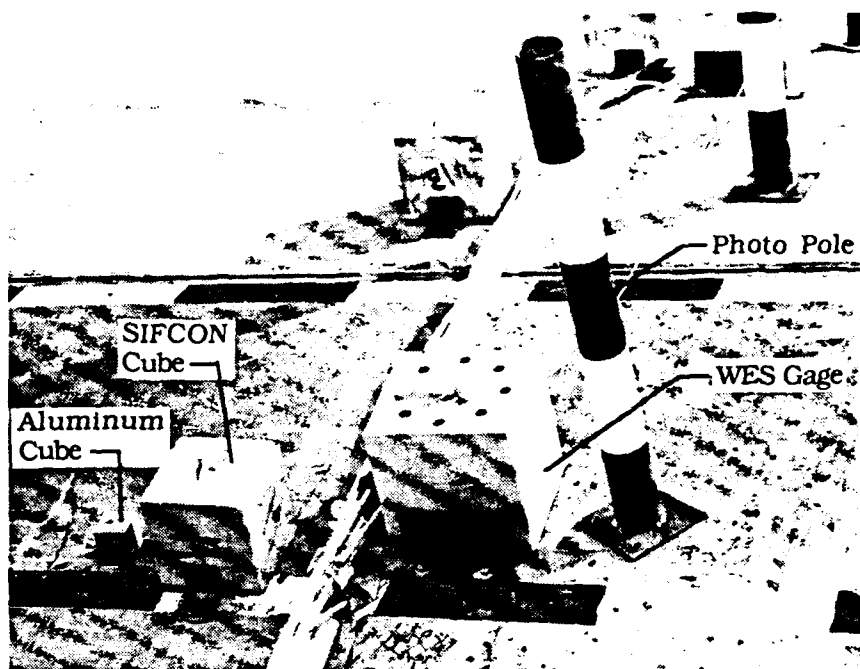


Figure 71. The WES self-recording accelerometer.

Twenty-five high-speed motion picture and sequential still cameras were provided at seven camera stations. One station was located in a helicopter hovering over the test site. The locations of the six ground stations for the PAS-3 event are shown in Figure 72. Motion picture data were recorded at rates of 500 and 1000 frames per second. All the ground stations were located at a range of 228 m from the structure.

4.2 TEST RESULTS

4.2.1 Structural Damage Survey

The test structure was destroyed in the PAS-3 event. Figures 3 and 4 present a key for identifying the various components of the model in the following discussion of structural damage. The estimated debris velocities were calculated on the basis of observed object motion in one plane. The actual velocities could be somewhat higher due to the out-of-plane motion of the object.

The front door was blown out of the structure very quickly. It bowed outward as gases escaped around its edges at 6 ms. The top edge of the door separated from the door frame at 16 to 18 ms. The door then rotated about its lower edge and was flat on the apron at 110 ms. It skidded outward along the ground surface until its top edge struck the ground at about 23 m from the front of the structure (Fig. 73). After its impact with the ground surface, the door became airborne and began rotating about all three centroidal axes. It impacted the ground again at 90 and 100 m before finally coming to rest at approximately 120 m in front of the structure (Fig. 74). The destroyed PAS-3 structure is also shown in the background of this photograph. Since the door left the fields of view of the ground cameras, it was not possible to determine the maximum height of its flight. Because it was partially obscured at early times, it was also difficult to determine exactly when the door started its horizontal motion away from the shelter. Time counted from the moment the door was flat on the apron indicated an average velocity to the first ground marker of about 98 ms. If counted from $t = 0$, its average velocity was about 66 ms.

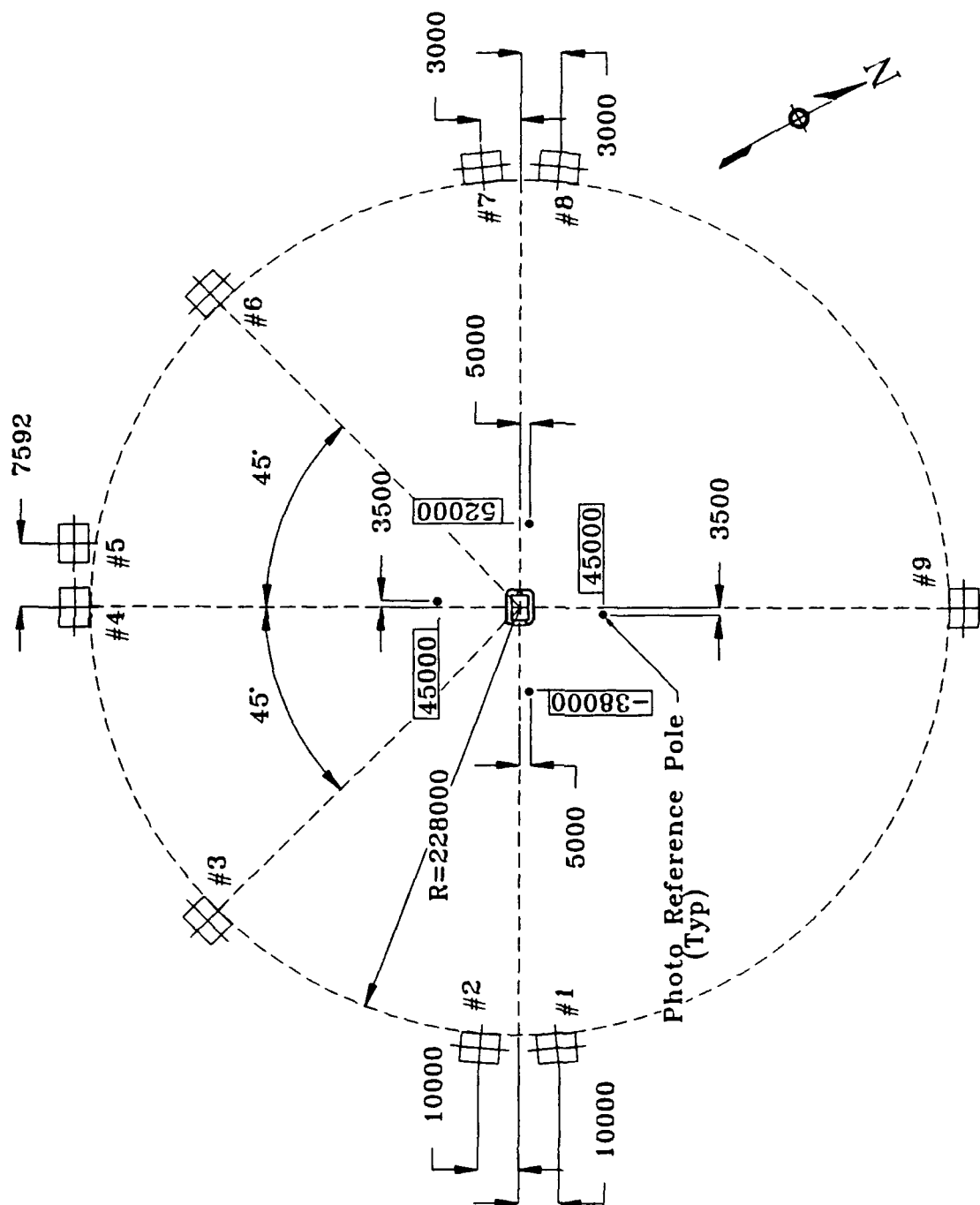
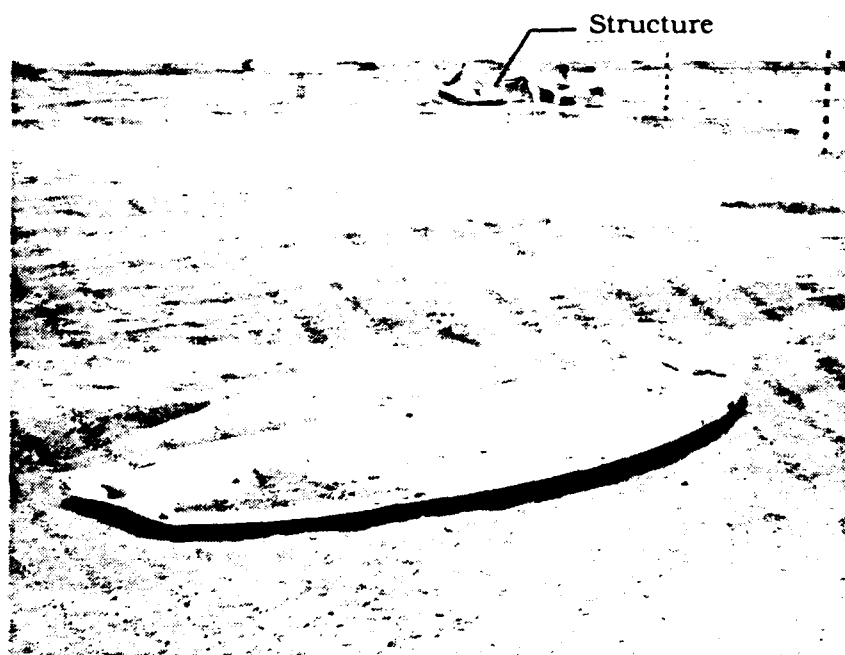


Figure 72. Camera station locations, PAS-3.



Figure 73. Impact of front door at 23 m from the structure, PAS-3.



(a) Posttest location.



(b) Posttest condition of inside surface.

Figure 74. Front door, PAS-3.

The door was bent its full width about a horizontal line with a maximum permanent deflection of 185 mm at the center. The edges at both sides of the door were also bent inward at approximately 140 mm. The inside plate was dished inward between each of the vertical ribs. The inside plate was also buckled in a 700 mm wide band along the horizontal centerline (Fig. 74b).

The personnel entrance vestibule was found intact, approximately 2.6 m in front of the left wingwall (Fig. 75). The personnel door, which had been located in a frame installed in the opening in the left front wall, was found near the vestibule. The door was bent in half about its vertical centerline (Fig. 75). All the welds simulating the door hinges and latches were broken. The door frame remained welded to the steel liner (Fig. 76).

A section of the left wingwall was found connected to a section of the left front wall and resting 11 m in front of the structure (Fig. 77). Only the outer portion of the left wingwall beyond the personnel door opening was found intact on its foundation. A failure plane ran diagonally upward and away from the upper corner of the opening (Fig. 78). All the reinforcing bars crossing the failure plane were found to be broken. This failure plane corresponded to one of the cracks in the left wingwall noted following the PAS-1 test (see Section 3.0).

A large section of the arch fell back onto and covered the right wingwall. The high-speed photography suggests that the right wingwall failed in a manner similar to that of the left wingwall. However, the failure plane in this wall ran diagonally upward and away from a point near the base of the front wall foundation (Fig. 79).

The front walls and parapet remained connected to a front section of the arch. The right front wall appeared to have broken off the large arch section upon impact with the floor slab (Fig. 80). About two-thirds of the dowels extending from the right front wall into the wingwall were broken. The unbroken dowel bars appeared to have pulled out of the wingwall and remained in the front wall (Fig. 81).



Figure 75. Vestibule and personnel door (foreground), PAS-3.

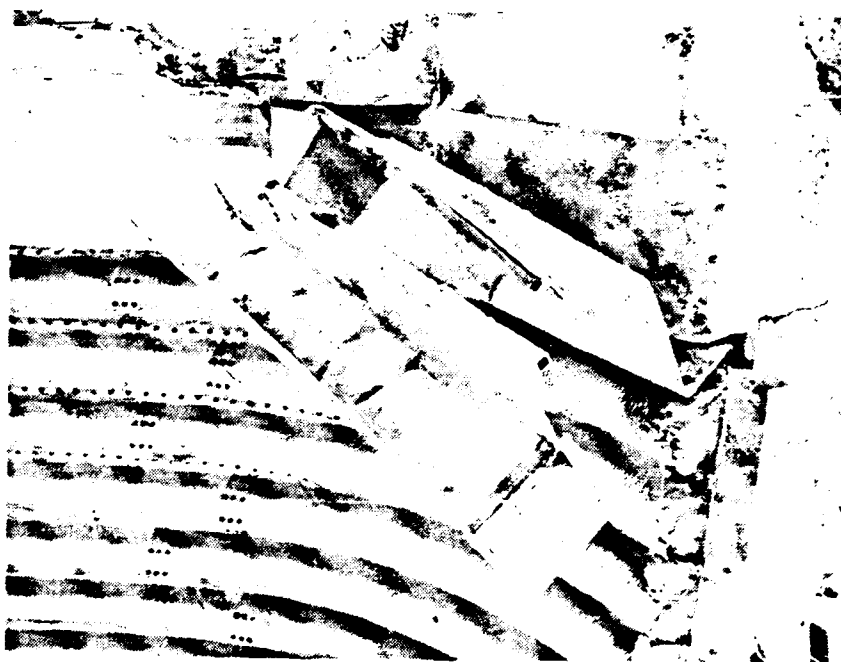


Figure 76. Steel liner at personnel door opening, PAS-3.



Figure 77. Part of left wingwall and left front wall, PAS-3.

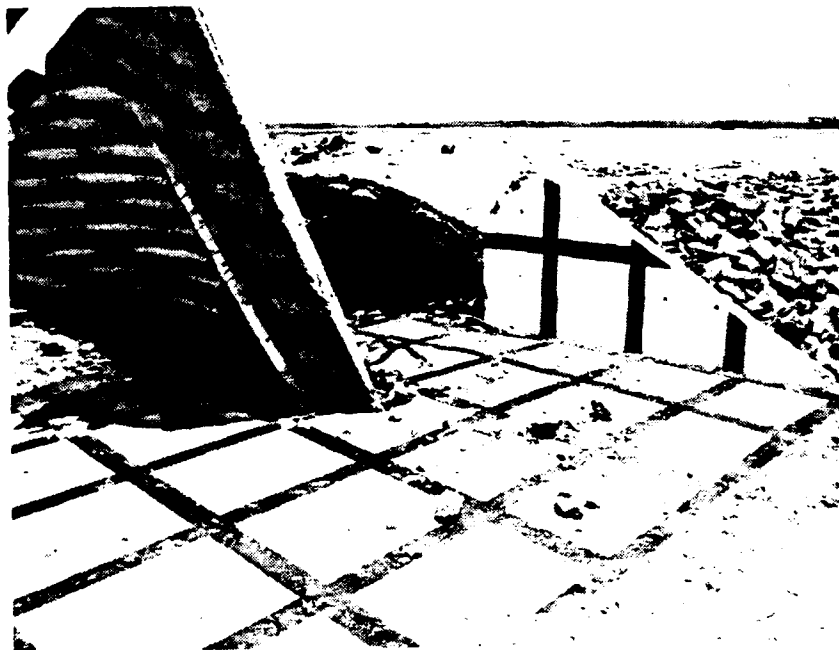


Figure 78. Left wingwall, PAS-3.

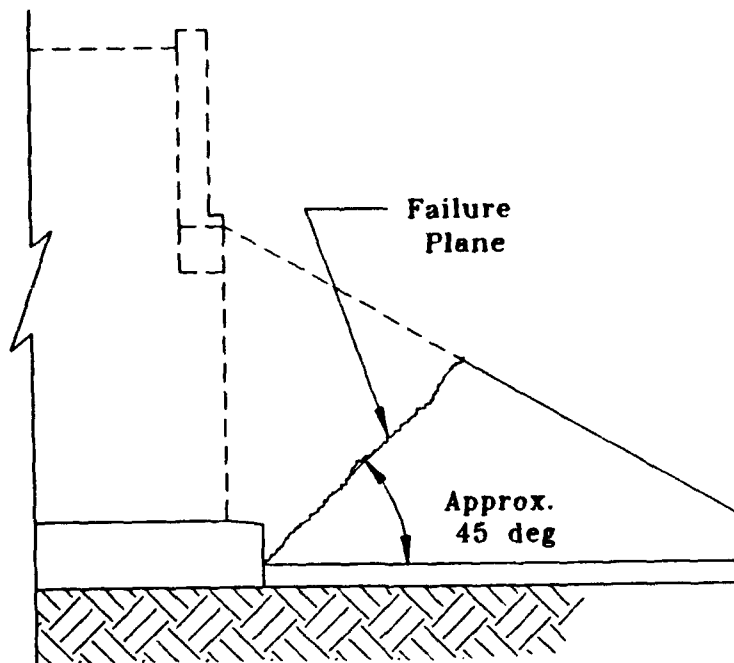


Figure 79. Elevation: Right wingwall failure plane, PAS-3.

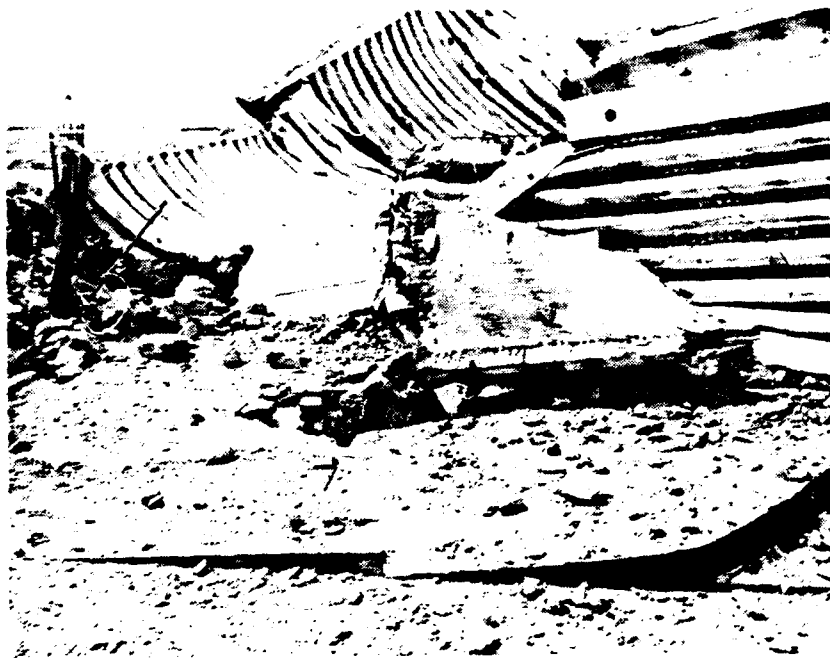


Figure 80. Final location of right front wall, PAS-3.



Figure 81. Dowel bars in right front wall, PAS-3.

The heavily reinforced column, between the left side of the front door opening and the personnel door, and part of the left wingwall broke away from the parapet (Fig. 76). All the reinforcing dowel bars were pulled out of the base of the column and remained embedded in the foundation. The rest of the left front wall broke away from the arch and pulled out of the steel plate liner, breaking every headed anchor stud in the process.

Two major breaks were observed in the welds joining the sections of the steel door frame at the top of the front door opening. The broken welds were located adjacent to each of the two brackets located along the front edge of the door slot (Fig. 82). Significant damage also occurred to the concrete in the front parapet at these two locations. No break occurred in the welded joint near the location of the third bracket, which was broken off in the PAS-1 test (Fig. 83). There was also no damage to the parapet concrete at this location.

The first detectable upward movement at the crown of the arch occurred at about 6 ms, and the first venting of gases at the crown was observed at 20 ms. Venting of gases along the springline of the arch began at about 28 ms; the major breakup of the arch began at about 34 ms. The arch was broken into seven large sections, which were launched vertically upward at gradually increasing velocities (Fig. 84). Analysis of the high-speed photography indicates the front portion of the arch was moving upward at a velocity of 9.4 m/s at 30 ms, 11.3 m/s at 50 ms, and 14.2 m/s at 100 ms. The upward velocity of the middle portion of the arch was 18.0 m/s at 30 ms, 22.7 m/s at 50 ms, and 23.1 m/s at 100 ms. The rear portion of the arch was moving upward at a velocity of 13.9 m/s at 30 ms and 15.0 m/s at 50 ms. Because this portion was obscured by smoke and other detonation products, its velocity could not be determined at 100 ms. These velocities were averages for large pieces of debris, which rotated about horizontal and vertical axes while moving upward. They are higher than those indicated by integrated accelerometer records. The trajectory of the larger pieces of debris was nearly vertical, and all seven large sections of the arch fell back within the limits of the structure foundation and the perimeter of the rock rubble berm (Fig. 85). The maximum height

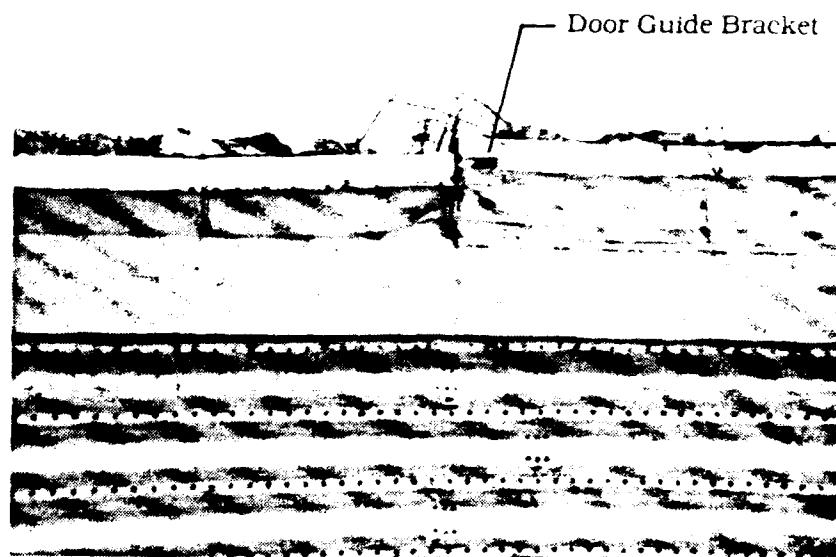


Figure 82. Welded joint in steel plate liner and parapet damage at location of door guide bracket, PAS-3.

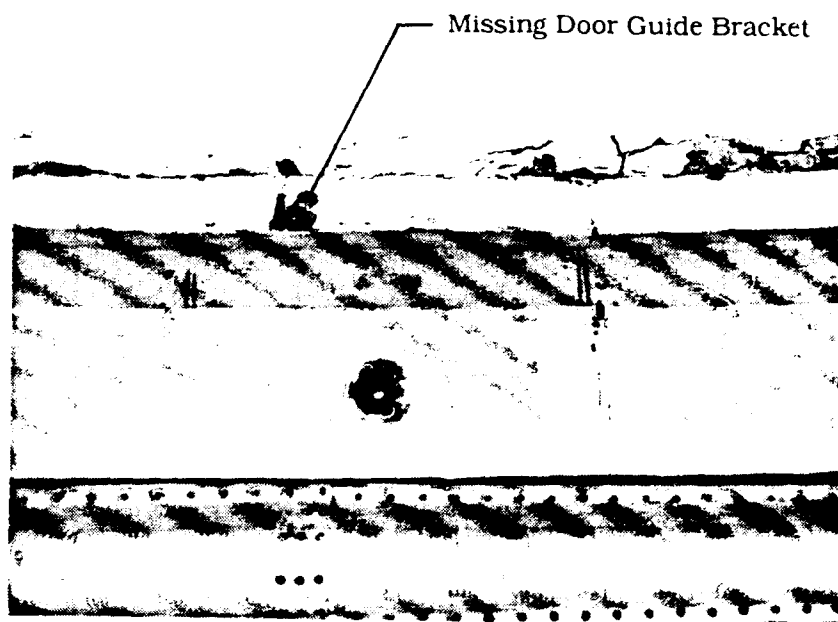
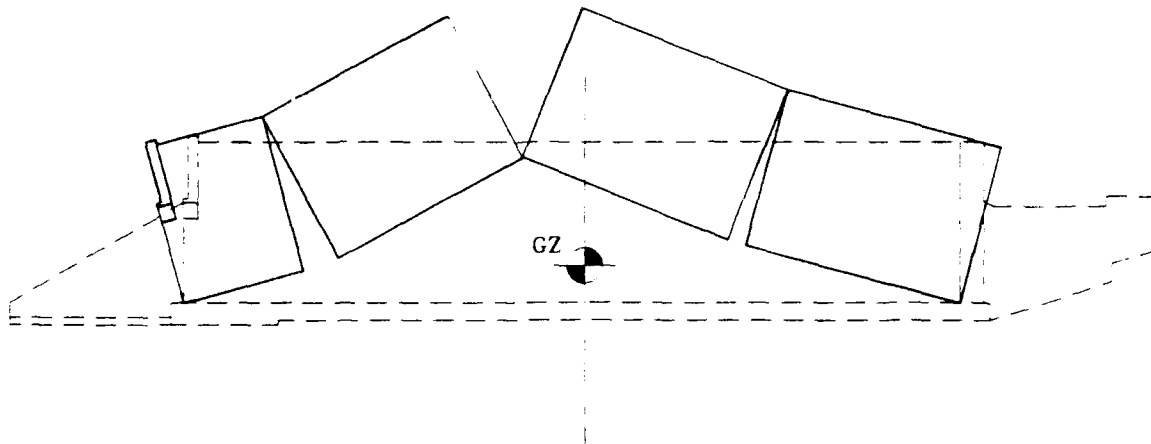
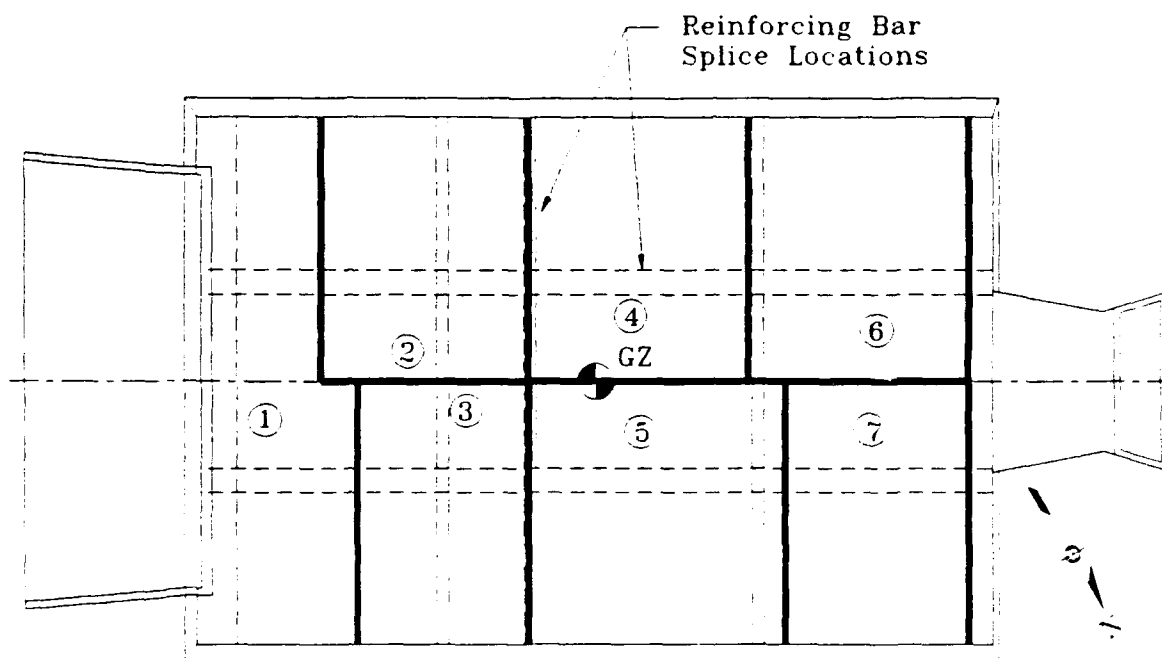


Figure 83. Steel plate liner and parapet at location of missing door guide bracket, PAS-3.



(a) Crack Pattern.



(b) Breakup into seven sections.

Figure 84. Breakup of the arch, PAS-3.

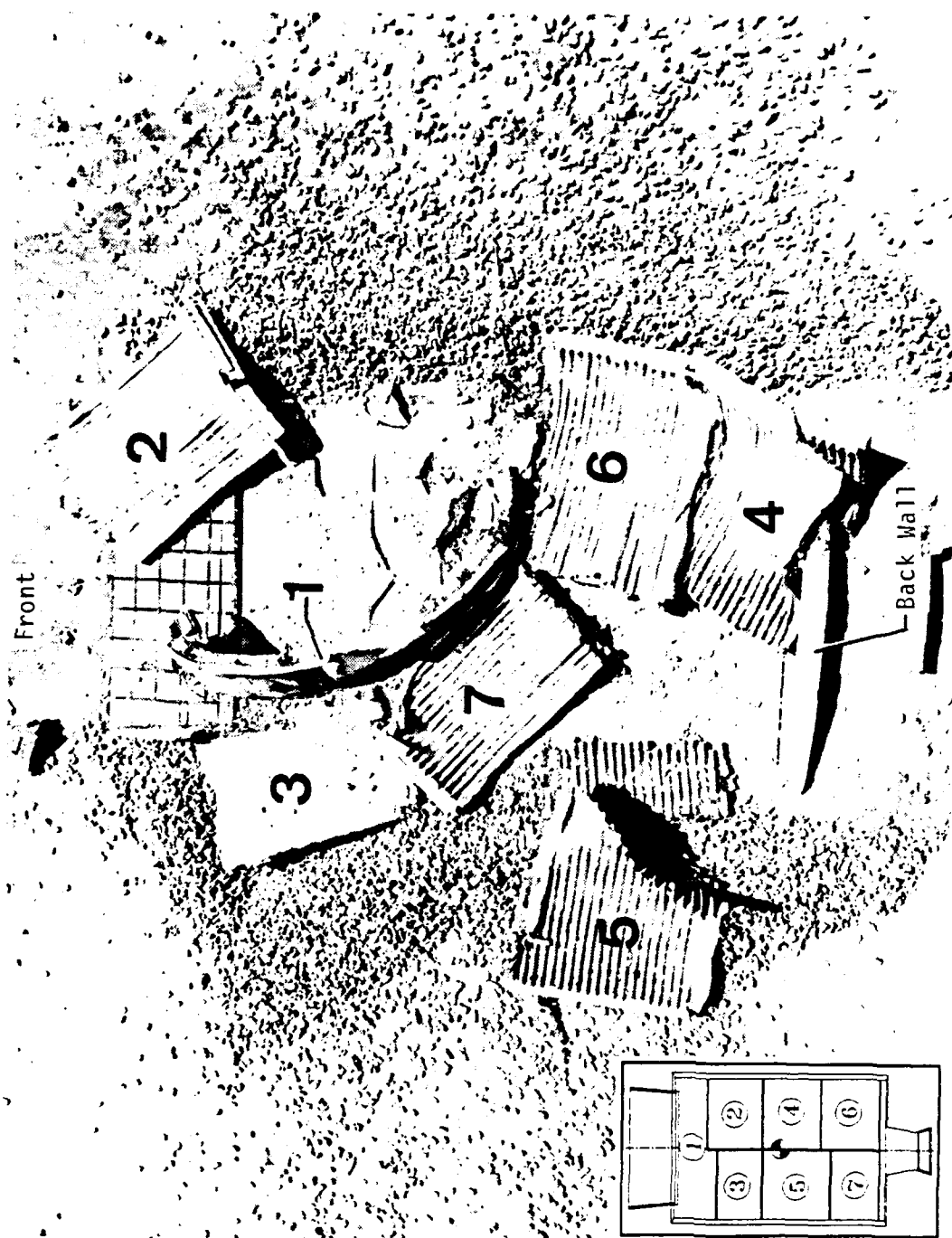


Figure 85. Posttest overhead view of PAS-3 test structure.

of their trajectory could not be determined, because the pieces moved out of camera range. The front portion reached a height in excess of 6.6 m; the center portion reached a height in excess of 17.2 m. All of the larger pieces of debris had returned to the ground within 4.0 s. One SIFCON cube was observed returning to the ground at 5.9 s, and the last small piece of debris observed returned to the ground at 9.0 s. In most instances the corrugated metal liner remained attached to the concrete. The ground impact velocities of several large pieces of debris were estimated from high-speed photography to be about 15.7 m/s. One SIFCON cube was observed falling at a velocity of 14.3 m/s.

A study of the seven arch sections revealed several common features. Failure in the transverse direction always occurred along a bolted liner joint. At the failure line, the corrugated liner material was almost always pulled over the nut of the bolt (Fig. 86). In only one instance, between Sections #2 and #1, was there some edge tear-out of the bolts (Fig. 87). Examination of the transverse failure line revealed a tension failure of the concrete. Between Sections #2 and #4, #3 and #5, and #4 and #6, the failure plane occurred near a line of splices in the reinforcing bars, and the bars pulled out of the adjacent piece (Fig. 88). Between Sections #1 and #2, #1 and #3, and #5 and #7, the reinforcing bars failed in tension at the fractured face of the concrete (Fig. 89).

Failure in the longitudinal direction occurred along the crown of the arch. Along the failure line the corrugated liner material failed in tension (Fig. 90). In no case did a failure occur in the bolted joints of the liner segments. At the failure plane the concrete failed in tension. All of the reinforcing bars in the failure plane also failed in tension at, or within a few millimeters either side of, the fractured face of the concrete.

An examination of the fractured face of the longitudinal failure plane revealed tension cracks at almost every transverse liner joint (Fig. 91). The cracks ranged from hairline to several millimeters in width. There were significantly fewer cracks at the base edge of the arch. These cracks were also narrower in width than those elsewhere on the arch and appeared to be randomly spaced along the edge.

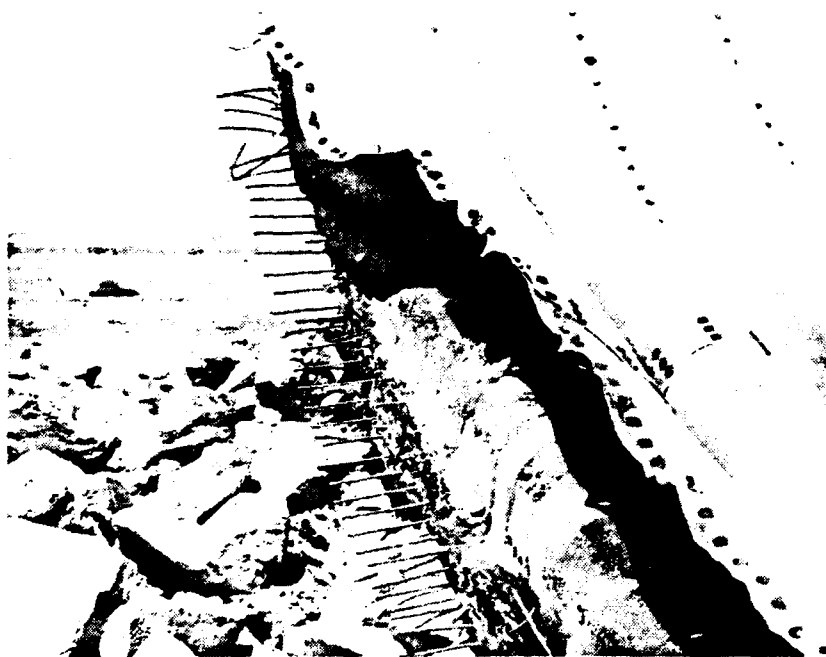


Figure 86. Typical bolt pull-out at liner joint, PAS-3.



Figure 87. Edge tear-out of bolts in liner of Section #2, PAS-3.



Figure 88. Pull-out of reinforcing bars at transverse failure plane, PAS-3.



Figure 89. Broken reinforcing bars at transverse failure plane, PAS-3.



Figure 90. Longitudinal failure plane, PAS-3.



Figure 91. Tension cracks, PAS-3.

The base channel for the corrugated liner remained attached to the base of the arch sections. In some cases it became detached from the inside plane of the corrugated liner and was bent downward (Fig. 92).

The backwall was found generally intact and upright on its foundation following the test. A slight outward tip was noted. It also appeared that it had been displaced backward about 50 mm. The earth against the outside of the backwall appeared to have been pushed away from the wall (Fig. 93). The position of the soil indicates a larger transient outward motion of the whole backwall and a rebound to its final position.

The arch portion had separated from the top edge of the backwall at the inside interface, breaking every dowel bar (Fig. 94). The failure plane then proceeded along a vertical plane corresponding to the step in the joint (Fig. 95). All the horizontal reinforcing bars crossing the vertical failure plane were also broken. Along the top one-third of the backwall the concrete covering the reinforcing bars was broken off. A crack corresponding to the inside interface was observed all along the top edge on the back surface of the wall (Fig. 96).

A wide vertical crack was observed at the left side of the backwall directly above the wall of the exhaust port. The portion of the backwall beyond the exhaust port was displaced outward relative to the rest of the wall at the wide crack (Fig. 97). A pattern of narrow cracks running diagonally upward from the upper corner of the exhaust port opening was seen on the right side of the backwall. The high-speed photography indicates that the wide crack and outward displacement may have been caused by the impact between a large section of the arch and the top of the wall as the arch section fell back on the structure.

Other than the diagonal cracks at the corners of the exhaust port, only a few small cracks were observed in the surface of the backwall above the exhaust port opening. No cracks were seen in the face of the backwall on either side of the exhaust port opening.



Figure 92. Base channel for corrugated liner, PAS-3.

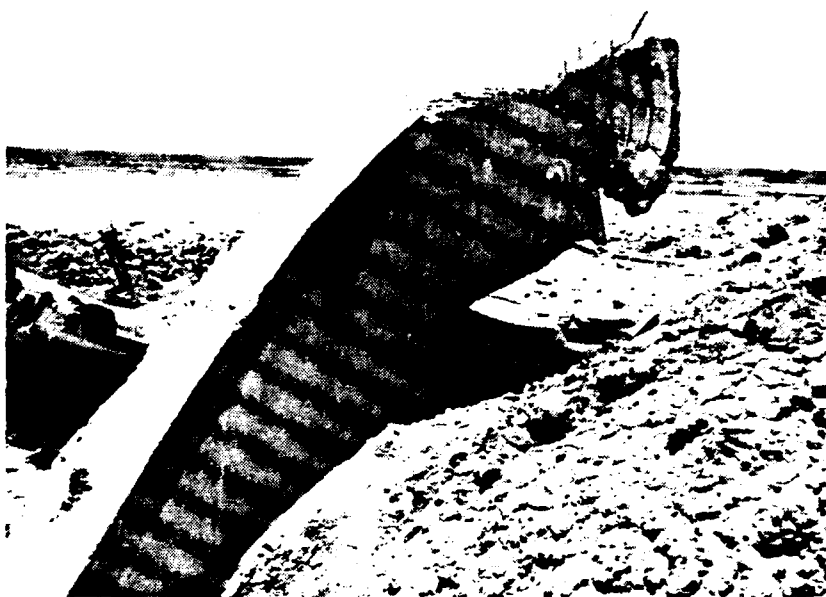


Figure 93. Displaced earth backfill, PAS-3.

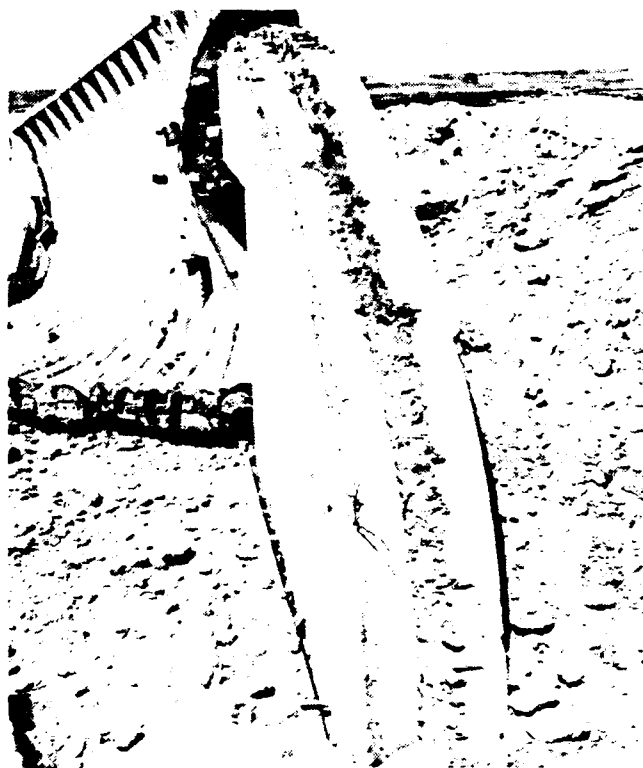


Figure 94. Top edge of backwall, PAS-3.

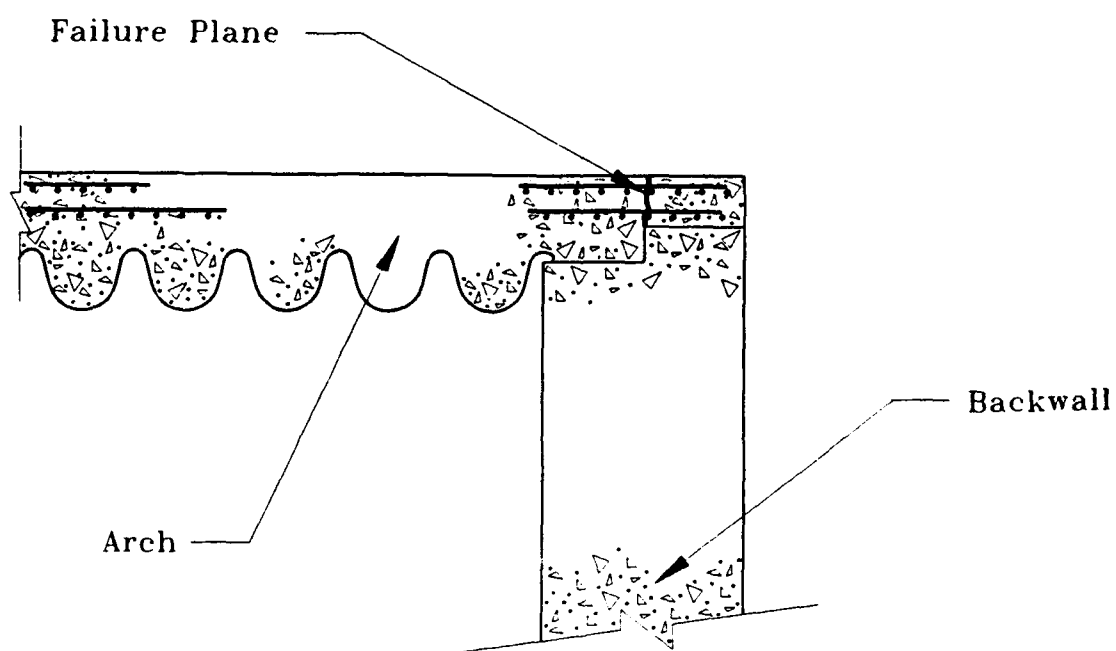


Figure 95. Section: Failure plane between the arch and backwall, PAS-3.

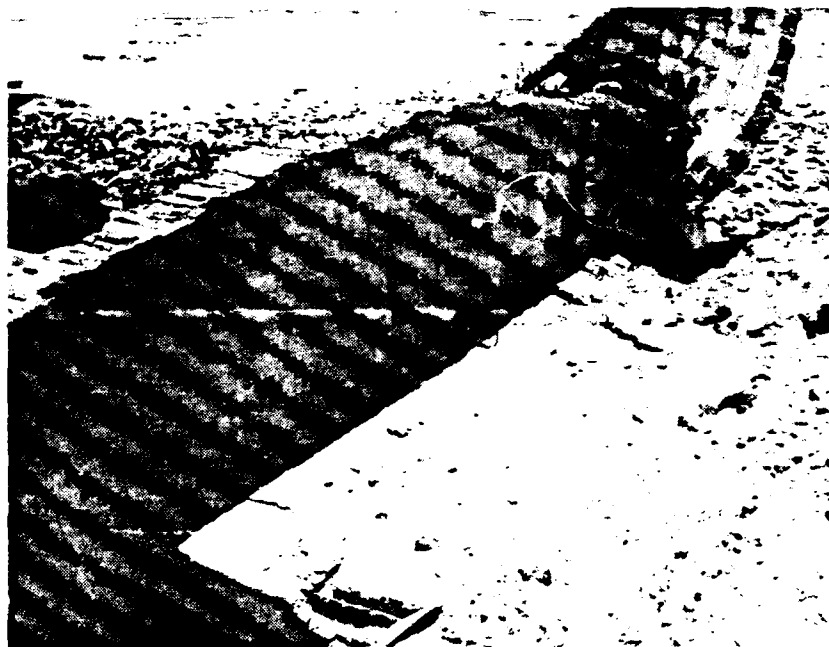


Figure 96. Back view of backwall, PAS-3.



Figure 97. Wide crack on left side of backwall, PAS-3.

The entire endwall of the exhaust port broke away from the sidewalls of the exhaust port (Fig. 98). Several large pieces were found as far as 32 m behind the structure (Fig. 99). The exhaust port experienced severe cracking and damage at every intersection of the structural elements (Fig. 100). Cracking to a somewhat lesser degree was also observed in the faces of the structural elements themselves. Despite the severe damage at the corners, all of the components, with the exception of the endwall, remained attached to each other and/or the backwall.

The two exhaust port doors were blown upward and out the back of the exhaust port and were found at distances of 76.5 and 155.7 m behind the structure. Both doors were bent about a horizontal line (Fig. 101). Abrasions on the doors indicate that they probably struck the exhaust port endwall as they were blown out. The two steel door frames originally embedded in the floor and the walls and roof of the exhaust port were also found in several pieces behind the structure (Fig. 102). The headed anchor studs used to secure the door frames to the exhaust port concrete had been pulled out of the concrete but remained welded to the frame. In some cases, the steel angles at the top and bottom of the doors were found still welded to the frame; in others the welds had failed and the angles adhered to the door.

Following the test, most of the arch foundation was covered with large pieces of the arch or with rock rubble. The only visible portion of the arch foundation was found intact with little indication of upward or outward displacement. The majority of the outside dowel bars (with the hooked ends) had either been broken at the top of the foundation or broken off inside the foundation and pulled out (Fig. 103). About one-third of the inner dowel bars (no hooked ends) were found broken at the top of the foundation; the rest appeared to have been pulled out of the base of the arch.

The floor slab was found in place against the arch foundation, with little indication of vertical displacement between the two components (Fig. 103). The floor was heavily damaged due to the impact of the large arch sections falling back down. A portion of a crater caused by the explosive charge was seen in the surface of the floor slab. The

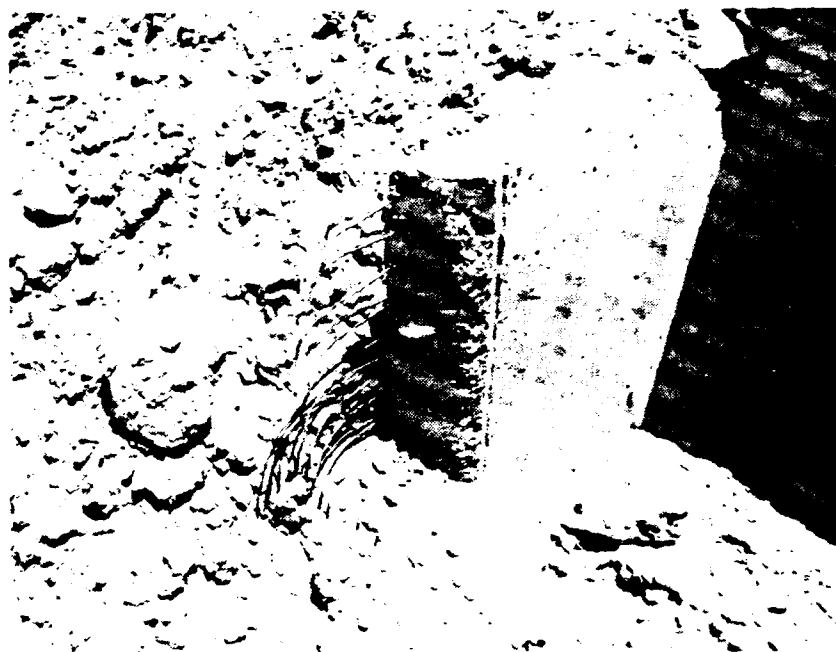


Figure 98. Exhaust port endwall failure at sidewall, PAS-3.



Figure 99. Final position of exhaust port endwall, PAS-3.

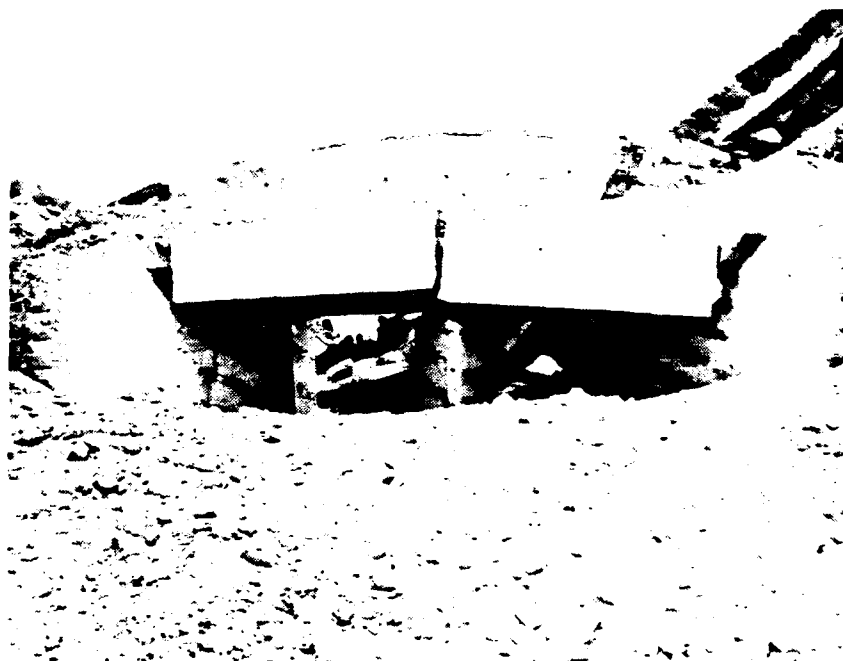


Figure 100. Posttest condition of exhaust port, PAS-3.



Figure 101. Exhaust port door, PAS-3.



Figure 102. Exhaust port door frame, PAS-3.



Figure 103. Broken dowel bars in top of the arch foundation, PAS-3.

exact size could not be determined because the corner of the front arch section hit almost at the GZ as it fell back. A large section of the arch partially covered the crater.

The joint between the floor slab and the heavily reinforced portion of the floor slab containing the door pit showed a relative separation of 25 mm of the two components. The fiber board expansion joint material was blown out of the joint for most of its length (Fig. 104).

Several large cracks were found at the left back corner of the floor slab, and the corner at the arch foundation and backwall appeared to be displaced slightly upward. Although the pattern of the cracks appeared to correspond with those observed in the PAS-1 test, no cracks were seen in the right back corner of the floor slab in the PAS-3 test.

The heavily reinforced portion of the floor slab around the door pit showed a few hairline cracks in addition to those observed following the PAS-1 test. The pre-existing cracks showed no indication of widening as a result of the PAS-3 test.

The major damage to the apron slab occurred when it was struck by the corner of the front wall and headworks section as it fell back (Fig. 105). A 30-mm wide gap was noted between the front foundation and the apron slab (Fig. 106). The gap ran the full length of the apron slab.

The front top plate of the door trench was found bent down and inward, resulting in a separation between the edge of the plate and the front foundation (Fig. 107). The area of damage was limited to the region between the door hinge pins. This damage is probably due to the forced rotation of the front door about its lower edge.

The front of the backwall foundation was still covered by the floor slab. Through a gap between the floor slab and backwall, the foundation was seen to have split vertically. The failure plane corresponded with an extended plane of the inside face of the

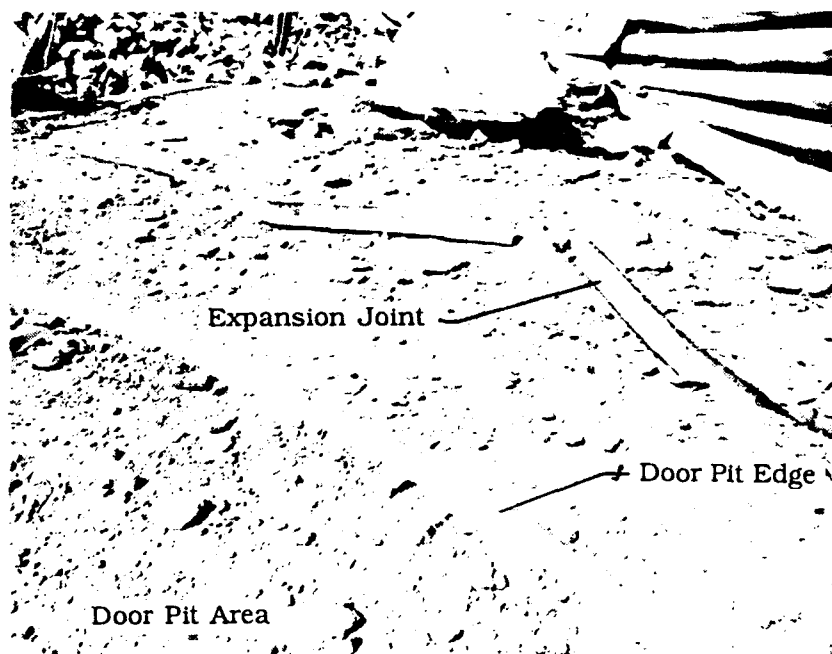


Figure 104. Floor slab expansion joint, PAS-3.



Figure 105. Damage to apron slab, PAS-3.



Figure 106. Gap between foundation and apron slab, PAS-3.



Figure 107. Top plate of door trench and front foundation, PAS-3.

backwall (Fig. 108). The top bars in the transverse stirrups crossing the plane were observed to have failed in tension at the face of the fractured concrete. There was no indication of upward movement of the backwall foundation.

A 50-mm gap was noted along the full length of the floor slab and the backwall (Fig. 109). As noted above, the backwall foundation had split, and the inside portion remained attached to the floor slab.

4.2.2 Data Obtained from Instrumentation

Data were obtained from all but one of the electronic sensors. Some baseline shifts were noted, and most of the gages mounted on the arch or front door failed at early times. No corrections have been made to data presented in this report. INBLAST and NMERI GUSH computer codes were used to make airblast predictions for selected points on the interior of the structure in the PAS-3 test. Where available these predictions are compared to the measured values.

The maximum pressure recorded inside the structure was 19.86 MPa at MN 604 (Fig. 110). This gage was located on the ceiling directly over the charge. This measurement failed at about 28 ms, probably as a result of the breakup of the structure. The INBLAST code predicted 28.8 MPa at this location. The GUSH code provided a value of 18.7 MPa.

Figures 111 and 112 show the pressures recorded on the floor near the sides of the structure in the same plane as MN 604. These two gages did not show the same degree of symmetry observed in PAS-1. Although the timing of the early peaks is similar, the magnitudes of the first two peaks are quite different. The first two peaks of MN 602 (Fig. 111) are 3.5 MPa and 5.0 MPa. This record also shows a positive baseline shift at $t = 0$. The corresponding peaks of MN 603 (Fig. 112) are 9.5 MPa and 3.4 MPa. The INBLAST and GUSH code predictions for the first peak at MN 603 were 5.0 and 9.6 MPa, respectively.

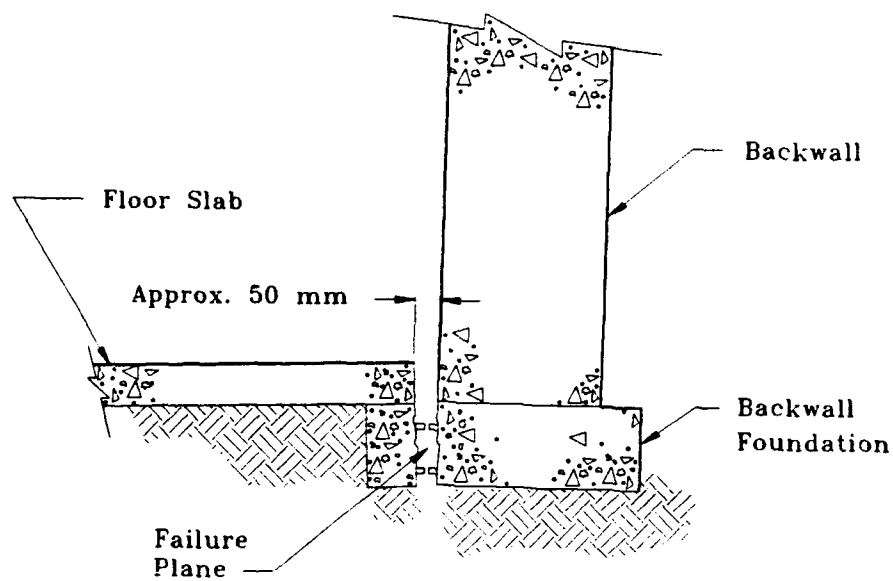


Figure 108. Section: Failure plane in backwall foundation, PAS-3.



Figure 109. Gap between floor slab and backwall, PAS-3.

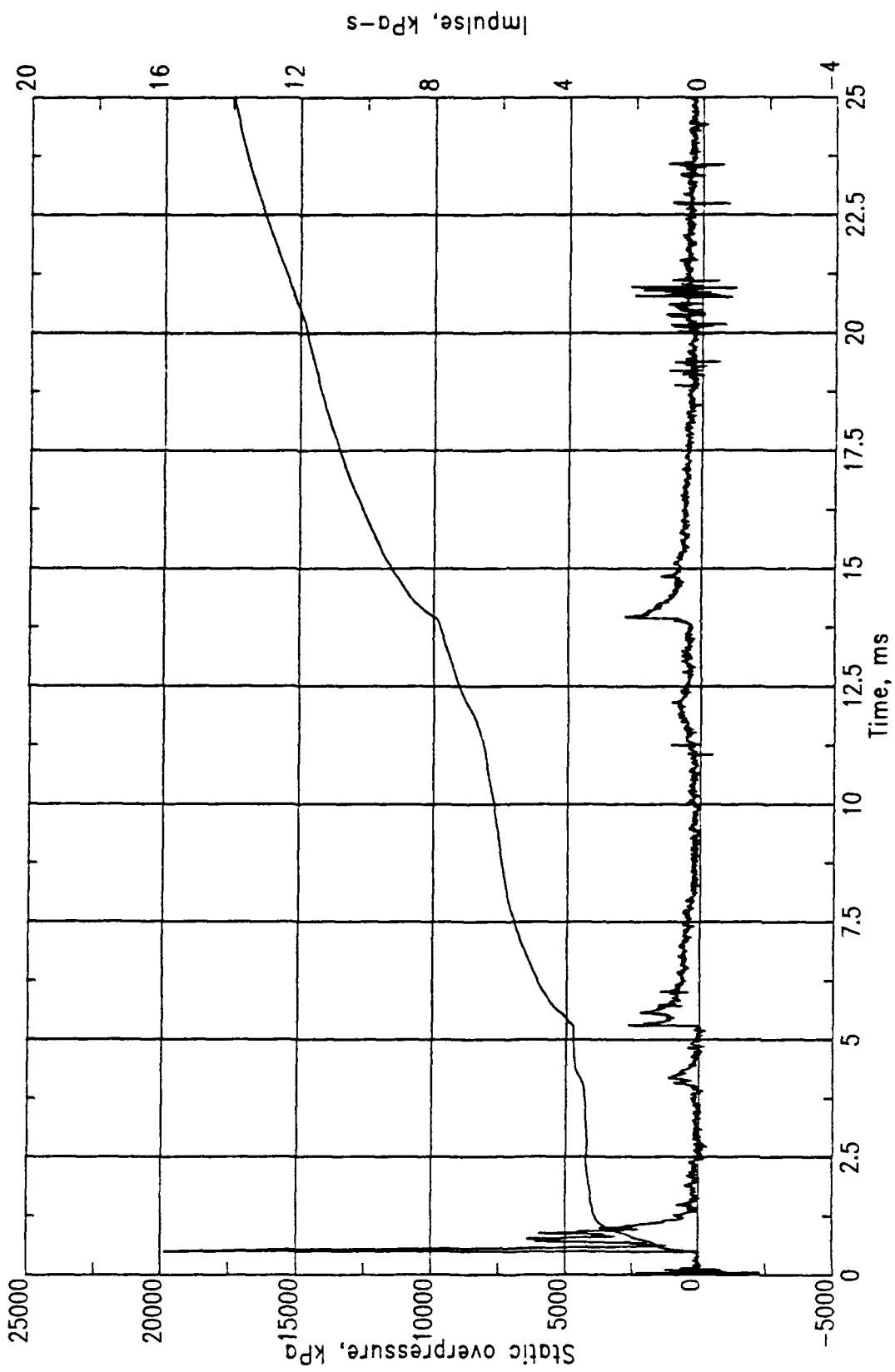


Figure 110. PAS-3, MN 0604.

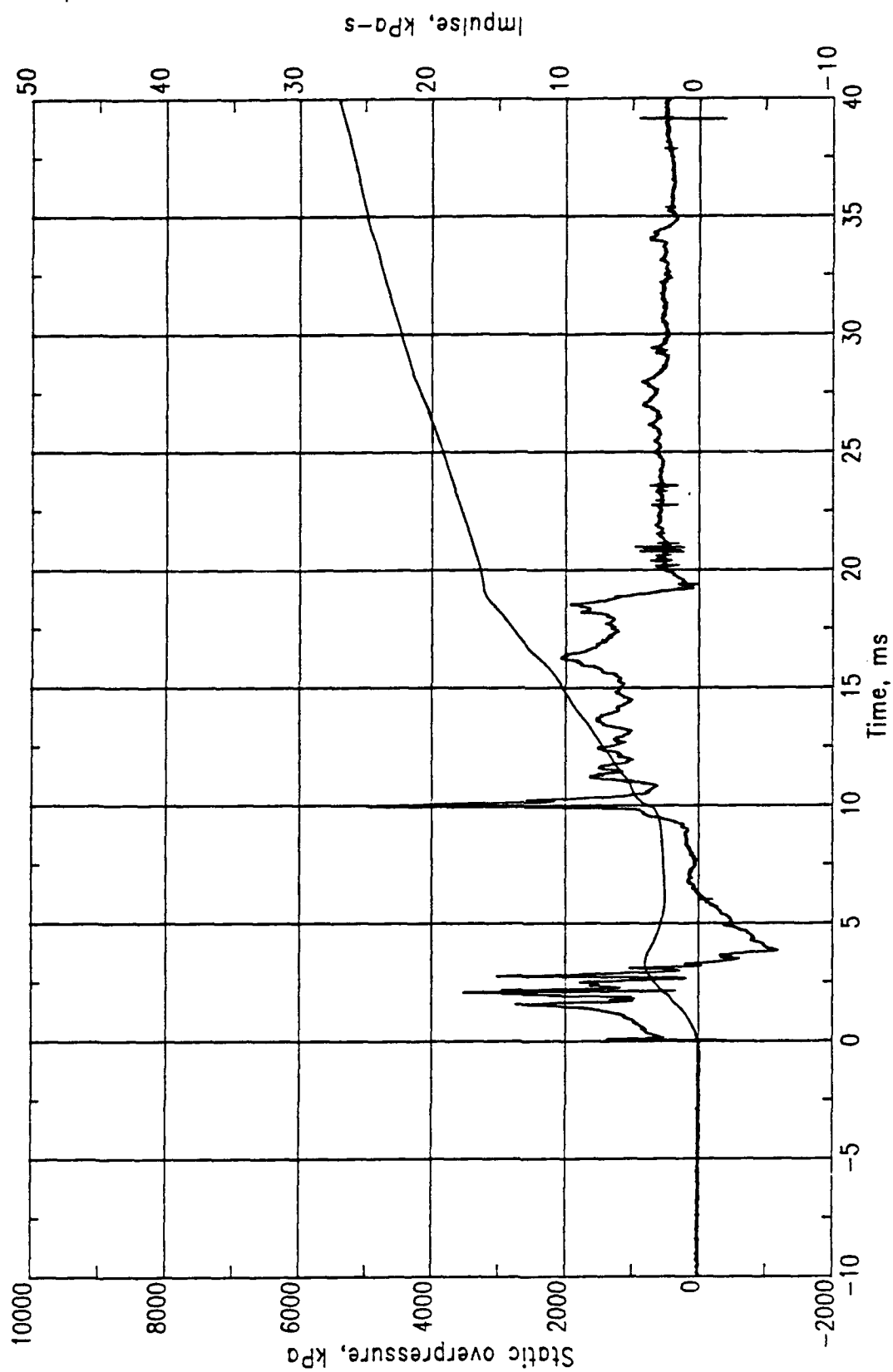


Figure 111. PAS-3, MN 0602.

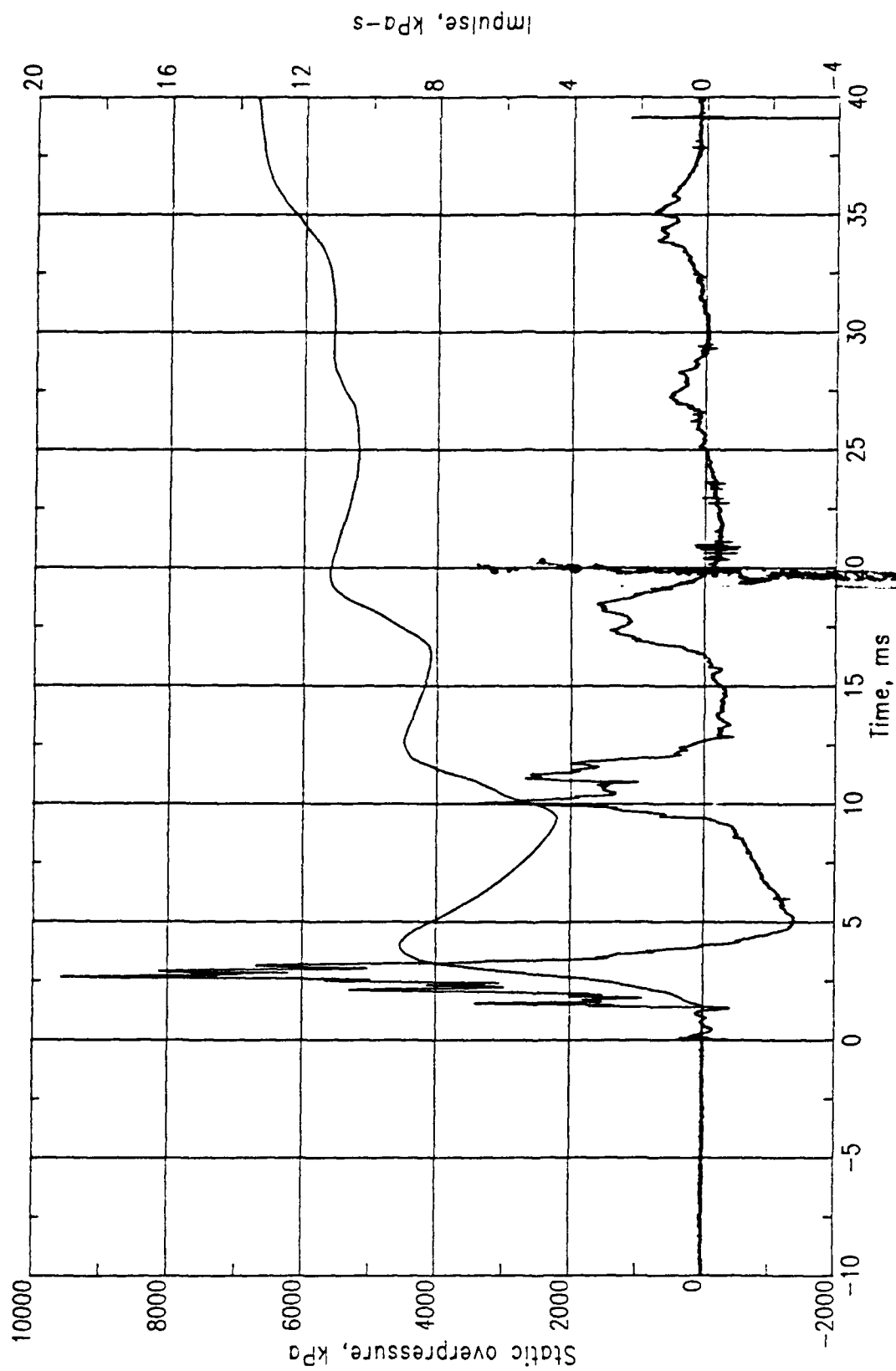


Figure 112. PAS-3, MN 0603.

The only pressure measurement made on the inside surface of the front door in the PAS-3 test was MN 402 (Fig. 113). This gage showed a peak pressure of 1.7 MPa, but a negative baseline shift at $t = 0$ makes this peak somewhat uncertain. The INBLAST code predicted 2.08 MPa at this location. Measurement Number 202 (Fig. 114) located in the backwall at about the same range and height from GZ, but off of the structure centerline, shows a peak of 1.8 MPa. The INBLAST prediction for this location was also 1.8 MPa. The spike that occurs in MN 202 at about 6 ms appears to be noise and not real data.

Measurement Number 501 (Fig. 115) located in the floor at the front corner of the shelter showed a peak pressure of 4.8 MPa. Measurement Number 102 (Fig. 116) located in the floor at the rear corner of the shelter showed a much higher peak of 7.9 MPa at the same time. Although the three peaks in both records occurred at about the same time, those of MN 102 were consistently higher than those of MN 501. The INBLAST prediction for these two locations was only 1.66 MPa.

Measurement Number 601 (Fig. 117) was made in the floor 1.85 m from GZ towards the side of the shelter. It shows a peak pressure of 3.7 MPa. The INBLAST code predicted 5.8 MPa at this location. Measurement Number 301 (Fig. 118) was made in the floor 2.84 m from GZ toward the front door. This record shows a peak of almost 5.0 MPa. However, MN 301 also shows a positive baseline shift of about 1.5 MPa at $t = 0$. If this shift were subtracted from the peak of MN 301, it would show better agreement with MN 601.

Table 8 summarizes selected peaks from interior pressure measurements. A complete set of pressure records from PAS-3 is presented in Volume III.

Although some of the free-field gage records were noisy, all but one gage provided usable data. The entire set of data appears to be internally consistent, i.e., TOAs increase and peak pressures decrease with increasing distances from GZ. All of the records were characterized by complex waveforms with multiple peaks. The records along each blast line showed many similar features, but details varied between blast

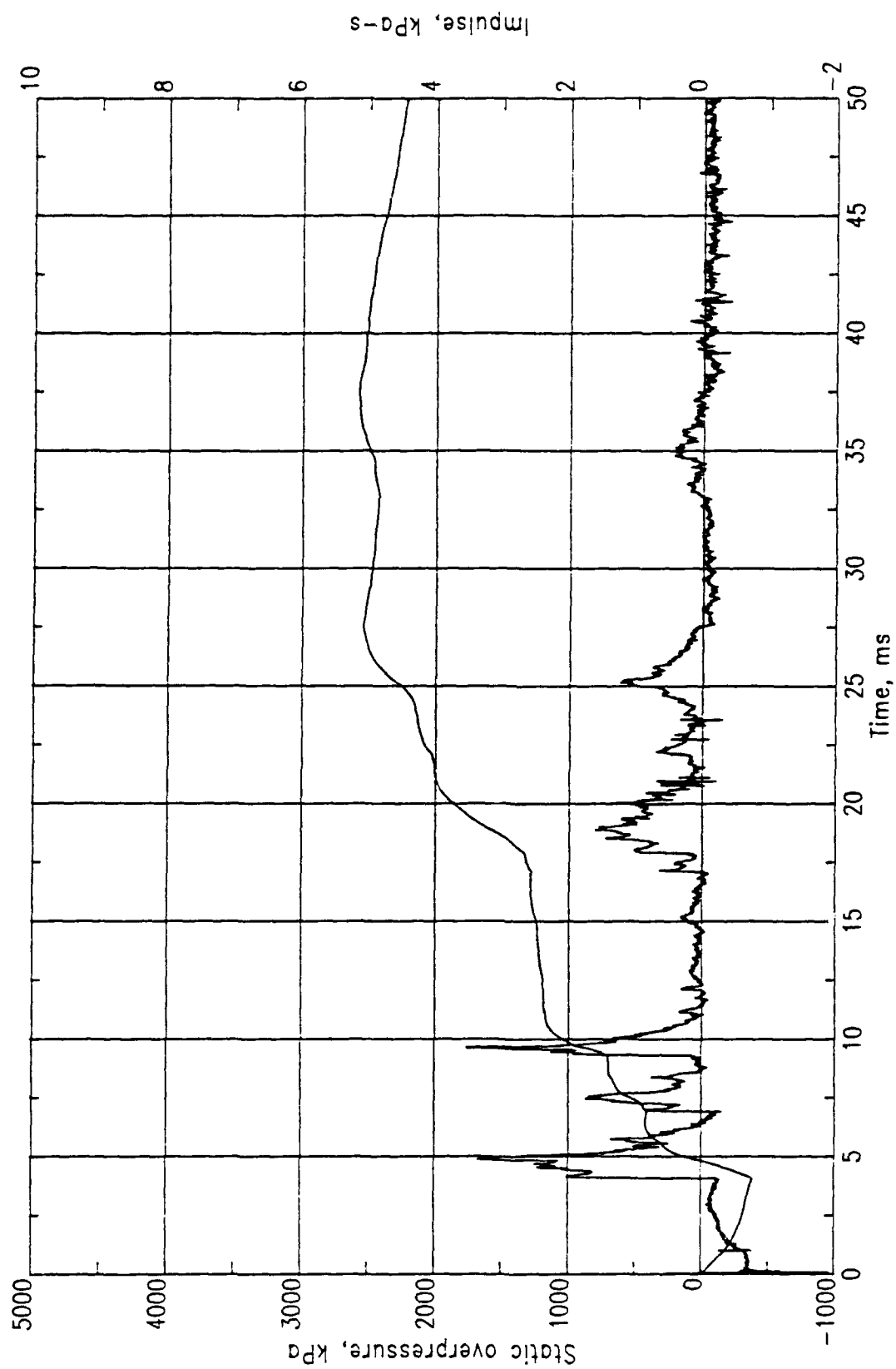


Figure 113. PAS-3, MN 0402.

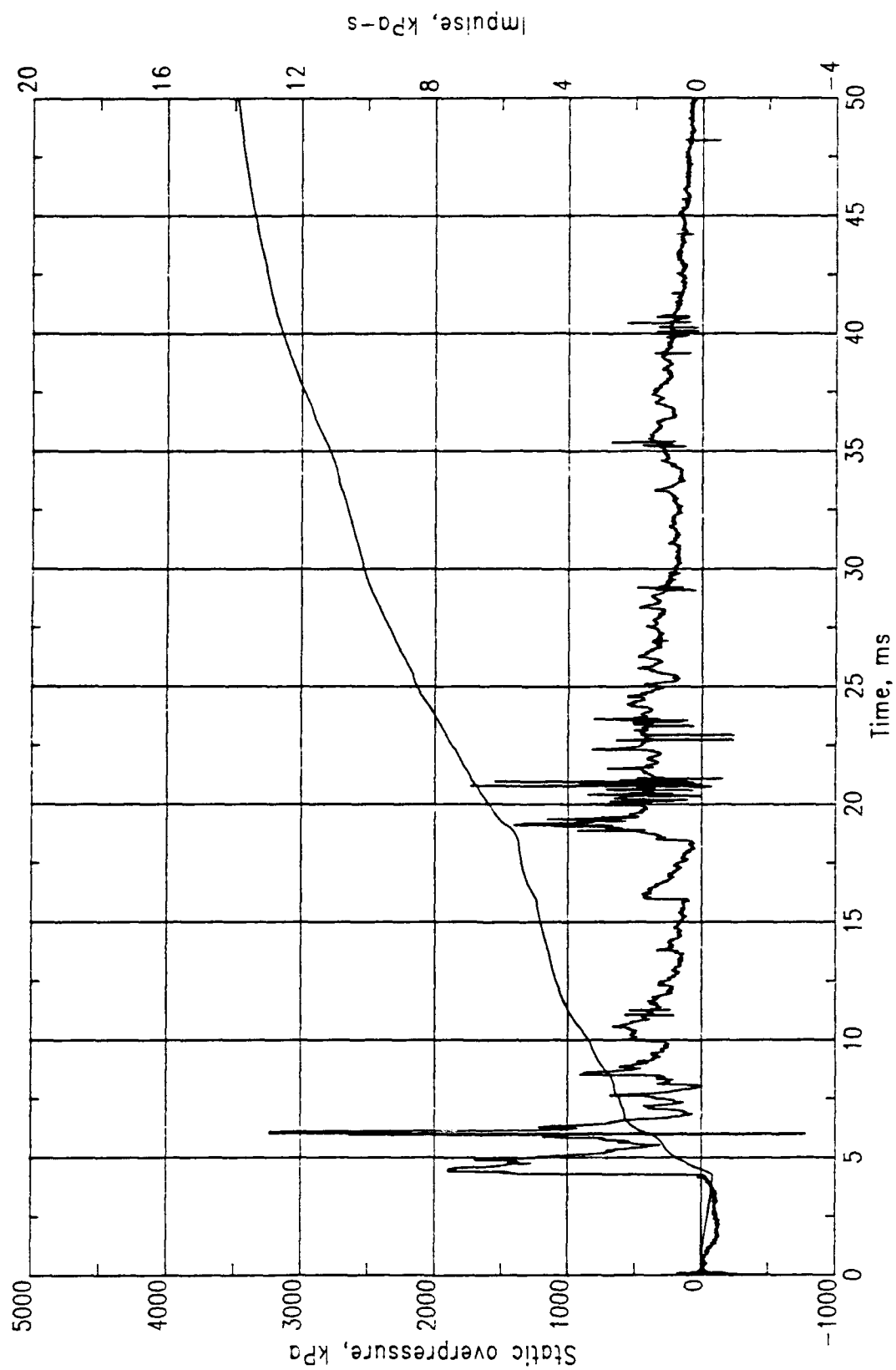


Figure 114. PAS-3, MN 0202.

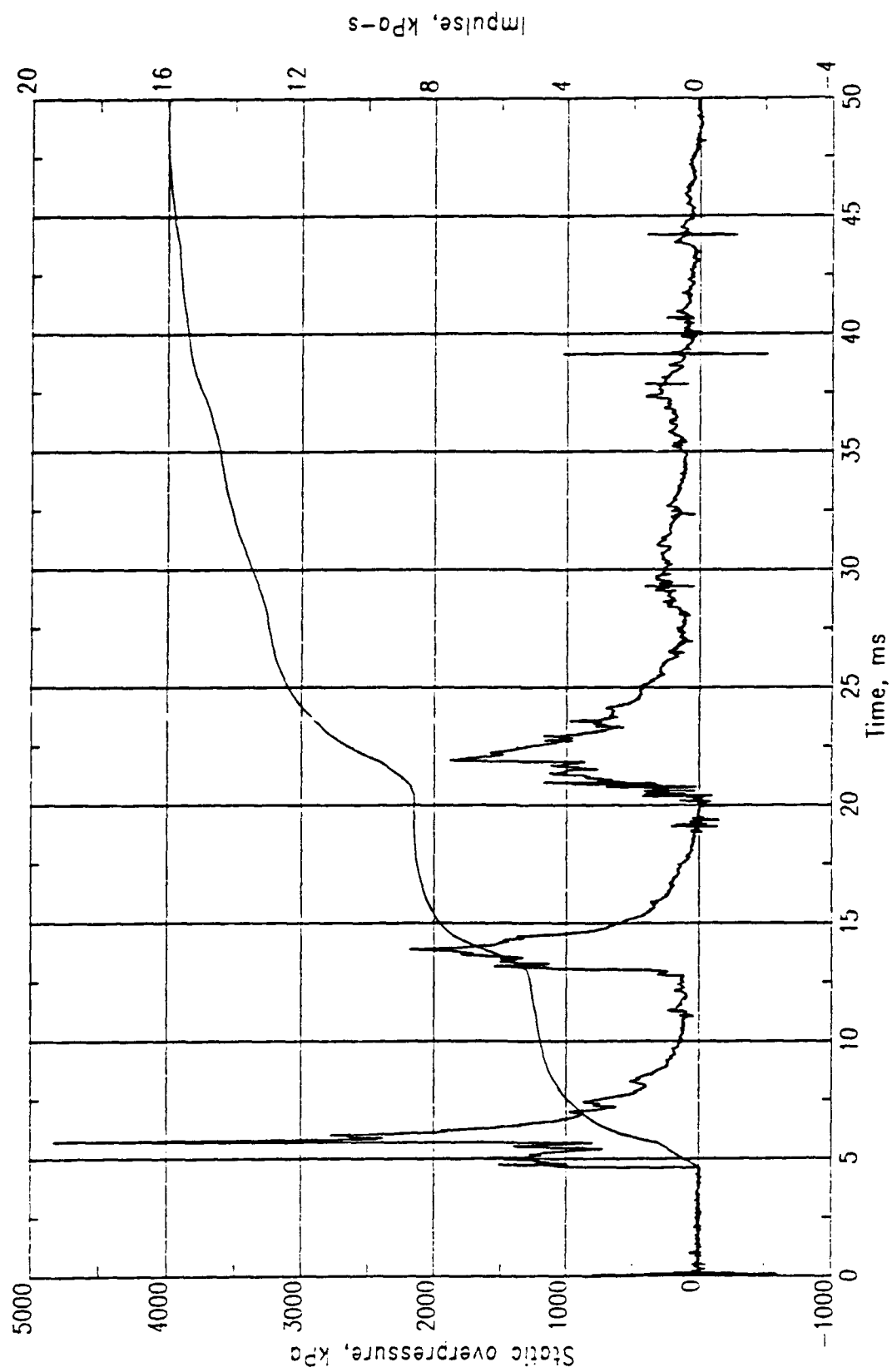


Figure 115. PAS-3, MN 0501.

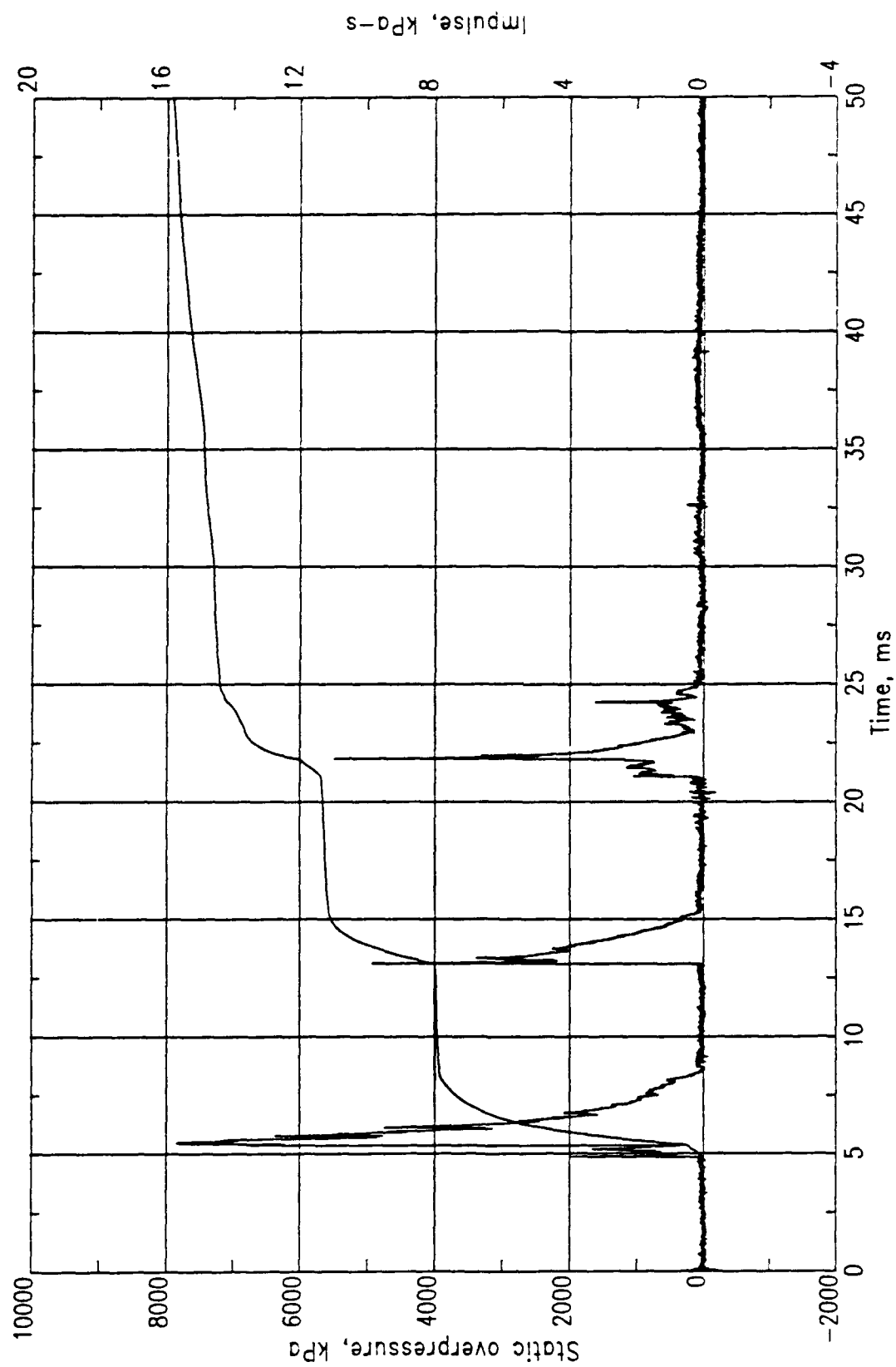


Figure 116. PAS-3, MN 0102.

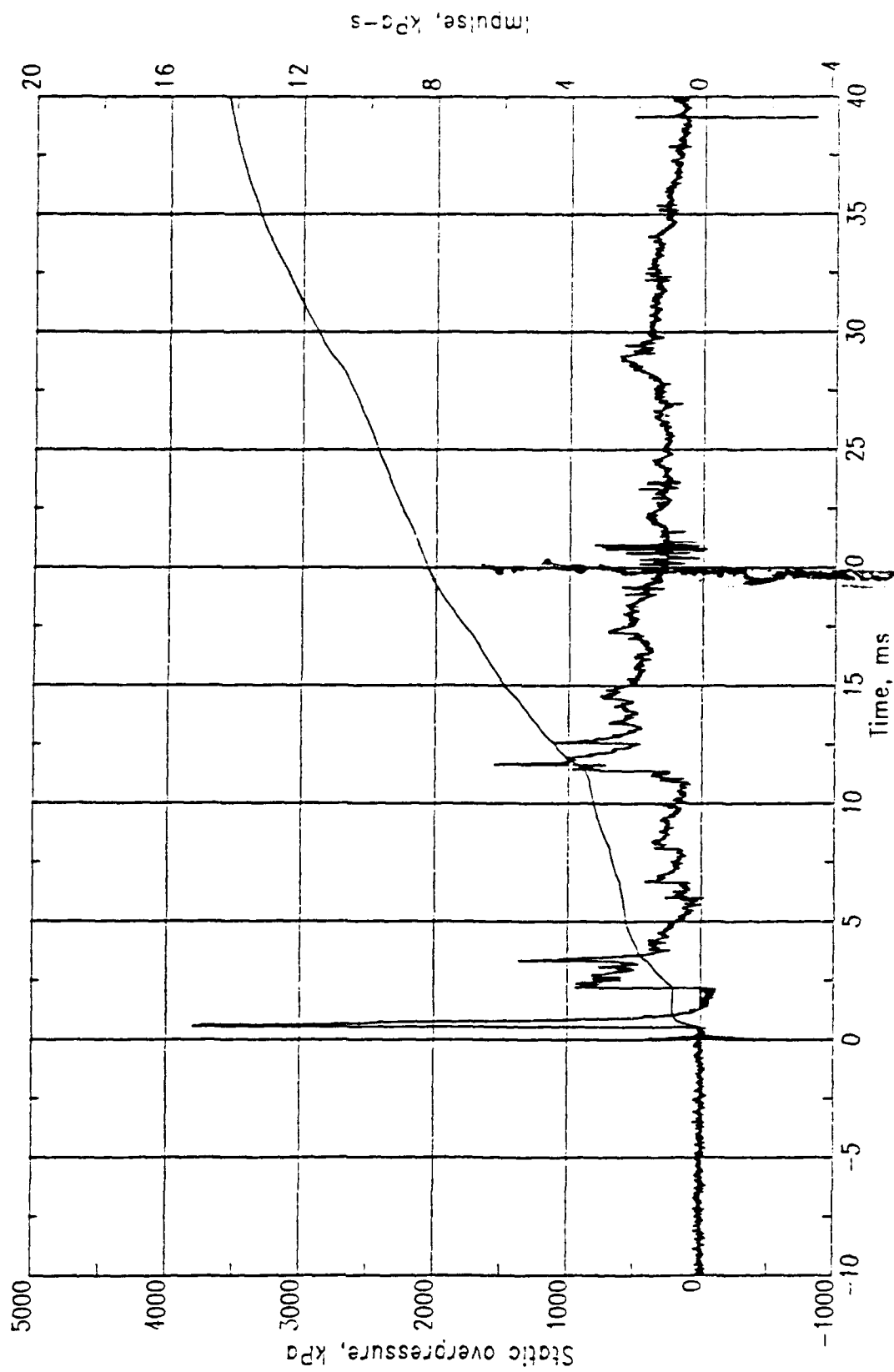


Figure 117. PAS-3, MN 0601.

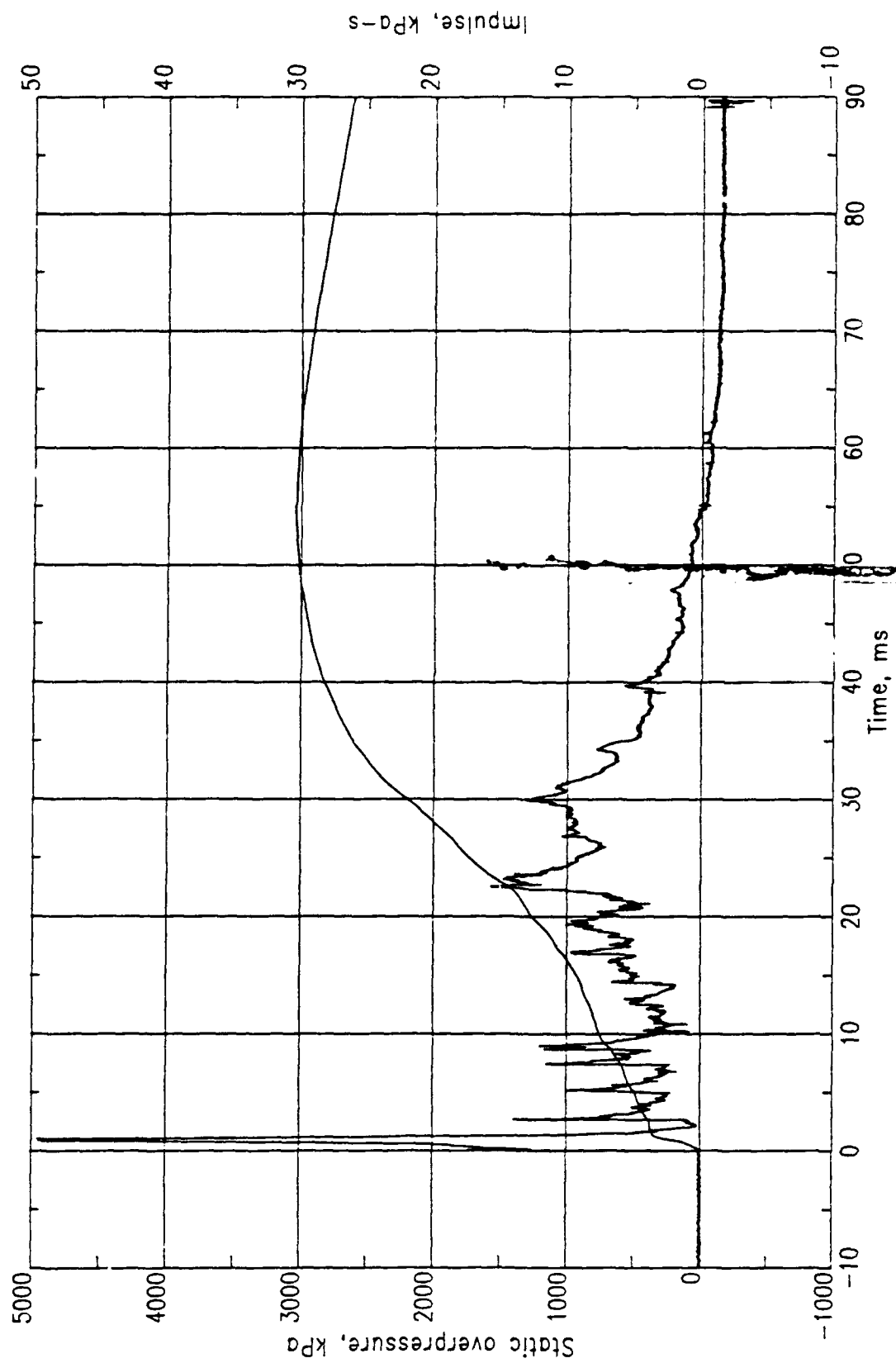


Figure 118. PAS-3, MN 0301.

Table 8. Summary of interior pressure measurements, PAS-3.

Meas. No.	Location	TOA (ms)	Peak (MPa)	Time (ms)	Peak (MPa)	Time (ms)	Peak (MPa)	Time (ms)	Peak (MPa)	Time (ms)
0101-3	SF	3.50	1.999	5.90	1.475	6.70	2.179	9.1	0.814	10.5
0102-3	SF	4.90	7.860	5.50	4.964	13.00	5.516	21.8	1.655	24.3
0202-3	BW	4.30	1.800	4.50	7.115	6.05	0.841	8.5	1.269	19.1
0301-3	SF	6.8	4.964	9.25	1.379	2.69	1.186	7.4	1.296	9.0
0302-3	SF	1.30	1.751	1.40	0.827	3.60	0.827	3.7	0.593	8.8
0303-3	SF	2.10	0.855	2.50	1.744	10.60	0.689	16.0	1.062	19.1
0402-3	FD	4.10	1.669	4.80	0.869	7.50	1.765	9.6	0.800	18.8
0501-3	SF	4.70	1.517	5.10	4.800	5.70	2.124	14.0	1.820	22.0
0601-3	SF	0.50	3.696	0.60	0.689	2.20	1.351	3.50	1.407	11.6
0602-3	SF	-	2.758	1.56	3.500	2.10	3.500	2.75	4.964	10.0
0603-3	SF	1.41	3.420	1.57	9.542	2.67	-1.379	5.1	3.378	10.0
0604-3	SC	0.49	19.857	0.50	6.371	0.77	2.758	5.3	2.758	14.0
										20.8

NOTES:

TOA range given for MN 301-3 as noise precludes exact time determination.

TOA for MN 602-3 cannot be determined. However, since 602-3 and 603-3 are symmetrical about the x and y axes,

TOA for MN 602-3 should be close to 1.41 ms, the TOA for MN 603-3.

First peak on MN 301-3 appears to have been truncated.

lines. Many of the measurements exceeded 6.9 kPa. The highest pressures were measured at the front of the structure. This is probably a result of the early failure of the front door. On the centerline of the structure at a range of 40.7 m from GZ, MN 703 recorded a peak pressure of 12.5 kPa (Fig. 119). At a range of 50.7 m from GZ, MN 704 showed the peak pressure had decreased to 8.9 kPa (Fig. 120). At the side of the structure the peak pressure had decreased to 5.9 kPa at a range of 40.0 m from GZ. At the rear of the structure the peak pressure had decreased to 6.5 kPa at a range of 30.3 m from GZ. The distribution of pressures at either side of the structure was nearly identical with only slight differences measured at the same ranges. The lowest pressures were measured at the side of the structure.

Table 9 summarizes selected peak pressures from the free-field measurements in PAS-3. A complete set of pressure records is presented in Volume III.

Only one accelerometer was mounted on the structure in the PAS-3 event. Measurement number 1601 (Fig. 121) was mounted at the crown of the arch directly over the explosive charge. It showed a peak radial acceleration of 4500 g. Integrated over the first 5 ms, this record shows a velocity of 8.0 m/s. This measurement failed at 27.5 ms. A WES self-recording accelerometer installed at the same location recorded a peak radial acceleration of 5500 g. The peak velocity obtained from integration of the WES gage record was 12.5 m/s. Data obtained from high-speed photography appear to support the higher velocity. Table 10 summarizes selected peak accelerations from MN 1601. The record from 1601 is also presented in Volume III.

Because of the severe damage to the front door, the data obtained from strain gages on the door were of limited usefulness. Individual gages failed at times varying from 11.5 to 100 ms. The peak strains recorded varied up to almost 50,000 microstrain. The type of gages used on the door is believed to be linear up to about 20,000 microstrain. Table 11 summarizes selected peak strains measured on the door. A complete set of strain records is presented in Volume III.

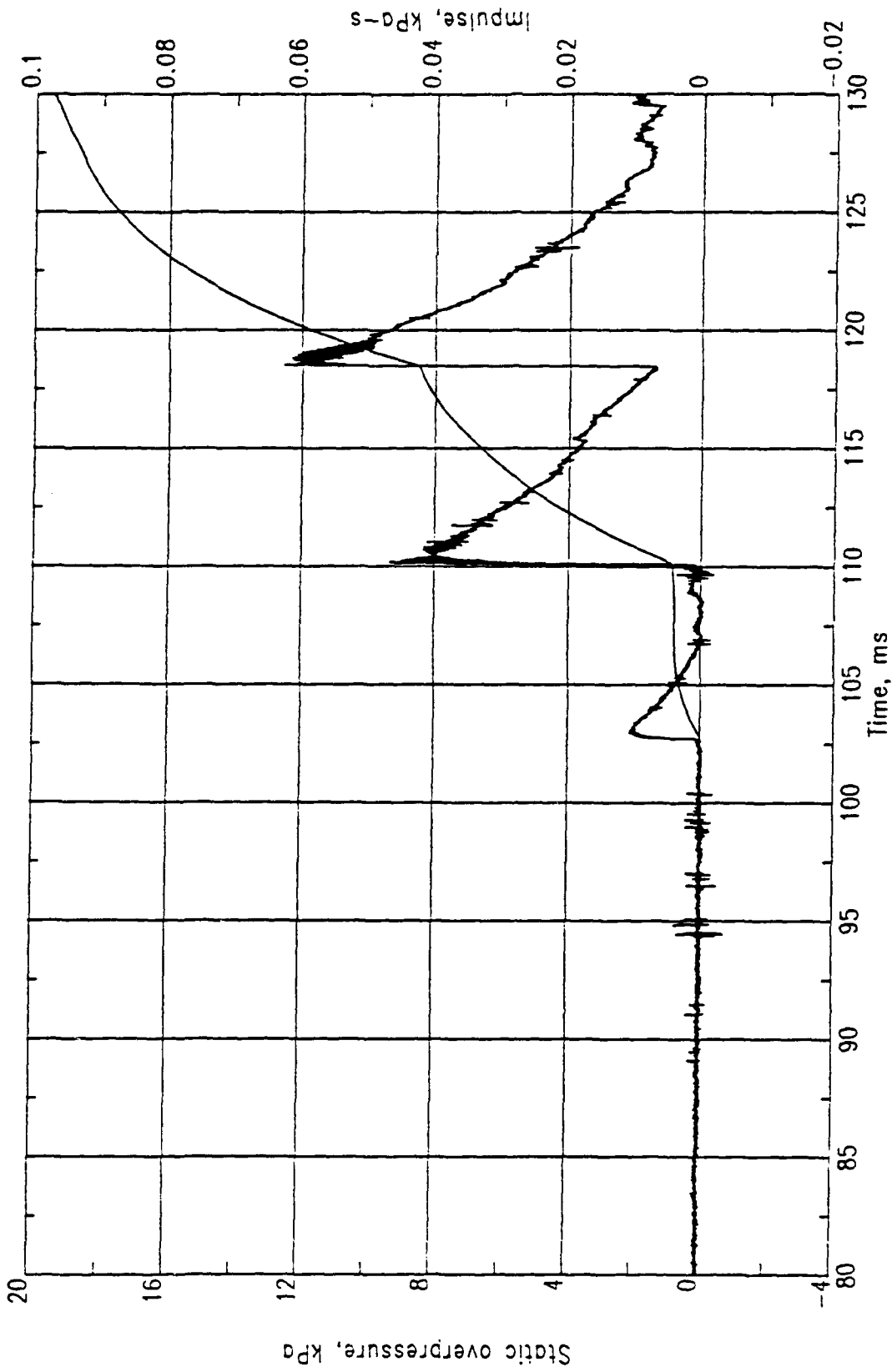


Figure 119. PAS-3, MN 0703.

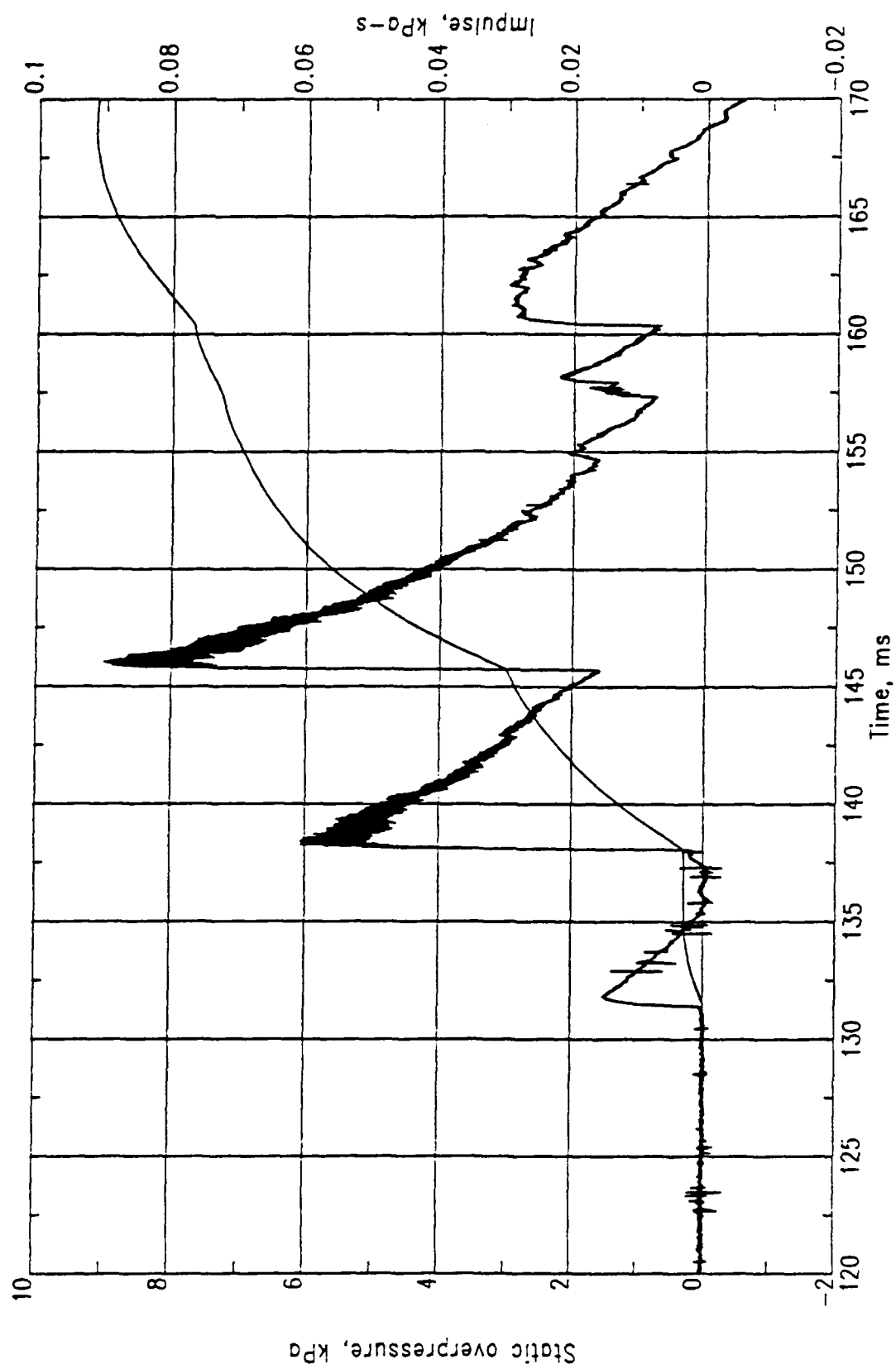


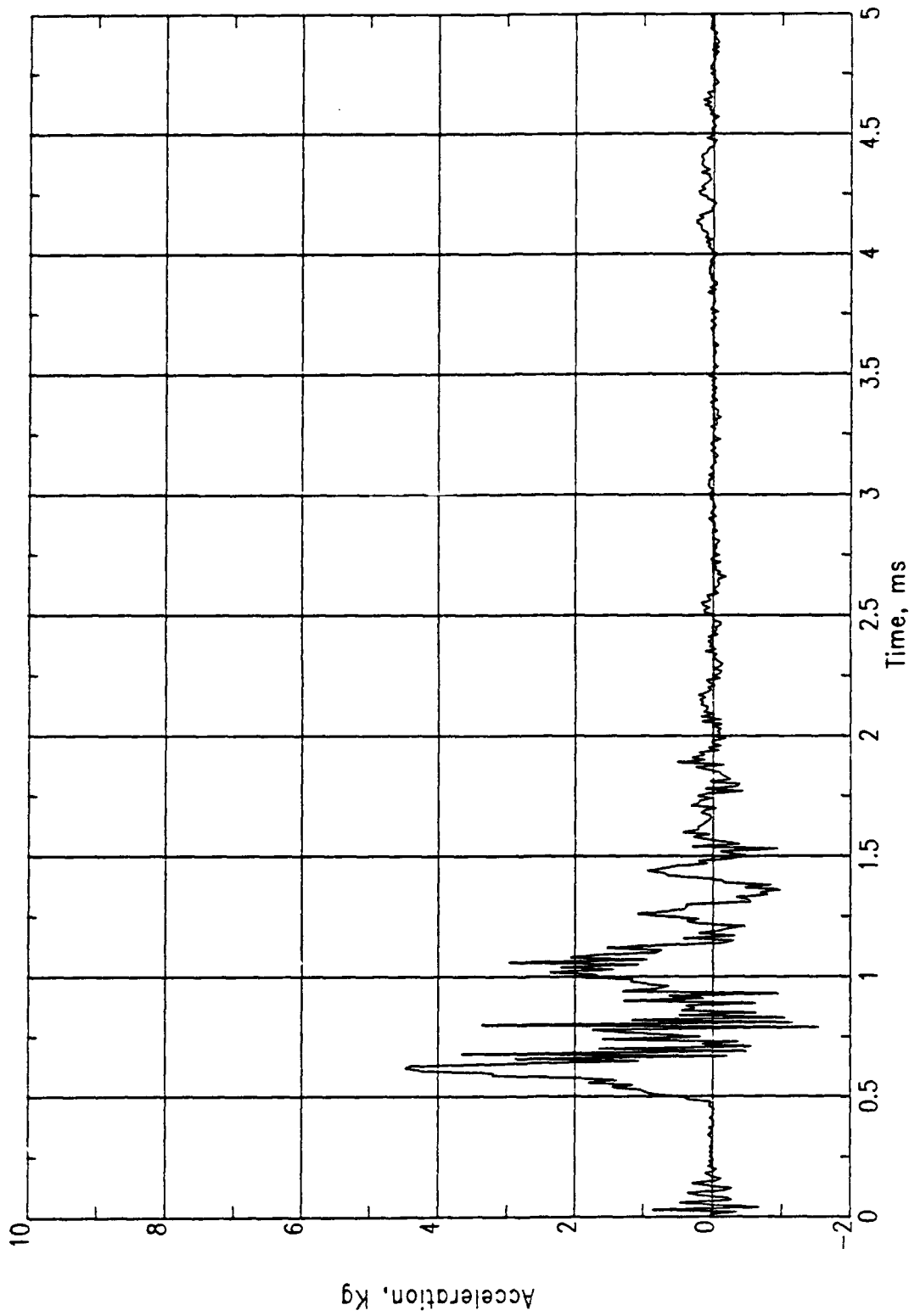
Figure 120. PAS-3, MN 0704.

Table 9. Summary of free-field measurements, PAS-3.

Meas. No.	Location	TOA (ms)	Peak (kPa)	Time (ms)	Peak (kPa)	Time (ms)	Peak (kPa)	Time (ms)	Peak (kPa)	Time (ms)
701-3	FF	31.25	15.858	31.3	47.436	44.5	34.474	53.8	27.166	67.4
702-3	FF	73.7	3.447	73.8	14.893	82.3	18.754	91.5	9.653	104.3
703-3	FF	102.8	2.068	103.0	9.377	110.2	12.549	118.5	5.171	132.0
704-3	FF	131.4	1.517	131.8	6.067	138.4	8.963	145.8	2.896	160.6
705-3	FF	161.6	0.896	162.4	3.654	168.3	5.861	175.4	2.068	191.2
706-3	FF	34.8	8.963	47.1	11.032	53.0	21.236	59.2	12.411	74.0
707-3	FF	87.7	6.343	90.6	11.583	96.8	4.137	106.7	6.895	112.4
708-3	FF	106.8	5.171	118.7	9.101	124.1	2.620	134.4	5.378	140.8
709-3	FF	136.0	3.585	147.7	5.930	152.2	2.413	161.5	3.447	169.6
710-3	FF	26.0	6.688	56.0	10.204	64.0	3.792	82.5	4.275	86.4
711-3	FF	117.0	3.310	132.0	5.998	138.7	5.861	140.6	2.413	159.0
712-3	FF	139.0	2.413	161.2	4.137	167.2	4.068	169.0	1.793	187.2
713-3	FF	29.0	8.274	44.8	14.341	51.3	6.757	53.0	7.171	57.0
714-3	FF	38.5	4.688	52.0	7.171	62.1	5.309	73.0	3.861	84.0
715-3	FF	-	-	-	-	-	-	-	-	-
716-3	FF	29.2	12.962	40.6	9.377	49.5	13.100	56.0	11.376	60.5
717-3	FF	69.4	4.137	80.0	4.137	89.0	6.550	95.2	5.240	101.9
718-3	FF	99.0	2.758	109.5	3.103	118.4	3.654	124.3	3.378	131.0
719-3	FF	128.0	1.724	138.6	1.586	147.5	2.551	153.5	2.551	159.8
720-3	FF	26.0	5.654	34.5	3.310	44.1	9.929	67.6	7.722	84.0
721-3	FF	138.5	1.103	139.4	1.655	156.2	3.861	164.2	2.137	184.0

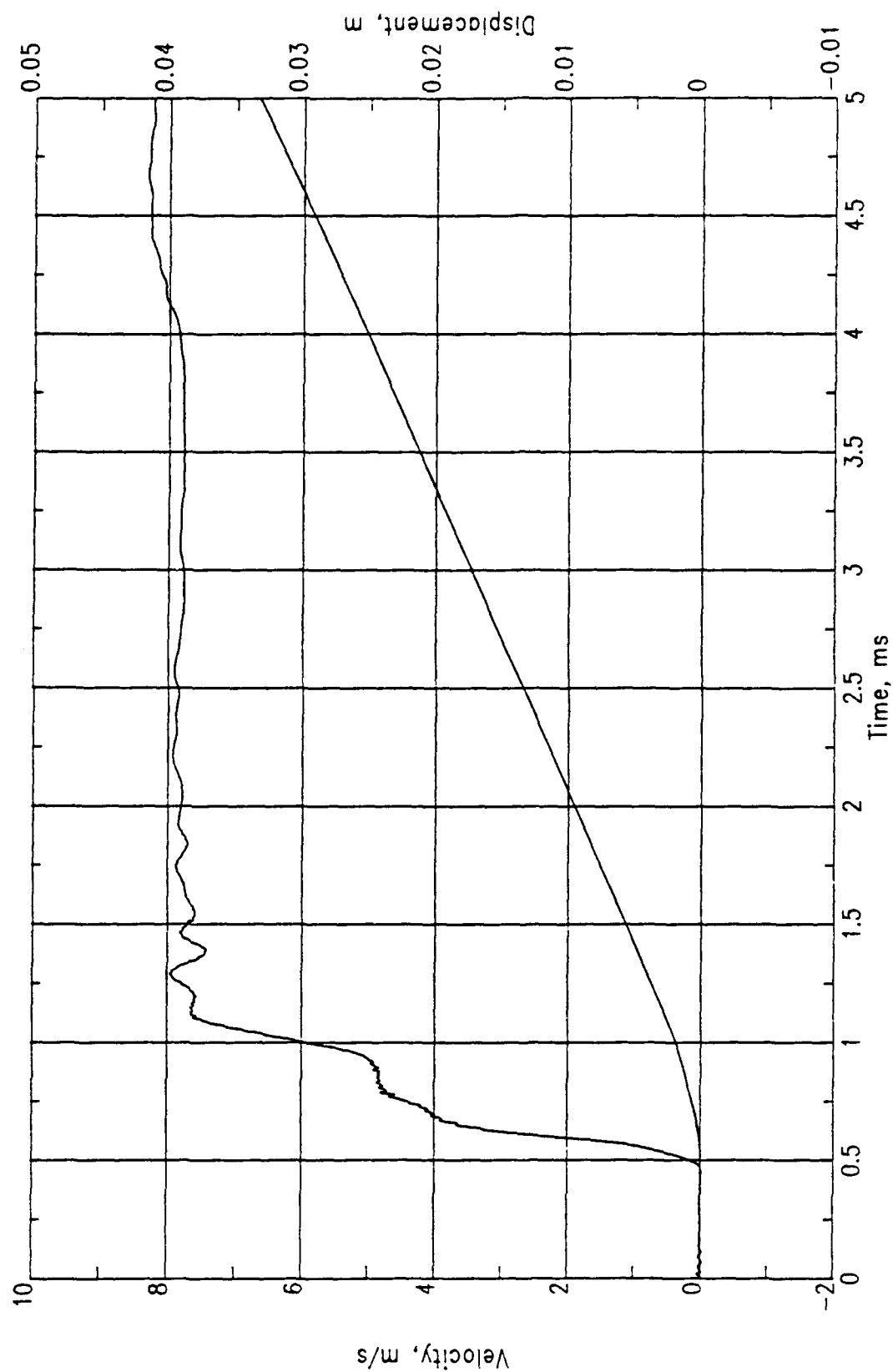
NOTE:

Due to an apparent malfunction, no data were recorded for MN 715-3.



(a) Acceleration.

Figure 121. PAS-3, MN 1601.



(b) Velocity and displacement.

Figure 121. Concluded.

Table 10. Summary of exterior acceleration measurements, PAS-3.

Meas. No.	Location	TOA (ms)	Peak (g)	Time (ms)	Peak (g)	Time (ms)	Peak (g)	Time (ms)
1601-3	SR	0.48	4440	0.61	-1520	0.79	2920	1.06
							1040	1.26
							920	1.44

Table 11. Summary of strain measurements, PAS-3

Meas. No.	Location	TOA (ms)	Peak (msn)	Time (ms)	Peak (msn)	Time (ms)	Peak (msn)	Time (ms)	Peak (msn)	Time (ms)
3401-3	FD	4.20	-664	4.90	960	6.50	-340	6.68	-1260	9.66
3402-3	FD	4.50	300	4.80	-3400	11.90	-6400	14.10	-200	36.00
3403-3	FD	4.00	-5000	5.00	-1200	5.45	-1300	6.32	<-27000	11.30
3404-3	FD	4.50	-620	5.00	>34000	12.00	-	-	-	-
3405-3	FD	4.20	-13000	5.10	-3700	5.71	-14000	6.23	-8500	6.82
3406-3	FD	4.50	-1060	5.30	>24000	12.00	-	-	-	-

NOTES:

A "greater than" sign indicates MN 3403, MN 3404, and MN 3406 may have temporarily bandedged.

msn = microstrain

4.2.3 Rock Rubble Berm

A portion of the rock rubble berm adjacent to the arch was blown upward and out during the test (Fig. 122). The rocks remaining in the berm were relatively undisturbed by the test. High-speed photography shows that the rocks at the sides of the structure were thrown out at trajectories of 75 deg or less. Individual pieces of rock were a little difficult to follow, but in a few instances their early upward velocities were on the order of 14 to 15 m/s. Ground-impact velocities of pieces of rock rubble varied from 7.5 to 11.5 m/s.

The rock berm along the left front side of the structure in the vicinity of the personnel entrance appeared to have been blown or pushed away to the front and side, probably resulting from the failure of the vestibule and the personnel door at this location. A more complete discussion of the distribution of the rock from the berm is presented next.

4.2.4 Debris Distribution

Three general classes of materials were included in the posttest debris distribution survey for PAS-3. The first class included those items placed at various locations on the surface of the shelter, e.g., SIFCON and aluminum cubes, the WES gages, and photo poles. The second class included pieces of the model structure, and the last was of rock from the rock rubble berm placed at the sides of the structure. The following paragraphs present data collected on the distribution of these three classes of debris in the PAS-3 test. Interpretation of the data in terms of quantity-distance criteria is beyond the scope of this report.

All coordinates are referenced to the Structure Coordinate System (SCS) (Fig. 123). All ranges and azimuths are given in the plane of the top surface of the floor slab of the structure and referenced from the surface GZ of the charge (Fig. 124).

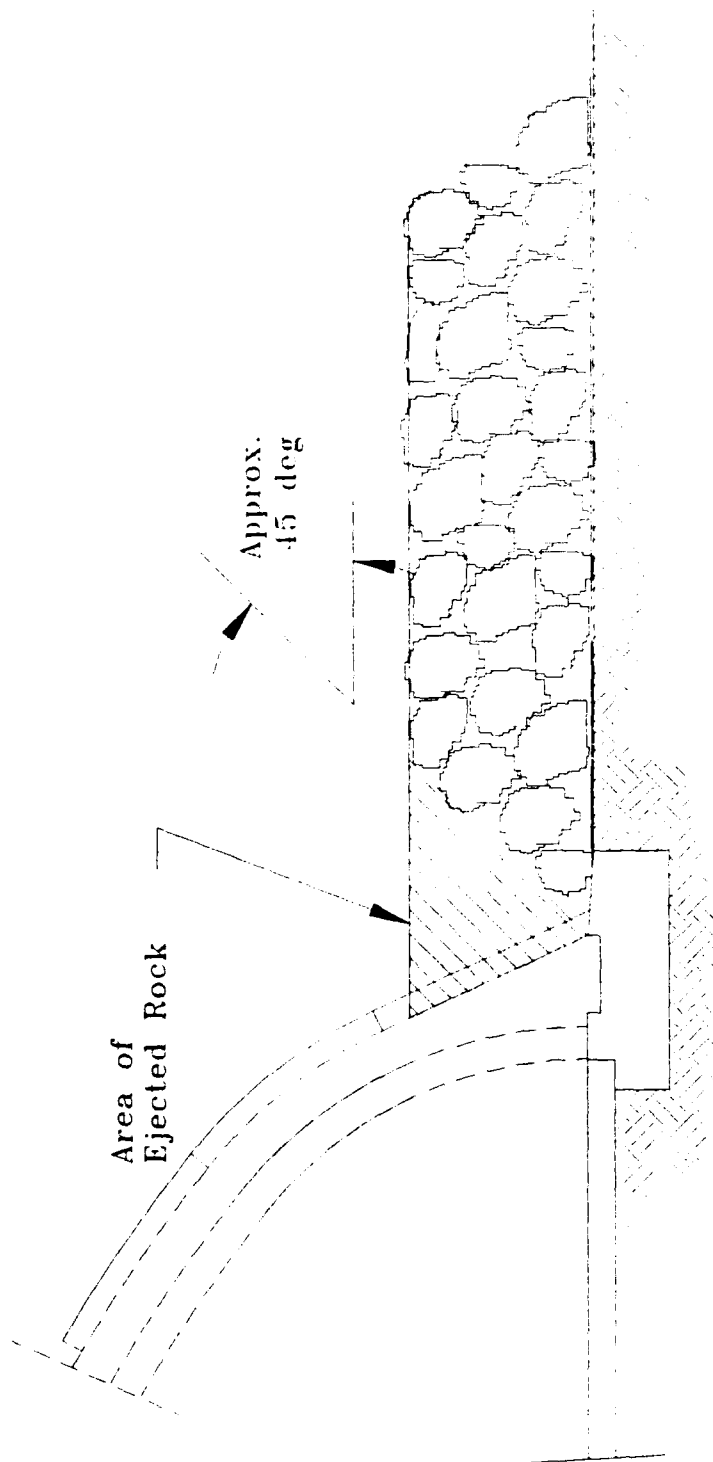
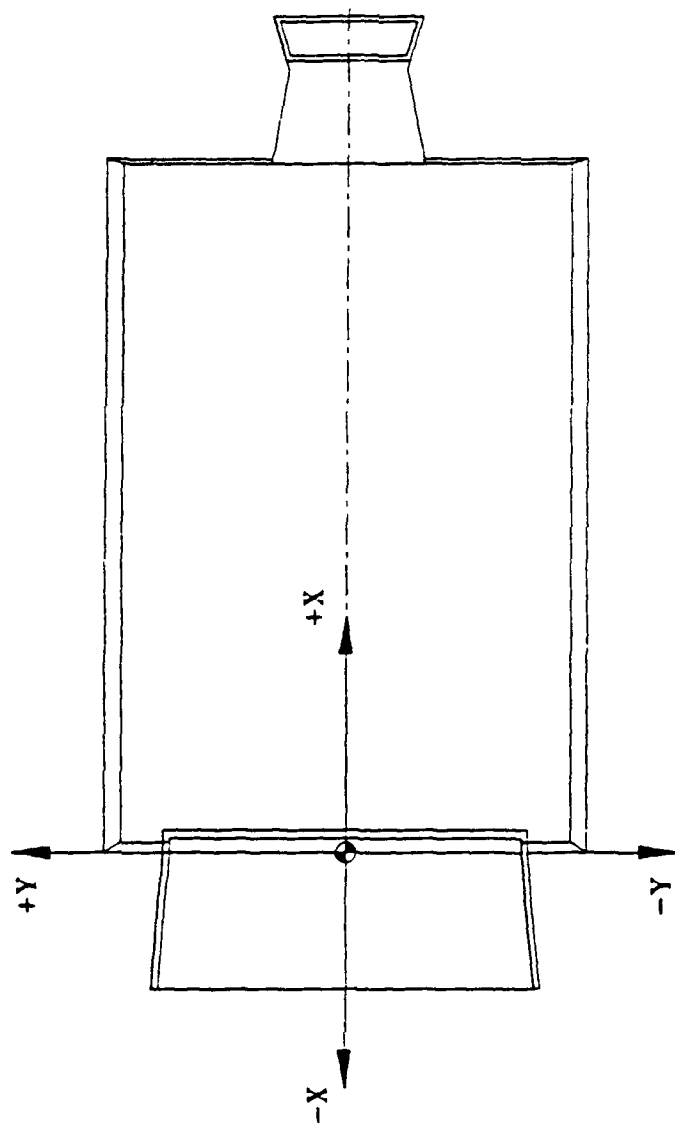
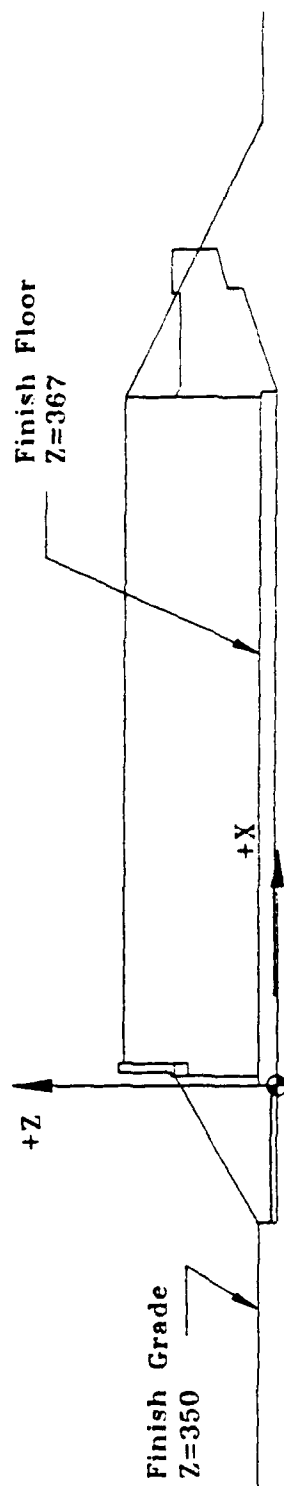


Figure 122. Section: Rock rubble berm, PAS-3.



(a) Plan.



(b) Elevation.

Figure 123. Structure coordinate system, PAS-3.

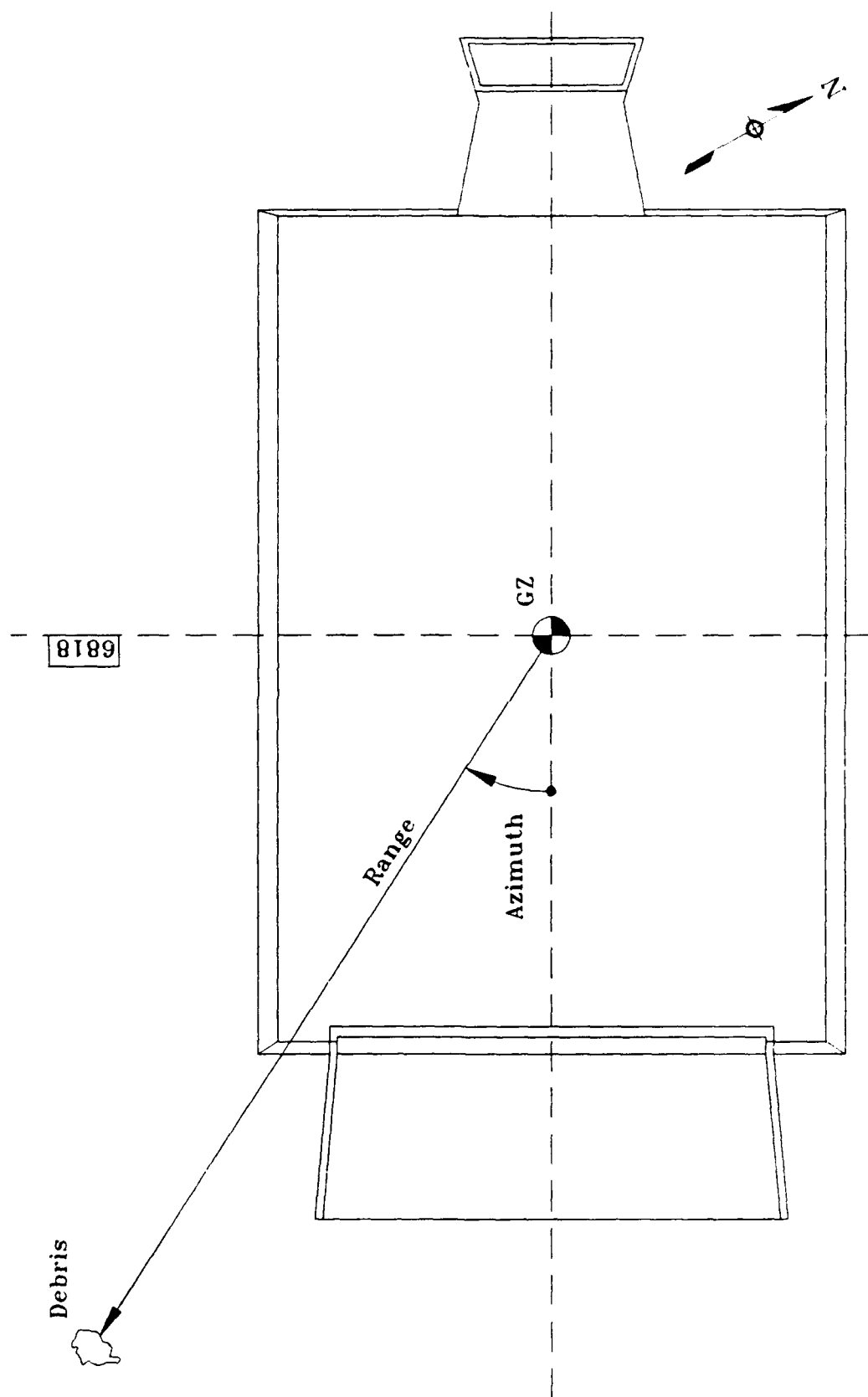


Figure 124. Range and azimuth reference system, PAS-3.

Tables 12 and 13 present the pretest and posttest coordinates of the SIFCON and aluminum cubes. Tables 14 and 15 present the pretest and posttest coordinates of the photo poles and WES gages.

The distribution of structural debris was of great significance in this test series and a major effort was expended in collecting these data. As an aid in identifying the origin of a piece of concrete debris from the arch, the concrete for the arch was dyed four different colors as illustrated in Figure 125a. In order to define further the source of debris from the arch, colored plastic beads were mixed with the concrete in four sections along the length of the arch. The faceted beads were 10 mm in diameter. They were added to the concrete at a rate not exceeding 0.5 percent by volume. A different color of bead was used in each quadrant (Fig. 125b).

Two different procedures were used to recover, identify, and measure concrete debris. The first method was the collection of the concrete debris from selected 5-deg sectors. Following the test, the boundaries of four circular sectors, each having a 5-deg angle and its center at GZ, were laid out on the testbed (Fig. 126). Beginning at 10 m from the GZ, and for every 5-m wide segment of the sector out to 100 m, all concrete debris with a maximum dimension less than about 50 mm was raked up and placed in a bucket. Larger debris was left in place. The material in each bucket was then passed through a series of screen sieves. After the material was sieved, all soil, sticks, stones, and other debris passing through the 10 mm sieve were discarded, and the pieces remaining on each sieve were counted. If the number of pieces on a sieve was estimated to be more than 200, a representative group of pieces was selected, weighed, and counted. The total number of pieces on the sieve was then calculated using the average weight of the representative group. Tables 16 through 19 summarize the data for four of the sectors. No debris was found in the 45-deg sector. A complete set of sieve data is presented in Volume III.

The second debris collection procedure included the location and collection of all pieces of debris with dimensions between 50 and 500 mm. After the smaller debris was collected from the four 5-deg sectors virtually all the pieces of debris in this size range

Table 12. Pretest and posttest locations of SIFCON cubes, PAS-3.

I.D. MARK	STARTING LOCATION COORDINATES			FINAL LOCATION COORDINATES		
	X (mm)	Y (mm)	Z (mm)	X (mm)	Y (mm)	Z (mm)
SC1	1260	0	2987	-3942	-1508	350
SC2	1260	1612	2752	-6253	-39	350
SC3	1260	2678	2311	-4046	9310	350
SC4	1260	3492	1777	321	14608	350
SC5	1260	3985	1188	522	9114	350
SC6	4060	0	2987	1538	4147	350
SC7	4060	1482	2789	-6464	14057	350
SC8	4060	2500	2403	-8205	16160	350
SC9	4060	3511	1761	-5040	16923	350
SC10	4060	3978	1201	1917	22703	350
SC11	7010	0	2987	1763	3755	350
SC12	7010	1674	2733	10522	22998	350
SC13	7010	2607	2349	11916	23689	350
SC14	7010	3531	1746	11057	40050	350
SC15	7010	3967	1223	5285	30075	350
SC16	9650	0	2987	9450	-1592	350
SC17	9650	1569	2764	12153	8710	350
SC18	9650	2589	2358	14273	10819	350
SC19	9650	3511	1761	12196	30827	350
SC20	9650	3952	1249	9313	24401	350
SC21	12310	0	2987	24680	-6700	350
SC22	12310	1588	2759	14902	1155	350
SC23	12310	2598	2353	15330	17981	350
SC24	12310	3550	1730	15964	25231	350
SC25	12310	3990	1179	13893	19027	350

Table 13. Pretest and posttest locations of aluminum cubes, PAS-3.

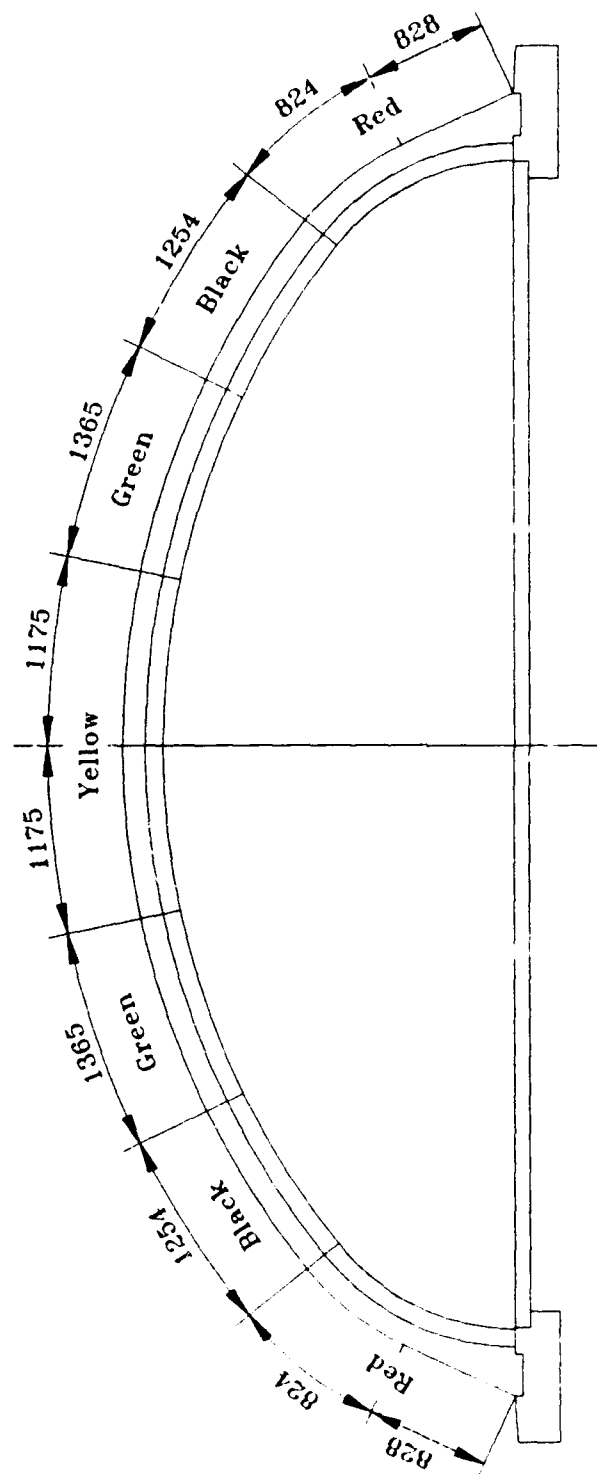
I.D. MARK	STARTING LOCATION COORDINATES			FINAL LOCATION COORDINATES		
	X (mm)	Y (mm)	Z (mm)	X (mm)	Y (mm)	Z (mm)
AL1	850	0	2987	-4155	2505	350
AL2	850	1559	2767	-7268	-2489	350
AL3	850	2564	2371	-8782	1086	350
AL4	850	3514	1759	-9330	7163	350
AL5	850	4020	1118	1837	14142	350
AL6	3875	0	2987	1770	3531	350
AL7	3875	1559	2767	-8625	10938	350
AL8	3875	2564	2371	-7433	11757	350
AL9	3875	3514	1759	-6376	12677	350
AL10	3875	4020	1118	-3759	11792	350
AL11	6900	0	2987	-13105	-52787	350
AL12	6900	1559	2767	4007	19230	350
AL13	6900	2564	2371	2237	24978	350
AL14	6900	3514	1759	12427	20706	350
AL15	6900	4020	1118	7484	24122	350
AL16	9525	0	2987	13333	-10509	350
AL17	9525	1559	2767	10595	7766	350
AL18	9525	2564	2371	13882	7311	350
AL19	9525	3514	1759	17520	10657	350
AL20	9525	4020	1118	10776	28728	350
AL21	12150	0	2987	Not Found		
AL22	12150	1559	2767	13014	-1028	350
AL23	12150	2564	2371	18088	2482	350
AL24	12150	3514	1759	18707	7971	350
AL25	12150	4020	1118	9543	13201	350

Table 14. Pretest and posttest locations of photo poles, PAS-3.

I.D. MARK	STARTING LOCATION COORDINATES			FINAL LOCATION COORDINATES		
	X (mm)	Y (mm)	Z (mm)	X (mm)	Y (mm)	Z (mm)
PP1	1060	-2511	2398	1629	-2038	350
PP2	1000	0	2987	Not Found		
PP3	940	1502	2783	5712	-378	350
PP4	1060	2511	2398	Not Found		
PP5	940	3810	1461	6816	809	350
PP6	6560	-2511	2398	Not Found		
PP7	6500	0	2987	9715	-22156	350
PP8	6440	1502	2783	6717	-75041	350
PP9	6560	2511	2398	Not Found		
PP10	6440	3810	1461	Not Found		
PP11	12060	-2511	2398	Not Found		
PP12	12000	0	2987	7744	262	350
PP13	11940	1502	2783	8207	1925	350
PP14	12060	2511	2398	Not Found		
PP15	11940	3810	1461	8800	4192	350

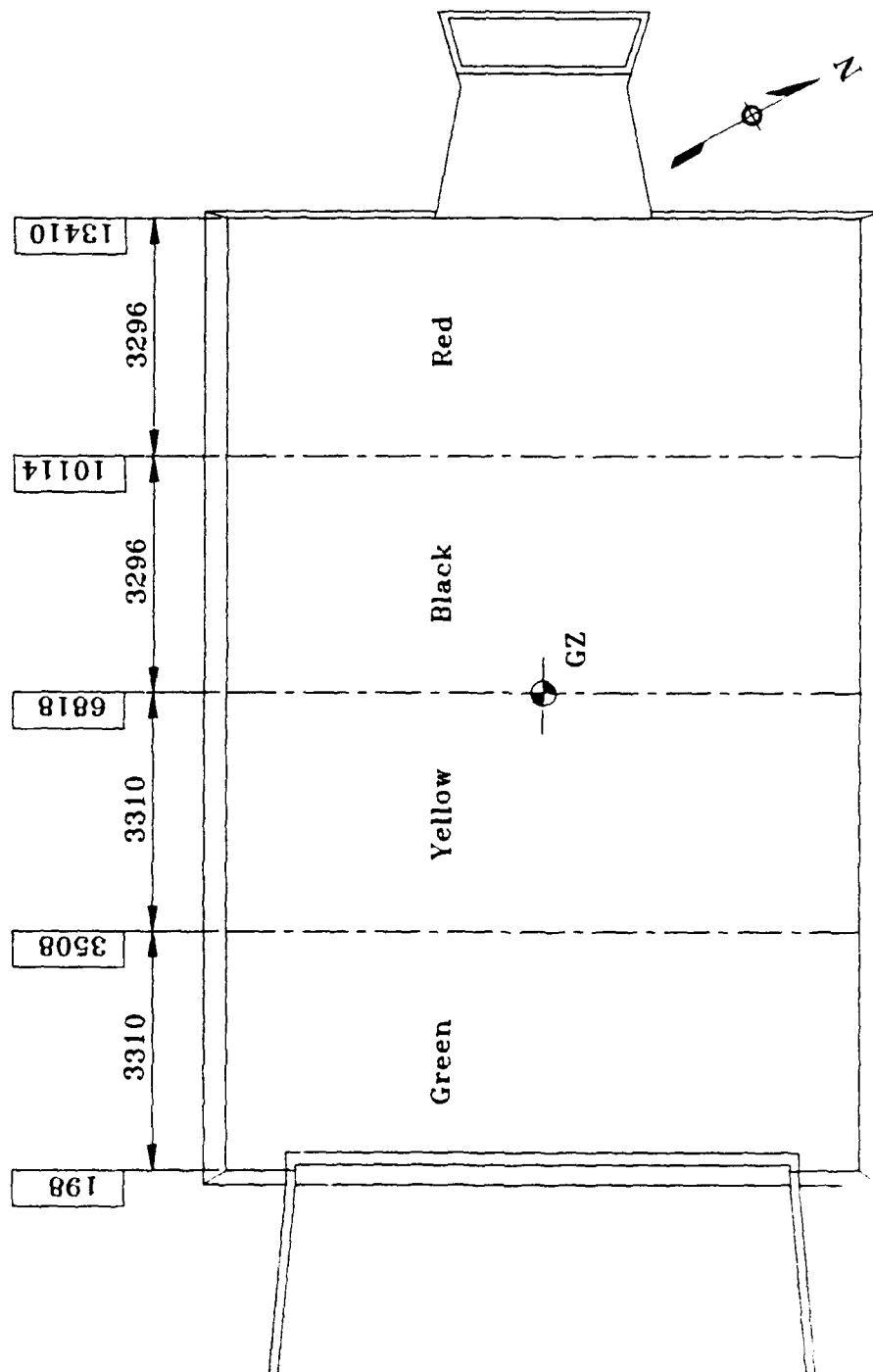
Table 15. Pretest and posttest locations of WES gages, PAS-3.

I.D. MARK	STARTING LOCATION COORDINATES			FINAL LOCATION COORDINATES		
	X (mm)	Y (mm)	Z (mm)	X (mm)	Y (mm)	Z (mm)
W1601	6695	0	2987	1449	-13727	350
W1603	6695	1855	2673	10747	24100	350
W1605	6695	3425	1829	14211	23342	350



(a) Section: Positions of colored bands on concrete of arch.

Figure 125. Dyed concrete and colored beads in arch, PAS-3.



(b) Plan: Colored bead zones on arch.

Figure 125. Concluded.

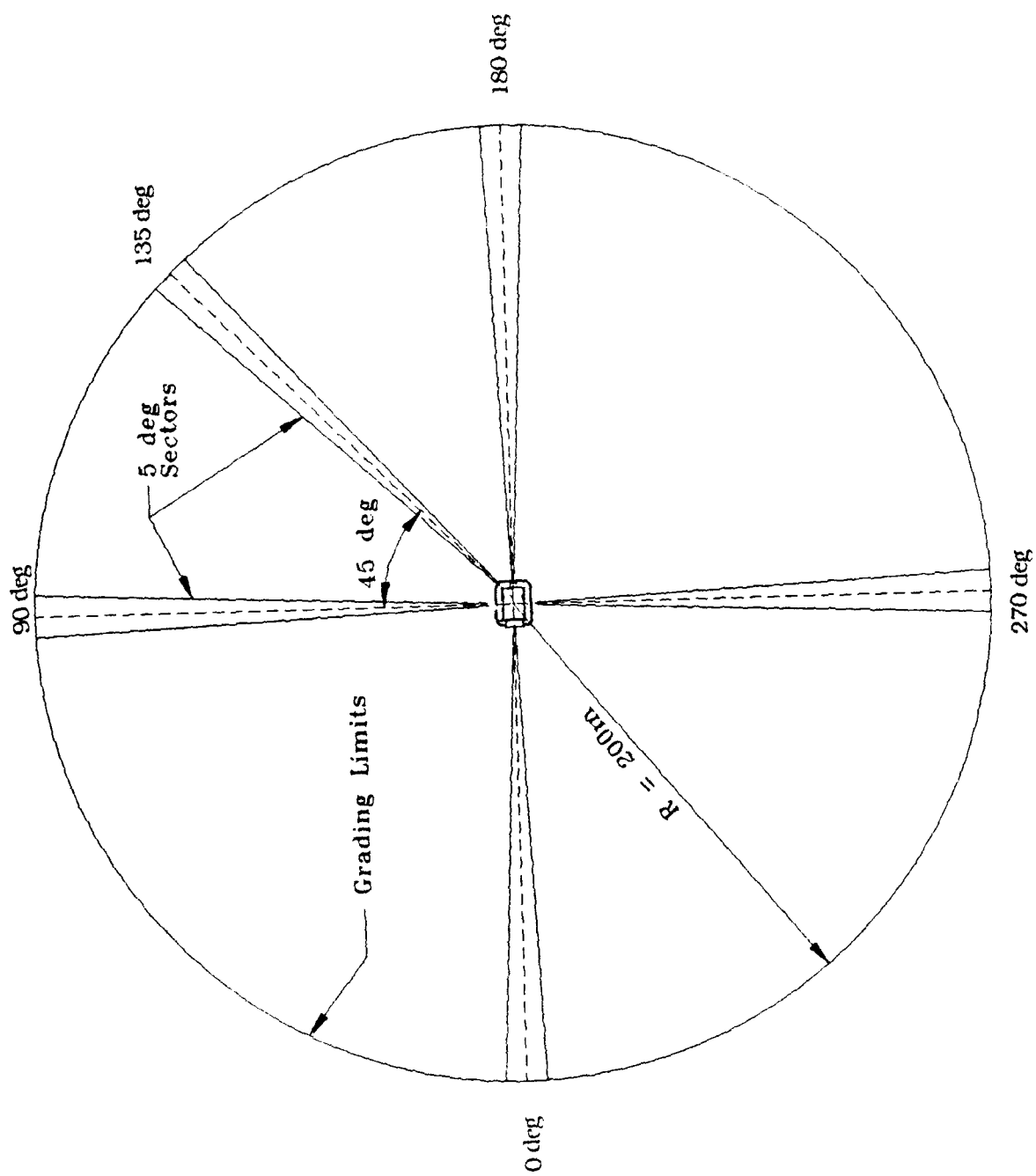


Figure 126. Five-degree debris collection sectors, PAS-3.

Table 16. Sieve data: 0-deg azimuth (front) sector, PAS-3.

ZONE	INSIDE RADIUS (m)	OUTSIDE RADIUS (m)	AVERAGE RADIUS (m)	ZONE AREA (m ²)	WEIGHT (gm)	NUMBER	WT./AREA (gm /m ²)	NO./AREA (no./m ²)
000AZ - 1	10.0	15.0	12.5	5.45	1443.9	170	264.7	31.2
000AZ - 2	15.0	20.0	17.5	7.64	774.4	90	101.4	11.8
000AZ - 3	20.0	25.0	22.5	9.82	494.1	70	50.3	7.1
000AZ - 4	25.0	30.0	27.5	12.00	325.6	39	27.1	3.3
000AZ - 5	30.0	35.0	32.5	14.18	118.8	17	8.4	1.2
000AZ - 6	35.0	40.0	37.5	16.36	46.0	7	2.8	0.4
000AZ - 7	40.0	45.0	42.5	18.54	315.5	31	17.0	1.7
000AZ - 8	45.0	50.0	47.5	20.73	160.7	19	7.8	0.9
000AZ - 9	50.0	55.0	52.5	22.91	264.2	18	11.5	0.8
000AZ - 10	55.0	60.0	57.5	25.09	110.4	11	4.4	0.4
000AZ - 11	60.0	65.0	62.5	27.27	70.1	12	2.6	0.4
000AZ - 12	65.0	70.0	67.5	29.45	120.6	12	4.1	0.4
000AZ - 13	70.0	75.0	72.5	31.63	76.4	11	2.4	0.3
000AZ - 14	75.0	80.0	77.5	33.82	19.5	3	0.6	0.1
000AZ - 15	80.0	85.0	82.5	36.00	23.4	4	0.7	0.1
000AZ - 16	85.0	90.0	87.5	38.18	44.4	6	1.2	0.2
000AZ - 17	90.0	95.0	92.5	40.36	198.0	13	4.9	0.3
000AZ - 18	95.0	100.0	97.5	42.54	40.2	3	0.9	0.1
Totals					4646.2	536		

Table 17. Sieve data: 90-deg azimuth (right side) sector, PAS-3.

ZONE	INSIDE RADIUS (m)	OUTSIDE RADIUS (m)	AVERAGE RADIUS (m)	ZONE AREA (m ²)	WEIGHT (gm)	NUMBER	WT./AREA (gm / m ²)	NO./AREA (no./m ²)
090AZ - 1	10.0	15.0	12.5	5.45	225.0	24	41.3	4.4
090AZ - 2	15.0	20.0	17.5	7.64	94.7	9	12.4	1.2
090AZ - 3	20.0	25.0	22.5	9.82	27.4	4	2.8	0.4
090AZ - 4	25.0	30.0	27.5	12.00	18.2	7	1.5	0.6
090AZ - 5	30.0	35.0	32.5	14.18	72.6	14	5.1	1.0
090AZ - 6	35.0	40.0	37.5	16.36	36.9	5	2.3	0.3
090AZ - 7	40.0	45.0	42.5	18.54	20.7	4	1.1	0.2
Totals					495.5	67		

Table 18. Sieve data: 180-deg azimuth (back) sector, PAS-3.

ZONE	INSIDE RADIUS (m)	OUTSIDE RADIUS (m)	AVERAGE RADIUS (m)	ZONE AREA (m ²)	WEIGHT (gm)	NUMBER	WT./AREA (gm / m ²)	NO./AREA (no./m ²)
180AZ - 2	15.0	20.0	17.5	7.64	2535.9	275	332.1	36.0
180AZ - 3	20.0	25.0	22.5	9.82	1689.2	235	172.1	23.9
180AZ - 4	25.0	30.0	27.5	12.00	2043.7	304	170.3	25.3
180AZ - 5	30.0	35.0	32.5	14.18	2950.9	326	208.1	23.0
180AZ - 6	35.0	40.0	37.5	16.36	1466.5	199	89.6	12.2
180AZ - 7	40.0	45.0	42.5	18.54	1159.1	128	62.0	6.9
180AZ - 8	45.0	50.0	47.5	20.73	853.1	80	41.4	3.9
180AZ - 9	50.0	55.0	52.5	22.91	866.6	61	37.8	2.7
180AZ - 10	55.0	60.0	57.5	25.09	339.0	21	13.2	0.8
180AZ - 11	60.0	65.0	62.5	27.27	357.3	23	13.1	0.8
180AZ - 12	65.0	70.0	67.5	29.45	374.3	20	11.4	0.7
180AZ - 13	70.0	75.0	72.5	31.63	0.0	0	0.0	0.0
180AZ - 14	75.0	80.0	77.5	33.82	0.0	0	0.0	0.0
180AZ - 15	80.0	85.0	82.5	36.00	0.0	0	0.0	0.0
180AZ - 16	85.0	90.0	87.5	38.18	46.3	5	1.2	0.1
180AZ - 17	90.0	95.0	92.5	40.36	41.4	6	1.0	0.1
Totals					14669.3	1683		

Table 19. Sieve data: 270-deg azimuth (left side) sector, PAS-3.

ZONE	INSIDE RADIUS (m)	OUTSIDE RADIUS (m)	AVERAGE RADIUS (m)	ZONE AREA (m ²)	WEIGHT (gm)	NUMBER	WT./AREA (gm/m ²)	NO./AREA (no./m ²)
270AZ - 1	10.0	15.0	12.5	5.45	1262.5	141	231.5	25.9
270AZ - 2	15.0	20.0	17.5	7.64	652.8	115	85.5	15.1
270AZ - 3	20.0	25.0	22.5	9.82	1144.4	152	116.6	15.5
270AZ - 4	25.0	30.0	27.5	12.00	697.4	94	57.8	7.8
270AZ - 5	30.0	35.0	32.5	14.18	319.3	44	22.5	3.1
270AZ - 6	35.0	40.0	37.5	16.36	207.8	58	12.7	3.5
270AZ - 7	40.0	45.0	42.5	18.54	18.5	2	1.0	0.1
270AZ - 8	45.0	50.0	47.5	20.73	47.6	3	2.3	0.1
Totals					4346.3	609		

surrounding the structure were located by standard surveying methods. Once the piece of debris was surveyed, it was marked with an identifying number and taken back to the lab. In the lab, each piece of debris recovered was weighed and its dimensions measured. The measuring procedure was based on determining the dimensions of the smallest rectangular box that could enclose the piece of debris. Other identifying features were noted, such as the color of the concrete, color of plastic beads in the piece, and whether the piece had a painted and/or a formed surface. The survey located and identified 623 pieces of concrete debris. A complete set of the data obtained from this survey is presented in Volume III.

The debris location and identification data were combined into a spreadsheet program (LOTUS 1-2-3) and sorted in various ways. The first data sort was by weight from lightest to heaviest. The weights were then scaled up to full-size by multiplying by 27. The scaled-up data were then grouped by weight intervals, and the number of pieces and total weight of debris in each weight interval were determined. A summary of the results is given in Table 20. Figure 127 is a graphical presentation of the information in Table 20. A complete set of data is presented in Volume III.

The second data sort of the debris was by range from GZ. The debris was sorted into zones of concentric rings 5 m wide. The number of pieces and total weight of debris in each zone were determined. From this data sort the weight densities and number densities could be calculated for each zone. Table 21 presents a summary of this information. Figures 128 and 129 are graphic presentations of the data in Table 21.

A second calculation of these data provided the cumulative weight and quantity distribution in the concentric zones, beginning at the structure and working outward. Table 22 presents a summary of this information. Figures 130 and 131 are graphic presentations of the data in Table 22.

The final data sort, presented in Volume III, was by color of concrete.

Table 20. Debris weights scaled up to full-size structure (no sieve data), PAS-3.

WEIGHT INTERVAL (Scaled-Up) (kg)	WEIGHT INTERVAL (Scaled-Up) (lb)	NUMBER OF PIECES	TOTAL WEIGHT (kg)	TOTAL WEIGHT (lb)
0.79 - 1.02	1.75 - 2.25	3	2.62	5.77
1.02 - 1.25	2.25 - 2.75	7	8.37	18.45
1.25 - 1.47	2.75 - 3.25	7	9.61	21.18
1.47 - 1.70	3.25 - 3.75	13	20.94	46.17
1.70 - 1.93	3.75 - 4.25	16	29.14	64.25
1.93 - 2.15	4.25 - 4.75	17	34.80	76.73
2.15 - 2.38	4.75 - 5.25	14	31.72	69.94
2.38 - 2.61	5.25 - 5.75	17	41.96	92.50
2.61 - 2.83	5.75 - 6.25	24	65.40	144.18
2.83 - 3.06	6.25 - 6.75	24	70.48	155.38
3.06 - 3.29	6.75 - 7.25	25	78.12	172.22
3.29 - 3.52	7.25 - 7.75	24	82.10	180.99
3.52 - 3.74	7.75 - 8.25	18	65.17	143.68
3.74 - 3.97	8.25 - 8.75	25	95.72	211.03
3.97 - 4.20	8.75 - 9.25	13	53.46	117.86
4.20 - 4.42	9.25 - 9.75	17	73.58	162.21
4.42 - 4.65	9.75 - 10.25	12	54.56	120.28
4.65 - 4.88	10.25 - 10.75	14	66.57	146.77
4.88 - 5.10	10.75 - 11.25	17	84.30	185.85
5.10 - 5.78	11.25 - 12.75	35	188.38	415.31
5.78 - 6.46	12.75 - 14.25	28	169.75	374.24
6.46 - 7.60	14.25 - 16.75	32	226.82	500.05
7.60 - 8.28	16.75 - 18.25	17	134.71	296.99
8.28 - 9.87	18.25 - 21.75	29	259.39	571.86
9.87 - 10.55	21.75 - 23.25	13	133.41	294.11
10.55 - 12.13	23.25 - 26.75	24	272.08	599.84
12.13 - 12.81	26.75 - 28.25	4	49.41	108.94
12.81 - 14.40	28.25 - 31.75	15	206.90	456.14
14.40 - 15.08	31.75 - 33.25	4	58.62	129.24
15.08 - 16.67	33.25 - 36.75	7	112.03	246.99
16.67 - 19.62	36.75 - 43.25	29	530.65	1169.88
19.62 - 25.74	43.25 - 56.75	20	434.47	957.84
25.74 - 28.69	56.75 - 63.25	6	160.30	353.40
28.69 - 34.81	63.25 - 76.75	18	560.83	1236.42
> 34.81	> 76.75	35	3361.23	7410.25
Totals		623	7827.62	17256.94

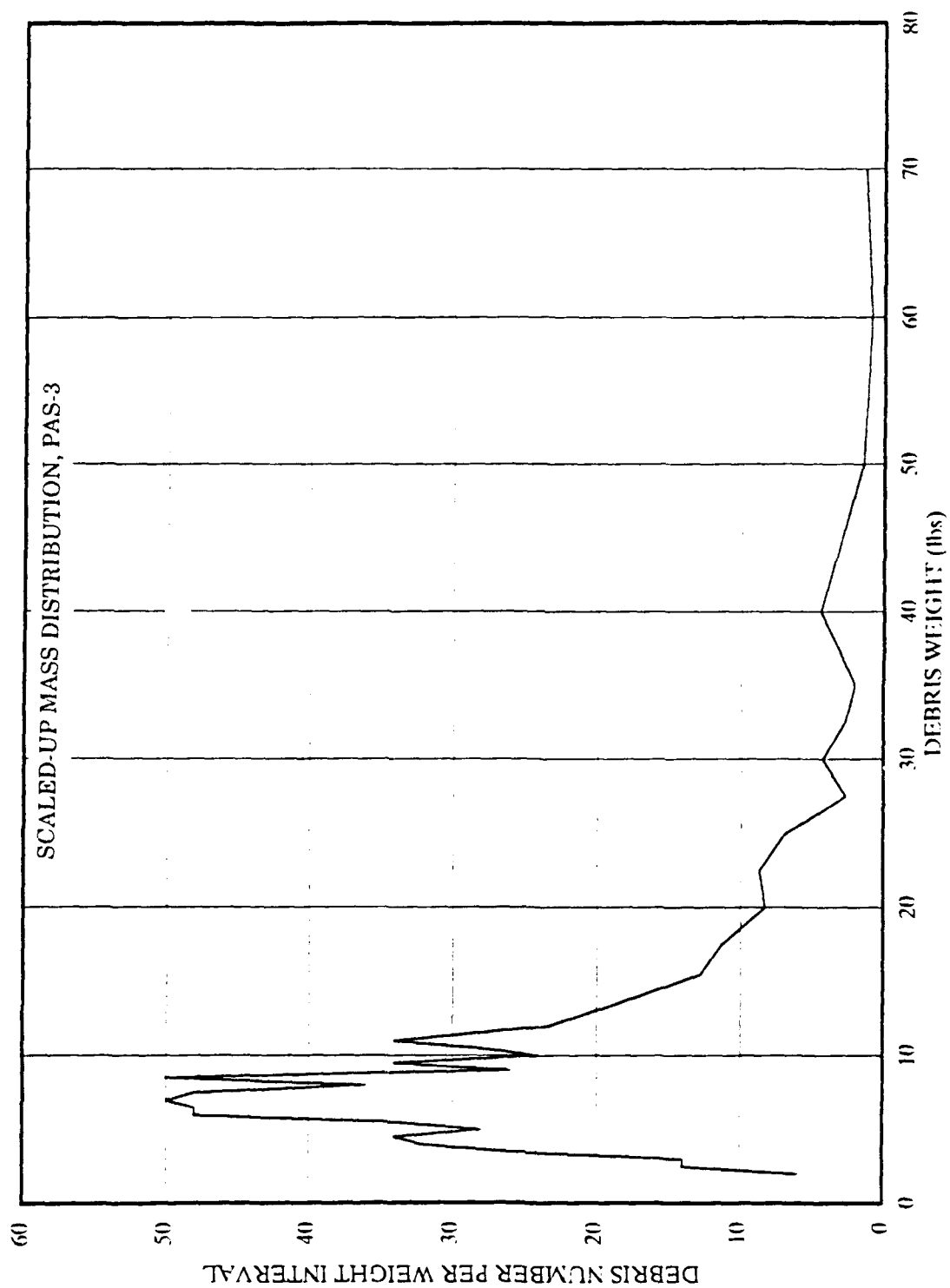


Figure 127. Number of pieces of debris in each weight interval (scaled to full-size structure).

Table 21. Number of pieces and total weight of debris in concentric zones, PAS-3.

ZONE R1 TO R2 (m) (m)		WEIGHT IN ZONE (gm)	NUMBER IN ZONE	ZONE AREA (m ²)	WT./AREA (gm/m ²)	NO./AREA (No./m ²)
0 TO 10		7166.66	8	314.16	22.812	0.02546
10 TO 15		34713.54	102	392.70	88.397	0.25974
15 TO 20		28032.84	75	549.78	50.989	0.13642
20 TO 25		47184.61	85	706.86	66.753	0.12025
25 TO 30		52561.76	97	863.94	60.840	0.11228
30 TO 35		20540.00	51	1021.02	20.117	0.04995
35 TO 40		12861.34	37	1178.10	10.917	0.03141
40 TO 45		7678.20	19	1335.18	5.751	0.01423
45 TO 50		20816.39	30	1492.26	13.950	0.02010
50 TO 55		3968.00	15	1649.34	2.406	0.00909
55 TO 60		6913.30	11	1806.42	3.827	0.00609
60 TO 65		6432.80	7	1963.50	3.276	0.00357
65 TO 70		4358.00	7	2120.58	2.055	0.00330
70 TO 75		2124.40	8	2277.65	0.933	0.00351
75 TO 80		3307.60	6	2434.73	1.359	0.00246
80 TO 85		7694.30	6	2591.81	2.969	0.00231
85 TO 90		1874.70	6	2748.89	0.682	0.00218
90 TO 95		649.60	4	2905.97	0.224	0.00138
95 TO 100		2471.90	5	3063.05	0.807	0.00163
100 TO 105		414.00	1	3220.13	0.129	0.00031
105 TO 110		7699.70	8	3377.21	2.280	0.00237
110 TO 115		1318.40	4	3534.29	0.373	0.00113
115 TO 120		655.00	4	3691.37	0.177	0.00108
120 TO 125		171.50	1	3848.45	0.045	0.00026
125 TO 130		181.10	1	4005.53	0.045	0.00025
130 TO 135		338.30	3	4162.61	0.081	0.00072
135 TO 140		515.00	4	4319.69	0.119	0.00093
140 TO 145		4722.52	4	4476.77	1.055	0.00089
145 TO 150		74.10	1	4633.85	0.016	0.00022
150 TO 155		644.36	3	4790.93	0.134	0.00063
155 TO 160		281.10	1	4948.01	0.057	0.00020
160 TO 165		560.20	2	5105.09	0.110	0.00039
165 TO 170		240.90	2	5262.17	0.046	0.00038
170 TO 175		206.00	1	5419.25	0.038	0.00018
175 TO 180		141.90	1	5576.33	0.025	0.00018
180 TO 185		0	0	5733.41	0.000	0.00000
185 TO 190		0	0	5890.49	0.000	0.00000
190 TO 195		164.90	1	6047.57	0.027	0.00017
195 TO 200		0	0	6204.65	0.000	0.00000
200 TO 205		292.30	2	6361.73	0.046	0.00031
Totals		289971.22	623			

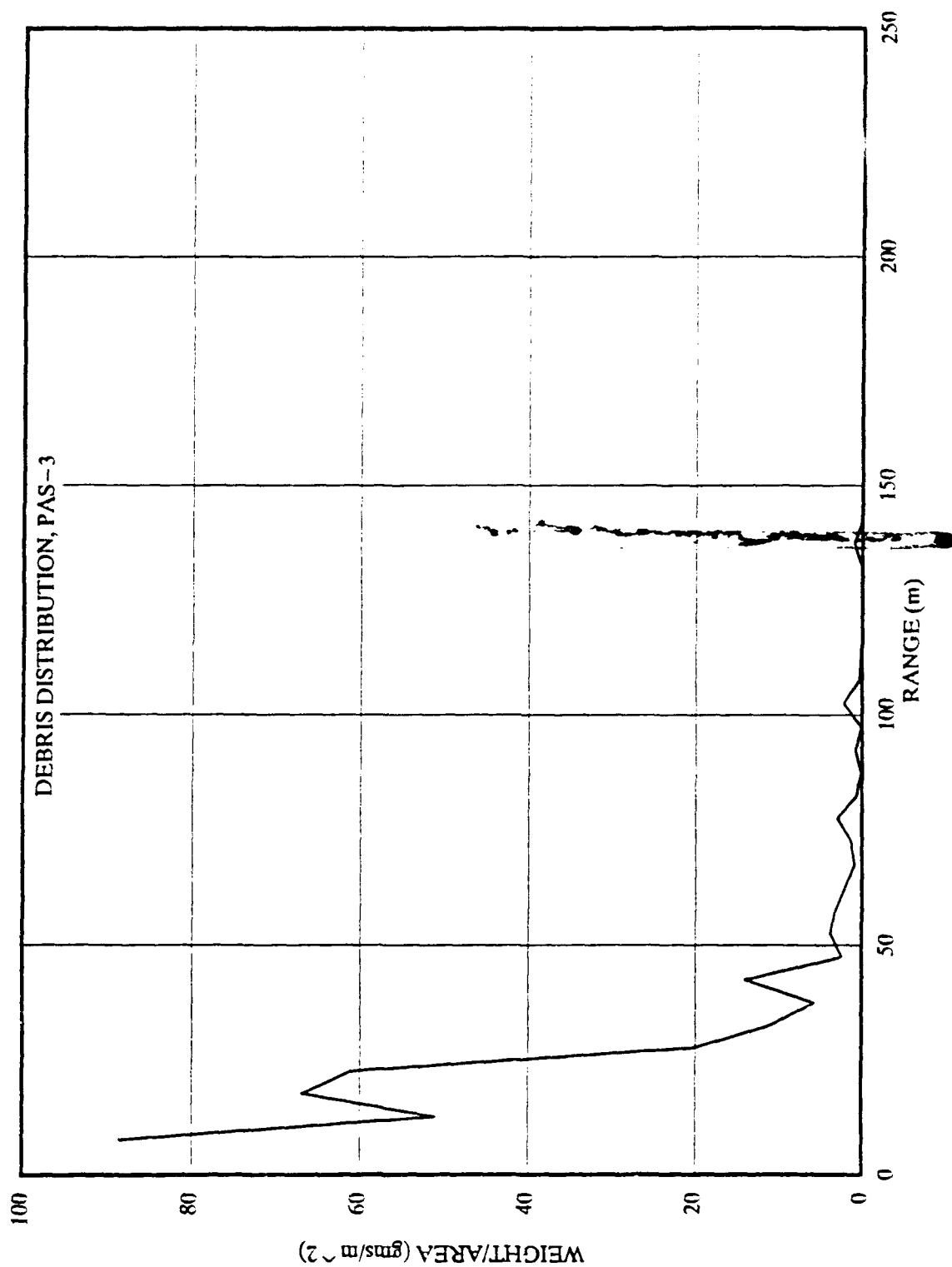


Figure 128. Plot of weight of debris versus range of concentric zone.

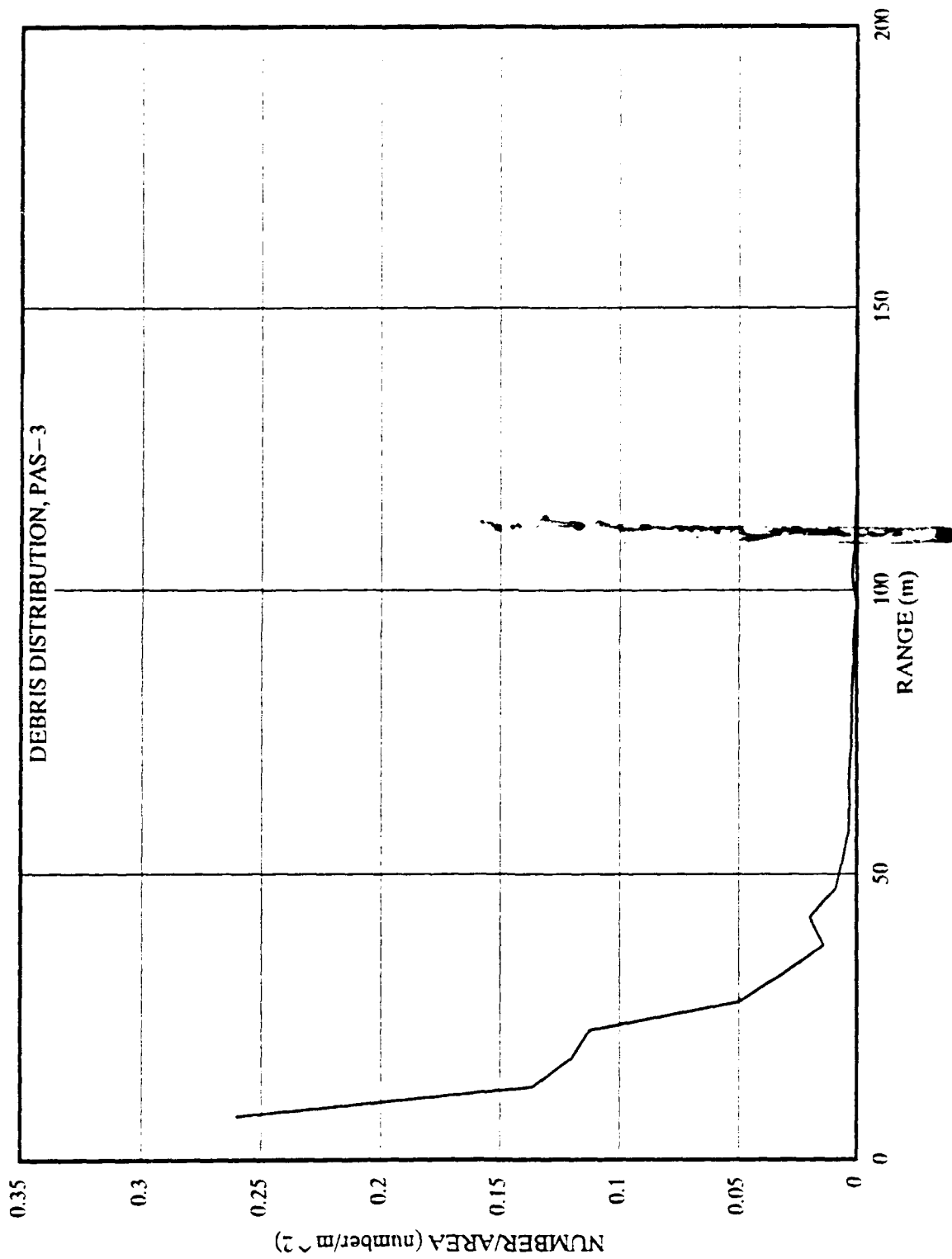


Figure 129. Plot of number of pieces of debris versus range of concentric zone.

Table 22. Cumulative weights and number of pieces of debris in concentric zones, PAS-3.

ZONE			CUMULATIVE WEIGHT (gm)	PERCENT OF TOTAL WEIGHT	CUMULATIVE NUMBER	PERCENT OF TOTAL NUMBER
R1 TO (m)	TO	R2 (m)				
0	TO	10	7166.7	2.47	8	1.28
10	TO	15	41880.2	14.44	110	17.66
15	TO	20	69913.0	24.11	185	29.70
20	TO	25	117097.7	40.38	270	43.34
25	TO	30	169659.4	58.51	367	58.91
30	TO	35	190199.4	65.59	418	67.09
35	TO	40	203060.8	70.03	455	73.03
40	TO	45	210739.0	72.68	474	76.08
45	TO	50	231555.3	79.85	504	80.90
50	TO	55	235523.3	81.22	519	83.31
55	TO	60	242436.6	83.61	530	85.07
60	TO	65	248869.4	85.83	537	86.20
65	TO	70	253227.4	87.33	544	87.32
70	TO	75	255351.8	88.06	552	88.60
75	TO	80	258659.4	89.20	558	89.57
80	TO	85	266353.7	91.86	564	90.53
85	TO	90	268228.4	92.50	570	91.49
90	TO	95	268878.0	92.73	574	92.13
95	TO	100	271349.9	93.58	579	92.94
100	TO	105	271763.9	93.72	580	93.10
105	TO	110	279463.6	96.38	588	94.38
110	TO	115	280782.0	96.83	592	95.02
115	TO	120	281437.0	97.06	596	95.67
120	TO	125	281608.5	97.12	597	95.83
125	TO	130	281789.6	97.18	598	95.99
130	TO	135	282127.9	97.30	601	96.47
135	TO	140	282642.9	97.47	605	97.11
140	TO	145	287365.5	99.10	609	97.75
145	TO	150	287439.6	99.13	610	97.91
150	TO	155	288083.9	99.35	613	98.39
155	TO	160	288365.0	99.45	614	98.56
160	TO	165	288925.2	99.64	616	98.88
165	TO	170	289166.1	99.72	618	99.20
170	TO	175	289372.1	99.79	619	99.36
175	TO	180	289514.0	99.84	620	99.52
180	TO	185	289514.0	99.84	620	99.52
185	TO	190	289514.0	99.84	620	99.52
190	TO	195	289678.9	99.90	621	99.68
195	TO	200	289678.9	99.90	621	99.68
200	TO	205	289971.2	100.00	623	100.00

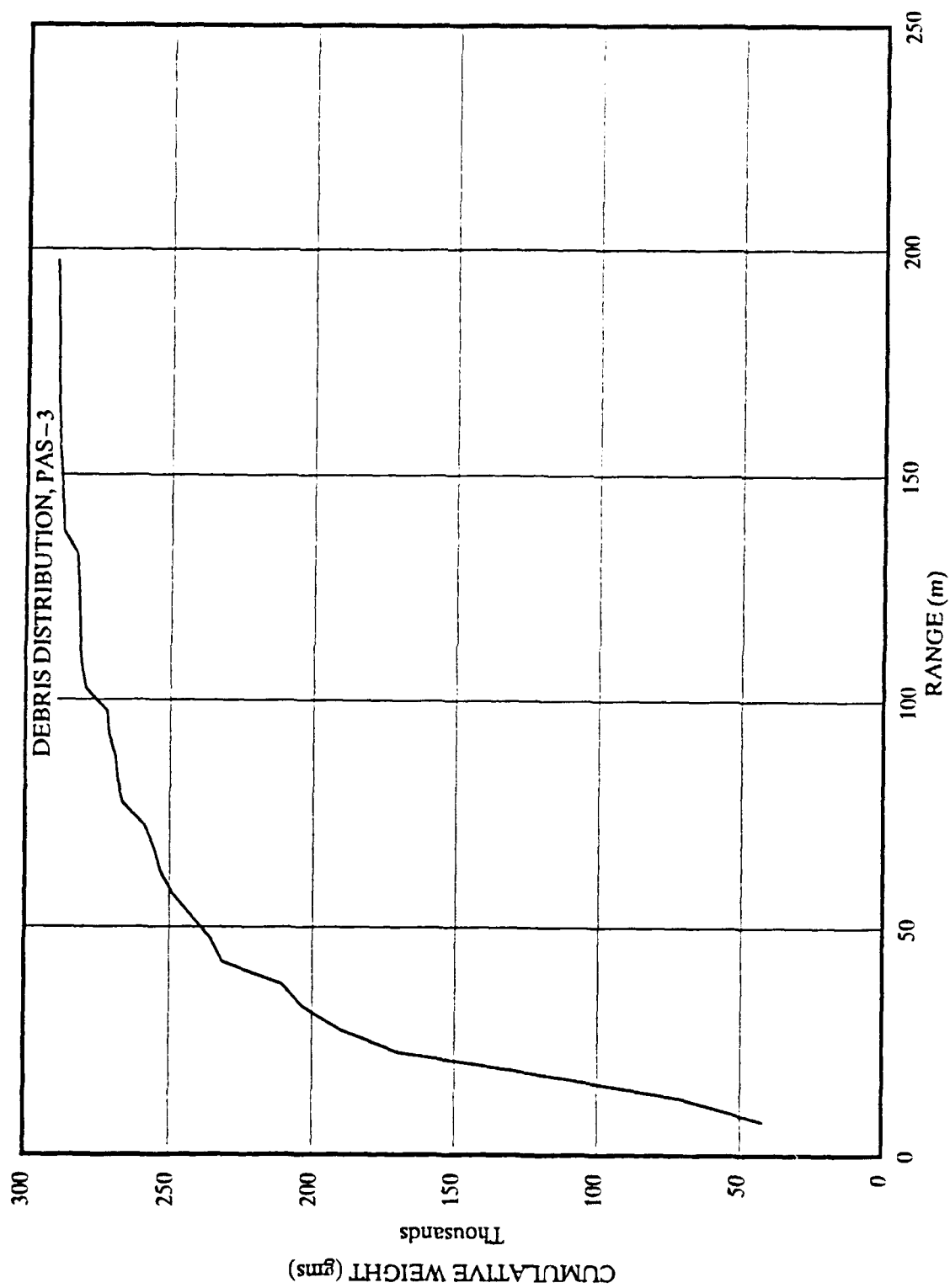


Figure 130. Cumulative weight of debris versus range of concentric zone.

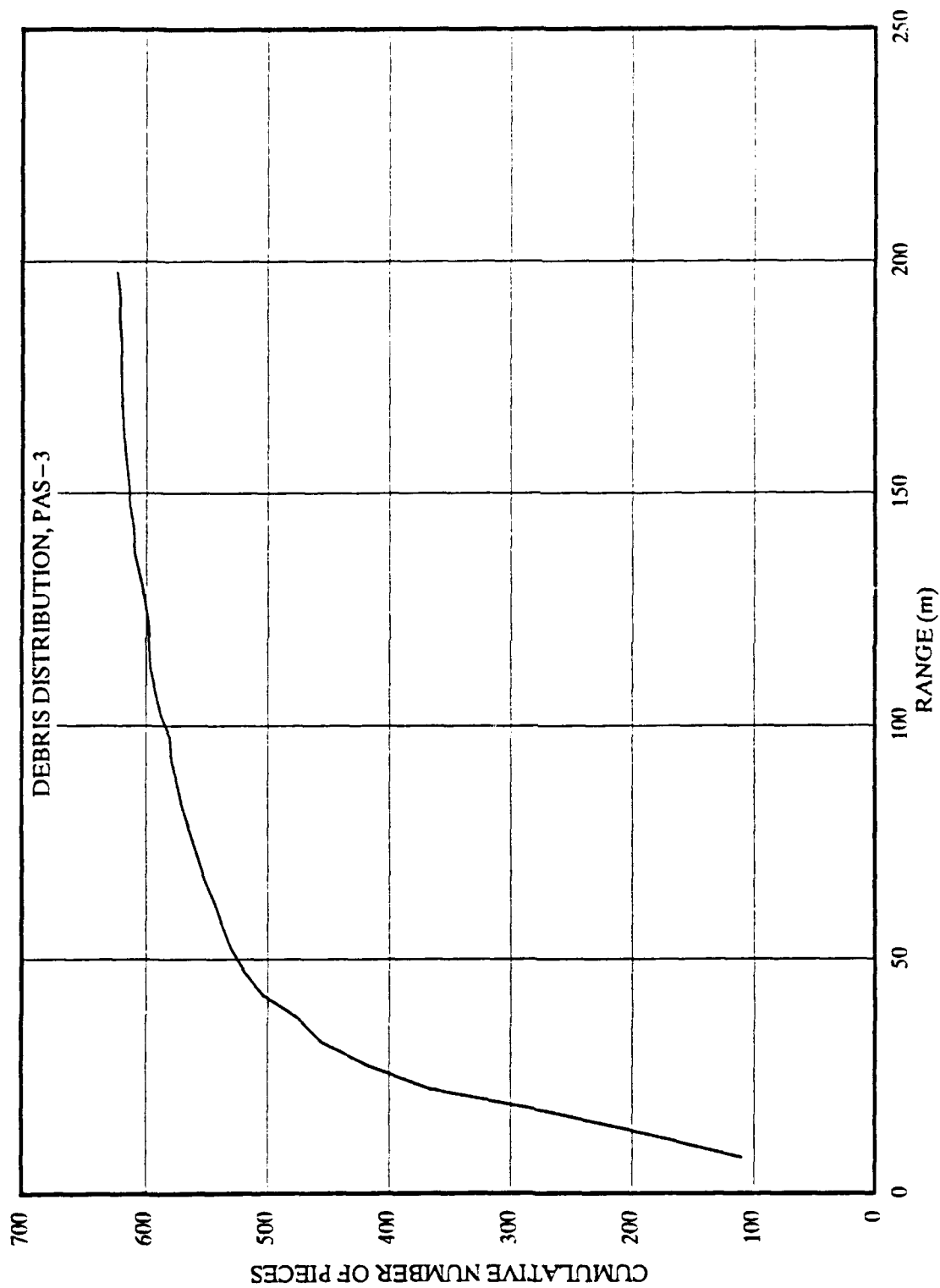


Figure 131. Cumulative number of pieces of debris versus range of concentric zone.

A Shape Factor (SF) was also calculated for each piece of debris using the following formula:

$$SF = M/(L*W*H*p)$$

where: M = Debris weight, g
L = Debris length, mm
W = Debris width, mm
H = Debris thickness, mm
p = Concrete density, 0.0024 g/mm³

A listing of the SF for all of the pieces of debris is presented in Volume III. The average SF for all pieces was calculated to be 0.4291.

Large pieces of debris included the front door, exhaust port doors and frames, the steel vestibule, and large sections of concrete from the wingwalls and the endwall of the exhaust port. The seven large arch sections were not included within this category because they all ended up generally within the limits of the structure and berm. Table 23 is a summary of the posttest locations of the large pieces of debris.

Only one piece of debris was recovered from the catcher bins. The SIFCON cube #SC14 was found in bin number 10.

A large amount of rock from the rock berm was scattered around the structure. The distribution density of the rock far exceeded that of the concrete debris, particularly at the sides of the structure. Figures 132a and 132b are overhead views showing the extent of the rock debris following the test. As noted in the discussion of the structural response, most of the rock debris came from an area adjacent to the structure. It is estimated that the volume of rock ejected during the test was about 15 to 20 percent of the total rock berm on either side of the arch. Within the limits of rock distribution there appeared to be two areas of significantly different densities. The limits of the

Table 23. Posttest locations of large pieces of structural debris, PAS-3.

ITEM	COORDINATES		FROM GZ:	
	X (mm)	Y (mm)	RANGE (mm)	AZIMUTH (deg)
FRONT DOOR	-112820	11781	120216	5.62
LEFT FRONT WALL	-10230	-5383	17877	342.48
PERSONNEL VESTIBULE	-4706	-4156	12251	340.17
EXHAUST PORT (E.P.) DOOR	83318	-636	76503	180.48
EXHAUST PORT (E.P.) DOOR	161607	-17292	155752	186.37
E.P. DOOR FRAME	30444	-2945	23809	187.11
E.P. DOOR FRAME	47997	-1551	41208	182.16
E.P. DOOR FRAME	48084	-1784	41305	182.48
1200x600x100 CONCRETE (E.P.)	44040	2848	37331	175.62
600x600x100 CONCRETE (E.P.)	20000	-4002	13777	196.89
370x235x75 CONCRETE (E.P.)	54836	-4186	48200	184.89

Table 24. Rock rubble from 5-deg sector, 90-deg azimuth, PAS-3.

ZONE	INSIDE RADIUS (m)	OUTSIDE RADIUS (m)	AVERAGE RADIUS (m)	ZONE AREA (m ²)	WEIGHT (kg)	NUMBER	WT./AREA (km/m ²)	NO./AREA (no./m ²)
090AZ - 1	10.0	15.0	12.5	5.45	68.9	80	12.6	14.7
090AZ - 2	15.0	20.0	17.5	7.64	88.4	60	11.6	7.9
090AZ - 3	20.0	25.0	22.5	9.82	86.6	28	8.8	2.9
090AZ - 4	25.0	30.0	27.5	12.00	37.5	9	3.1	0.8
090AZ - 5	30.0	35.0	32.5	14.18	7.6	3	0.5	0.2
Totals					289.0	180		



(a) Right side.



(b) Left side.

Figure 132. Rock rubble debris at structure, PAS-3.

rock distribution, and the boundary between the two areas of different densities were surveyed. This information is illustrated in Figure 133.

During the recovery of concrete debris from the 90-deg azimuth 5-deg sector, the rocks ejected from the berm were also collected within each zone. Table 24 presents the weight and number of rocks collected in each zone.

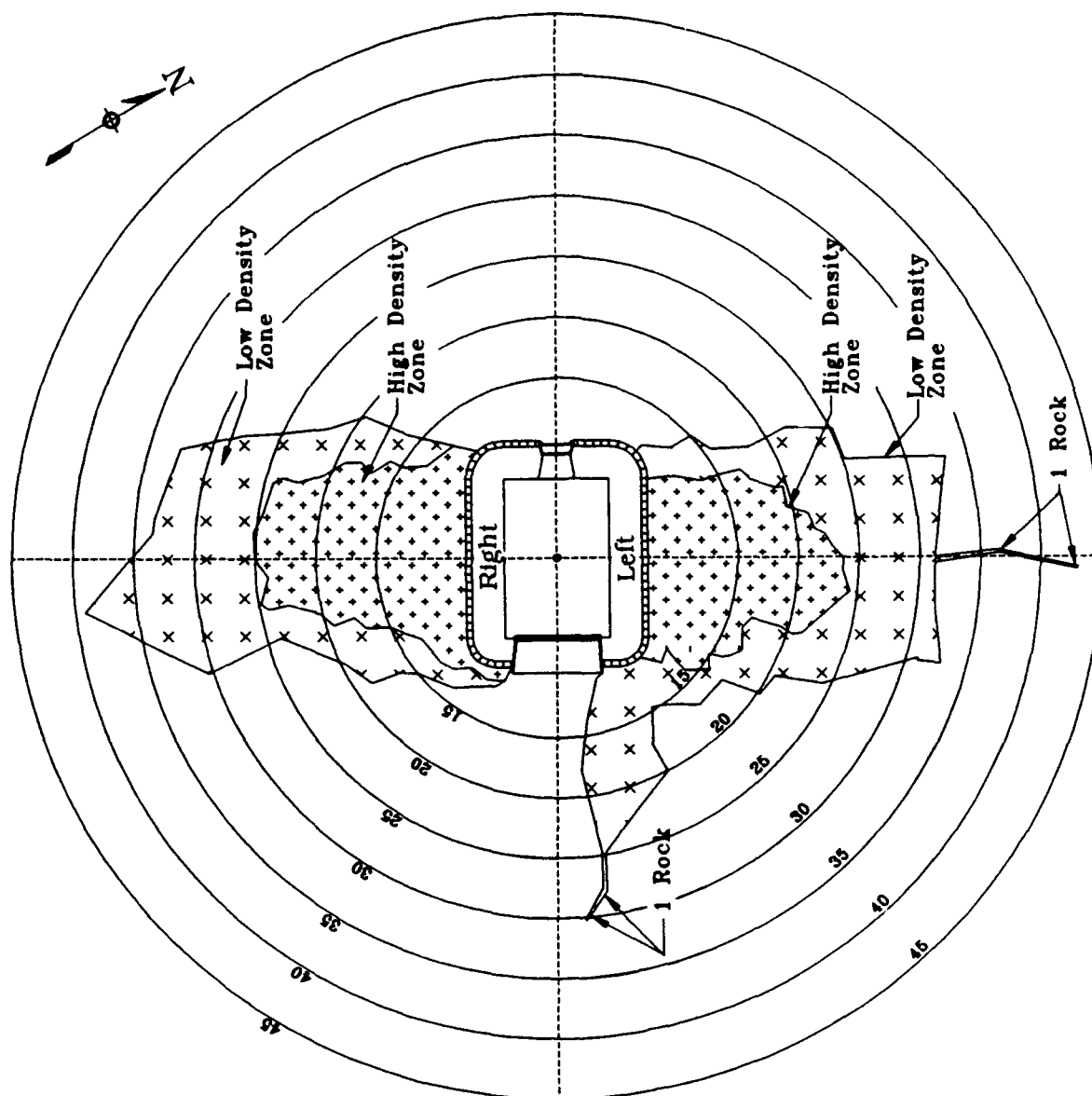


Figure 133. Distribution of debris from rock rubble berm, PAS-3.

5.0 PAS-2 TEST

5.1 TEST DESCRIPTION

5.1.1 General

The PAS-2 test was conducted on June 11, 1992. The explosive charge for this event was 11.1 kg of Composition C-4, which is the equivalent of 300 kg of the same explosive in the full-size structure. Figures 134 and 135 show the placement of the charge for this event. The center of the charge was placed 600 mm above the surface of the floor.

Figures 136, 137, and 138 show the placement of photo poles, aluminum cubes, and SIFCON cubes for the PAS-2 test. These items were identical to those used in the PAS-3 test (Fig. 71). The arrangement of plywood catcher bins for this event is shown in Figure 139. These bins were also identical to those used in the PAS-3 test (Fig. 62).

5.1.2 Instrumentation Plan

A total of 60 channels of electronic instrumentation were provided for the PAS-2 event. Included were 25 pressure measurements in the interior of the structure, 19 free-field pressure measurements around the exterior of the structure, 12 accelerometers mounted at various locations on the structure, and 4 strain measurements on the front door. Table 25 is a measurements list for the PAS-2 event. As for the previous events, the predicted maximum amplitudes shown in Table 25 are approximate values used for gage selection and setting recording bandwidths. The locations of the various on-structure measurements are shown in Figures 140 through 146—gages mounted in the floor of the structure (Fig. 140), strain gages on the outside surface of the front door (Fig. 141), sensors mounted on the inner surface of the door (Fig. 142), and sensors mounted at three sections through the arch (Figs. 143-145). The sensing axes of the accelerometers mounted at these locations were oriented to measure radial and tangential accelerations.

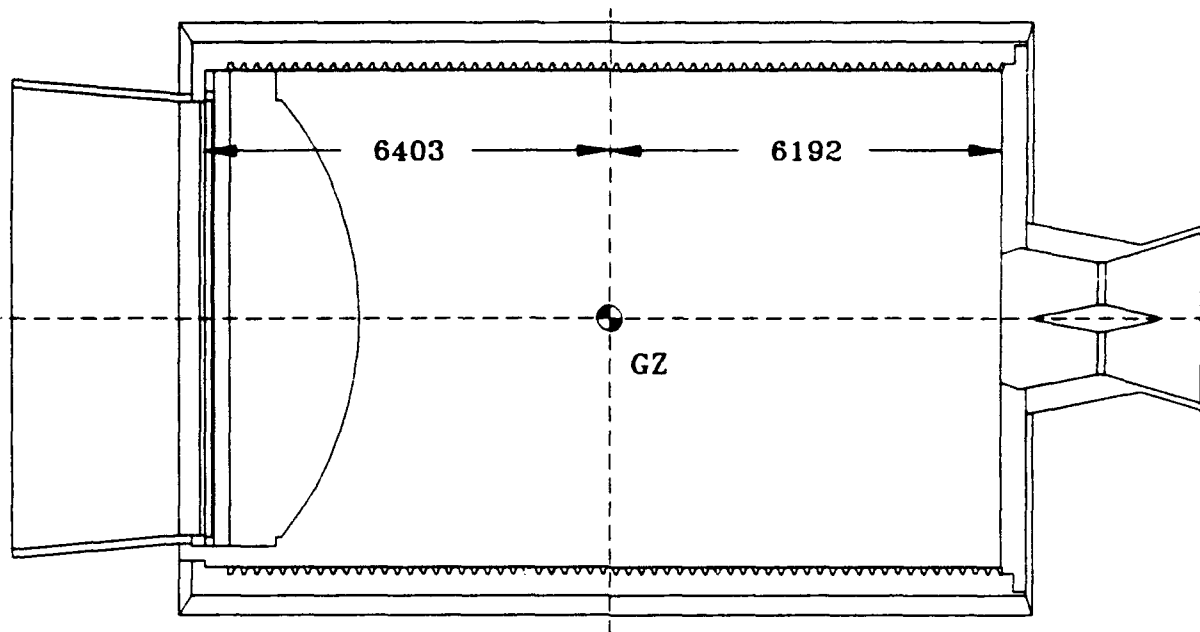


Figure 134. Location of GZ for PAS-2.

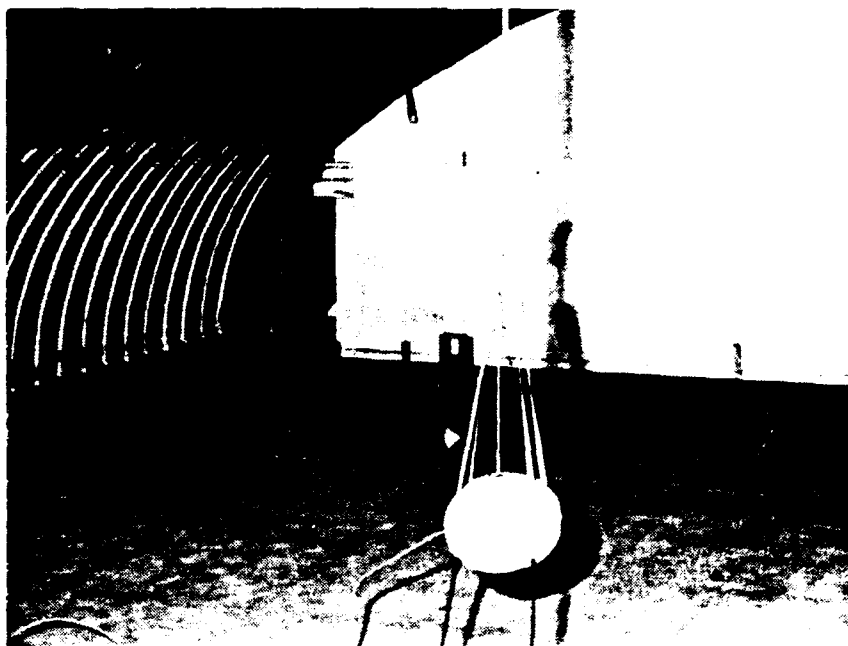
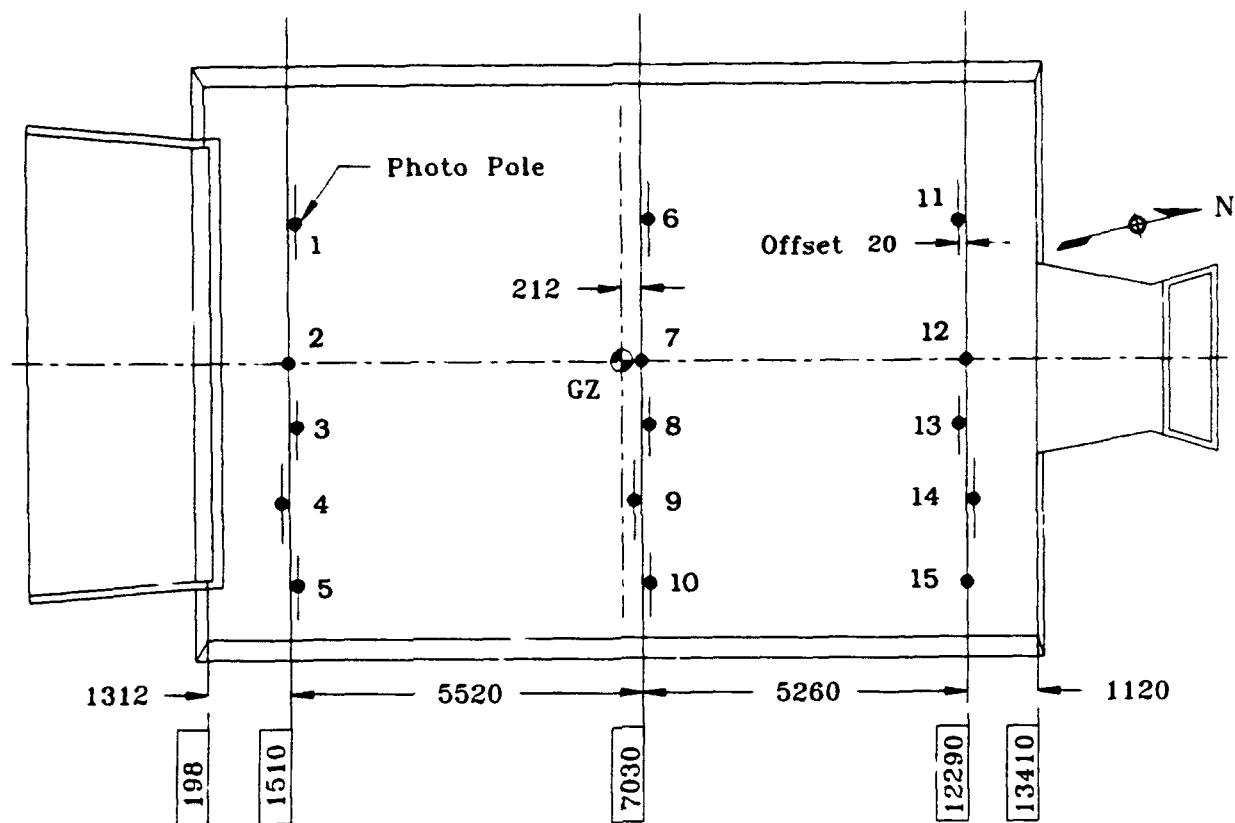
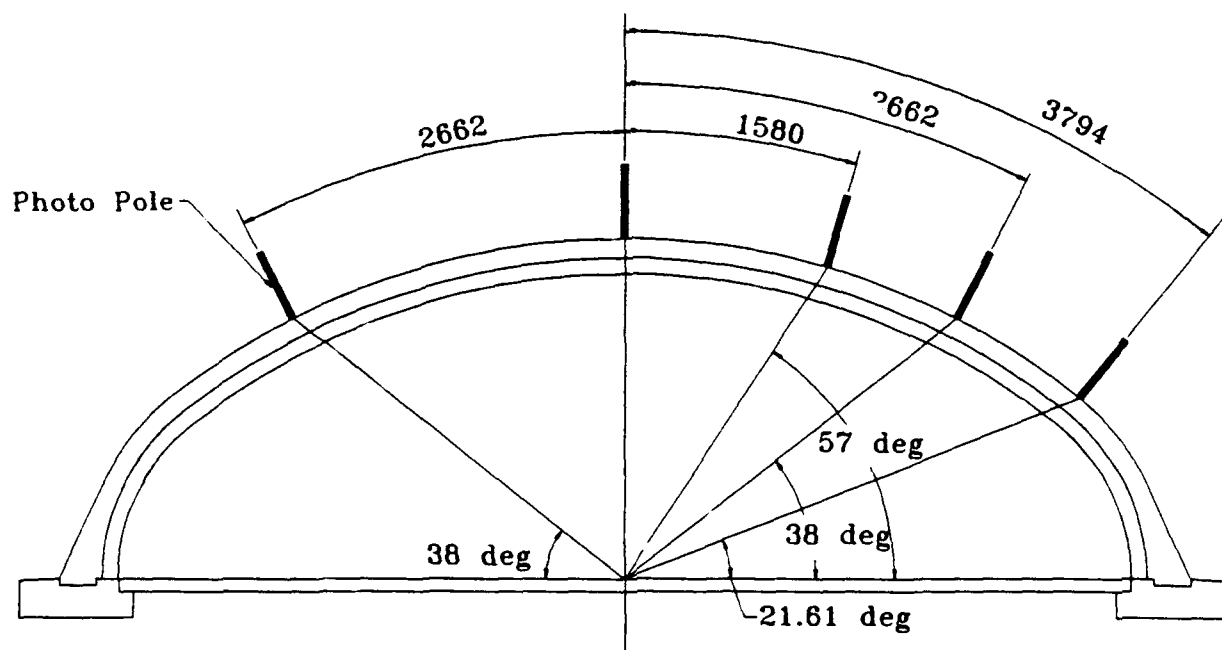


Figure 135. Explosive charge, 11.1 kg of C-4, PAS-2.

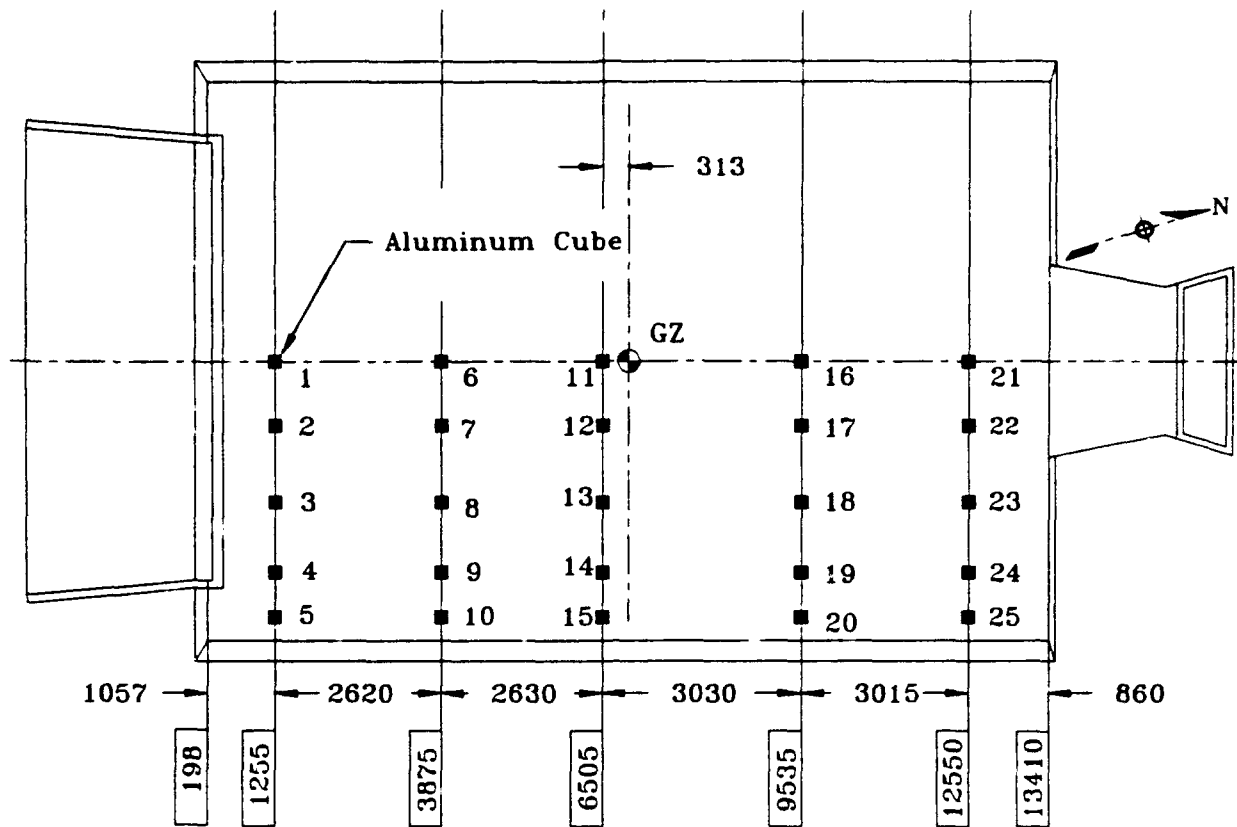


(a) Plan.

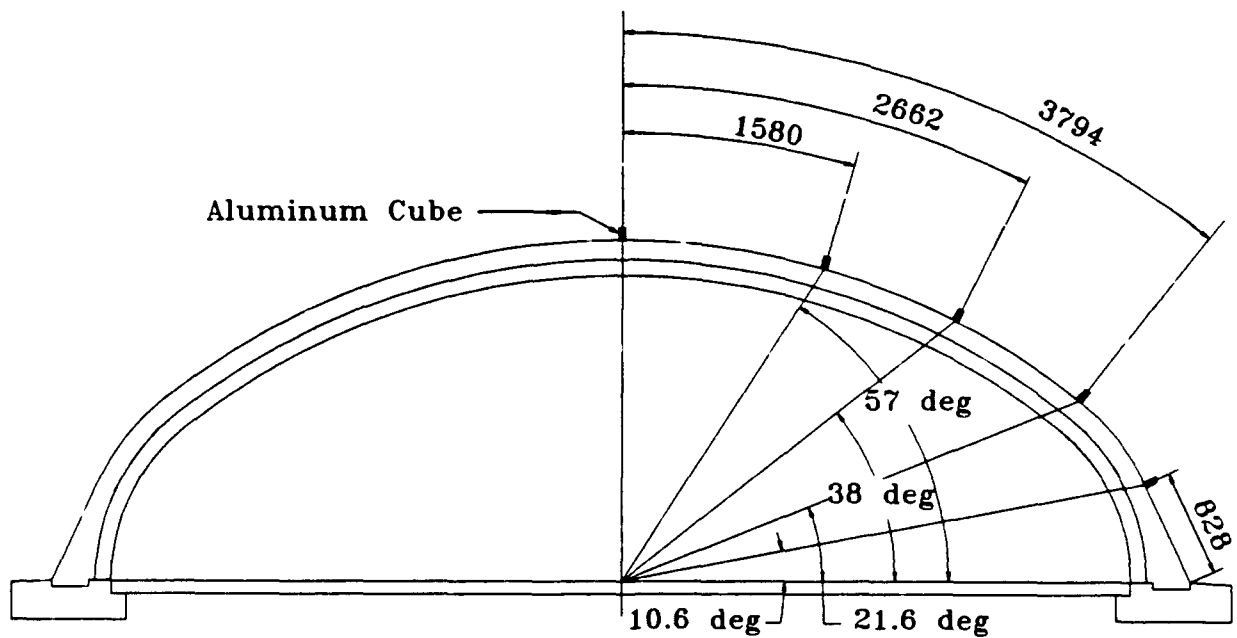


(b) Section.

Figure 136. Photo pole locations, PAS-2.

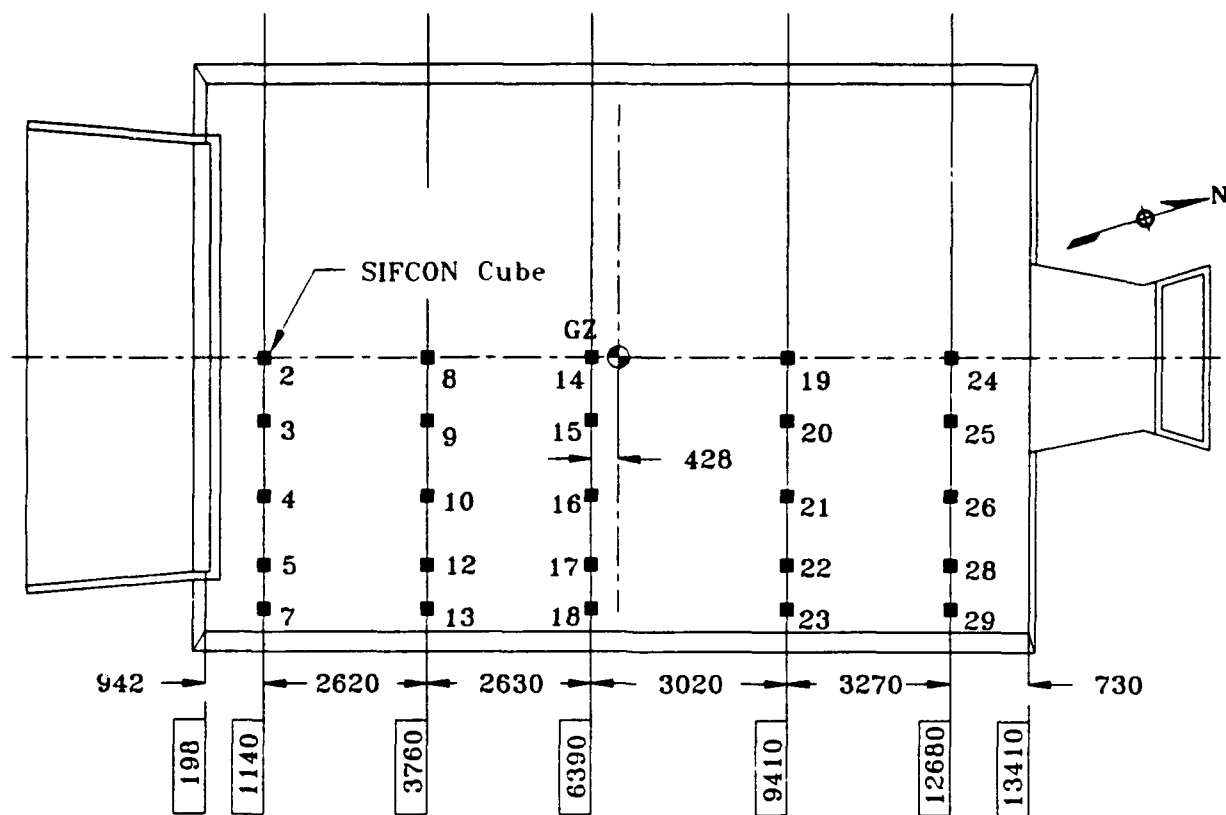


(a) Plan.

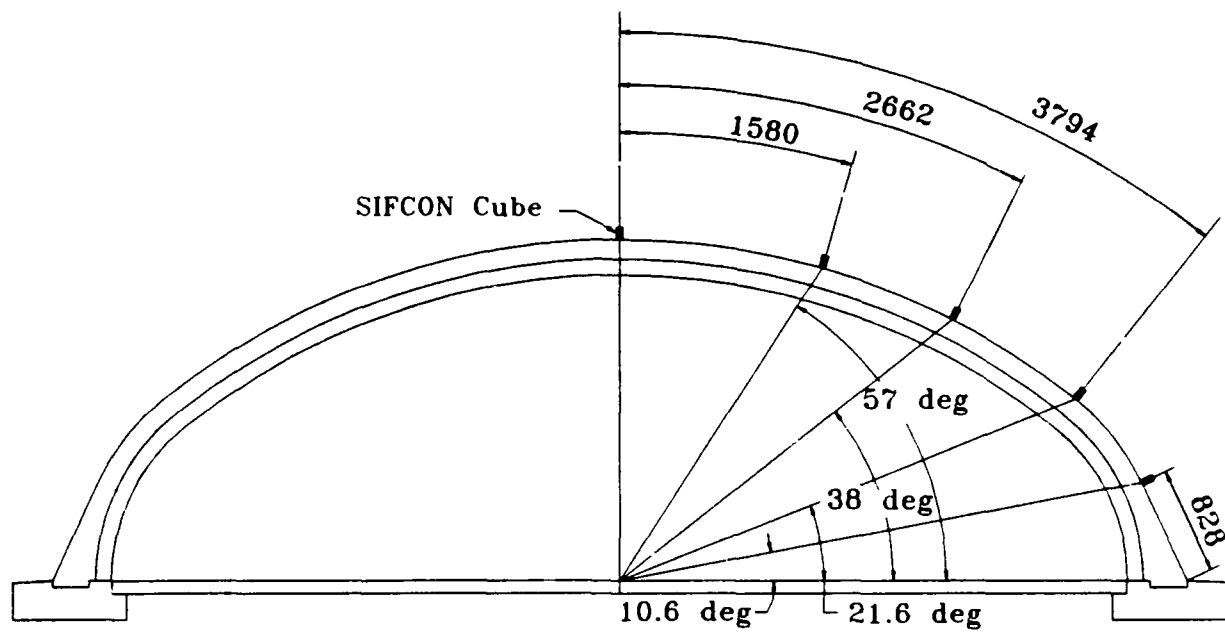


(b) Section.

Figure 137. Locations of aluminum cubes, PAS-2.



(a) Plan.



(b) Section.

Figure 138. The SIFCON cube placement, PAS-2.

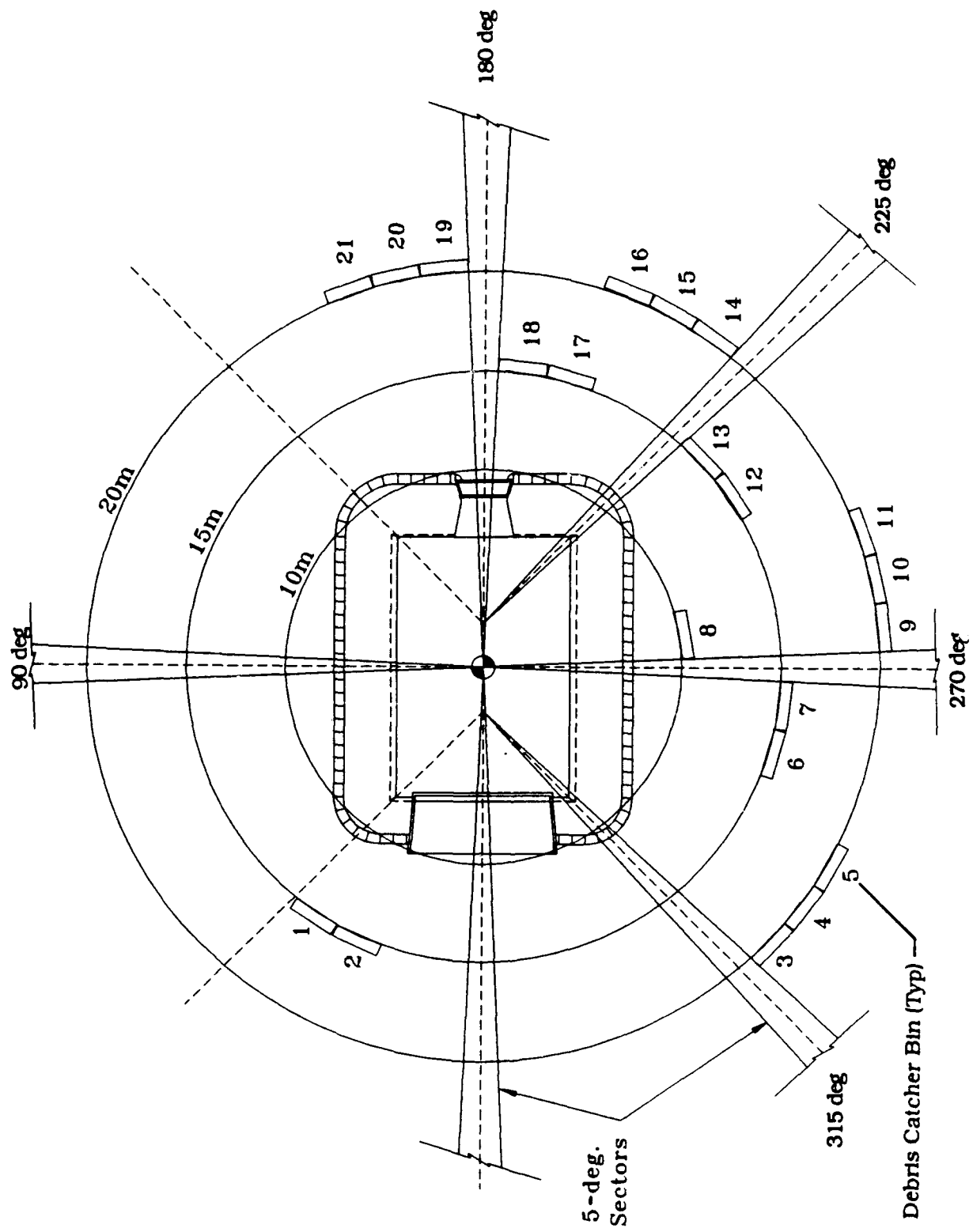


Figure 139. Locations of debris catcher bins, PAS-2.

Table 25. List of measurements for PAS-2.

MEASUREMENT LIST																	DATE	22 MAY 92	PAGE 1 OF 8 PAGES	
PAS-2																	KIRST			
TEST EVENT	MEAS NO.	LOCATION				SENS AXIS	PREC MAX	CONF LEVEL	TRANSDUCER		RANGE	TRANSDUCER TYPE	TRANSDUCER SERIAL NUMBER	CHANGES						
		BEN	X#	Y#	Z#				MODEL	ITEM				AUTH	DATE					
	0101-2	SF	12807	0	367	Z	0.896 MPa	50 %	KULITE XT-190		2.068 MPa	(Filter) PRESSURE	(1743-5-46) 6-75							
	0102-2	SF	12807	3700	367	Z	2.827 MPa	91 %	KULITE HKS-11-375		3.447 MPa	(Filter) PRESSURE	1400-2-16							
	0201-2	BW	13010	100	2500	X	1.241 MPa	100 %	KULITE XT-190		1.379 MPa	(Filter) PRESSURE	C6-19							
	0202-2	BW	13010	1700	1475	X	0.689 MPa	85 %	KULITE XT-190		1.379 MPa	(Filter) PRESSURE	(1743-5-40) Y6-6							
	0203-2	BW	13010	3700	930	X	2.137 MPa	61 %	KULITE HKS-11-375		6.895 MPa	(Filter) PRESSURE	117-7-23							
	0301-2	SF	3976	0	367	Z	0.931 MPa	90 %	KULITE XT-190		1.379 MPa	(Filter) PRESSURE	(1743-5-94) Z6-94							
	0302-2	SF	3976	1850	367	Z	0.689 MPa	95 %	KULITE XT-190		1.379 MPa	(Filter) PRESSURE	(1743-5-151) E7-1							
	0303-2	SF	3976	3700	367	Z	1.034 MPa	67 %	KULITE XT-190		2.068 MPa	(Filter) PRESSURE	(1743-5-72) D7-54							
	0304-2	SC	3976	0	2717	Z	0.724 MPa	79 %	KULITE XT-190		1.379 MPa	(Filter) PRESSURE	(1743-5-184) G7-37							
	0305-2	SC	3976	1749	2424	R1	1.172 MPa	89 %	KULITE XT-190		1.379 MPa	(Filter) PRESSURE	(1893-3-31) O7-30							
	0306-2	SC	3976	3346	1548	R2	0.965 MPa	75 %	KULITE XT-190		2.068 MPa	(Filter) PRESSURE	(1743-5-116) D7-53							
	0307-2	SC	3976	3763	1029	R3	0.896 MPa	88 %	KULITE XT-190		1.379 MPa	(Filter) PRESSURE	(1743-5-222) P7-73							
NOTES:																	SC = Shelter Ceiling			
# = Distance in millimeters																	SF = Shelter Floor			
																	BW = Backwall			

Table 25. Continued.

MEASUREMENT LIST														DATE	22 MAY 92	PAGE 2 OF 8 PAGES
TEST EVENT		PAS-2				IE		KIRST				TRANSDUCER		CHANGES		
MEAS NO.	LOCATION			SENS AXIS	PRED MAX	CONF LEVEL	TRANSDUCER		RANGE	TRANSDUCER TYPE	SERIAL NUMBER	ITEM	AUTH	DATE		
	GEN	X#	Y#				Z#	MODEL							MODEL	
0402-2	FD	498	100	1475	X	66	KULITE	XT-190	1.379 MPa	(Nylon Mount) PRESSURE	(1893-3-108) X8-86					
0405-2	FW	498	3700	930	X	47	KULITE	HKS-11-375	6.895 MPa	(Nylon Mount) PRESSURE	117-7-7					
0501-2	SF	645	3700	367	Z	100	KULITE	HKS-11-375	3.447 MPa	(Filter) PRESSURE	2014-3-2					
0502-2	SC	645	0	2717	Z	100	KULITE	XT-190	1.379 MPa	(Filter) PRESSURE	(543-5-39) M5-84					
0503-2	SC	645	1749	2424	R1	100	KULITE	XT-190	1.379 MPa	(Filter) PRESSURE	(2200-2-83) G10-98					
0504-2	SC	645	3346	1548	R2	90	KULITE	XT-190	2.068 MPa	(Filter) PRESSURE	(1743-5-85) D7-47					
0601-2	SF	6818	1850	367	Z	95	KULITE	HKS-11-375	3.447 MPa	(Filter) PRESSURE	2013-2-18					
0602-2	SF	6818	3700	367	Z	69	KULITE	XT-190	1.379 MPa	(Filter) PRESSURE	(1743-5-112) D7-39					
0603-2	SF	6818	-3700	367	Z	69	KULITE	XT-190	1.379 MPa	(Filter) PRESSURE	(1743-5-242) P7-76					
0604-2	SC	6818	0	2717	Z	34	KULITE	HKS-11-375	13.79 MPa	(Filter) PRESSURE	118-7-26					
0605-2	SC	6818	1749	2424	R1	93	KULITE	HKS-11-375	6.895 MPa	(Filter) PRESSURE	117-7-19					
0606-2	SC	6818	3346	1548	R2	80	KULITE	HKS-11-375	3.447 MPa	(Filter) PRESSURE	2013-2-15					
NOTES:														SF = Shelter floor		
														SC = Shelter Ceiling		
														FD = Front Door		
														FW = Front Wall		

Table 25. Continued.

MEASUREMENT LIST																	DATE	22 MAY 92	PAGE 3 OF 8 PAGES
PAS-2										IE		KIRST							
TEST EVENT	MEAS NO.	LOCATION			Z#	ENS AXIS	PREC MAX	CONF LEVEL	TRANSDUCER		RANGE	TRANSDUCER TYPE	SERIAL NUMBER	CHANGES					
		GEN	X#	Y#					MODEL	ITEM				AUTH	DATE				
0607-2	SC		6818	3763	1029	R3	1.931 MPa	82 %	KULITE	HKS-11-375	3.447 MPa	(Filter) PRESSURE	2013-2-13						
0701-2	FF		-5000	0	350	Z	48.264 kPa	70 %	KULITE	XT-190	172.4 kPa	PRESSURE	(2710-1-15) A9-57	GADE	J.K.	8/10			
0702-2	FF		-9000	0	350	Z	17.237 kPa	63 %	KULITE	XT-190	68.95 kPa	PRESSURE	(2907-3-114) K9-35	GADE	J.K.	8/27			
0703-2	FF		-14000	0	350	Z	8.274 kPa	50 %	KULITE	XT-190	34.74 kPa	PRESSURE	(1495-7-75) K7-7						
0704-2	FF		-24000	0	350	Z	1.724 kPa	50 %	ENDEVCO	8510B	13.79 kPa	PRESSURE	C61M						
0705-2	FF		-3433	8000	350	Z	20.684 kPa	60 %	KULITE	XT-190	68.95 kPa	PRESSURE	(3827-4-19) L18-92						
0706-2	FF		-6233	10800	350	Z	6.895 kPa	50 %	ENDEVCO	8510B	13.79 kPa	PRESSURE	RF93	GADE	J.K.	8/27			
0707-2	FF		-16433	21000	350	Z	1.724 kPa	50 %	KULITE	XT-190	34.74 kPa	PRESSURE	(4263-5-135) Y18-25	GADE	J.K.	8/8			
0708-2	FF		6818	8000	350	Z	6.895 kPa	67 %	KULITE	XT-190	34.74 kPa	PRESSURE	(1495-7-76) K7-6						
0709-2	FF		6818	12000	350	Z	5.171 kPa	60 %	KULITE	XT-190	34.74 kPa	PRESSURE	(1491-2-46) U6-16						
0710-2	FF		6818	16000	350	Z	3.447 kPa	50 %	KULITE	XT-190	34.74 kPa	PRESSURE	(4363-5-139) X18-22	GADE	J.K.	8/10			
0711-2	FF		6818	24000	350	Z	1.724 kPa	50 %	ENDEVCO	8510B	13.79 kPa	PRESSURE	RF87						
NOTES: # = Distance in millimeters																			
FF = Free Field																			
SC = Shelter Ceiling																			

Table 25. Continued.

MEASUREMENT LIST														DATE	22 MAY 92	PAGE 4 OF 8 PAGES
TEST EVENT		PAS-2				IE		KIRST								
MEAS NO.	LOCATION			SENS AXIS	PREC MAX	CONF LEVEL	TRANSDUCER		TRANSDUCER TYPE	TRANSDUCER SERIAL NUMBER	CHANGES					
	GEN	X#	Y#				Z#	MODEL			RANGE	ITEM	AUTH	DATE		
0712-2	FF	17041	8000	350	Z	5.171 kPa	60	KULITE XT-190	34.74 kPa	PRESSURE	(4263-5-140) Y18-26	QAGE	J.K.	9/8		
0713-2	FF	19841	10800	350	Z	3.447 kPa	50	KULITE XT-190	34.74 kPa	PRESSURE	{RF91} (4363-5-151) X18-26	QAGE	J.K.	9/7		
0714-2	FF	21000	21000	350	Z	0.689 kPa	33	ENDEVCO 8510B	13.79 kPa	PRESSURE	C93M	QAGE	J.K.	9/10		
0715-2	FF	19000	0	350	Z	6.895 kPa	50	ENDEVCO 8510B	34.74 kPa	PRESSURE	RF77					
0716-2	FF	23000	0	350	Z	3.447 kPa	63	KULITE XT-190	13.79 kPa	PRESSURE	(4363-5-184) X18-31	QAGE	J.K.	9/10		
0717-2	FF	37000	0	350	Z	1.379 kPa	67	ENDEVCO 8510B	13.79 kPa	PRESSURE	WC95					
0718-2	FF	6818	-8000	350	Z	6.895 kPa	67	KULITE XT-190	34.74 kPa	PRESSURE	(4363-5-137) K18-21	QAGE	J.K.	9/10		
0719-2	FF	6818	-24000	350	Z	1.724 kPa	50	ENDEVCO 8510B	13.79 kPa	PRESSURE	RF86					
1301-2	SR	3976	0	2987	Z	1000 g	50	ENDEVCO 2264A	2000 g	ACCELEROMETER	CA90A					
1302-2	SR	3976	0	2987	Y	250 g	100	ENDEVCO 2260A	250 g	ACCELEROMETER	AR93F					
1303-2	SR	3976	1837	2680	R1	500 g	50	ENDEVCO 2264A	2000 g	ACCELEROMETER	BW72A					
1304-2	SR	3976	1837	2680	T1	150 g	60	ENDEVCO 2260A	250 g	ACCELEROMETER	AR80F					
NOTES:														■ = Distance in millimeters		
														FF = Free Field		
														SR = Structure Roof		

Table 25. Concluded.

MEASUREMENT LIST														DATE	22 MAY 92	PAGE 8 OF 8 PAGES
TEST EQUIP		PAS-2				IE		KIRST								
MEAS NO.	GEN	LOCATION			SENS AXIS	PRED MAX	CONF LEVEL	TRANSDUCER		RANGE	TRANSDUCER TYPE	TRANSDUCER SERIAL NUMBER	CHANGES			
		X#	Y#	Z#				MODEL	ITEM				AUTH	DATE		
1305-2	SR	3976	3514	1759	R2	500 g	50 %	ENDEVCO	2264A	2000 g	ACCELEROMETER	CA65A				
1306-2	SR	3976	3514	1759	T2	150 g	60 %	ENDEVCO	2260A	250 g	ACCELEROMETER	AQ95F				
1601-2	SR	6818	0	2987	Z	3500 g	70 %	ENDEVCO	2264A	5000 g	ACCELEROMETER	BY90B				
1602-2	SR	6818	0	2987	Y	500 g	50 %	ENDEVCO	2262C	1000 g	ACCELEROMETER	KT55				
1603-2	SR	6818	1837	2680	R1	1500 g	50 %	ENDEVCO	2264A	5000 g	ACCELEROMETER	CA20B				
1604-2	SR	6818	1837	2680	T1	300 g	50 %	ENDEVCO	2262C	1000 g	ACCELEROMETER	KA17				
1605-2	SR	6818	3514	1759	R2	1000 g	50 %	ENDEVCO	2264A	5000 g	ACCELEROMETER	BT06A				
1606-2	SR	6818	3514	1759	T2	250 g	50 %	ENDEVCO	2262C	1000 g	ACCELEROMETER	KA38				
3401-2	FD	415	0	1475	Z	5000 msn	25 %	AILTECH	SG159-11-10-6S	+/-20000 msn	STRAIN GAGE	N/A				
3402-2	FD	415	0	1475	Z	5000 msn	25 %	AILTECH	SG159-11-10-6S	+/-20000 msn	STRAIN GAGE	N/A				
3403-2	FD	498	0	1475	Z	5000 msn	25 %	AILTECH	SG159-11-10-6S	+/-20000 msn	STRAIN GAGE	N/A				
3404-2	FD	498	0	1475	Z	5000 msn	25 %	AILTECH	SG159-11-10-6S	+/-20000 msn	STRAIN GAGE	N/A				
NOTES: # = Distance in millimeters msn = microstrains																
SR = Shelter Roof																
FD = Front Door																

NOTES: # = Distance in millimeters
 SR = Shelter Roof
 FD = Front Door

msn = microstrains

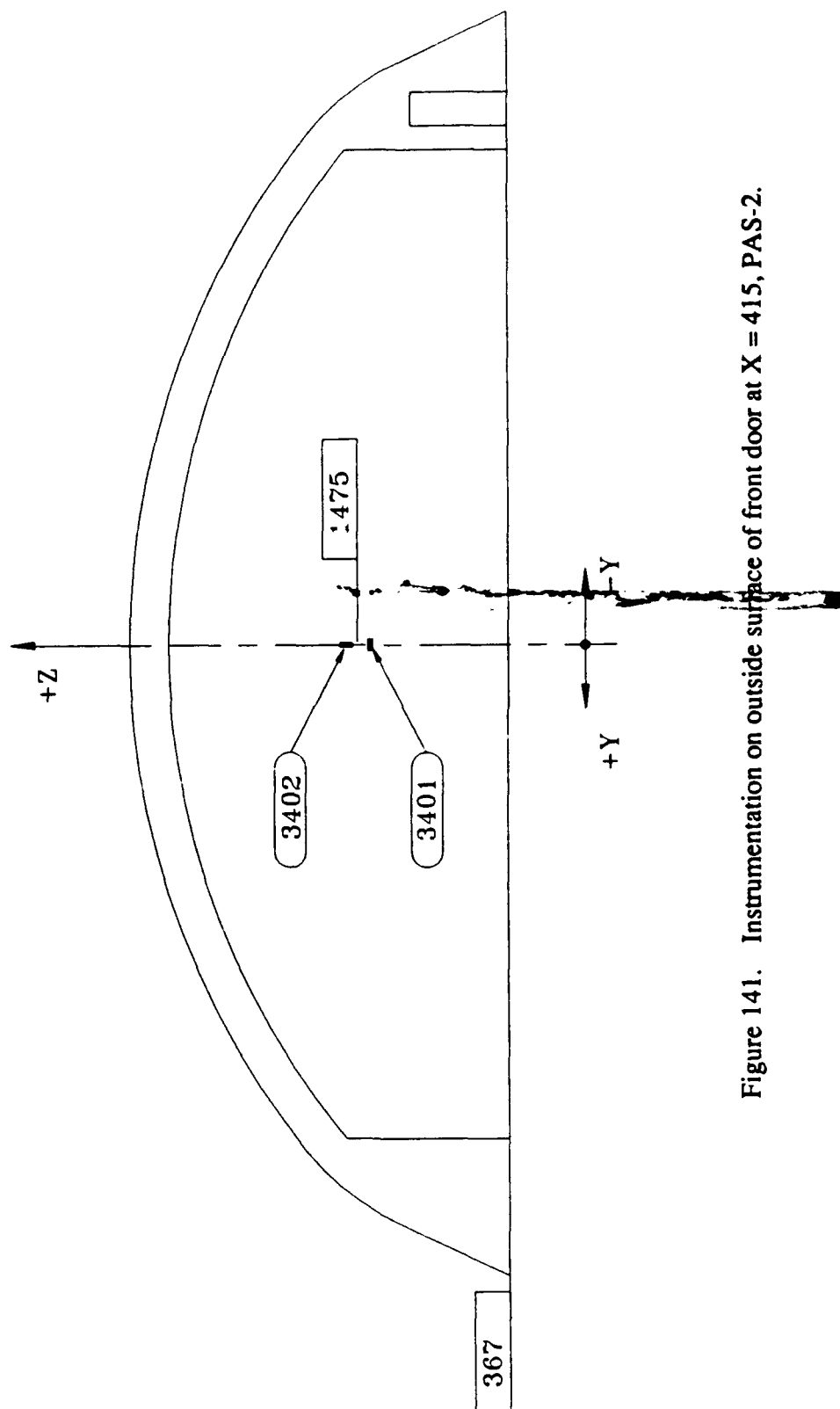


Figure 141. Instrumentation on outside surface of front door at $X = 415$, PAS-2.

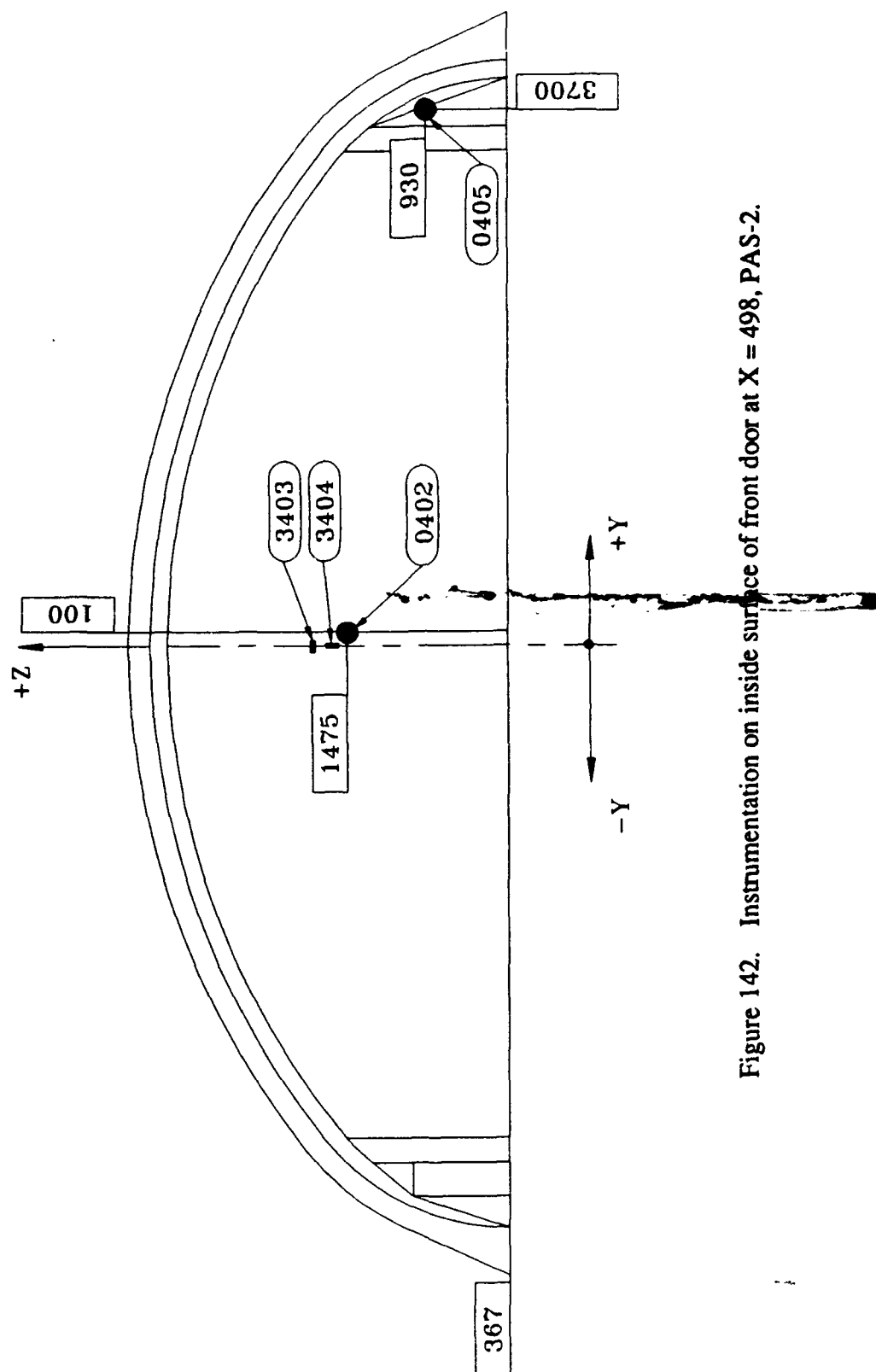


Figure 142. Instrumentation on inside surface of front door at $X = 498$, PAS-2.

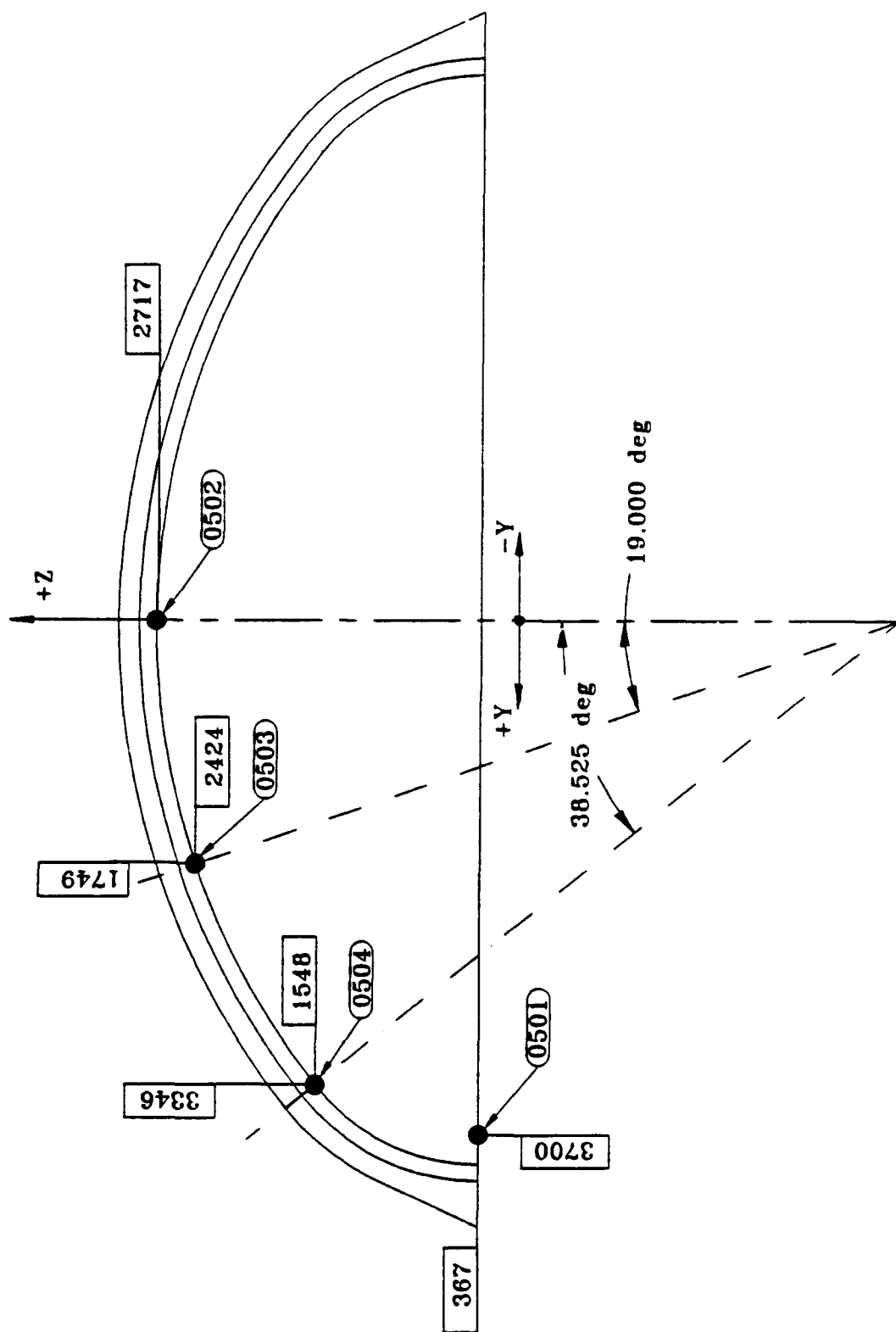


Figure 143. Instrumentation on arch at $X = 645$, PAS-2.

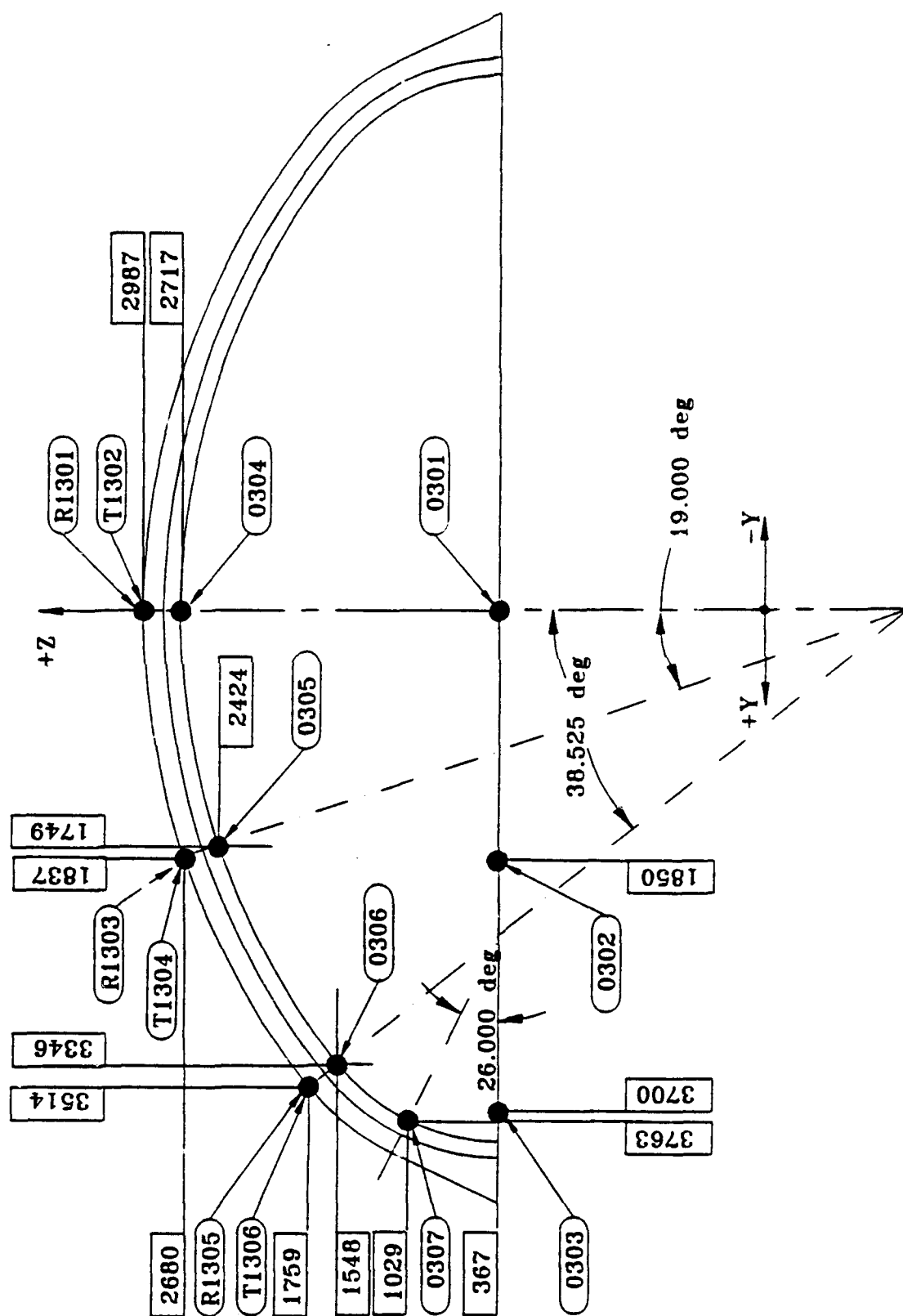


Figure 144. Instrumentation on arch at $X = 3976$, PAS 2.

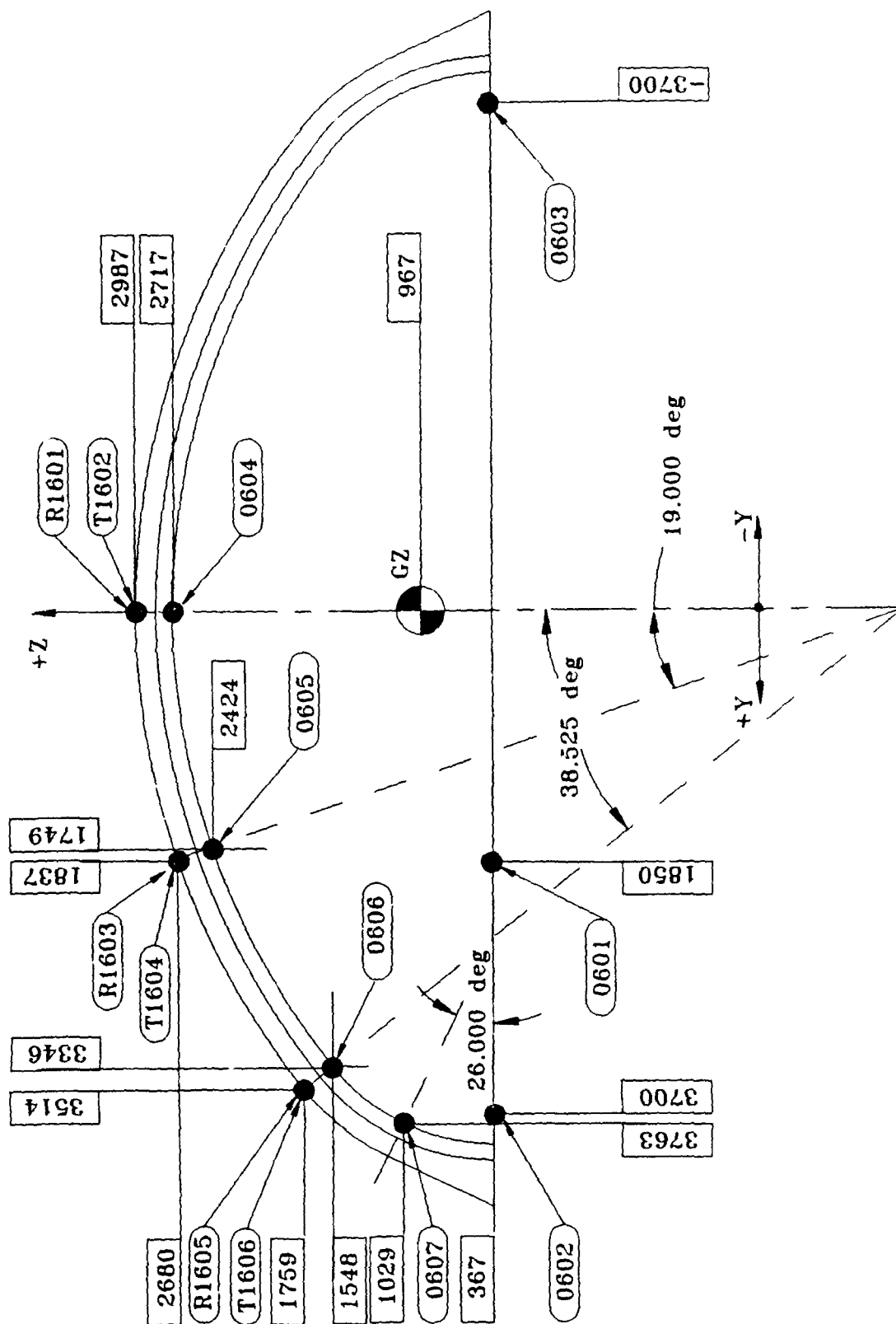


Figure 145. Instrumentation on arch at X = 6818, PAS-2.

Figure 146 shows the locations of airblast gages mounted in the backwall. Figure 147 shows the locations of the free-field airblast gages.

Fourteen high-speed motion picture and sequential still cameras were provided at five camera stations. The locations of these stations for the PAS-2 event are shown in Figure 148. Motion picture data were recorded at rates of 500 and 1000 frames per second.

5.2 TEST RESULTS

5.2.1 Structural Damage Survey

The test structure was severely damaged in the PAS-2 event, but the arch and backwall remained standing. Figures 3 and 4 present a key for identifying the various components of the model shelter in the following discussion of structural damage. As in the discussion of PAS-3 results, estimated debris velocities were calculated on the basis of observed object motion in one plane. The actual velocities could be somewhat higher due to out-of-plane motion of the object. In the few instances where out-of-plane motion was checked for a specific piece of debris, it did not appear to be a significant factor.

The front door was again blown out of the structure very quickly. Smoke was observed along the top edge of the door at about 6 ms, and it appeared to separate from the door frame at about 25 ms. The door rotated about its lower edge and was flat on the front apron at about 140 ms. It then skidded outward along the ground and came to rest at about 19 m from the front of the structure (Fig. 149). The velocity of the door could not be determined because its early movement was obscured by smoke, flame, and dust.

The door was bent its full length about a horizontal line and had a maximum deflection of 125 mm at the center (Fig. 150). The inside plate was dished inward between each

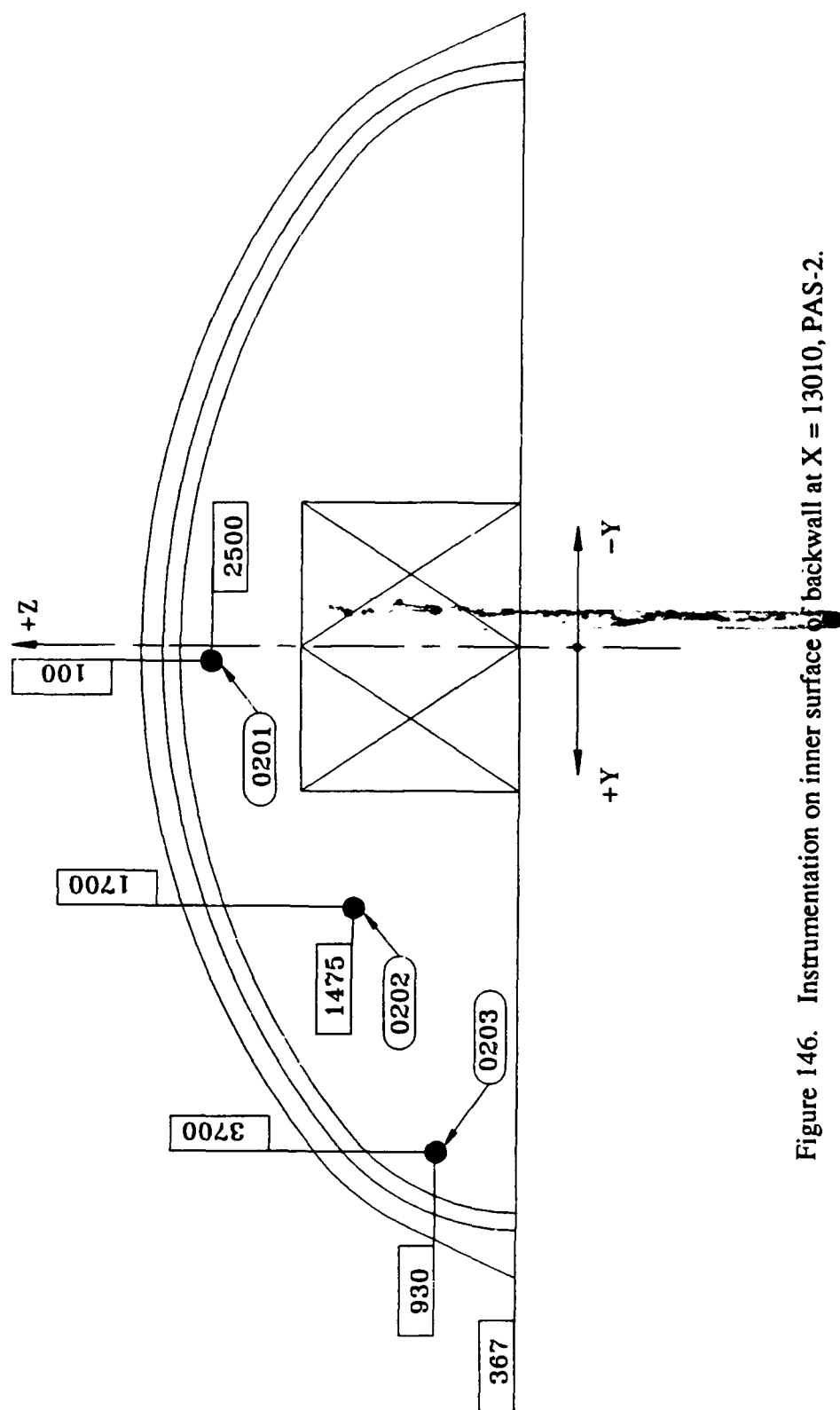


Figure 146. Instrumentation on inner surface of backwall at X = 13010, PAS-2.

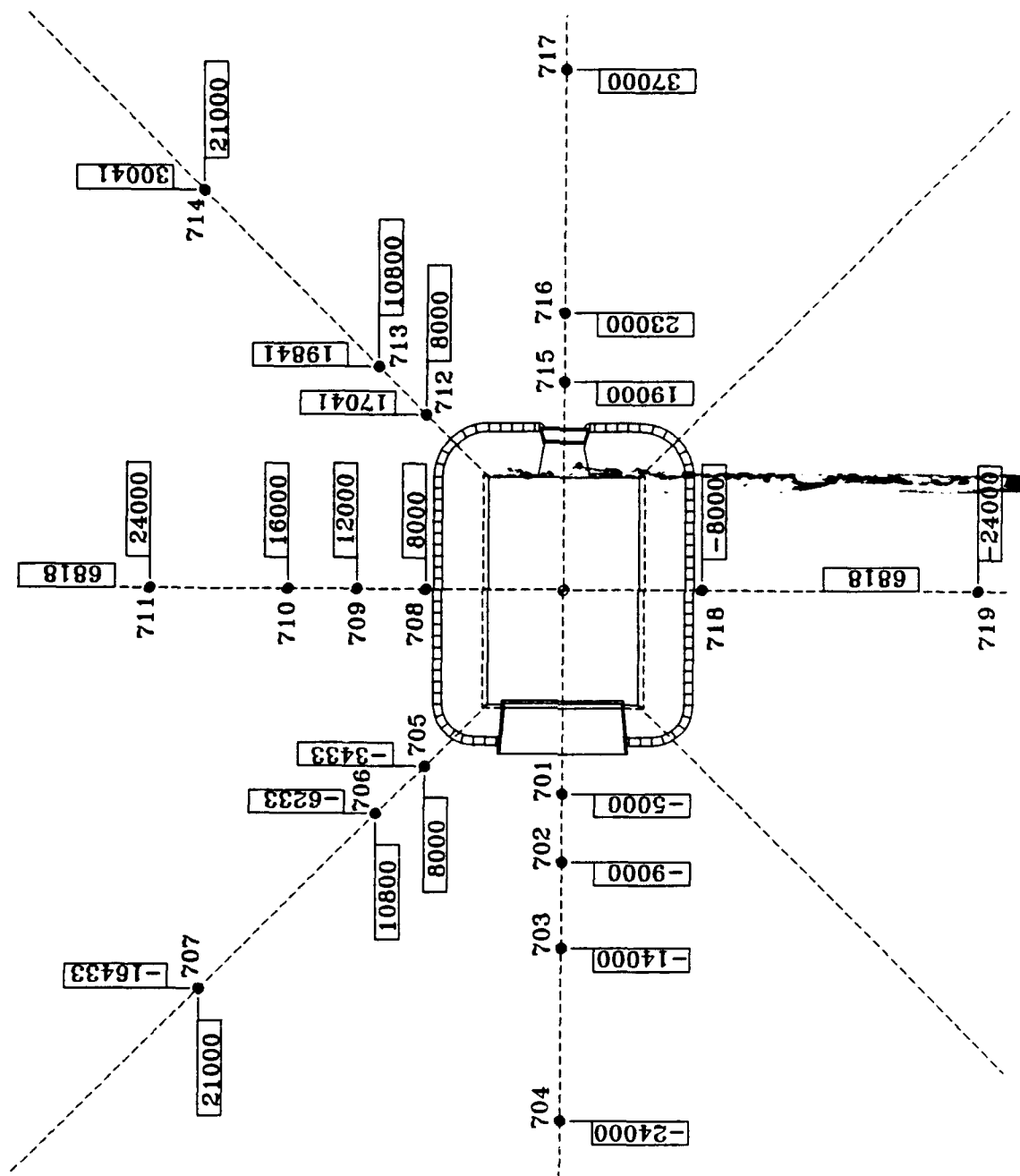


Figure 147. Free-field airblast gage locations, PAS-2.

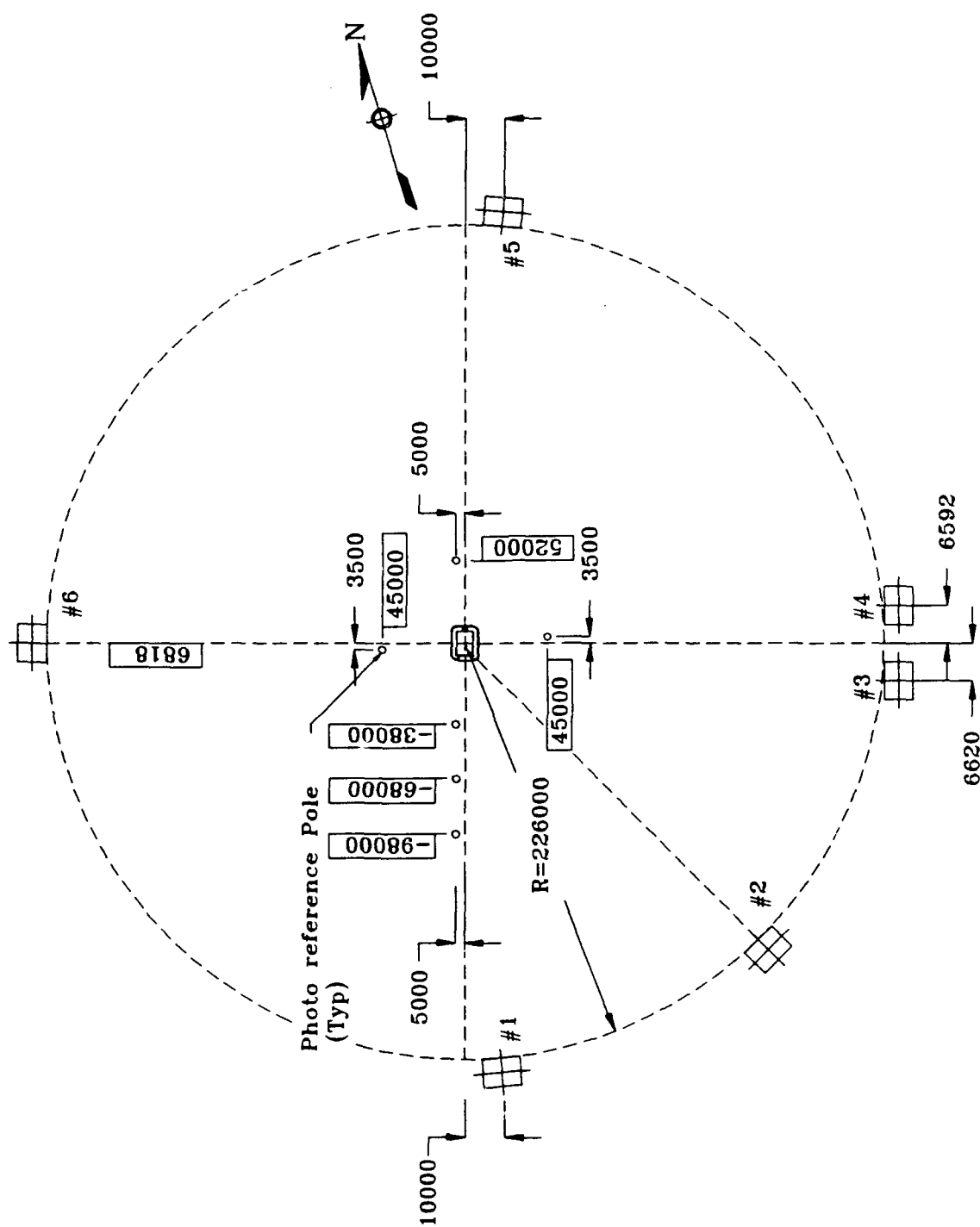


Figure 148. Camera station locations, PAS-2.

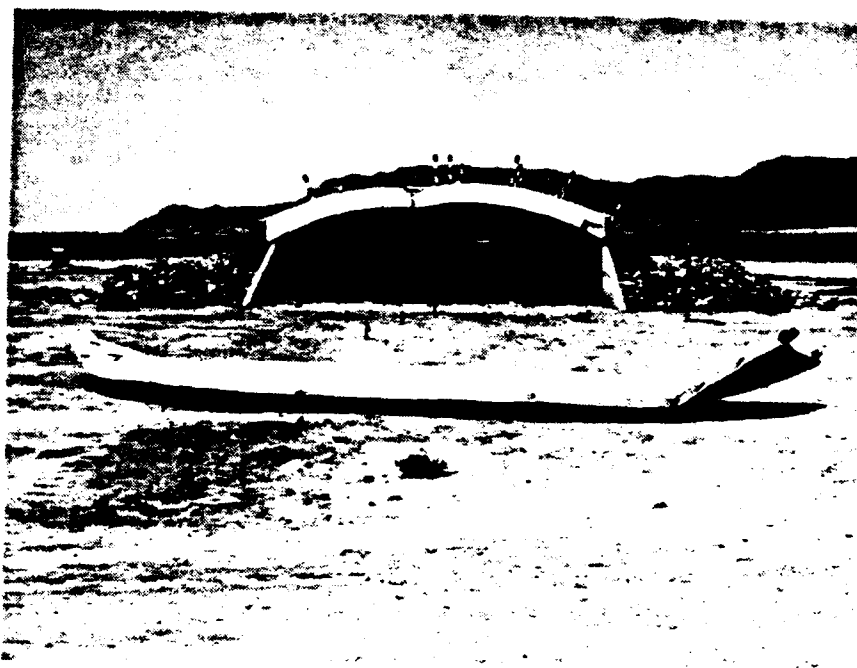


Figure 149. Posttest location of front door, PAS-2.



Figure 150. Posttest condition of inside surface of front door, PAS-2.

of the vertical ribs. The inside plate was also buckled in a 500- to 900-mm-wide band along the horizontal centerline. The sides of the door were bent inward approximately 470 mm at the left edge and 250 mm at the right edge (Fig. 151). No broken welds were detected.

The personnel vestibule was found in its original location against the left wingwall. The personnel door was blown out of its frame in the left front wall and was found inside the vestibule (Fig. 152). The door was bent in half about its vertical centerline. The welds simulating the hinges and latches were all broken. The door frame remained welded to the steel liner.

Although the wingwalls were still in place following the test, both were damaged when the front section of the arch fell back on top of them (Fig. 153). This figure also shows a slight separation between the wingwalls and the front walls. There was some spalling of the concrete on the inside face of the left wingwall at the door opening, but this damage was probably due to the impact of the arch section on the wingwall.

The front apron slab was slightly damaged when it was struck by a lifting lug on the front door (Fig. 154). No other cracks were observed in the apron slab, and there was no separation in the joint between the apron slab and the front foundation and wingwalls.

The front walls remained attached to the foundation, but the top of the headworks and the parapet broke away from the front wall with the front arch section (Fig. 155). The separation in the headworks steel liner assembly occurred at or near the welded joint in the liner. In some instances the weld was broken, in others the failure occurred in the base metal of the liner. The door stop at the top of the door frame was broken off of the frame. A series of radial cracks were observed in the front face of the parapet (Fig. 156). The crack pattern was virtually identical to that observed in the PAS-1 test. The large crack at the center of the parapet is consistent with a flexure failure, and probably a result of the front section of the arch falling back onto the wingwalls. There did not appear to be any significant damage to the front wall foundation.

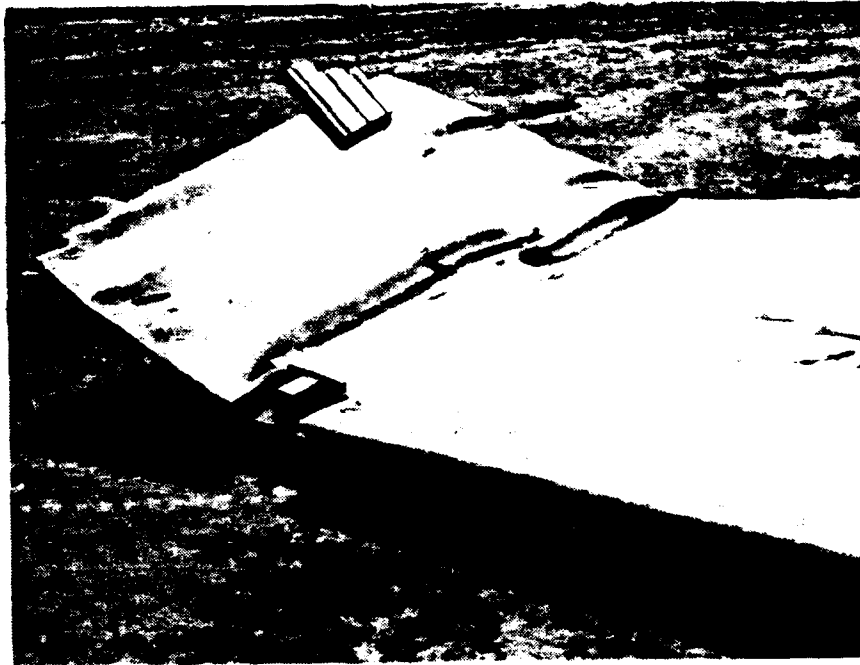


Figure 151. Bent ends of front door, PAS-2.



Figure 152. Personnel door inside vestibule, PAS-2.



Figure 153. Damage to left wingwall, PAS-2.



Figure 154. Impact damage to edge of apron slab, PAS-2.

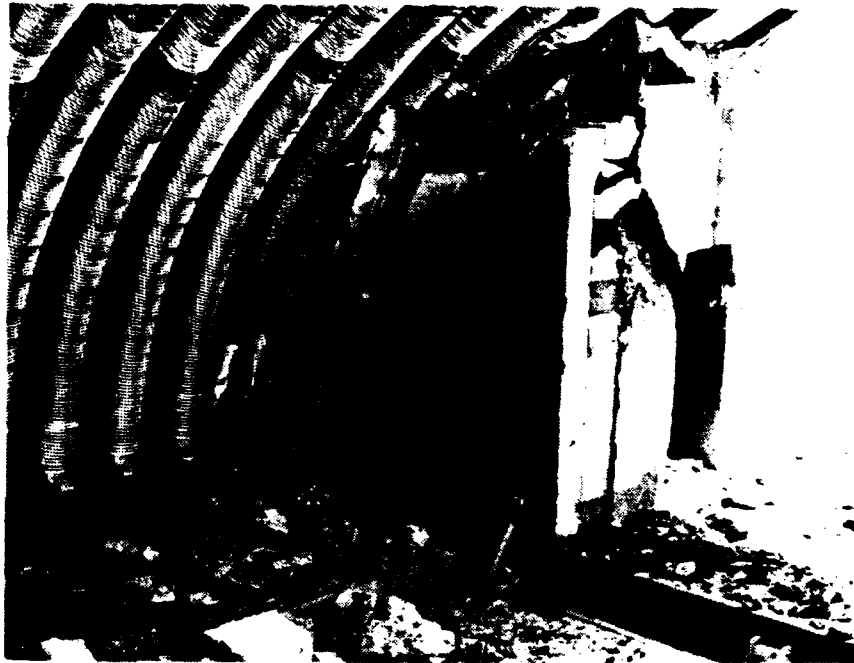


Figure 155. Posttest view of left front wall, PAS-2.

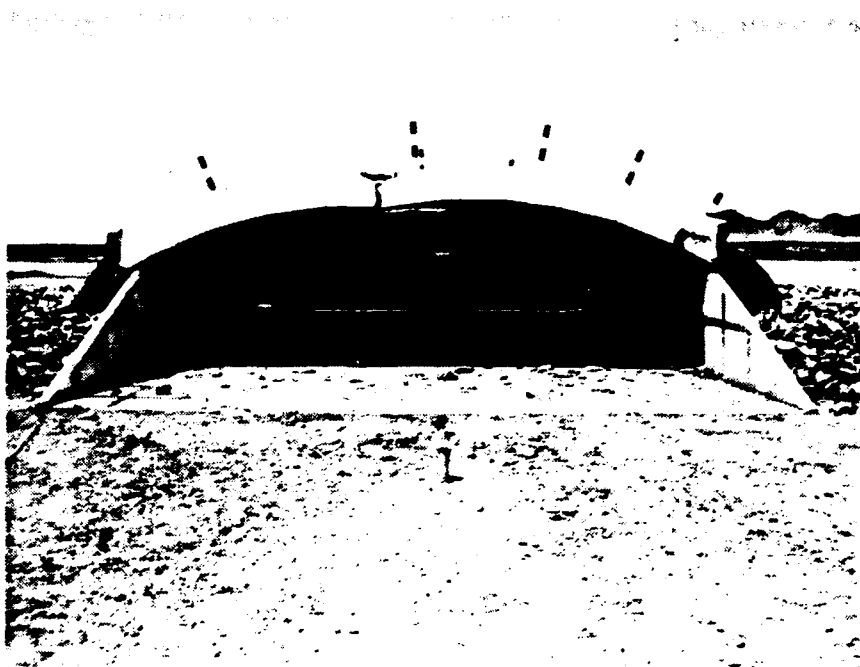


Figure 156. Crack pattern in front face of parapet, PAS-2.

The first detectable upward motion of the arch portion of the structure occurred at about 25 ms. The arch broke away from the foundation and into two sections along a transverse line approximately 9.1 m from the front of the structure. Figure 157 shows an overall view of the transverse failure plane in the arch. The front section moved upward uniformly for about 200 ms to a height of about 0.85 m. This section then began to rotate about the break point, and its front edge reached a maximum height of about 3.7 m. It came back down on top of the wingwalls (Fig. 153) about 1.0 m forward of its original position. The rear arch section remained attached to, and rotated about, the lower edge of the backwall. The front edge of this section reached a maximum height of about 0.75 m. The trajectory of the arch was vertical with no detectable sideways motion. The vertical velocity of the front section was about 6.3 m/s at 160 ms after $t = 0$ and decreased to 5.7 m/s at 230 ms. At 230 ms the vertical velocity of the front edge of the rear section was 1.6 m/s.

The transverse failure plane in the arch occurred along a bolted liner joint (Fig. 158). Examination of the failure line showed an edge tear-out of the bolts in the liner material and a tension failure in the concrete. The failure plane occurred at the only location where the splices for both layers of the longitudinal reinforcing bars are in close proximity. Almost all the reinforcing bars crossing the failure plane were found to have been pulled out of the concrete (Fig. 159). Transverse cracks were observed all along the arch (Fig. 160). Measurements indicated that the location of these cracks corresponded closely with the transverse bolt lines of the steel liner.

A longitudinal crack was observed along the crown of the arch. The crack began at the front parapet and extended to a point 2.64 m down the arch (Fig. 161). The appearance of the top surface of the concrete along the crack was consistent with a flexure compression failure. The steel liner had been partially pulled apart at some of the bolted joints on the inside surface of the structure opposite the crack (Fig. 162).

The arch was severely fractured and rubbleized on both sides where it broke away from the front walls (Fig. 163). The damage was more severe and extensive on the left corner than on the right. The diagonal crack pattern seen in these areas of the arch in

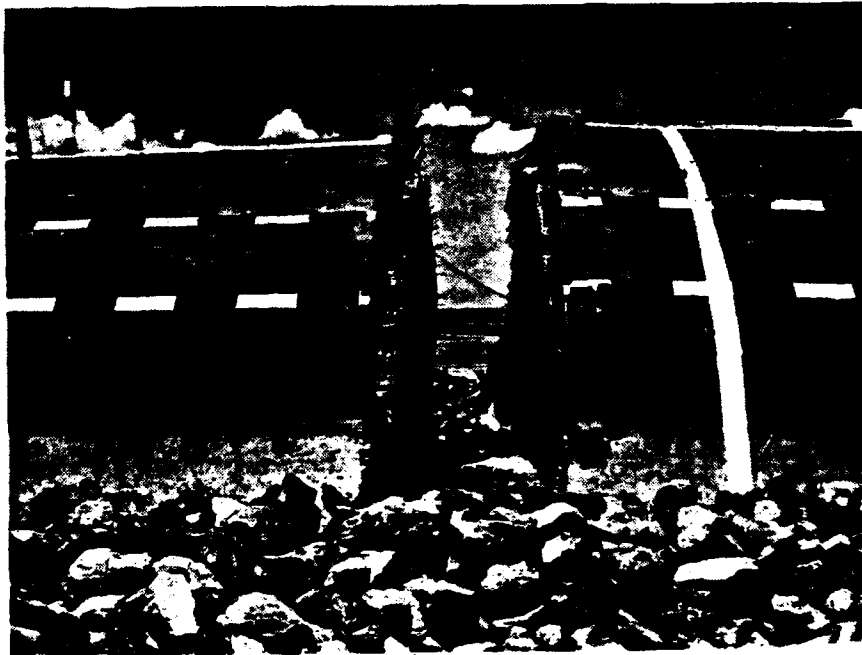


Figure 157. View of transverse failure plane in arch, PAS-2.

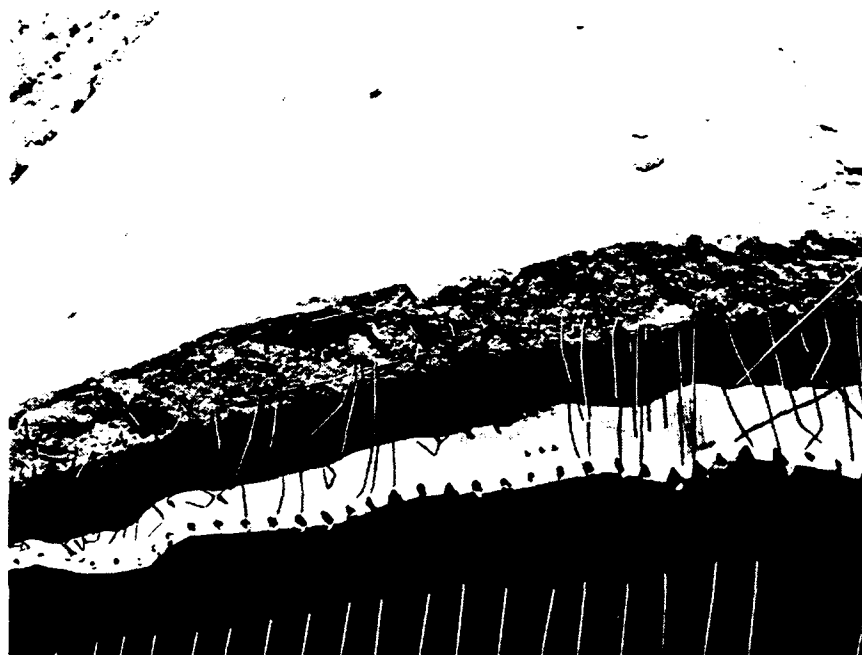


Figure 158. Edge tear-out of bolts in line at transverse failure plane, PAS-2.



Figure 159. Pull-out of reinforcing bars at transverse failure plane, PAS-2.

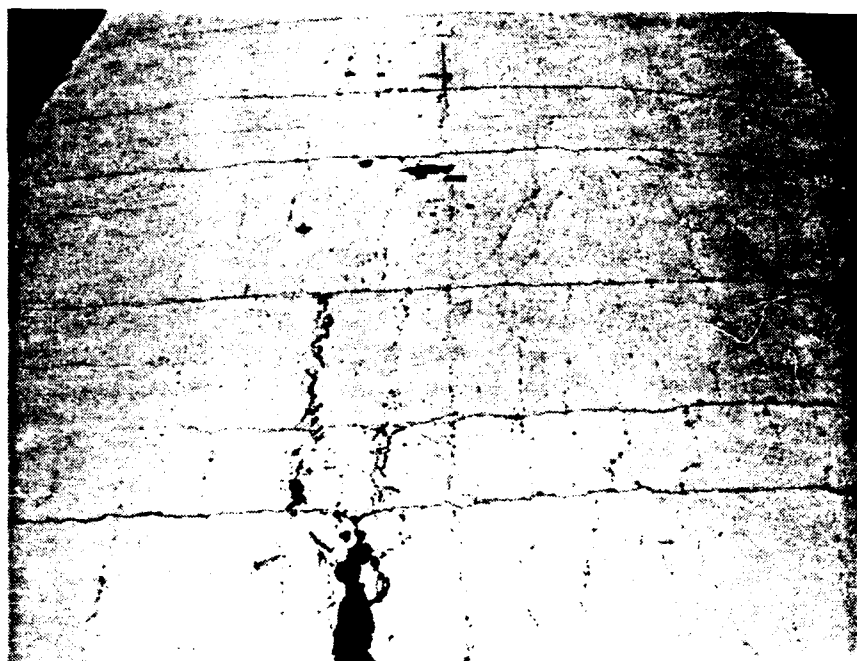


Figure 160. Transverse cracking pattern in arch, PAS-2.

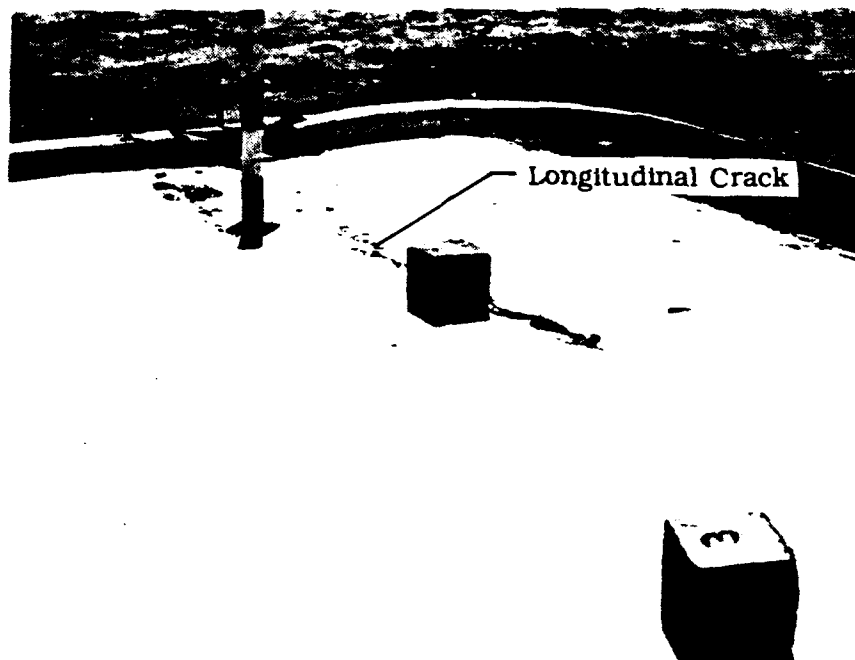


Figure 161. Longitudinal cracks at crown of arch, PAS-2.



Figure 162. Condition of liner joints opposite longitudinal cracks, PAS-2.



Figure 163. Damage at left front corner of arch, PAS-2.

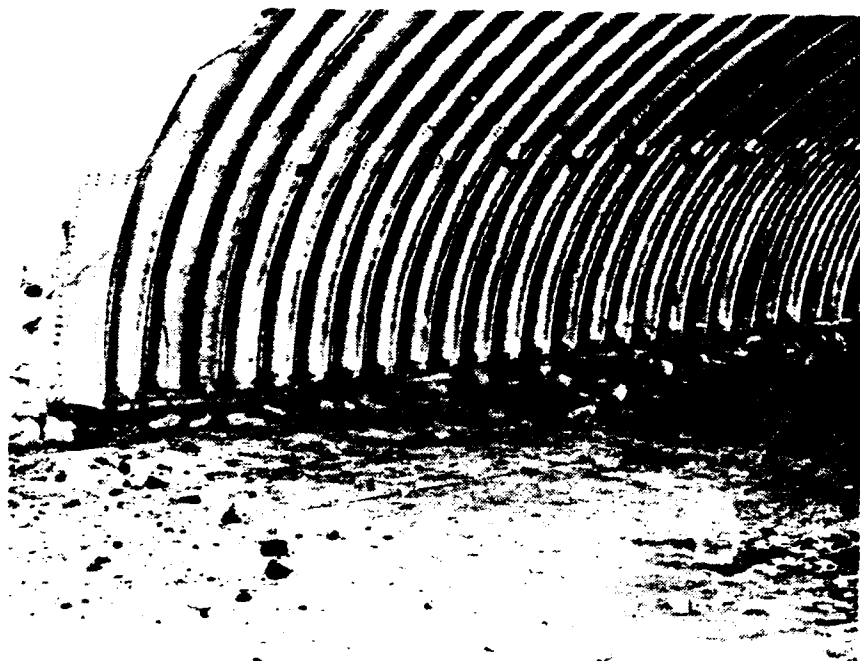


Figure 164. Arch resting on rock rubble, PAS-2.

PAS-2 is clearly similar to the one observed in the PAS-1 test at the same locations but much more severe.

Most of the arch foundation was found covered with rock rubble, with the arch sections resting on the rock rubble (Fig. 164). The only visible portion of the arch foundation was at the opening between the two arch sections. In this area the foundation showed virtually no outward displacement, but a posttest survey showed 50 to 150 mm of residual upward displacement. In the open area between the two arch sections, all the outside dowel bars in the joint between the arch and foundation were either broken off at the top of the foundation or broken inside the foundation and pulled out (Fig. 165). Most of the inner dowel bars were found broken at the top of the foundation or pulled out of the base of the arch. The outer dowel bars had hooked ends, and the inner dowels did not.

About half of the anchor bolts for the arch liner base channel were found still embedded in the foundation. The channel had been pulled up over the bolts and remained attached to the sections of the arch. The rest of the anchor bolts had pulled out of the foundation, along with the channel, and were still attached to the base edge of the arch sections (Fig. 166).

Figure 166 also shows a crack in the floor slab running parallel to, and about 550 mm from, both sides of the arch and the backwall. The crack varied in width from a few millimeters up to about 50 mm, and the average vertical displacement between the two sides of the crack was 15 mm. The concrete at the edges of the crack was severely fractured and crushed. The floor slab sloped upward from the crack to the arch foundation and backwall. The joint between the floor slab and arch foundations was still tightly closed. At both back corners, another large crack ran diagonally from the intersection of the cracks (parallel to the sides) back to the corner of the arch and backwall (Fig. 167).

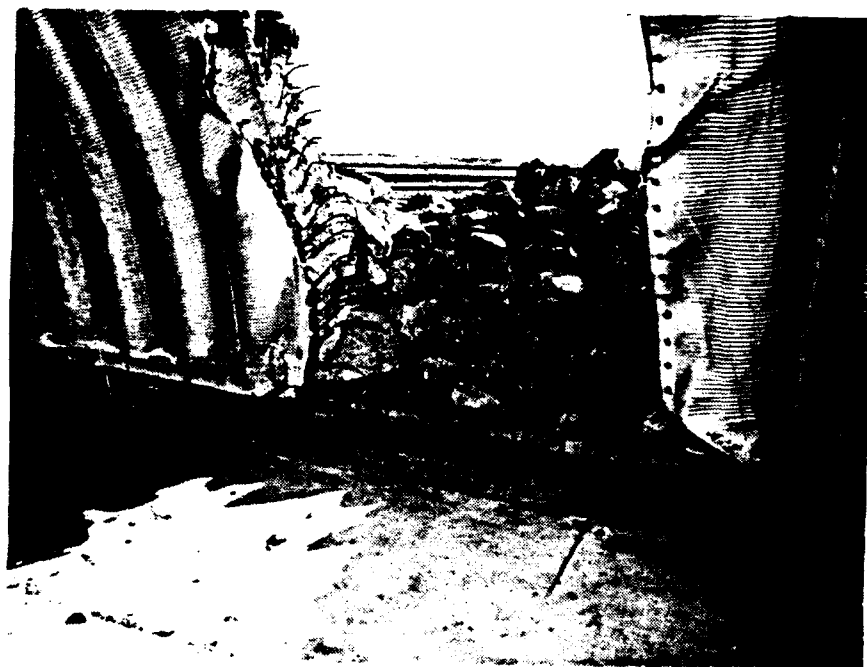


Figure 165. Broken dowel bars in arch foundation, PAS-2.

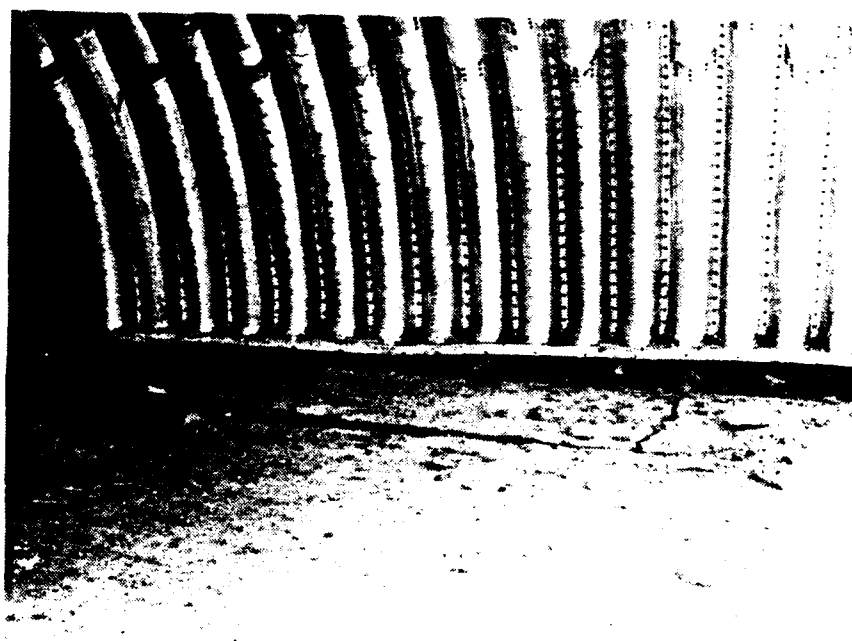


Figure 166. Anchor bolt pull-out at base of arch, PAS-2.

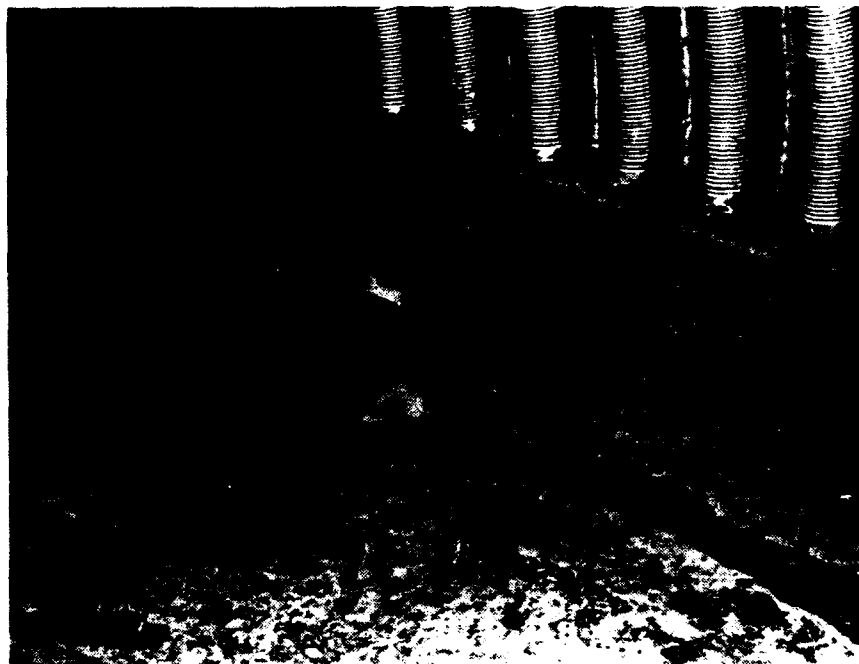


Figure 167. Crack at back corners of floor slab, PAS-2.



Figure 168. Crack pattern in left side of arch at backwall, PAS-2.

The backwall was found upright on its foundation. An outward tip of about 1.5 deg was noted. The backwall also appeared to have been displaced backward. The arch was still attached to the top of the backwall. Figure 168 shows a single crack running parallel to the plane of the backwall on the outside surface of the arch on the left side. The crack varied in width from about 8 mm near the top of the rock rubble to zero near the crown. Some crushing of the concrete was observed along the crack line near the top of the rock rubble. There was no similar crack pattern on the right side. The position of the crack tended to correspond with the vertical offset in the top of the backwall (Fig. 169). There were no cracks on the inside surface of the backwall.

A gap was noted between the outside surface of the backwall and the earth berm. This gap is probably due to the rebound of the backwall from its maximum outward displacement and motion induced to the soil.

The front portion of the backwall foundation was still covered by the floor slab. The crack pattern in the floor slab suggested an upward movement and a backward rotation of the backwall foundation. Although not as easily observable as in the PAS-3 test, it appears that the backwall foundation fractured along a vertical plane corresponding to the inside face of the backwall (Fig. 170).

A gap was noted along the full length of the joint between the floor slab and the backwall. The gap ranged in width from a few millimeters at the back corners to 25 mm at the opening of the exhaust port (Fig. 171).

The heavily reinforced portion of the floor slab between the door pit and the expansion joint showed a few randomly spaced hairline cracks running parallel to the longitudinal axis of the structure. The joint between the floor slab and the heavily reinforced portion of the floor slab containing the door pit showed a slight separation of the two components. The fiberboard expansion joint filler was still in place along the length of the joint.

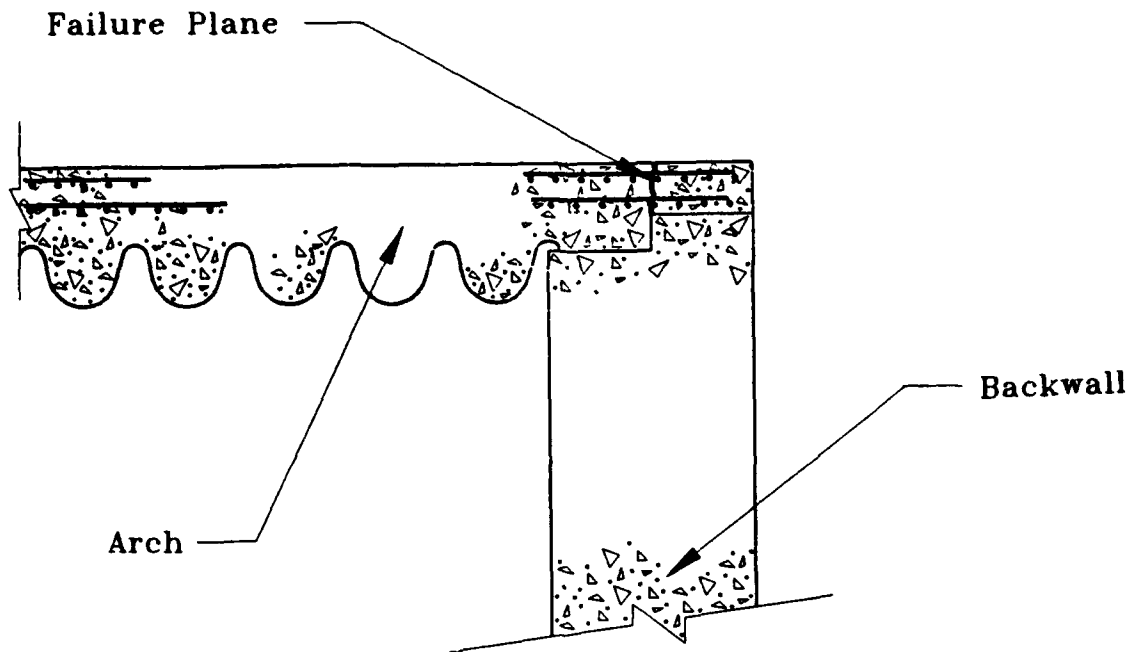


Figure 169. Section: Failure plane between the arch and backwall, PAS-2.

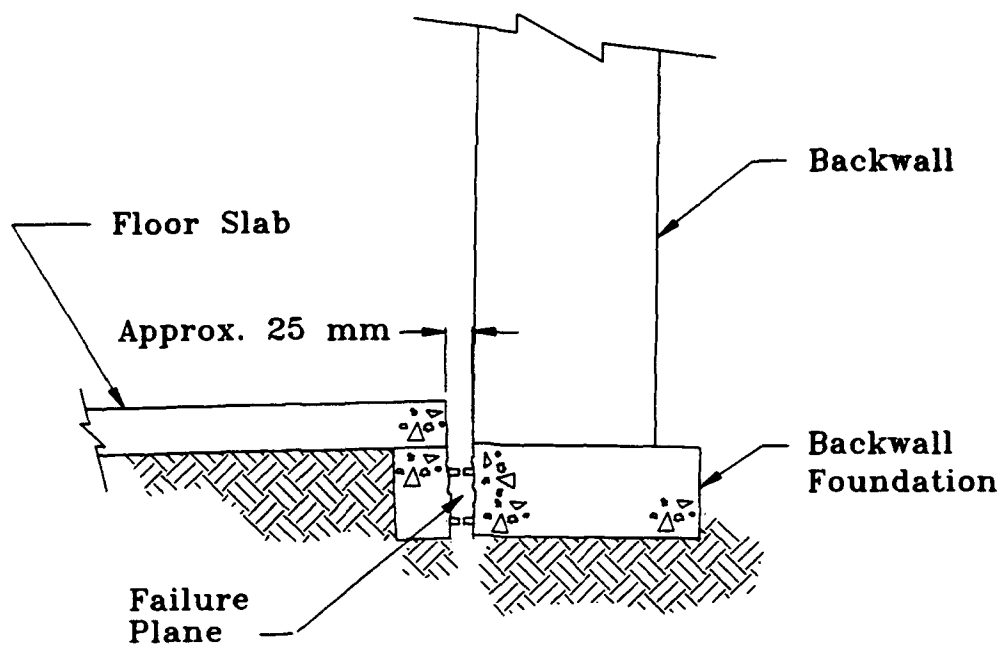


Figure 170. Section: Failure plane in backwall foundation, PAS-2.



Figure 171. Gap between floor slab and backwall, PAS-2.

A small area of spalling was observed in the underside of the roof slab of the exhaust port at its junction with the center wall. The crack pattern suggests that the roof had been pushed upward from the wall. No other major cracking was seen in the exhaust port, either at the corners or in the structural elements themselves. No cracking or separation was observed between the exhaust port and the backwall.

The steel door on the right side of the exhaust port was bent about a horizontal axis, but held its place in the frame (Fig. 172). The other exhaust port door was blown out of its frame, but remained inside the exhaust port (Fig. 173). Some of the earth backfill had fallen into the exhaust port covering the left door. When uncovered, it was noted that the left door was also bent about its horizontal centerline. The steel frames for both doors were still tightly embedded in the concrete floor, walls, and roof of the exhaust port.

5.2.2 Data Obtained from Instrumentation

Data were obtained from all of the electronic sensors. Although some baseline shifts were noted and a few of the data channels failed at later times, useful data appeared to have been obtained from most measurements. No corrections have been made to data presented in this report.

The maximum pressure recorded inside the structure was 8.2 MPa at MN 604 (Fig. 174b). This gage was located on the ceiling directly over the charge. The INBLAST code predicted 12.2 MPa at this location. Figures 175 and 176 show the pressures recorded on the floor near the opposite sides of the structure in the same plane as MN 604. These two gages showed symmetry in the magnitudes and TOAs of the first few peaks of the two records. The first peak of MN 602 was 1.22 MPa (Fig. 175); the first peak of MN 603 was 1.29 MPa (Fig. 176).

The only pressure measurement made on the inside surface of the front door in the PAS-2 test was MN 402 (Fig. 177). This gage was located near the center of the door, and it recorded a peak pressure of 0.74 MPa at 24 ms. The INBLAST code predicted a



Figure 172. Steel door in right side of exhaust port, PAS-2.



Figure 173. Steel door in left side of exhaust port, covered with backfill, PAS-2.

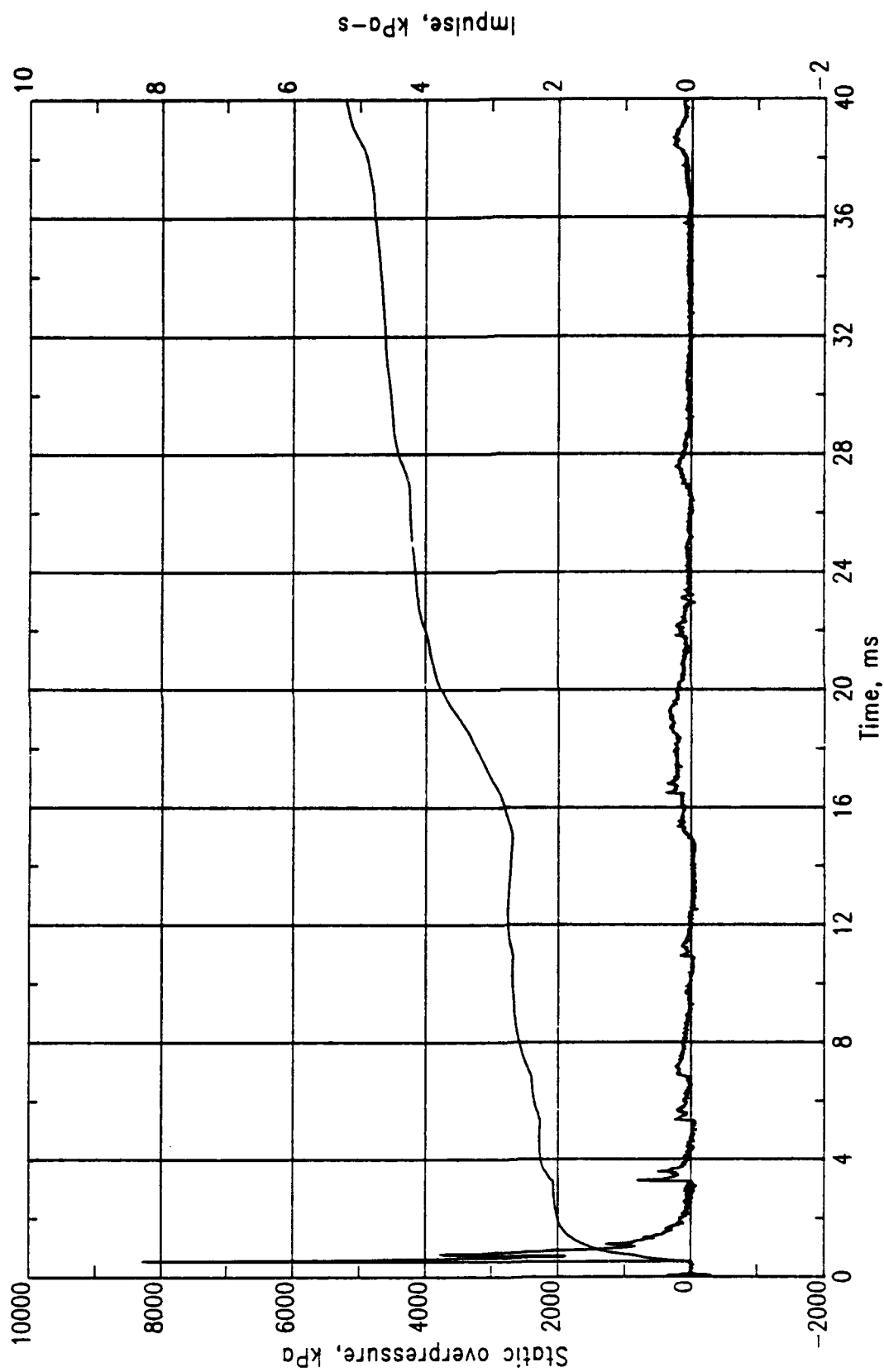


Figure 174. PAS-2, MN 0604.

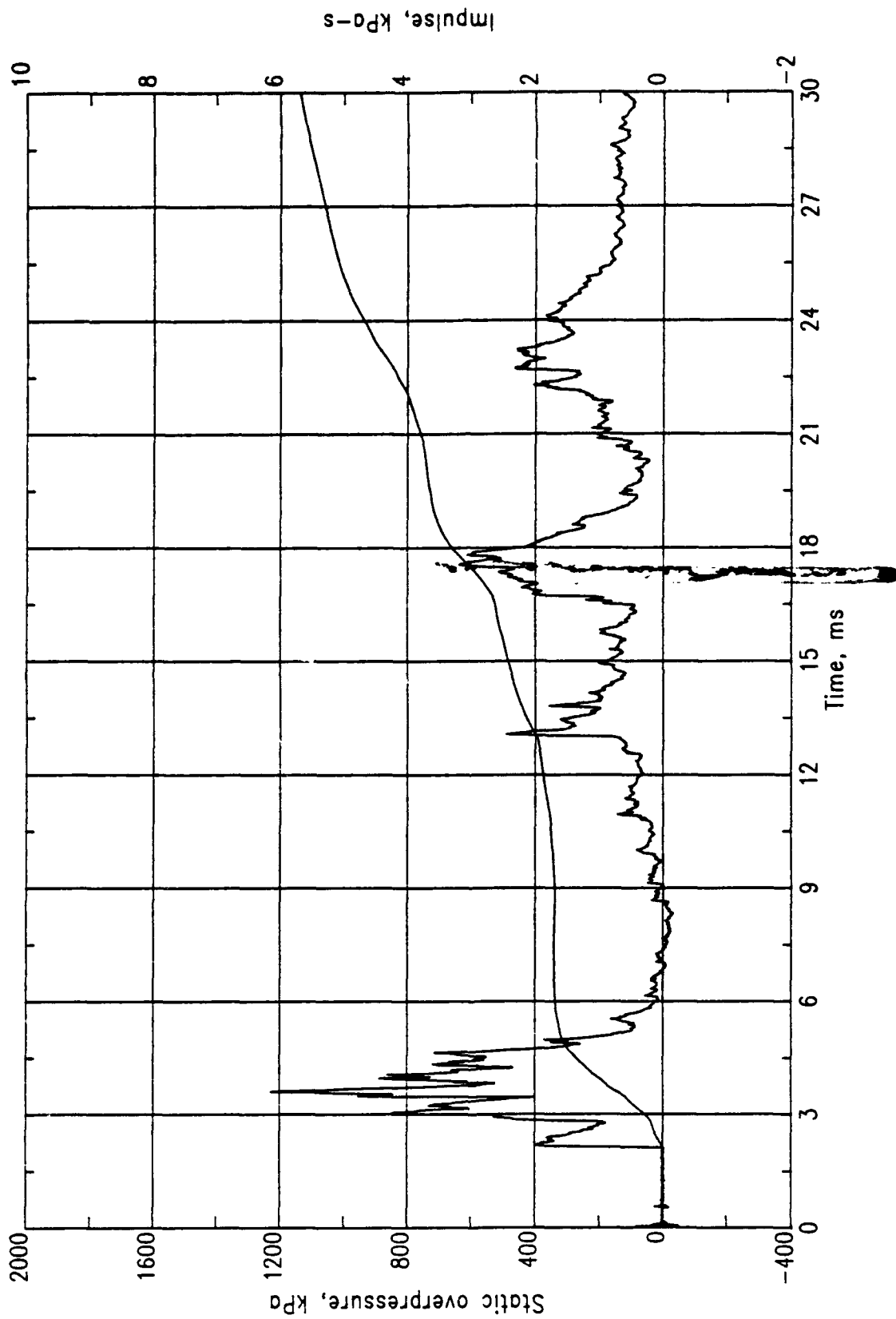


Figure 175. PAS-2, MN 0602.

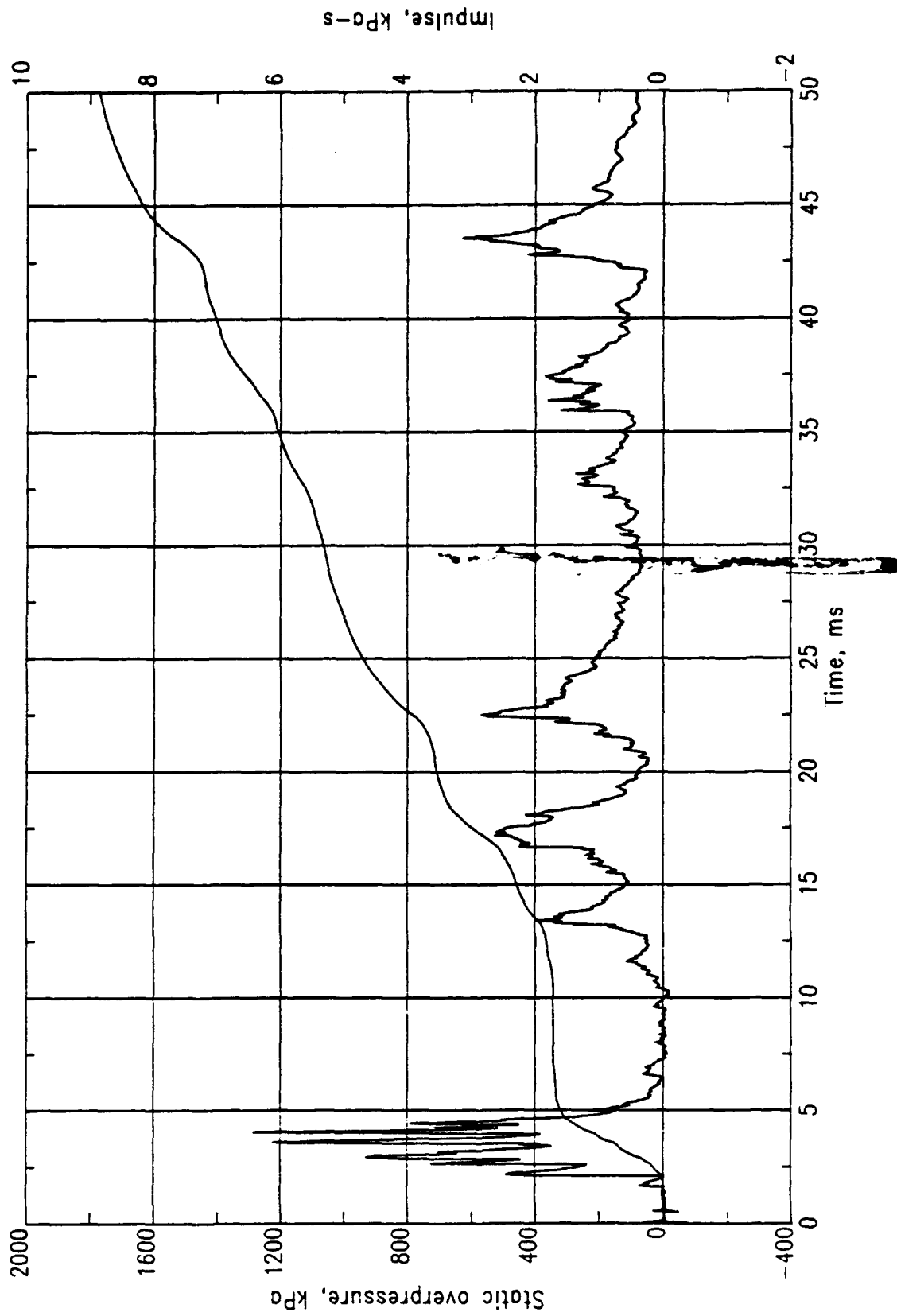


Figure 176. PAS-2, MN 0603.

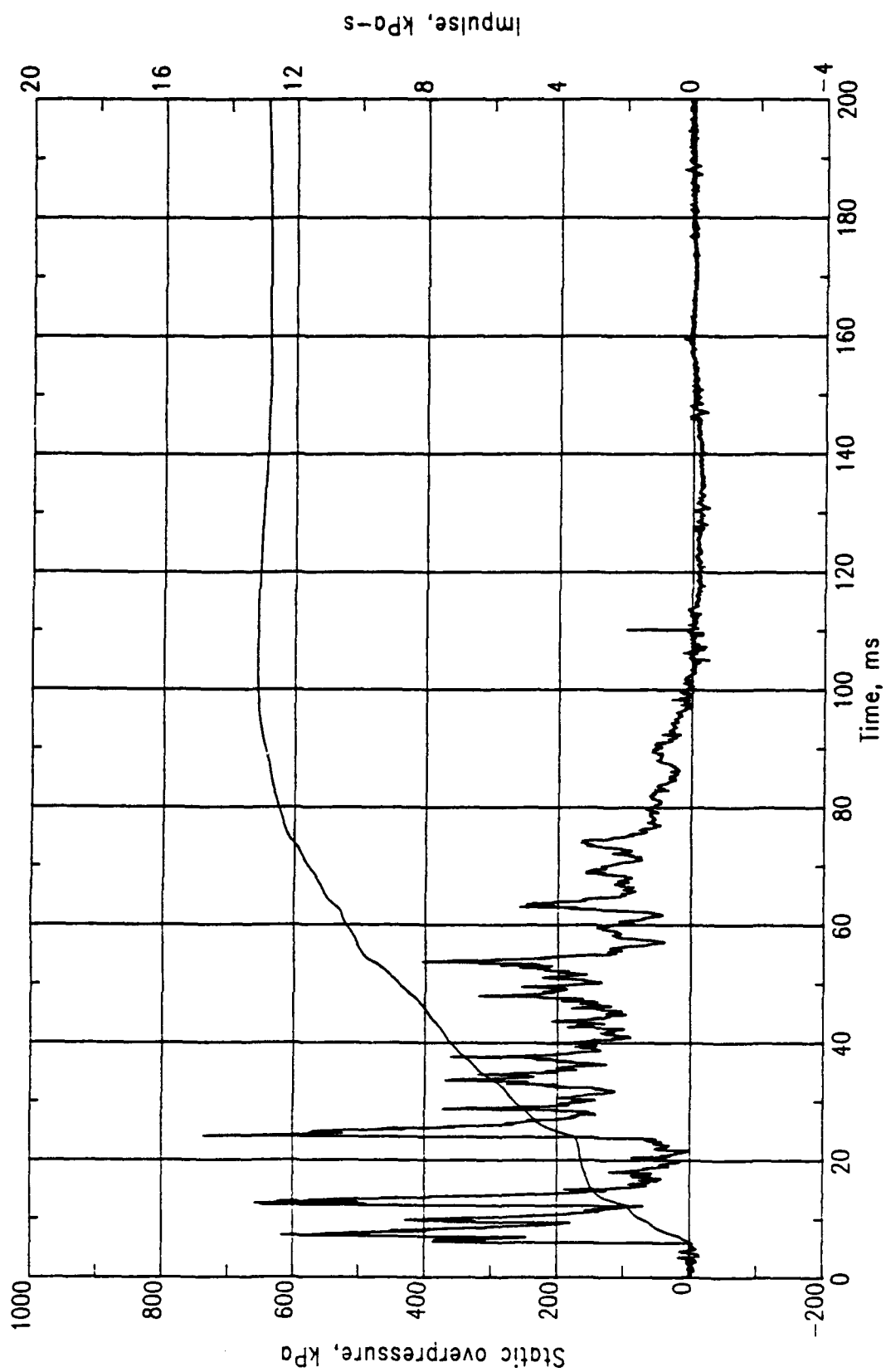


Figure 177. PAS-2, MN 0402.

peak of 0.76 MPa at 7.5 ms at this location. The recorded peak at this time was 0.63 MPa. Measurement Number 201, located in the backwall at about the same range and distance off the structure centerline but at a slightly greater height, shows a peak of 1.27 MPa (Fig. 178). Amplitude differences are also noted between MN 405 in the front wall and MN 203 at a similar location in the backwall. The peak pressure recorded at MN 405 was 2.26 MPa (Fig. 179); at MN 203 it was 6.2 MPa (Fig. 180). These two records had similar characteristics, except for the amplitude of their peaks.

Measurement Number 501 located in the floor at the front corner of the shelter showed a peak pressure of 1.5 MPa (Fig. 181). Measurement Number 102 located in the floor at the rear corner of the shelter shows a higher peak of 1.95 MPa at the same time (Fig. 182).

Measurement Number 601 was made in the floor 1.85 m from GZ towards the side of the shelter (Fig. 183). It shows a peak pressure of 1.7 MPa. The INBLAST code predicted 2.7 MPa at this location. Measurement Number 301, made in the floor 2.84 m from GZ towards the front door, shows a peak of only 0.5 MPa (Fig. 184).

Table 26 summarizes selected peaks from interior pressure measurements. A complete set of pressure records from PAS-2 is presented in Volume IV.

All free-field gages appear to have provided usable data, but in most instances the maximum values occurred at later times. All of the records were characterized by complex waveforms with multiple peaks. Many of the free-field data traces still showed large amplitude signals at 200 ms. Several records were plotted out to 1 s to determine how long this activity continued. All records checked returned to a zero baseline within 250 to 350 ms after $t = 0$. The records along each blast line showed some similar features, but details varied between blast lines. Both the first peaks and maximum values appeared to be internally consistent, i.e., TOAs increase and peak pressures decrease with increasing distances from GZ.

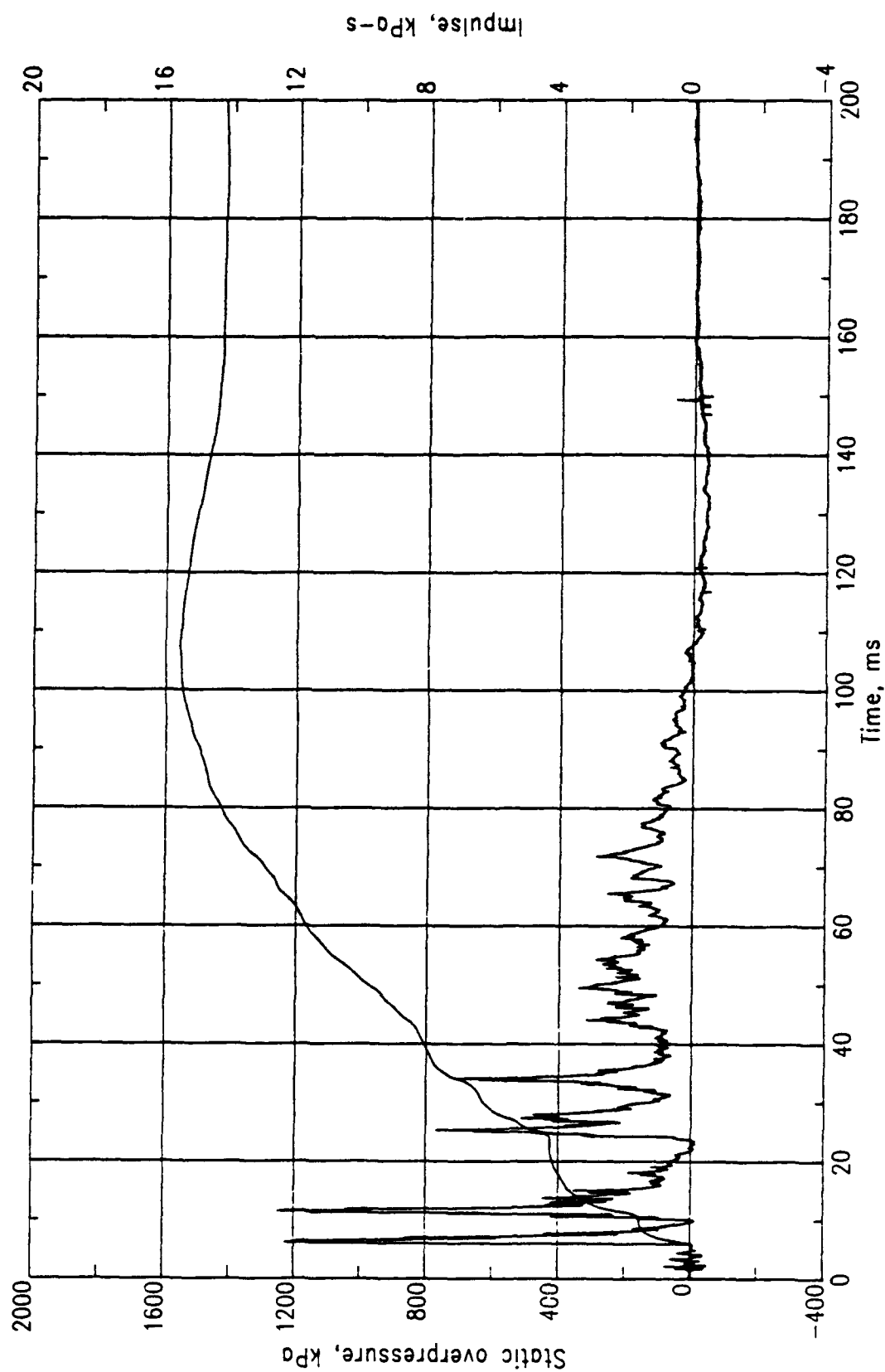


Figure 178. PAS-2, MN 0201.

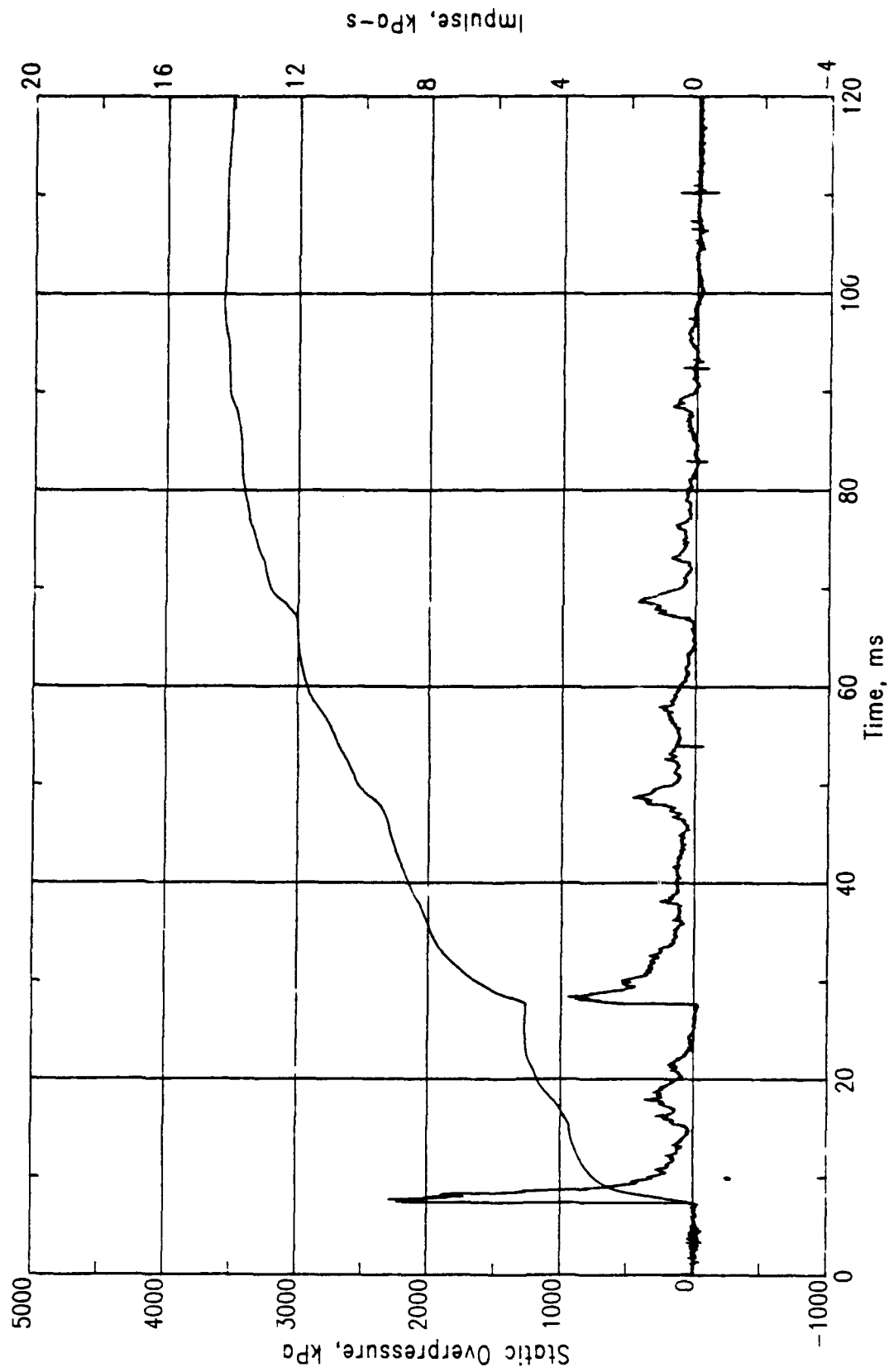


Figure 179. PAS-2, MN 0405.

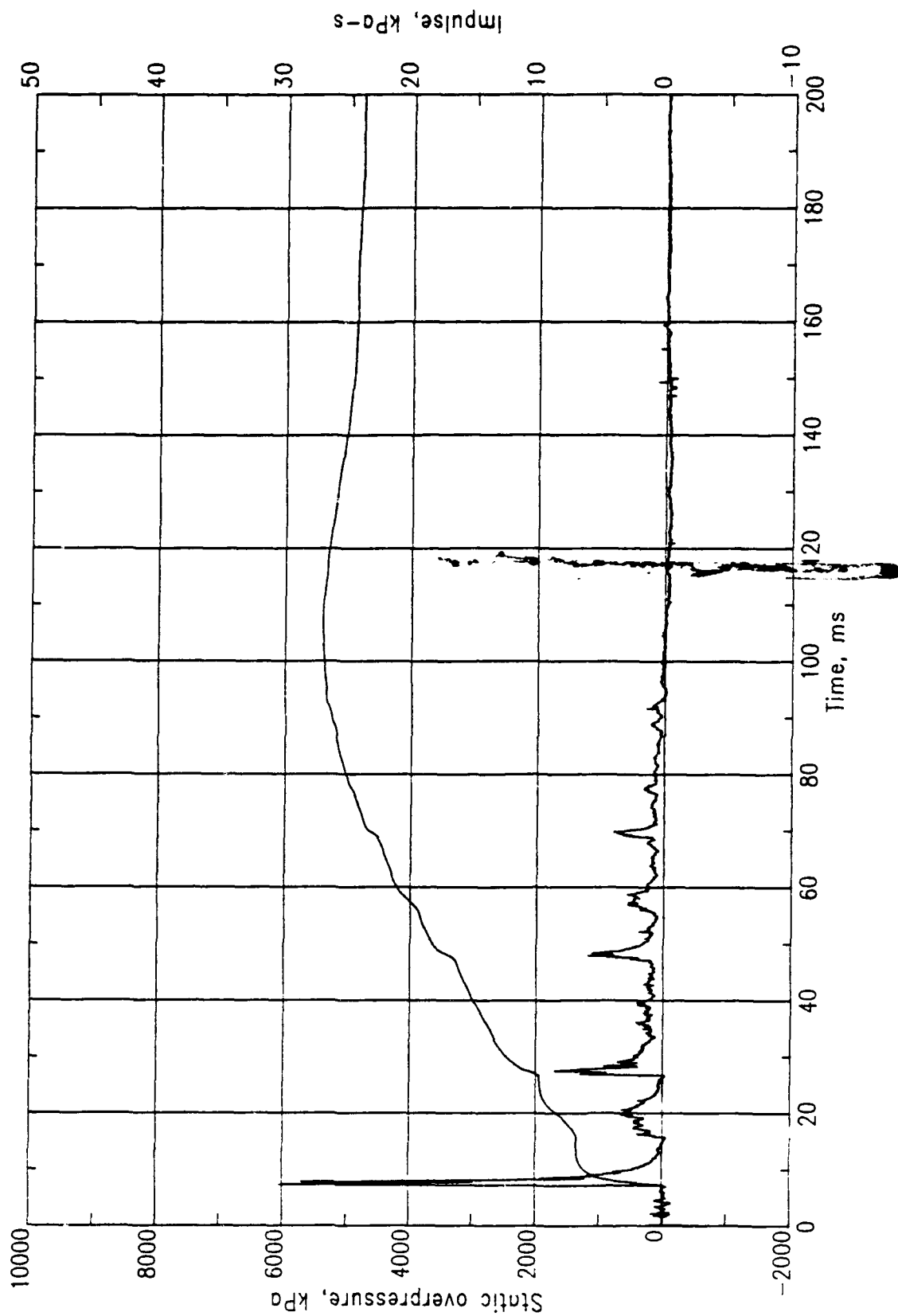


Figure 180. PAS-2, MN 0203.

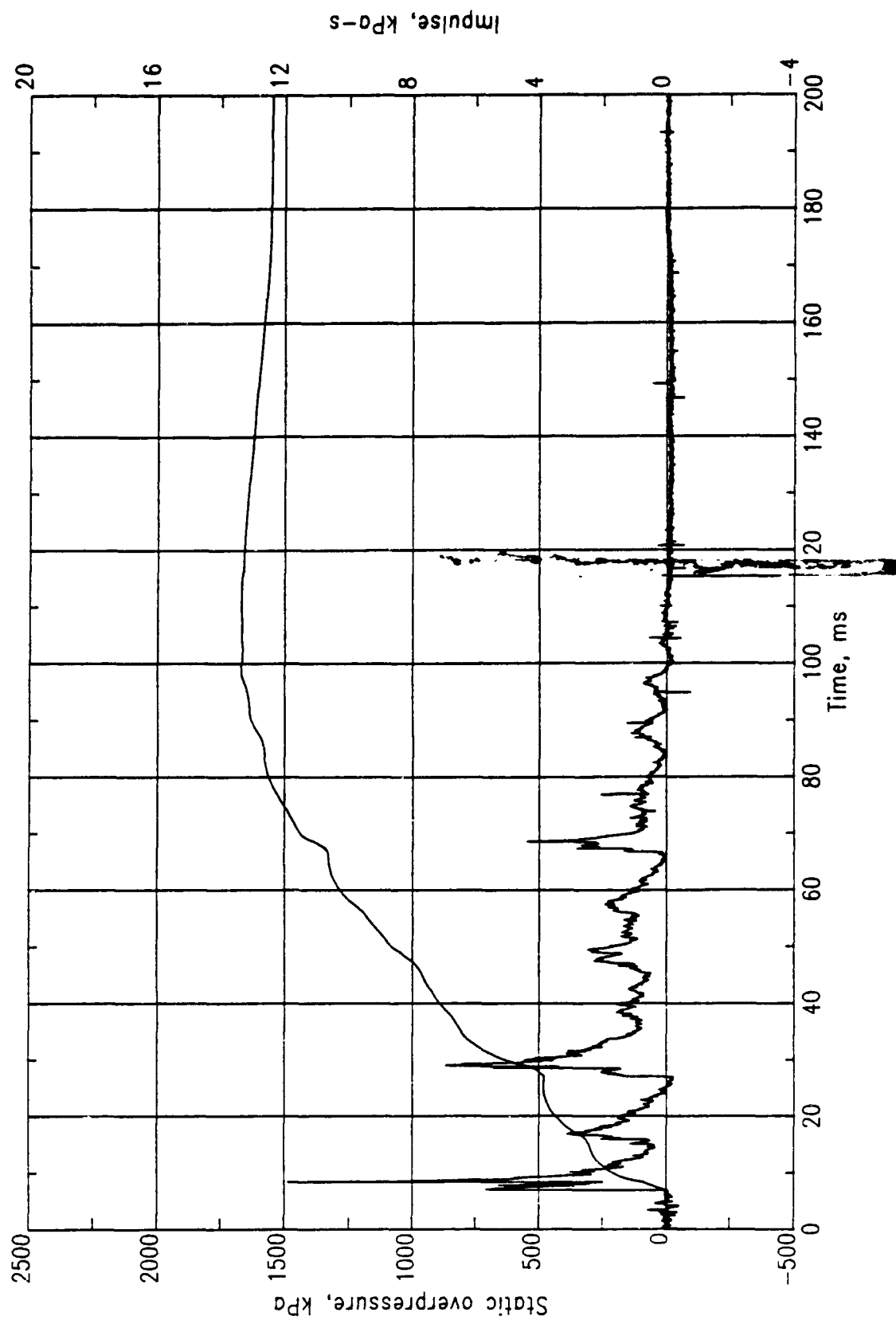


Figure 181. PAS-2, MN 0501.

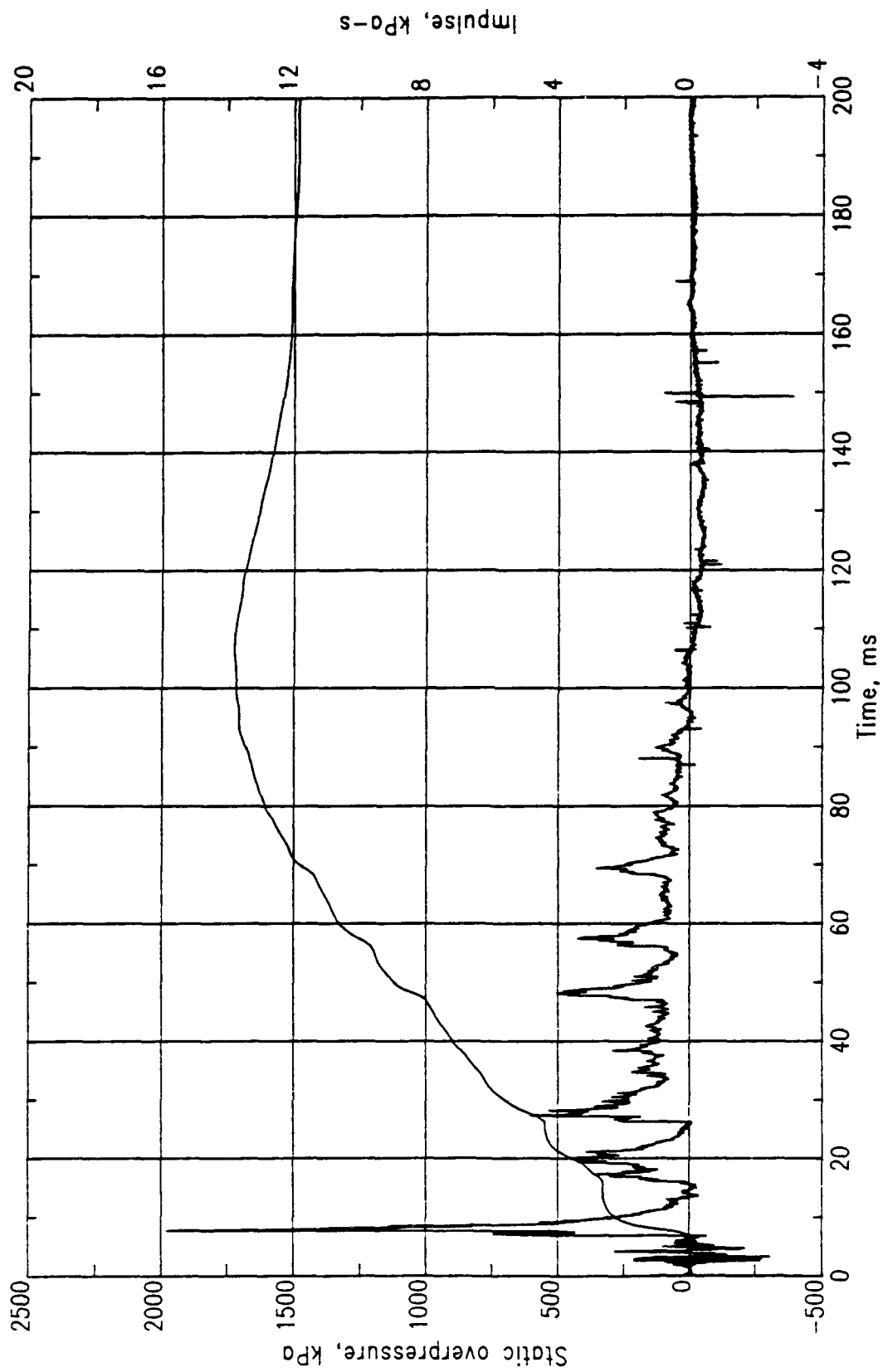


Figure 182. PAS-2, MN 0102.

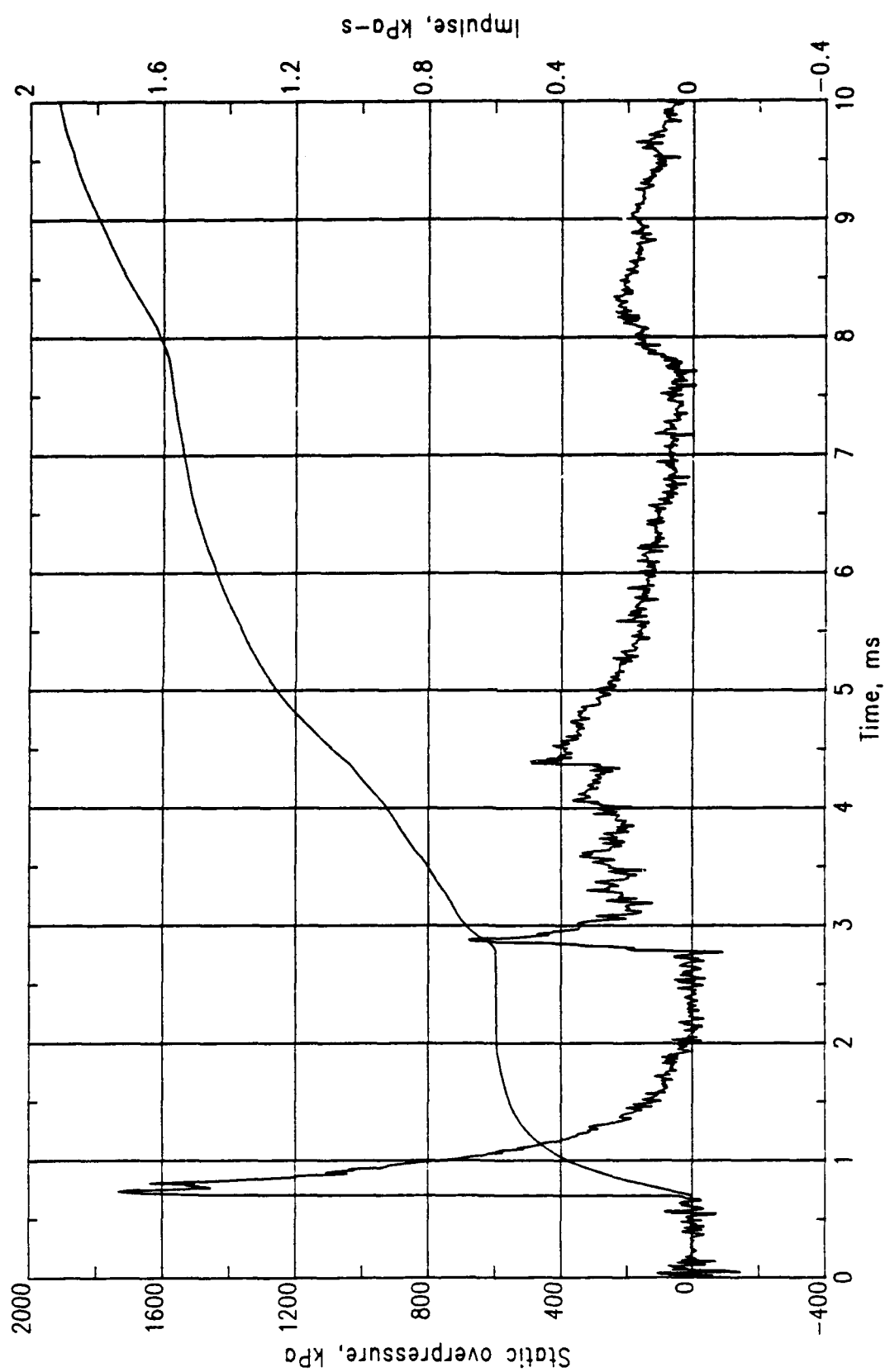


Figure 183. PAS-2, MN 0601.

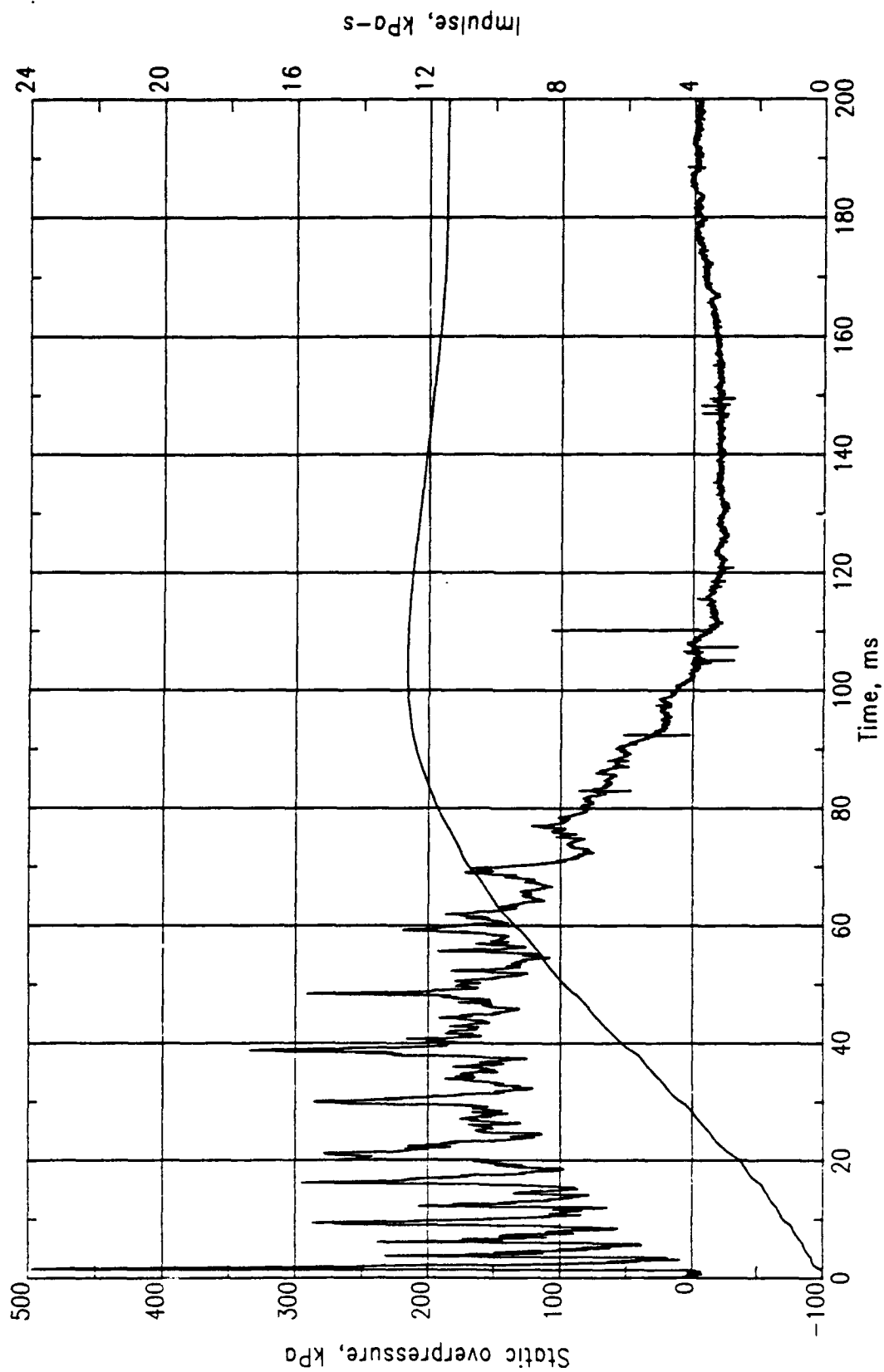


Figure 184. PAS-2, MN 0301.

Table 26. Summary of interior pressure measurements, PAS-2.

Meas. No.	Location	TOA (ms)	Peak (kPa)	Time (ms)	Peak (kPa)	Time (ms)	Peak (kPa)	Time (ms)	Peak (kPa)	Time (ms)
0101-2	SF	5.0	434.4	10.00	372.3	11.50	482.6	13.3	420.6	28.3
0102-2	SF	6.9	786.0	7.20	1985.7	7.70	620.5	27.4	510.2	48.1
0201-2	BW	6.0	1275.5	6.50	1289.3	11.60	779.1	25.5	544.7	27.6
0202-2	BW	5.9	455.1	6.20	820.5	6.90	496.4	10.8	351.6	11.9
0203-2	BW	7.2	6136.4	7.40	5681.3	7.80	1689.2	27.5	1241.1	48.3
0301-2	SF	1.2	496.4	1.60	289.6	9.40	299.9	16.3	289.6	30.2
0302-2	SF	1.8	437.8	1.90	375.8	5.00	334.4	14.9	317.2	20.7
0303-2	SF	3.2	1117.0	4.04	627.4	14.20	472.3	22.4	1268.6	33.9
0304-2	SC	2.0	737.7	2.32	517.1	2.70	379.2	7.9	344.7	19.0
0305-2	SC	2.5	1048.0	2.70	413.7	6.60	331.0	17.4	372.3	19.8
0306-2	SC	3.0	923.9	3.49	599.8	6.20	530.9	13.5	482.6	35.5
0307-2	SC	3.2	1551.3	3.80	772.2	13.50	620.5	34.1	-	-
0402-2	FD	6.0	627.4	7.10	441.3	9.70	682.6	12.7	737.7	24.1
0405-2	FD	7.4	2289.1	7.80	965.3	28.40	482.6	48.6	434.4	69.0
0501-2	SF	6.9	1482.4	8.50	413.7	16.80	910.1	29.1	551.6	68.5
0502-2	SC	6.0	915.6	6.70	1356.9	11.30	888.1	24.8	-	-
0503-2	SC	6.3	915.6	7.00	606.7	12.00	455.1	27.8	393.0	34.1
0504-2	SC	7.0	1180.4	7.80	670.2	28.20	490.9	48.8	275.8	70.0
0601-2	SF	0.7	1737.5	0.75	689.5	2.90	496.4	4.4	482.6	16.7
0602-2	SF	2.2	1227.3	3.60	496.4	13.00	639.8	17.5	468.8	22.6
0603-2	SF	1.6	1289.3	4.10	386.1	13.50	524.0	17.3	565.4	22.5
0604-2	SC	0.5	8273.8	0.55	3792.1	0.78	827.4	3.3	-	-
0605-2	SC	1.0	3585.3	1.05	2757.9	1.26	930.8	6.1	-	-
0606-2	SC	2.0	2371.8	2.10	2171.9	2.40	551.6	5.4	1075.6	16.5
0607-2	SC	2.3	1723.7	2.30	2013.3	2.75	965.3	17.1	-	-

NOTE:

Due to noise and/or possible cable problems, peak values on MN 307 may not be exact.

The initial peak of only one free-field measurement exceeded 6.9 kPa. Measurement Number 701 located 11.8 m from the GZ recorded a peak of 11.5 kPa (Fig. 185). Measurement Number 702 located at 15.8 m from GZ recorded 6.5 kPa (Fig. 186). However, MN 701 showed a peak of 25 kPa at 83 ms and MN 702 a peak of 16.2 kPa at 93 ms. If the maximum values are considered, the 6.9-kPa contour would occur at about 30 m from GZ at the front of the structure. Measurement Number 704 at a range of 30.8 m recorded a peak of 6.5 kPa.

The highest pressures were measured at the front of the structure and the lowest at the sides. The highest pressure recorded at the side of the structure was 3.1 kPa at 12 m from GZ. The maximum pressure recorded at the rear of the structure was 5.5 kPa at 12.2 m from GZ. The distribution of pressures at either side of the structure was nearly identical with only slight differences measured at the same ranges.

Table 27 summarizes selected peak pressures from the free-field measurements in PAS-2. A complete set of pressure records is presented in Volume IV.

Six pairs of accelerometers were mounted on the exterior surface of the arch. Three of these pairs were in the same cross-sectional plane that included the GZ. The remaining three pairs were in a cross-sectional plane 2.8 m from GZ toward the front door. One accelerometer in each pair had its sensing axis oriented to measure radial accelerations, while the sensing axis of the other was oriented to measure tangential accelerations.

Measurement Numbers 1601 and 1602 were made at the crown of the arch directly above GZ. Although numerous noise spikes made it difficult to read a peak from the record of MN 1601 (Fig. 187a), expansion of the first 5 ms of this record indicates a peak radial acceleration of about 7000 g. The higher negative peaks between 1 and 2 ms appear to be noise rather than real data. A similar expansion of the time base for MN 1602 indicates a peak tangential acceleration of 540 g. Figure 187b, a plot of the first and second integrals of the accelerometer record for MN 1601, shows a peak radial velocity of 5.4 m/s during the first 10 ms of the record. This velocity is slightly lower than the 6.3 m/s derived from high-speed photography for the entire front portion of the

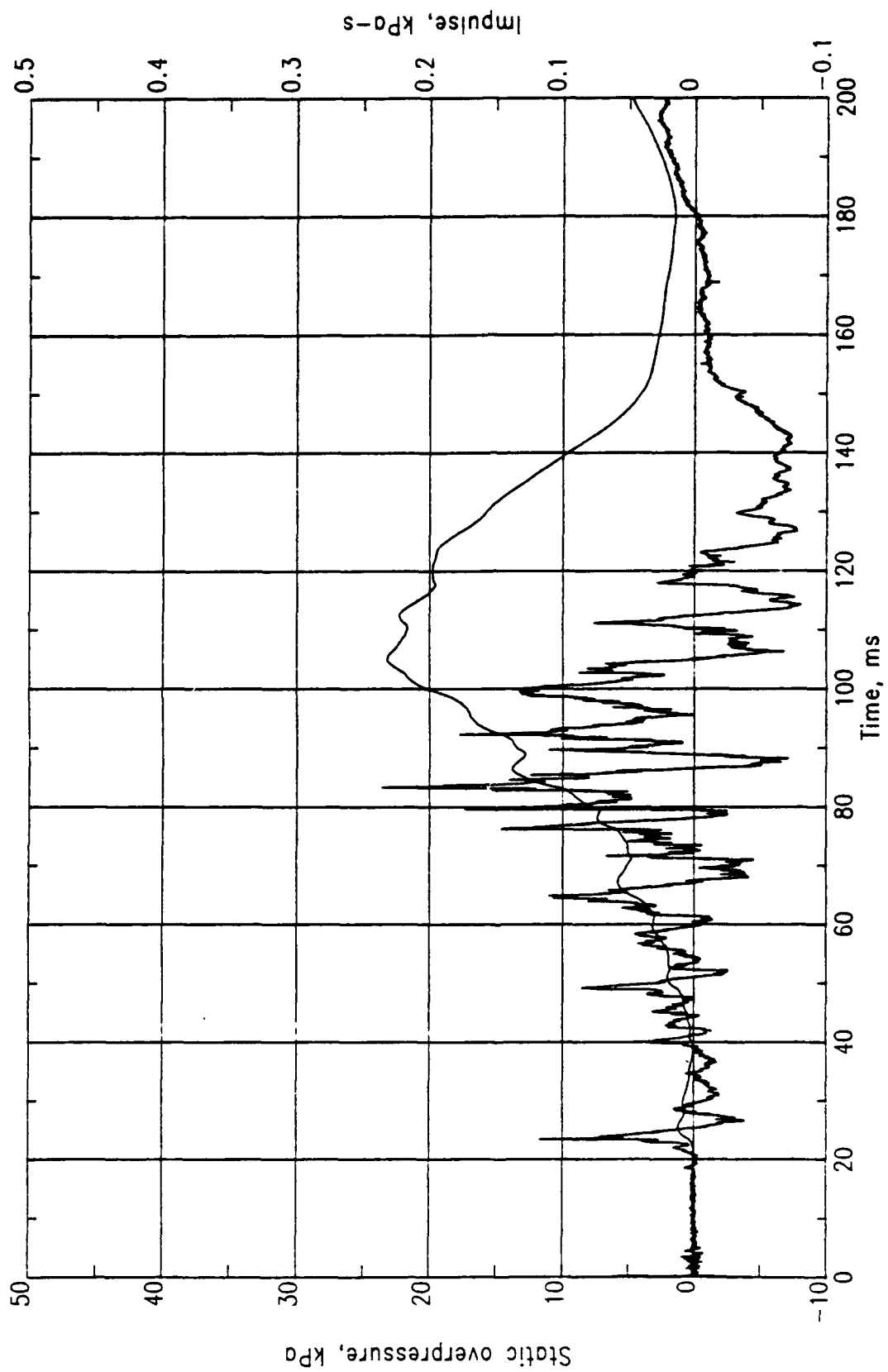


Figure 185. PAS-2, MN 0701.

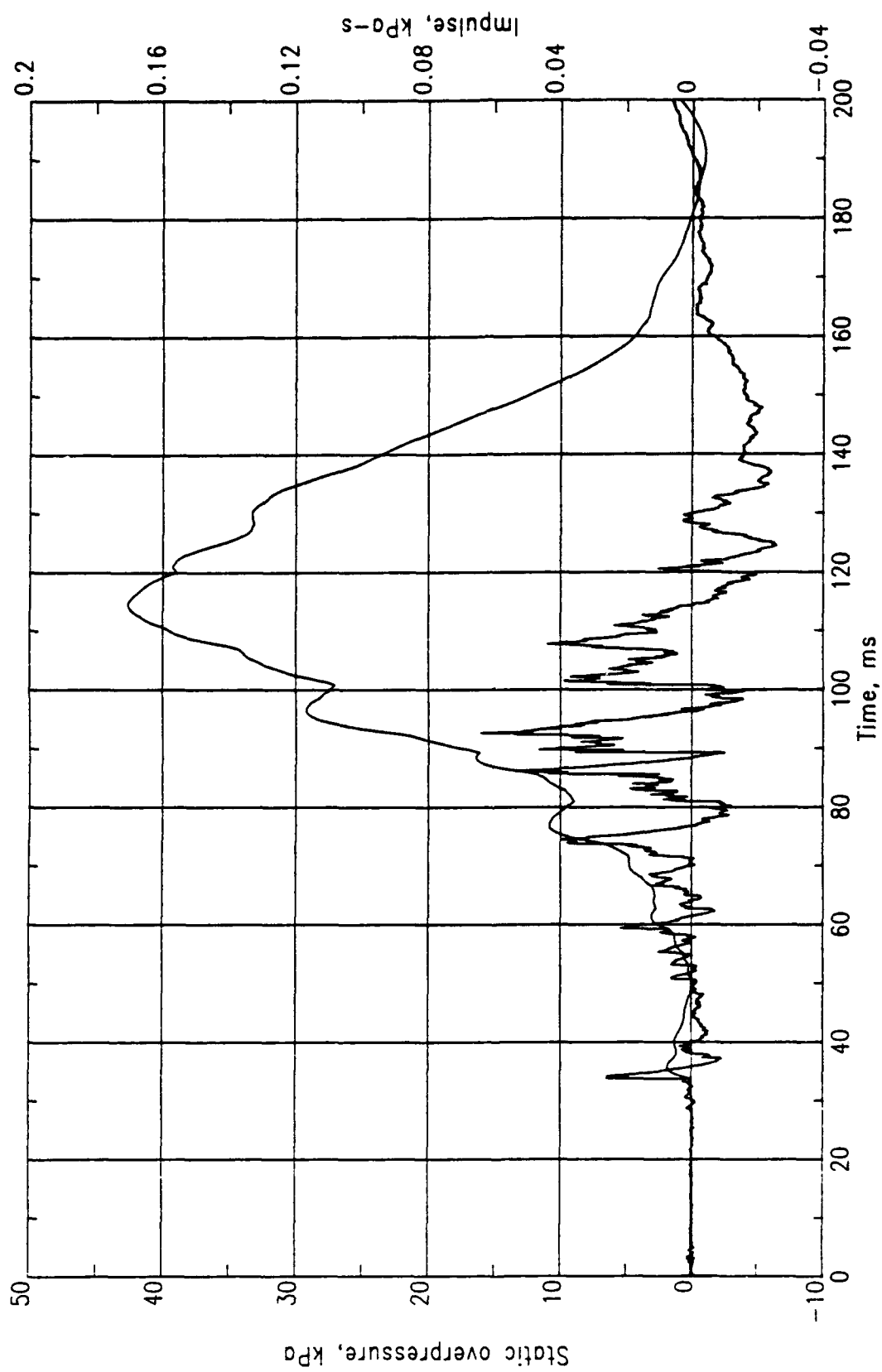
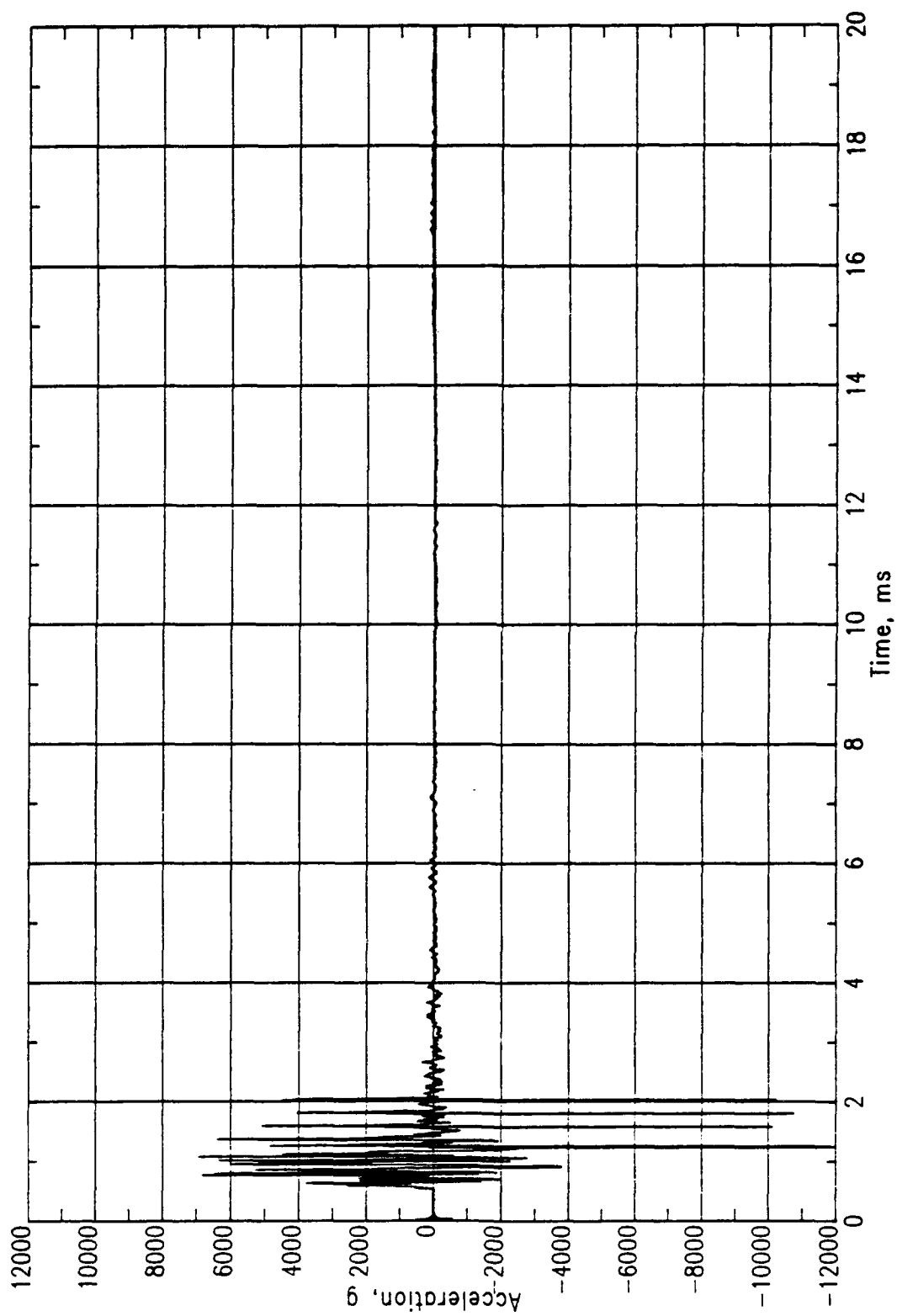


Figure 186. PAS-2, MN 0702.

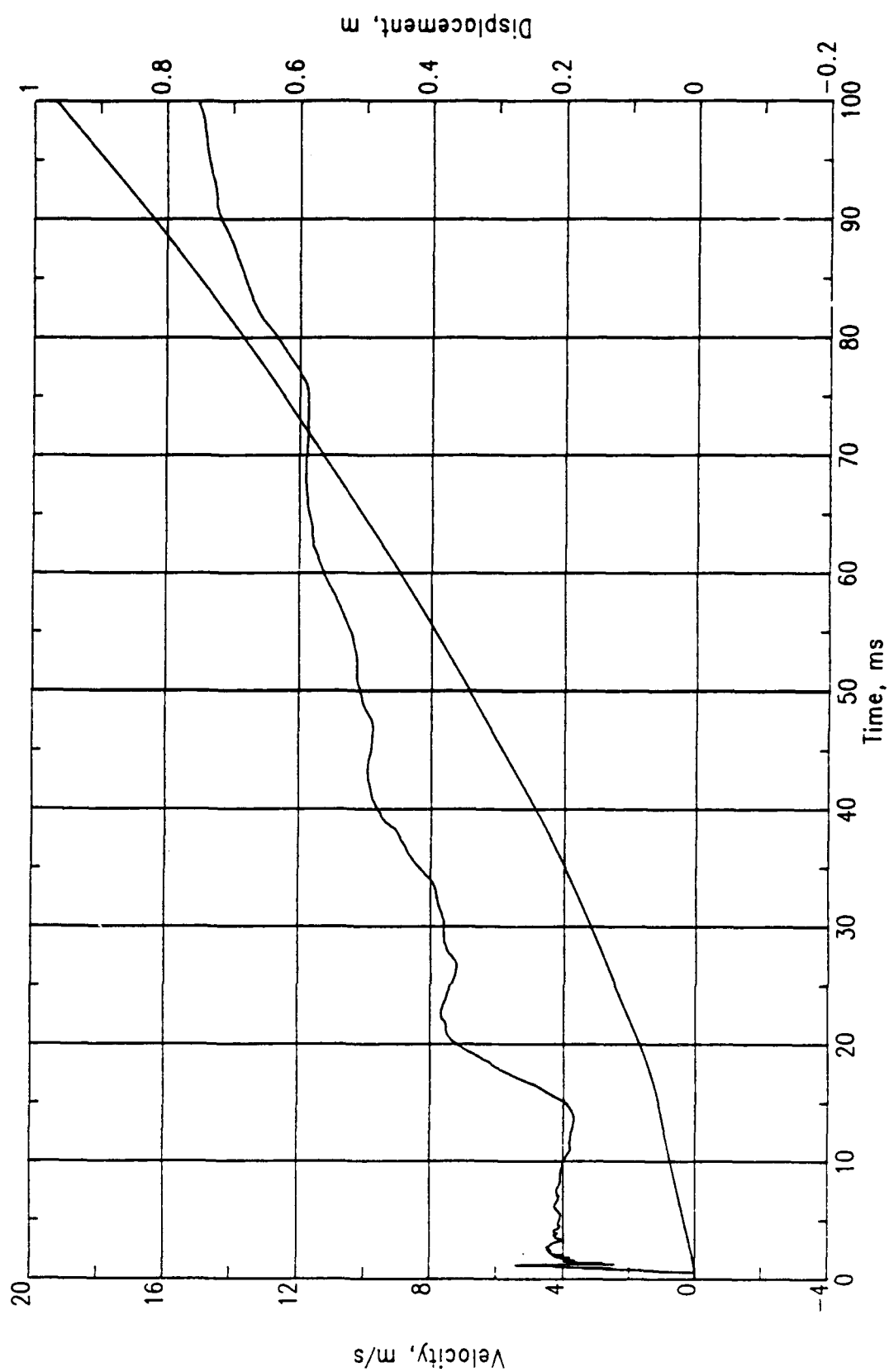
Table 27. Summary of free-field pressure measurements, PAS-2.

Meas. No.	Location	TOA (ms)	Peak (kPa)	Time (ms)	Peak (kPa)	Time (ms)	Peak (kPa)	Time (ms)	Peak (kPa)	Time (ms)	Peak (kPa)	Time (ms)
701-2	FF	18.3	11.80	23.5	14.60	76.0	23.50	83.0	17.90	93.0	13.20	99.0
702-2	FF	28.6	6.50	33.8	10.00	74.0	13.50	86.0	16.00	92.3	11.00	108.0
703-2	FF	42.4	3.90	47.8	7.60	87.0	14.80	98.5	13.60	102.2	9.50	114.5
704-2	FF	71.0	2.00	76.0	4.60	114.2	6.00	125.7	6.50	132.2	4.90	142.0
705-2	FF	26.0	1.10	26.4	6.20	73.2	7.90	82.8	7.30	90.5	6.40	104.0
706-2	FF	36.8	4.10	83.5	7.00	93.1	6.10	100.8	3.60	108.8	5.00	113.3
707-2	FF	78.0	2.05	123.8	3.35	133.8	3.10	141.5	2.15	148.0	2.80	155.2
708-2	FF	14.5	0.84	48.5	2.35	89.5	2.40	90.8	1.30	95.2	0.90	106.2
709-2	FF	25.9	1.30	88.8	3.10	98.5	2.00	100.0	1.25	106.8	1.25	111.8
710-2	FF	37.0	1.29	98.2	2.73	108.0	2.59	108.5	1.32	115.2	1.55	127.5
711-2	FF	60.0	0.73	118.9	1.33	128.2	0.82	132.0	0.80	139.0	1.07	148.5
712-2	FF	31.9	0.85	35.3	0.98	53.9	1.72	74.0	1.48	76.0	1.00	97.9
713-2	FF	42.0	0.70	45.0	0.89	63.5	1.60	83.5	0.76	105.0	1.04	131.0
714-2	FF	81.8	0.28	84.3	0.77	122.0	0.48	147.0	0.61	163.9	0.60	187.0
715-2	FF	22.0	5.50	22.8	5.30	41.0	3.80	60.8	3.00	68.6	2.70	106.0
716-2	FF	32.5	3.50	33.2	3.40	51.8	3.45	70.8	2.10	79.0	1.75	116.5
717-2	FF	72.0	0.80	72.5	1.05	109.8	0.82	91.0	0.90	111.0	0.70	114.0
718-2	FF	14.1	1.88	51.8	1.42	71.8	1.60	82.0	2.80	92.0	2.50	92.8
719-2	FF	60.0	1.00	89.0	0.85	120.5	1.82	129.5	1.28	141.8	0.92	148.2



(a). Acceleration.

Figure 187. PAS-2, MN 1601.



(b). Velocity and displacement.

Figure 187. Concluded.

structure. Integration of the record for MN 1602 showed a peak velocity of -0.4 m/s during the same time period. Peak velocities shown for times later than 10 ms are subject to greater uncertainties because of baseline shifts in the accelerometer records.

Measurement Numbers 1605 and 1606 were mounted on the side of the arch at a point close to where the radius of curvature changes. Peak accelerations at this point were 2600 g radial and 280 g tangential, respectively. Corresponding peak velocities were 1.50 m/s and -0.5 m/s. Measurement Numbers 1603 and 1604 were mounted on the arch between MN 1601 and MN 1605. At this point the peak accelerations were 3700 g radial and -540 g tangential. The corresponding peak velocities were 2.9 and -0.6 m/s.

The peak structural motions measured in a plane 2.8 m from GZ were much lower than those measured in the plane through GZ. Measurement Number 1301 recorded a peak radial acceleration of 1100 g at the crown of the arch. The peak radial velocity was 0.7 m/s. Table 28 summarizes selected peak accelerations from all of the accelerometer records for the PAS-2 event. A complete set of records is presented in Volume IV.

Two pairs of strain gages were mounted about mid-height on the centerline of the door. One gage of each pair was mounted on the inner surface of the door and the other on the outer surface. One pair was oriented to measure vertical strains (MN 3402 and MN 3404) and the other to measure horizontal strains (MN 3401 and MN 3403). At about 20 ms MN 3401 shows a horizontal tensile strain of 5000 microstrain in the outside plate of the door (Fig. 188). At the same time MN 3403 shows a horizontal tensile strain of 25,000 microstrain in the inner plate (Fig. 189). Measurement Number 3402 shows a vertical tensile strain of 3500 microstrain in the outer plate at 19 ms (Fig. 190). At about the same time MN 3404 exceeded its recording bandwidth, but it shows a compressive strain in excess of 35,000 microstrain in the inner plate (Fig. 191). The linear range for all gages is 20,000 microstrain. Greater recorded values are subject to some uncertainty.

Table 28. Summary of acceleration measurements, PAS-2.

Meas. No.	Location	TOA (ms)	Peak (g)	Time (ms)	Peak (g)	Time (ms)	Peak (g)	Time (ms)	Peak (g)	Time (ms)	Peak (g)	Time (ms)
1301-2	SR	1.33	72.00	1.42	168.00	1.51	496.00	1.61	1087.00	2.63	-875.00	2.46
1302-2	SR	1.30	24.00	1.40	100.00	1.48	288.00	1.55	460.00	1.77	-292.00	1.67
1303-2	SR	1.33	92.00	1.64	480.00	2.82	-444.00	3.25	220.00	2.23	420.00	2.39
1304-2	SR	1.35	144.00	1.80	100.00	1.86	-264.00	1.90	344.00	2.30	188.00	2.09
1305-2	SR	1.68	144.00	2.12	440.00	2.73	-464.00	2.77	1664.00	3.46	-1904.00	3.48
1306-2	SR	1.65	124.00	1.85	-264.00	2.06	128.00	2.28	560.00	3.55	-350.00	2.42
1601-2	SR	0.54	2600.00	0.60	3800.00	0.63	-1400.00	0.66	7250.00	1.02	-12000.00	1.24
1602-2	SR	0.57	425.00	0.66	-535.00	0.79	-430.00	1.00	338.00	1.22	350.00	1.75
1603-2	SR	0.91	-800.00	1.02	3200.00	1.10	-880.00	1.15	3640.00	1.35	-2300.00	1.41
1604-2	SR	0.85	345.00	1.17	-445.00	1.36	-550.00	1.50	200.00	1.68	130.00	2.45
1605-2	SR	1.45	640.00	1.90	-800.00	2.08	2140.00	2.15	2550.00	2.29	-1920.00	2.36
1606-2	SR	1.30	-192.00	1.85	290.00	2.22	199.00	2.63	-194.00	3.04	-	-

NOTE:

The last peak for MN 1302 appears to be truncated.

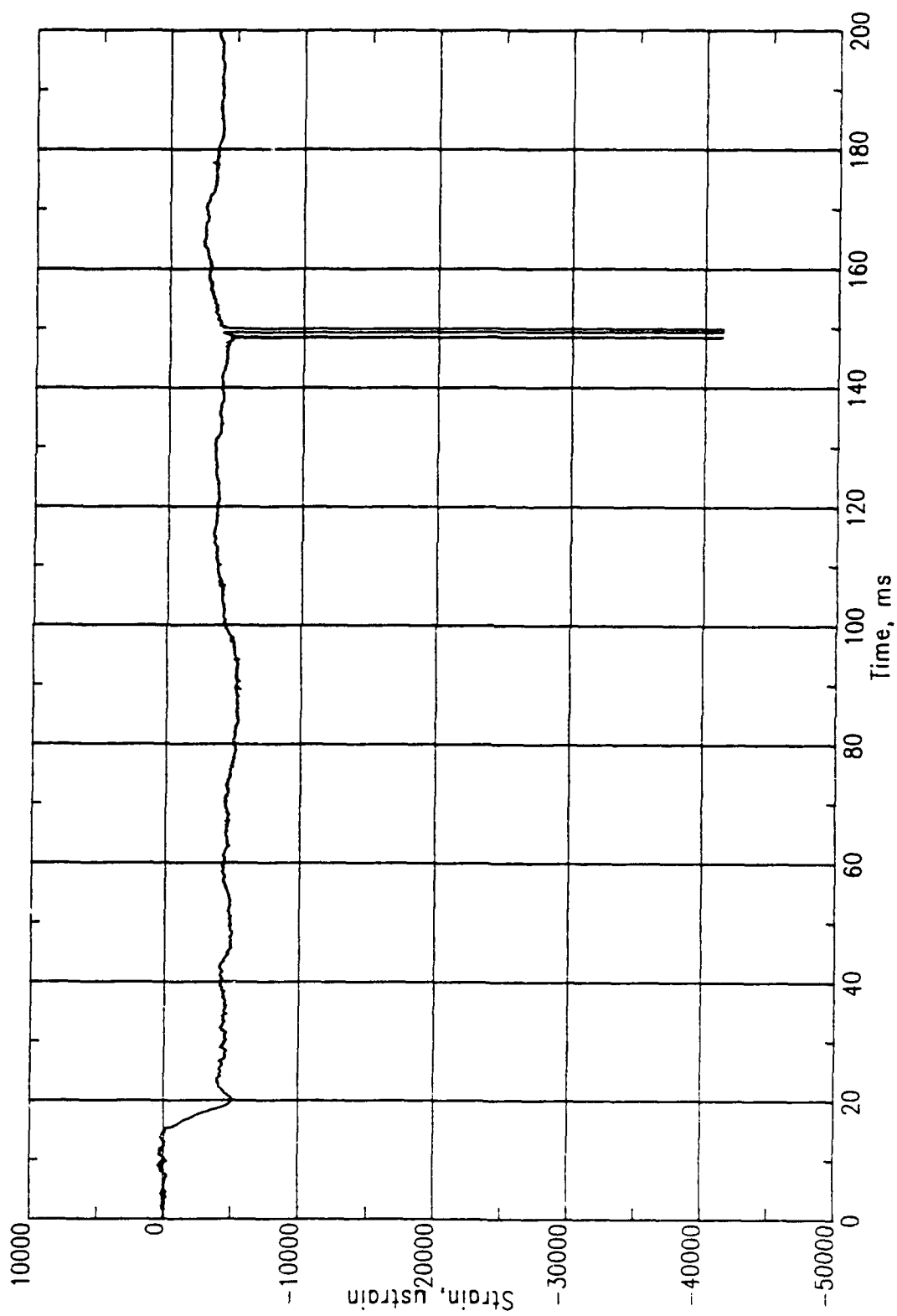


Figure 188. PAS-2, MN 3401.

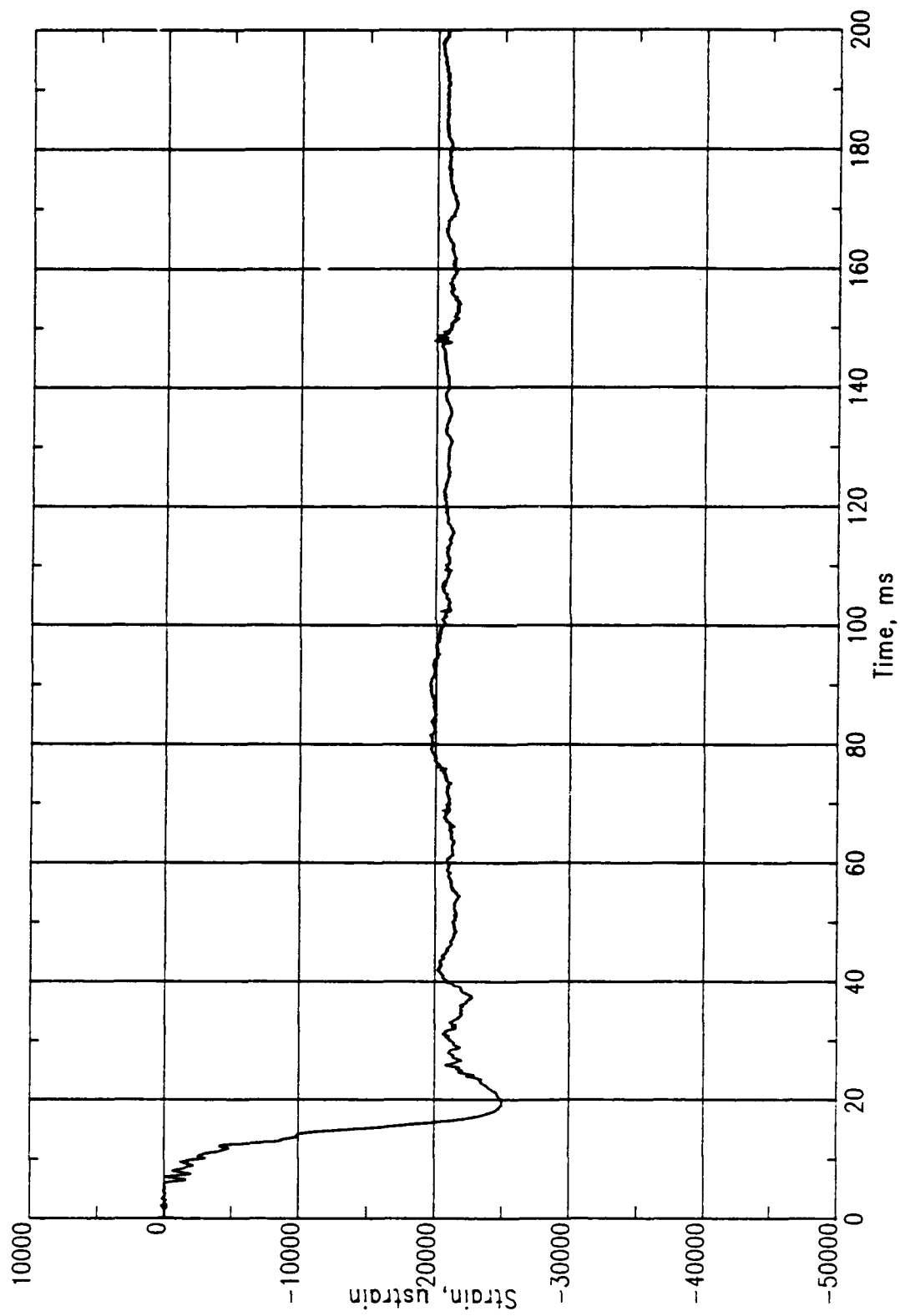


Figure 189. PAS-2, MN 3403.

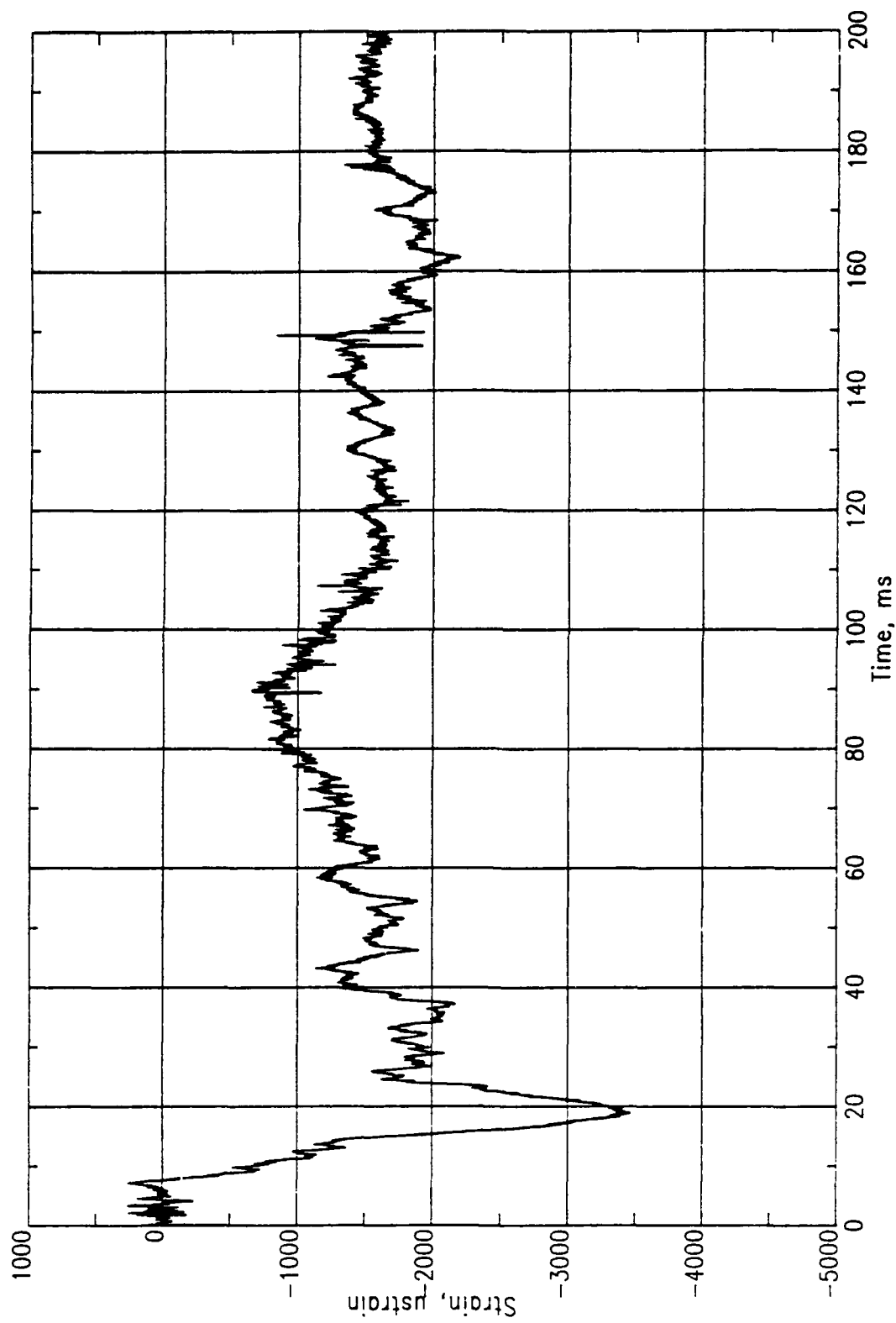


Figure 190. PAS-2, MN 3402.

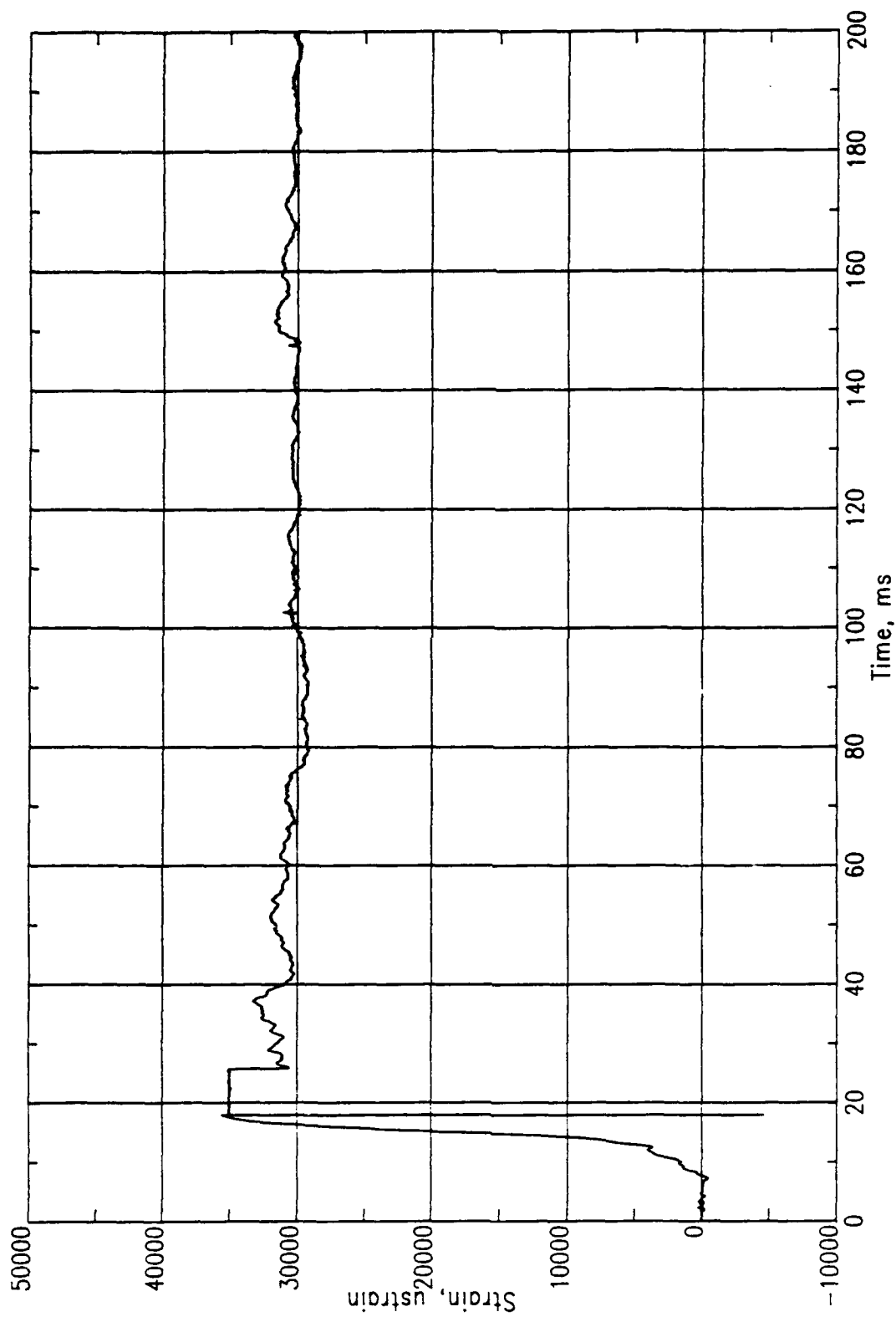


Figure 191. PAS-2, MN 3404.

Although the observed general characteristics of vertical strains are consistent with outward bending of the door, they are not consistent with pure bending. The higher compressive strains in the inner plate would normally indicate an axial compressive force had been applied to the door. This does not appear to be a probable explanation of this measurement discrepancy. The horizontal strains are also inconsistent with outward bending of the door. For the observed mode of response, i.e., outward bending, no combination of bending plus axial loads would produce greater tensile strains in the inner plate of the door. There was some buckling of the inner plate of the door in the vicinity of the gages, and this buckling could have affected the recorded strains. The strains recorded in PAS-2 are consistent with results observed in PAS-1 and PAS-3.

Table 29 summarizes selected peak strains from all strain gages for the PAS-2 event. A complete set of records is presented in Volume IV.

5.2.3 Rock Rubble Berm

The trajectory of the rocks from the rock rubble berm was nearly vertical with very little lateral motion. Only those rocks close to the arch were ejected outward during the test (Fig. 192). The greatest portion of the rocks remained relatively undisturbed.

Representative upward velocities varied from 4.7 to 6.3 m/s with the greater velocities occurring in the vicinity of the break in the arch. The maximum height reached by the rock rubble was 4.25 m. An additional discussion of the distribution patterns of the rock in the berm is presented next.

5.2.4 Debris Distribution

As in the case of PAS-3 there were three general classes of materials included in the posttest debris distribution survey for PAS-2. The first class included those items placed at various locations on the surface of the shelter, i.e., SIFCON and aluminum cubes and photo poles. The second class included pieces of the model structure, and the last was of rock from the rock rubble berm placed at the sides of the structure. The following

Table 29. Summary of strain measurements, PAS-2.

Meas. No.	Location	TOA (ms)	Peak (msn)	Time (ms)
3401-2	FD	6.00	-5100.00	20.25
3402-2	FD	6.50	-3500.00	19.20
3403-2	FD	6.10	-25000.00	19.50
3404-2	FD	6.80	35600.00	17.90

NOTE:

msn = microstrain



Figure 192. Rock rubble ejected from the berm, PAS-2.

paragraphs present data collected on the distribution of these three classes of debris in the PAS-2 test. The procedures used for collecting, processing, and characterization of the structural debris from the PAS-2 test were identical to those described in Section 4.2.4 for the PAS-3 event. Interpretation of the data in terms of quantity-distance criteria is beyond the scope of this report.

All coordinates presented in this section are referenced to the Structure Coordinate System (SCS) as illustrated in Figure 193. All ranges and azimuths are given in the plane of the top surface of the floor slab of the structure and referenced from the surface GZ (Fig. 194).

Table 30 presents the pretest and posttest coordinates of the SIFCON cubes placed on the PAS-2 structure. Several of the SIFCON cubes placed on the arch appeared to separate from the arch at about 150 to 160 ms. One placed at the crown of the arch at its mid-length reached a maximum height of 3.94 m. The point on the arch where this cube was placed only reached a height of 2.06 m.

Table 31 presents the pretest and posttest coordinates of the aluminum cubes placed on the arch in PAS-2. These cubes could not be observed in high-speed photography, so no data were collected on their transient motions.

All the photo poles remained attached to the arch sections at the locations shown in Figure 136.

As an aid in identifying the origin of a piece of concrete debris from the arch, the arch concrete was dyed in four different colors as shown in Figure 195a. This coloring scheme was changed from that used for the PAS-3 test structure in order to increase the contrast between adjacent bands of concrete. Figure 195b shows the color of beads used in each quadrant along the length of the arch.

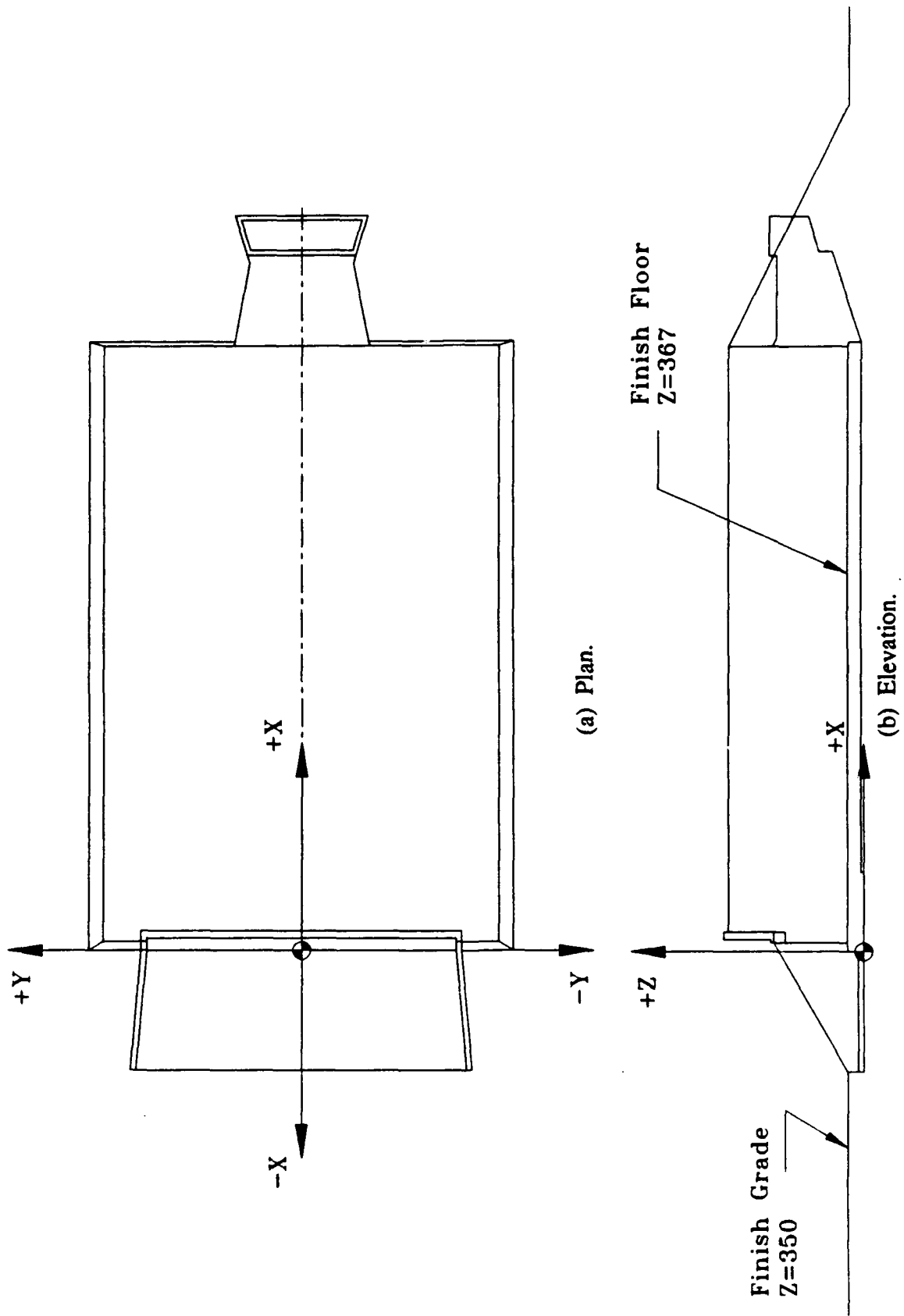


Figure 193. Structure coordinate system, PAS-2.

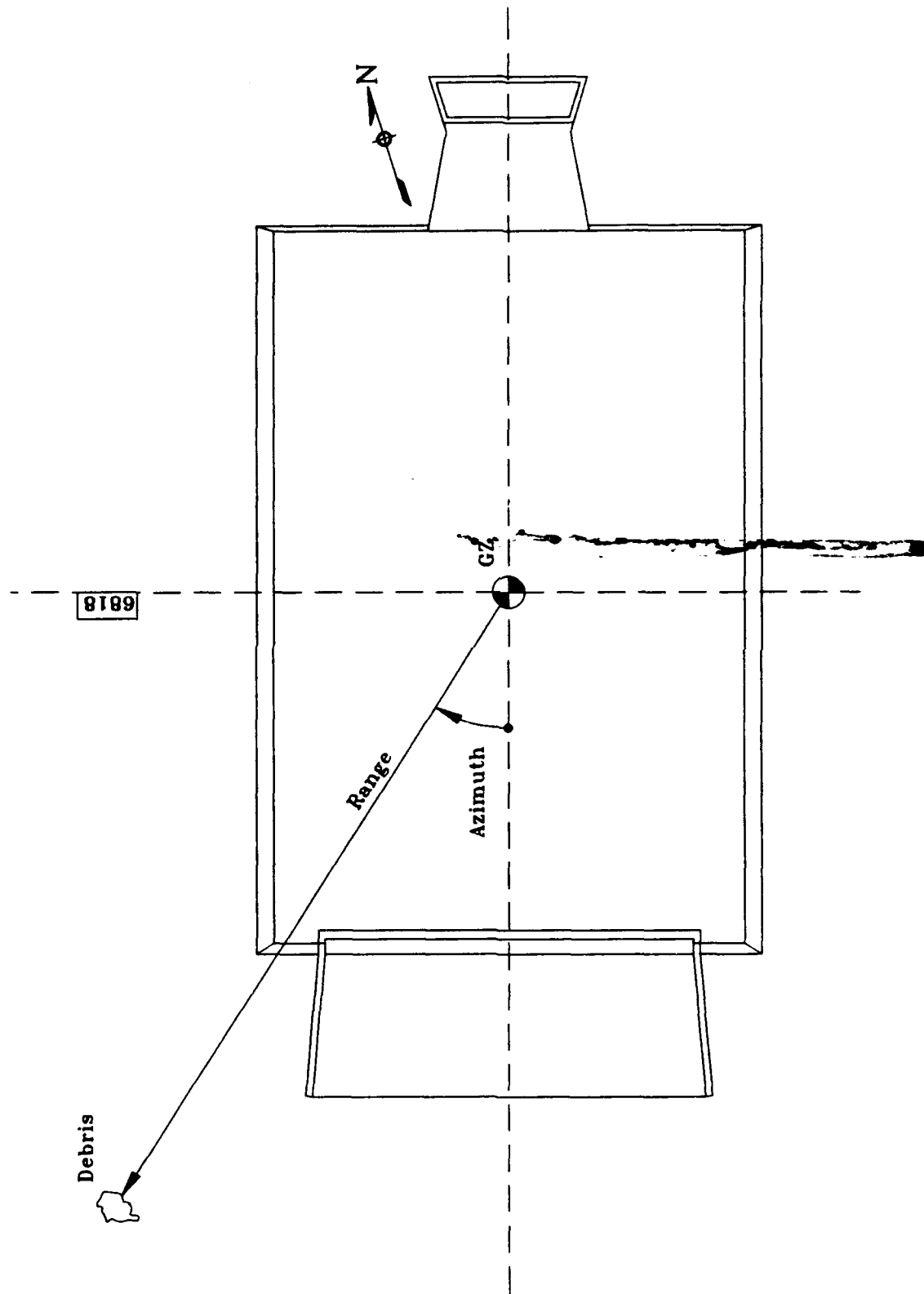


Figure 194. Range and azimuth reference system, PAS-2.

Table 30. Pretest and posttest locations of SIFCON cubes, PAS-2.

I.D. MARK	STARTING LOCATION COORDINATES			FINAL LOCATION COORDINATES		
	X (mm)	Y (mm)	Z (mm)	X (mm)	Y (mm)	Z (mm)
SC2	1140	0	2987	1516	225	2600 ^a
SC3	1140	1559	2767	3016	-219	2700 ^a
SC4	1140	2564	2371	1428	-4576	1017
SC5	1140	3514	1759	1582	-4580	1017
SC7	1140	4020	1118	1617	-4717	1017
SC8	3760	0	2987	3445	-118	2800 ^a
SC9	3760	1559	2767	3329	-4557	1017
SC10	3760	2564	2371	4689	-4937	1017
SC12	3760	3514	1759	4641	-4557	1017
SC13	3760	4020	1118	4197	-4797	1017
SC14	6390	0	2987	7377	-4521	1017
SC15	6390	1559	2767	6552	-4535	1017
SC16	6390	2564	2371	5395	-4522	1017
SC17	6390	3514	1759	6232	-4524	1017
SC18	6390	4020	1118	7415	-6553	1017
SC19	9410	0	2987	11863	480	3060 ^a
SC20	9410	1559	2767	10075	-4437	1017
SC21	9410	2564	2371	13757	-3385	1017 ^b
SC22	9410	3514	1759	14458	-4828	1017
SC23	9410	4020	1118	13373	-5743	1017
SC24	12680	0	2987	20082	976	350
SC25	12680	1559	2767	13856	-1840	1017 ^b
SC26	12680	2564	2371	14212	-2865	1017 ^b
SC28	12680	3514	1759	13804	-4668	1017
SC29	12680	4020	1118	13410	-4194	1017

NOTES:

^aOn crown of arch

^bOn earth backfill

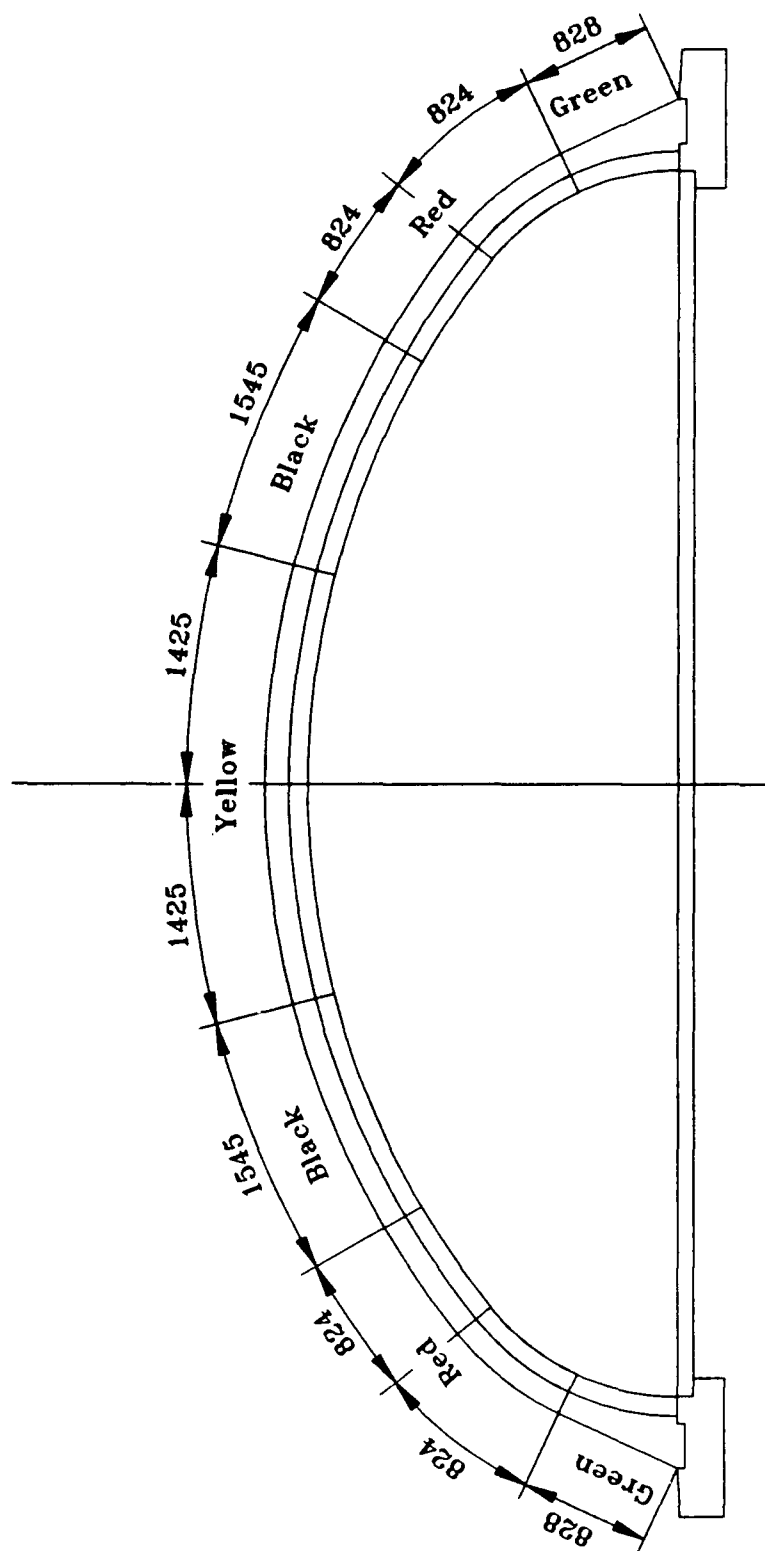
Table 31. Pretest and posttest locations of aluminum cubes, PAS-2.

I.D. MARK	STARTING LOCATION COORDINATES			FINAL LOCATION COORDINATES		
	X (mm)	Y (mm)	Z (mm)	X (mm)	Y (mm)	Z (mm)
AL1	1255	0	2987	6425	-4506	1017
AL2	1255	1559	2767	3208	-4480	1017
AL3	1255	2564	2371	3063	-4609	1017
AL4	1255	3514	1759	1700	-4731	1017
AL5	1255	4020	1118	1350	-4653	1017
AL6	3875	0	2987	3853	159	2900 ^a
AL7	3875	1559	2767	3759	-1180	2875 ^a
AL8	3875	2564	2371	4281	-4567	1017
AL9	3875	3514	1759	459	-4901	1017
AL10	3875	4020	1118	4784	-4491	1017
AL11	6505	0	2987	6119	-418	2950 ^a
AL12	6505	1559	2767	6008	-4435	1017
AL13	6505	2564	2371	6923	-4647	1017
AL14	6505	3514	1759	6647	-4498	1017
AL15	6505	4020	1118	7611	-6572	1017
AL16	9535	0	2987	13964	-868	1017 ^b
AL17	9535	1559	2767	14413	-2903	1017 ^b
AL18	9535	2564	2371	17945	-5374	350 ^b
AL19	9535	3514	1759	14151	-4442	1017 ^b
AL20	9535	4020	1118	12261	-6023	1017
AL21	12550	0	2987	13897	2048	1017 ^b
AL22	12550	1559	2767	13606	-2795	1017 ^b
AL23	12550	2564	2371	13897	-4253	1017 ^b
AL24	12550	3514	1759	14727	-4993	1017 ^b
AL25	12550	4020	1118	12873	-3719	1017

NOTES:

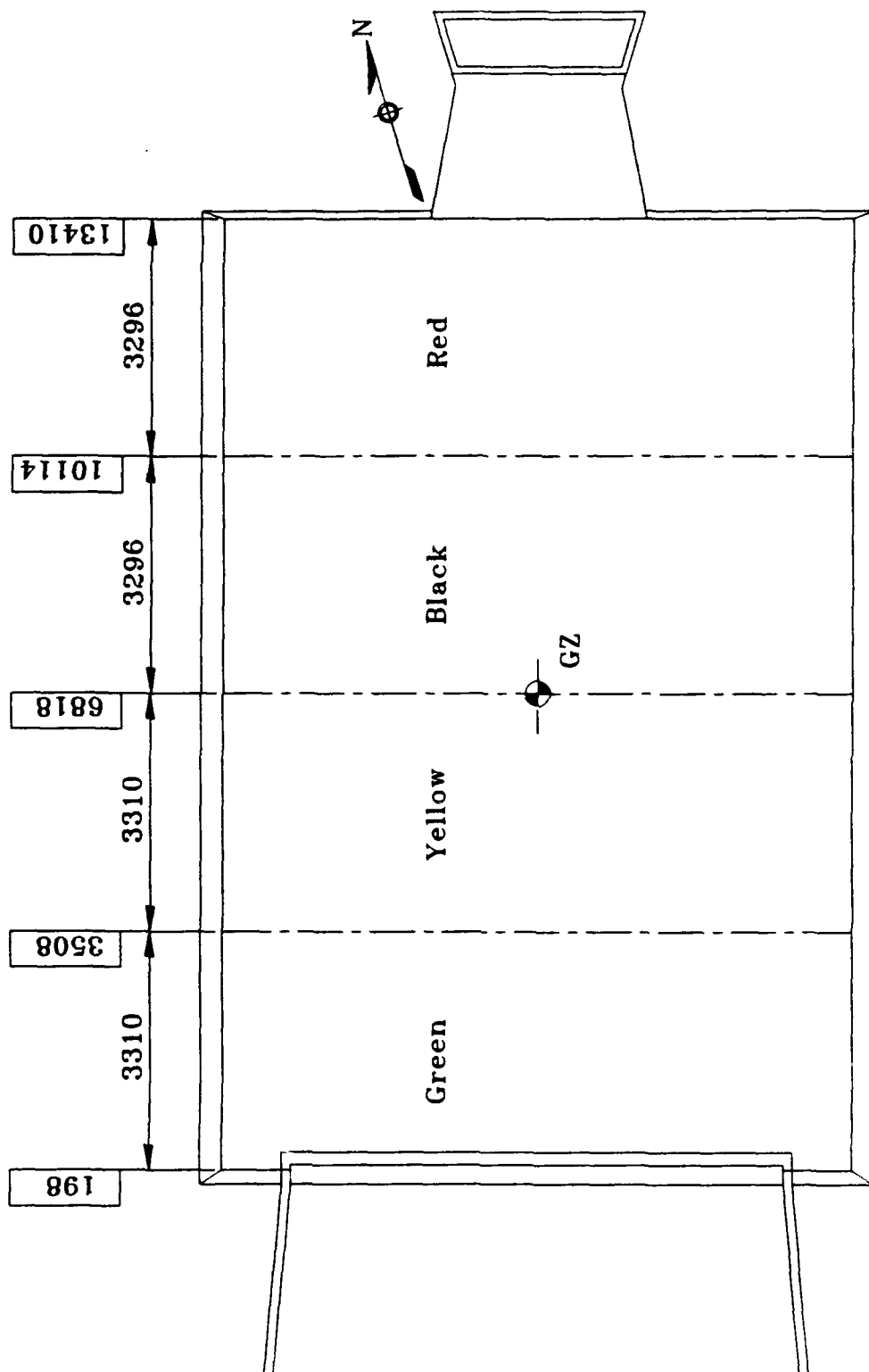
^aOn crown of arch

^bOn earth backfill



(a) Section: Positions of colored bands on concrete of arch.

Figure 195. Dyed concrete and colored beads in arch, PAS-2.



(b) Plan: Colored bead zones on arch.

Figure 195. Concluded.

Following the test, the boundaries of four 5-deg circular sectors were laid out on the testbed (Fig. 196). Virtually no small debris was found in the 5-deg collection sectors beyond a range of 10 m from GZ. As a result no sieve analysis was conducted. All larger debris was left in place and recovered during the 360-deg survey.

Virtually all of the larger debris surrounding the structure was located by standard surveying methods. Once the piece of debris was surveyed, it was marked with an identifying number and taken back to the lab where each piece of debris recovered was weighed and its dimensions measured. The measuring procedure was based on determining the smallest rectangular box that could enclose the piece of debris. Other identifying features were also noted, such as color of concrete, color of plastic beads in the piece, and whether the piece had a painted and/or a formed surface. The 360-deg survey located and identified only 30 pieces of concrete debris. Table 32 presents the survey data, and Table 33 presents the identification data of the concrete debris. Table 33 also gives shape factors (SF) for all the pieces of debris. These SF were determined using the procedure described in Section 4.2.4. The average SF for all the pieces was calculated to be 0.4361.

The debris location and identification data were entered into a spreadsheet computer program (LOTUS 1-2-3); however, because the small number of pieces recovered, no manipulation or sorting of the data was done.

Only 49 pieces of debris were recovered from the catcher bins. The characteristics of this debris are presented in Table 34.

All the rock ejected from the berm remained within a range of 15 m of GZ. The limits of the ejected rock were surveyed and are shown in Figure 197.

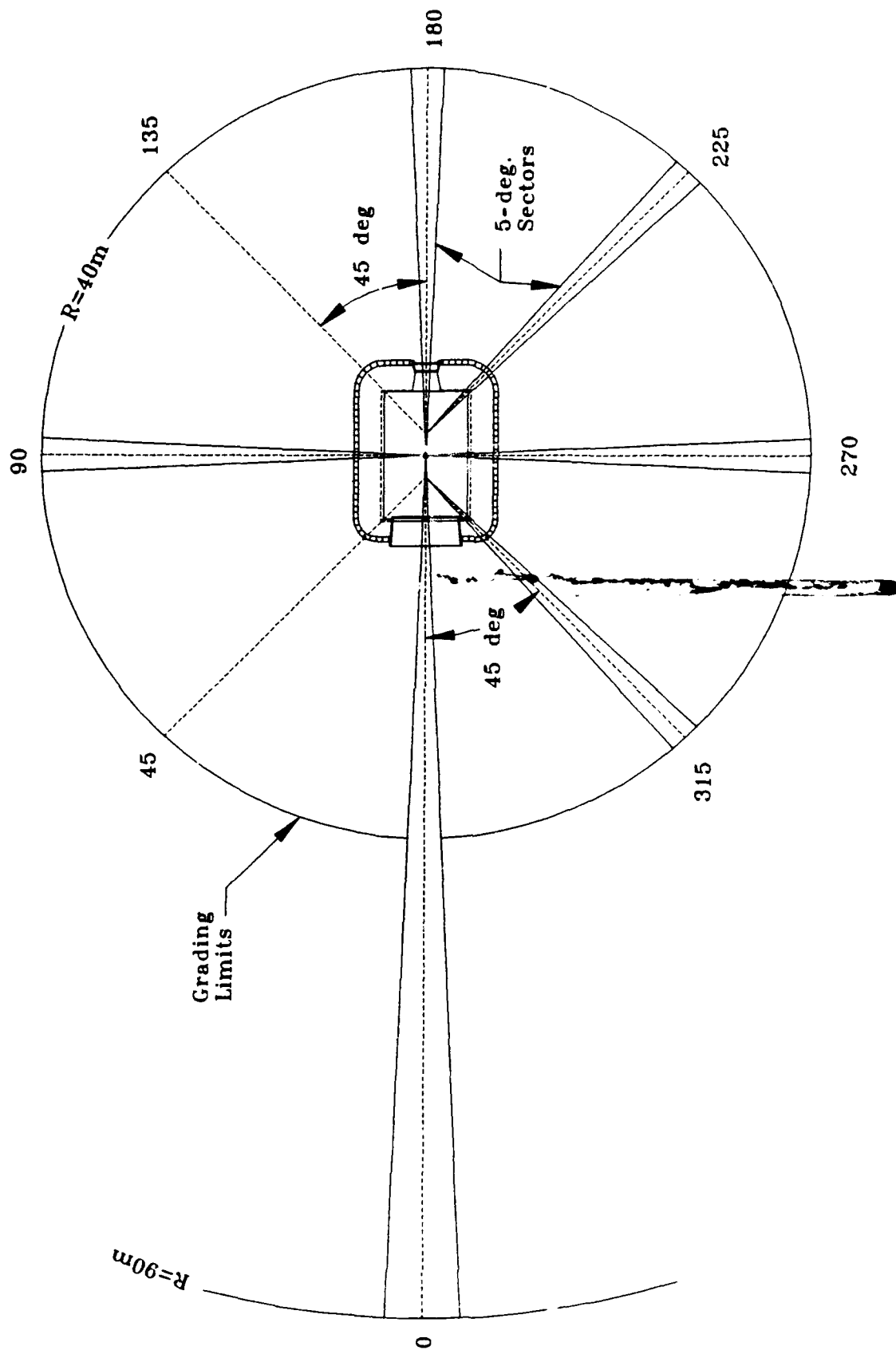


Figure 196. Five-degree debris collection sectors, PAS-2.

Table 32. Concrete debris location data, PAS-2.

I.D. MARK	COORDINATES		FROM GZ:	
	X (mm)	Y (mm)	RANGE (mm)	AZIMUTH (deg)
1	-2872	-3106	10175	342.23
2	-2884	-3118	10191	342.18
3	-2903	-3253	10250	341.50
4	-5492	-2787	12621	347.24
5	-5596	-2939	12758	346.68
6	-6045	-2399	13085	349.44
7	-6337	-2717	13432	348.33
8	-7151	-3686	14447	345.22
9	-6279	-5647	14262	336.68
10	-6370	-12636	18264	316.23
11	-2026	-15700	18020	299.39
12	-10053	-11644	20499	325.39
13	-14305	-1939	21212	354.76
14	-14728	-20032	29419	317.08
15	-54784	-65286	89761	313.34
16	-56828	-44362	77581	325.12
17	-72032	-31989	85092	337.92
18	-40326	-18505	50646	338.57
19	-31675	-13787	40887	340.29
101	-3015	3866	10566	21.46
102	-4474	244	11294	1.24
103	-4733	936	11589	4.63
104	-6568	1819	13508	7.74
105	-9329	351	16151	1.24
106	-67383	4406	74332	3.40
107	-13709	14933	25384	36.04
108	-4908	14971	19016	51.93
110	-5059	7972	14304	33.87
111	4976	34374	34423	86.93
112	3278	28688	28905	82.97

Table 33. Concrete debris characteristics data, PAS-2.

I.D. MARK	DIMENSIONS			WEIGHT (gm)	COLOR		OTHER IDENTIFYING MARKS	SHAPE FACTOR
	LENGTH (mm)	WIDTH (mm)	HEIGHT (mm)		CONCRETE	BEAD		
1	130	100	52	726.0	N			0.4475
2	80	47	19	57.6	R	G	1 Flat, White Side	0.3357
3	90	67	29	169.3	R			0.4033
4	220	120	132	3127.0	R			0.3739
5	80	50	27	121.8	R			0.4699
6	65	30	25	58.9	R		1 Flat, White Side	0.5032
7	130	50	27	168.5	R		1 Flat, White Side	0.4000
8	130	62	25	246.1	R		1 Flat Side	0.5088
9	58	32	18	43.8	R		1 Flat, White Side	0.5460
10	95	43	22	113.0	R		1 Flat Side	0.5240
11	120	70	40	403.7	R		1 Flat, White Side	0.5006
12	70	65	33	122.5	R		1 Flat, White Side	0.3400
13	78	48	20	82.7	R		1 Flat Side	0.4600
14	71	52	25	100.8	R		1 Flat Side	0.4551
15	80	57	47	252.4	R			0.4907
16	67	65	15	53.3	R		1 Flat Side	0.3402
17	103	60	44	190.1	R		1 Flat, White Side	0.2913
18	77	60	25	120.1	N			0.4332
19	75	59	14	43.4	N		1 Flat, White Side	0.2920
20	90	80	26	165.9	R			0.3692
101	77	92	31	170.9	N		2 Flat, White Sides	0.3242
102	52	32	21	61.9	R		1 Flat, White Side	0.7384
103	87	50	30	89.1	R			0.2844
104	77	30	29	66.9	R	G	1 Flat Side	0.4159
105	63	33	29	58.5	R		1 Flat Side	0.4042
106	102	81	23	163.1	R		1 Flat, White Side	0.3576
107	73	43	48	150.0	R		1 Flat, White Side	0.4147
108	49	41	18	40.5	R		1 Flat, White Side	0.4669
110	75	67	40	173.6	R		1 Flat, White Side	0.3598
111	40	29	29	60.4	R		3 Flat Sides	0.7486
112	60	46	22	77.4	R	G	2 Flat Sides	0.5314
Totals				6753.0				0.4361

Table 34. Characteristics of debris collected from catcher bins, PAS-2.

BIN NO.	WEIGHT (gm)	NUMBER
BIN- 1	56.80	16
BIN- 2	56.50	13
BIN- 3	22.50	3
BIN- 4	0.04	2
BIN- 5	0.00	0
BIN- 6	0.00	0
BIN- 7	0.01	1
BIN- 8	70.70	16
BIN- 9	0.00	0
BIN- 10	0.00	0
BIN- 11	0.00	0
BIN- 12	0.00	0
BIN- 13	0.00	0
BIN- 14	0.00	0
BIN- 15	0.00	0
BIN- 16	0.00	0
BIN- 17	1.20	2
BIN- 18	711.80	2
BIN- 19	0.00	0
BIN- 20	0.00	0
BIN- 21	0.00	0
BIN- 22	0.00	0
BIN- 23	0.00	0
BIN- 24	0.00	0
BIN- 25	0.00	0
BIN- 26	0.00	0
Totals	919.55	55

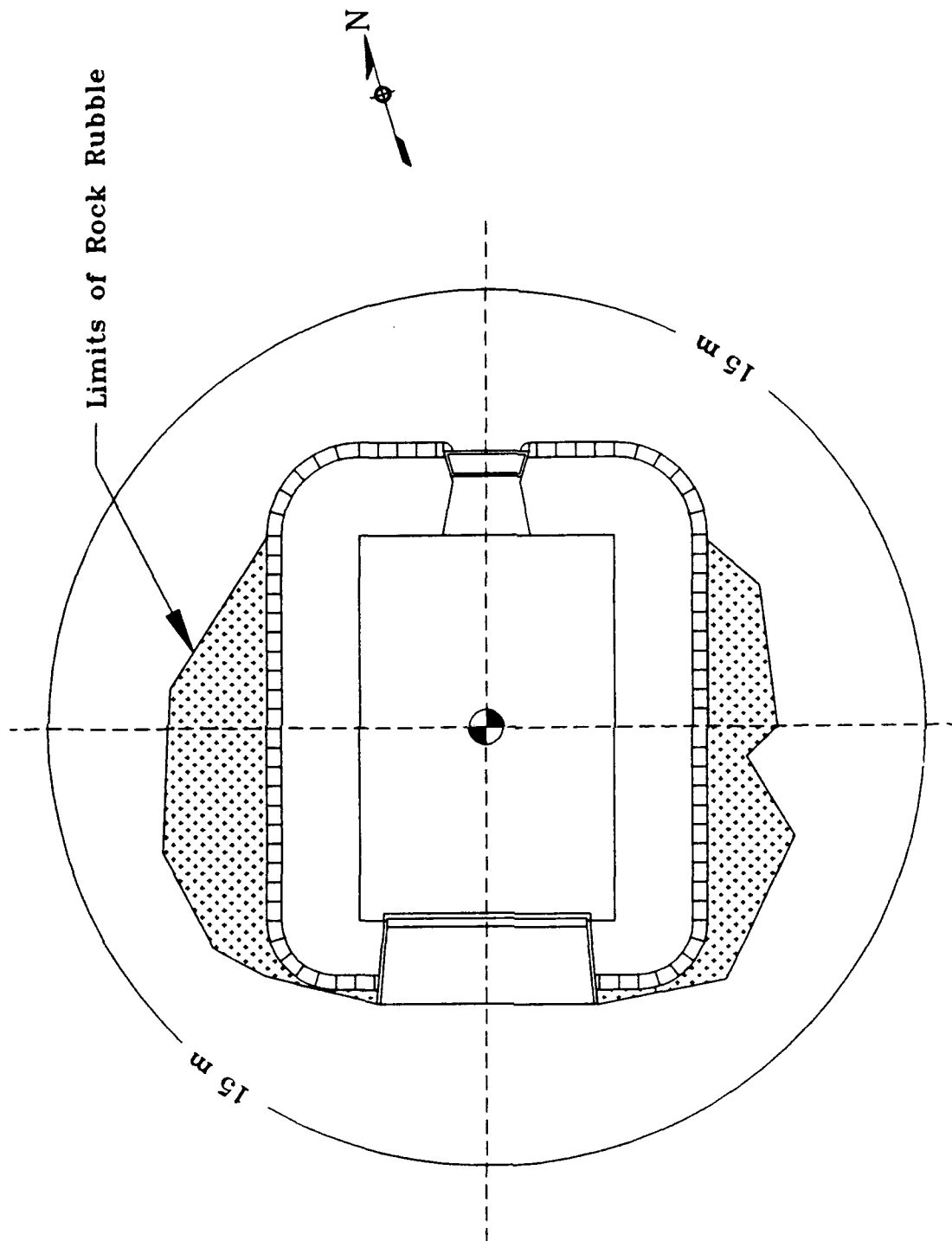


Figure 197. Rock rubble distribution, PAS-2.

6.0 PAS-4 TEST

6.1 TEST DESCRIPTION

6.1.1 General

The PAS-4 test was conducted on July 16, 1992. The explosive charge for this event was 100 kg of Composition C-4. This is the equivalent of 2700 kg of the same explosive in the full-size structure. Figures 198 and 199 show the placement of the charge for this event. The center of the charge was placed 600 mm above the surface of the floor.

Figures 200-202 show the placement of photo poles, aluminum cubes, and SIFCON cubes for the PAS-4 test. The photo poles and cubes used in the PAS-4 test were identical to those used in the PAS-3 test (Fig. 71). The arrangement of plywood catcher bins for this event is shown in Figure 203. These bins were also identical to those used in the PAS-3 test (Fig. 62).

6.1.2 Instrumentation Plan

A total of 37 channels of electronic instrumentation were provided for the PAS-4 event. Because the structure was expected to fail very quickly, only a few measurements were made on the arch. Most of the pressure measurements were made in the floor or the free-field around the structure. The instrumentation plan included 12 pressure measurements inside the structure, 22 free-field pressure measurements, and 3 accelerometers mounted on the structure at $X = 6818$ in the same plane as the explosive charge. No strain or deflection measurements were taken on the front door. The measurements list for the PAS-4 event gives the measurement number, the general location, coordinates, type of sensor and its sensing axis, and the predicted maximum amplitude of the recorded data (Table 35). As for the previous events, the predicted maximum amplitudes are approximate values used for gage selection and setting recording bandwidths. They are based on pretest calculations, but do not correspond exactly to the results of these calculations.

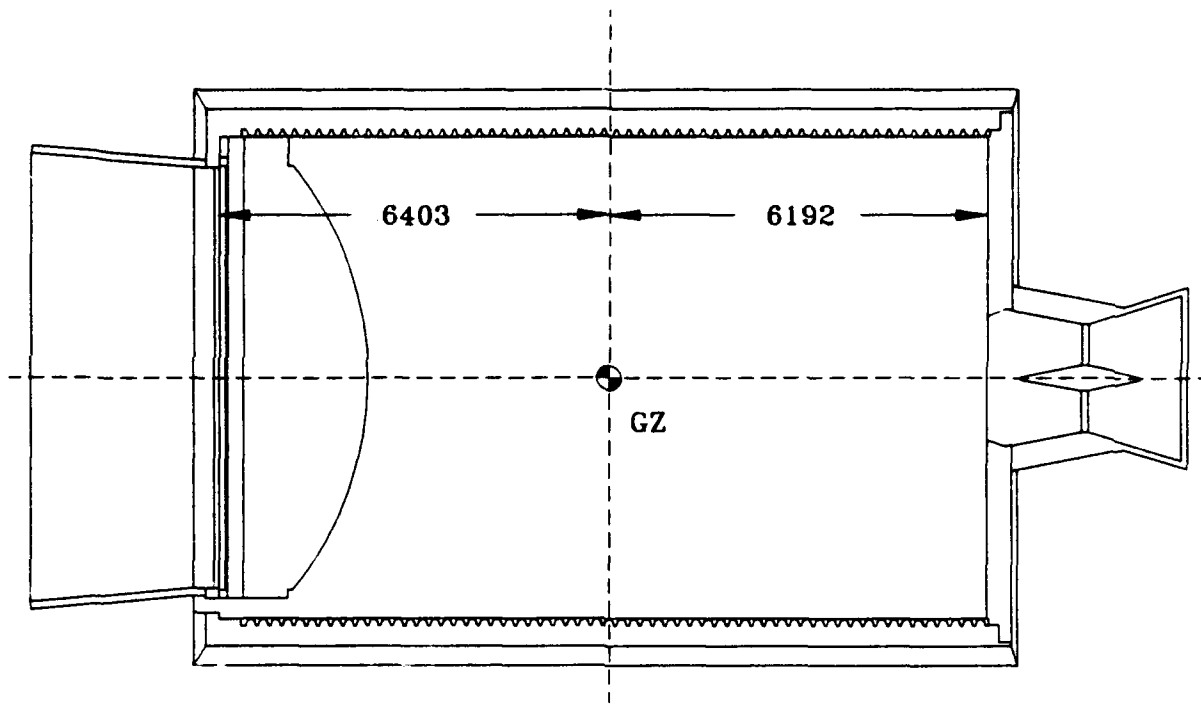


Figure 198. Location of GZ for PAS-4.

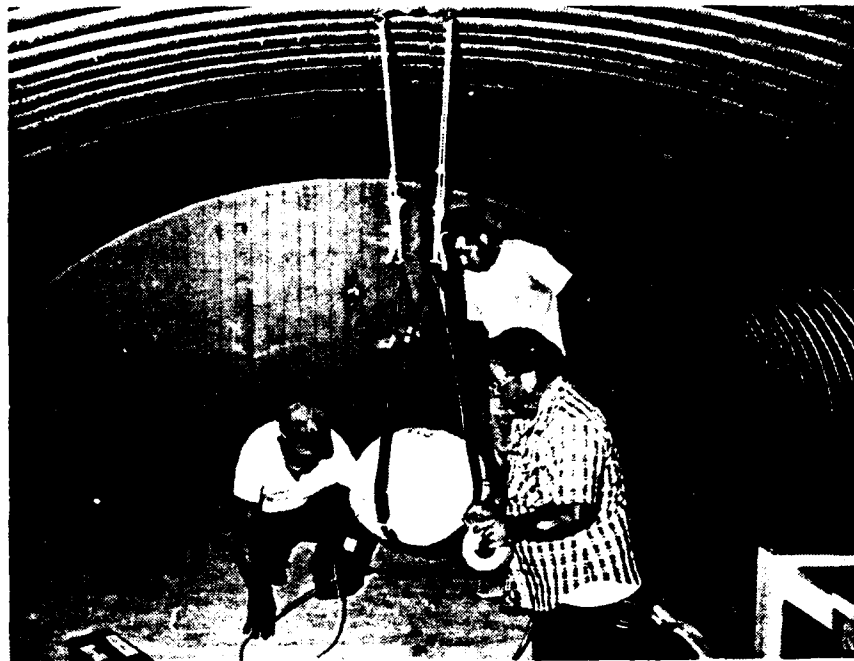
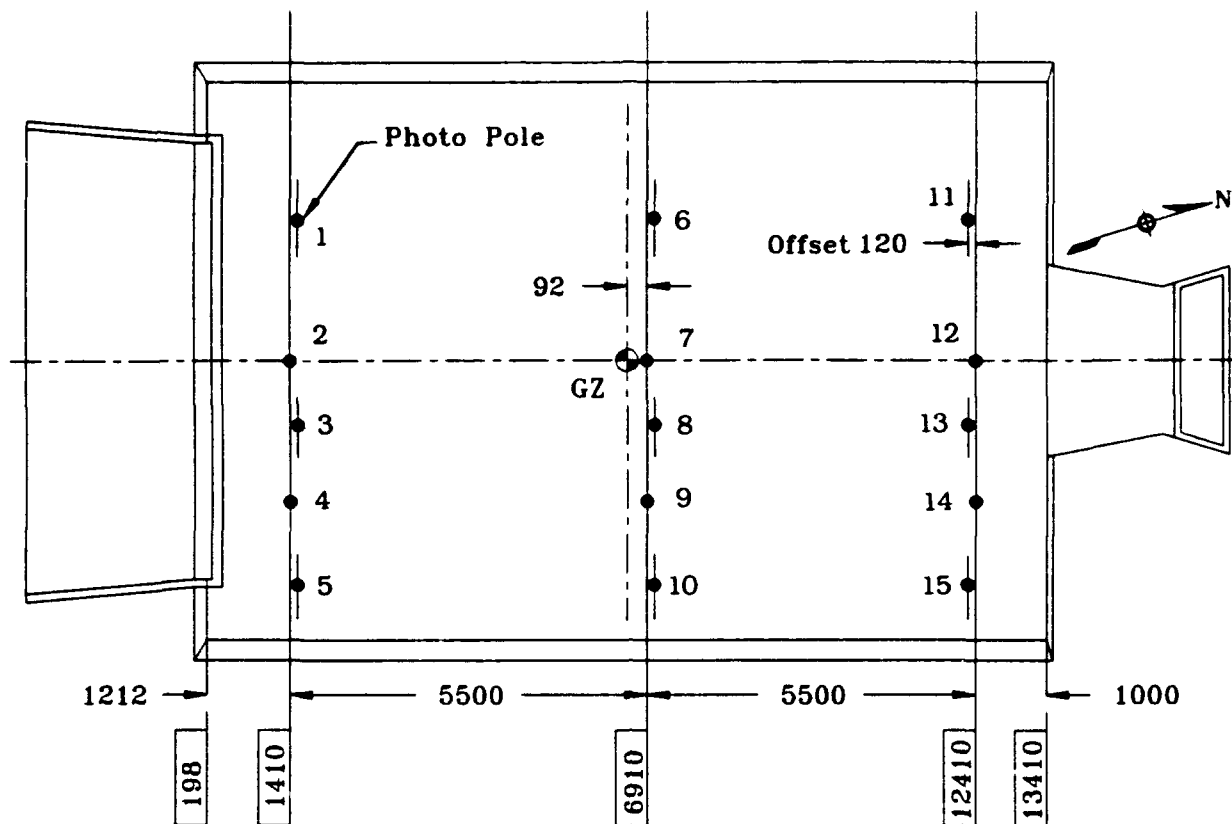
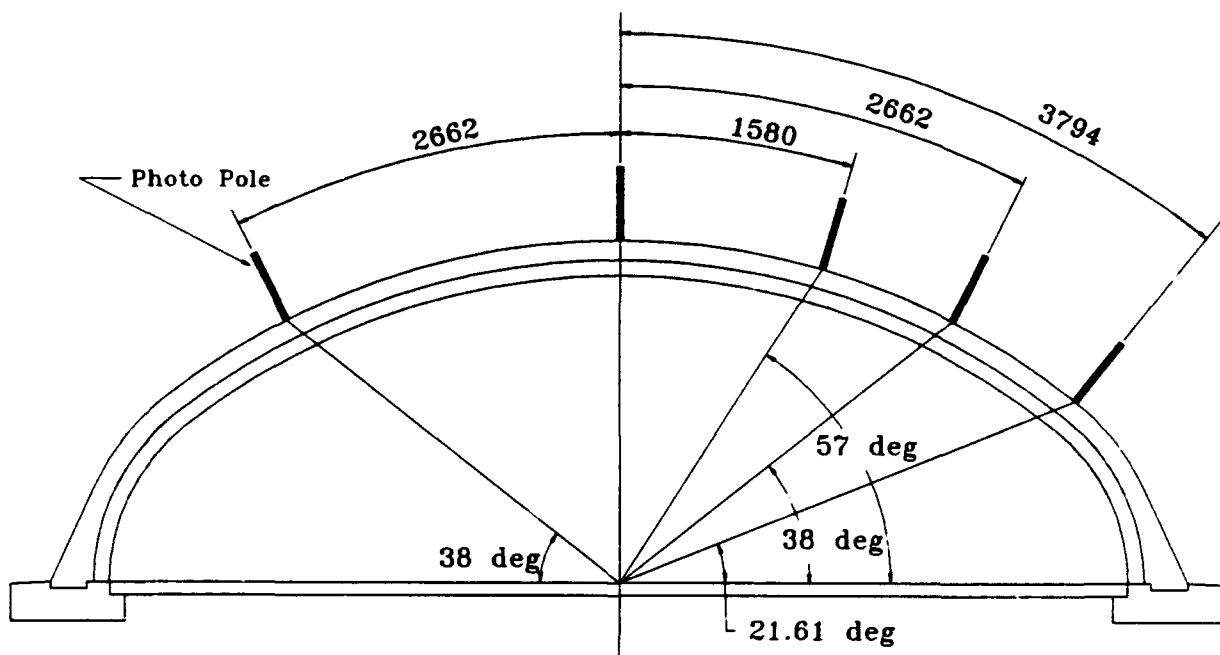


Figure 199. Explosive charge, 100 kg of C-4, PAS-4.

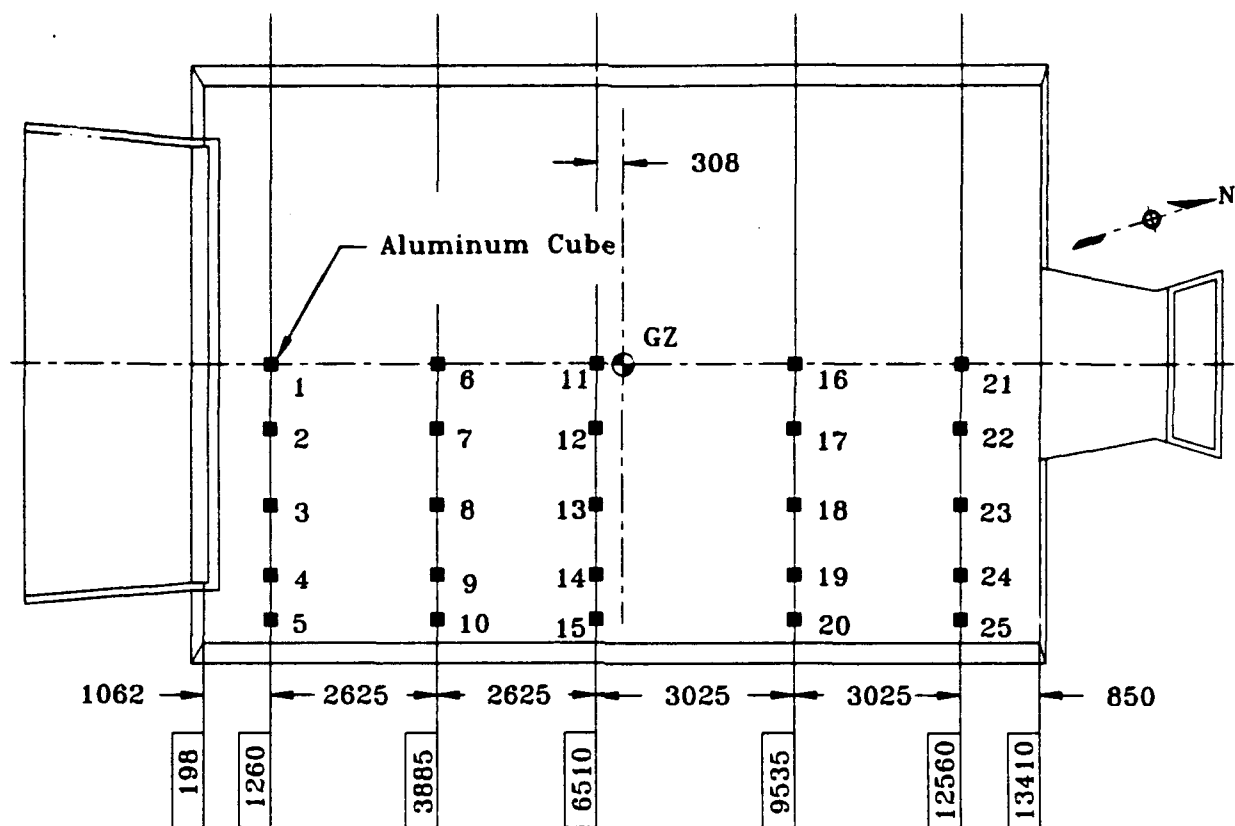


(a) Plan.

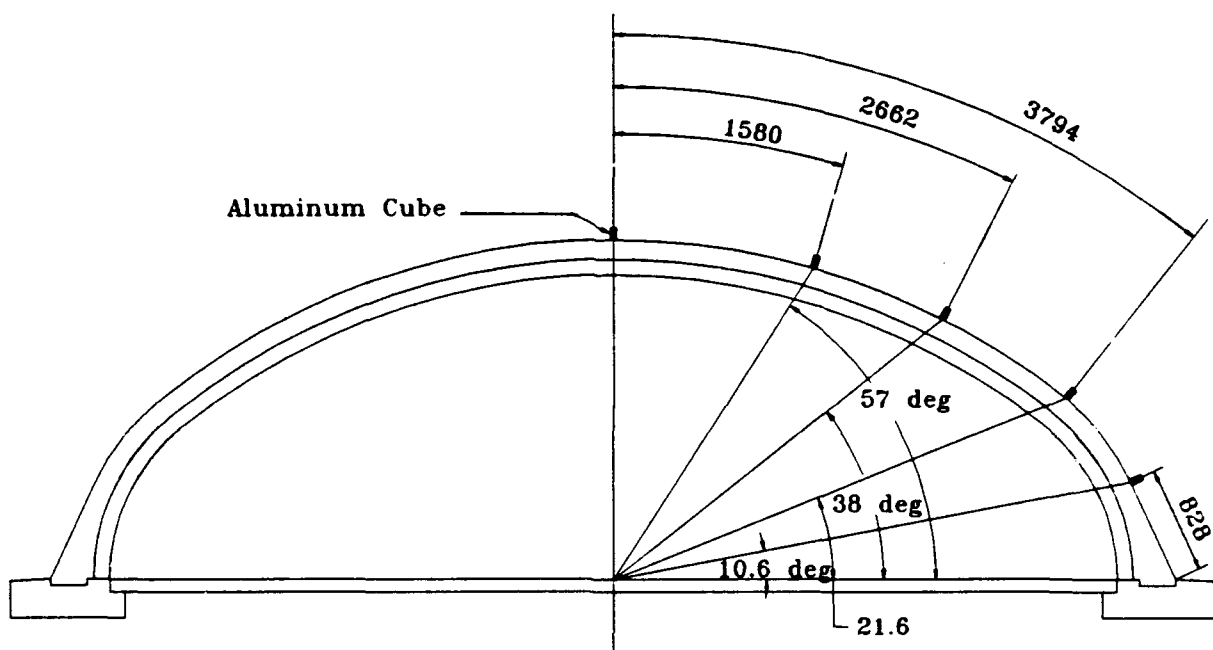


(b) Section.

Figure 200. Photo pole locations, PAS-4.

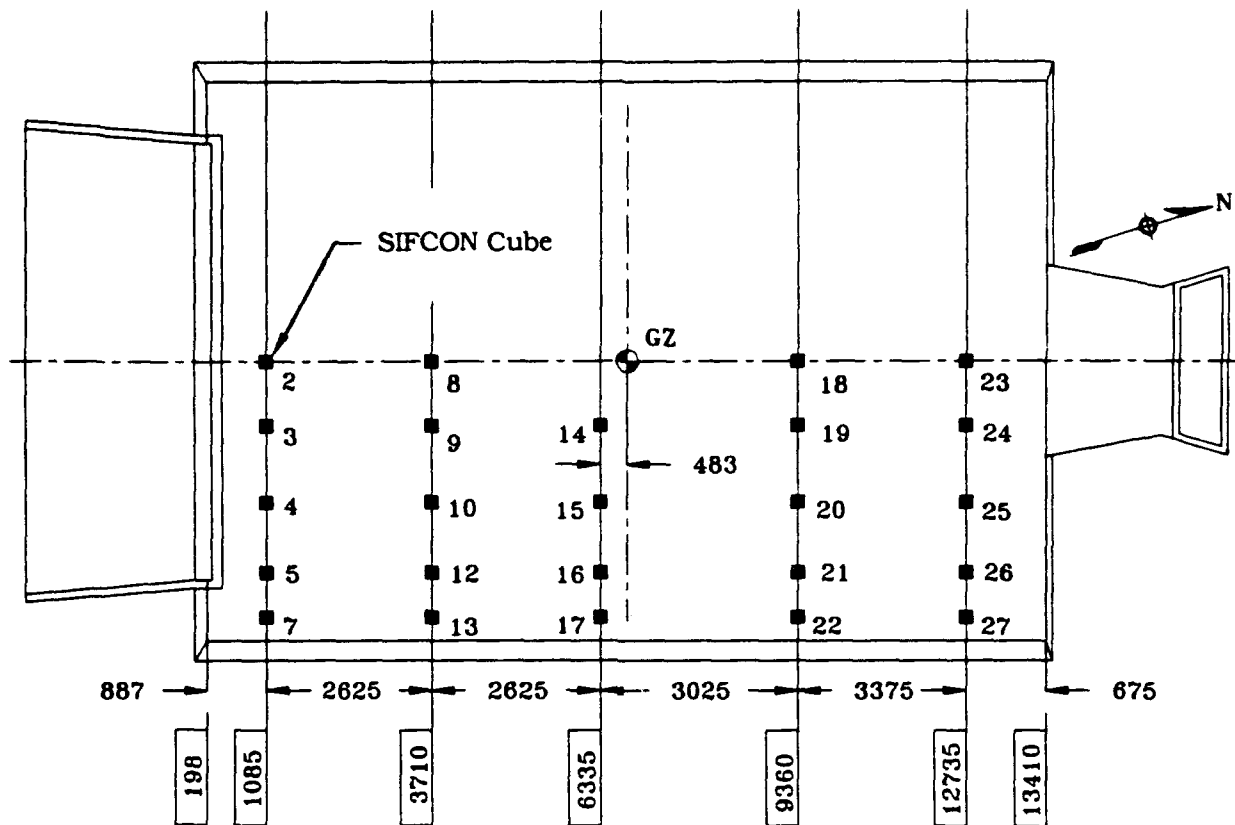


(a) Plan.

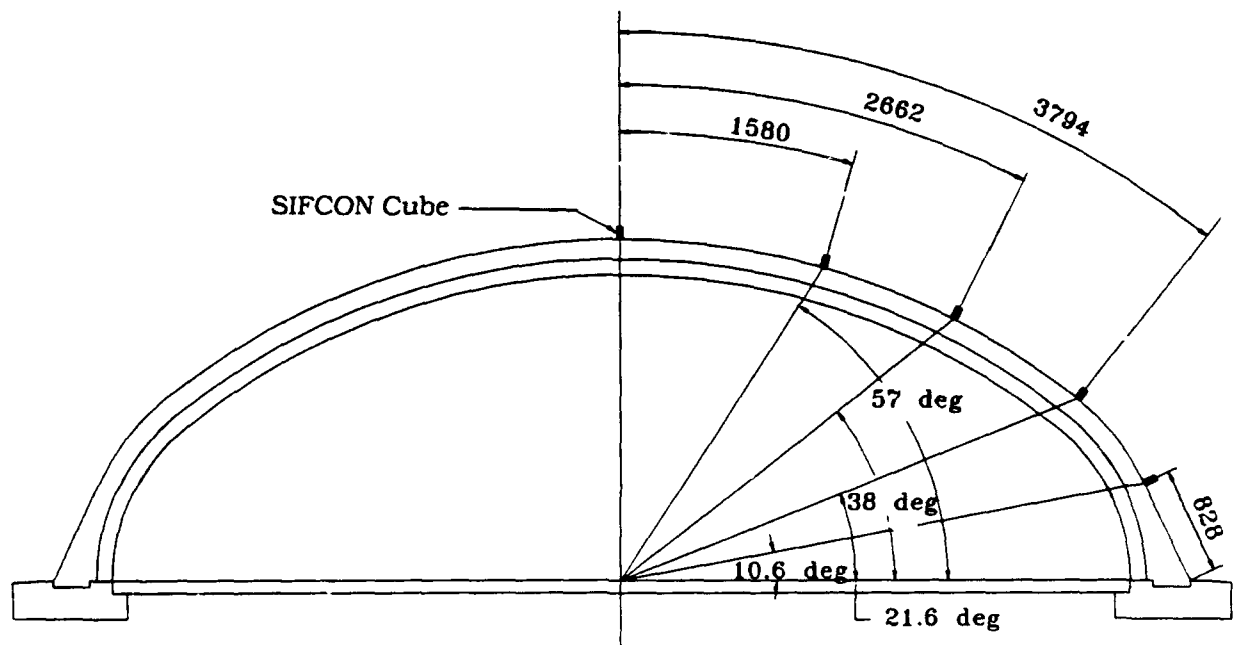


(b) Section.

Figure 201. Locations of aluminum cubes, PAS-4.



(a) Plan.



(b) Section.

Figure 202. The SIFCON cube placement, PAS-4.

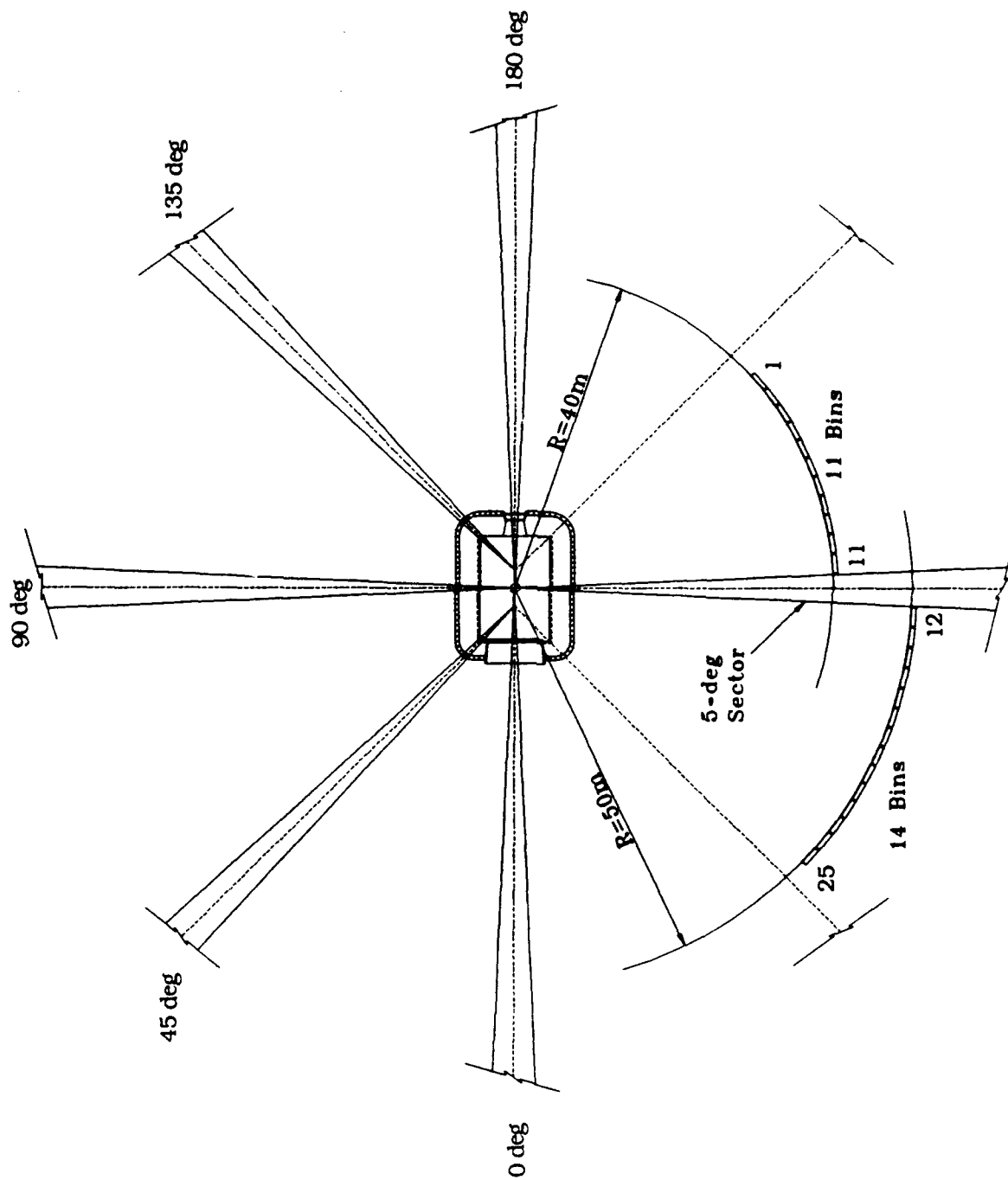


Figure 203. Locations of debris catcher bins, PAS-4.

Table 35. List of measurements for PAS-4.

MEASUREMENT LIST																	DATE	7 JUL 92	PAGE 1 OF 4 PAGES
PAS-4										KIRST							IE		
TEST EVENT		LOCATION				SENS		PREC	CONF	TRANSDUCER		TRANSDUCER	TRANSDUCER		CHANGES				
MEAS NO.	SEN	X#	Y#	Z#	AXIS	MAX	LEVEL	MODEL	RANGE	TYPE	SERIAL NUMBER	ITEM	AUTH	DATE					
0101-4	SF	12807	0	367	Z	5.171 MPa	70 %	KULITE	13.79 MPa	(Filter)	102-7-13								
0102-4	SF	12807	3700	367	Z	13.790 MPa	70 %	KULITE	34.47 MPa	(Filter)	3668-1-4								
0202-4	BW	13010	1700	1475	X	6.895 MPa	70 %	KULITE	13.79 MPa	(Filter)	102-9-1								
0301-4	SF	3976	0	367	Z	4.826 MPa	70 %	KULITE	13.79 MPa	(Filter)	102-9-10								
0302-4	SF	3976	1850	367	Z	4.826 MPa	70 %	KULITE	6.89 MPa	(Filter)	455-2-4								
0303-4	SF	3976	3700	367	Z	11.032 MPa	70 %	KULITE	34.47 MPa	(Filter)	5242-1-6	GAGE	J.K.	7/1					
0402-4	FD	498	100	1475	X	5.654 MPa	70 %	KULITE	13.79 MPa	(Nylon Mount)	102-9-2								
0501-4	SF	645	3700	367	Z	13.790 MPa	70 %	KULITE	34.47 MPa	(Filter)	5246-4-24								
0601-4	SF	6818	1850	367	Z	8.274 MPa	70 %	KULITE	13.79 MPa	(Filter)	103-3-1								
0602-4	SF	6818	3700	367	Z	13.790 MPa	70 %	KULITE	34.47 MPa	(Filter)	5047-1-4								
0603-4	SF	6818	3700	367	Z	13.790 MPa	70 %	KULITE	34.47 MPa	(Filter)	5241-3-4								
0604-4	SC	6818	0	2717	Z	13.790 MPa	100 %	KULITE	137.9 MPa	(Filter)	4319-1-19								
NOTES:																	FD = Front Door		
																	SF = Shelter Floor		
																	BW = Backwall		
																	SC = Shelter Ceiling		

Table 35. Continued.

MEASUREMENT LIST														DATE 8 JUL 92		PAGE 2 OF 4 PAGES	
PAS-4														KIRST			
TEST EVENT		LOCATION				SENS		PRED		CONF		TRANSDUCER		TRANSDUCER		CHANGES	
MEAS NO.	GEN	X#	Y#	Z#	AXIS	MAX	LEVEL	MODEL	RANGE	TYPE	SERIAL NUMBER	ITEM	AUTH	DATE			
RDT 0604-4	SC	12807	0	2717	Z	55.16 MPa	57.2 %	KULITE HKS-11-375	137.9 MPa	(Filter) PRESSURE	4319-1-19						
0701-4	FF	-9000	0	350	Z	106.87 kPa	100 %	KULITE XT-190	172.4 kPa	PRESSURE	(3549-1-175) O15-43						
0702-4	FF	-24000	0	350	Z	34.474 kPa	100 %	KULITE XT-190	68.9 kPa	PRESSURE	(2650-2-112) X8-19						
0703-4	FF	-44000	0	350	Z	13.790 kPa	100 %	KULITE XT-190	34.5 kPa	PRESSURE	(4363-5-137) X18-21						
0704-4	FF	-74000	0	350	Z	6.895 kPa	100 %	ENDEVCO 8510B	13.8 kPa	PRESSURE	D44T						
0705-4	FF	-84000	0	350	Z	5.861 kPa	100 %	ENDEVCO 8510B	13.8 kPa	PRESSURE	C93M		J.K.	8/23			
0706-4	FF	-6233	10800	350	Z	96.527 kPa	50 %	KULITE XT-190	172.4 kPa	PRESSURE	(3549-1-174) O15-42						
0707-4	FF	-16433	21000	350	Z	20.684 kPa	50 %	KULITE XT-190	34.5 kPa	PRESSURE	(4263-5-135) Y18-25						
0708-4	FF	-30433	35000	350	Z	6.895 kPa	50 %	ENDEVCO 8510B	13.8 kPa	PRESSURE	RF77						
0709-4	FF	-37433	42000	350	Z	4.826 kPa	50 %	ENDEVCO 8510B	6.9 kPa	PRESSURE	L11K						
0710-4	FF	6818	12000	350	Z	34.474 kPa	50 %	KULITE XT-190	68.9 kPa	PRESSURE	(2907-3-91) N9-69						
0711-4	FF	6818	40000	350	Z	6.895 kPa	50 %	ENDEVCO 8510B	13.8 kPa	PRESSURE	RF93						

NOTES:

= Distance in millimeters

SC = Structure Ceiling

FF = Free field

RDT = Redundant

NOTES: # = Distance in millimeters RDT = Redundant
 SC = Structure Ceiling
 ff = Free Field

Table 35. Continued.

MEASUREMENT LIST														
PAS-4										KIRST				
TEST EVENT		LOCATION			SENS AXIS	PRED MAX	CONF LEVEL	TRANSDUCER		TRANSDUCER TYPE	TRANSDUCER SERIAL NUMBER	CHANGES		
MEAS NO.	GEN	X#	Y#	Z#				MODEL	RANGE			ITEM	AUTH	DATE
0712-4	FF	6818	50000	350	Z	4.137 kPa	50	ENDEVCO 8510B	6.9 kPa	PRESSURE	L53F			
0713-4	FF	19841	10800	350	Z	55.158 kPa	50	KULITE XT-190	172.4 kPa	PRESSURE	(2710-1-15) A9-57			
0714-4	FF	30041	21000	350	Z	11.721 kPa	50	KULITE XT-190	34.5 kPa	PRESSURE	(4263-5-140) Y18-26	GAUGE	J.K.	7/1
0715-4	FF	44041	35000	350	Z	3.447 kPa	50	ENDEVCO 8510B	6.9 kPa	PRESSURE	L23K			
0716-4	FF	23000	0	350	Z	103.422 kPa	100	KULITE XT-190	172.4 kPa	PRESSURE	(2710-1-10) A9-60			
0717-4	FF	37000	0	350	Z	34.474 kPa	100	KULITE XT-190	68.9 kPa	PRESSURE	(3827-4-19) L18-92			
0718-4	FF	57000	0	350	Z	13.790 kPa	100	KULITE XT-190	34.5 kPa	PRESSURE	(4363-5-139) X18-22			
0719-4	FF	77000	0	350	Z	5.516 kPa	100	ENDEVCO 8510B	6.9 kPa	PRESSURE	L08K			
0720-4	FF	6818	-12000	350	Z	34.474 kPa	50	KULITE XT-190	68.9 kPa	PRESSURE	(2650-2-49) W8-91			
0721-4	FF	6818	-40000	350	Z	6.895 kPa	50	ENDEVCO 8510B	13.8 kPa	PRESSURE	C61M			
0722-4	FF	6818	-50000	350	Z	4.137 kPa	50	ENDEVCO 8510B	6.9 kPa	PRESSURE	L01K			
1601-4	SR	6818	0	2987	Z	20000 g	50	ENDEVCO 2264A	50000 g	ACCELEROMETER	CH03E			
NOTES:														
* = Distance in millimeters														
FF = Free field														
SR = Structure Roof														

Table 35. Concluded.

[illegible]

The locations of the various on-structure measurements are shown in Figures 204 through 208—gages mounted in the floor of the structure (Fig. 204), one pressure gage mounted on the inner surface of the front door (Fig. 205), gages in the plane through $X = 3976$ (Fig. 206), and sensors mounted on the arch in a plane through GZ (Fig. 207). The sensing axes of the accelerometers mounted at these locations were oriented to measure radial accelerations. Figure 208 shows the location of the one airblast gage mounted in the backwall; Figure 209 shows the locations of the free-field airblast gages.

Waterways Experiment Station (WES) installed three self-recording accelerometers on the structure. These gages were identical to those installed in the PAS-3 test. The three gages were placed on narrow brackets attached to the outside of the arch (Fig. 210).

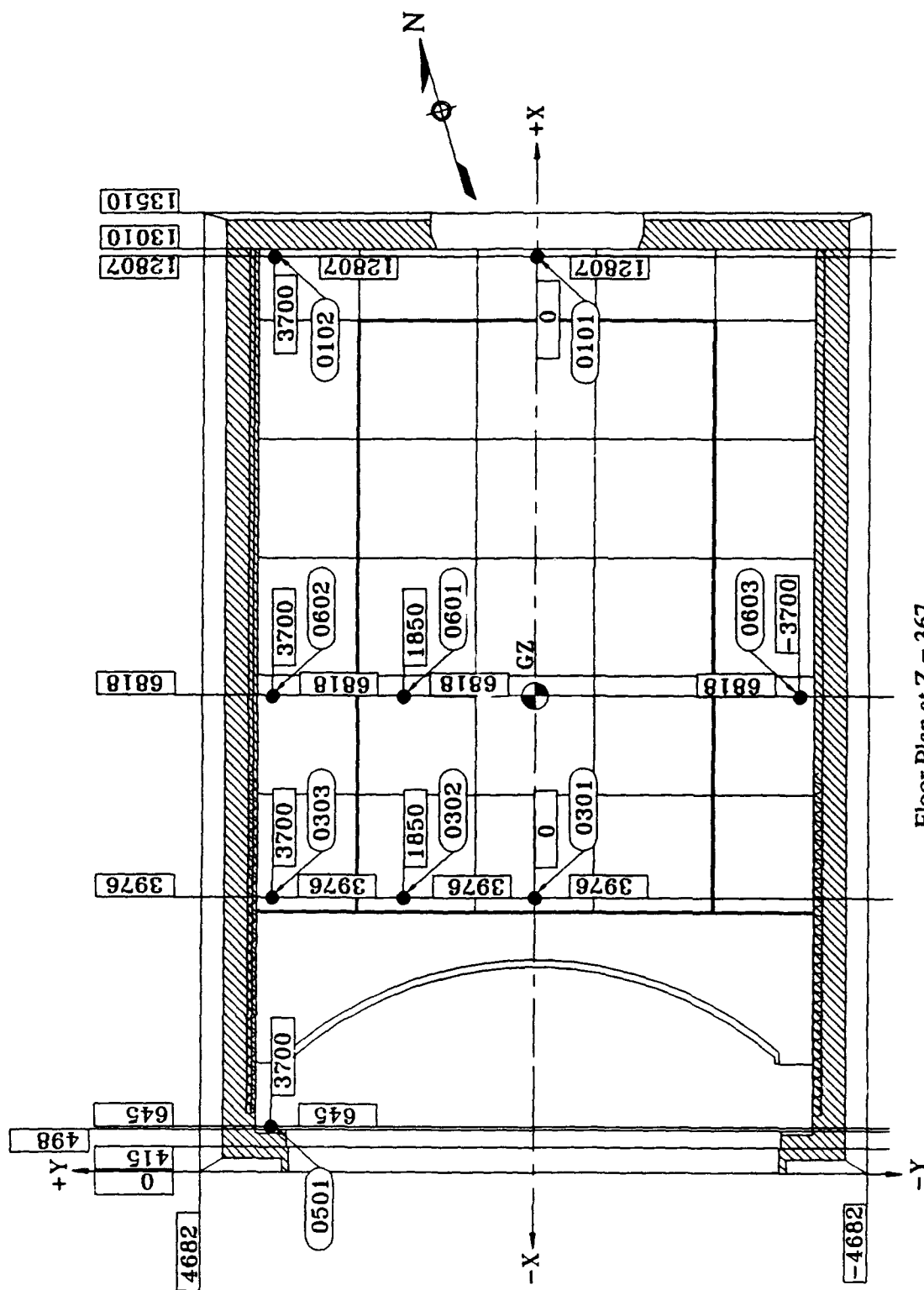
Twenty-one high-speed motion picture, sequential still, and video cameras were provided at one aerial and five ground-level camera stations. The locations of the ground stations for the PAS-4 event are shown in Figure 211. Motion picture data were recorded at rates of 400, 500, and 2000 frames per second.

6.2 TEST RESULTS

6.2.1 Structural Damage Survey

The test structure was destroyed in the PAS-4 event. Figures 3 and 4 present a key for identifying the various components of the model in the following discussion of structural damage. Estimated debris velocities given in the following paragraphs were calculated on the basis of observed object motion in one plane. The actual velocities could be somewhat higher due to out-of-plane motion of the object.

The front door was blown out of the structure at about 20 ms. It rotated about its lower edge until it was down on the ground surface. It then moved horizontally away from the structure at a velocity of about 140 m/s, until it became airborne at about



Floor Plan at Z = 367

Figure 204. Instrumentation in floor of structure, PAS-4.

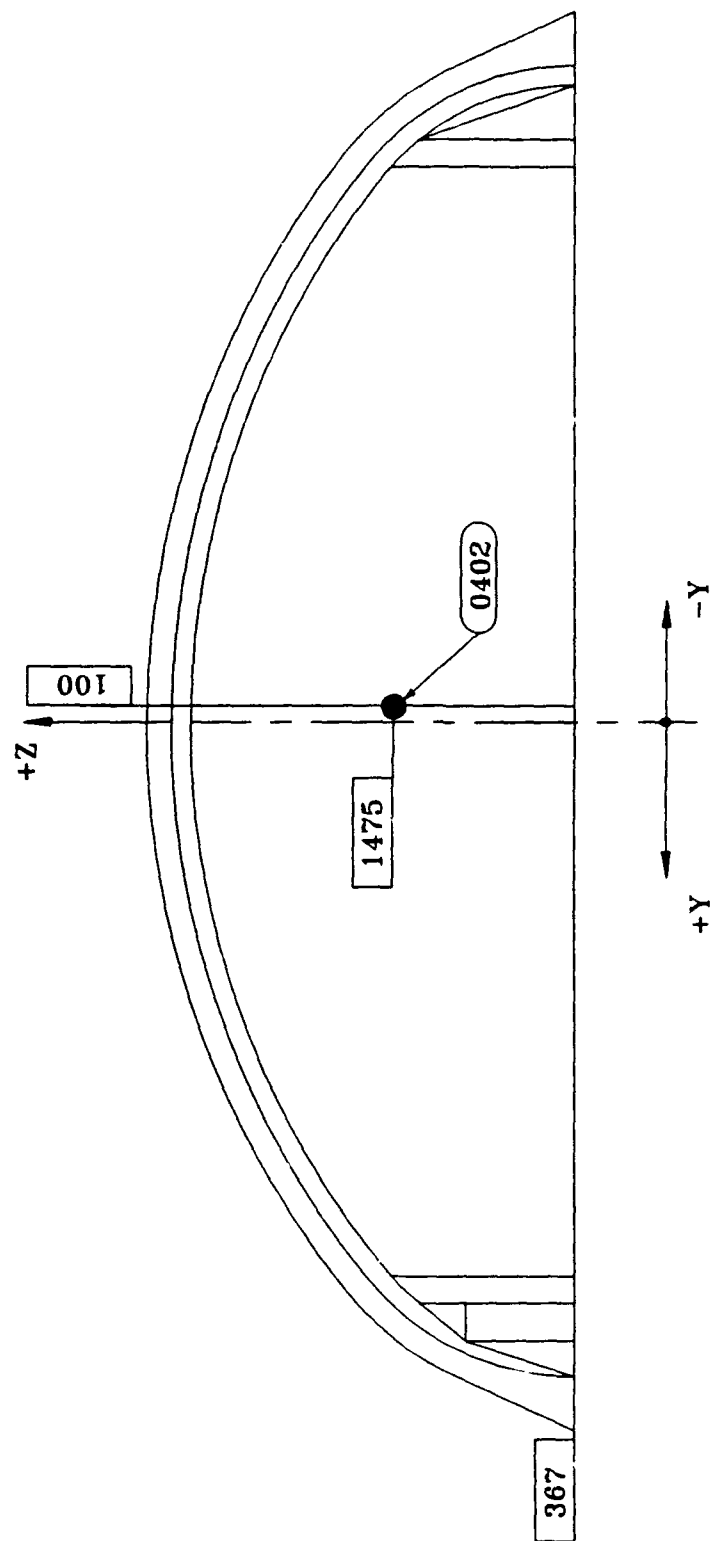


Figure 205. Instrumentation on inside surface of front door X = 498, PAS-4.

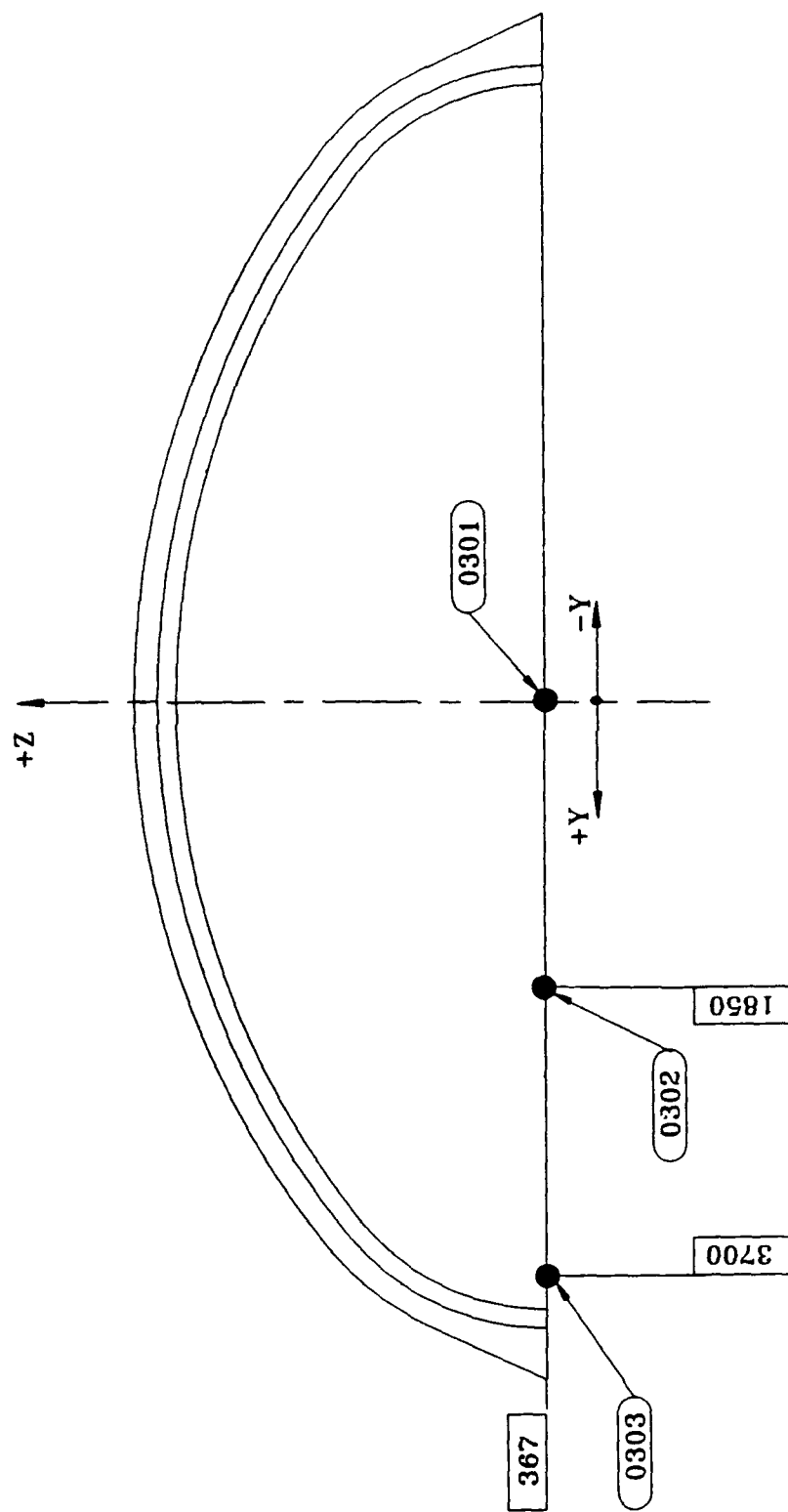


Figure 206. Instrumentation on arch at X = 3976, PAS-4.

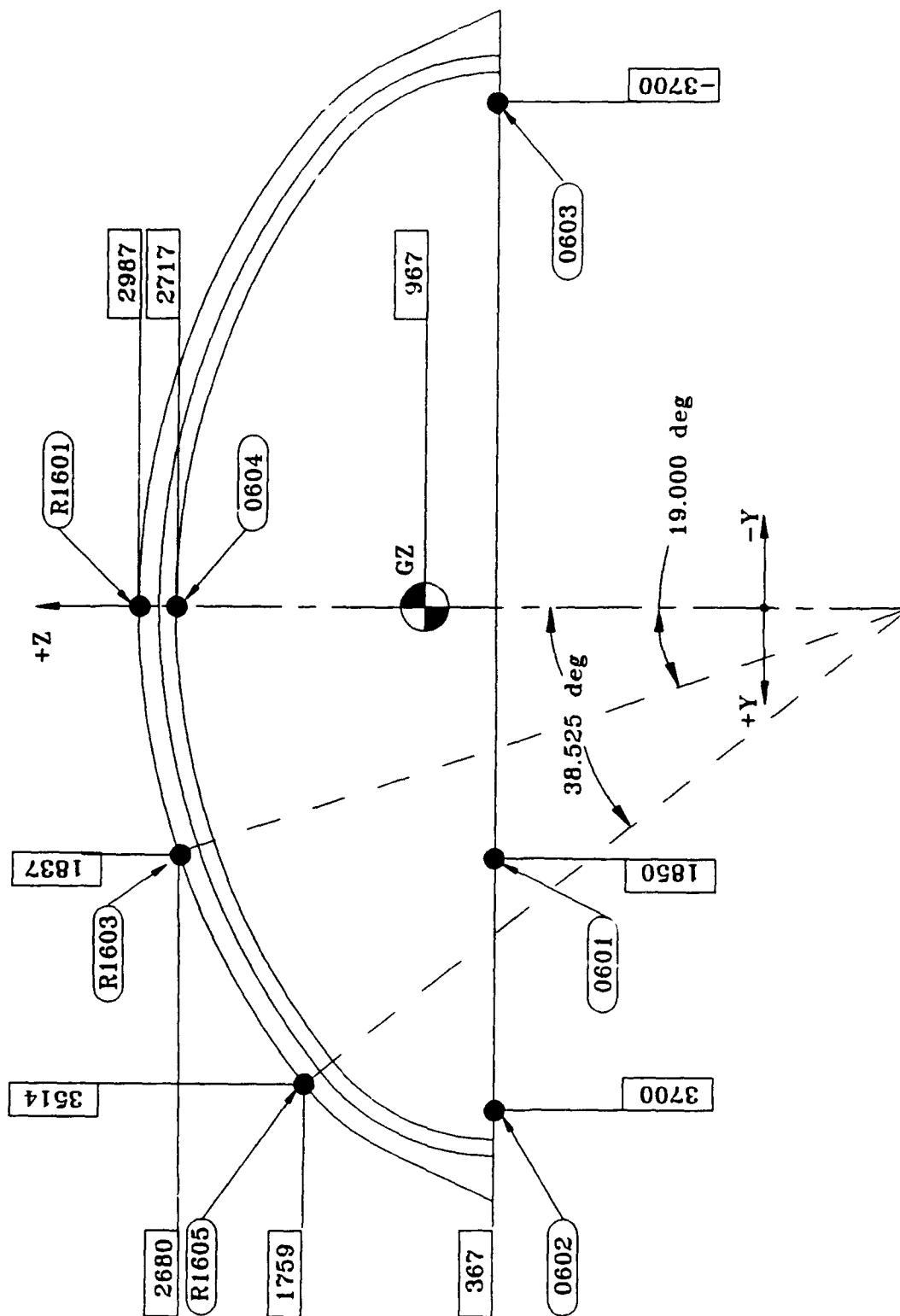


Figure 207. Instrumentation on arch at X = 6818, PAS-4.

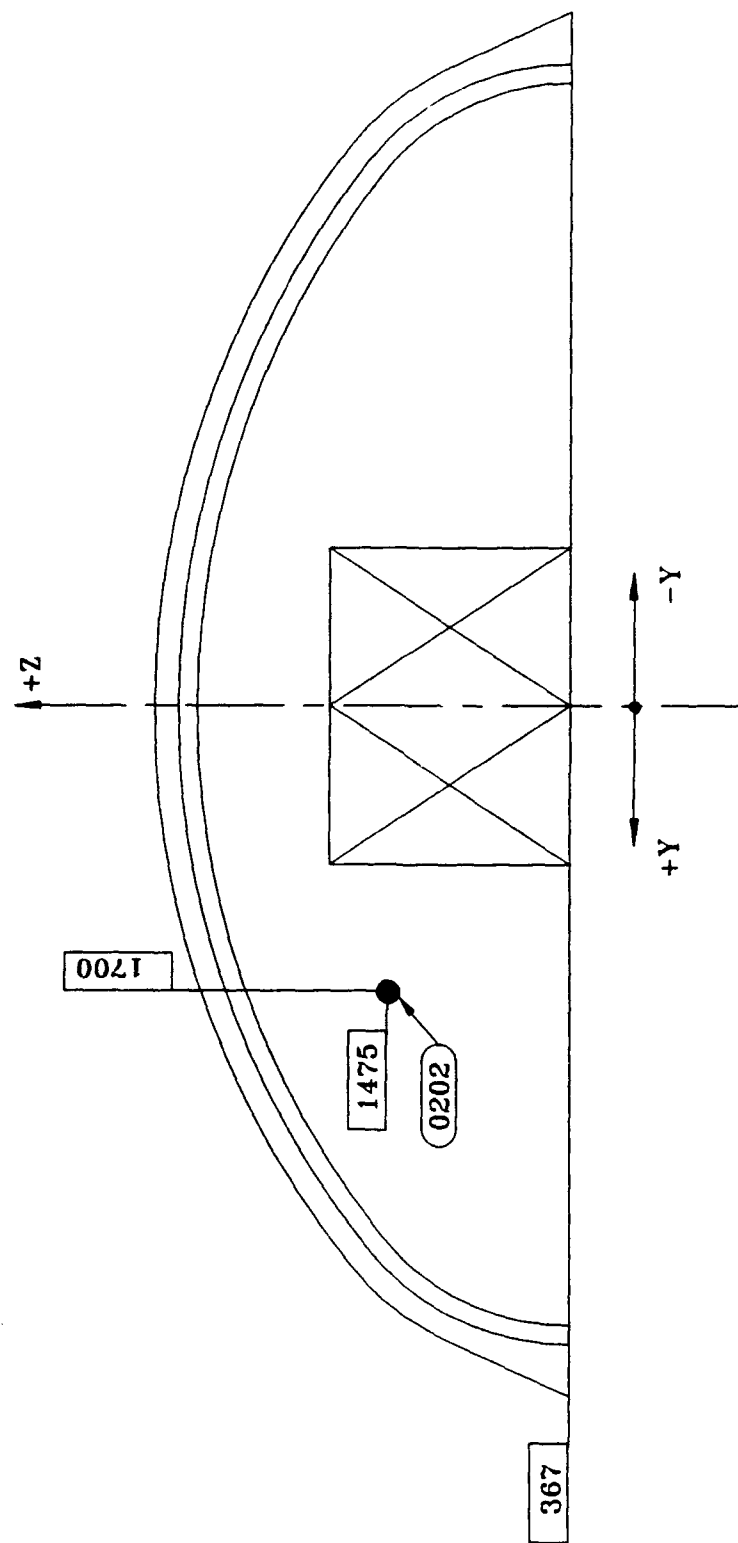
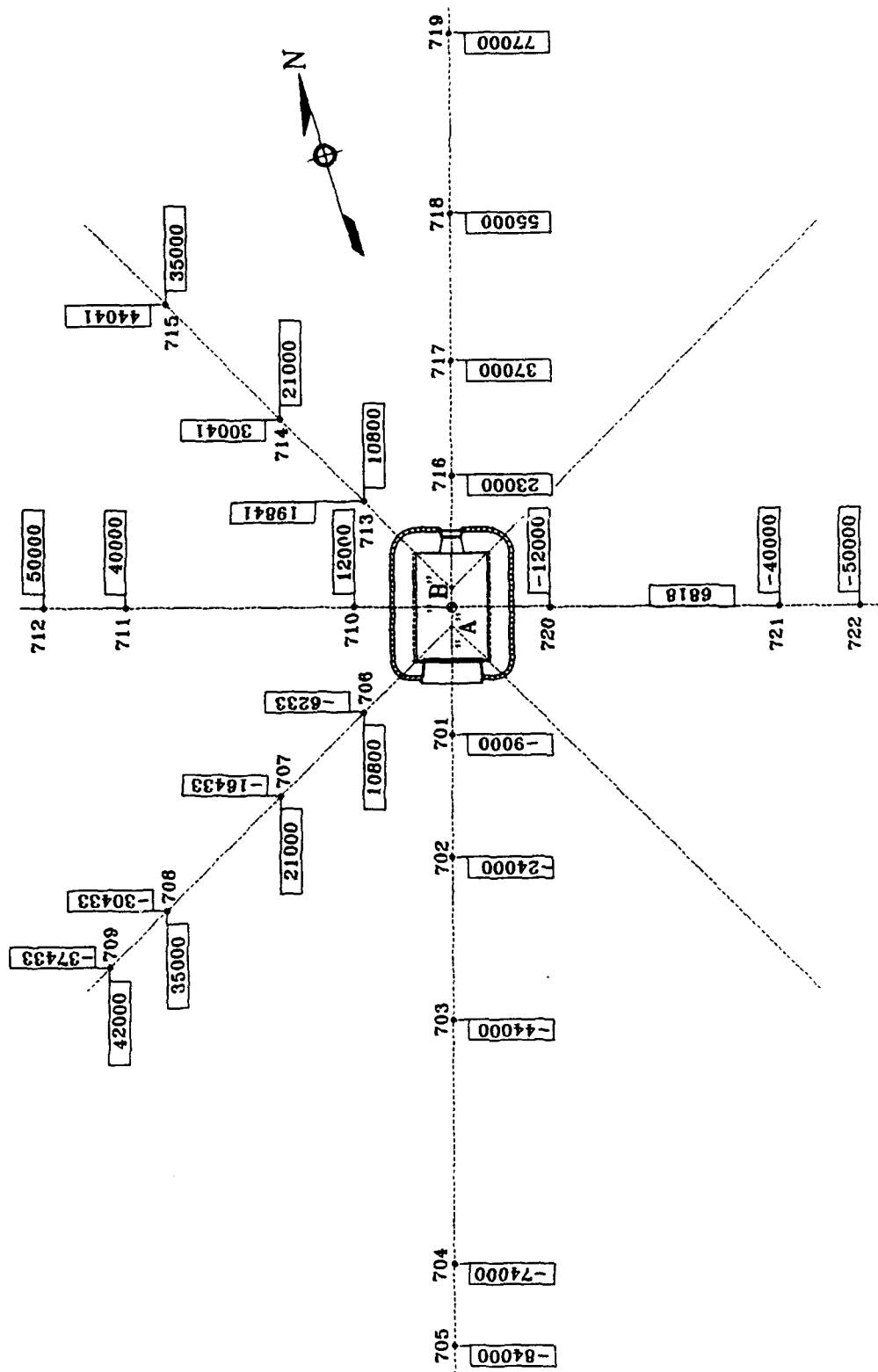
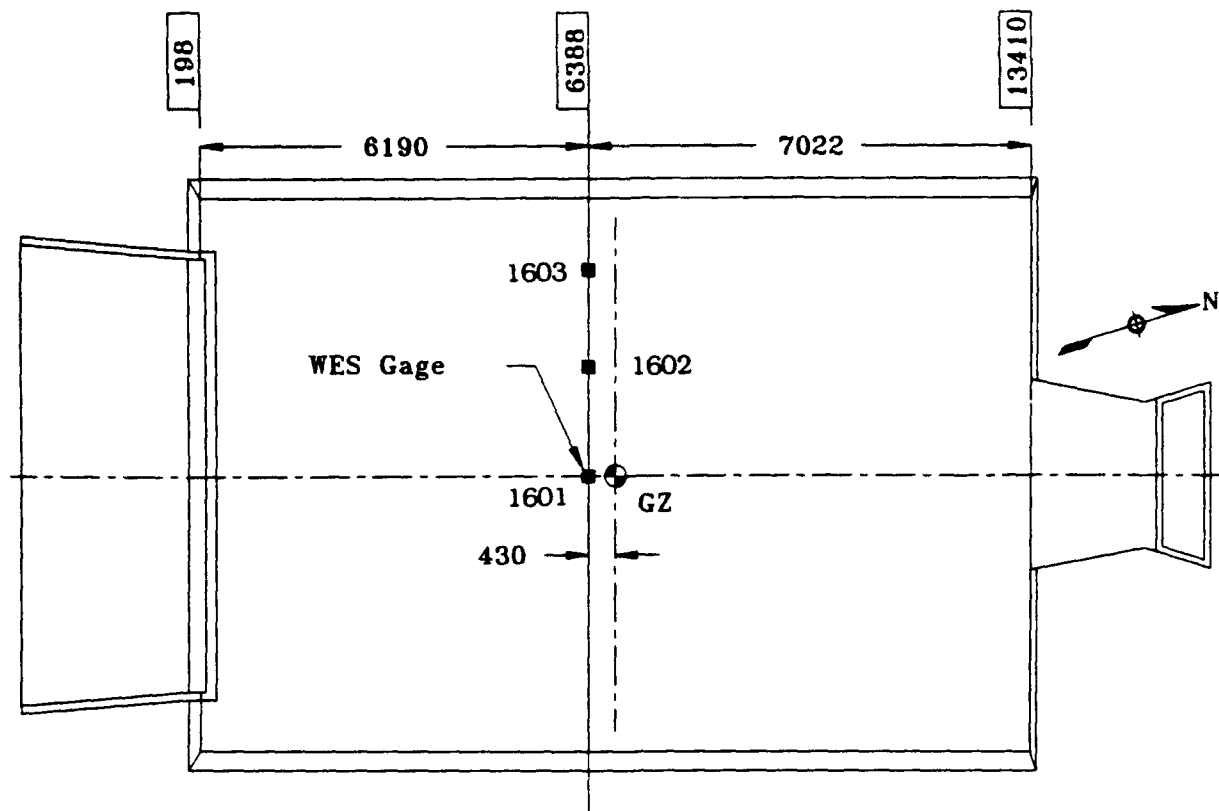


Figure 208. Instrumentation on inner surface of backwall at $X = 13010$, PAS-4.

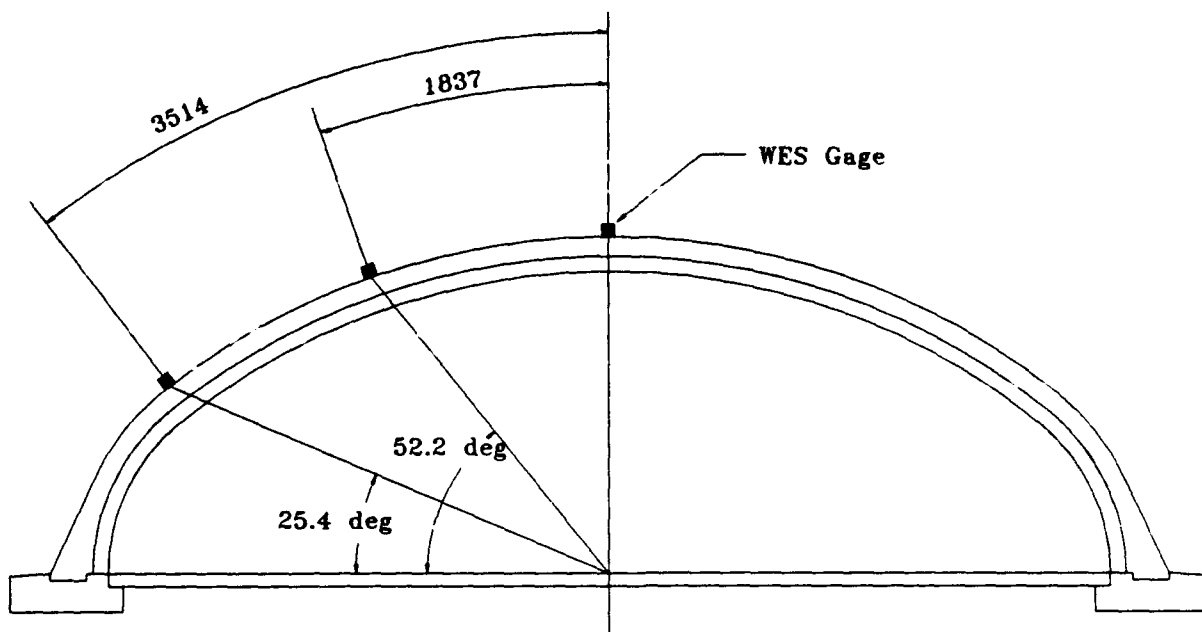


TEST BED GRADE AT Z=350

Figure 209. Free-field airblast gage locations, PAS-4.



(a) Plan.



(b) Section.

Figure 210. Locations of WES self-recording accelerometers, PAS-4.

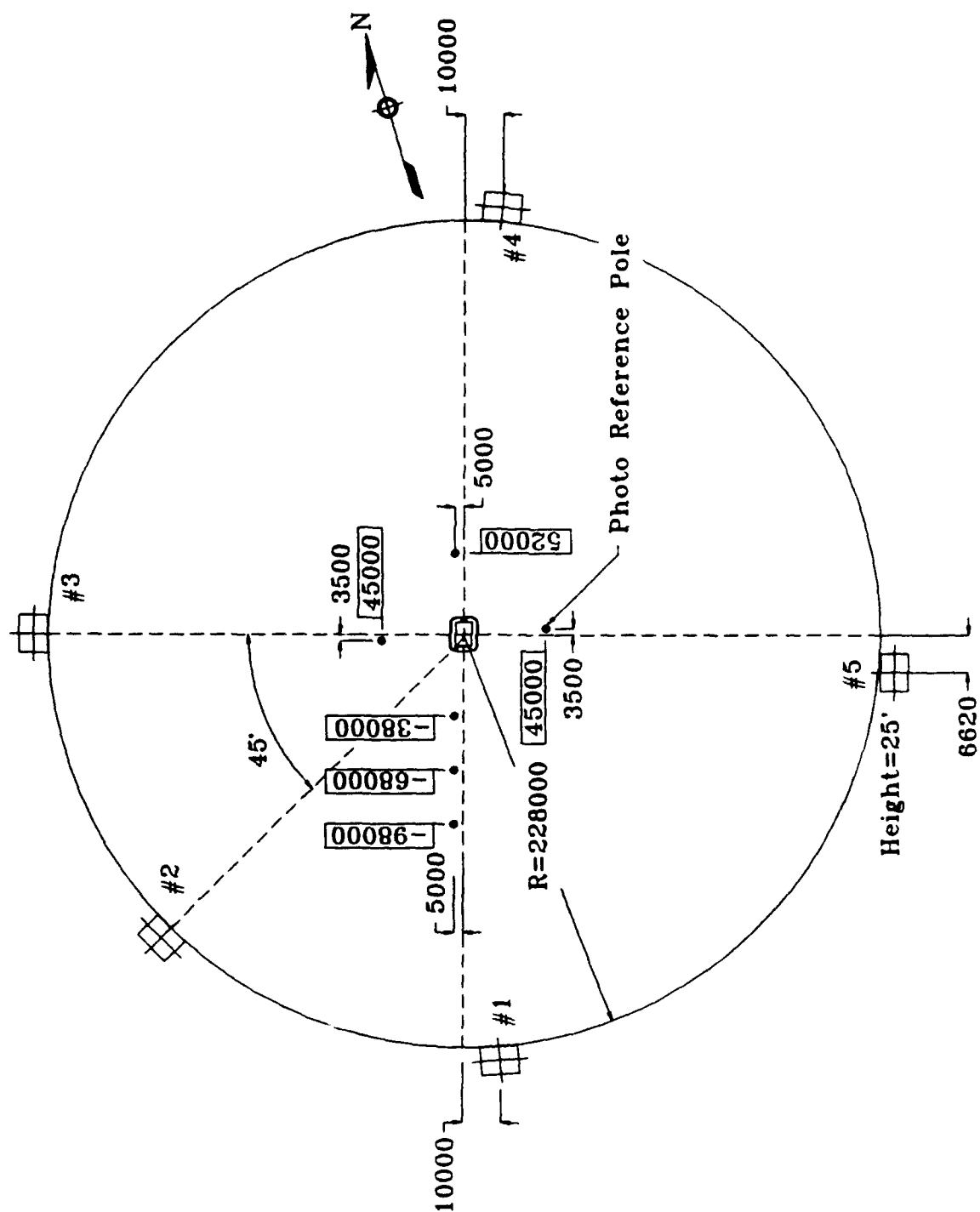


Figure 211. Camera station locations, PAS-4.

160 ms after $t = 0$. Its maximum height of flight could not be determined as it left the field of view of most ground-level cameras. It came to rest at 402 m in front of the structure (Fig. 212).

The door was bent its full length about a horizontal line and had a maximum deflection of 420 mm at the center (Fig. 213). The inside plate was dished inward approximately 15-20 mm between each of the vertical ribs. The inside plate was also buckled in a 700- to 1150-mm wide band along the horizontal centerline. The sides of the door were bent inward approximately 170 mm at the east edge and 340 mm at the west edge (Fig. 214).

The entire edge piece above the support bracket and a section of the inner plate to the first internal stiffener rib, including the heavy plate at the upper corner, were torn away along the weld line and were missing from the left side of the door (Fig. 215). The three sections of inner plate adjacent to the missing piece were also torn from the internal stiffeners, but they remained attached to the door at the top and bottom edges.

At several locations on the inside surface, the welds joining the inner plate to the internal stiffeners had areas of longitudinal tensile cracks. At two locations near the top center of the door, the inner plate was torn from the internal stiffener along the weld line (Fig. 216). At one location the tear was 620 mm long, and at the other it was 315 mm long. There were also some isolated locations of torn welds in the inner plate around both of the hinges.

The personnel entrance vestibule was found intact, but severely damaged, approximately 28 m in front of the left wingwall (Fig. 217). The personnel door was found inside the vestibule. It had impacted the inner wall of the vestibule, fracturing the 6-mm-thick steel plate in several places (Fig. 218). The personnel door was deformed to the point of being almost unrecognizable. Although the welds simulating the hinges and latches had all been broken, the door frame remained welded to the steel liner of the headworks.

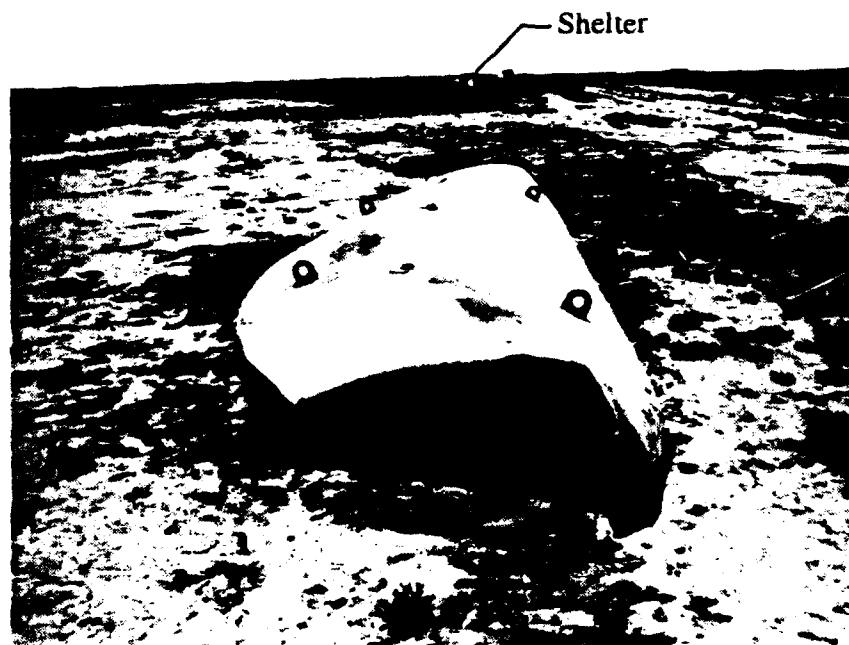


Figure 212. Posttest location of front door, PAS-4.

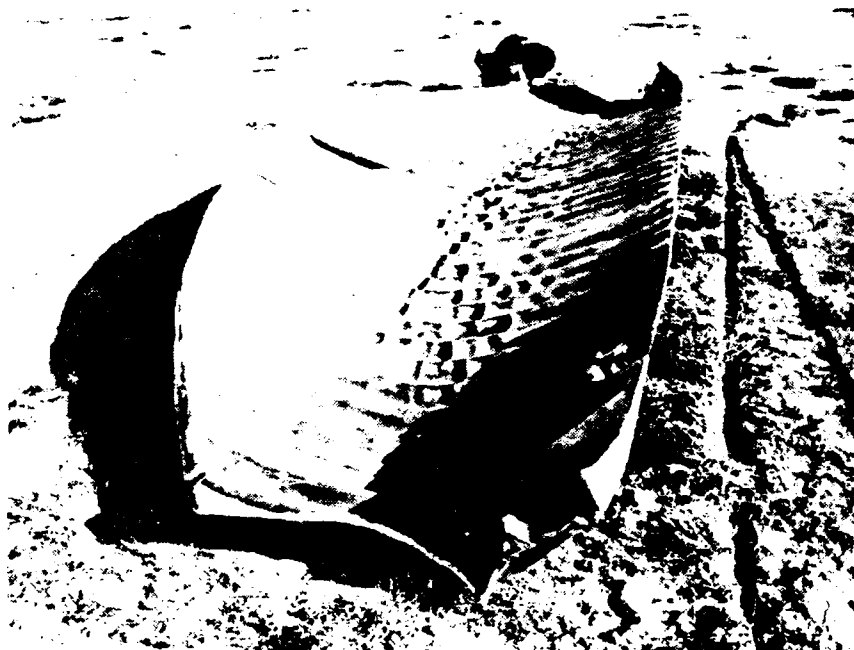


Figure 213. Posttest condition of inside surfaces of front door, PAS-4.

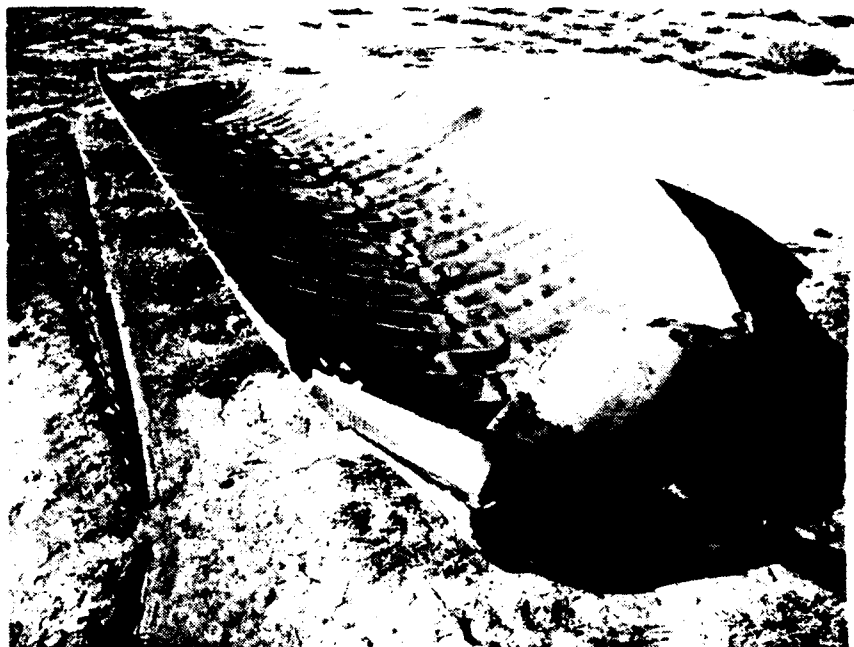


Figure 214. Bent edges of front door, PAS-4.

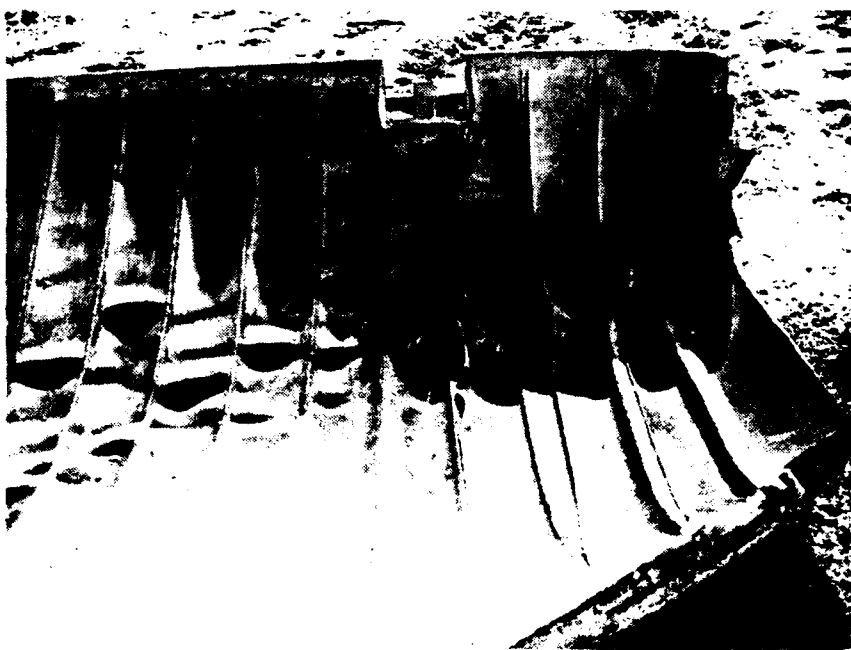


Figure 215. Left edge of front door, inside surface, PAS-4.



Figure 216. Tom weld at inside plate and internal stiffener, PAS-4.



Figure 217. Posttest location of vestibule. PAS-4.

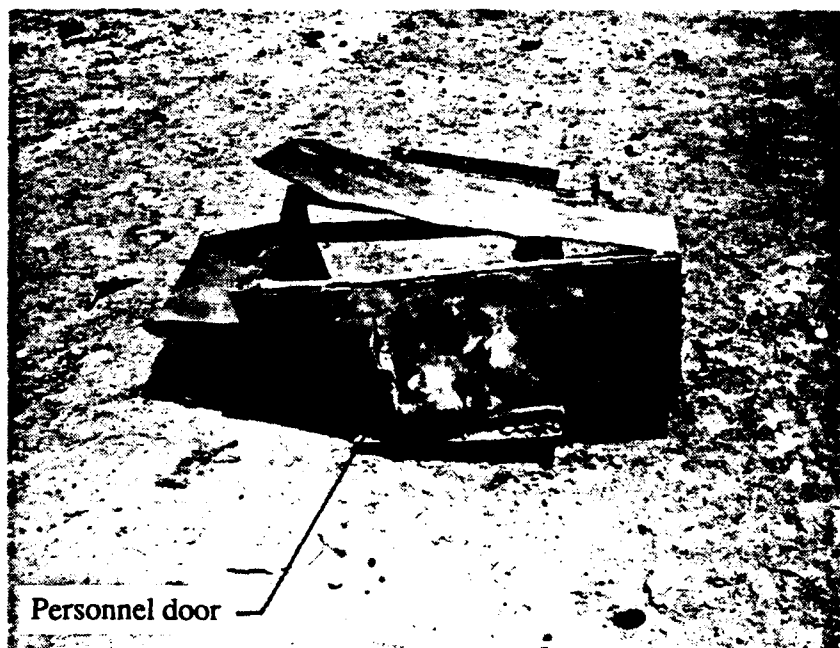


Figure 218. Vestibule and personnel door (foreground), PAS-4.

The lower portions of both wingwalls were found in place on their foundations (Figs. 219 and 220). Most of the top portion of the right wingwall was found as a single piece of debris about 29 m from the side of the shelter. A large piece of the top portion of the left wingwall was found 45 m in front of the shelter. All of the reinforcing bars crossing the failure planes had broken in tension. Both wingwalls and their foundations had broken away from the front foundation and moved forward about 65 mm.

The front apron slab was relatively undamaged with only a few abrasions caused when the front door was blown out. The slab had moved away from the front foundation 12 mm.

The top plate of the door trench was found slightly deformed along its length, and the concrete adjacent to the outside edge of the top plate had spalled away (Fig. 221). The heaviest spalling was located near the door hinge pins.

The right front wall was found intact 25 m from the right side of the shelter (Fig. 222). The left front wall, including the heavily reinforced column next to the personnel entrance opening, was found attached to the adjacent section of the arch. All of the reinforcing dowel bars were pulled out of the base of the column and remained in the front foundation. Both of the front walls were pulled out of the steel plate liner, breaking every headed anchor stud in the process. Most of the dowels between the wingwalls and the front walls remained in the front walls.

The headworks liner was torn in half along a welded joint near the crown of the arch. The two pieces remained attached to the adjacent large sections of the arch. The top parts of the liner were bent outward (Fig. 223). The concrete in the parapet was rubbleized, exposing the large threaded bars, most of which remained attached to the pair of channels welded to the liner plate (Fig. 224).

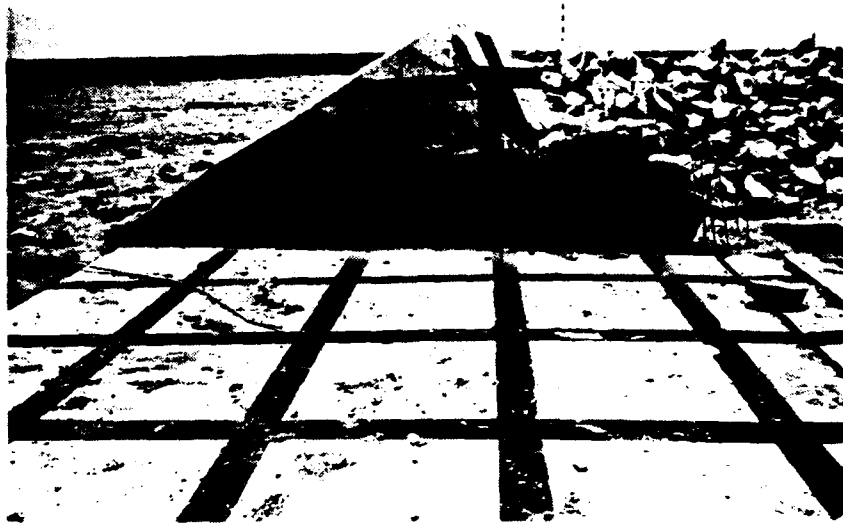


Figure 219. Right wingwall, PAS-4.

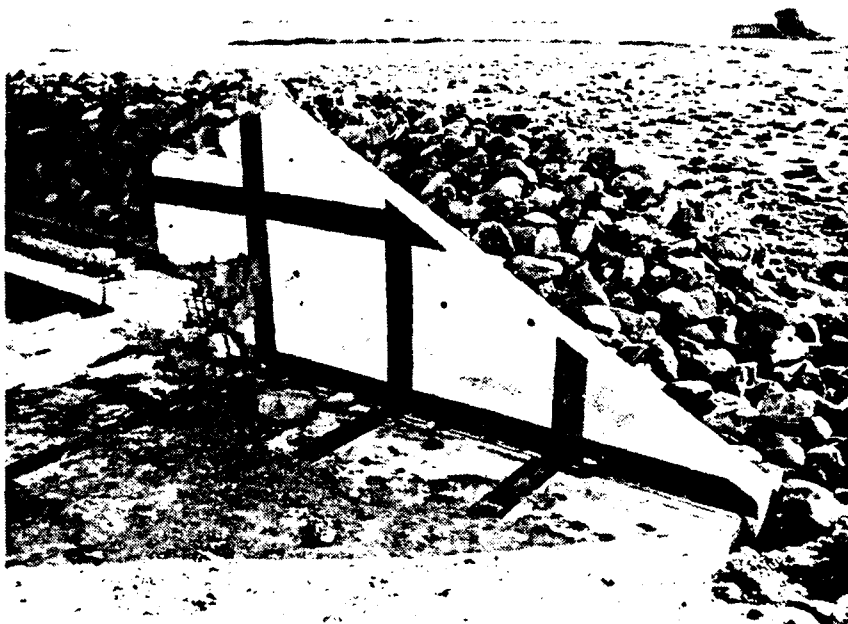


Figure 220. Left wingwall, PAS-4.



Figure 221. Top plate of door trench and front foundation, PAS-4.

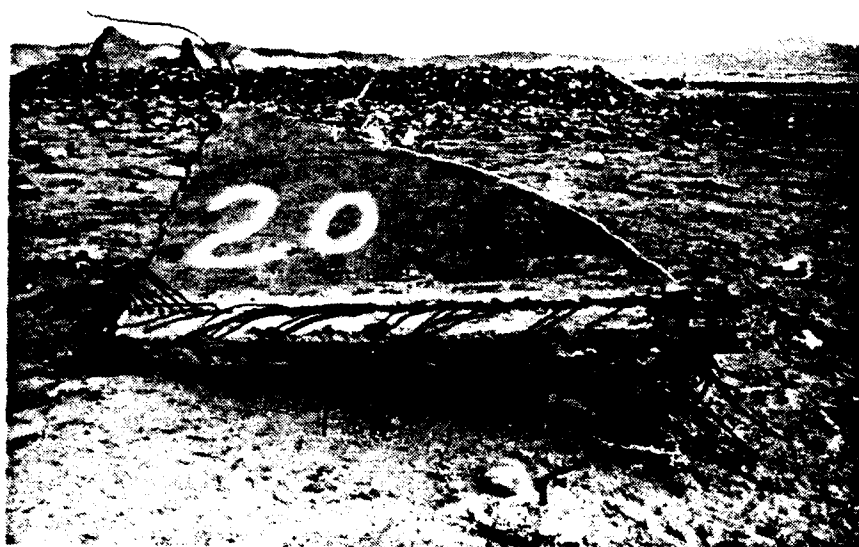


Figure 222. Final location of right front wall, PAS-4.



Figure 223. Deformed steel plate headworks liner, PAS-4.

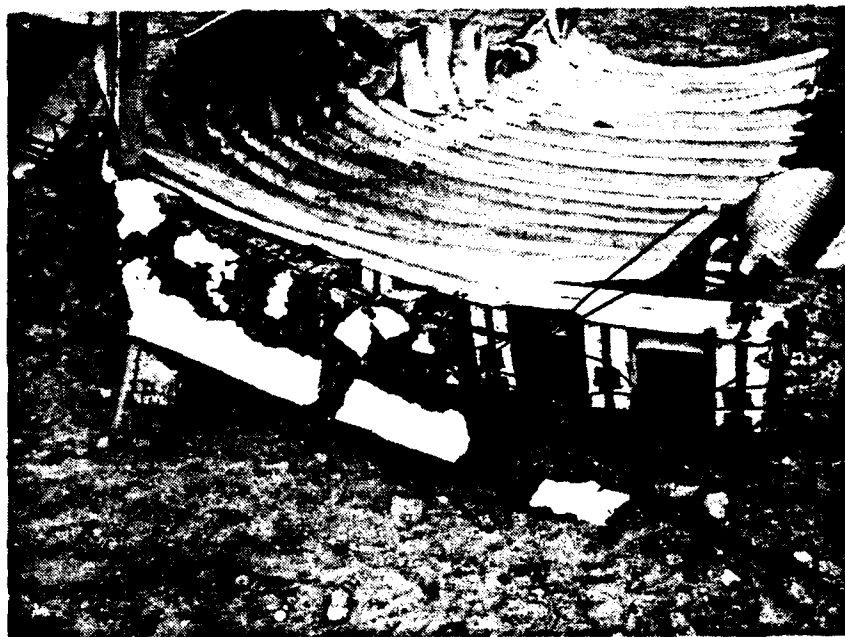


Figure 224. Rubbleized concrete in parapet, PAS-4.

The first detectable bulge in the arch occurred over the charge at about 5 ms, rupturing at about 10 ms. The arch portion of the structure broke into 23 large sections (Fig. 225) which were launched upward and away from the structure. The initial trajectory of side portions of the arch was 45 deg. The initial trajectory of the upper portions of the arch was 75 deg. Analysis of high-speed photography indicated upward arch debris velocities ranging from 28.5 to 55.3 m/s. The average velocity for upper portions of the arch was 38 m/s. The average velocity for side pieces was 33.3 m/s. Debris from the top portion of the arch departed the field of view of the cameras, but the maximum height of the trajectory of this debris was in excess of 57 m in height. The maximum height reached by debris from the sides of the arch was about 40 m. Large sections of the arch were found as far as 120 m from the structure. Figure 226 shows the final location of the 23 sections in relation to the shelter.

Arch failure in the transverse direction always occurred along a bolted liner joint. At the failure line, the concrete failed in tension, and the corrugated liner material was almost always pulled over the nut and washer of the bolt (Fig. 227). Figure 228 shows the location of the transverse failure planes in relation to the location of the splices in the two layers of longitudinal reinforcing bars. Where the failure plane was at, or near, a line of splices in the reinforcing bars, the bars pulled out of the adjacent piece (Fig. 229). At the other failure planes the reinforcing bars were found to have failed in tension at the fractured face of the concrete (Fig. 230).

Five longitudinal failure planes in the arch were identified (Fig. 231). One of the longitudinal failure planes was along the crown of the arch. Two occurred at or near the splices in the transverse reinforcing bars. The remaining two were found at or near the location where the upper arch section begins to thicken near the foundation. At each of the failure lines, the corrugated liner material was ripped apart in tension (Fig. 232). Although the upper three failure lines occurred near the bolted joints between liner segments, the presence of the joints did not appear to influence the formation of the failure planes or the tearing of the liner. The liner was observed to have torn exactly at a bolted joint in only a few isolated locations. At the longitudinal failure plane, the concrete failed in tension. Along the failure plane at the crown and at

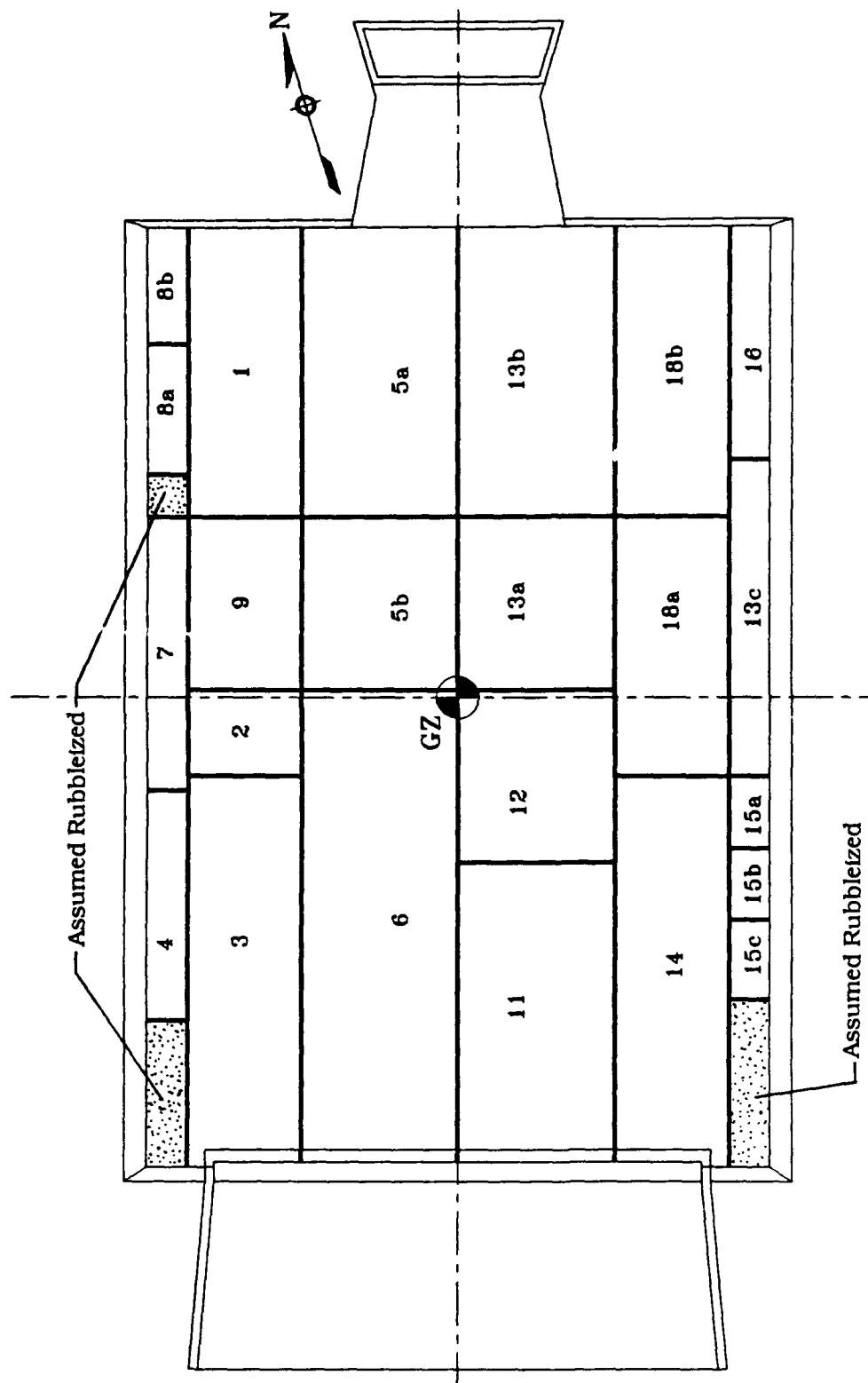


Figure 225. Crack pattern in arch, PAS-4.

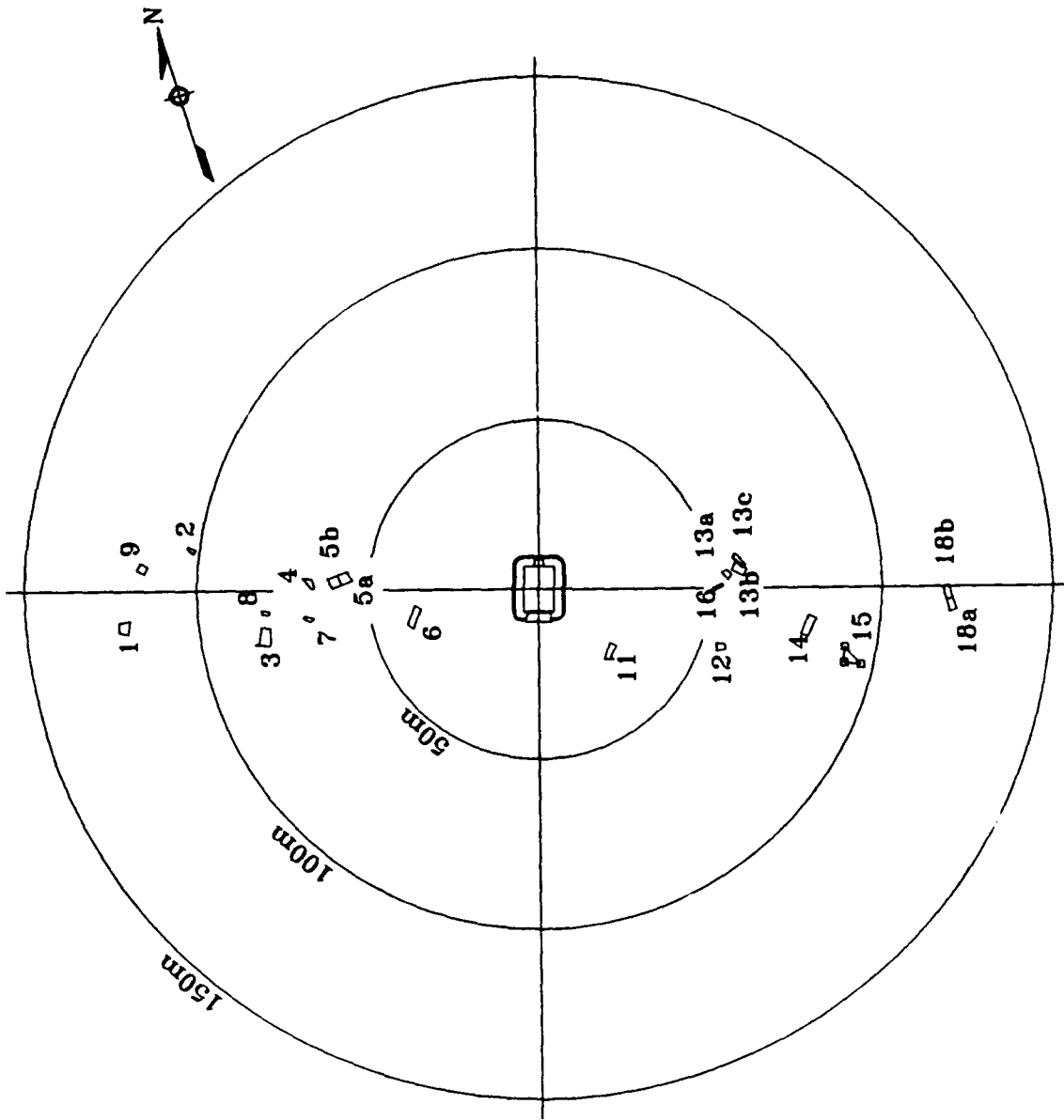


Figure 226. Posttest locations of large arch sections, PAS-4.



Figure 227. Typical bolt pull-out at liner joint, PAS-4.

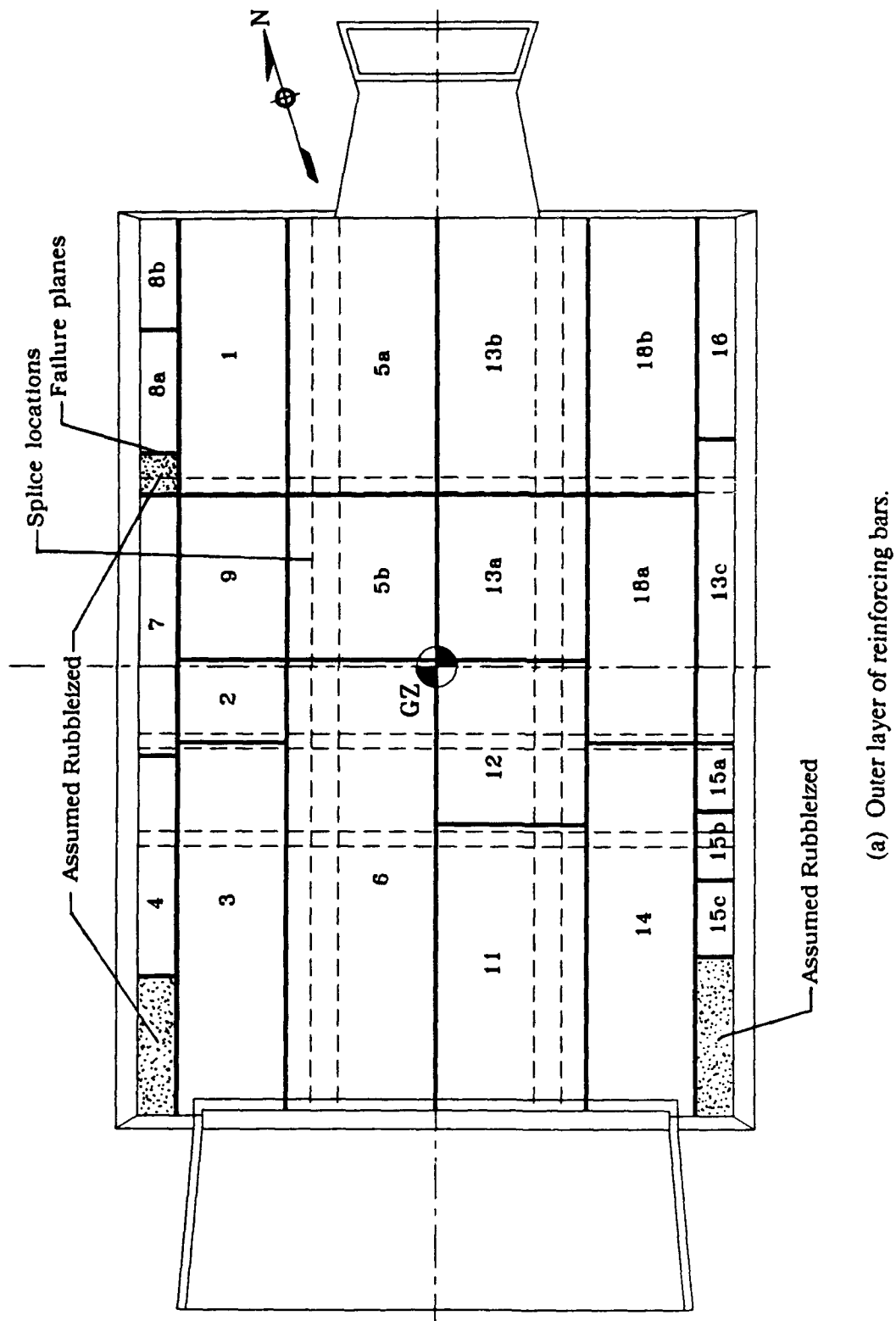
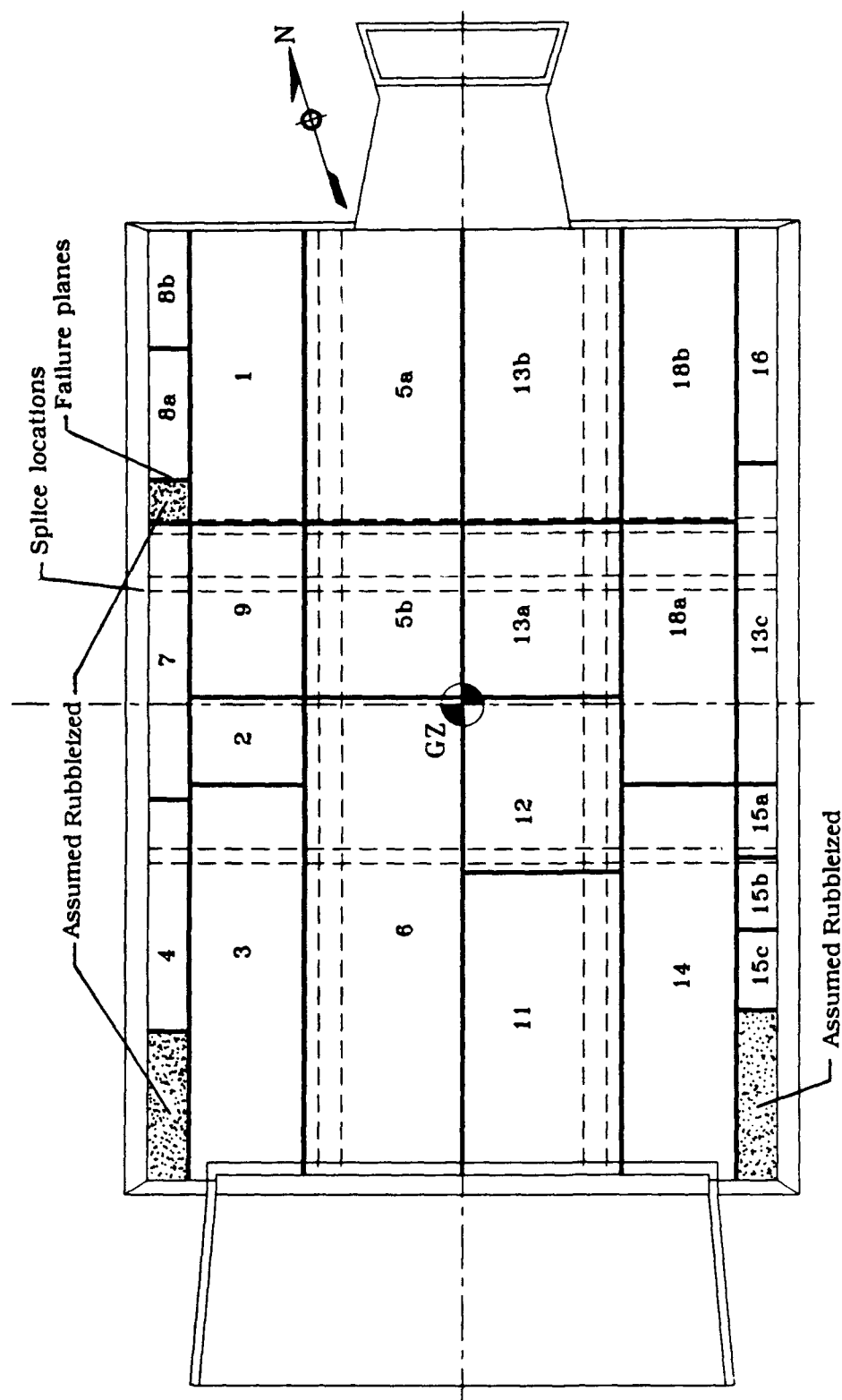


Figure 228. Failure planes and splice locations, PAS-4.



(b) Inner layer of reinforcing bars.

Figure 228. Concluded.



Figure 229. Pull-out of reinforcing bars at transverse failure plane, PAS-4.

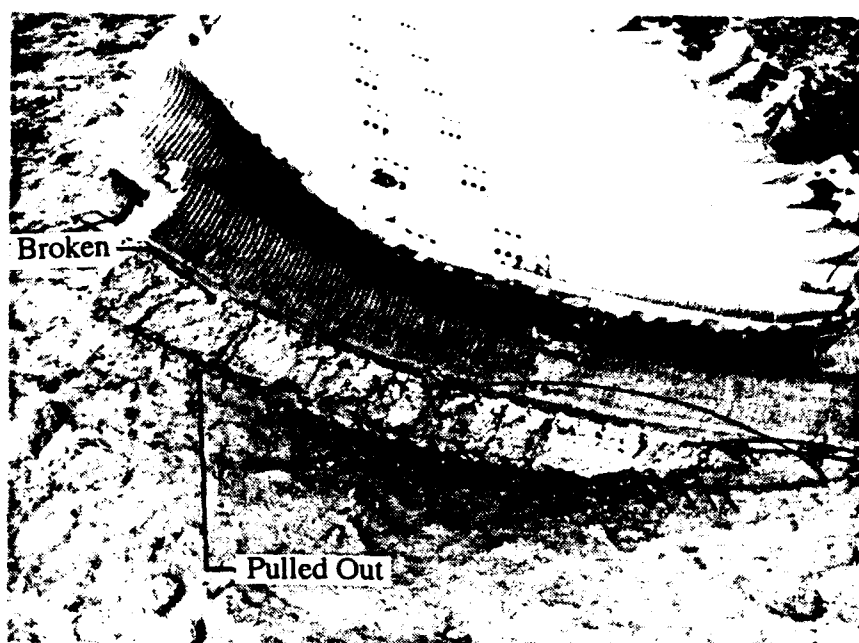


Figure 230. Broken reinforcing bars in transverse failure plane, PAS-4.

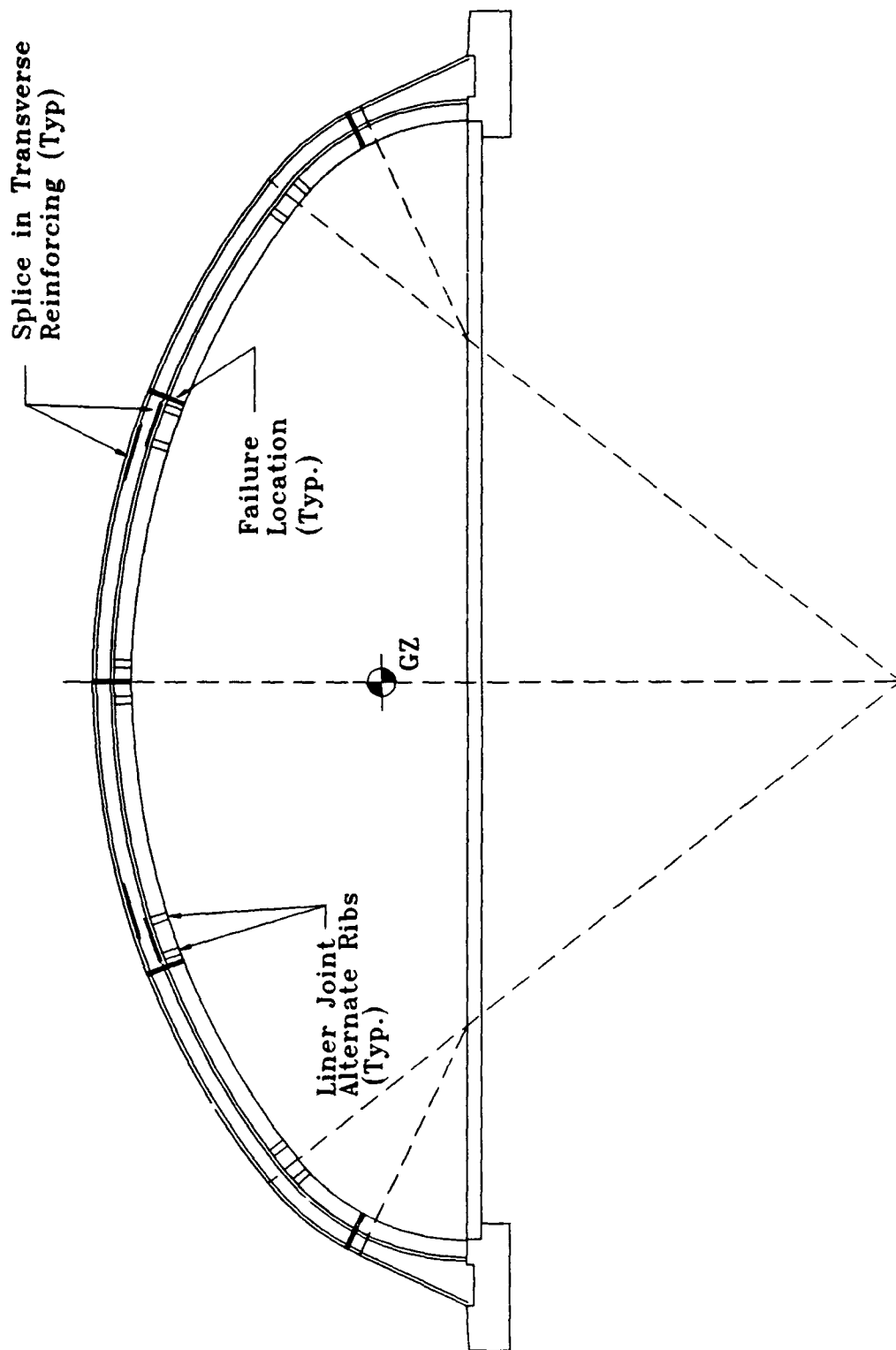


Figure 231. Locations of longitudinal failure plane, PAS-4.

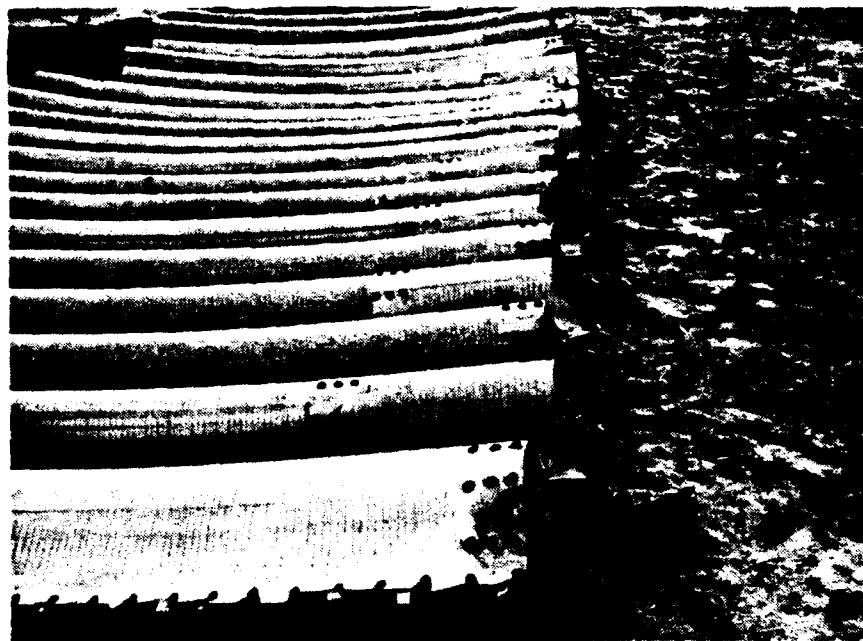


Figure 232. Liner failure at longitudinal failure plane, PAS-4.

the two failure planes near the foundation, the transverse reinforcing bars failed in tension at, or within a few millimeters either side of, the fractured face of the concrete. At the two failure planes near the splices in the transverse reinforcing bars, most of the bars were found to have pulled out of the lower arch sections (Fig. 233); however, a few longitudinal failure planes at this location had a combination of both failed and pulled-out bars.

An examination of the fractured face of the longitudinal failure plane revealed tension cracks ranging from hairline to several millimeters in width at almost every transverse liner joint (Fig. 234). There were fewer of them in the thickened arch sections near the foundation. The tension cracks in these sections were also narrower in width and randomly spaced along the edge as compared to those associated with the liner joints. Transverse cracks were also seen on the surface of the arch sections (Fig. 235).

The high-speed photography shows that most of the large arch sections generally maintained their initial breakup geometry during the flight. The arch sections impacted the ground in a variety of positions. Some of the sections maintained their curved arch geometry after impact, and others were flattened or folded. In some cases the corrugated liner was still attached to the concrete. In several cases the sections broke up and produced various amounts of secondary debris. Two sections were almost totally rubbleized with very little secondary debris surrounding them (Fig. 236).

The arch foundation was found generally free of debris or rock rubble (Fig. 237). There was little indication of upward or outward displacement of the arch foundation. All of the outside dowel bars had either been broken at the top of the foundation or broken off inside the foundation and pulled out (Fig. 238). About one-fifth of the inner dowel bars were broken at the top of the foundation. The rest appeared to have been pulled out of the base of the arch and remained in the arch foundation. No transverse cracks were noted in the arch foundation.



Figure 233. Pull-out of reinforcing bars at transverse failure plane, PAS-4.

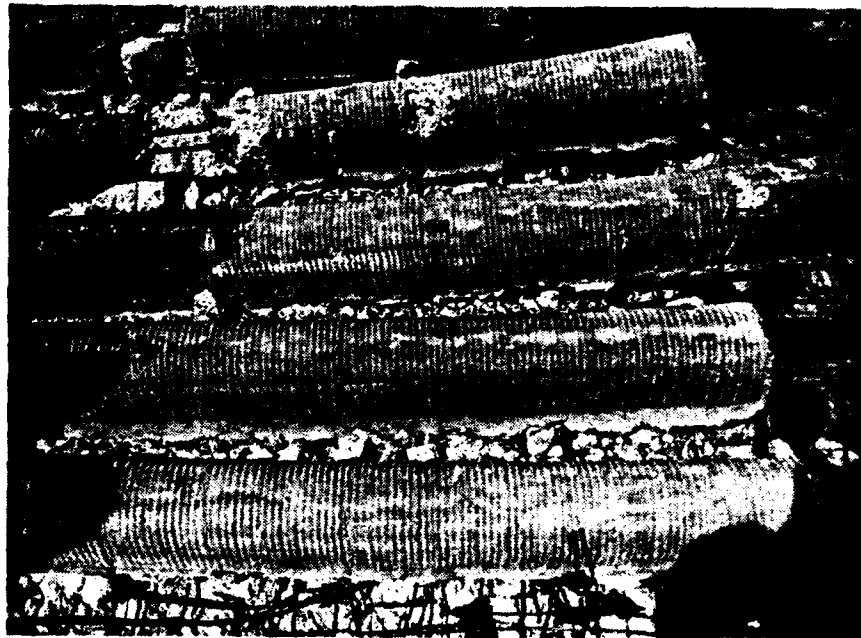


Figure 234. Tension cracks at transverse failure plane, PAS-4.



Figure 235. Typical transverse cracks on surface of arch sections, PAS-4.



Figure 236. Rubbleized arch section, PAS-4.



Figure 237. Top of arch foundation, PAS-4.



Figure 238. Broken dowel bars in top of arch foundation, PAS-4.

Most of the anchor bolts from the base channel of the arch liner were still embedded in the foundation. The channel had been pulled up over the bolts and remained attached to the sections of the arch. The remainder of the anchor bolts had pulled out of the foundation, along with the channel, but were found still attached to the base edge of the arch sections. The embedded end hook had been straightened when the anchor bolt pulled out.

The floor slab appeared to have been pushed downward relative to the arch foundation, which resulted in a 3-mm-wide crack running the length of the floor slab about 100 mm from the face of the arch liner base channels (Fig. 239). A second parallel crack, about 360 mm from the liner base channel, was also seen in the floor slab (Fig. 240). The floor slab remained tight against the arch foundation.

The floor slab was cratered at the GZ to a depth of 280 mm (Fig. 241). The damaged area of the floor slab was generally confined to a 1.66- x 2.01-m area between construction joints in the floor. The concrete inside the cratered area was rubbleized and pushed down into the soil subgrade.

A 220-mm-wide gap was noted along the full width of the floor slab in front of the backwall (Fig. 242). The break occurred about 330 mm from the face of the backwall. Bars of the reinforcing mesh in the floor slab were broken on either side of the gap. There was also a 20-mm-wide crack running parallel to the large gap about 110 mm from the inside face of the backwall. The large gap appeared to correspond to the ends of the reinforcing bars running from the backwall foundation into the floor slab. The smaller crack corresponded to the inside edge of the foundation (Fig. 243).

At the expansion joint between the floor slab and the heavily reinforced door pit area, the expansion material had been pushed up out of the joint (Fig. 244). The floor slab had been pushed downward relative to the door pit slab by about 15 mm. There was no horizontal displacement between these two components.



Figure 239. Floor slab at arch foundation, PAS-4.

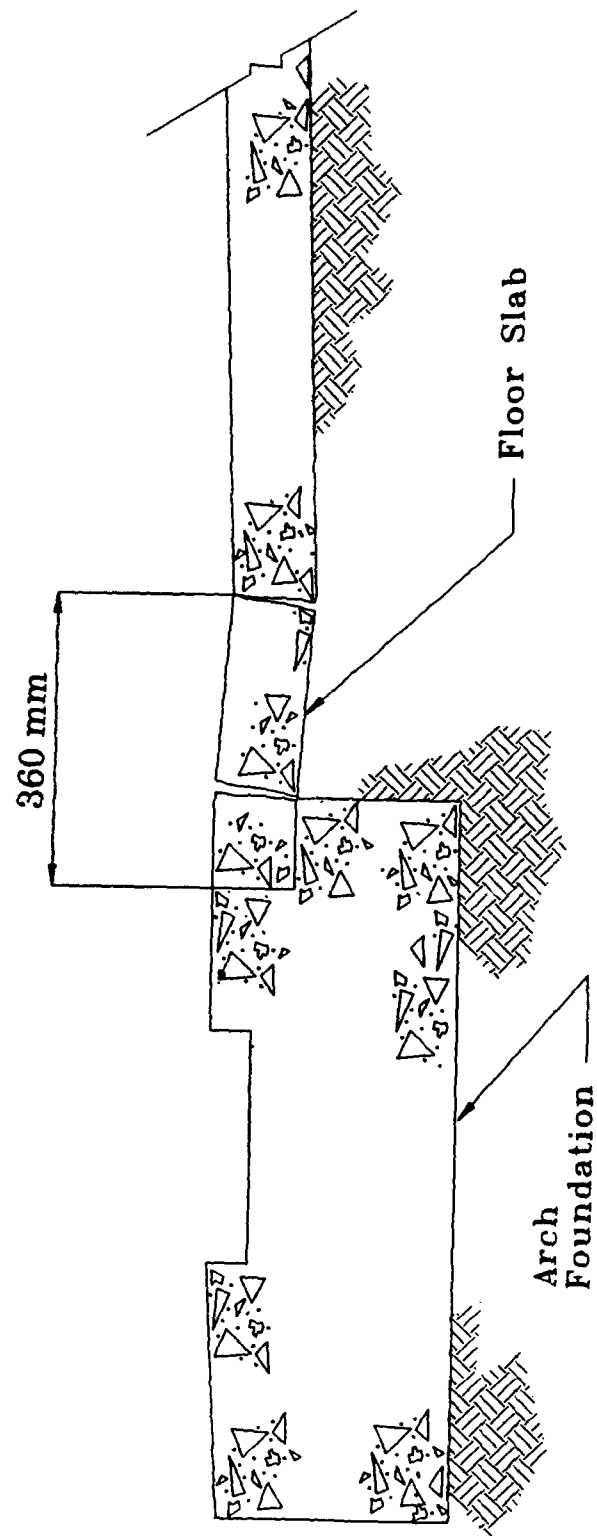


Figure 240. Section: Crack pattern in floor slab at arch foundation, PAS-4.

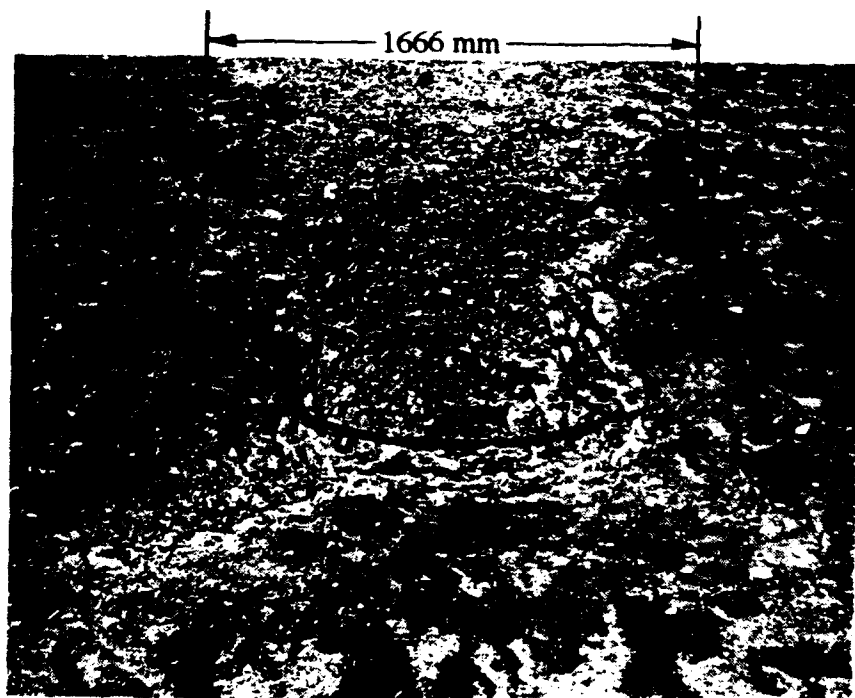


Figure 241. Crater in floor slab, PAS-4.



Figure 242. Gap between floor slab and backwall, PAS-4.

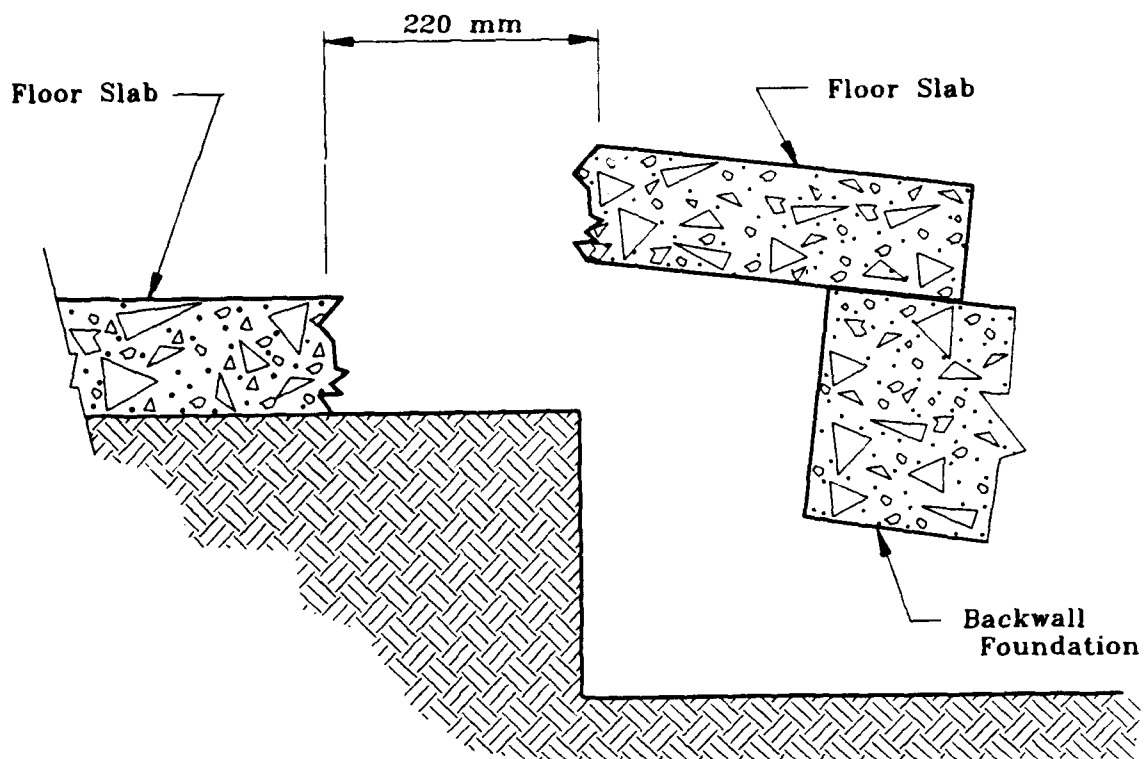


Figure 243. Crack pattern in floor slab at backwall foundation, PAS-4.

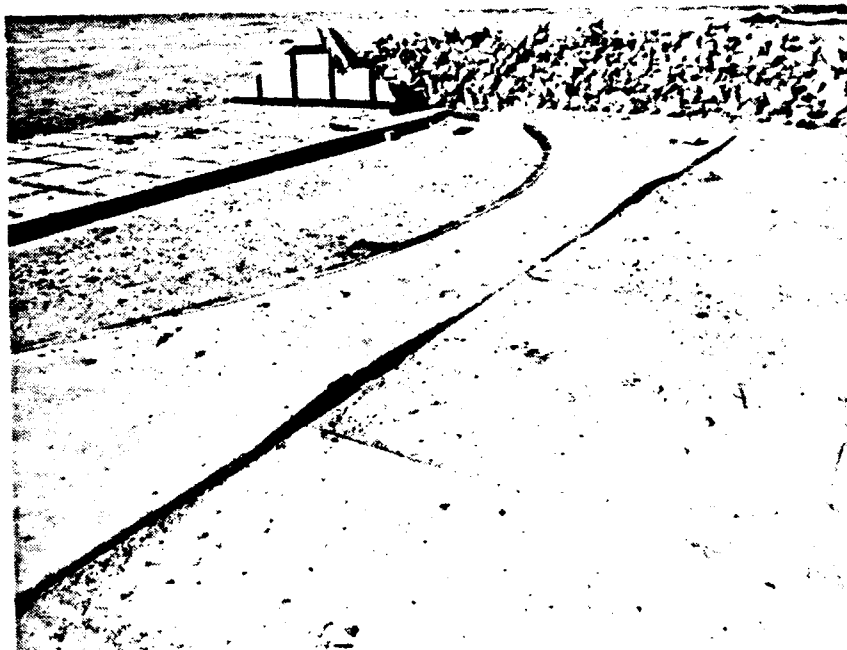


Figure 244. Posttest condition of expansion joint, PAS-4.

The center section of the backwall over the exhaust port opening had broken away along diagonal lines running from the upper corners of the exhaust port opening (Fig. 245). This section was found in two pieces about 9.1 m behind the shelter. The two remaining sections of the backwall on either side of the opening had broken away from the foundation and were pushed backwards about 200 mm. These walls had tipped backward approximately 30 deg (Fig. 246).

The arch had separated from the top edge of the backwall at the inside horizontal interface. The failure plane then proceeded along a vertical plane corresponding to the step in the joint (Fig. 247). Most of the arch concrete beyond the vertical step remained on the backwall. About half of the reinforcing bars crossing the failure planes had failed in tension; the rest of the bars pulled out of the arch concrete and remained in the top of the backwall (Fig. 248).

The earth backfill originally against the outside of the backwall had been thrown back behind the shelter. Figure 249 shows the limits of the displaced earth backfill.

The backwall foundation had a large vertical crack running its full length about 100 mm from its front face. Although the front edge of the backwall had pulled off the foundation, these two components remained together at the back edge of the wall. The foundation was also pushed back about 220 mm, and the front edge had lifted and rotated upward about 145 mm. Most of the dowel bars on the inside face were broken at the base of the backwall. The posttest condition of the foundation is shown in Figure 250. The backwall foundation also failed at its junction with both sides of the arch foundation (Fig. 251).

The exhaust port was displaced backward and severely damaged during the test. The roof and a portion of the backwall, had broken away from the top of the walls and was found in three pieces approximately 24.7 m behind the shelter (Fig. 252). Figure 253 shows the breakup pattern of the roof. The dowels connecting the roof and the walls all failed in tension. Both of the sidewalls had broken away from the floor slab and the backwall and tipped upward at the backwall. Both sidewalls also had large open areas



Figure 245. Posttest view of backwall, PAS-4.



Figure 246. Thirty-degree backward rotation of backwall, PAS-4.

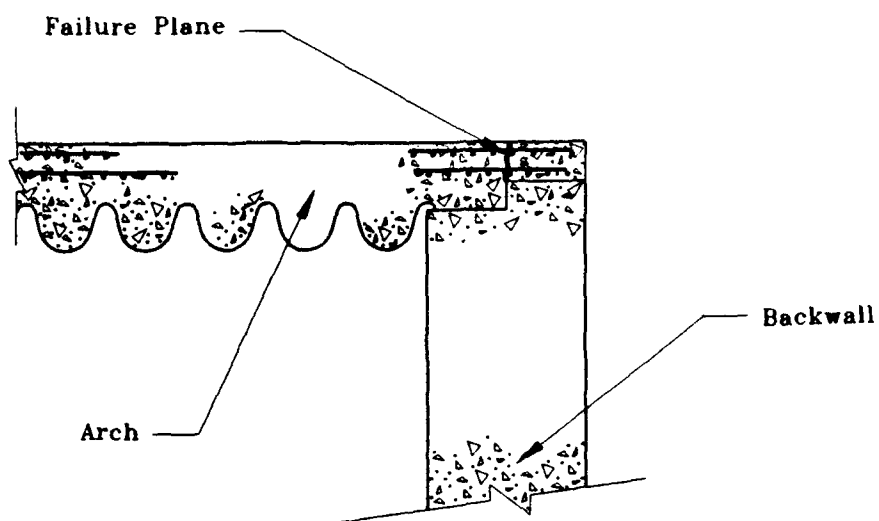


Figure 247. Section: Failure plane between arch and backwall, PAS-4.



Figure 248. Top edge of backwall, PAS-4.

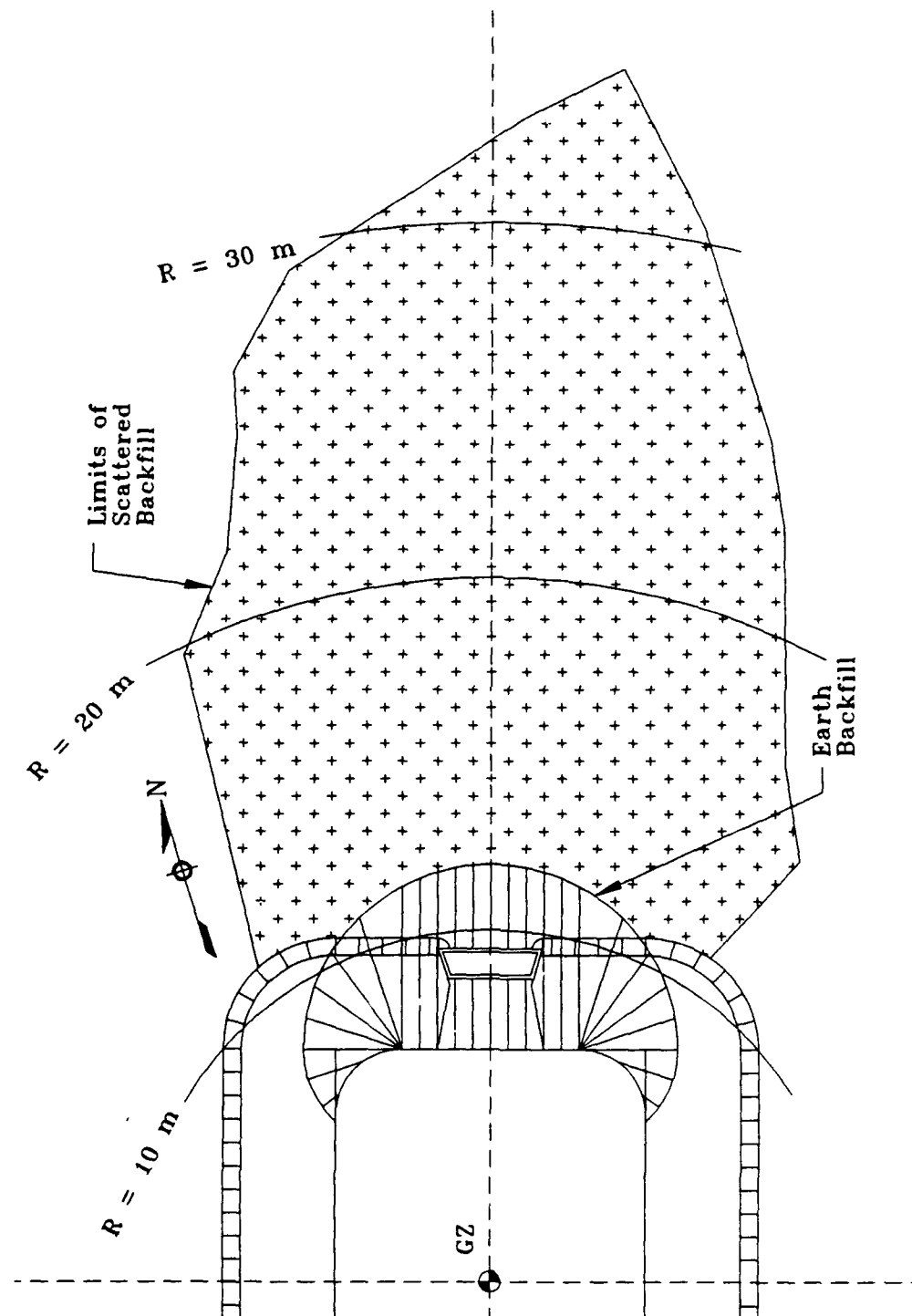


Figure 249. Limits of ejected earth backfill, PAS-4.

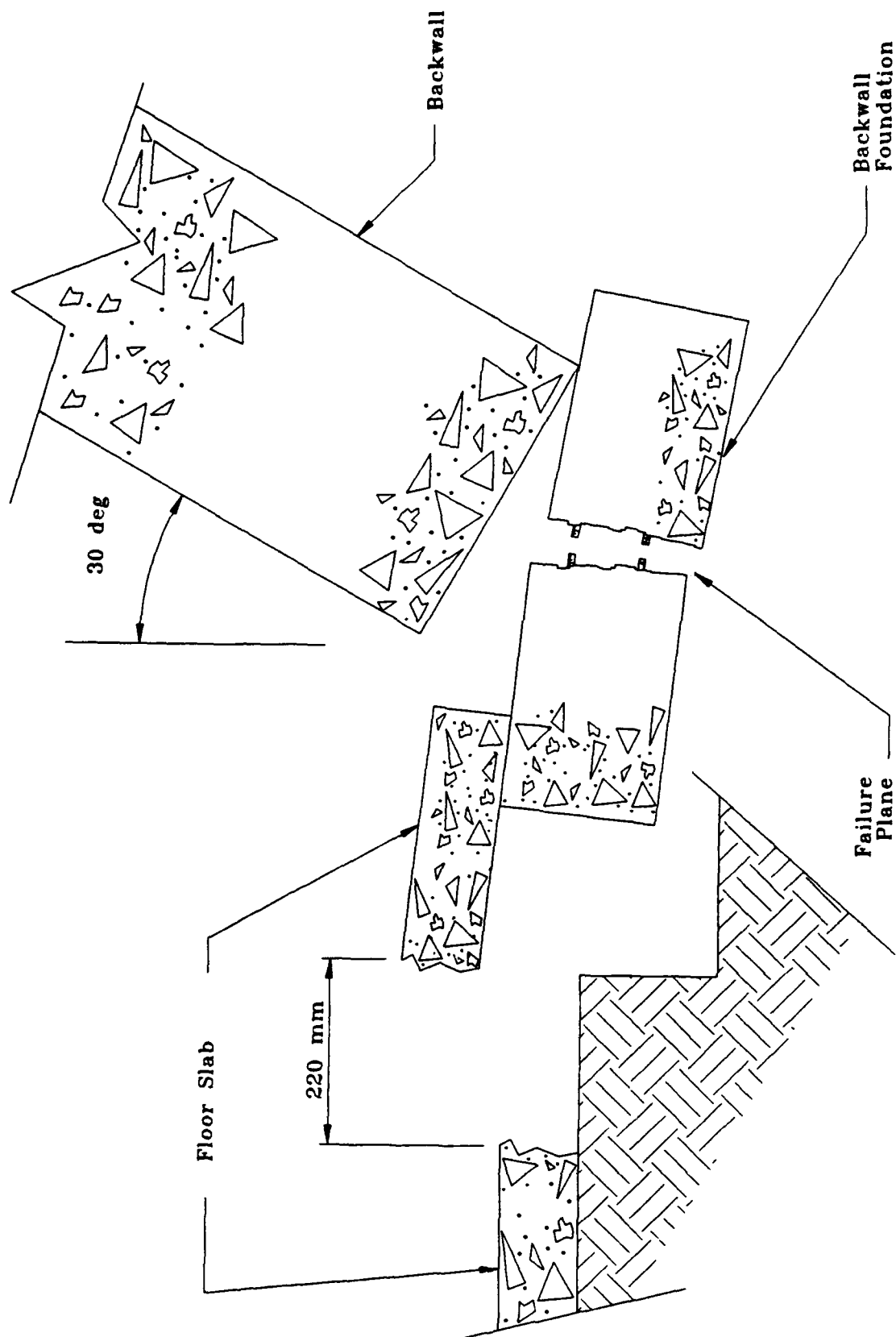


Figure 250. Section: Breakup pattern of backwall foundation, PAS-4.

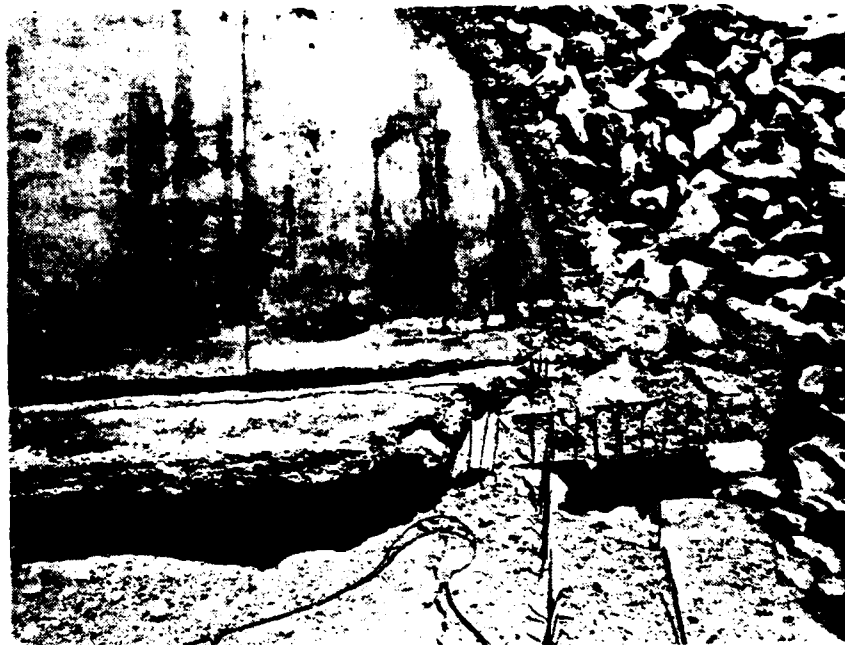


Figure 251. Failure of backwall foundation at junction with arch foundation, PAS-4.

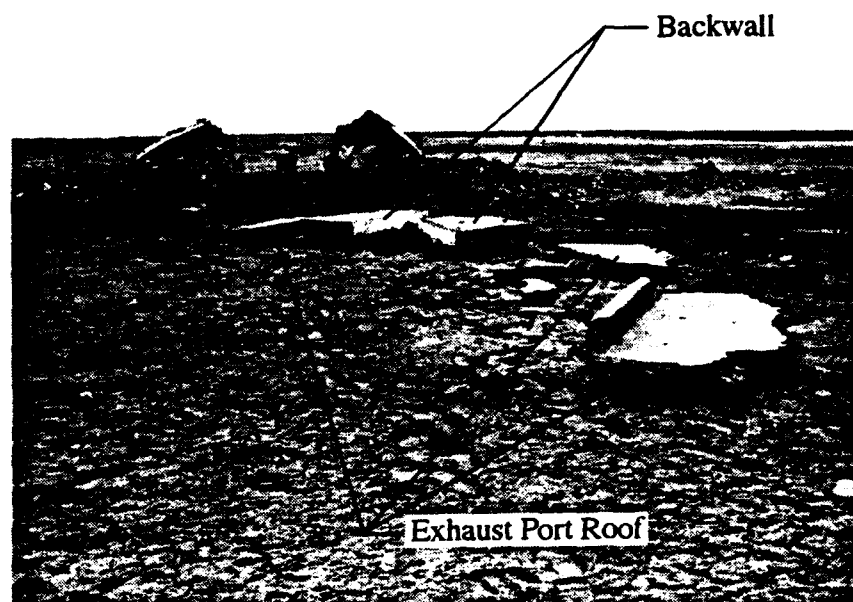


Figure 252. Exhaust port roof and center section of backwall, PAS-4.

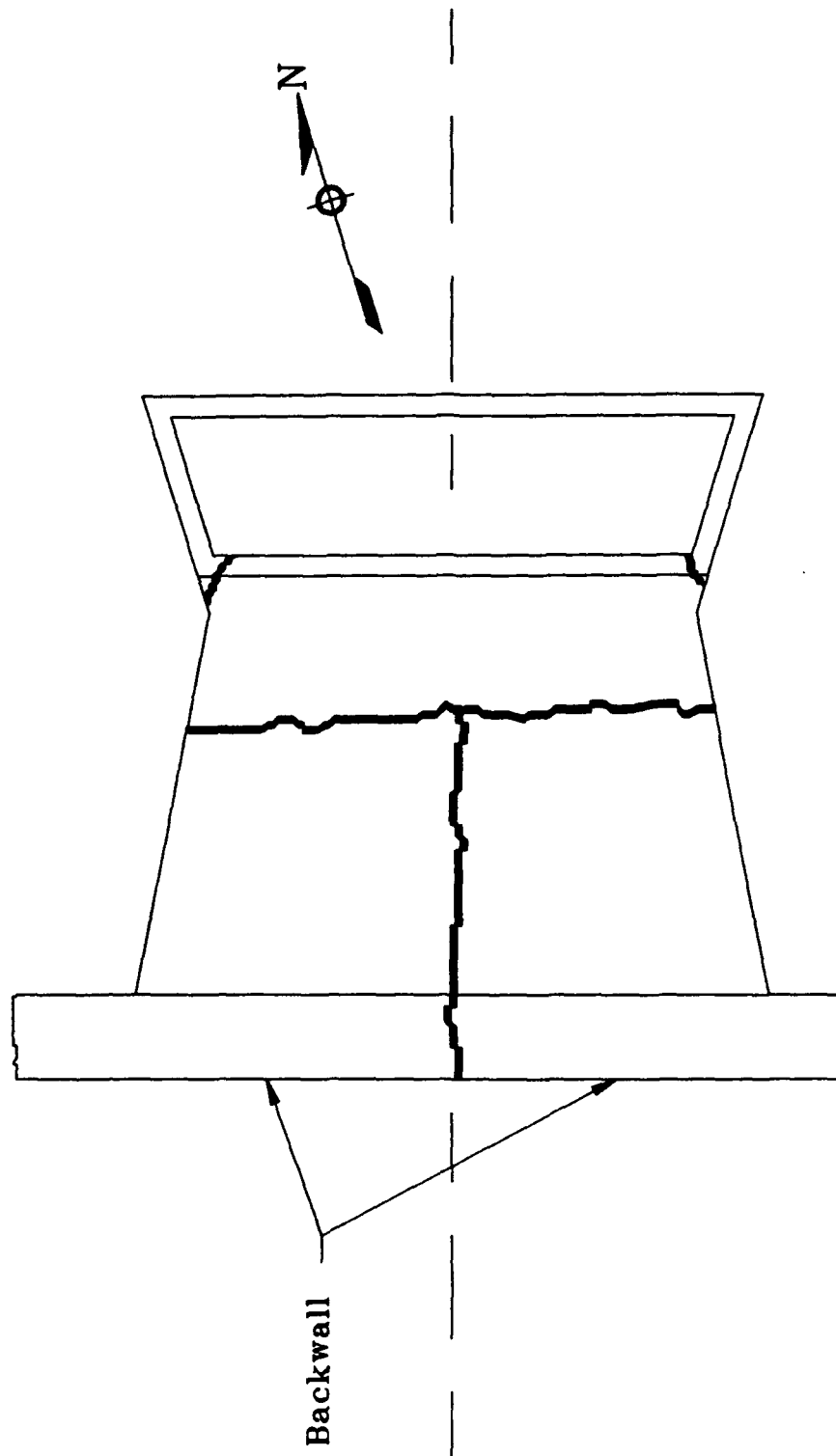


Figure 253. Plan: Breakup pattern of exhaust port roof, PAS-4.

of rubbleized concrete at the location where the wall thickness changed (Figs. 254 and 255). The reinforcing bars in these rubbleized areas were broken and severely deformed. Although the center wall was also broken from the floor slab, it remained relatively undamaged (Fig. 256).

The exhaust port endwall broke away at its junction with both the sidewalls, and it was found in several pieces 9.1 m behind the shelter. Concrete from most of the pieces was rubbleized leaving only the reinforcing steel mat. Most of the corner dowels from the sidewalls were pulled out of the endwall section.

The floor of the exhaust port was displaced backwards and had several large cracks at the back corners where it joined with the sides and endwall.

The two steel doors in the exhaust port were found folded tightly in half about a horizontal line (Figs. 257 and 258). The doors had been blown upward and out the back of the exhaust port and were found at 121.2 and 116.2 m behind the structure. Abrasions on the doors may indicate that the doors struck the exhaust port endwall as they were blown out.

The two steel door frames originally embedded in the floor, walls, and roof of the exhaust port were also found in several pieces behind the structure (Fig. 259). The headed anchor studs were broken near the welds attaching them to the frames and remained embedded in the concrete walls, roof, and floor. In all cases the steel angles at the top and bottom of the doors were found still welded to the frame.

6.2.2 Data Obtained from Instrumentation

Data were obtained from all but one of the electronic sensors. Although some baseline shifts were noted and a few of the data channels failed at later times, useful data appeared to have been obtained from most measurements. No corrections have been made to data presented in this report.



Figure 254. Left sidewall of exhaust port, PAS-4.



Figure 255. Right sidewall of exhaust port, PAS-4.

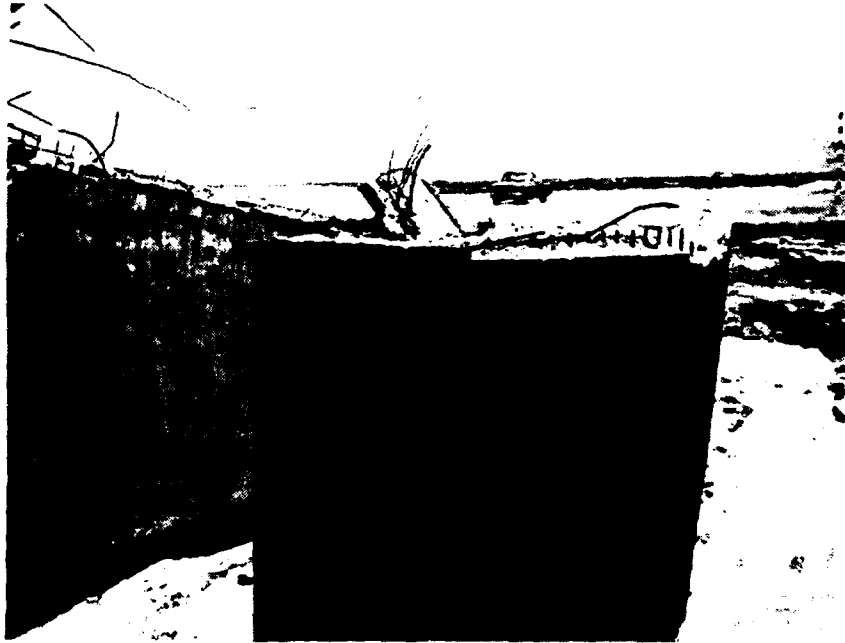


Figure 256. Center wall of exhaust port, PAS-4.

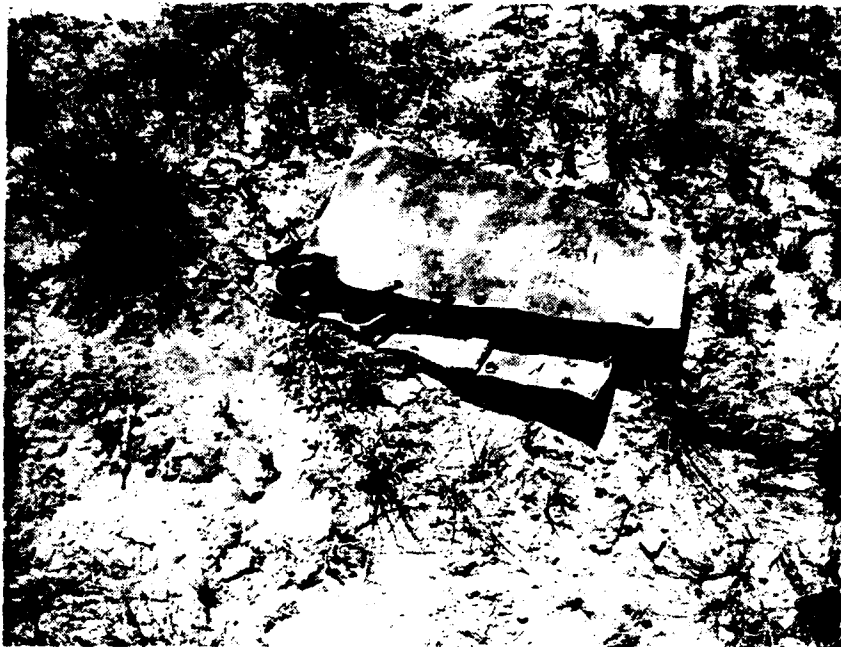


Figure 257. Steel door from left side of exhaust port, PAS-4.

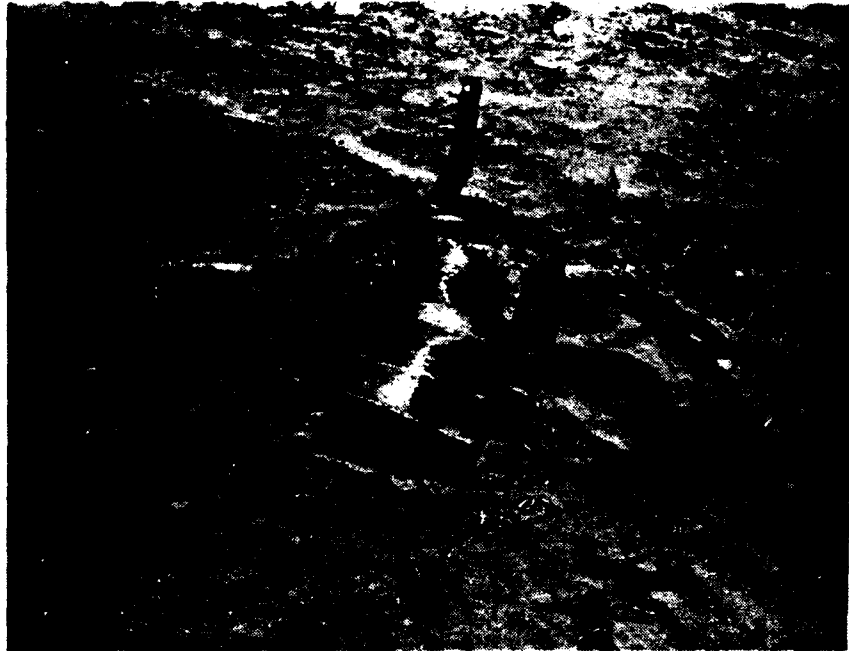


Figure 258. Steel door from right side of exhaust port, PAS-4.



Figure 259. Steel frame for exhaust port door, PAS-4.

Multiple peaks were observed in most of the airblast records obtained from gages inside and outside the structure. In some instances the maximum recorded value was the second, third, or even later peak.

Measurement Number 604 was located on the ceiling of the arch directly over the explosive charge. This measurement was expected to record the maximum pressure inside the structure, but it failed at 0.4 ms. A peak reflected pressure of about 93 MPa was predicted to occur at this location at about 0.4 ms.

Measurement Numbers 602 (Fig. 260) and 603 (Fig. 261) show the pressures recorded on the floor near the sides of the structure in the same plane as MN 604. The peaks at these two locations were 13.2 and 15.0 Mpa. Although the peaks differ slightly, the characters of the records are similar. The INBLAST code predicted a peak of 10.1 MPa at these locations.

Measurement Number 601 was made in the floor 1.85 m from GZ towards the side of the shelter. It shows a peak pressure of 8.59 MPa (Fig. 262). The INBLAST code predicted 1.16 MPa at this location. Measurement Number 301, made in the floor 2.84 m from GZ towards the front door, shows a peak of 5.18 MPa (Fig. 263).

The only pressure measurement made on the inside surface of the front door in the PAS-4 test was MN 402 (Fig. 264). This gage was located near the center of the door, and it recorded a peak pressure of 5.32 MPa at 3.0 ms. The INBLAST code predicted a peak of 5.06 MPa at 3.3 ms at this location. Measurement Number 202 located in the backwall at a little shorter range (same height off the floor but greater distance off the structure centerline) shows a peak of 6.29 MPa (Fig. 265). The first peak of MN 202 was 6.0 MPa at 3.0 ms. Measurement Number 501 located in the floor of the shelter near the front left corner recorded a peak pressure of 10.2 MPa (Fig. 266).

Measurement Number 102, at about the same location near the left rear corner of the shelter, recorded a peak of 8.95 MPa (Fig. 267).

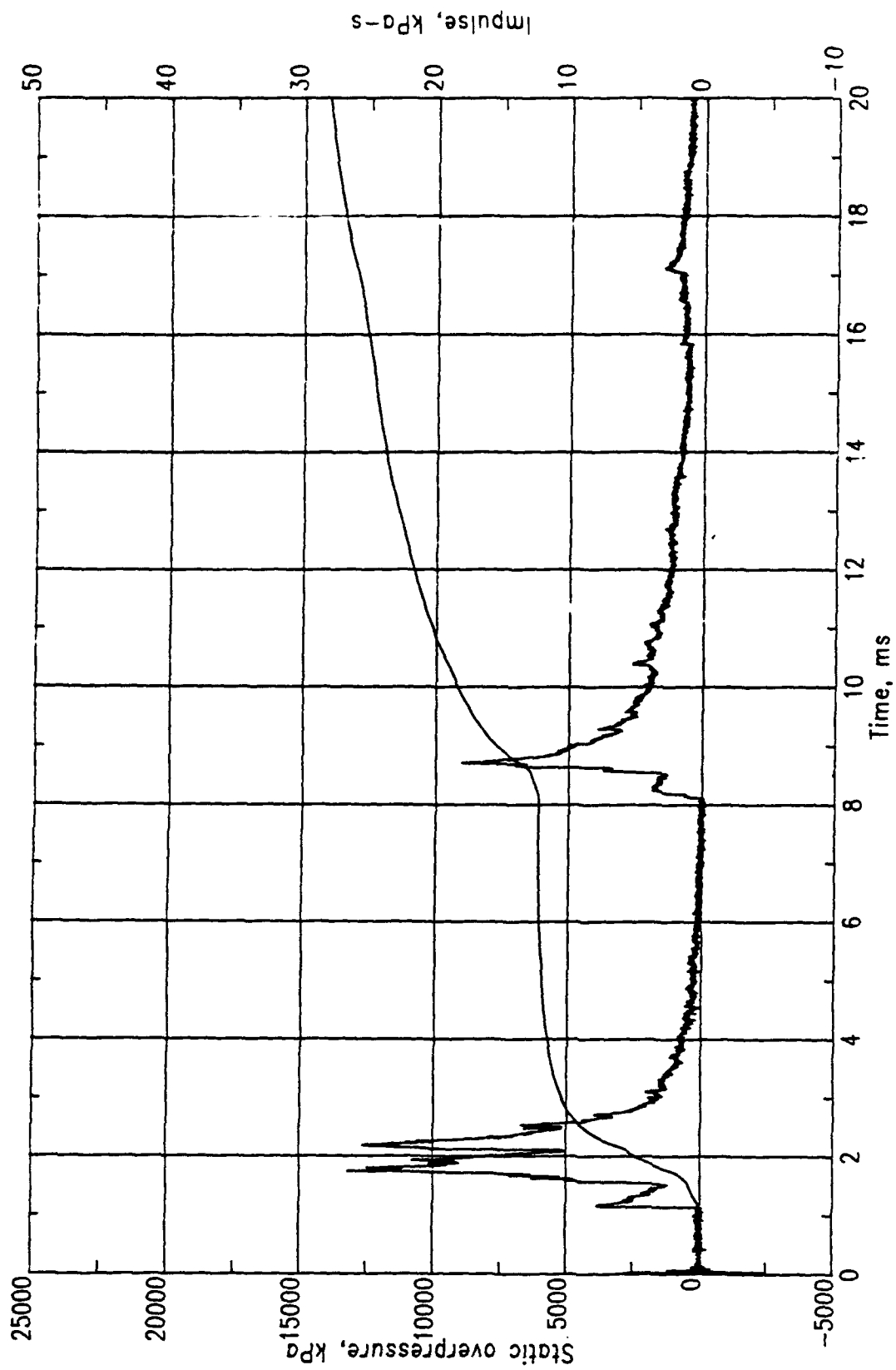


Figure 260. PAS-4, MN 0602.

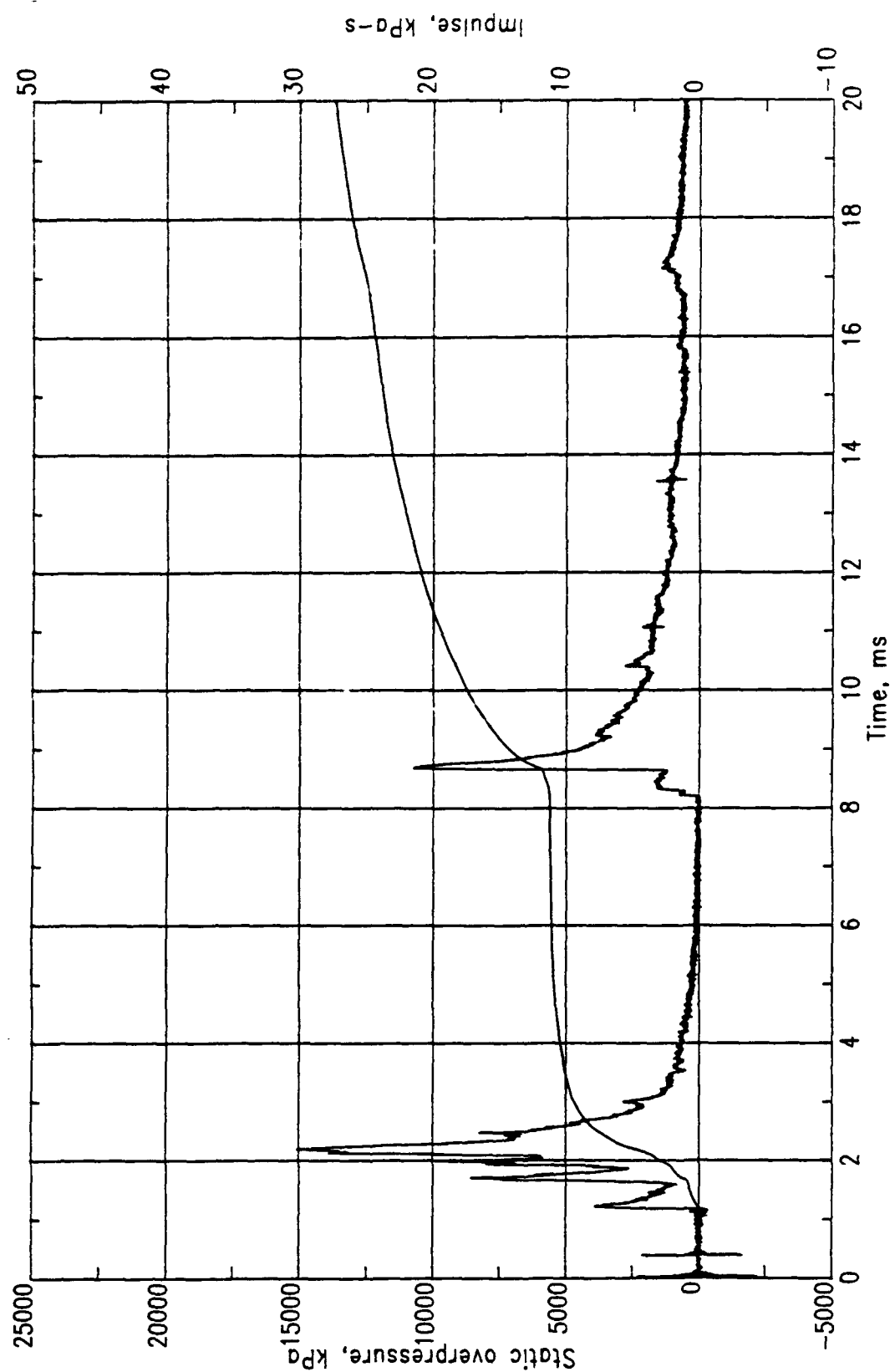


Figure 261. PAS-4, MN 0603.

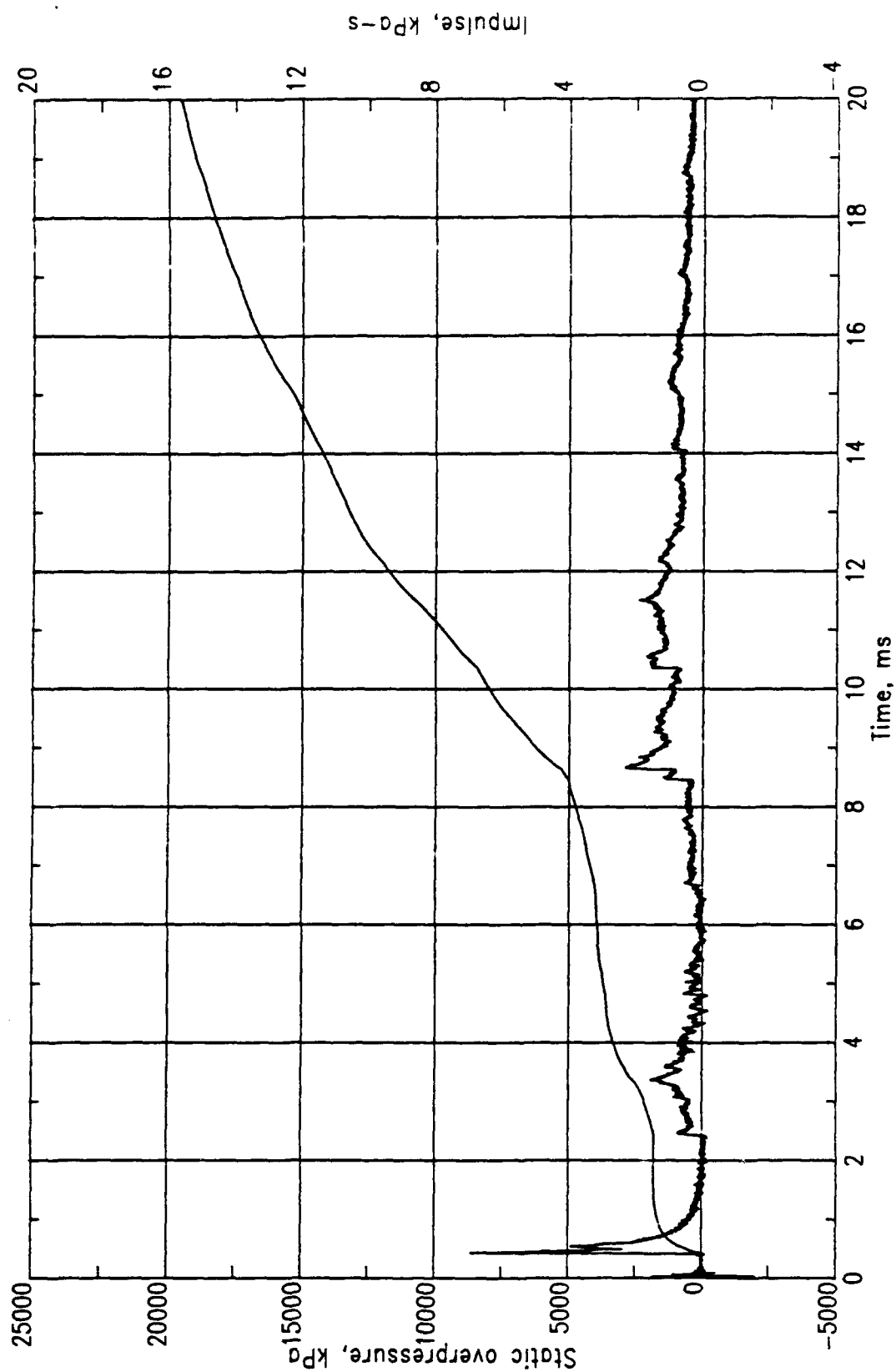


Figure 262. PAS-4, MN 0601.

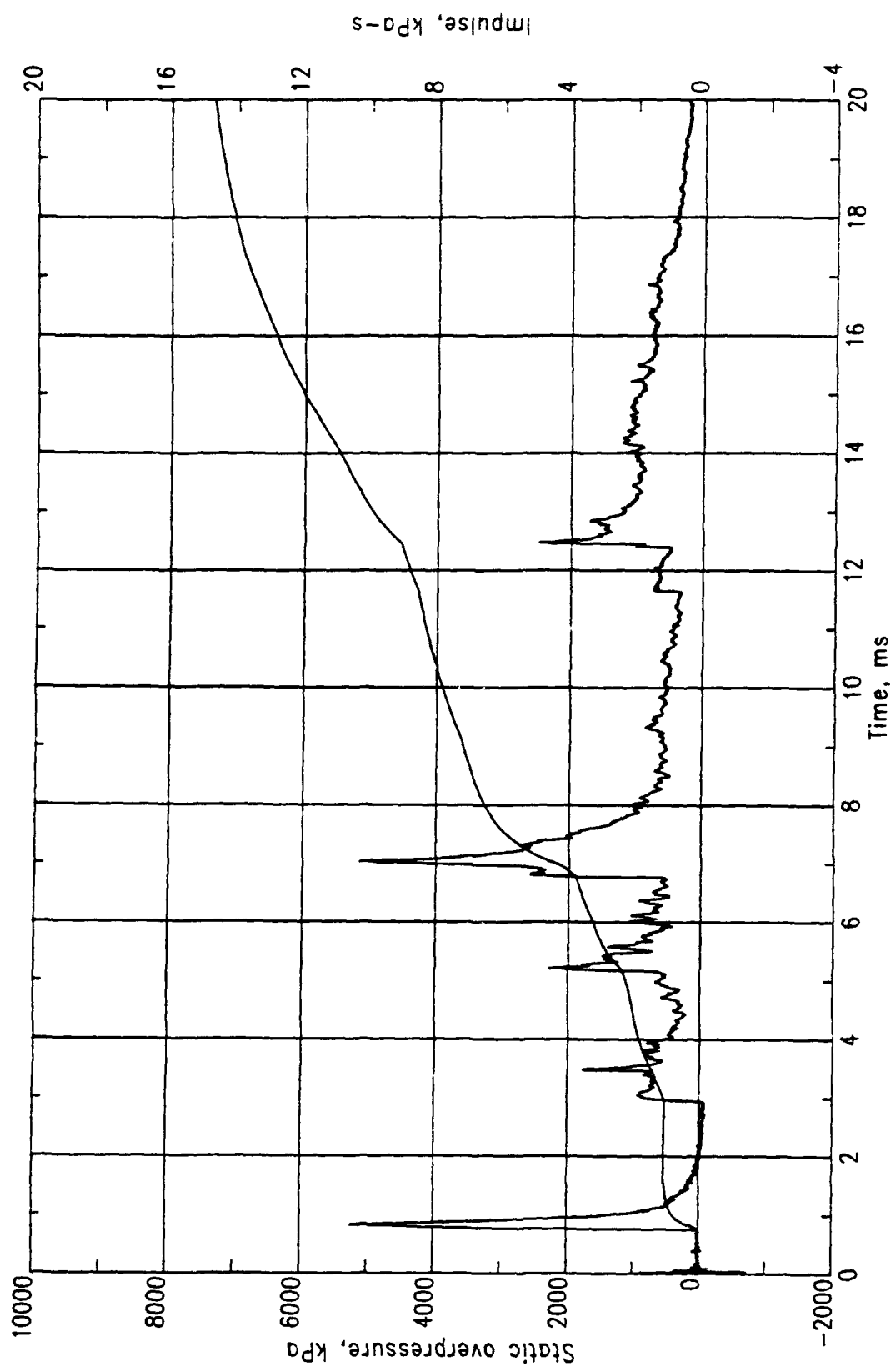


Figure 263. PAS-4, MN 0301.

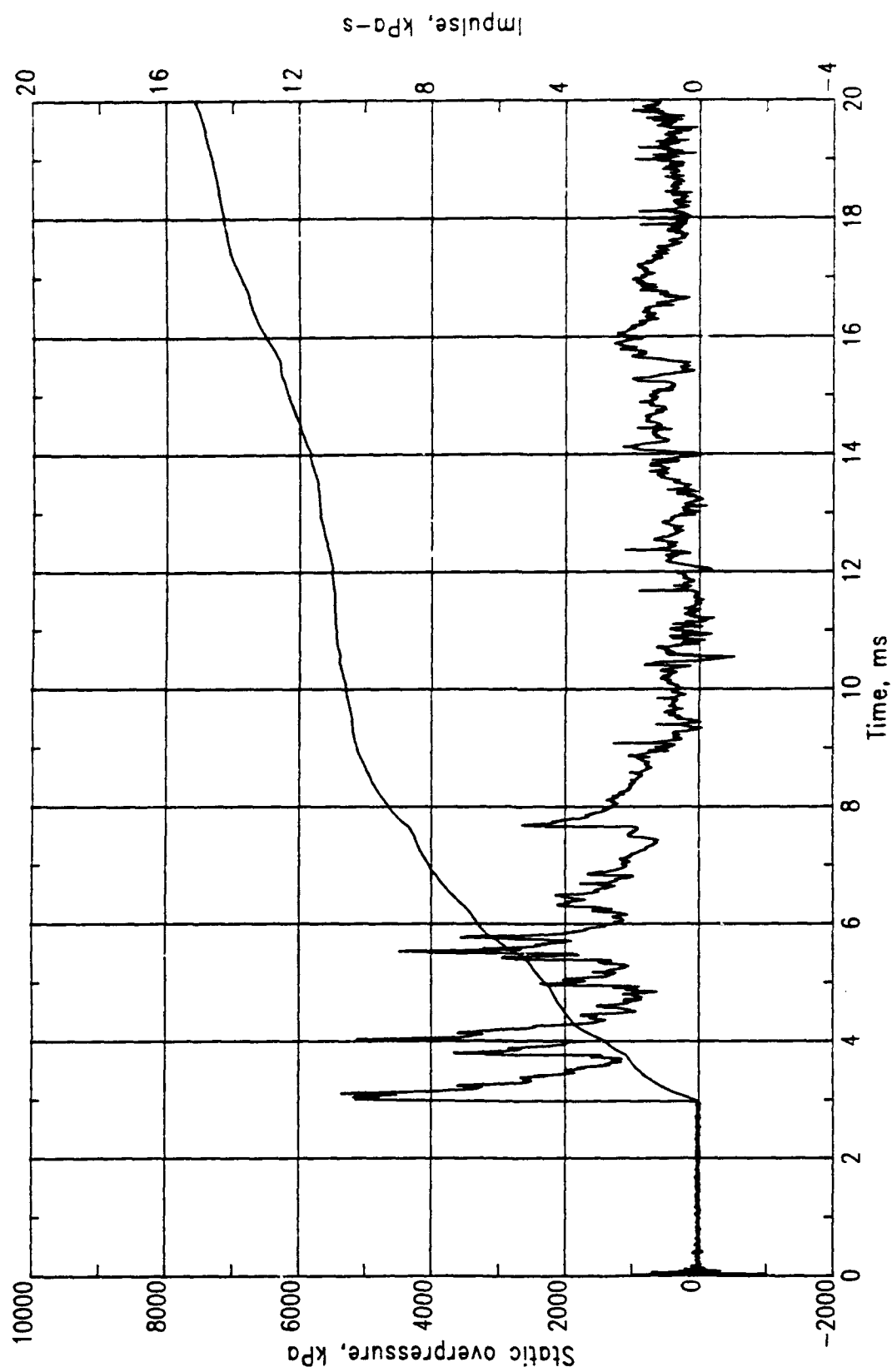


Figure 264. PAS-4, MN 0402.

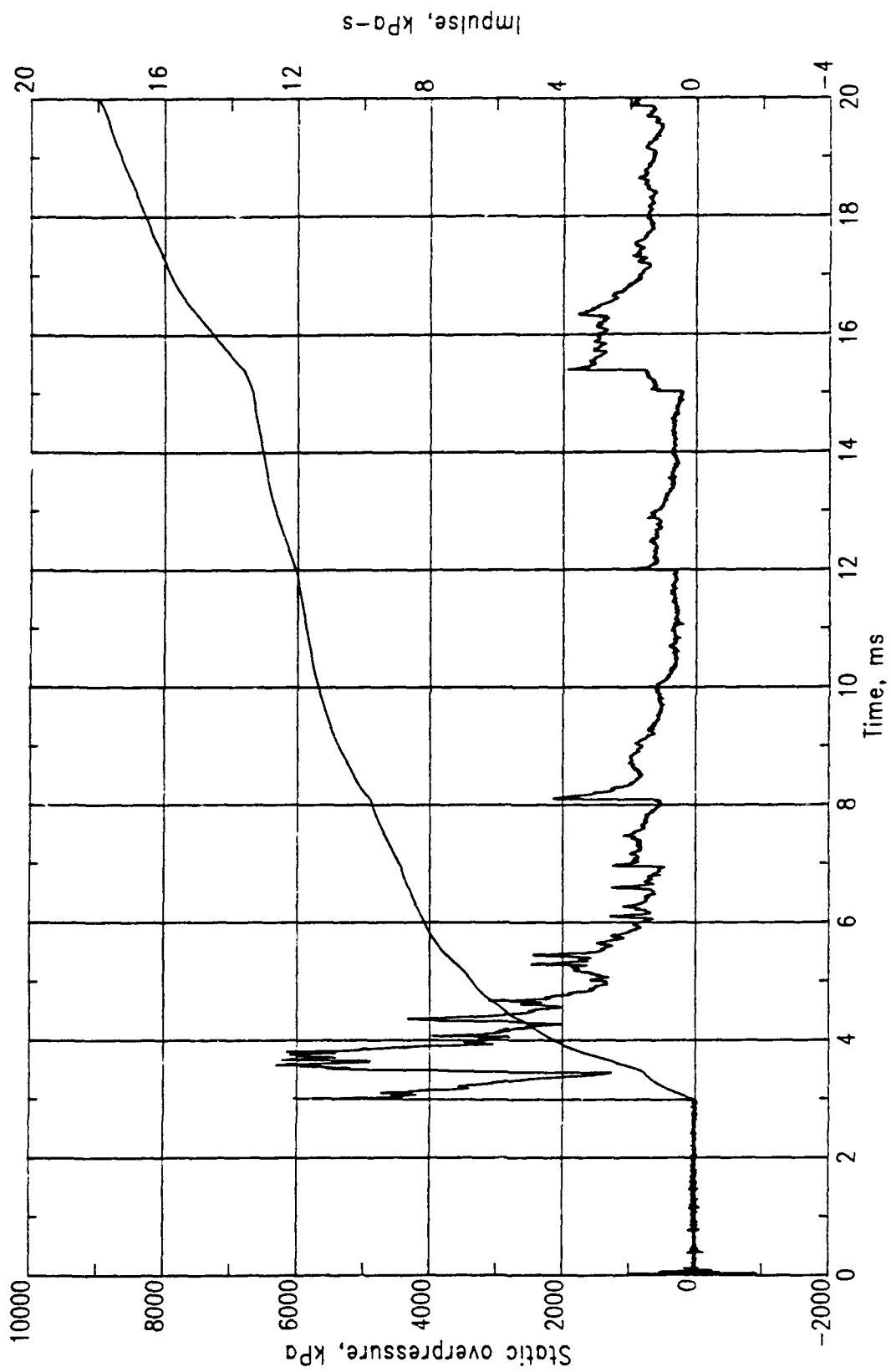


Figure 265. PAS-4, MN 0202.

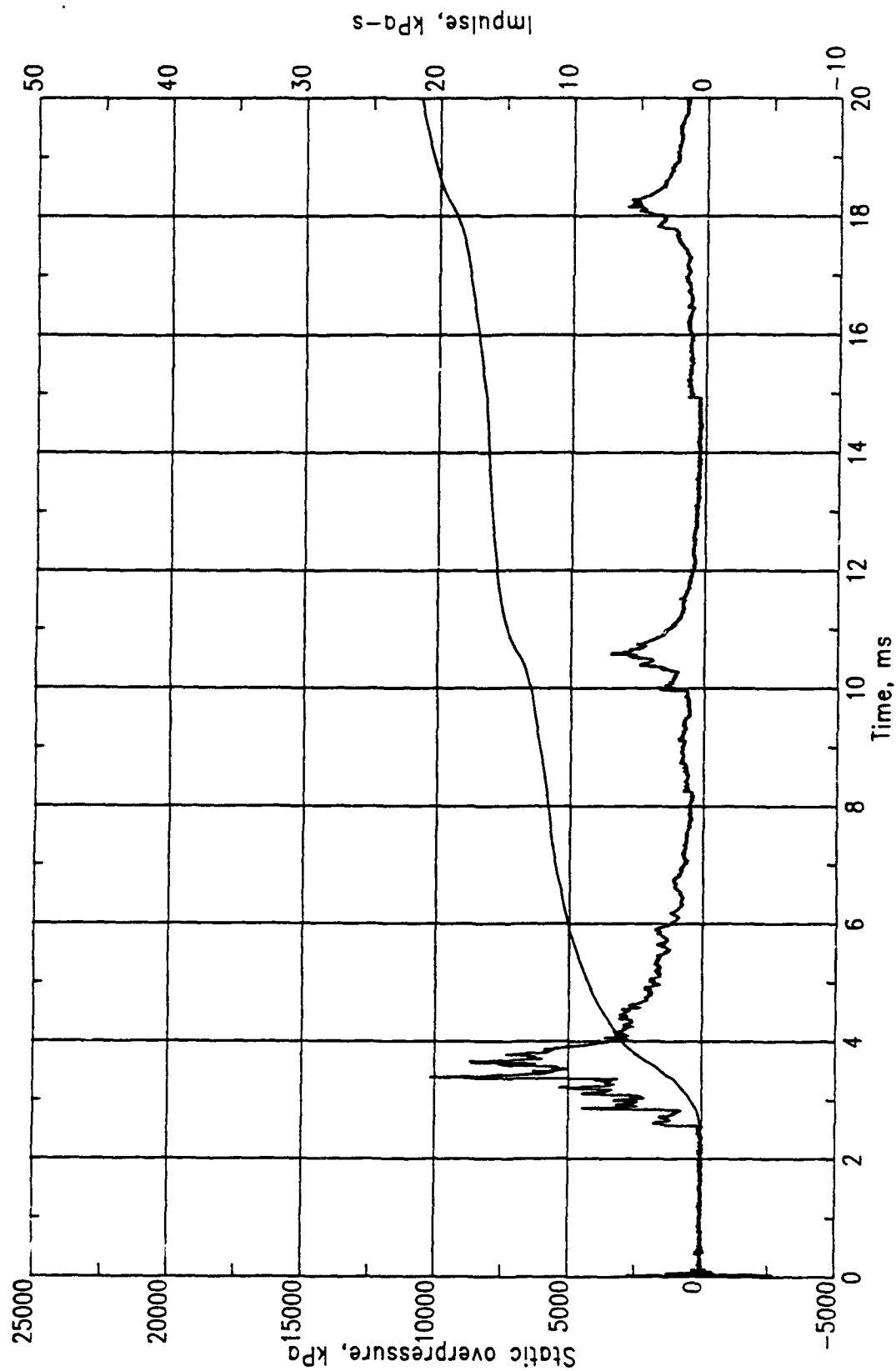


Figure 266. PAS-4, MN 0501.

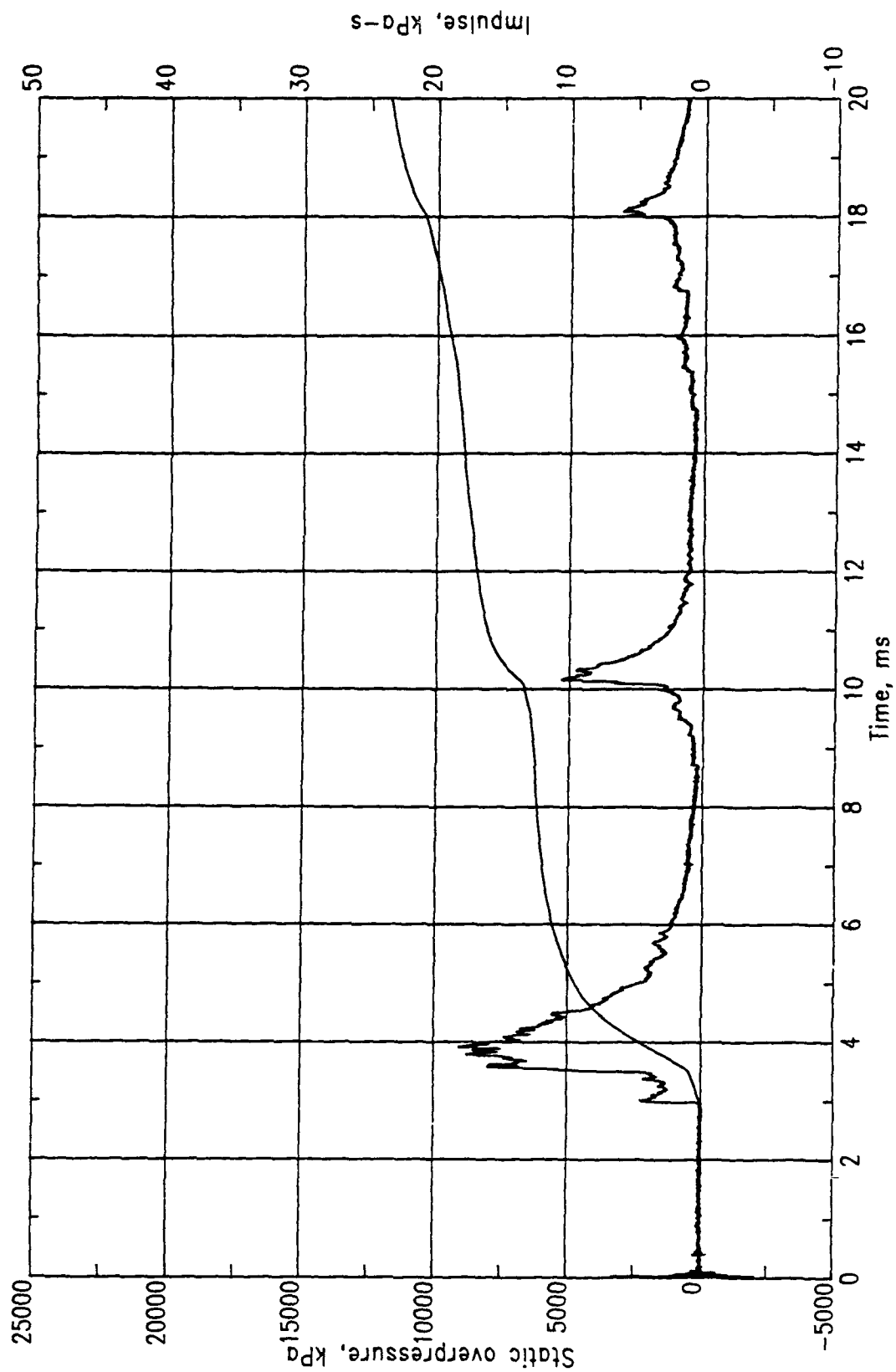


Figure 267. PAS-4, MN 0102.

Table 36 summarizes selected peaks from interior pressure measurements. A complete set of pressure records from PAS-4 is presented in Volume V.

Although there were a few noise spikes and baseline shifts, all of the free-field gage records provided usable data. The entire set of data again appeared to be internally consistent, i.e., TOAs increase and peak pressures decrease with increasing distances from GZ. All of the records were characterized by complex waveforms with multiple peaks. The records along each blastline showed similar features. The larger charge for the PAS-4 event resulted in higher pressures at a given range from GZ, and many of the measurements exceeded 6.9 kPa. The highest pressures were again measured at the front of the structure, but the differences were not as great as in earlier events with smaller charges. Measurement Number 703, at the front of the structure, recorded a peak pressure of 11.5 kPa at a range of 50.8 m from GZ (Fig. 268). At a range of 50.0 m from the left and right sides of the structure, the peak pressures were 11.0 and 10.2 kPa, respectively. At 50.2 m from GZ the peak pressure at the rear of the structure was 8.3 kPa. At 80.8 m from GZ the peak pressure at the front of the structure had dropped to 6.0 kPa. At 70.2 m from GZ the peak pressure at the rear of the structure had dropped to 5.0 kPa. In the PAS-4 event, the highest pressures were measured at the front of the structure while the lowest pressures were measured at the rear.

Table 37 summarizes selected peak pressures from the free-field measurements in the PAS-4 test. A complete set of pressure records is presented in Volume V.

Three accelerometers were mounted on the exterior surface of the arch in the same cross-sectional plane that included the GZ. The sensing axes of all accelerometers were oriented to measure radial accelerations. Measurement Number 1601 was made at the crown of the arch right over GZ. Figure 269a shows a peak radial acceleration of about 14,000 g for MN 1601. Figure 269b, a plot of the first and second integrals of the accelerometer record for MN 1601, shows a peak radial velocity of 15.8 m/s during the

Table 36. Summary of interior pressure measurements, PAS-4.

Meas. No.	Location	TOA (ms)	Peak (kPa)	Time (ms)	Peak (kPa)	Time (ms)	Peak (kPa)	Time (ms)	Peak (kPa)	Time (ms)
0101-1	SF	2.50	7725	4.75	5400	5.25	7900	7.05	2650	8.30
0102-1	SF	3.00	2300	3.00	8000	3.60	8950	3.90	5300	10.15
0202-1	BW	3.00	6050	3.00	6300	3.60	4325	4.35	2150	8.10
0301-1	SF	0.70	5250	0.80	1775	3.50	2300	5.20	5150	7.05
0302-1	SF	0.75	5150	0.82	2550	2.70	1650	6.75	1800	8.10
0303-1	SF	1.55	2800	1.60	8600	2.00	6600	2.60	3800	3.50
0402-1	FD	3.00	5350	3.10	5100	4.05	4500	5.55	3550	5.80
0501-1	SF	2.55	1800	2.60	10200	3.40	8700	3.64	3500	10.60
0601-1	SF	0.40	8600	0.45	1900	3.40	2900	8.70	2100	10.55
0602-1	SF	1.10	3800	1.15	13200	1.75	12600	2.20	9000	8.70
0603-1	SF	1.15	4000	1.20	8600	1.75	15000	2.20	10700	8.70
0604-1	SC	-	-	-	-	-	-	-	-	-

NOTE:

No data were recorded for MN 604 due to gage or instrumentation failure.

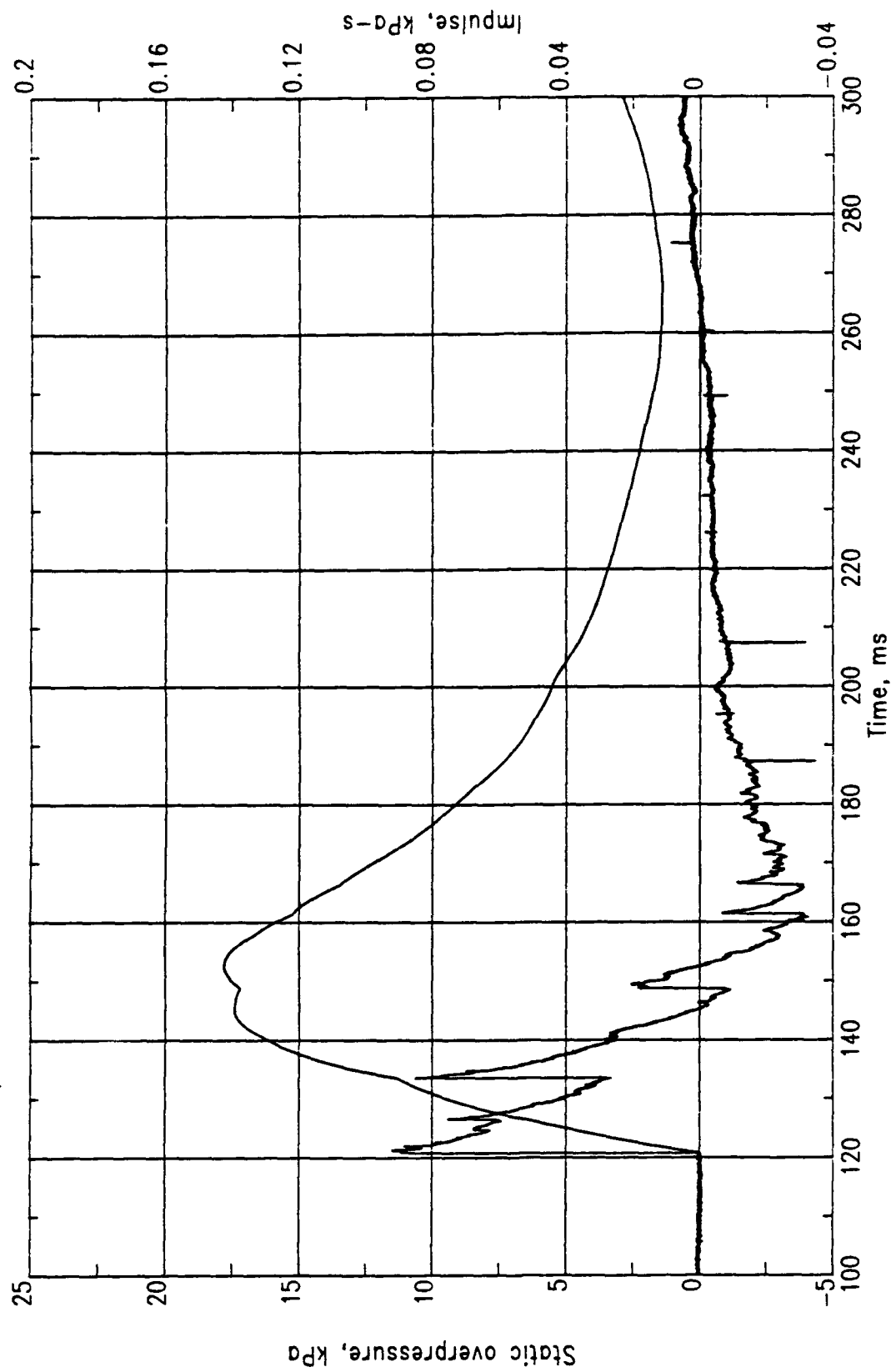
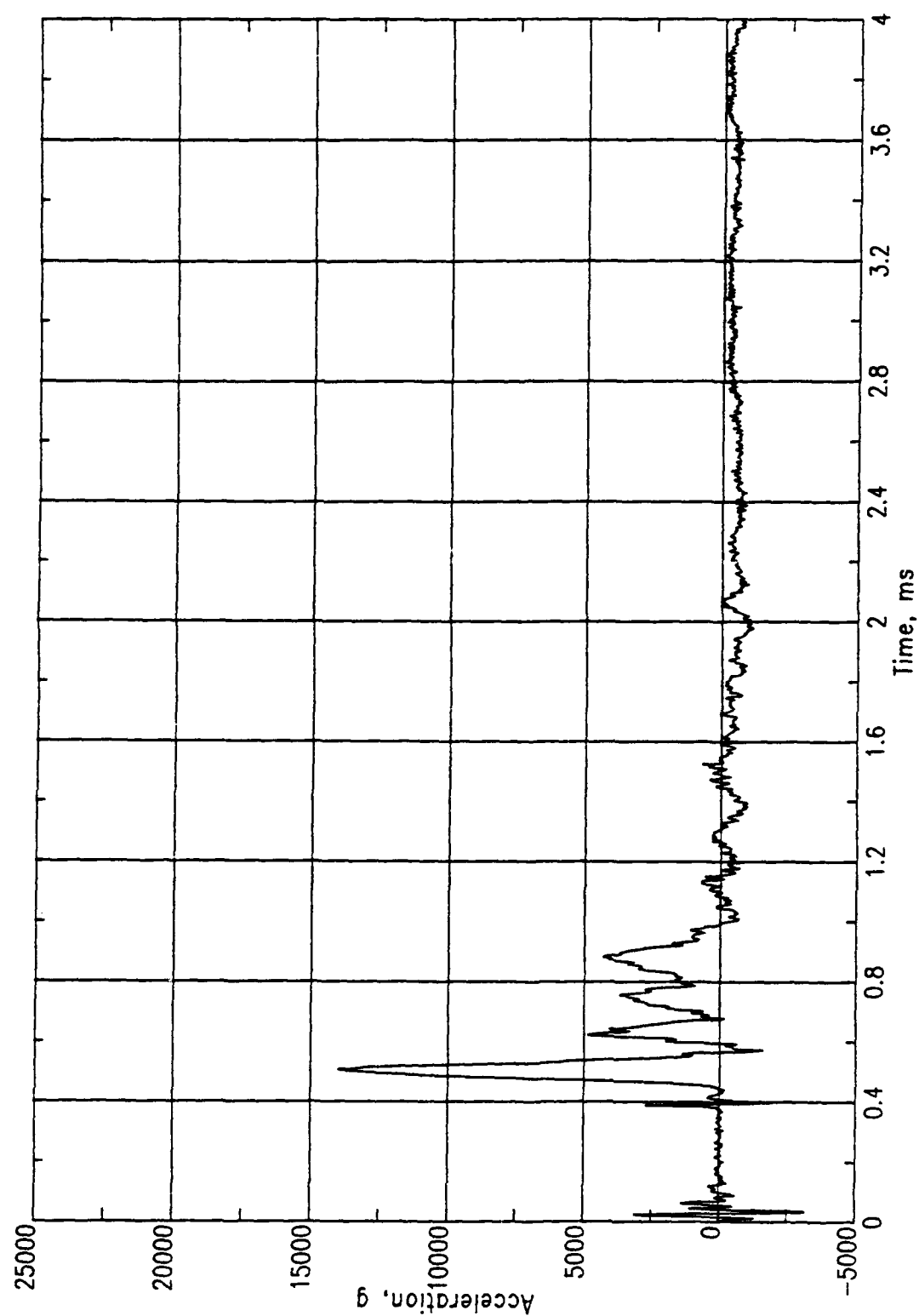


Figure 268. PAS-4, MN 0703.

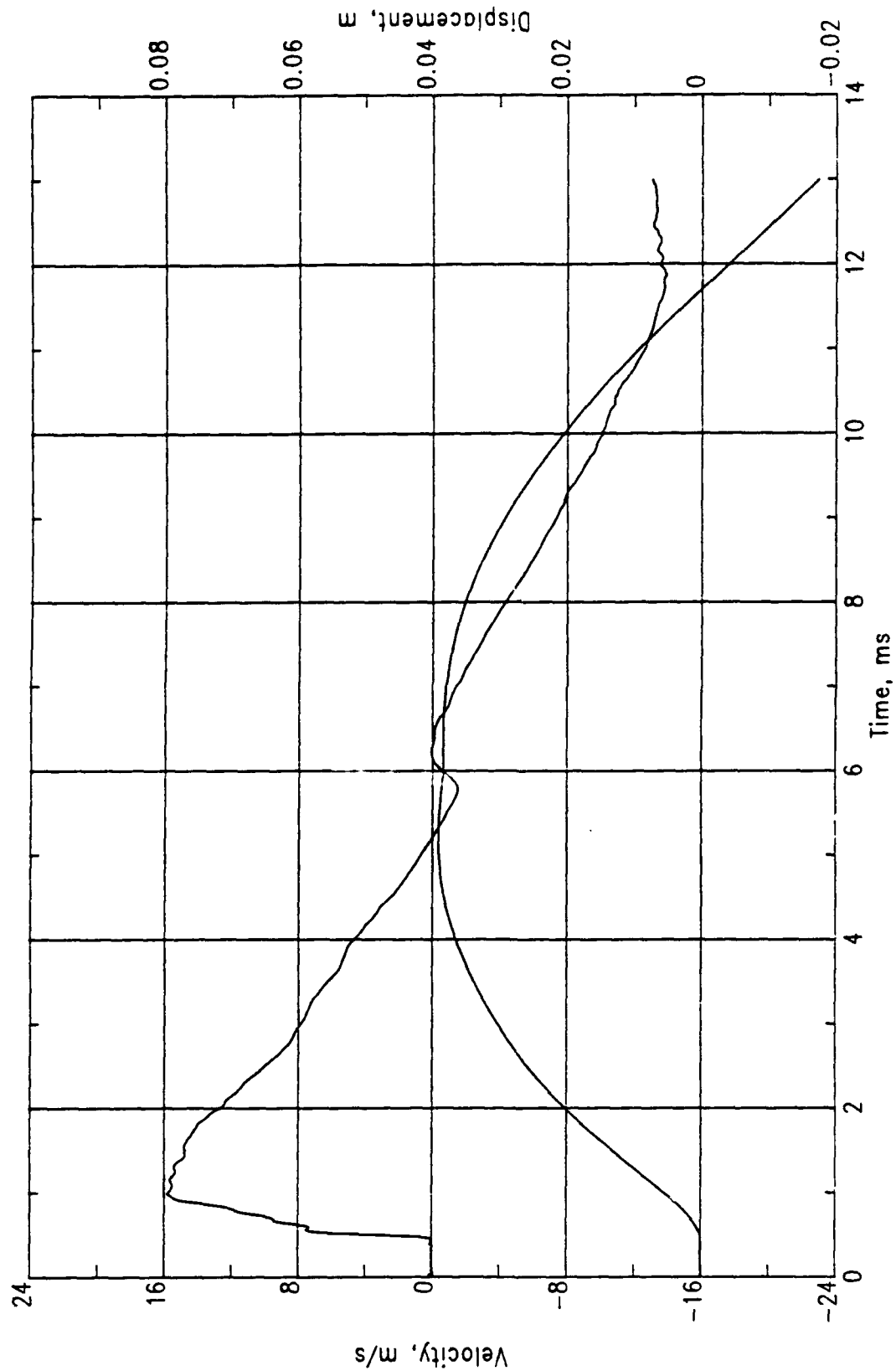
Table 37. Summary of free-field measurements, PAS-4.

Meas. No.	Location	TOA (ms)	Peak (kPa)	Time (ms)	Peak (kPa)	Time (ms)	Peak (kPa)	Time (ms)	Peak (kPa)	Time (ms)	Peak (kPa)	Time (ms)
701-4	FF	28.8	47.0	29.5	105.0	33.5	45.0	39.5	50.0	45.5	20.0	54.5
702-4	FF	67.0	27.0	67.5	15.5	75.0	28.0	81.0	6.5	93.0	4.0	192.0
703-4	FF	121.0	11.5	121.6	9.3	127.0	10.5	134.0	2.5	149.0	-	-
704-4	FF	204.5	5.9	205.0	5.1	209.0	5.0	216.4	1.6	235.0	-	-
705-4	FF	233.0	5.1	234.0	4.9	236.5	4.5	245.0	1.3	264.0	-	-
706-4	FF	32.0	14.0	32.4	39.0	35.0	27.5	42.0	21.5	50.0	12.5	62.0
707-4	FF	72.0	13.0	72.5	14.5	75.0	13.8	84.0	1.6	101.0	4.8	108.0
708-4	FF	126.5	8.2	127.0	6.6	138.0	4.1	163.0	-	-	-	-
709-4	FF	154.0	7.3	154.5	5.7	164.5	0.9	186.0	3.3	190.5	-	-
710-4	FF	24.0	42.0	43.0	34.0	44.0	27.0	51.0	9.0	60.5	-	-
711-4	FF	105.5	14.7	112.5	11.9	116.0	9.5	124.0	-	-	-	-
712-4	FF	134.5	10.8	140.0	7.6	150.4	-	-	-	-	-	-
713-4	FF	34.0	24.6	38.5	19.4	43.0	14.4	45.5	11.0	58.0	4.9	69.0
714-4	FF	74.5	7.2	77.0	8.4	82.0	8.2	91.5	7.2	105.5	2.7	134.4
715-4	FF	132.0	5.2	134.5	4.6	140.0	4.5	144.0	4.0	159.5	3.0	167.0
716-4	FF	44.5	9.8	44.5	12.3	52.0	29.6	56.0	20.2	68.0	-	-
717-4	FF	84.0	4.0	84.0	7.5	90.5	14.5	92.0	9.5	104.0	1.5	115.0
718-4	FF	135.0	2.2	135.5	8.3	141.0	5.8	152.5	0.7	165.0	-	-
719-4	FF	192.5	1.3	193.0	4.9	197.0	3.6	208.0	0.3	223.0	-	-
720-4	FF	24.0	11.5	31.0	10.0	38.0	46.5	42.0	43.5	43.0	32.0	51.0
721-4	FF	104.0	2.6	104.5	11.2	111.0	13.0	114.0	11.2	124.0	-	-
722-4	FF	132.5	2.0	133.0	7.8	138.5	10.3	140.5	9.3	150.0	-	-



(a) Acceleration.

Figure 269. PAS-4, MN 1601.



(b) Velocity and displacement.

Figure 269. Concluded.

first 2 ms of the record. This data channel failed at 13.6 ms. Measurement Number 1603 failed at 15.2 ms, but it recorded a peak acceleration of 4800 g (Fig. 270a). Figure 270b shows a peak velocity of 4.7 m/s within the first 2 ms for this gage. Measurement Number 1605 recorded a peak of 7000 g before failing at 34 ms (Fig. 271a). Figure 271b shows a peak velocity of 8.8 m/s in the first 4 ms for MN 1605. All of the peak velocities obtained from integration of accelerometer records are much lower than those obtained from analysis of high-speed photography. Since these velocity peaks occur before structure breakup, their validity is questionable. Peak velocities shown for later times are subject to even greater uncertainties because of baseline shifts in the accelerometer records.

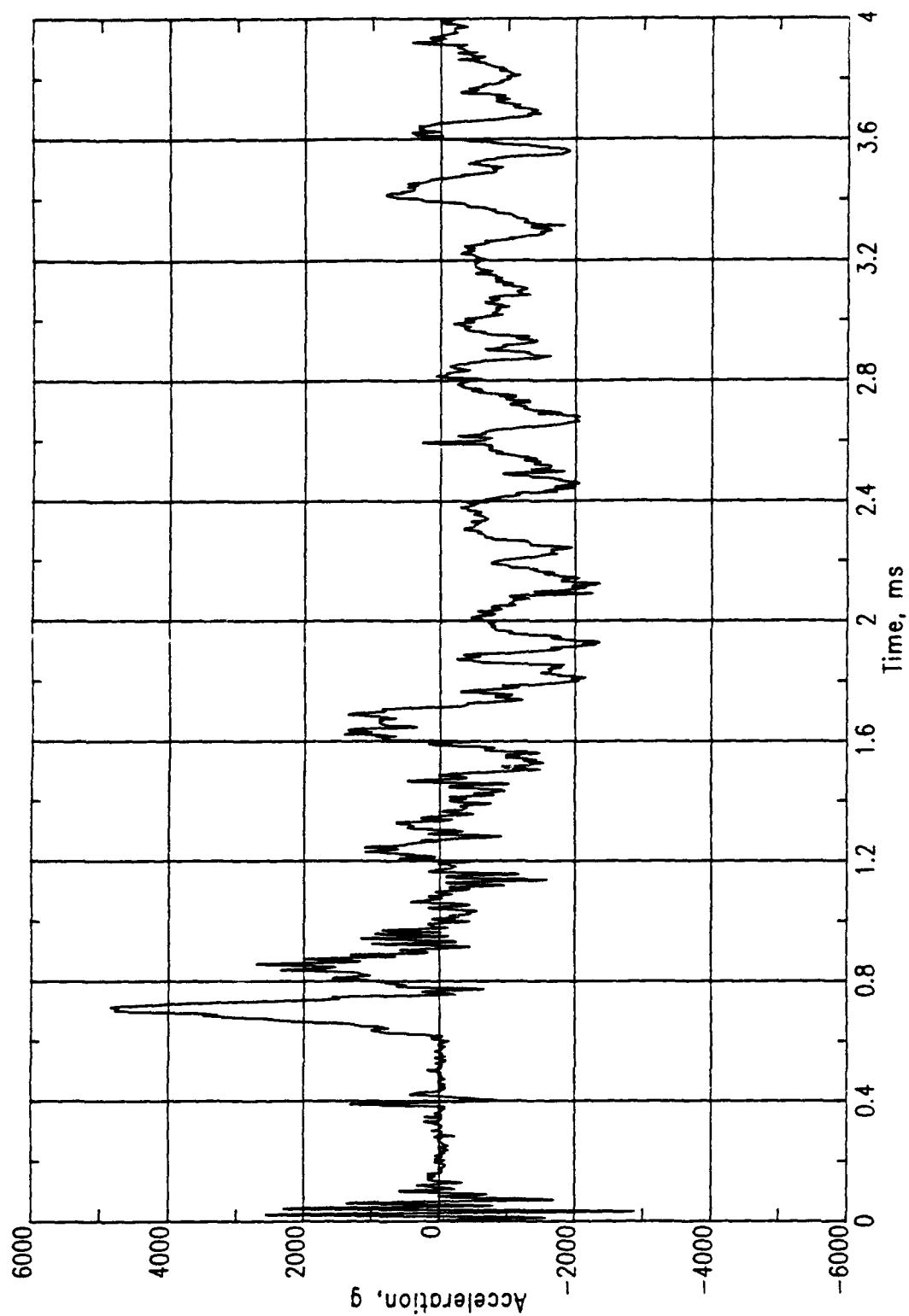
Table 38 summarizes selected peak accelerations from all of the accelerometer records for the PAS-4 event, and a complete set of records is presented in Volume V.

Data from the WES self-recording accelerometers were not available for inclusion in this report.

6.2.3 Rock Rubble Berm

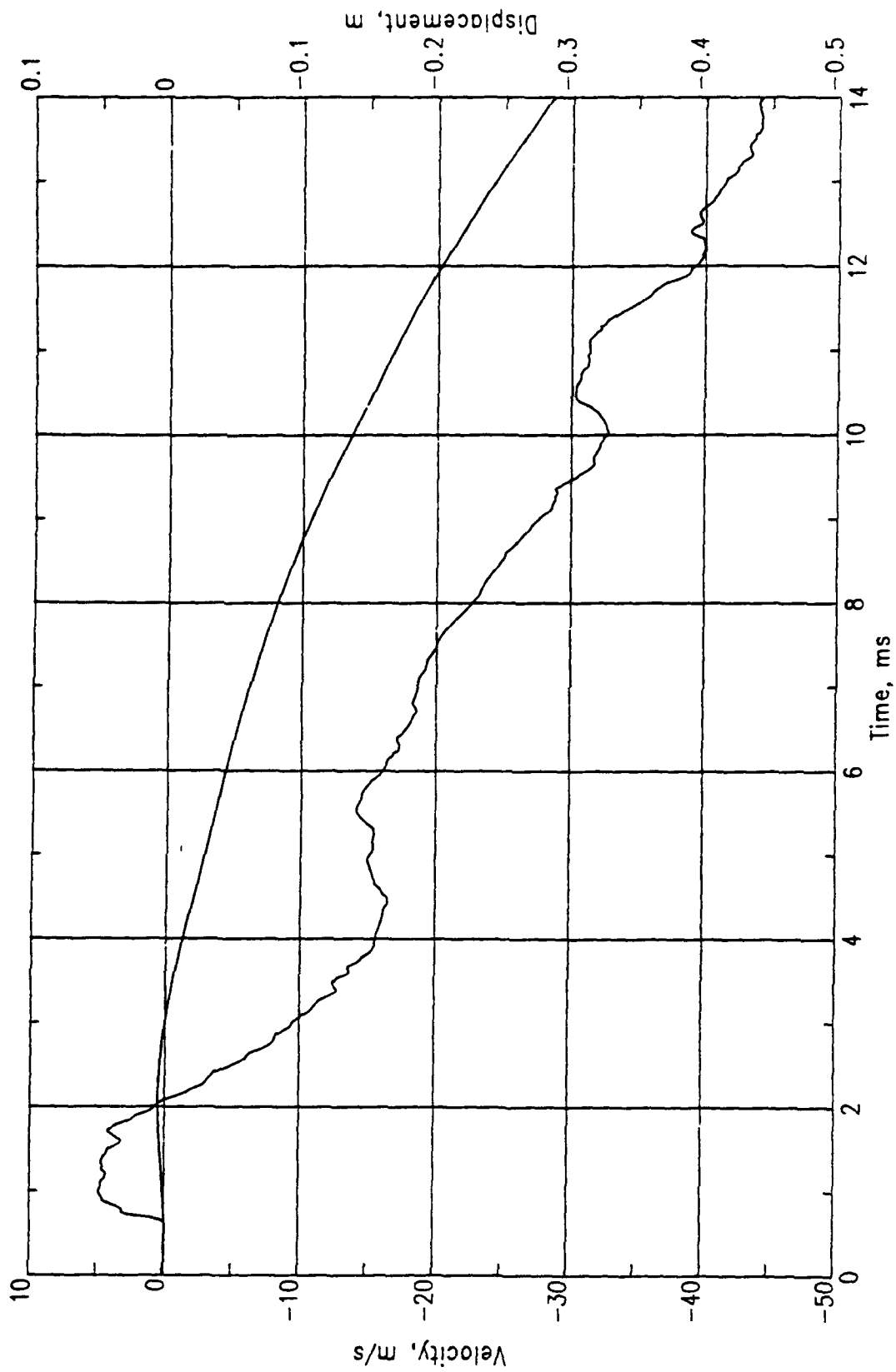
A portion of the rock rubble berm adjacent to the arch was blown upward and out during the test while the remainder of the rocks were relatively undisturbed (Figs. 272 and 273). The upward trajectory of the rock varied from 20 to about 80 deg. Rock velocities estimated from high-speed photography varied from 25.1 to 55.3 m/s.

The higher trajectory rock showed higher velocities with an average of 55 m/s. The lower trajectory rock averaged about 25 m/s. That portion of the berm behind an extended plane of the backwall was also undisturbed. A complete description of the limits of the rock ejected from the berm is presented in the section on debris recovery.



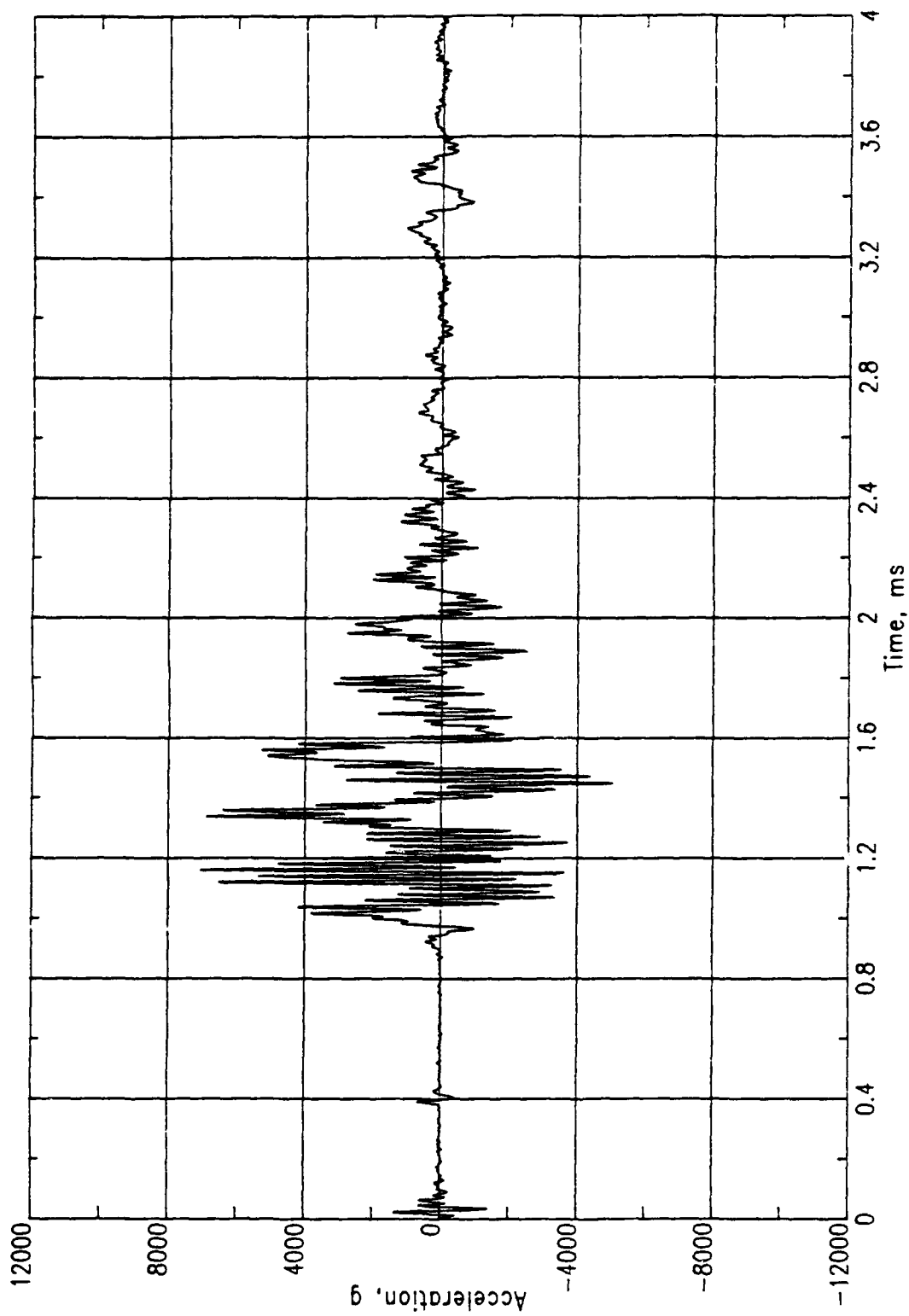
(a) Acceleration.

Figure 270. PAS-4, MN 1603.



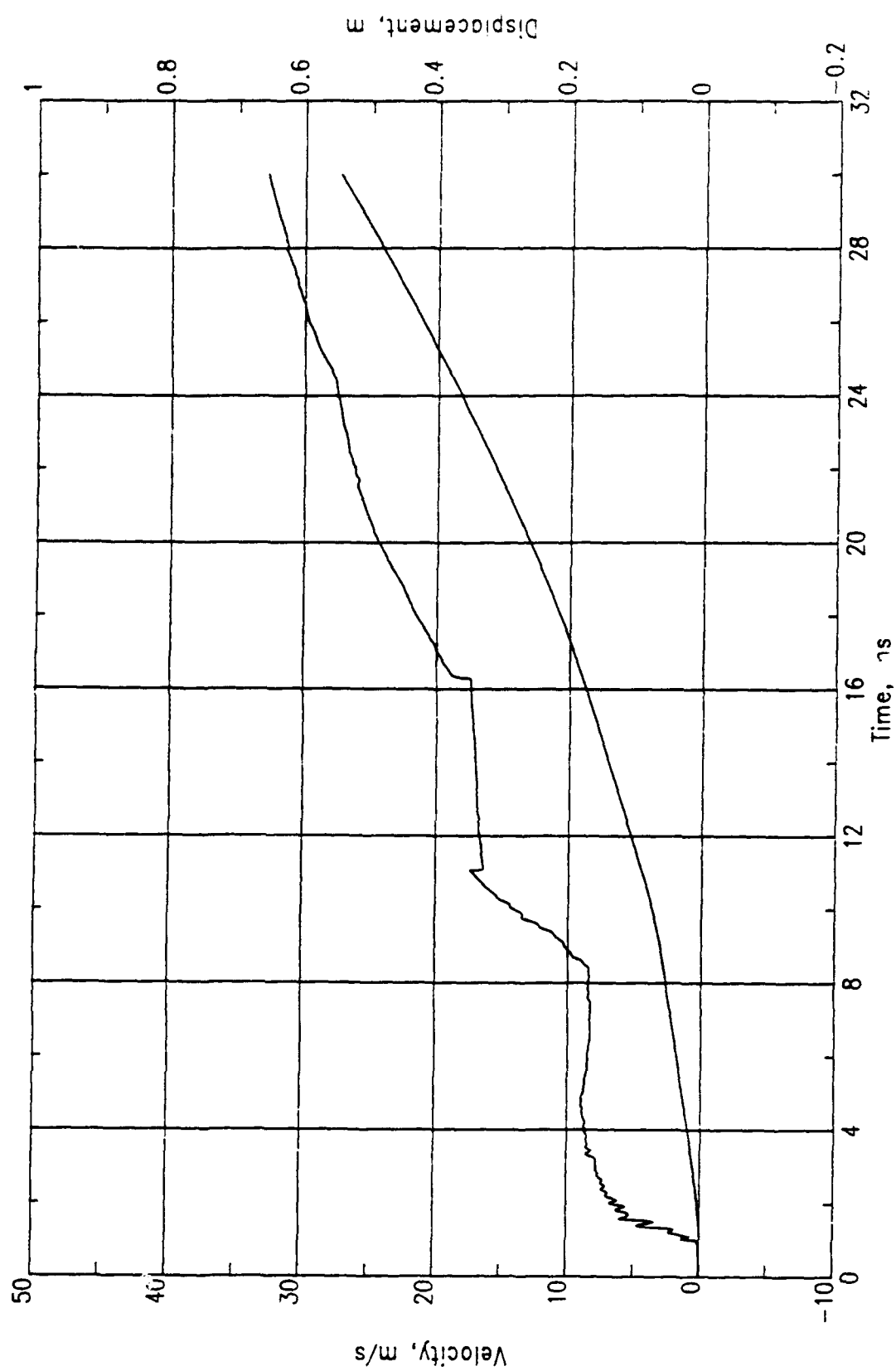
(b) Velocity and displacement.

Figure 270. Concluded.



(a) Acceleration.

Figure 271. PAS-4, MN 1605.



(b) Velocity and displacement.

Figure 271. Concluded.

Table 38. Summary of exterior acceleration measurements, PAS-4.

Meas. No.	Location	TOA (ms)	Peak (g)	Time (ms)	Peak (g)	Time (ms)	Peak (g)	Time (ms)	Peak (g)	Time (ms)
1601-4	SR	0.444	14000	0.505	4900	0.623	3700	0.76	4300	0.88
1603-4	SR	0.620	4850	0.713	2700	0.854	-2400	1.93	800	3.42
1605-4	SR	0.860	4200	1.040	6500	1.120	7000	1.16	-3300	1.07
									-3600	1.15

NOTES:

Start time of MN 1601-4 is approximate since the data start is mixed with the end of the second fidu.

Ringling phenomena are apparent in 1605-4 data..



Figure 272. Posttest view of rock rubble berm adjacent to arch foundation, PAS-4.

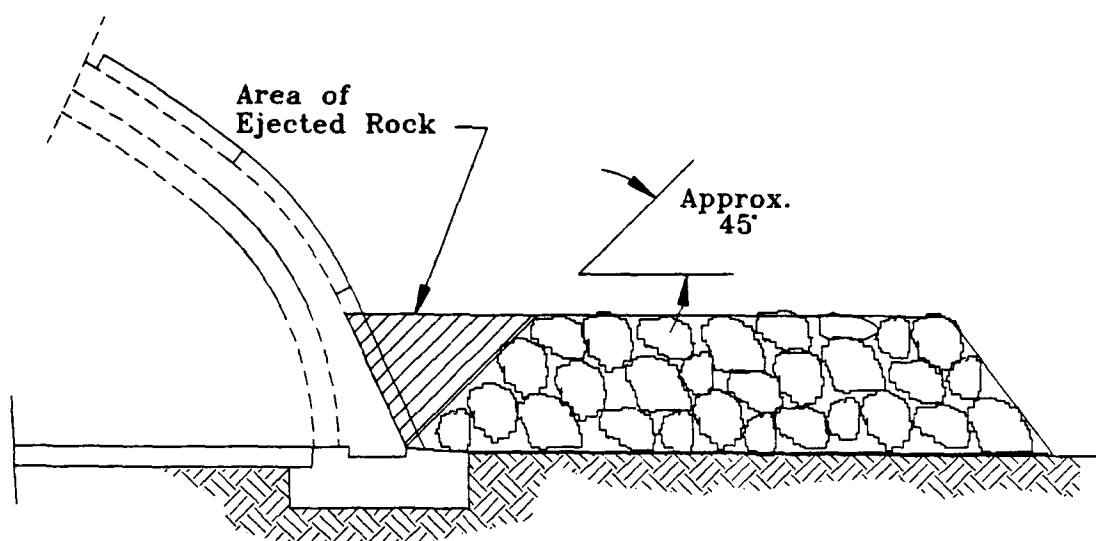


Figure 273. Portion of rock rubble berm ejected during test, PAS-4.

6.2.4 Debris Distribution

As in the case of PAS-3 and PAS-2, three general classes of materials were included in the posttest debris distribution survey for PAS-4. The first class included those items placed at various locations on the surface of the shelter, i.e., SIFCON and aluminum cubes and photo poles. The second class included pieces of the model structure, and the last was of rock from the rock rubble berm placed at the sides of the structure. The following paragraphs present data collected on the distribution of these three classes of debris in the PAS-4 test. The procedures used for collecting, processing, and characterizing the structural debris from the PAS-4 test were similar to those described in Section 4.2.4 for the PAS-3 event. Interpretation of the data in terms of quantity-distance criteria is beyond the scope of this report.

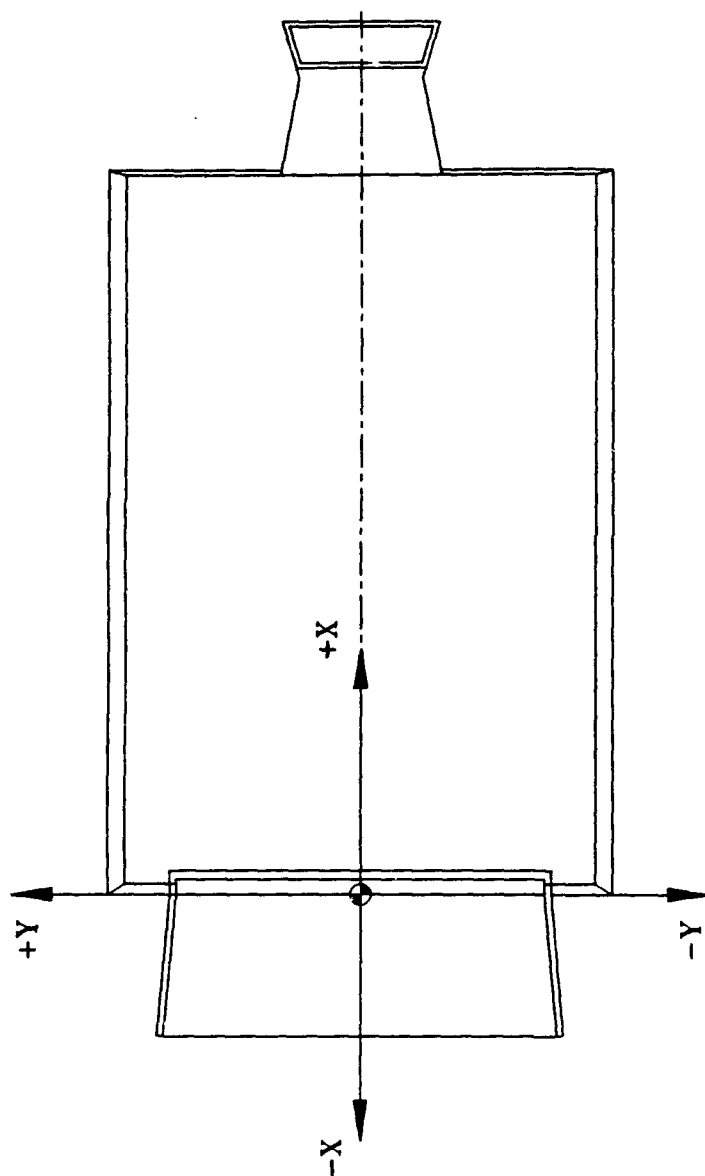
All coordinates presented in this section are referenced to the Structure Coordinate System (SCS) shown in Figure 274. All ranges and azimuths are given in the plane of the top surface of the floor slab of the structure and referenced from the surface GZ of the charge (Fig. 275).

Table 39 presents the pretest and posttest coordinates of the SIFCON cubes placed on the structure for the PAS-4 test.

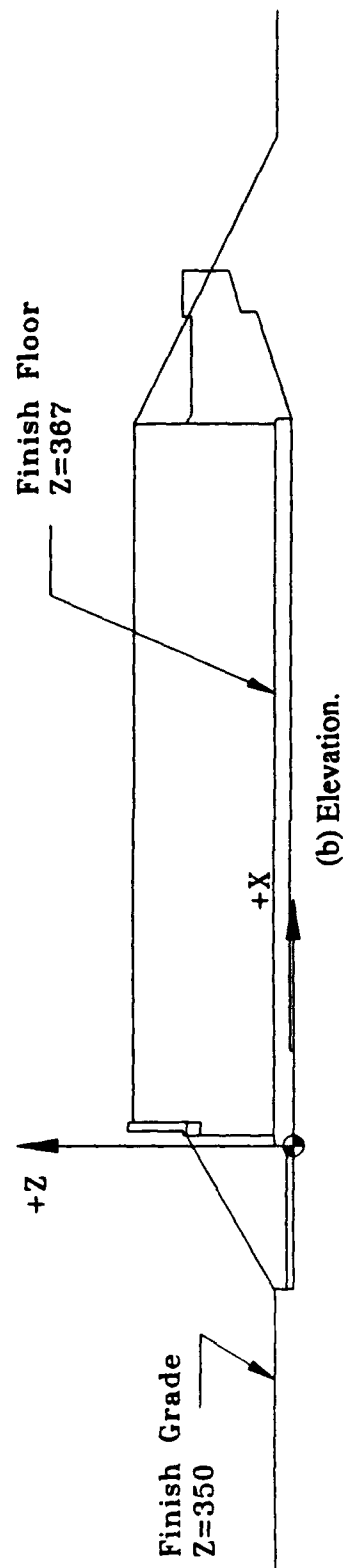
Table 40 presents the pretest and posttest coordinates of the aluminum cubes placed on the structure. Because of their small size, no attempt was made to use the aluminum cubes in a photographic analysis.

Table 41 presents the pretest and posttest coordinates of the photo poles placed on the structure. Because the structure was so quickly obscured in smoke and dust, the photo poles were not considered useful in determining debris velocities from photographic analysis.

Table 42 presents the pretest and posttest coordinates of the three WES self-recording accelerometers placed on the structure.



(a) Plan.



(b) Elevation.

Figure 274. Structure coordinate system, PAS-4.

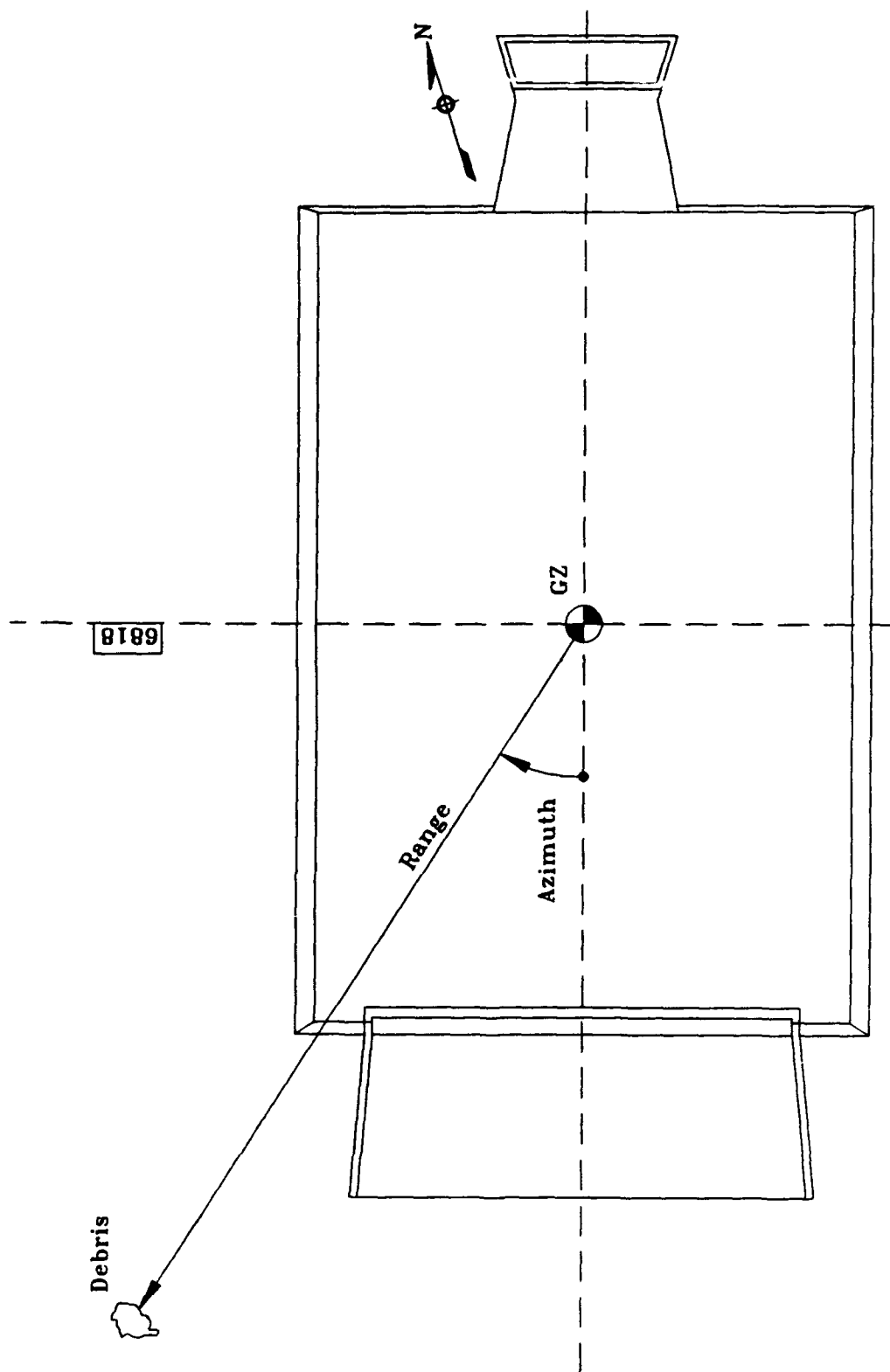


Figure 275. Range and azimuth reference system, PAS-4.

Table 39. Pretest and posttest locations of SIFCON cubes, PAS-4.

I.D. MARK	STARTING LOCATION COORDINATES			FINAL LOCATION COORDINATES		
	X (mm)	Y (mm)	Z (mm)	X (mm)	Y (mm)	Z (mm)
SC2	1085	0	2987	-34081	21659	350
SC3	1085	-1559	2767	-26682	-21044	350
SC4	1085	-2564	2371	-18143	-72914	350
SC5	1085	-3514	1759	-14623	-55851	350
SC7	1085	-4020	-384	-8516	-47259	350
SC8	3710	0	2987	-21191	-33328	350
SC9	3710	-1559	2767	-11977	-25254	350
SC10	3710	-2564	2371	-45169	-140219	350
SC12	3710	-3514	1759	-30286	-91616	350
SC13	3710	-4020	-384	-6333	-74698	350
SC14	6335	-1559	2767	-35330	-78036	350
SC15	6335	-2564	2371	3246	-161789	350
SC16	6335	-3514	1759	8472	-169726	350
SC17	6335	-4020	-384	7720	-114662	350
SC18	9360	0	2987	26027	-12640	350
SC19	9360	-1559	2767	14894	-50177	350
SC20	9360	-2564	2371	10273	-113051	350
SC21	9360	-3514	1759	12115	-116502	350
SC22	9360	-4020	-384	13302	-78505	350
SC23	12735	0	2987	23409	15207	350
SC24	12735	-1559	2767	17636	-68324	350
SC25	12735	-2564	2371	15350	-107152	350
SC26	12735	-3514	1759	13669	-111631	350
SC28	12735	-4020	-384	7618	-75094	350

Table 40. Pretest and posttest locations of aluminum cubes, PAS-4.

I.D. MARK	STARTING LOCATION COORDINATES			FINAL LOCATION COORDINATES		
	X (mm)	Y (mm)	Z (mm)	X (mm)	Y (mm)	Z (mm)
AL1	1260	0	2987	-27295	10256	350
AL2	1260	-1559	2767	-29038	-22928	350
AL3	1260	-2564	2371	-17680	-63250	350
AL4	1260	-3514	1759	-11333	-47599	350
AL5	1260	-4020	1118	-10922	-46386	350
AL6	3885	0	2987	-16527	-20402	350
AL7	3885	-1559	2767	5524	-23702	350
AL8	3885	-2564	2371	-23507	-106300	350
AL9	3885	-3514	1759	Not Found		
AL10	3885	-4020	1118	-5093	-58078	350
AL11	6510	0	2987	Not Found		
AL12	6510	-1559	2767	-19378	-71807	350
AL13	6510	-2564	2371	5895	-127078	350
AL14	6510	-3514	1759	7441	-133988	350
AL15	6510	-4020	1118	4541	-76455	350
AL16	9535	0	2987	16443	-13005	350
AL17	9535	-1559	2767	16190	-51215	350
AL18	9535	-2564	2371	16680	-99924	350
AL25	9535	-3514	1759	11276	-102740	350
AL20	9535	-4020	1118	7089	-71941	350
AL21	12560	0	2987	19310	12761	350
AL22	12560	-1559	2767	17964	-57733	350
AL23	12560	-2564	2371	18103	-90991	350
AL24	12560	-3514	1759	14177	-97023	350

Table 41. Pretest and posttest locations of photo poles, PAS-4.

I.D. MARK	STARTING LOCATION COORDINATES			FINAL LOCATION COORDINATES		
	X (mm)	Y (mm)	Z (mm)	X (mm)	Y (mm)	Z (mm)
PP1	1530	2564	2371	Not Found		
PP2	1410	0	2987	-26857	13147	350
PP3	1530	-1559	2767	-102352	-4136	350
PP4	1410	-2564	2371	-1229	-66818	350
PP5	1530	-3798	-742	-3919	-41286	350
PP6	7030	2564	2371	Not Found		
PP7	6910	0	2987	-10637	-11465	350
PP8	7030	-1559	2767	36077	-55485	350
PP9	6910	-2564	2371	Not Found		
PP10	7030	-3798	-742	-20161	1202	350
PP11	12290	2564	2371	-1495	120431	350
PP12	12410	0	2987	Not Found		
PP13	12290	-1559	2767	15758	-52467	350
PP14	12410	-2564	2371	Not Found		
PP15	12290	-3798	-742	5198	-117796	350

Table 42. Pretest and posttest locations of WES accelerometers, PAS-4.

I.D. MARK	STARTING LOCATION COORDINATES			FINAL LOCATION COORDINATES		
	X (mm)	Y (mm)	Z (mm)	X (mm)	Y (mm)	Z (mm)
W1601	6388	0	2987	-21253	-11040	350
W1603	6388	1805	2691	-4270	103597	350
W1605	6388	3291	1928	64	161588	350

As an aid in identifying the origin of a piece of concrete debris from the arch, the arch concrete was dyed in four different colors. Figure 276 also shows the color of beads used in each quadrant along the length of the arch.

Three different procedures were used to recover, identify, and measure concrete debris. The first was the collection of concrete debris from 5-deg sectors. A sieve analysis was conducted on the debris collected from these sectors to determine the size distribution range. The second procedure was to identify areas of secondary debris produced as a result of the large arch sections impacting the ground. The number and size distributions of the debris within these areas were also determined by a sieve analysis. This second procedure was not used in the preceding tests of this series. The third procedure included locating and collecting larger pieces of debris from around the structure. The collected debris was then measured, weighed, and identified. Pieces within the secondary debris areas were not included in this survey.

Following the test, the boundaries of six 5-deg circular sectors were surveyed on the testbed (Fig. 277). All concrete debris smaller than 50 mm found within these sectors was collected, sieved, and counted using the procedures described for the PAS-3 test in Section 4.2.4. Tables 43 through 48 summarize the data for the six sectors of PAS-4.

It was fairly easy to locate the areas of secondary debris produced when the sections of the arch impacted the ground (Fig. 278). Where two or more arch sections were close to each other, one area including all the pieces could be defined. Ten areas containing secondary debris were identified. The boundaries of the areas were marked and surveyed. The boundary surveys for the 10 areas are shown in Figure 279.

Within each secondary debris area, at least one region measuring 3 x 3 m was laid out and surveyed. All concrete debris smaller than 50 mm within each region was raked up and placed in a bucket. Debris larger than 50 mm was left in place. Following the procedures used for the 5-deg sectors, a sieve analysis was conducted on the collected

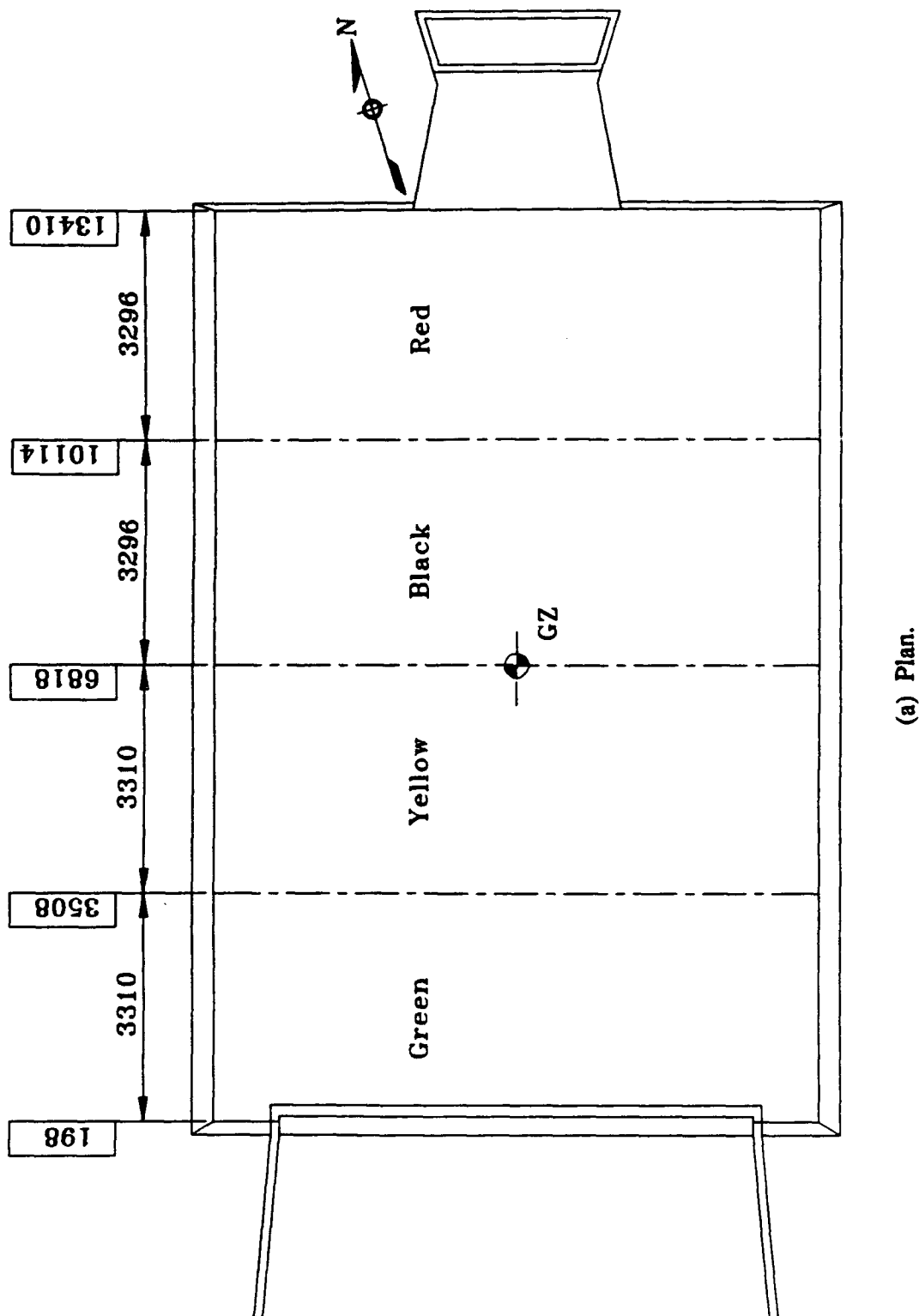
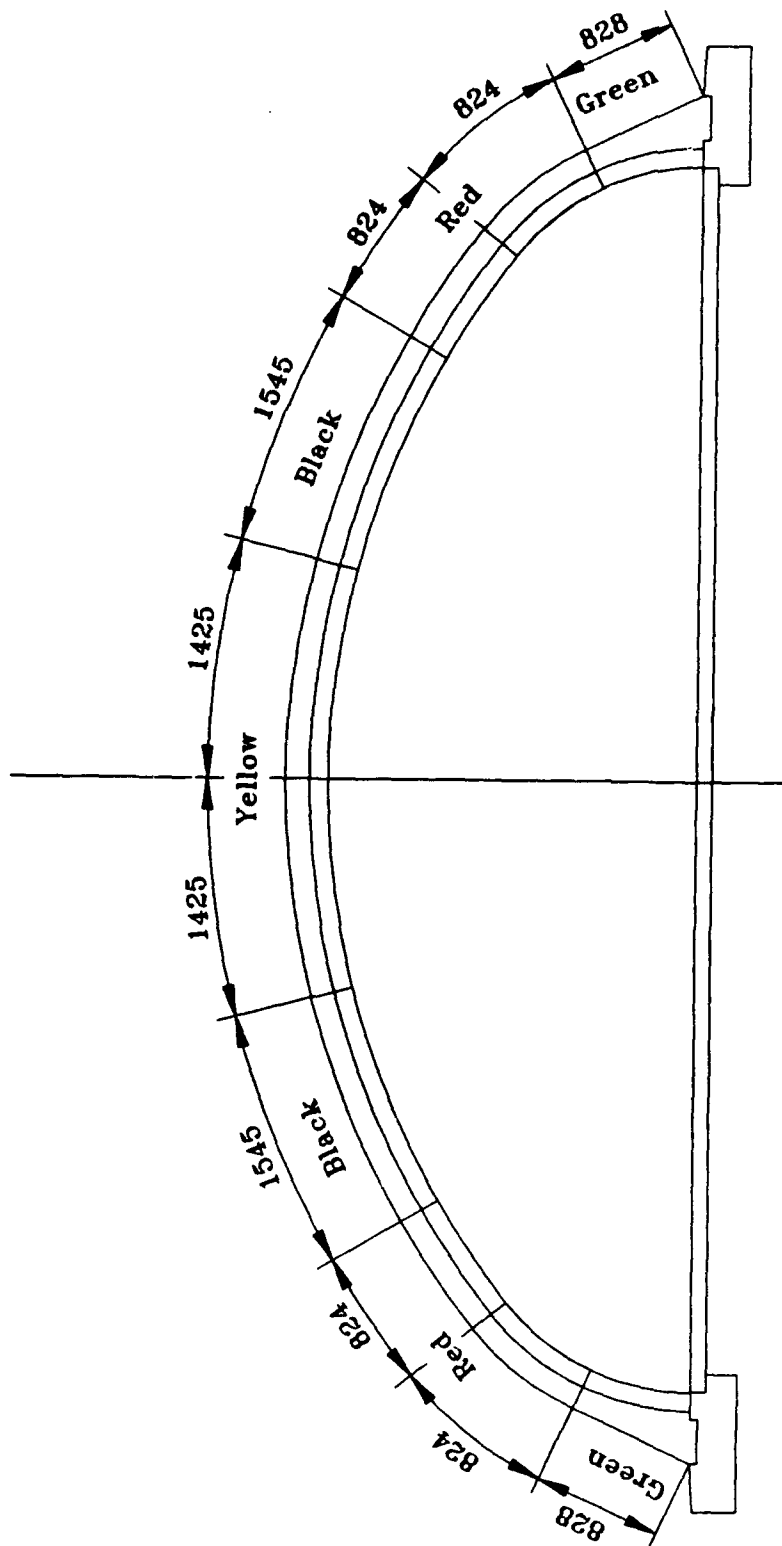


Figure 276. Dyed concrete and colored beads in arch, PAS-4.



(b) Section.

Figure 276. Concluded.

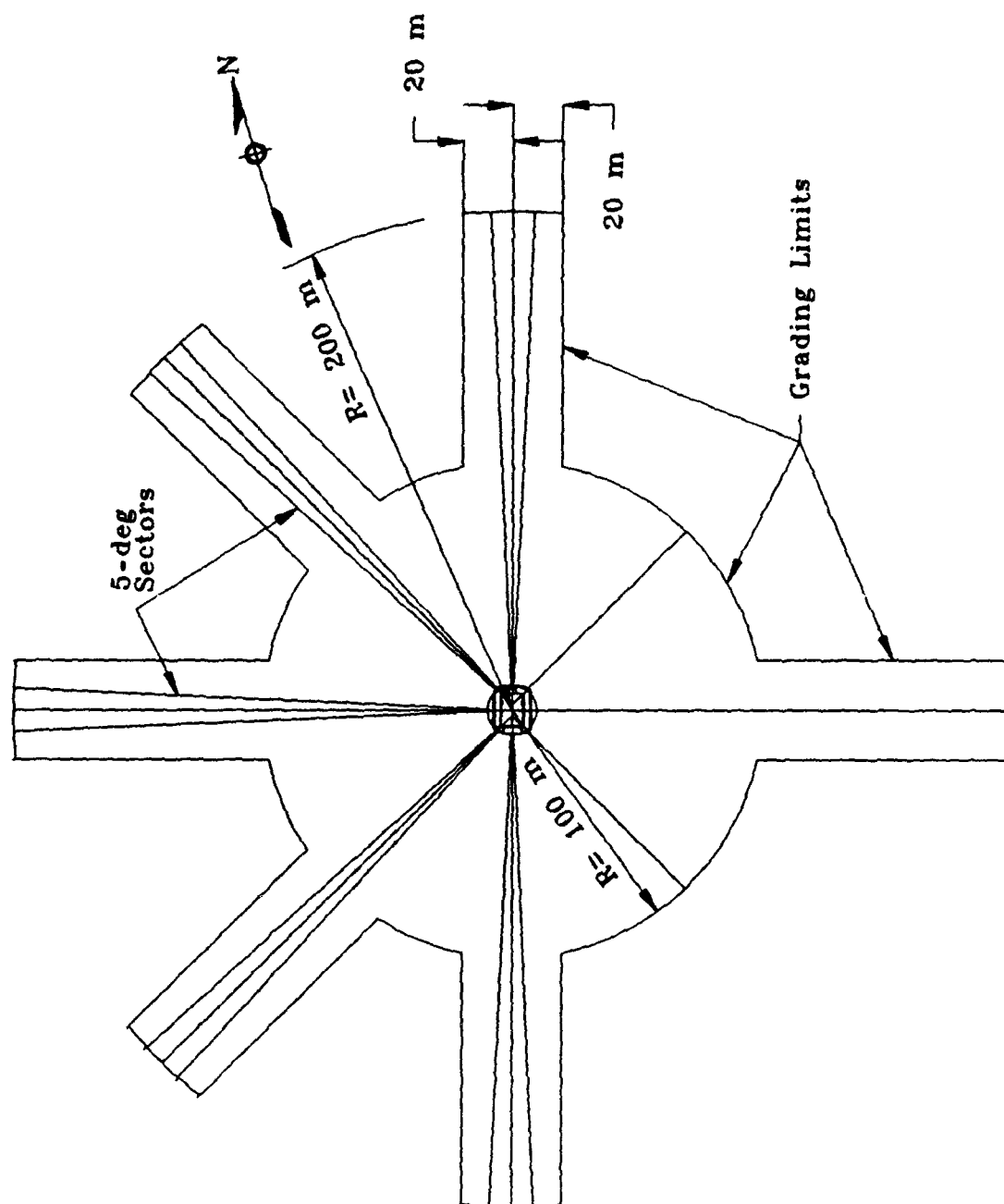


Figure 277. Five-degree debris collection sectors, PAS-4.

Table 43. Sieve data: 0-deg azimuth (front) sector, PAS-4.

ZONE	INSIDE RADIUS (m)	OUTSIDE RADIUS (m)	AVERAGE RADIUS (m)	ZONE AREA (m ²)	WEIGHT (gm)	NUMBER	WT./AREA (gm /m ²)	NO./AREA (no./m ²)
000AZ- 1	10.0	15.0	12.5	5.45	501.1	70	91.9	12.8
000AZ- 2	15.0	20.0	17.5	7.64	505.0	108	66.1	14.1
000AZ- 3	20.0	25.0	22.5	9.82	1020.9	170	104.0	17.3
000AZ- 4	25.0	30.0	27.5	12.00	599.3	95	49.9	7.9
000AZ- 5	30.0	35.0	32.5	14.18	948.5	115	66.9	8.1
000AZ- 6	35.0	40.0	37.5	16.36	753.2	77	46.0	4.7
000AZ- 7	40.0	45.0	42.5	18.54	578.5	49	31.2	2.6
000AZ- 8	45.0	50.0	47.5	20.73	590.8	48	28.5	2.3
000AZ- 9	50.0	55.0	52.5	22.91	620.1	29	27.1	1.3
000AZ- 10	55.0	60.0	57.5	25.09	162.7	12	6.5	0.5
000AZ- 11	60.0	65.0	62.5	27.27	173.9	9	6.4	0.3
000AZ- 12	65.0	70.0	67.5	29.45	193.4	10	6.6	0.3
000AZ- 13	70.0	75.0	72.5	31.63	456.2	8	14.4	0.3
000AZ- 14	75.0	80.0	77.5	33.82	0.0	0	0.0	0.0
000AZ- 15	80.0	85.0	82.5	36.00	0.0	0	0.0	0.0
000AZ- 16	85.0	90.0	87.5	38.18	0.0	0	0.0	0.0
000AZ- 17	90.0	95.0	92.5	40.36	0.0	0	0.0	0.0
000AZ- 18	95.0	100.0	97.5	42.54	0.0	0	0.0	0.0
Totals					7103.6	800		

Table 44. Sieve data: 45-deg azimuth (right, front corner) sector, PAS-4.

ZONE	INSIDE RADIUS (m)	OUTSIDE RADIUS (m)	AVERAGE RADIUS (m)	ZONE AREA (m ²)	WEIGHT (gm)	NUMBER	WT./AREA (gm /m ²)	NO./AREA (no./m ²)
045AZ-1	10.0	15.0	12.5	5.45	0.0	0	0.0	0.0
045AZ-2	15.0	20.0	17.5	7.64	459.6	77	60.2	10.1
045AZ-3	20.0	25.0	22.5	9.82	1032.6	126	105.2	12.8
045AZ-4	25.0	30.0	27.5	12.00	1195.4	110	99.6	9.2
045AZ-5	30.0	35.0	32.5	14.18	1403.1	90	98.9	6.3
045AZ-6	35.0	40.0	37.5	16.36	1114.1	67	68.1	4.1
045AZ-7	40.0	45.0	42.5	18.54	1254.4	127	67.6	6.8
045AZ-8	45.0	50.0	47.5	20.73	1841.1	95	88.8	4.6
045AZ-9	50.0	55.0	52.5	22.91	173.2	19	7.6	0.8
045AZ-10	55.0	60.0	57.5	25.09	540.9	18	21.6	0.7
045AZ-11	60.0	65.0	62.5	27.27	0.0	0	0.0	0.0
045AZ-12	65.0	70.0	67.5	29.45	0.0	0	0.0	0.0
045AZ-13	70.0	75.0	72.5	31.63	0.0	0	0.0	0.0
045AZ-14	75.0	80.0	77.5	33.82	0.0	0	0.0	0.0
045AZ-15	80.0	85.0	82.5	36.00	0.0	0	0.0	0.0
045AZ-16	85.0	90.0	87.5	38.18	0.0	0	0.0	0.0
045AZ-17	90.0	95.0	92.5	40.36	0.0	0	0.0	0.0
045AZ-18	95.0	100.0	97.5	42.54	0.0	0	0.0	0.0
Totals					9014.4	729		

Table 45. Sieve data: 90-deg azimuth (right side) sector, PAS-4.

ZONE	INSIDE RADIUS (m)	OUTSIDE RADIUS (m)	AVERAGE RADIUS (m)	ZONE AREA (m ²)	WEIGHT (gm)	NUMBER	WT./AREA (gm./m ²)	NO./AREA (no./m ²)
090AZ-1	10.0	15.0	12.5	5.45	0.0	0	0.0	0.0
090AZ-2	15.0	20.0	17.5	7.64	1093.5	162	143.2	21.2
090AZ-3	20.0	25.0	22.5	9.82	2396.8	208	244.1	21.2
090AZ-4	25.0	30.0	27.5	12.00	2611.8	242	217.7	20.2
090AZ-5	30.0	35.0	32.5	14.18	2439.2	381	172.0	26.9
090AZ-6	35.0	40.0	37.5	16.36	3254.0	276	198.9	16.9
090AZ-7	40.0	45.0	42.5	18.54	2894.3	272	156.1	14.7
090AZ-8	45.0	50.0	47.5	20.73	2926.4	227	141.2	11.0
090AZ-9	50.0	55.0	52.5	22.91	3503.3	221	152.9	9.6
090AZ-10	55.0	60.0	57.5	25.09	0.0	0	0.0	0.0
090AZ-11	60.0	65.0	62.5	27.27	0.0	0	0.0	0.0
090AZ-12	65.0	70.0	67.5	29.45	0.0	0	0.0	0.0
090AZ-13	70.0	75.0	72.5	31.63	0.0	0	0.0	0.0
090AZ-14	75.0	80.0	77.5	33.82	2159.5	118	63.9	3.5
090AZ-15	80.0	85.0	82.5	36.00	2330.9	121	64.8	3.4
090AZ-16	85.0	90.0	87.5	38.18	3000.6	115	78.6	3.0
090AZ-17	90.0	95.0	92.5	40.36	2107.9	106	52.2	2.6
090AZ-18	95.0	100.0	97.5	42.54	1536.8	68	36.1	1.6
Totals					32255.0	2517		

Table 46. Sieve data: 135-deg azimuth (right, back corner) sector, PAS-4.

ZONE	INSIDE RADIUS (m)	OUTSIDE RADIUS (m)	AVERAGE RADIUS (m)	ZONE AREA (m ²)	WEIGHT (gm.)	NUMBER	WT./AREA (gm /m ²)	NO./AREA (no./m ²)
135AZ - 1	10.0	15.0	12.5	5.45	214.3	40	39.3	7.3
135AZ - 2	15.0	20.0	17.5	7.64	541.0	84	70.9	11.0
135AZ - 3	20.0	25.0	22.5	9.82	329.3	42	33.5	4.3
135AZ - 4	25.0	30.0	27.5	12.00	638.3	40	53.2	3.3
135AZ - 5	30.0	35.0	32.5	14.18	234.0	25	16.5	1.8
135AZ - 6	35.0	40.0	37.5	16.36	0.0	0	0.0	0.0
135AZ - 7	40.0	45.0	42.5	18.54	0.0	0	0.0	0.0
135AZ - 8	45.0	50.0	47.5	20.73	0.0	0	0.0	0.0
135AZ - 9	50.0	55.0	52.5	22.91	0.0	0	0.0	0.0
135AZ - 10	55.0	60.0	57.5	25.09	0.0	0	0.0	0.0
135AZ - 11	60.0	65.0	62.5	27.27	0.0	0	0.0	0.0
135AZ - 12	65.0	70.0	67.5	29.45	0.0	0	0.0	0.0
135AZ - 13	70.0	75.0	72.5	31.63	0.0	0	0.0	0.0
135AZ - 14	75.0	80.0	77.5	33.82	0.0	0	0.0	0.0
135AZ - 15	80.0	85.0	82.5	36.00	0.0	0	0.0	0.0
135AZ - 16	85.0	90.0	87.5	38.18	0.0	0	0.0	0.0
135AZ - 17	90.0	95.0	92.5	40.36	0.0	0	0.0	0.0
135AZ - 18	95.0	100.0	97.5	42.54	0.0	0	0.0	0.0
Totals					1956.9	231		

Table 47. Sieve data: 180-deg azimuth (back) sector, PAS-4.

ZONE	INSIDE RADIUS (m)	OUTSIDE RADIUS (m)	AVERAGE RADIUS (m)	ZONE AREA (m ²)	WEIGHT (gms)	NUMBER	WT./AREA (gms/m ²)	NO./AREA (no./m ²)
180AZ-1	10.0	15.0	12.5	5.45	0.0	0	0.0	0.0
180AZ-2	15.0	20.0	17.5	7.64	0.0	0	0.0	0.0
180AZ-3	20.0	25.0	22.5	9.82	0.0	0	0.0	0.0
180AZ-4	25.0	30.0	27.5	12.00	0.0	0	0.0	0.0
180AZ-5	30.0	35.0	32.5	14.18	837.2	75	59.0	5.3
180AZ-6	35.0	40.0	37.5	16.36	636.8	82	38.9	5.0
180AZ-7	40.0	45.0	42.5	18.54	0.0	0	0.0	0.0
180AZ-8	45.0	50.0	47.5	20.73	546.7	111	26.4	5.4
180AZ-9	50.0	55.0	52.5	22.91	848.0	149	37.0	6.5
180AZ-10	55.0	60.0	57.5	25.09	831.7	113	33.1	4.5
180AZ-11	60.0	65.0	62.5	27.27	1248.7	157	45.8	5.8
180AZ-12	65.0	70.0	67.5	29.45	723.9	127	24.6	4.3
180AZ-13	70.0	75.0	72.5	31.63	0.0	0	0.0	0.0
180AZ-14	75.0	80.0	77.5	33.82	0.0	0	0.0	0.0
180AZ-15	80.0	85.0	82.5	36.00	0.0	0	0.0	0.0
180AZ-16	85.0	90.0	87.5	38.18	0.0	0	0.0	0.0
180AZ-17	90.0	95.0	92.5	40.36	0.0	0	0.0	0.0
180AZ-18	95.0	100.0	97.5	42.54	0.0	0	0.0	0.0
Totals					5673.0	814		

Table 48. Sieve data: 270-deg azimuth (left side) sector, PAS-4.

ZONE	INSIDE RADIUS (m)	OUTSIDE RADIUS (m)	AVERAGE RADIUS (m)	ZONE AREA (m ²)	WEIGHT (gm.)	NUMBER	WT./AREA (gm./m ²)	NO./AREA (no./m ²)
270AZ-1	10.0	15.0	12.5	5.45	0.0	0	0.0	0.0
270AZ-2	15.0	20.0	17.5	7.64	826.3	157	108.2	20.6
270AZ-3	20.0	25.0	22.5	9.82	1180.0	144	120.2	14.7
270AZ-4	25.0	30.0	27.5	12.00	1526.1	160	127.2	13.3
270AZ-5	30.0	35.0	32.5	14.18	2339.6	209	165.0	14.7
270AZ-6	35.0	40.0	37.5	16.36	1535.3	152	93.8	9.3
270AZ-7	40.0	45.0	42.5	18.54	1785.0	174	96.3	9.4
270AZ-8	45.0	50.0	47.5	20.73	1491.0	193	71.9	9.3
270AZ-9	50.0	55.0	52.5	22.91	0.0	0	0.0	0.0
270AZ-10	55.0	60.0	57.5	25.09	0.0	0	0.0	0.0
270AZ-11	60.0	65.0	62.5	27.27	18733.3	1251	686.9	45.9
270AZ-12	65.0	70.0	67.5	29.45	6377.0	317	216.5	10.8
270AZ-13	70.0	75.0	72.5	31.63	4395.1	139	138.9	4.4
270AZ-14	75.0	80.0	77.5	33.82	3785.5	150	111.9	4.4
270AZ-15	80.0	85.0	82.5	36.00	2255.4	103	62.7	2.9
270AZ-16	85.0	90.0	87.5	38.18	2862.1	139	75.0	3.6
270AZ-17	90.0	95.0	92.5	40.36	1809.0	59	44.8	1.5
270AZ-18	95.0	100.0	97.5	42.54	1406.4	68	33.1	1.6
Totals					52307.1	3415		



Figure 278. Secondary debris from large arch section, PAS-4.

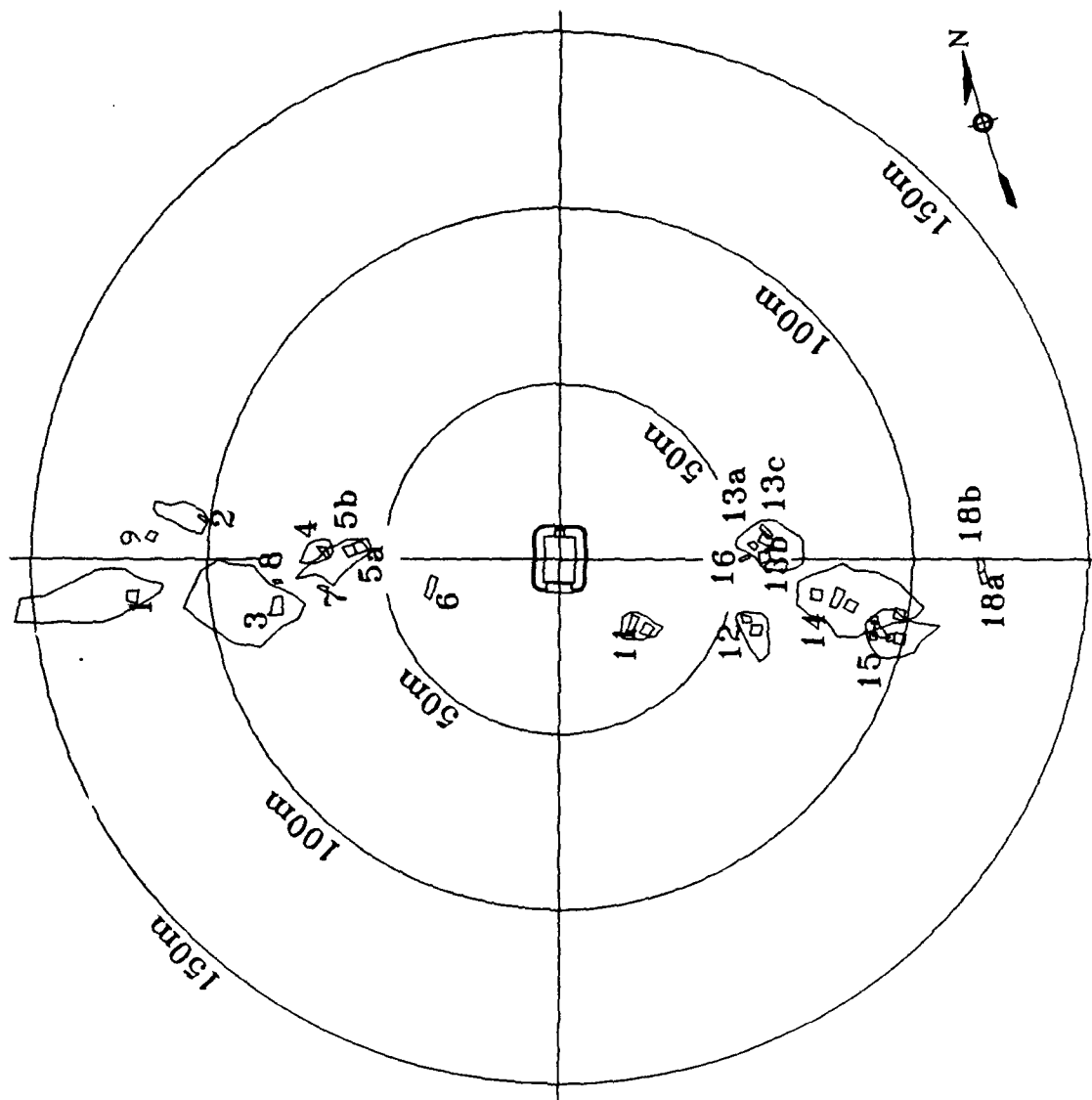


Figure 279. Boundaries of secondary debris from large arch sections, PAS-4.

material. A complete set of this sieve data is presented in Volume V. Tables 49 and 50 are summaries of the data from the 16 3- x 3-m regions within the 12 secondary debris areas.

After the smaller debris from the 3- x 3-m regions was recovered, the larger remaining pieces were marked with an identifying number and taken back to the lab for weighing and measuring. Other identifying features such as color of concrete and color of plastic beads in each piece were noted. These data are summarized in Tables 51 and 52.

Tables 53 and 54 present the weight and number density of the secondary debris in each region.

After the debris from the 6 5-deg sectors and 16 secondary debris regions was recovered, most of the debris larger than 50 mm was located by standard surveying methods. Once the piece of debris was surveyed, it was marked with an identifying number and taken back to the lab for weighing, measuring, and other characterization. The 360-deg survey located and identified 852 pieces of concrete debris. The average shape factor for all pieces was 0.4930. Volume V includes summaries of these concrete debris survey data.

The debris location and identification data were combined into a spreadsheet computer program (LOTUS 1-2-3) and sorted in various ways. The first data sort was by weight from lightest to heaviest. The weights were then scaled up to full-size by multiplying by 27. The scaled-up data were then grouped by weight intervals, and the number of pieces and total weight of debris in each weight interval were determined. A summary of the results is given in Table 55. Figure 280 is a graphical presentation of the information in Table 55. A complete set of data is presented in Volume V.

The second data sort sorted the debris by range from GZ. The debris was sorted into zones of concentric rings 5 m wide. The number of pieces and total weight of debris in each zone were determined. From this data sort the weight densities and number densities could be calculated for each zone. Table 56 presents a summary of this information. Figures 281 and 282 are graphic presentations of the data in Table 56.

Table 49. Weight distribution data from secondary debris regions, PAS-4.

AREA I.D.	WEIGHT RETAINED ON SIEVE (gm)										TOTALS
	SIEVE SIZE (mm)										
	64-51	51-38	38-32	32-25	25-22	22-19	19-16	16-13	13-10		
ARCH 1- 1	0.0	0.0	323.1	974.9	529.0	442.2	342.6	393.5	583.8	3589.1	
ARCH 1- 2	0.0	0.0	76.2	21.0	98.5	112.6	55.2	65.7	85.8	515.0	
ARCH 1- 3	0.0	0.0	51.4	124.3	12.5	22.7	26.2	20.8	7.1	265.0	
ARCH 2- 1	0.0	0.0	186.6	434.9	475.9	438.4	189.3	430.7	435.5	2591.3	
ARCH 3- 1	0.0	0.0	722.8	897.8	275.4	347.0	310.9	268.5	304.1	3126.5	
ARCH 3- 2	0.0	163.0	192.5	260.0	100.0	75.4	94.3	73.8	53.9	1012.9	
ARCH 3- 3	0.0	0.0	405.0	152.1	23.1	16.7	6.3	27.7	0.0	630.9	
ARCH 4- 1	0.0	0.0	460.5	740.6	430.7	335.6	302.6	259.5	202.6	2732.1	
ARCH 5- 1	0.0	1667.0	2367.6	1688.8	1336.3	1313.4	1322.1	1651.8	1848.6	13195.6	
ARCH 11- 1	0.0	0.0	61.0	260.8	167.1	59.9	80.3	87.5	84.1	800.7	
ARCH 12- 1	0.0	0.0	50.1	85.5	55.5	40.2	50.1	24.6	33.4	339.4	
ARCH 13- 1	0.0	0.0	1163.3	2014.1	797.9	843.6	934.5	1192.1	1940.2	8885.7	
ARCH 14- 1	356.6	934.6	1680.2	2297.1	1337.0	1433.9	1276.9	1246.3	2184.4	12747.0	
ARCH 14- 2	0.0	0.0	613.1	1175.3	566.4	714.2	425.9	573.5	930.9	4999.3	
ARCH 14- 3	0.0	0.0	51.4	56.5	33.3	36.8	28.8	60.1	28.3	295.2	
ARCH 15- 1	0.0	0.0	263.4	194.9	86.4	149.2	161.2	80.4	115.7	1051.2	
Totals	356.6	2764.6	8668.2	11378.6	6325.0	6381.8	5607.2	6456.5	8838.4	56776.9	

Table 50. Number distribution data from secondary debris regions, PAS-4.

AREA I.D.	NUMBER RETAINED ON SIEVE (gm.)											TOTALS
	SIEVE SIZE (mm)											
	64-51	51-38	38-32	32-25	25-22	22-19	19-16	16-13	13-10			
ARCH 1-1	0	0	6	31	28	40	47	95	247		494	
ARCH 1-2	0	0	1	1	5	9	7	16	46		85	
ARCH 1-3	0	0	1	4	1	2	4	5	3		20	
ARCH 2-1	0	0	3	13	23	34	25	98	202		398	
ARCH 3-1	0	0	13	27	15	29	41	67	167		359	
ARCH 3-2	0	2	6	8	5	7	13	18	23		82	
ARCH 3-3	0	0	5	4	1	1	1	6	0		18	
ARCH 4-1	0	0	9	22	24	27	41	65	103		291	
ARCH 5-1	0	19	46	59	70	108	167	380	732		1581	
ARCH 11-1	0	0	1	8	8	6	10	23	46		102	
ARCH 12-1	0	0	1	3	3	4	7	6	14		38	
ARCH 13-1	0	0	23	64	42	76	128	286	820		1439	
ARCH 14-1	2	10	30	68	73	117	164	235	913		1612	
ARCH 14-2	0	0	12	37	30	64	59	138	213		553	
ARCH 14-3	0	0	1	2	2	3	4	14	12		38	
ARCH 15-1	0	0	5	6	5	13	22	19	49		119	
Totals	2	31	163	357	335	540	740	1471	3590		7229	
AVE. WT.	178.3	89.2	53.2	31.9	18.9	11.8	7.6	4.4	2.5		7.9	
S.F	0.39	0.42	0.52	0.57	0.61	0.57	0.59	0.60	0.67		0.57	

Table 51. Weight distribution of large pieces from secondary debris regions, PAS-4.

AREA I.D.	WEIGHT OF PIECES IN WEIGHT INTERVAL (gm)															
	WEIGHT INTERVAL (kg)															
	<0.05	0.05-0.1	0.1-0.2	0.2-0.3	0.3-0.4	0.4-0.5	0.5-1.0	1.0-2.0	2.0-3.0	3.0-4.0	>4.0	TOTALS				
ARCH 1-1	87.0	1041.0	1047.8	726.8	772.6	851.5	1626.9	0.0	0.0	3467.5	0.0	9621.1				
ARCH 1-2	90.4	68.1	756.3	291.3	0.0	475.5	1439.3	0.0	0.0	0.0	0.0	3120.9				
ARCH 1-3	0.0	59.0	0.0	216.7	0.0	0.0	576.4	1737.9	0.0	0.0	0.0	2590.0				
ARCH 2-1	137.9	412.5	1193.8	275.0	691.0	0.0	1860.5	0.0	4894.4	3218.2	0.0	12683.3				
ARCH 3-1	135.4	878.2	817.7	249.6	330.4	0.0	765.2	1234.2	0.0	0.0	0.0	4410.7				
ARCH 3-2	47.0	246.5	605.0	244.2	1010.1	0.0	0.0	0.0	4442.3	3099.8	0.0	9694.9				
ARCH 3-3	0.0	95.3	0.0	0.0	0.0	0.0	845.3	1042.4	0.0	0.0	0.0	1983.0				
ARCH 4-1	77.2	938.1	767.7	722.5	335.0	0.0	529.7	1100.1	0.0	0.0	0.0	4470.3				
ARCH 5-1	40.7	1708.9	3665.6	1717.6	725.6	416.8	2001.8	1936.8	4393.2	0.0	0.0	16607.0				
ARCH 11-2	43.4	193.1	263.2	0.0	324.3	404.0	0.0	1682.3	0.0	0.0	0.0	2910.3				
ARCH 12-1	38.8	157.9	0.0	0.0	0.0	0.0	0.0	0.0	0.0	0.0	0.0	196.7				
ARCH 13-1	82.5	1282.4	2980.1	1229.8	667.1	1291.6	3081.6	3137.7	0.0	0.0	0.0	13752.8				
ARCH 14-1	126.2	1020.0	1848.6	776.7	1138.5	1383.4	2979.6	1968.0	2074.3	0.0	0.0	13315.3				
ARCH 14-2	141.7	964.6	2384.5	439.3	1058.2	1385.1	1275.2	0.0	0.0	0.0	0.0	7648.6				
ARCH 14-3	0.0	0.0	0.0	0.0	0.0	452.5	570.2	1118.1	0.0	0.0	0.0	2140.8				
ARCH 15-1	33.4	201.6	490.1	0.0	0.0	0.0	0.0	3291.5	2438.0	0.0	0.0	6454.6				
Totals	1081.6	9267.2	16820.4	6889.5	7052.8	6660.4	17551.7	18249.0	18242.2	9785.5	0.0	111600.3				

Table 52. Number distribution of large pieces from secondary debris regions, PAS-4.

AREA I.D.	NUMBER OF PIECES IN WEIGHT INTERVAL														
	WEIGHT INTERVAL (kg)														
	<0.05	0.05-0.1	0.1-0.2	0.2-0.3	0.3-0.4	0.4-0.5	0.5-1.0	1.0-2.0	2.0-3.0	3.0-4.0	>4.0	TOTALS			
ARCH 1-1	2	15	7	3	2	2	2	0	0	1	0	34			
ARCH 1-2	2	1	6	1	0	1	2	0	0	0	0	13			
ARCH 1-3	0	1	0	1	0	0	1	1	0	0	0	4			
ARCH 2-1	3	6	9	1	2	0	3	0	2	1	0	27			
ARCH 3-1	3	11	7	1	1	0	1	1	0	0	0	25			
ARCH 3-2	1	3	4	1	3	0	0	0	2	1	0	15			
ARCH 3-3	0	1	0	0	0	0	1	1	0	0	0	3			
ARCH 4-1	2	13	6	3	1	0	1	1	0	0	0	27			
ARCH 5-1	1	21	26	7	2	1	3	1	2	0	0	64			
ARCH 11-2	1	3	2	0	1	1	0	1	0	0	0	9			
ARCH 12-1	1	2	0	0	0	0	0	0	0	0	0	3			
ARCH 13-1	2	18	22	5	2	3	4	2	0	0	0	58			
ARCH 14-1	3	12	13	3	3	3	4	1	1	0	0	43			
ARCH 14-2	4	13	17	2	3	3	2	0	0	0	0	44			
ARCH 14-3	0	0	0	0	0	1	1	1	0	0	0	3			
ARCH 15-1	1	3	3	0	0	0	0	2	1	0	0	10			
Totals	26	123	122	28	20	15	25	12	8	3	0	382			
AVE. WT	41.6	75.3	137.9	246.1	352.6	444.0	702.1	1520.8	2280.3	3261.8		292.1			

Table 53. Weight and number densities of small pieces from secondary debris, PAS-4.

ZONE	DISTANCE FROM ARCH SECTION, (m)	ZONE AREA (m ²)	WEIGHT (gm)	NUMBER	WT./AREA (gm /m ²)	NO./AREA (no./m ²)
ARCH 1- 1	6.3	9.00	3589.1	494	398.8	54.9
ARCH 1- 2	13.7	9.00	515.0	85	57.2	9.4
ARCH 1- 3	21.5	9.00	265.0	20	29.4	2.2
ARCH 2- 1	5.5	9.00	2591.3	398	287.9	44.2
ARCH 3- 1	5.2	9.00	3126.5	359	347.4	39.9
ARCH 3- 2	11.7	9.00	1012.9	82	112.5	9.1
ARCH 3- 3	17.8	9.00	630.9	18	70.1	2.0
ARCH 4- 1	4.6	9.00	2732.1	291	303.6	32.3
ARCH 5- 1	5.5	9.00	13195.6	1581	1466.2	175.7
ARCH 11- 1	4.8	9.00	800.7	102	89.0	11.3
ARCH 12- 1	4.1	9.00	339.4	38	37.7	4.2
ARCH 13- 1	5.0	9.00	8885.7	1439	987.3	159.9
ARCH 14- 1	6.0	9.00	12747.0	1612	1416.3	179.1
ARCH 14- 2	4.6	9.00	4999.3	553	555.5	61.4
ARCH 14- 3	18.7	9.00	295.2	38	32.8	4.2
ARCH 15- 1	6.4	9.00	1051.2	119	116.8	13.2
Totals			56776.9	7229		

Table 54. Weight and number densities of large pieces from secondary debris, PAS-4.

ZONE	DISTANCE FROM ARCH SECTION, (m)	ZONE AREA (m ²)	WEIGHT (gm)	NUMBER	WT./AREA (gm /m ²)	NO./AREA (no./m ²)
ARCH 1- 1	6.3	9.00	9621.1	34	1069.0	3.8
ARCH 1- 2	13.7	9.00	3120.9	13	346.8	1.4
ARCH 1- 3	21.5	9.00	2590.0	4	287.8	0.4
ARCH 2- 1	5.5	9.00	12683.3	27	1409.3	3.0
ARCH 3- 1	5.2	9.00	4410.7	25	490.1	2.8
ARCH 3- 2	11.7	9.00	9694.9	15	1077.2	1.7
ARCH 3- 3	17.8	9.00	1983.0	3	220.3	0.3
ARCH 4- 1	4.6	9.00	4470.3	27	496.7	3.0
ARCH 5- 1	5.5	9.00	16607.0	64	1845.2	7.1
ARCH 11- 1	4.8	9.00	2910.3	9	323.4	1.0
ARCH 12- 1	4.1	9.00	196.7	3	21.9	0.3
ARCH 13- 1	5.0	9.00	13752.8	58	1528.1	6.4
ARCH 14- 1	6.0	9.00	13315.3	43	1479.5	4.8
ARCH 14- 2	4.6	9.00	7648.6	44	849.8	4.9
ARCH 14- 3	18.7	9.00	2140.8	3	237.9	0.3
ARCH 15- 1	6.4	9.00	6454.6	10	717.2	1.1
Totals			111600.3	382		

Table 55. Scaled-up mass distribution (no sieve data), PAS-4.

WEIGHT INTERVAL (kg)	WEIGHT INTERVAL (lb)	NUMBER OF PIECES	TOTAL WEIGHT (kg)	TOTAL WEIGHT (lb)
0.79 - 1.47	1.75 - 3.25	5	5.10	11.24
1.47 - 2.15	3.25 - 4.75	10	18.07	39.83
2.15 - 3.06	4.75 - 6.75	14	38.73	85.38
3.06 - 4.20	6.75 - 9.25	32	117.26	258.52
4.20 - 5.56	9.25 - 12.25	61	300.20	661.82
5.56 - 7.60	12.25 - 16.75	82	520.64	1147.82
7.60 - 8.28	16.75 - 18.25	34	264.07	582.18
8.28 - 9.87	18.25 - 21.75	72	647.77	1428.08
9.87 - 10.55	21.75 - 23.25	30	307.64	678.23
10.55 - 12.13	23.25 - 26.75	59	666.52	1469.41
12.13 - 12.81	26.75 - 28.25	19	238.60	526.02
12.81 - 14.40	28.25 - 31.75	38	518.83	1143.83
14.40 - 15.08	31.75 - 33.25	17	249.96	551.07
15.08 - 16.67	33.25 - 36.75	43	680.32	1499.86
16.67 - 19.62	36.75 - 43.25	47	850.03	1873.99
19.62 - 25.74	43.25 - 56.75	91	2045.36	4509.25
25.74 - 28.69	56.75 - 63.25	20	547.73	1207.53
28.69 - 34.81	63.25 - 76.75	44	1378.97	3040.10
34.81 - 40.94	76.75 - 90.25	28	1063.44	2344.49
40.94 - 47.06	90.25 - 103.75	27	1178.70	2598.58
47.06 - 59.08	103.75 - 130.25	27	1425.95	3143.67
59.08 - 71.10	130.25 - 156.75	20	1265.71	2790.41
71.10 - 95.37	156.75 - 210.25	14	1131.12	2493.68
>95.37	>210.25	18	2975.08	6558.92
Totals		852	18435.78	40643.93

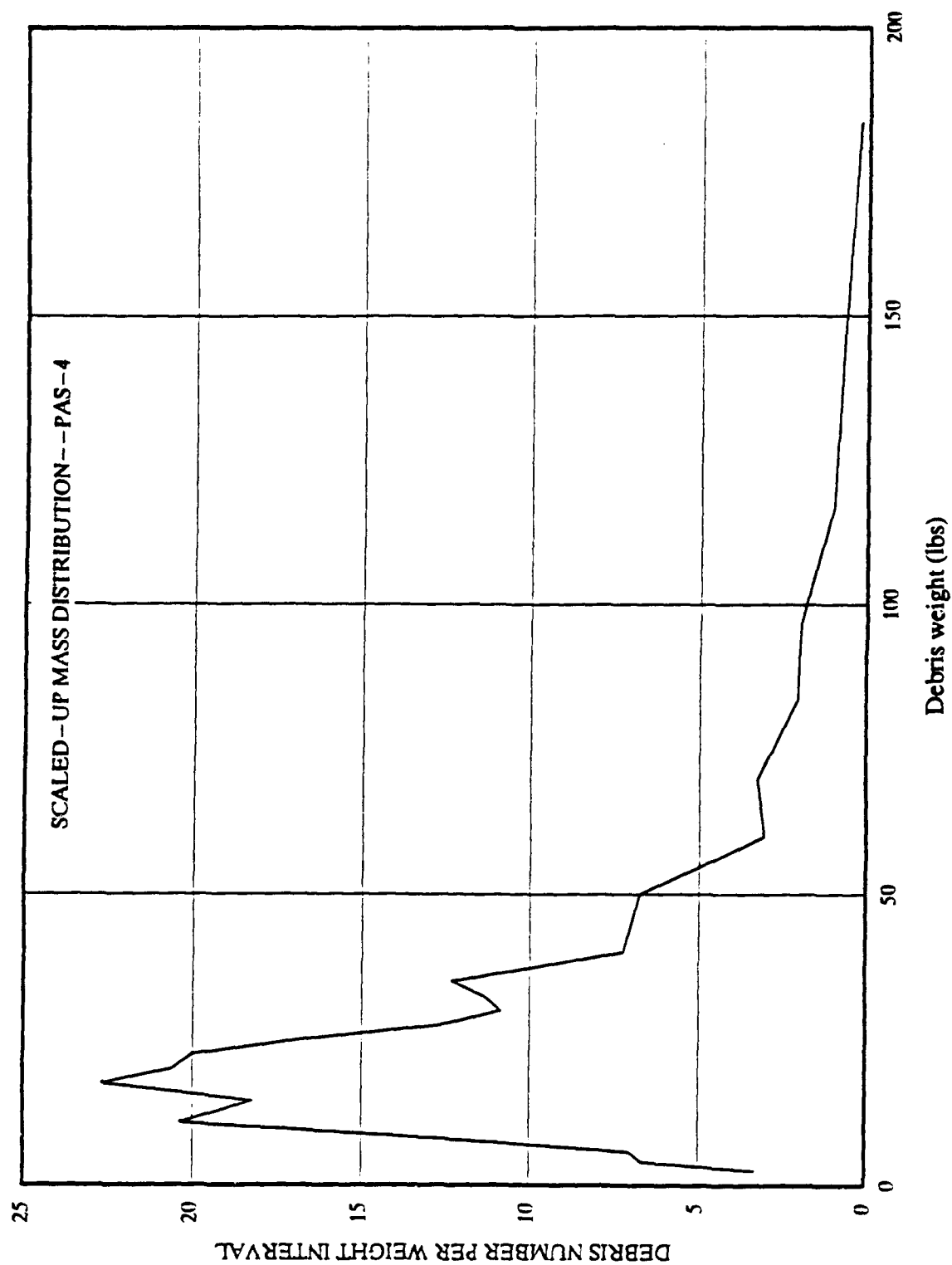


Figure 280. Scaled-up mass distribution (no sieve data).

Table 56. Weight and quantity distribution (no sieve data), PAS-4.

ZONE R1 TO R2 (m) (m)		WEIGHT IN ZONE (gm)	NUMBER IN ZONE	ZONE AREA (m ²)	WT./AREA (gm/m ²)	NO./AREA (No./m ²)
0 TO 10		0.0	0	314.16	0.000	0.00000
10 TO 15		7737.8	6	392.70	19.704	0.01528
15 TO 20		22087.9	24	549.78	40.176	0.04365
20 TO 25		33682.0	29	706.86	47.650	0.04103
25 TO 30		58490.7	68	863.94	67.702	0.07871
30 TO 35		48811.8	54	1021.02	47.807	0.05289
35 TO 40		41228.8	60	1178.10	34.996	0.05093
40 TO 45		47040.4	67	1335.18	35.232	0.05018
45 TO 50		57732.2	75	1492.26	38.688	0.05026
50 TO 55		37416.6	51	1649.34	22.686	0.03092
55 TO 60		40001.6	68	1806.42	22.144	0.03764
60 TO 65		20432.9	49	1963.50	10.406	0.02496
65 TO 70		42979.8	45	2120.58	20.268	0.02122
70 TO 75		36145.5	37	2277.65	15.870	0.01624
75 TO 80		20649.5	25	2434.73	8.481	0.01027
80 TO 85		26268.0	28	2591.81	10.135	0.01080
85 TO 90		16339.8	17	2748.89	5.944	0.00618
90 TO 95		49147.0	17	2905.97	16.912	0.00585
95 TO 100		9944.0	13	3063.05	3.246	0.00424
100 TO 105		6473.3	12	3220.13	2.010	0.00373
105 TO 110		5933.8	12	3377.21	1.757	0.00355
110 TO 115		10044.5	12	3534.29	2.842	0.00340
115 TO 120		7069.4	12	3691.37	1.915	0.00325
120 TO 125		5619.6	8	3848.45	1.460	0.00208
125 TO 130		3964.4	8	4005.53	0.990	0.00200
130 TO 135		5939.4	13	4162.61	1.427	0.00312
135 TO 140		2253.2	6	4319.69	0.522	0.00139
140 TO 145		5254.4	7	4476.77	1.174	0.00156
145 TO 150		4098.5	5	4633.85	0.884	0.00108
150 TO 155		353.8	2	4790.93	0.074	0.00042
155 TO 160		936.5	3	4948.01	0.189	0.00061
160 TO 165		3928.1	4	5105.09	0.769	0.00078
165 TO 170		547.0	2	5262.17	0.104	0.00038
170 TO 175		194.7	1	5419.25	0.036	0.00018
175 TO 180		1253.6	3	5576.33	0.225	0.00054
180 TO 185		54.7	1	5733.41	0.010	0.00017
185 TO 190		0.0	0	5890.49	0.000	0.00000
190 TO 195		884.1	1	6047.57	0.146	0.00017
195 TO 200		61.0	1	6204.65	0.010	0.00016

Table 56. Concluded.

ZONE R1 TO R2 (m) (m)			WEIGHT IN ZONE (gm.)	NUMBER IN ZONE	ZONE AREA (m ²)	WT./AREA (gm/m ²)	NO./AREA (No./m ²)
200	TO	205	0.0	0	6361.73	0.000	0.00000
205	TO	210	0.0	0	6518.80	0.000	0.00000
210	TO	215	0.0	0	6675.88	0.000	0.00000
215	TO	220	0.0	0	6832.96	0.000	0.00000
220	TO	225	0.0	0	6990.04	0.000	0.00000
225	TO	230	636.4	2	7147.12	0.089	0.00028
230	TO	235	0.0	0	7304.20	0.000	0.00000
235	TO	240	0.0	0	7461.28	0.000	0.00000
240	TO	245	218.9	1	7618.36	0.029	0.00013
245	TO	250	0.0	0	7775.44	0.000	0.00000
250	TO	255	572.5	2	7932.52	0.072	0.00025
255	TO	260	0.0	0	8089.60	0.000	0.00000
260	TO	265	0.0	0	8246.68	0.000	0.00000
265	TO	270	0.0	0	8403.76	0.000	0.00000
270	TO	275	0.0	0	8560.84	0.000	0.00000
275	TO	280	261.5	1	8717.92	0.030	0.00011
Totals			682689.6	852			

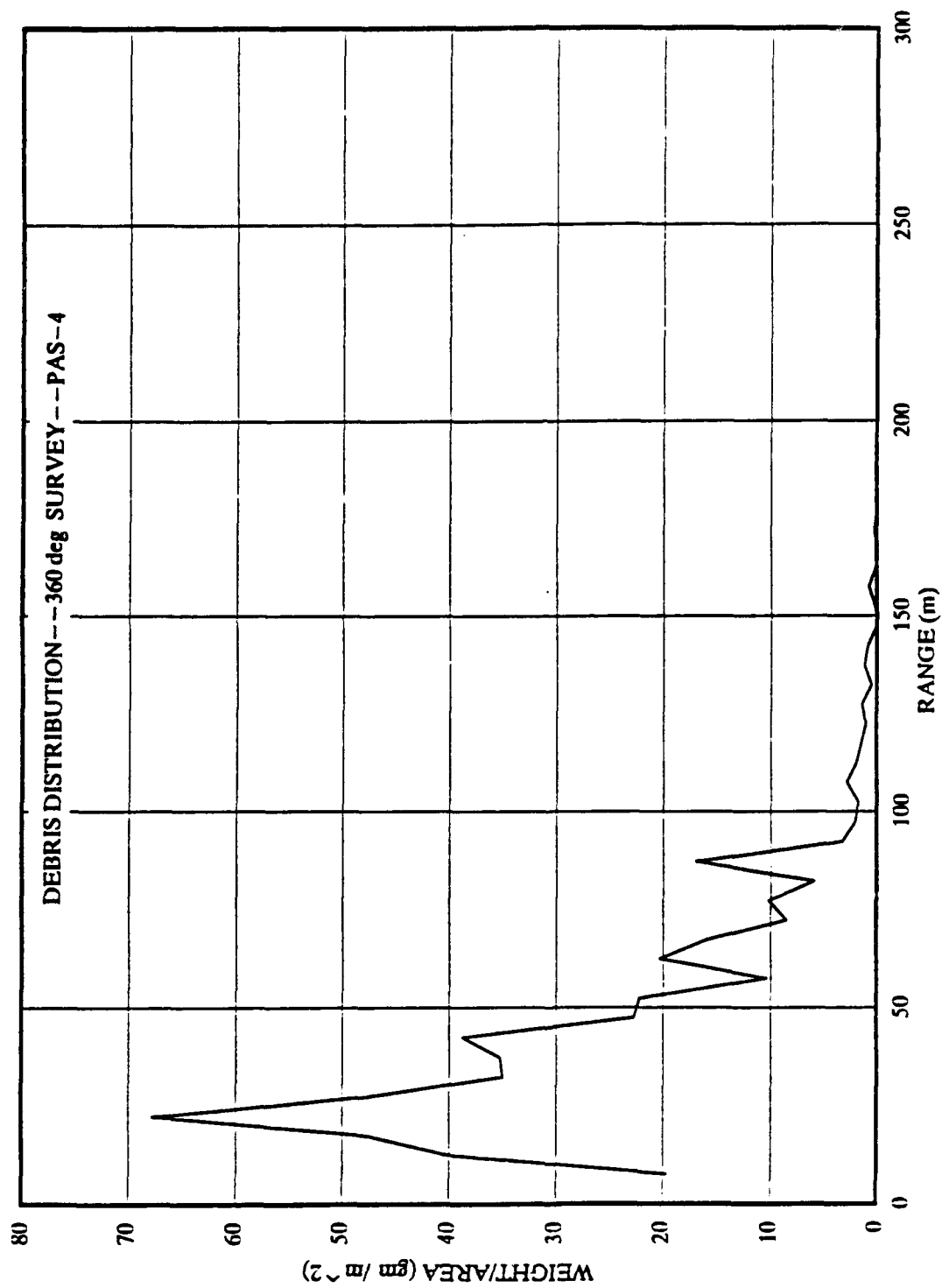


Figure 281. Plot of weight of debris versus range of concentric zone.

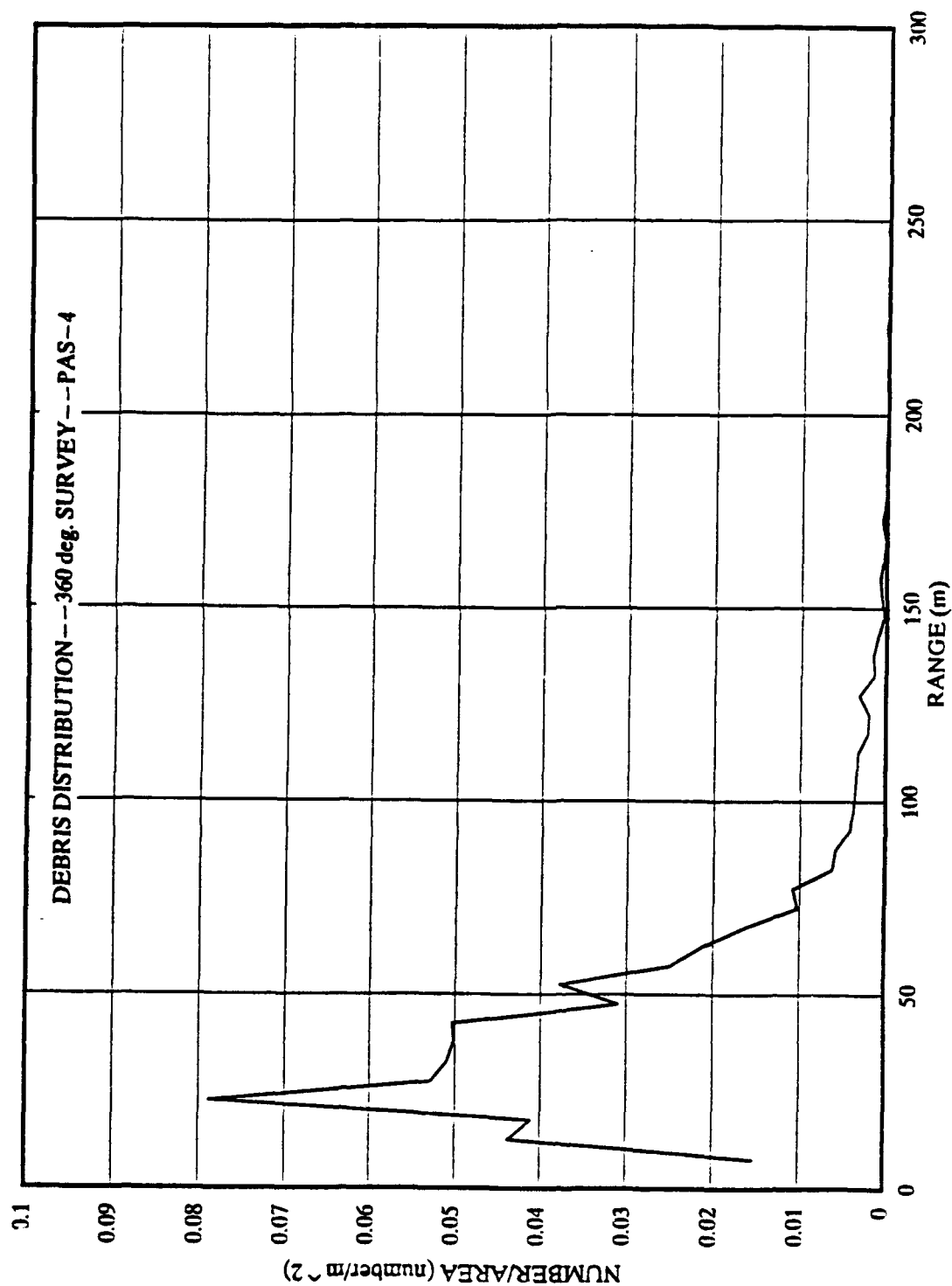


Figure 282. Plot of number of pieces of debris versus range of concentric zone.

A second calculation on these data provided the cumulative weight and quantity distribution in the concentric zones, beginning at the structure and working outward. Table 57 presents a summary of this information. Figures 283 and 284 are graphic presentations of the data in Table 57.

The database was sorted a third time by color of concrete. This information is presented in Volume V.

A sieve analysis was made of all debris recovered from the catcher bins that was smaller than 50 mm. Tables 58 and 59 present the results of that sieve analysis. Larger pieces of debris were measured, weighed, and identified. Table 60 presents the data on the larger pieces of debris found in the catcher bins.

Large debris included the front door, exhaust port doors and frames, the steel vestibule, the 23 arch sections, and large pieces of concrete from the wingwalls, front walls, and exhaust port. Table 61 is a summary of the locations of the large pieces of debris in PAS-4.

One of the more noticeable results of the test was the relatively large amount of rock from the berm scattered around the structure (Fig. 285). The distribution density of the rock far exceeded the concrete debris, particularly to the sides of the structure. As noted in the discussion of structural response, most of the rock debris came from an area adjacent to the structure. It is estimated that the volume of rock ejected during the test was about 15-20 percent of the total rock berm on either side of the arch. The limits of the rock distribution were surveyed and are illustrated in Figure 286.

During the recovery of concrete debris from the 5-deg sector (90- and 270-deg azimuth), the rocks ejected from the berm within each segment were also collected. Tables 62 and 63 present the weights and number of rocks collected in each segment.

Table 57. Cumulative weight and quantity distribution, PAS-4.

ZONE R1 TO R2 (m) (m)		CUMULATIVE WEIGHT (gm)	PERCENT OF TOTAL WEIGHT	CUMULATIVE NUMBER	PERCENT OF TOTAL NUMBER
0 TO 10		0.0	0.00	0	0.00
10 TO 15		7737.8	1.13	6	0.70
15 TO 20		29825.7	4.37	30	3.52
20 TO 25		63507.7	9.30	59	6.92
25 TO 30		121998.4	17.87	127	14.91
30 TO 35		170810.2	25.02	181	21.24
35 TO 40		212039.0	31.06	241	28.29
40 TO 45		259079.4	37.95	308	36.15
45 TO 50		316811.6	46.41	383	44.95
50 TO 55		354228.2	51.89	434	50.94
55 TO 60		394229.8	57.75	502	58.92
60 TO 65		414662.7	60.74	551	64.67
65 TO 70		457642.5	67.04	596	69.95
70 TO 75		493788.0	72.33	633	74.30
75 TO 80		514437.5	75.35	658	77.23
80 TO 85		540705.5	79.20	686	80.52
85 TO 90		557045.3	81.60	703	82.51
90 TO 95		606192.3	88.79	720	84.51
95 TO 100		616136.3	90.25	733	86.03
100 TO 105		622609.6	91.20	745	87.44
105 TO 110		628543.4	92.07	757	88.85
110 TO 115		638587.9	93.54	769	90.26
115 TO 120		645657.3	94.58	781	91.67
120 TO 125		651276.9	95.40	789	92.61
125 TO 130		655241.3	95.98	797	93.54
130 TO 135		661180.7	96.85	810	95.07
135 TO 140		663433.9	97.18	816	95.77
140 TO 145		668688.3	97.95	823	96.60
145 TO 150		672786.8	98.55	828	97.18
150 TO 155		673140.6	98.60	830	97.42
155 TO 160		674077.1	98.74	833	97.77
160 TO 165		678005.2	99.31	837	98.24
165 TO 170		678552.2	99.39	839	98.47
170 TO 175		678746.9	99.42	840	98.59
175 TO 180		680000.5	99.61	843	98.94
180 TO 185		680055.2	99.61	844	99.06
185 TO 190		680055.2	99.61	844	99.06
190 TO 195		680939.3	99.74	845	99.18
195 TO 200		681000.3	99.75	846	99.30

Table 57. Concluded.

ZONE R1 TO R2 (m) (m)			CUMULATIVE WEIGHT (gm)	PERCENT OF TOTAL WEIGHT	CUMULATIVE NUMBER	PERCENT OF TOTAL NUMBER
200	TO	205	681000.3	99.75	846	99.30
205	TO	210	681000.3	99.75	846	99.30
210	TO	215	681000.3	99.75	846	99.30
215	TO	220	681000.3	99.75	846	99.30
220	TO	225	681000.3	99.75	846	99.30
225	TO	230	681636.7	99.85	848	99.53
230	TO	235	681636.7	99.85	848	99.53
235	TO	240	681636.7	99.85	848	99.53
240	TO	245	681855.6	99.88	849	99.65
245	TO	250	681855.6	99.88	849	99.65
250	TO	255	682428.1	99.96	851	99.88
255	TO	260	682428.1	99.96	851	99.88
260	TO	265	682428.1	99.96	851	99.88
265	TO	270	682428.1	99.96	851	99.88
270	TO	275	682428.1	99.96	851	99.88
275	TO	280	682689.6	100.00	852	100.00

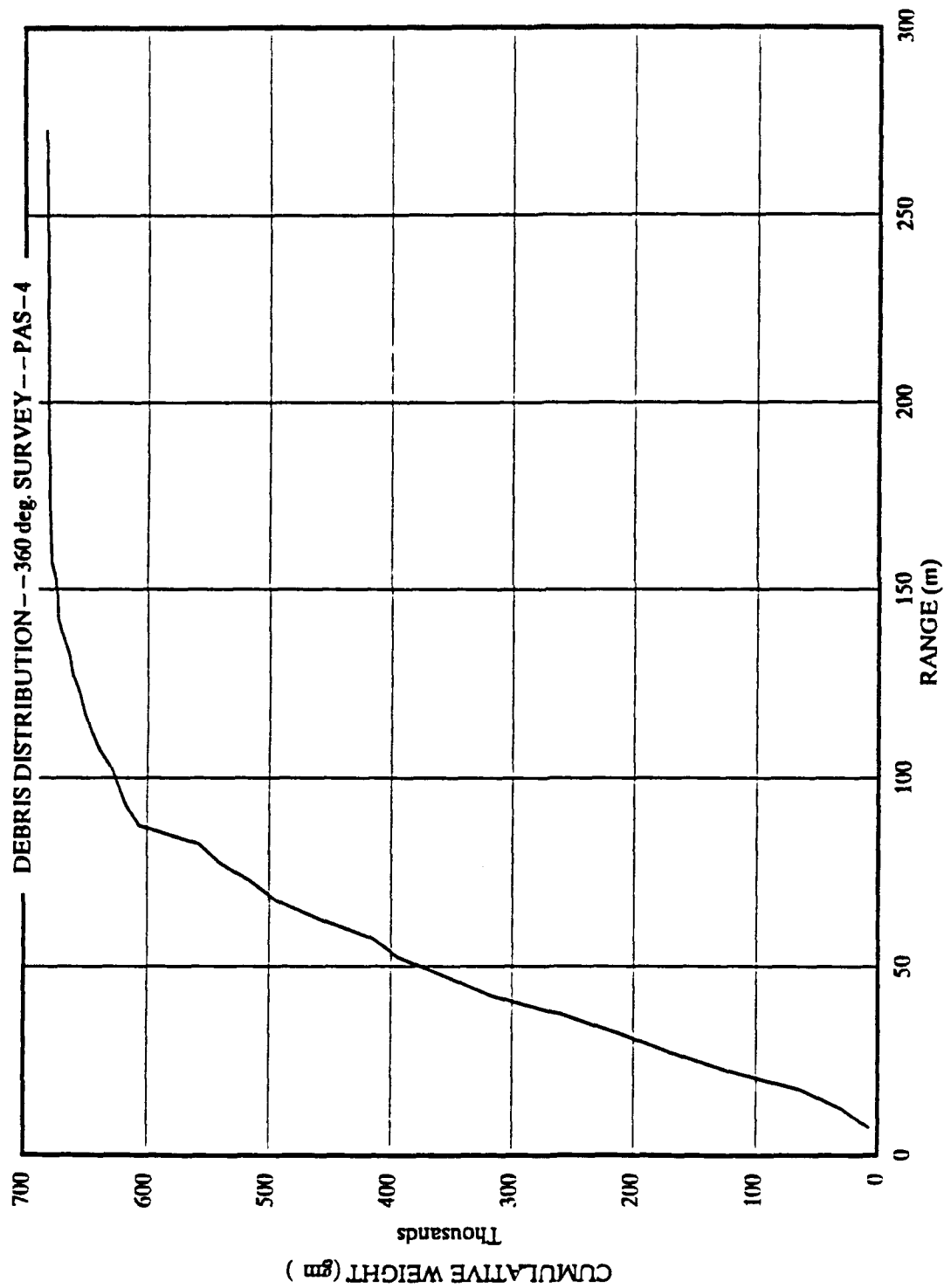


Figure 283. Cumulative weight of debris versus range of concentric zone.

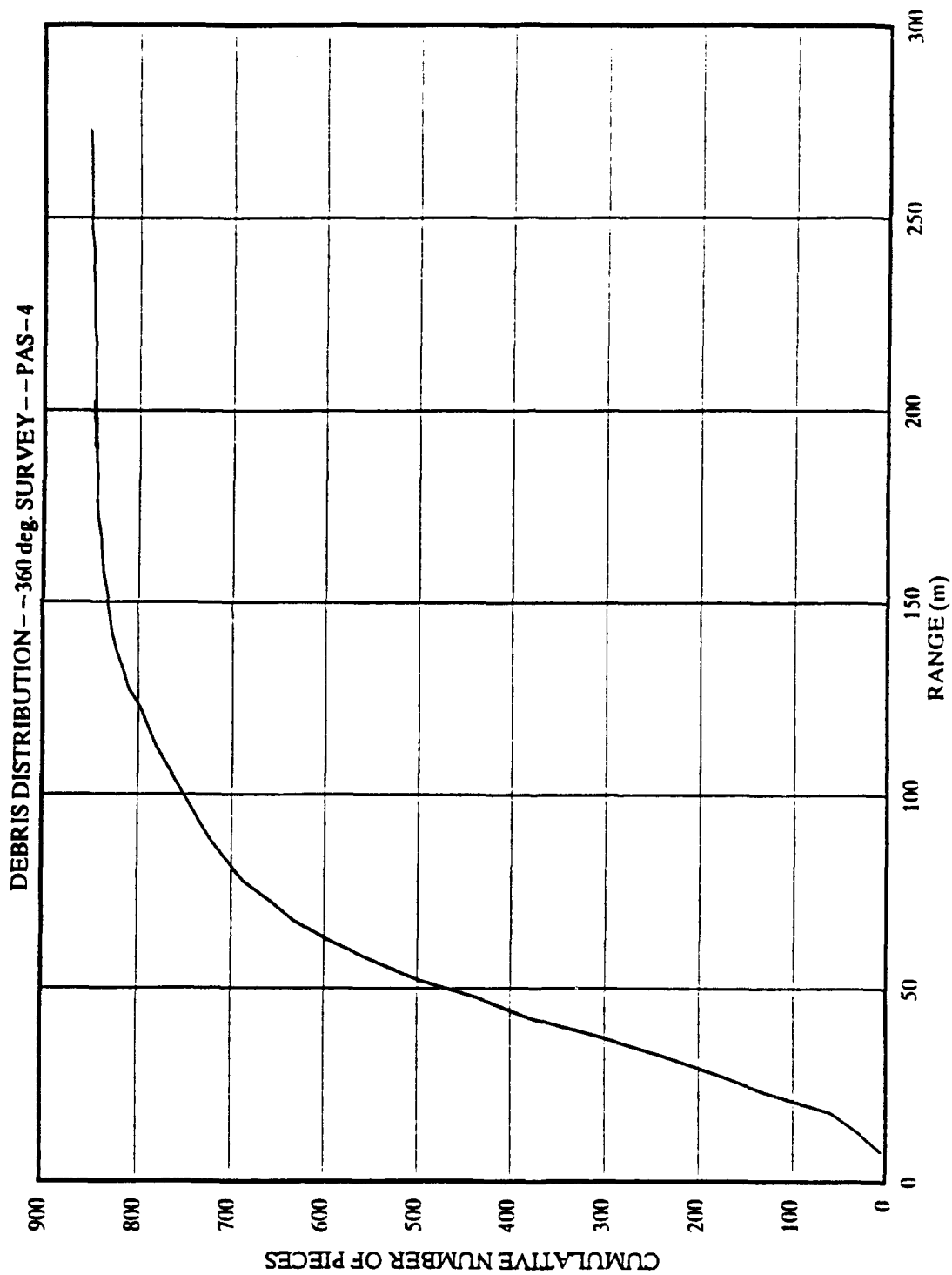


Figure 284. Cumulative number of pieces of debris versus range of concentric zone.

Table 58. Weight distribution of debris from catcher bins, PAS-4.

BIN No.		WEIGHT RETAINED ON SIEVE (gm)													TOTALS
		SIEVE SIZE (mm)													
		102-76	76-64	64-51	51-38	38-32	32-25	25-22	22-19	19-16	16-13	13-10			
BIN- 1	0.0	0.0	0.0	0.0	0.0	0.0	0.0	0.0	0.0	14.9	3.3	15.6	33.8		
BIN- 2	0.0	0.0	0.0	112.7	61.5	0.0	0.0	0.0	0.0	19.3	12.2	14.6	220.3		
BIN- 3	0.0	0.0	0.0	0.0	0.0	28.5	0.0	13.2	26.9	26.9	17.0	7.2	92.8		
BIN- 4	0.0	0.0	0.0	0.0	134.0	107.0	28.9	24.1	8.8	39.6	20.4	362.8			
BIN- 5	0.0	0.0	0.0	0.0	0.0	0.0	0.0	31.2	12.8	23.7	16.8	84.5			
BIN- 6	0.0	0.0	0.0	0.0	0.0	64.7	15.5	0.0	8.8	10.1	22.2	121.3			
BIN- 7	0.0	0.0	0.0	167.8	0.0	0.0	17.9	12.5	14.3	9.8	25.5	247.8			
BIN- 8	0.0	259.8	161.5	0.0	52.3	123.9	15.6	20.3	18.1	16.8	9.7	678.0			
BIN- 9	0.0	0.0	213.3	0.0	248.5	35.8	35.2	41.5	57.8	39.8	34.1	706.0			
BIN- 10	941.3	0.0	0.0	122.0	202.8	43.2	38.8	35.6	35.5	10.1	25.4	1454.7			
BIN- 11	0.0	0.0	0.0	0.0	198.1	101.3	60.8	73.9	15.5	24.5	34.9	509.0			
BIN- 12	0.0	0.0	0.0	246.0	0.0	42.5	0.0	23.4	11.9	24.1	11.5	359.4			
BIN- 13	0.0	0.0	0.0	0.0	0.0	29.7	0.0	0.0	13.4	20.7	23.3	87.1			
BIN- 14	0.0	0.0	0.0	93.8	0.0	27.5	22.3	37.1	6.9	10.5	11.1	209.2			
BIN- 15	0.0	540.3	0.0	190.6	53.0	145.7	69.3	40.9	0.0	31.3	30.5	1101.6			
BIN- 16	0.0	0.0	0.0	0.0	145.9	23.3	0.0	19.9	11.0	13.8	13.3	227.2			
BIN- 17	700.0	0.0	0.0	195.7	102.6	177.7	13.7	12.7	13.1	18.4	19.0	1252.9			
BIN- 18	0.0	0.0	0.0	0.0	43.9	104.6	0.0	25.4	22.2	5.3	10.9	212.3			
BIN- 19	0.0	0.0	0.0	0.0	43.8	93.4	18.9	26.0	0.0	6.9	4.1	193.1			
BIN- 20	0.0	681.1	0.0	80.7	0.0	55.4	0.0	0.0	0.0	2.4	8.1	827.7			
BIN- 21	0.0	0.0	0.0	176.0	0.0	31.5	0.0	0.0	0.0	5.5	0.0	213.0			
BIN- 22	0.0	0.0	0.0	0.0	0.0	0.0	20.2	9.1	0.0	4.2	6.5	40.0			
BIN- 23	0.0	503.3	0.0	0.0	84.5	0.0	15.0	0.0	15.2	3.6	3.4	625.0			
BIN- 24	0.0	706.3	0.0	0.0	53.6	82.5	0.0	0.0	0.0	3.9	4.6	850.9			
BIN- 25	0.0	0.0	290.6	0.0	0.0	0.0	0.0	10.3	5.4	0.0	1.4	307.7			
Totals	1641.3	2690.8	665.4	1385.3	1424.5	1318.2	372.1	457.1	331.8	357.5	374.1	11018.1			

Table 59. Number distribution of debris from catcher bins, PAS-4.

BIN No.	NUMBER RETAINED ON SIEVE (gm)													TOTALS
	SIEVE SIZE (mm)													
	102-76	76-64	64-51	51-38	38-32	32-25	25-22	22-19	19-16	16-13	13-10			
BIN-1	0	0	0	0	0	0	0	0	2	1	8	11		
BIN-2	0	0	0	1	1	0	0	0	3	3	7	15		
BIN-3	0	0	0	0	0	1	0	1	4	4	4	14		
BIN-4	0	0	0	0	2	3	2	2	1	10	10	30		
BIN-5	0	0	0	0	0	0	0	3	2	6	9	20		
BIN-6	0	0	0	0	0	2	1	0	1	3	12	19		
BIN-7	0	0	0	2	0	0	1	1	2	3	13	22		
BIN-8	0	1	1	0	1	4	1	2	3	4	5	22		
BIN-9	0	0	1	0	4	1	2	4	8	10	17	47		
BIN-10	1	0	0	1	4	1	2	3	5	3	13	33		
BIN-11	0	0	0	0	4	3	3	6	2	6	18	42		
BIN-12	0	0	0	2	0	1	0	2	2	6	6	19		
BIN-13	0	0	0	0	0	1	0	0	2	5	12	20		
BIN-14	0	0	0	1	0	1	1	3	1	3	5	15		
BIN-15	0	1	0	2	1	5	4	4	0	8	15	40		
BIN-16	0	0	0	0	3	1	0	2	2	4	7	19		
BIN-17	1	0	0	2	2	5	1	1	2	5	9	28		
BIN-18	0	0	0	0	1	3	0	2	3	1	5	15		
BIN-19	0	0	0	0	1	3	1	2	0	2	2	11		
BIN-20	0	2	0	1	0	2	0	0	0	1	4	10		
BIN-21	0	0	0	2	0	1	0	0	0	1	0	4		
BIN-22	0	0	0	0	0	0	1	1	0	1	3	6		
BIN-23	0	1	0	0	2	0	1	0	2	1	2	9		
BIN-24	0	2	0	0	1	2	0	0	0	1	2	8		
BIN-25	0	0	1	0	0	0	0	1	1	0	1	4		
Totals	2	7	3	14	27	40	21	40	48	92	189	483		
AVE. WT.	820.7	384.4	221.8	99.0	52.8	33.0	17.7	11.4	6.9	3.9	2.0	22.8		
S.F	0.49	0.47	0.49	0.47	0.51	0.59	0.57	0.55	0.54	0.53	0.54	0.54		

Table 60. Larger pieces of debris from catcher bins, PAS-4.

BIN NO.	RADIUS (m)	WEIGHT (kg)
BIN- 1	40.0	0.0
BIN- 2	40.0	0.0
BIN- 3	40.0	0.0
BIN- 4	40.0	0.0
BIN- 5	40.0	0.0
BIN- 6	40.0	0.0
BIN- 7	40.0	0.0
BIN- 8	40.0	5.0
BIN- 9	40.0	13.7
BIN- 10	40.0	42.3
BIN- 11	40.0	65.6
BIN- 12	50.0	8.6
BIN- 13	50.0	15.2
BIN- 14	50.0	27.9
BIN- 15	50.0	11.3
BIN- 16	50.0	9.8
BIN- 17	50.0	3.9
BIN- 18	50.0	0.0
BIN- 19	50.0	0.0
BIN- 20	50.0	0.0
BIN- 21	50.0	0.0
BIN- 22	50.0	0.0
BIN- 23	50.0	0.0
BIN- 24	50.0	0.0
BIN- 25	50.0	0.0
BIN- 26	50.0	0.0
Totals		203.3



Figure 285. Posttest distribution of rocks from left berm, PAS-4.

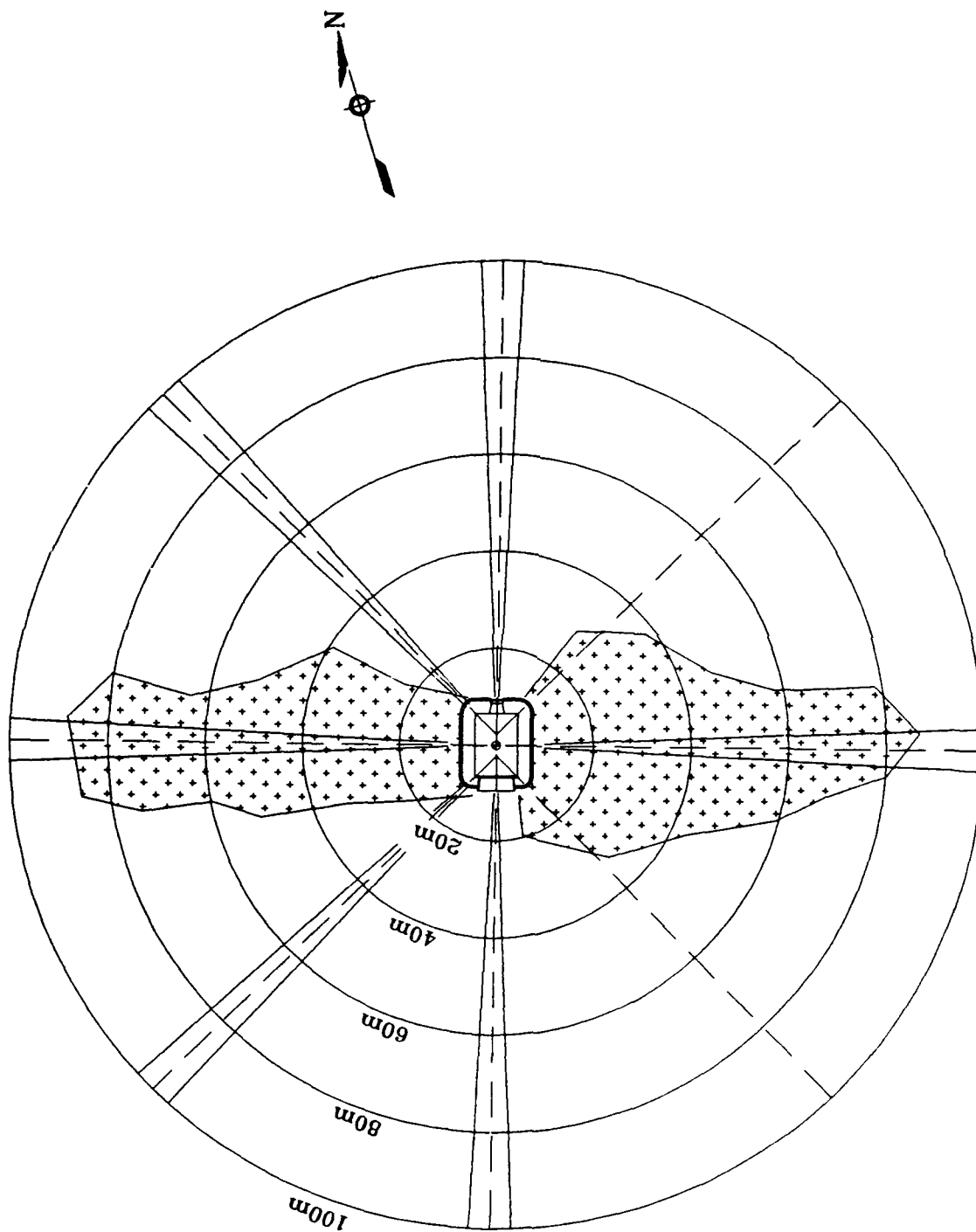


Figure 286. Distribution of rocks from berm, PAS-4.

Table 61. Locations of large debris, PAS-4.

ITEM	COORDINATES		FROM GZ:	
	X (mm)	Y (mm)	RANGE (mm)	AZIMUTH (deg)
FRONT DOOR	-398168	57669	409071	8.10
RIGHT FRONT WALL (#20)	-1716	23865	25345	70.32
PART OF LEFT FRONT WALL (#17)	-3933	75431	76193	278.11
PERSONNEL VESTIBULE	-20409	-16318	28118	322.23
TOP SECTION OF BACKWALL ("B")	23771	61	16953	179.79
TOP SECTION OF BACKWALL ("C")	25363	1228	18585	176.21
EXHAUST PORT ROOF ("A")	23110	-1385	16350	184.86
EXHAUST PORT ROOF ("D")	27981	2022	21260	174.54
EXHAUST PORT ROOF ("E")	31479	660	24670	178.47
Rt. EXHAUST PORT DOOR (416)	121276	12622	115151	173.71
Lt. EXHAUST PORT DOOR	113766	-23739	109551	192.51
E.P. DOOR FRAME (422)	49566	383	42750	179.49
E.P. DOOR FRAME (415)	88924	5831	82313	175.94
E.P. DOOR FRAME (1390)	82456	-33437	82699	203.85
E.P. DOOR FRAME (1395)	85160	-14961	79758	190.81
E.P. DOOR FRAME (1398)	77393	-10232	71313	188.25
E.P. DOOR FRAME (1399)	77386	-8559	71085	186.92
E.P. DOOR FRAME (1403)	107348	-1629	100543	180.93
1200x600x100 E.P. CONCRETE (1385)	51215	-18080	47937	202.16
760x850x100 E.P. CONCRETE (1409)	69089	7766	62753	172.89
880x480x180 E.P. CONCRETE ("F")	28190	961	21394	177.43
600x300x140 E.P. CONCRETE ("G")	29190	473	22377	178.79
700x520x140 E.P. CONCRETE ("H")	29852	828	23049	177.94
770x770x100 E.P. CONCRETE ("I")	82442	2981	75683	177.74
1250x150x150 ARCH CONCRETE ("J")	33048	-21734	34065	219.65
460x220x90 ARCH CONCRETE (1425)	33928	73284	78137	110.30
630x760x140 Lt. W.W. CONCRETE (723)	-19304	-36385	44791	305.68
1150x830x130 Rt. W.W. CONCRETE (#19)	-9342	23973	28911	56.02

Table 61. Concluded.

ITEM	COORDINATES		FROM GZ:	
	X (mm)	Y (mm)	RANGE (mm)	AZIMUTH (deg)
ARCH #1	-3773	121258	121720	85.01
ARCH #2	18846	101831	102539	96.73
ARCH #3	-6938	80705	81869	80.33
ARCH #4	8815	66878	66908	91.71
ARCH #5 A&B	10015	57778	57866	93.17
ARCH #6	-1133	36467	37324	77.70
ARCH #7	-1359	67459	67953	83.09
ARCH #8	377	79967	80226	85.40
ARCH #9	13466	115933	116123	93.28
ARCH #11	-12190	-21179	28458	311.91
ARCH #12	-10286	-53059	55748	287.87
ARCH #13A	10918	-54886	55039	265.72
ARCH #13 B&C	12663	-58189	58482	264.26
ARCH #14	-4320	-78564	79350	278.07
ARCH #15A	-15221	-88957	91646	283.91
ARCH #15B	-15690	-93737	96401	283.50
ARCH #15C	-10604	-89086	90774	281.07
ARCH #16	7081	-52150	52151	269.71
ARCH #18 A&B	3512	119559	119605	271.58

Table 62. Rock rubble from 5-deg sector, 90-deg azimuth, PAS-4.

ZONE	INSIDE RADIUS (m)	OUTSIDE RADIUS (m)	AVERAGE RADIUS (m)	ZONE AREA (m ²)	WEIGHT (kg)	NUMBER	WT./AREA (kg/m ²)	NO./AREA (no./m ²)
090AZ-1	10.0	15.0	12.5	5.45	0.0	0	0.00	0.0000
090AZ-2	15.0	20.0	17.5	7.64	72.9	33	9.55	4.3217
090AZ-3	20.0	25.0	22.5	9.82	55.7	28	5.67	2.8521
090AZ-4	25.0	30.0	27.5	12.00	87.6	30	7.30	2.5002
090AZ-5	30.0	35.0	32.5	14.18	46.2	23	3.26	1.6219
090AZ-6	35.0	40.0	37.5	16.36	48.0	28	2.93	1.7112
090AZ-7	40.0	45.0	42.5	18.54	78.6	30	4.24	1.6178
090AZ-8	45.0	50.0	47.5	20.73	60.1	30	2.90	1.4475
090AZ-9	50.0	55.0	52.5	22.91	53.7	33	2.34	1.4406
090AZ-10	55.0	60.0	57.5	25.09	0.0	0	0.00	0.0000
090AZ-11	60.0	65.0	62.5	27.27	0.0	0	0.00	0.0000
090AZ-12	65.0	70.0	67.5	29.45	0.0	0	0.00	0.0000
090AZ-13	70.0	75.0	72.5	31.63	0.0	0	0.00	0.0000
090AZ-14	75.0	80.0	77.5	33.82	0.0	0	0.00	0.0000
090AZ-15	80.0	85.0	82.5	36.00	0.0	0	0.00	0.0000
090AZ-16	85.0	90.0	87.5	38.18	0.0	0	0.00	0.0000
090AZ-17	90.0	95.0	92.5	40.36	0.0	0	0.00	0.0000
090AZ-18	95.0	100.0	97.5	42.54	0.0	0	0.00	0.0000
Totals					502.8	235		

Table 63. Rock rubble from 5-deg sector, 270-deg azimuth, PAS-4.

ZONE	INSIDE RADIUS (m)	OUTSIDE RADIUS (m)	AVERAGE RADIUS (m)	ZONE AREA (m ²)	WEIGHT (kg)	NUMBER	WT./AREA (kg/m ²)	NO./AREA (no./m ²)
270AZ-1	10.0	15.0	12.5	5.45	0.0	0	0.00	0.0000
270AZ-2	15.0	20.0	17.5	7.64	65.4	30	8.56	3.9289
270AZ-3	20.0	25.0	22.5	9.82	64.2	31	6.54	3.1576
270AZ-4	25.0	30.0	27.5	12.00	105.0	40	8.75	3.3336
270AZ-5	30.0	35.0	32.5	14.18	58.8	34	4.15	2.3976
270AZ-6	35.0	40.0	37.5	16.36	141.5	49	8.65	2.9947
270AZ-7	40.0	45.0	42.5	18.54	112.4	39	6.06	2.1031
270AZ-8	45.0	50.0	47.5	20.73	92.6	24	4.47	1.1580
270AZ-9	50.0	55.0	52.5	22.91	0.0	0	0.00	0.0000
270AZ-10	55.0	60.0	57.5	25.09	0.0	0	0.00	0.0000
270AZ-11	60.0	65.0	62.5	27.27	0.0	0	0.00	0.0000
270AZ-12	65.0	70.0	67.5	29.45	0.0	0	0.00	0.0000
270AZ-13	70.0	75.0	72.5	31.63	0.0	0	0.00	0.0000
270AZ-14	75.0	80.0	77.5	33.82	0.0	0	0.00	0.0000
270AZ-15	80.0	85.0	82.5	36.00	0.0	0	0.00	0.0000
270AZ-16	85.0	90.0	87.5	38.18	0.0	0	0.00	0.0000
270AZ-17	90.0	95.0	92.5	40.36	0.0	0	0.00	0.0000
270AZ-18	95.0	100.0	97.5	42.54	0.0	0	0.00	0.0000
Totals					639.9	247		

7.0 CONCLUSIONS AND RECOMMENDATIONS

The following is a summary of the observed response of each of the major structural elements of the shelter. Throughout the summary, probable causes for the particular response are presented. Also included are conclusions concerning the hazards that could be expected from full-size shelters with equivalent explosives loadings.

Recommendations for future structural design concepts of similar structural systems, which could reduce the hazard potential of debris, are given following the review. The reader should be familiar with the details of the structural response of each of the four tests described earlier.

Very general qualitative comments are also made concerning the distribution of the smaller debris (dimensions less than 500 mm for 1/3-scale), from the tests. Suggested geometries to define the hazard zones are presented for equivalent full-size shelters. These suggestions should not be construed as recommendations for the hazard zones or Quantity-Distance criteria. Development of such criteria would be based on a detailed analysis of the debris, which was beyond the scope of this project.

7.1 STRUCTURAL RESPONSE

7.1.1 Summary

All structures exhibited the same patterns of response under the effects of a detonation of a bare, centrally-located, explosive charge. The level of damage experienced by the structure was a function of the amount of explosives used. In each case the structure began as a relatively tightly closed system. Upon detonation of the charge, the structure was internally pressurized with the blast and quasi-static pressures. Under the effects of the internal pressure, the door and backwall were pushed outward causing the arch to be in tension in the longitudinal direction. In addition, internal radial pressure placed the arch in hoop tension.

7.1.1.1 Front door—Under pressure, the door was bent about a horizontal centerline as it reacted against the slots in the parapet and floor and against the wingwalls at the sides of the opening. If the pressure and impulse was large enough (e.g., PAS -2, -3, and -4), the combination of the bending of the door and the outward deformation of the arch under radial pressure allowed the door to blow out of the structure. As it blew out, the side edges were bent inward as it moved past the wingwalls. In all cases the door became airborne in a relatively short time after leaving the structure. In PAS-3, the door tumbled end-over-end during its flight; in PAS-4, it appeared to exhibit aerodynamic characteristics for part of its flight. In all cases where the door was blown out of the structure, it generally traveled farther than most of the other pieces of debris from the structure. It was also observed that all the doors ended up within a circular area having an angle not exceeding 10 deg from the extended axis of the structure.

7.1.1.2 Exhaust port doors—In PAS -1 and -2, the exhaust port doors remained within the shelter. In PAS -3 and -4, the exhaust port doors were blown out the back of the structure as single units. The exit trajectory angle was equal to, or greater than, the slope of the floor in the exhaust port. In all four tests the doors were bent in half about a horizontal line. The final location of all the exhaust port doors was within 15 deg of the extended center line of the structure.

7.1.1.3 Arch—The same breakup patterns of the arch were observed in all four tests. Even though the arch of the PAS-1 structure did not break up into individual pieces, it did exhibit some crack patterns similar to those observed in PAS -2, -3, and -4. The quantity of explosives that determined the range that the pieces of the arch traveled.

Transverse cracks in arch: With the arch in tension from the internal pressure against the door and backwall, the concrete failed in tension at the transverse liner joints where the cross-sectional area was the smallest. In every structure, the transverse cracks observed corresponded directly to a liner joint. If the energy from the blast was sufficiently large, some of these transverse cracks developed into lines of failure in the arch. In almost every case, these failure planes corresponded with a line of splices in one or both of the reinforcing bar layers.

In every test where the arch broke apart, there were three common locations for the transverse failure planes. One location was about 4000 mm from the backwall and corresponded to the only location where a line of splices in the inner layer of those bars existed near a similar line of splices in the outer layer of those bars. Even in the PAS-1 test a transverse crack was observed at this location.

Another common location for a transverse failure plane was at or near the center of the arch, over GZ. This failure plane location often corresponded with a splice location in the longitudinal reinforcing bars. Failure planes were observed at this general location for PAS -3 and -4; a transverse crack was observed at this location in PAS -1 and -2. The third common transverse failure plane was generated at the junction of the arch and backwall as the arch tore off its foundation and began to move upward.

Depending upon the energy from the blast, additional transverse failure planes developed first at or near a line of splices in the longitudinal reinforcing bars, and then at other locations as a function of the bending of the arch system as it was blown upward.

Longitudinal cracks in arch: With the arch in hoop tension from the internal radial pressure on the arch, the concrete also cracked in tension along longitudinal lines. If the energy from the blast was large enough, some of these longitudinal cracks developed into failure planes. For those structures in which the arch broke up, two common longitudinal failure lines were observed. One was at the centerline of the crown of the arch, and the other was at the foundation-arch joint on both sides of the shelter. Two additional lines were observed in PAS-4. One corresponded to the location on both sides of the arch where the line of splices in the inner layer of transverse reinforcing bars existed near the similar line of splices in the outer layer of those bars. The second additional line was seen on both sides near the base where the thickness of the arch began to increase.

Breakup patterns in arch: The combination of the major transverse and longitudinal failure planes caused the arch to break up into several large rectangular pieces (see

Sections 4.2.1, 5.2.1, and 6.2.1). The quantity of explosives used influenced the total number of pieces produced. The smaller the explosive quantity, the fewer pieces were generated. PAS-1 produced no large pieces, PAS-2 produced only 2 large pieces, PAS-3 produced 7 large pieces, and PAS-4 produced 23 large pieces.

As a general observation, the breakup pattern in the arch was directly influenced by the presence of the lines of splices in the reinforcing bars. The presence of the bolted connections joining the individual segments of a single rib of the corrugated steel liner did not appear to affect the breakup pattern of the arch.

Final locations of arch pieces: Under the impulse from the blast, the large pieces were launched upward and outward from the structure. The distance the pieces traveled was a function of the quantity of explosives used. As the quantity increased, the pieces traveled farther. The arches of PAS -1 and -2 remained virtually in their original positions. Although PAS-3 broke apart, the pieces fell back within the limits of the structure. The pieces of PAS-4 traveled as far as 122 m from the model structure. Neglecting the effects of gravity, this would be equivalent to 366 m in a full-size shelter.

In the case of PAS-4 where the arch pieces were thrown beyond the structure, the direction of travel was confined to either side of the structure. No large arch piece was directed to the front or back of the structure.

7.1.1.4 Backwall—The backwall was observed to have the same general pattern of damage in all tests. In the PAS -1 and -2 tests, the backwall suffered only minor cracking. The cracks extended from the upper corners of the exhaust port opening, diagonally upward toward the top edge of the backwall. In PAS-3, the cracks were much larger but in the same location. The section of the PAS-4 backwall above the opening was blown off, failing along the same diagonal lines seen in the other three structures. It should be noted that a line of splices in the horizontal reinforcing bars above the opening was located on either side of the opening and probably contributed to the similar cracking and failure pattern observed in all tests. The backwall on either side of the exhaust port opening suffered little or no damage in each test.

In all tests the backwall was observed to have been tipped backward, rotating at the foundation. The amount of rotation was a function of the quantity of explosives used. In PAS-1, the rotation was small but observable. In PAS-2, the angle of rotation was less than 2 deg. In PAS-3, the angle was about 5 deg; in PAS-4, the wall was rotated backward 30 deg. In observing the high-speed films and the posttest conditions in the field, it was seen that the backwall was rotated backward as the arch section moved upward. The arch first broke away at the center, near GZ, and then continued to "peel" off the foundation toward the back and front. The relatively large stiffness of the arch section, as compared to the backwall, caused the backwall to rotate backward with the arch as the arch moved upward. The backwall continued to rotate backward until stopped by resistance from the soil berm and the exhaust port elements, and the arch broke away from the top of the backwall. Internal pressure against the backwall probably contributed to the backward movement of the wall as well.

In the PAS-3 test, the debris produced was generally from the top edge of the backwall. In addition, some debris from the area of the two large diagonal cracks was found. In the PAS-4 test, where the top section of the backwall above the opening broke away, it broke into two pieces and was found behind the shelter. In this test, the pieces were found within 12 m of the back of the structure. Neglecting gravity effects this would be 36 m for a full-size shelter.

7.1.1.5 Exhaust port—During the detonation, the volume inside the exhaust port up to the doors was pressurized from the blast. If the energy was large enough, as in the case of PAS -3 and -4, the exhaust port roof lifted off the side and center walls. In the PAS-3 test, the exhaust port roof was lifted several millimeters above the walls and, though heavily fractured, remained near the shelter. In PAS-4, the exhaust port roof was blown off the walls and was found heavily fractured behind the shelter near the top portion of the backwall.

As the exhaust port roof was being lifted up, the exhaust port walls were also lifted off their foundation slab and pushed outward to the side. In the PAS-4 test, each side wall was also broken along a vertical line corresponding to the location where the wall

thicknesses changed abruptly. In the PAS -3 and -4 tests, the exhaust port walls also broke away from the backwall. However, in no test were the side walls of the exhaust port found much beyond the edge of their foundation slab.

The exhaust port doors were bent backward and as noted above, some broke away from their steel frames embedded in the concrete walls, roof, and floor. If the energy was great enough, as in the PAS -3 and -4 tests, the doors and frames were blown back and impacted the endwall of the exhaust port. The endwall was broken from the sidewalls and blown back behind the shelter. In both tests, the endwall was also broken into several smaller pieces. These pieces were found behind the shelter at distances less than the final locations of the exhaust port doors.

7.1.1.6 Foundation—In every test the arch foundation was found relatively undamaged. In the PAS -2, -3, and -4 tests, the dowel bars connecting the arch to the foundation were broken or had pulled out of the arch.

The backwall foundation was found damaged in the PAS -2, -3, and -4 tests. In all cases the damage was a longitudinal crack running the full length of the foundation. In addition, various degrees of cracking were observed at the junction of the backwall and arch foundations. The size of the cracking was observed to be directly related to how much the backwall was rotated backward during the test.

In all the tests, virtually no damage was observed to the front foundation and door pit area. In addition, no tie beams were found broken in any of the four tests. No debris was produced by the foundations.

7.1.1.7 Floor slab—In all four tests, the floor slab experienced varying degrees of damage at the GZ location depending on the size of the charge used. In PAS-1, the floor slab had minor cracking and was pushed down into the soil. In the other three tests, the detonation produced a crater of rubbleized concrete at the GZ. In these tests, the craters were relatively small compared to the total floor area and produced no debris beyond the structure.

The only other major damage to the floor slab occurred in the PAS-4 test when the backwall and foundation were rotated backward. As the backwall was rotated backward, the front edge of the foundation was lifted upward, cracking and breaking the floor slab. This cracking pattern was also observed to lesser degrees in the other three tests.

7.1.2 Conclusions

7.1.2.1 In front of the shelter—In terms of size, weight, and range traveled, the front door could be considered the "biggest" hazard to other structures in front of the shelter. Neglecting the effects of gravity for the purposes of comparison, the final position of doors from full-size shelters having 300 kg, 900 kg, and 2700 kg of explosives would be 60 m, 340 m, and 1200 m respectively. Assets within the range of the door would clearly be at risk of being destroyed or significantly damaged by the door. Fortunately, the area influenced by the door is relatively small, since it is a sector with an angle of only 10 deg on either side of the centerline of the shelter. It should be noted that the ranges observed could possibly be reduced because of the effects of the cables of the door-lifting systems. However, the same cable system could also cause the door to be directed at a greater angle to either side of the shelter than that observed in these tests.

7.1.2.2 In back of the shelter—The exhaust port doors could be considered the biggest hazard to assets located behind the PAS. Again, neglecting gravity effects, the full-scale distances for the exhaust port doors would be 450 m and 325 m for full-size structures with 300 kg and 2700 kg of explosives respectively. However, like the front, the area influenced by the exhaust port doors is relatively small, for it is a sector with an angle of less than 15 deg to either side of the centerline. The curved geometry of the full-size exhaust port in the area outside the doors differs somewhat from the test model. This curvature might possibly reduce the maximum range the doors could travel by directing them upward as they are blown out. In addition, the hydraulic lifting mechanisms could influence the maximum range the doors would travel.

In comparison to the exhaust port doors, the pieces of the backwall and exhaust port could not be considered a major hazard at the back of the shelter. However, in the

range between the shelter and the final locations of the exhaust port doors, the pieces from the backwall and exhaust port could be considered as the major hazard.

7.1.2.3 To the sides of the shelter—As in the case of the front door and exhaust port doors, the large arch pieces could be considered a major hazard to the sides of the structure. Whether the arch would break up and be directed away from the structure was dependent on the quantity of explosives used. The quantity used in PAS-3 (an amount equivalent to 900 kg for a full-size shelter) could be considered as an upper limit where the large arch pieces do not constitute a hazard at the sides of the shelter.

7.1.3 Recommendations for Future Structural Improvements

7.1.3.1 Arch-foundation connection—The size of the reinforcing bars connecting the arch to the foundation appears to influence the way the arch breaks up and the pieces are dispersed around the shelter. Because the percentage of reinforcing is relatively small, the connection is easily broken as the arch is subjected to the internal radial pressure from the blast. Once the bars are broken, the arch sections are unrestrained and are free to be blown away from the shelter.

If the percentage of reinforcing were greater, it might restrain the arch sections for a longer time and prevent them from being blown a great distance from the shelter. Instead, the longitudinal failure plane would be developed only at the crown. The arch would open up along this line, venting the pressure. The two sides of the arch would be pushed outward, pivoting about the strong foundation joint. Instead of being blown several hundred meters from the shelter, the arch sections would remain relatively close. The process could be enhanced by creating a "weak" line along the crown by locating a line of splices of the transverse reinforcing bars there. In addition, the breakup of the two arch sides into smaller pieces could be minimized by staggering all the splice locations of the reinforcing bars in both directions.

7.1.3.2 Frangible structural elements—The fact that the structure begins as a tightly enclosed system appears to influence the distances the front door and exhaust port

doors travel. In addition, the enclosed system influences the formation of the transverse and longitudinal cracks, which then determines the breakup pattern of the arch. If in future designs, the concepts of a tightly enclosed system could be eliminated, in favor of a simply closed system, the range of debris could probably be reduced. For example, if the headworks at the front door could be designed to provide resistance for external loads but be unrestrained for internal blast pressure, the door could act like a frangible element, by not allowing the internal pressure to reach and maintain the levels seen in the tightly closed system of the model PAS test structures. Instead, the door would be quickly blown down on the apron slab under a relatively small value of impulse, reducing the distance it would be driven. This early venting of the blast pressure would also reduce the total impulse on the backwall and the arch, which in turn would minimize both transverse and longitudinal cracking and the formation of failure planes in the arch, as well as reduce the energy available to launch the pieces of the arch great distances. A similar type of design could also be provided for the exhaust port doors, one which would allow them to be blown down early, helping to further reduce the peak pressures and total impulse on the shelter.

7.2 CONCRETE DEBRIS

7.2.1 Summary of Debris Distribution

7.2.1.1 PAS-1—No debris was produced, which would correspond to 100 kg of explosives in a full-size shelter.

7.2.1.2 PAS-2—Only 29 pieces of small-size debris having a dimension of less than 500 mm were recovered, corresponding to 300 kg of explosives in a full-size shelter. The front door and all but two pieces of the debris recovered were found in the front of the structure. Of the debris in front, only six pieces were found beyond 25 m, with the maximum range of 72 m from the front of the model, or 216 m for a full-size structure. All the debris in front of the shelter was from the parapet and wingwalls and resulted from damage when the door was blown out.

The maximum range for the two pieces found at the side of the PAS-2 model was 34 m, which corresponds to a range of about 100 m for a full-size shelter. If the ranges of the PAS-2 debris were multiplied by three to represent similar ranges from a full-scale structure with 300 kg of explosives, the door and all but the farthest six pieces of debris generated in the test would fall within a circle having a radius of 100 m.

7.2.1.3 PAS-3—The majority of the debris recovered was generally distributed along the longitudinal axis of the shelter, rather than to the sides. For example, a diamond drawn with one axis 140 m long from the center of the shelter toward the front, one axis 170 m from the center to the back of the shelter, and the two side axes 50 m long from the center, would encompass 95 percent of all the debris produced (Fig. 287).

Neglecting the effects of gravity, these dimensions should be multiplied by three to represent a full-size structure.

It would appear that over half of the debris found to the sides of the shelter originated at the failure planes of the large arch pieces, at which planes the concrete was rubbleized as the reinforcing bars broke or were pulled out of the adjacent piece. Broken concrete was also produced as the arch was lifted upward crushing the concrete at the failure planes.

Debris to the back of the shelter originated mainly from the exhaust port and the failure plane at the junction of the arch and the backwall. Debris to the front appeared to originate from the parapet and wingwalls.

7.2.1.4 PAS-4—In comparison to PAS-3, the debris from this test was distributed about the same distances to the front and back of the shelter but almost three times as far to the sides. For example, a diamond drawn with axes of 170 m to the front, 115 m to the back, and 200 m to the sides, would enclose 98 percent of the debris (Fig. 288).

Like PAS-3, the debris recovered at the sides of the PAS-4 shelter appeared to originate from the arch. The debris to the back came from the exhaust port and backwall; the debris found toward the front came from the parapet and wingwalls.

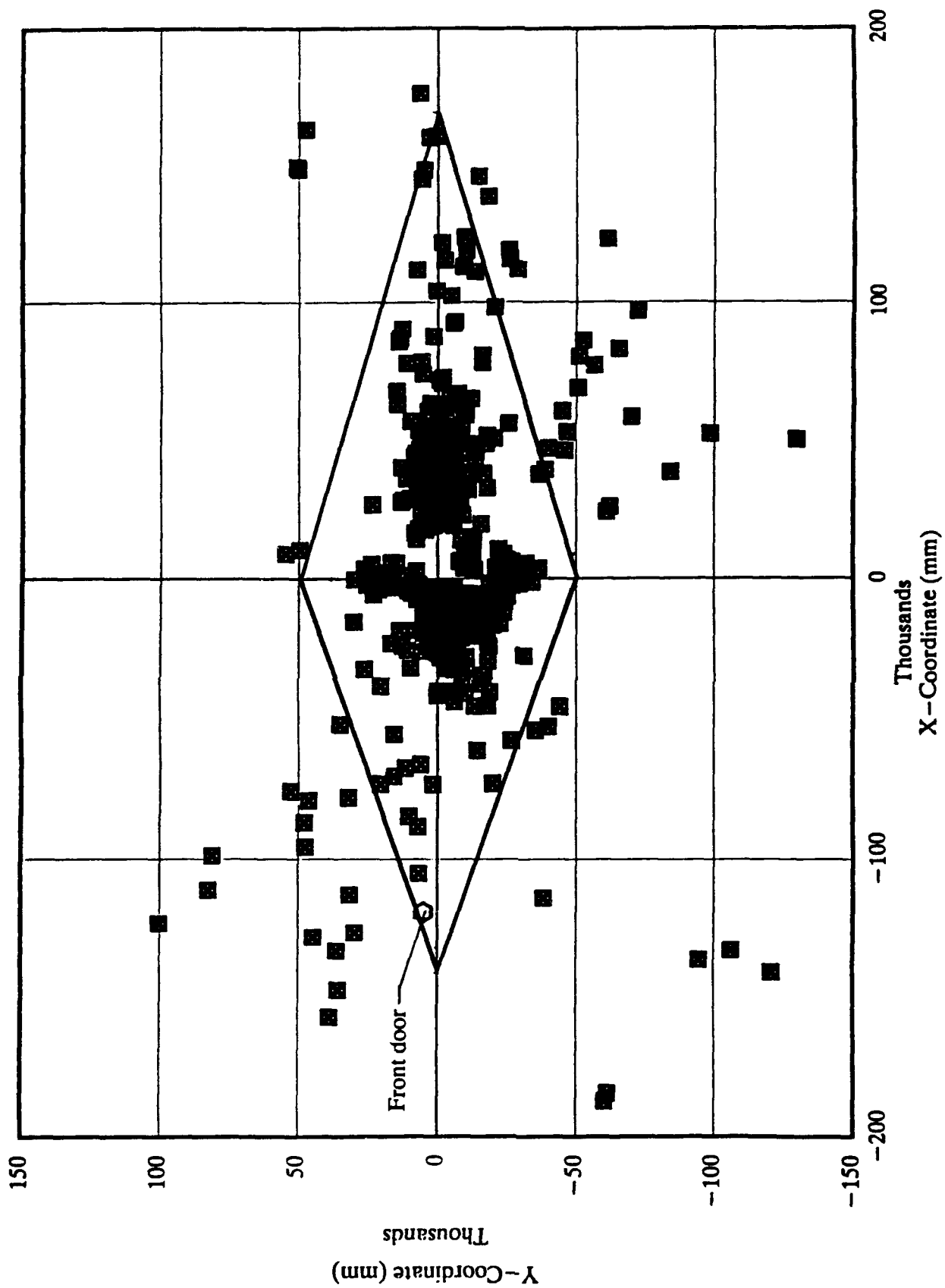


Figure 287. Suggested hazard boundary geometry, PAS-3.

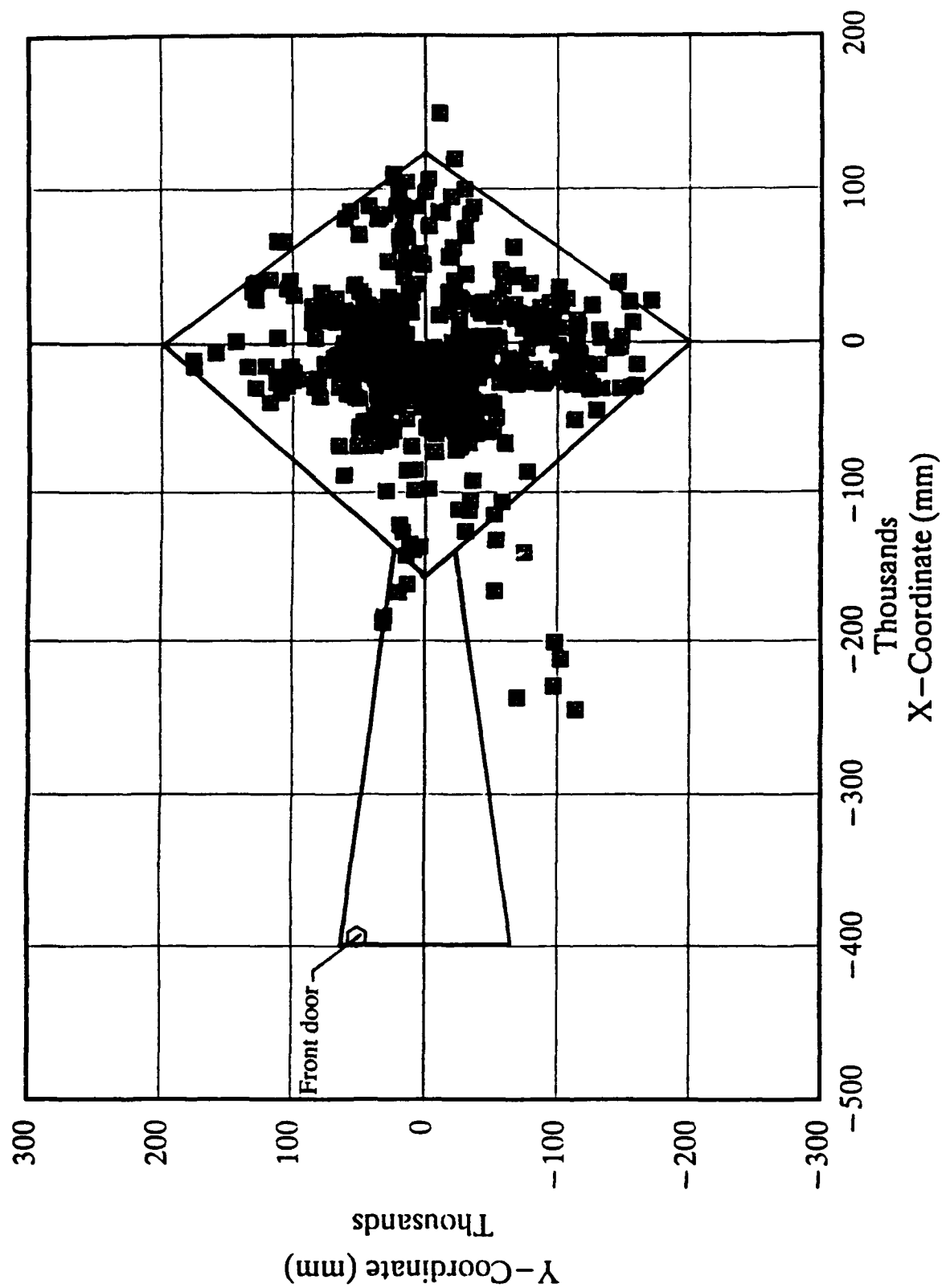


Figure 288. Suggested hazard boundary geometry, PAS-4.

For the PAS -2, -3, and -4 tests, the distribution of small debris generally followed the distribution of the large components such as the front door or the large arch pieces. For example, the large arch sections in PAS-3 remained close to the shelter, and there was correspondingly little distribution of the small debris to the sides of the structure. The large arch sections in PAS-4 were blown some distance to the sides of the shelter, and there was a large amount of small pieces of debris at the sides.

7.2.2 Conclusions

For a full-size shelter having an amount of explosives equal to or less than 100 kg (PAS-1), one would not expect to see any debris generated. If the quantity of explosives in the full-size shelter is increased to 300 kg (PAS-2), the amount of debris produced could still be considered insignificant. A quantity of explosives near 300 kg could be considered as an upper boundary for zero debris, especially to the back and sides of the shelter.

Neglecting the effects of gravity, a circle having a radius of 100 m for a full-size shelter would encompass over 95 percent of the debris produced from the explosions of 100 kg and 300 kg and could be considered as the boundary of a minimum hazard zone for shelters having any amount of explosives.

The diamond shape described above appears to encompass efficiently over 95 percent of the debris produced in the PAS -3 and -4 tests, and appears to be the appropriate geometry to describe the boundaries of the hazard areas for full-size shelters having amounts of explosives greater than 300 kg. An alternative to the diamond shape could be an ellipse having the same axes as the diamond.

If a diamond with dimensions three times those noted above were used to represent the hazard area of a full-size shelter with 900 kg of explosives (PAS-3), the area enclosed would be about 140,000 m² (Fig. 287). A circle, with a diameter equal to the long axis of the diamond, would have an area almost five times larger and include only 2 percent

more (or 97 percent) of the debris. It should be noted that this geometric shape also encompasses the front door, the exhaust port doors, and all the large arch pieces.

In some cases, attempting to draw a diamond geometry to include all of the large sections, such as the front door in the PAS-4 test, results in a distorted pattern having one relatively long axis. This distorted diamond shape also encompasses a large area without any debris potential. In such cases, a pie-shaped sector, encompassing the large piece that produced the distorted pattern, would be added to a diamond geometry, which efficiently encloses the other pieces of debris defined as hazardous.

For 2700 kg of explosives in a full-size shelter (PAS-4), one could consider a diamond geometry having dimensions three times as large as those discussed above to define the hazard area. This particular geometry encompasses 98 percent of the debris, but not the front door. To include the area affected by the front door, a pie-shaped sector having a radius of 1200 m and an angle of 10 deg on either side of the center line of the shelter would be added to the diamond (Fig. 288). This configuration results in an area encompassing about 40 percent of a circular area and about 75 percent of a standard diamond.

As noted at the beginning of this section, the exact geometries of the hazard areas can only be determined by a detailed analysis of the debris distribution data and the operational conditions for the shelters. Consequently, the geometries proposed above should be considered as suggestions.

ABBREVIATIONS AND ACRONYMS

deg	degrees
g	gravity
gm	gram
kg	kilograms
kPa	kilopascals
m	meters
mm	millimeters
MPa	megapascals
PAS	Protective Aircraft Shelter
SCS	Shelter Coordinate System
SF	Space Factor
SIFCON	Slurry-Infiltrated Fiber Concrete
WES	Waterways Experiment Station (US Army Corps of Engineers)